

AD-A216 445

FILE COPY

(2)

AFOSR/ONR Contractors Meeting

**COMBUSTION
ROCKET PROPULSION
DIAGNOSTICS OF
REACTING FLOW**

June 13 - 17 1988

DTIC
ELECTED
DEC 20 1989
S E D

Division of Engineering and Applied Science
Pasadena, California 91125

California Institute of Technology

Unclassified

SECURITY CLASSIFICATION OF THIS PAGE

Form Approved
OMB No. 0704-0188

REPORT DOCUMENTATION PAGE

1a. REPORT SECURITY CLASSIFICATION Unclassified		1b. RESTRICTIVE MARKINGS										
2a. SECURITY CLASSIFICATION AUTHORITY		3. DISTRIBUTION/AVAILABILITY OF REPORT Approved for public release; distribution is unlimited.										
2b. DECLASSIFICATION/DOWNGRADING SCHEDULE												
4. PERFORMING ORGANIZATION REPORT NUMBER(S)		5. MONITORING ORGANIZATION REPORT NUMBER(S) AFOSR-TR-89-1710										
6a. NAME OF PERFORMING ORGANIZATION Air Force Office of Scientific Research	6b. OFFICE SYMBOL (If applicable) AFOSR/NA	7a. NAME OF MONITORING ORGANIZATION AFOSR/NA										
6c. ADDRESS (City, State, and ZIP Code) Bolling AFB DC 20332-6448	7b. ADDRESS (City, State, and ZIP Code) Building 410, Bolling AFB DC 20332-6448											
8a. NAME OF FUNDING/SPONSORING ORGANIZATION AFOSR/NA	8b. OFFICE SYMBOL (If applicable) NA	9. PROCUREMENT INSTRUMENT IDENTIFICATION NUMBER <i>AFOSR-DO-0337</i>										
8c. ADDRESS (City, State, and ZIP Code) Building 410, Bolling AFB DC 20332-6448	10. SOURCE OF FUNDING NUMBERS <table border="1"><tr><td>PROGRAM ELEMENT NO. 61102F</td><td>PROJECT NO. 2308</td><td>TASK NO.</td><td>WORK UNIT ACCESSION NO.</td></tr></table>			PROGRAM ELEMENT NO. 61102F	PROJECT NO. 2308	TASK NO.	WORK UNIT ACCESSION NO.					
PROGRAM ELEMENT NO. 61102F	PROJECT NO. 2308	TASK NO.	WORK UNIT ACCESSION NO.									
11. TITLE (Include Security Classification) (U) AFOSR/ONR Contractors Meeting - Combustion, Rocket Propulsion, Diagnostics of Reacting Flow												
12. PERSONAL AUTHOR(S) J M Tishkoff, M A Birkan, G S Roy, and S G Lekoudis												
13a. TYPE OF REPORT Technical Report	13b. TIME COVERED FROM _____ TO _____	14. DATE OF REPORT (Year, Month, Day) 1988, June, 13	15. PAGE COUNT 358									
16. SUPPLEMENTARY NOTATION												
17. COSATI CODES <table border="1"><tr><th>FIELD</th><th>GROUP</th><th>SUB-GROUP</th></tr><tr><td> </td><td> </td><td> </td></tr><tr><td> </td><td> </td><td> </td></tr></table>		FIELD	GROUP	SUB-GROUP							18. SUBJECT TERMS (Continue on reverse if necessary and identify by block number) Combustion, Shear Layers, Supersonic, Soot, Sprays, Boron Lasers, Rocket, Nitramines, Turbulence, Plasmas, Instability	
FIELD	GROUP	SUB-GROUP										
19. ABSTRACT (Continue on reverse if necessary and identify by block number) Abstracts are given for research efforts on airbreathing combustion, rocket propulsion, and diagnostics of reacting flows supported by the Air Force Office of Scientific Research and the Office of Naval Research. <i>R&D Keldysh (S)</i>												
89 12 20 015												
20. DISTRIBUTION/AVAILABILITY OF ABSTRACT <input checked="" type="checkbox"/> UNCLASSIFIED/UNLIMITED <input checked="" type="checkbox"/> SAME AS RPT <input type="checkbox"/> DTIC USERS		21. ABSTRACT SECURITY CLASSIFICATION Unclassified										
22a. NAME OF RESPONSIBLE INDIVIDUAL Julian M Tishkoff		22b. TELEPHONE (Include Area Code) (202)767-0465	22c. OFFICE SYMBOL AFOSR/NA									

AFOSR/ONR CONTRACTORS MEETING
ROCKET PROPULSION – DIAGNOSTICS – COMBUSTION
CALIFORNIA INSTITUTE OF TECHNOLOGY

June 13 – 17, 1988

Approved for public release;
 Distribution is unlimited.

CONTENTS

AIR FORCE OFFICE OF SCIENTIFIC RESEARCH
 NOTICE OF TRANSMITTAL TO DTIC
 This technical report has been reviewed and
 approved for public release IAW AFR 190-12.
 Distribution is unlimited.
 MATTHEW J. KEEFER
 Chief, Technical Information Division

**(A) AFOSR CONTRACTORS MEETING ON ROCKET
 PROPULSION**

1. Agenda	1
2. Abstracts Of Work Presented	7
3. Abstracts Of Work Not Presented	105
4. List Of Invitees	117

**(B) AFOSR CONTRACTORS MEETING ON DIAGNOSTICS
 OF REACTING FLOW**

1. Agenda	131
2. Abstracts Of Work Presented	135
3. List Of Invitees	183

(C) AFOSR/ONR CONTRACTORS MEETING ON COMBUSTION

1. Agenda	187
2. Abstracts Of Work Presented	193
3. Abstracts Of Work Not Presented	289
4. List Of Invitees	345

AGENDA

1988 AFOSR CONTRACTORS MEETING ON ROCKET PROPULSION

13-15 June 1988

Howard Johnson Plaza-Hotel
Monrovia CA

Monday, 13 June

8:15	Welcome and Administrative Announcements	
Session Topic:	Electromagnetic Propulsion	
Chairman:	Seetharam Deevi, University of California, Davis	
8:30	Basic Processes of Plasma Propulsion H. O. Schrade, Universitat Stuttgart	7
9:30	Fundamental Research on Erosion Magnetoplasmadynamic Thrusters V. V. Subramaniam, Ohio State University	11
9:55	Physical Fluid Dynamics in MPD Thrusters M. Martinez-Sanchez, Massachusetts Institute of Technology	15
10:20	BREAK	
10:40	MPD Arcjet Thrust Chambers Flow Dynamics P. Turchi, R & D Associates	19
11:05	Electron-Cyclotron-Resonance Plasma Acceleration F. E. C. Culick, J. Sercel, California Institute of Technology	25
11:30	Plasma Inductive Thruster Clamped Discharge Evaluation C. L. Dailey, TRW Space and Technology Group	29
11:55	A Numerical Study of the Physics and Engineering of the Hybrid Plume Plasma Rocket T. F. Yang, Massachusetts Institute of Technology	33
12:20	LUNCH	

(cont'd)
Keywords:)

Session Topic:	Electrothermal Propulsion	
Chairman:	Leanne Pitchford, GTE Laboratories	
2:00	Laser Thermal Propulsion D. Keefer, University of Tennessee Space Institute	39
3:00	Effects of Turbulence on Stationary and Nonstationary Processes in C-Systems R. Beddini, University of Illinois	43
3:25	BREAK	
3:45	Coupling Between Radiation and Gas Dynamics C. L. Merkle and M. M. Micci, Pennsylvania State University	47
4:10	Heating of a Liquid/Vapor Mixture by a Pulsed Electric Discharge R. L. Burton, GT Devices	55
4:35	Plasma Initiation Mechanisms for CW Propulsion H. Krier, University of Illinois	59
5:00	RECESS	

Tuesday, 14 June

8:15	Administrative Announcements	
Session Topic:	Propellants	
Chairman:	Arthur Fontijn, Rensselaer Polytechnic Institute	
8:30	Propellants T. B. Brill, University of Delaware	63
9:30	Combustion Technology J. T. Edwards, AFAL	67
9:55	Chemical Kinetics of Nitramines Propellant Combustion M. Branch, Colorado University	71
10:20	BREAK	
10:40	Basic Research in the Chemistry and Combustion of Nitroform Compounds M. Frankel and D. O. Woolery, Rocketdyne	Abstract Not Available

11:05	Combustion of Hydrogen and Hydrocarbons in Fluorine M. Kaufman, Emory University	75
11:30	Plume Technology D. P. Weaver, AFAL	79
12:15	LUNCH	
Session Topic:	Instability	
Chairman:	Jay Levine, AFAL	
1:30	Instability R. S. Brown, United Technologies Chemical Systems Division	83
2:30	Particle Combustion in Solid Propellants M. Beckstead, Brigham Young University	85
2:55	Energy Exchange Mechanisms Between the Mean and Acoustic Flow Fields in Solid Rocket Combustion Chambers J. D. Baum, Naval Research Laboratory	89
3:20	BREAK	
3:45	Investigation of the Flame-Acoustic Waves, Interaction During Axial Solid Rocket Instabilities B. T. Zinn, Georgia Institute of Technology	93
4:10	Solid Fuel Combustion J. S. Tien, Case Western Reserve University	97
4:35	Fractal Image Compression of Rayleigh, Raman, LIF and LV Data in Turbulent Reacting Flow W. C. Strahle, Georgia Institute of Technology	101
5:00	recess	

Wednesday, 15 June

8:45	Administrative Announcements
9:00 - 12:00	WORKSHOPS (Locations To Be Announced)
	Space Power
	MPD Models and Diagnostics
12:00	LUNCH

Administrative Session

1:30	AFAL Research Interests R. R. Weiss, Chief Scientist, AFAL	
2:15	Dr. Michael J. Salkind, AFOSR/NA	
2:30	BREAK	
3:00	AFOSR Rocket Propulsion Interests M. A. Birkan, AFOSR/NA	
3:20	AFOSR Interests in Airbreathing Propulsion and Diagnostics of Reacting Flow J. M. Tishkoff, AFOSR/NA	179
3:40	Open Discussion of Government Support for Propulsion Research	
4:30	GENERAL ADJOURNMENT	
4:30	Business Meeting AFOSR Contractors Only	
7:00 - ?	BANQUET	

Accession For	
NTIS Serial	_____
DDIC Ref.	_____
Unpublished	_____
Justification	_____
Event	
Distribution	_____
Availability Notes	
Comments	_____
Dist	_____
<i>A-1</i>	

ABSTRACTS OF RESEARCH NOT
PRESENTED

Physics of Positively Biased Conductors Surrounded by Dielectrics in Contact with A Plasma D. E. Hastings, Massachusetts Institute of Technology	105
Asymptotic Methods Applied to Plasma of Knudsen Thermionic Converters G. L. Main, Georgia Institute of Technology	109
Diagnostics for Intelligent Adaptive Control of MPD Engines R. Shoureshi, Purdue University	113

BASIC PROCESSES OF PLASMA PROPULSION

(AFOSR Grant No. 86-0337)

Principal Investigator: Herbert O. Schrade

Institut für Raumfahrtssysteme
University of Stuttgart
Pfaaffentaldring 31
D-7000 Stuttgart 80
Federal Republic of Germany

OVERVIEW:

H. O. Schrade, M. Auweter-Kurtz, H. L. Kurtz, and P. C. Sleziona
The proposed research addresses itself to the not fully understood processes and problem areas in magnetoplasmadynamic thruster devices, in order to predict and improve their performance. These problem areas are a) the knowledge of the interphase area between current carrying plasma and the surrounding cold gas and/or walls, b) the discharge behavior within the plasma region and c) the electrode attachment and erosion processes.

TECHNICAL DISCUSSION:

a) The interphase area between the electrically active and heated plasma region and the surrounding cold gas and/or walls is characterized by heat conduction, radiation and convection. Depending on the overall pressure, the cold gas flow and the chamber geometry, this interphase area or surface area of the heated plasma body proper assumes a certain configuration or shape. It is of interest now to know this shape in order to predict heat loads to the walls and/or to avoid overheating of the chamber and nozzle walls. Besides the electrode attachment area, one of the most crucial regimes with respect to overheating is the nozzle throat walls. The goal is now to determine the size of the discharge channel within the throat and the heat load to the inner walls as a function of mass flow rate and current. In a first step, based on a new semiempirical analytical approach, the shape of a discharge channel in an axial flow tube has been calculated. Moreover, under the assumption that the arc fills the nozzle throat, the radial heat flux to the walls were calculated for a paraboloid shaped current density profile of grade n and the results compared with caloric measurements on the Stuttgart nozzle type MPD thruster. They showed good agreement at a current range of about 4000 A but at lower currents (1000 A) the experimental values dropped to half of the calculated ones, which is an indication that the arc size may not entirely fill the throat (see Fig. 1).

b) Based on a semi-two-dimensional model approach, a numerical analysis was developed to predict the overall performance of a nozzle type MPD thruster. A nonequilibrium nozzle flow was taken, which distinguishes between an isothermal behavior of the electrons and an adiabatic behavior of the ions. Input data are geometry of the thruster, mass flow rate and electric current; the output data are current contour lines, thrust and specific impulse. Comparison between calculated and measured thrust shows good agreement. This analysis has been improved by a more rigorous two-component approach, which accounts first for the energy exchange between the electrons and ions, second for the heat conduction of the electron component and the heat losses to the walls and third for the radial Lorentz force effects on the

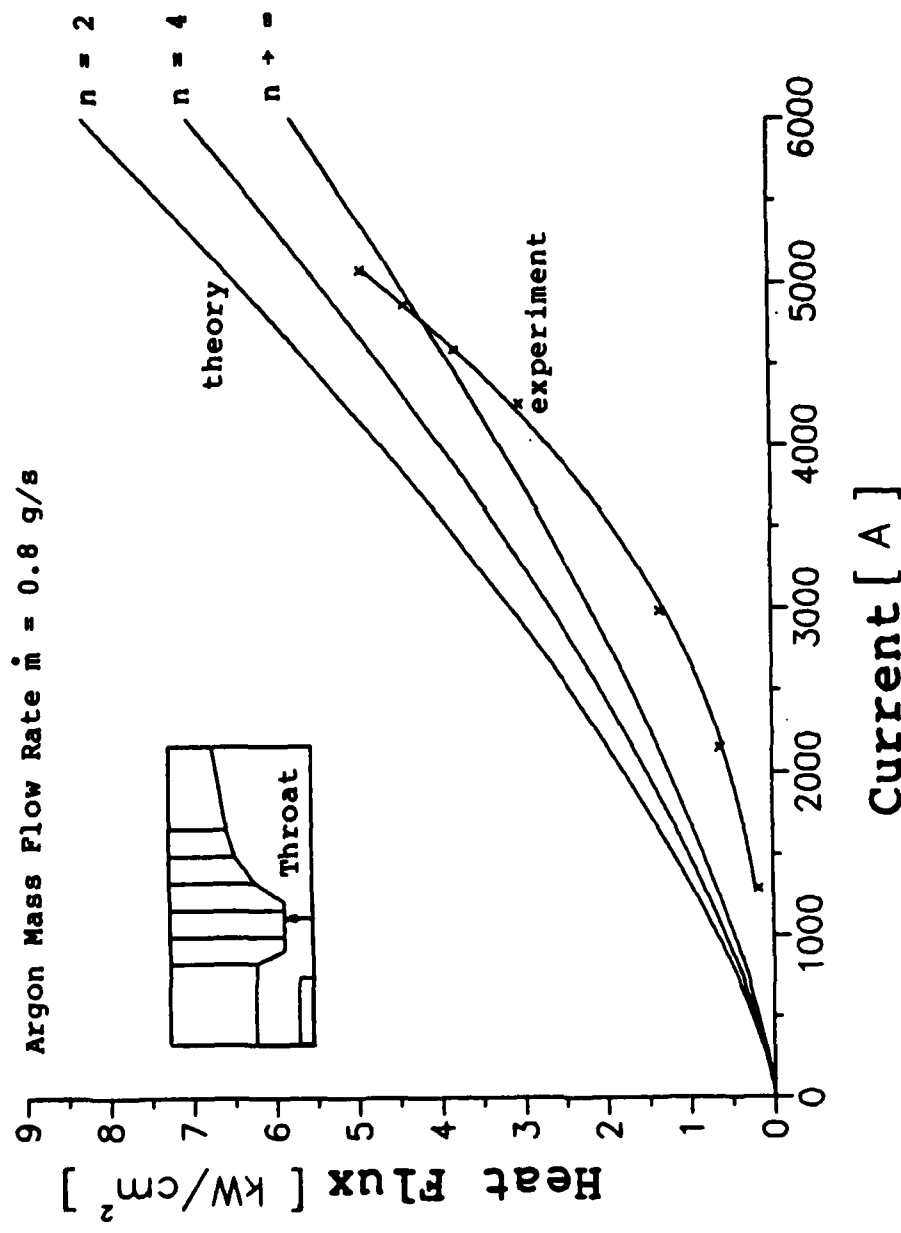


Fig. 1 Radial heat flux per unit channel length within nozzle throat.

plasma density. In Fig. 2 the calculated electron temperature distribution is plotted within the rz -plane of the Stuttgart MPD nozzle type thruster. For this thruster type a reevaluation of Hügel's* "onset" explanation by plasma starvation at the anode has been conducted. Excellent agreement with experimentally found onset conditions was achieved when, according to the calculations of the innermost anode point, the plasma density dropped to zero. In addition to this more heuristic approach, it was shown by means of a unique stability theory that any rotationally symmetric flow discharge configuration should become asymmetrical if the quotient of the axial impulse transport divided by the square of the electric current drops below a certain value. More detailed calculations revealed so far that a helically shaped discharge channel (or several of them) resemble(s) a more stable discharge configuration. These calculations will be continued, since they may have an impact on the behavior of high power MPD thrusters when operated beyond "onset." In addition, a computational code for a time dependent, fully two-dimensional, cylindrical MPD channel flow has been set up and is being tested for different exhaust conditions. In this numerical analysis (the plasma is considered to be a one-component mixture; friction is neglected) one calculates for a given current versus time curve, after each small time step, the time dependent flow and pressure field by means of an improved MacCormack code and then for these fields the corresponding current contour lines by a finite differential code (Gauss-Seidel). So far, several calculations for a current rise curve proportional to $\sin^2 \omega t$ up to a given plateau at $\omega t = \pi/2$ have been conducted.

c) Processes on the electrodes decisively determine the entire discharge behavior of almost all arc devices and therefore also of MPD and/or arcjet thrusters. The cathode attachment of cold metal electrodes (average temperature far below that of thermionic emission) consists of one or more microscopically small, current carrying plasma jets which emanate(s) from a high temperature, electron emitting spot. The current density within these spots amounts to 10^{12} A/m^2 and more. Depending on the electrode material (oxidized surface layer, surface chemistry) surface roughness, overall temperature and type and pressure of the atmosphere, these spots cluster together to macrosots of different sizes with different erosion rates. The erosion rate or material loss of such a spot discharge stems mainly from two mechanisms: a) evaporation of cathode material and b) ejection of droplets and molten material (see Fig. 3). While evaporation (a) starts from the beginning of the spot discharge, the second mechanism (b) occurs after a molten layer has formed and been affected by the high plasma pressure, is thrown out at the rim of the spot crater and/or, after several unstable spots, causes splashing on a preheated molten area. These last mechanisms need a certain time to develop, but they are most destructive and cause not only a dramatic material loss but also quite severe damage to the cathode surface. A model calculation to account for this damage has been developed and will be implemented in the overall spot life cycle analysis. In addition, a new electrode test stand has been built, in which cathode erosion measurements under various operating conditions are conducted.

* H. Hügel, "Zur Funktionsweise der Anode im Eigenfeldbeschleuniger", DFVLR report FB-80-20, 1980

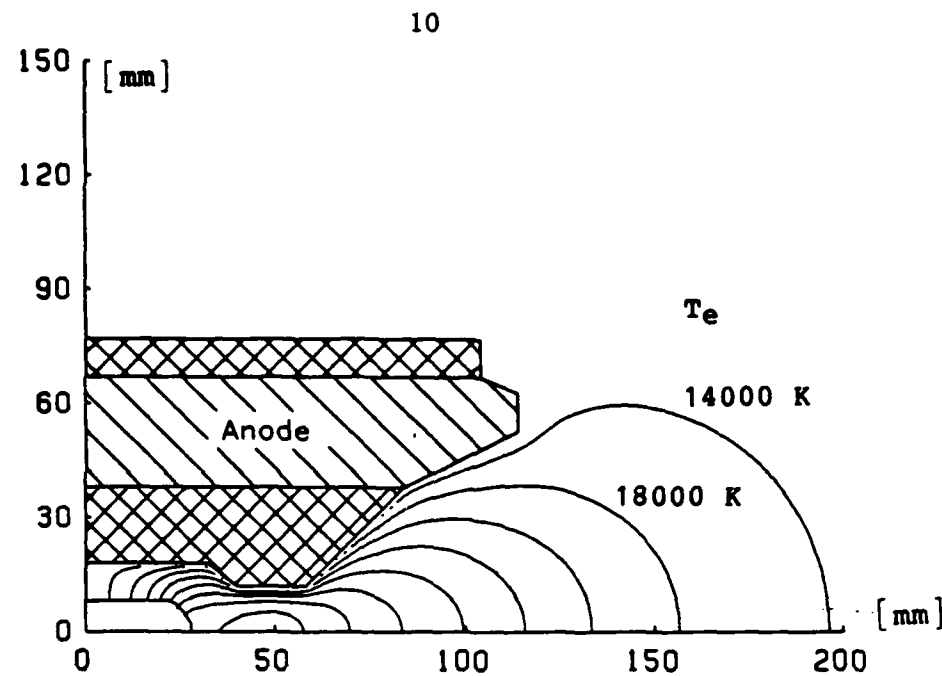


Fig. 2 Lines of constant electron temperature at $I = 3000 \text{ A}$.

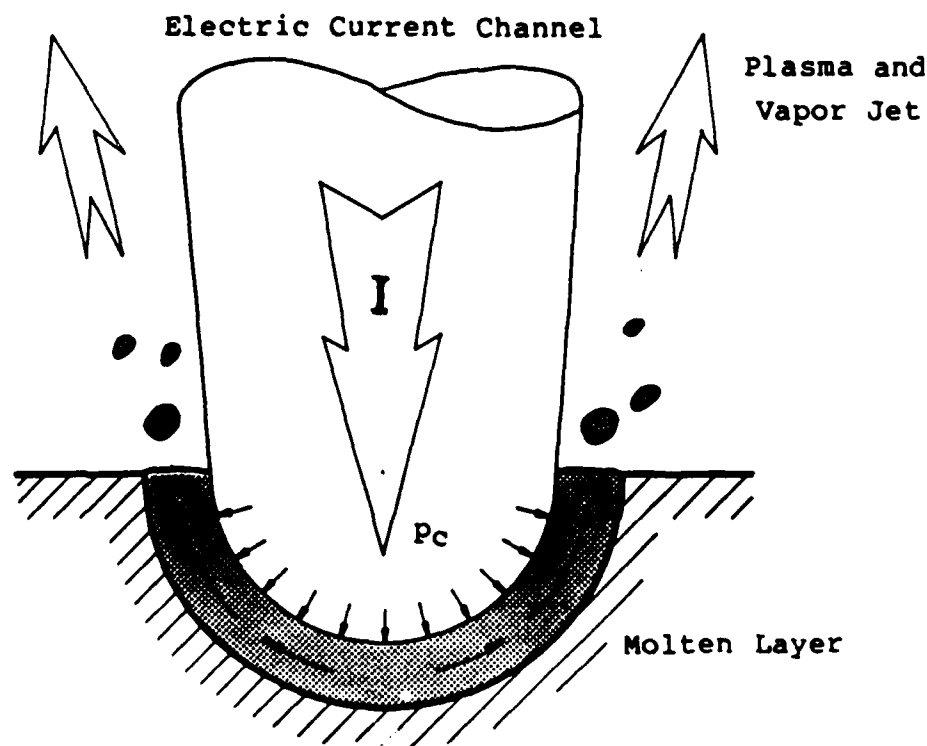


Fig. 3 Scheme of cathode spot.

FUNDAMENTAL RESEARCH ON EROSION IN MAGNETOPLASMADYNAMIC THRUSTERS

AFOSR Grant No. 87-0360

Principal Investigators : V. V. Subramaniam and J. W. Rich

Department of Mechanical Engineering
The Ohio State University
Columbus, Ohio 43210

SUMMARY/OVERVIEW:

The purpose of this research is to understand and quantify the mechanisms responsible for erosion in magnetoplasmadynamic (MPD) thrusters. This is an important step in being able to predict thruster lifetimes. The two major mechanisms of erosion are evaporative erosion and erosion by sputtering. At present, it is not known which of the two is more dominant and in which regions of the thruster. This analytical work aims to understand these mechanisms, their limits, and to provide quantitative models in order to estimate the lifetime of the cathode.

TECHNICAL DISCUSSION

The problem of cathode erosion in the MPD thruster involves a complex interaction between the electrode, the sheath, and the plasma outside the sheath. A detailed understanding of this coupled electrode-sheath-plasma interaction is necessary in order to calculate erosion rates due to evaporation and sputtering. A necessary first step to achieve this understanding is the prediction of electrode surface temperatures. The simplest steady state model to calculate cathode surface temperatures is discussed here, followed by a brief summary of ongoing and planned research.

Consider an energy balance on the cathode surface at steady state. This consists of a balance between electron bombardment, ion bombardment, ion surface recombinant heating, surface emission cooling,

radiative transfer to the anode, and heat transfer to an external coolant:

$$\frac{en_{\infty}C_e}{4}(\phi_c + \frac{2kT_{\infty}}{e})\exp(-eV_c/kT_{\infty}) + en_{\infty}C_i(V_c + \epsilon_i - \phi_c) = j_E(\phi_c + \frac{2kT}{e}) + \frac{5}{14}\sigma_{SB}(T^4 - T_A^4) + h(T - T_c) \quad (1)$$

where e is the electronic charge, n_{∞} is the plasma electron number density at the edge of the sheath, C_i is the ion speed based on the Bohm criterion, j_E is the surface emission current density, C_e is the electron mean thermal speed, k is Boltzmann's constant, T_{∞} is the electron temperature at the edge of the sheath, V_c is the cathode fall, ϕ_c is the cathode work function, ϵ_i is the ionization potential of the propellant, T is the cathode surface temperature, σ_{SB} is the Stefan-Boltzmann constant, T_A is the anode inner surface temperature, and h is the heat transfer coefficient for external cooling due to a coolant at temperature T_c .

The sheath voltage drop V_c must be determined from current conservation:

$$j_{\infty} = en_{\infty}C_i + j_E - \frac{en_{\infty}C_e}{4}\exp(-eV_c/kT_{\infty}) \quad (2)$$

Solving for V_c from equation (2) and substituting in equation (1) yields an implicit nonlinear equation for the cathode surface temperature T , with the charged particle number density n_{∞} , plasma current density j_{∞} , electron temperature T_{∞} , and electrode work function ϕ_c as parameters.

It has been found that the solution of equations (1) and (2) yields two steady state solutions for the cathode surface temperature, of which only one is a stable operating point. The other is an unstable thermal runaway point. Fig. 1 shows the typical variation of the heat defect (i.e. the net heat *into* the cathode surface) versus the surface temperature. The two possible steady state solutions are the intersections of the curve with the horizontal axis. It is apparent from this figure that the unstable root gives thermal runaway temperatures. Physically, this means that if the surface temperature increases just above the value given by the second root, the steady state energy balance indicates a further increase in temperature. This is because the only possible way of losing energy is through radiation, thermionic emission, and heat transfer to an external coolant, all of which increase with increasing temperature. This results in thermal runaway with eventual local melting of the surface.

The stable steady state solution may not exist for a certain range of values of the current density, electron and ion number densities at the sheath edge, temperatures, and the electrode material work function. This is a strong indication that stable steady state electrode operation depends on plasma discharge characteristics. Variations of the solutions of (1) and (2) with respect to the plasma discharge and electrode parameters are shown in Figs. 2-4. The lower branches in these figures correspond to stable

operation while the upper branches correspond to the thermal runaway.

In the remaining portion of this first year, we are studying the thermal response of a cylindrical cathode in the unsteady state in order to explore the possibility that the thermal runaway that has been found may represent a transition from diffuse to spot mode. This unsteady theory will include a model of the electrode adjacent sheath as well in order to correctly describe the boundary conditions. Further, research toward development of a theory of sputter erosion is being initiated. Once quantitative models of evaporative and sputter erosion are developed, the calculations will be compared with erosion measurements (specifically those of D. Q. King at the Jet Propulsion Laboratory, and H. O. Schrade at Universitat Stuttgart).

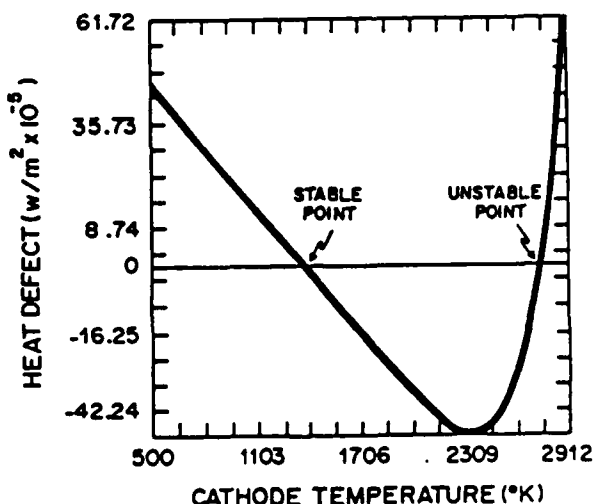


Fig. 1: The net heat into the cathode surface is shown here as a function of the surface temperature.

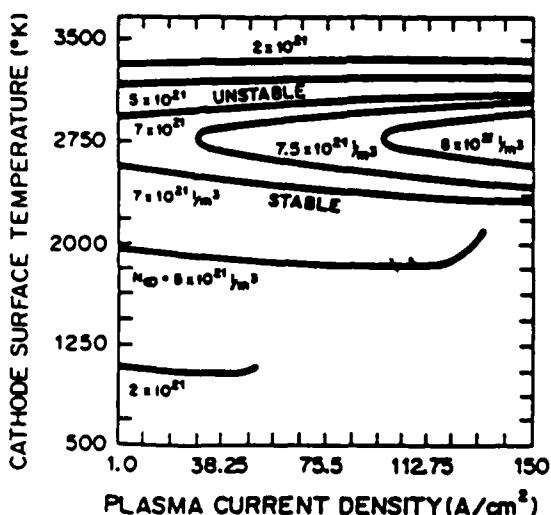


Fig. 2: The surface temperature calculated from the solution of equations (1) and (2), is shown here versus the plasma current density for various values of the charged particle number density at the sheath edge.

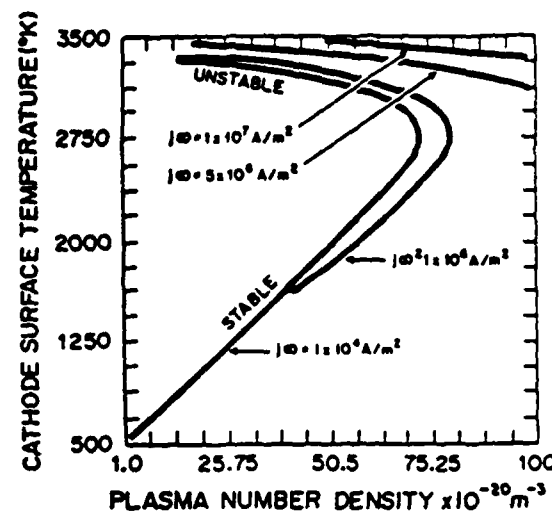


Fig. 3: The surface temperature calculated from the solution of equations (1) and (2), is shown here versus the charged particle number density at the sheath edge for various values of the plasma current density.

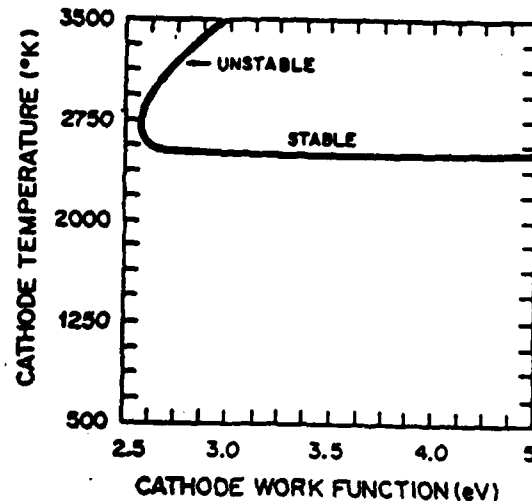


Fig. 4: The surface temperature calculated from the solution of equations (1) and (2), is shown here versus the cathode work function for a given plasma current density and a given charged particle number density at the sheath edge.

PHYSICAL FLUID-DYNAMICS IN MPD THRUSTERS

AFOSR Grant 86-0119

Principal Investigator: Manuel Martinez-Sanchez

M.I.T., Department of Aeronautics and Astronautics
Cambridge, Massachusetts 02139

SUMMARY:

Experimental results are reported on the effects of geometry variations on the performance of MPD thrusters. It is shown that convergent-divergent channels lead to more nearly uniform current and to reduced dissipation. Plasma data were also obtained spectroscopically, and ion temperatures of 3-6 eV were found, compared to 1-1.6 eV for the electrons. Theoretical work on these topics is underway.

TECHNICAL DISCUSSION:

The general objective of one work for this year has been to further understanding of the strong interactions between fluid dynamics, electromagnetic fields and atomic physics which seem inherent in the MPD regime of operation. This has been done through analysis, experiment and numerical work.

Our starting point was the analytical models reported previously (1), (2) in which the effects of channel contouring on accelerator performance were studied. One finding was that the Ohmic dissipation could be reduced for a given thrust level by favoring a uniform distribution of current density, which in turn could be achieved by adopting a convergent-divergent geometry. This could also have lifetime benefits, by reducing the strong inlet and exit current concentrations.

Three test channels were built to investigate these effects, one with a constant area, one with a flared downstream section and one with a convergent-divergent geometry. The latter was contoured using the simplified 2-D theory of Ref.(1), and a large cathode radius (5.5 cm maximum) and narrow throat width (2 cm) were used to approach 2-D conditions. The channels were tested at the R&D Associates Washington Laboratory, using 4 g/sec of Argon in 0.5 msec pulses. Probes were used to map the internal current and voltage distributions, and, in addition, spectral information was obtained at the exit plane using a 1.26 m spectrometer coupled to a digitizing camera. Possibly due to the large perimeter of the flow channel, some difficulty was experienced in obtaining azimuthally uniform ignition, except at current levels above ~35 KA. The theory predicted anode depletion at about 40 KA, and the data (Fig.1) show a strong rise of the anode drop between 30 and 40 KA, which seems to substantiate this. However, no increase in unsteadiness was observed until much higher currents (55 KA), when large voltage spikes appeared at intervals roughly corresponding to one flow passage time. These were visually associated with strong anode arcs.

The measured current density near the cathode is shown in Fig. 2 for the three channels. The constant area channel (CAC) shows the usual very strong

inlet and exit peaks. Partial flaring (PFC) eliminates the exit peak, and full flaring (FFC) does the same, and also reduces the inlet peak.

Electron temperature was measured at the exit plane from the slope of a Boltzmann plot using 6 AII high-lying lines. Values between 1 and 1.6 eV were measured, with little transverse variation (Fig. 3). Argon ion temperature and H neutral temperature (H_2 was added in some tests) were obtained from Doppler linewidths, and were found to be very high (Figs. 4,5) and different from each other. Attempts at Stark-width measurement of n_e failed due to the Doppler competition.

The unexpected heavy particle temperatures have prompted questions about possible strong viscous dissipation or internal shock layers around the cathode. Analysis is now underway on these points. A theoretical difficulty is the very strong drop in plasma viscosity as ionization sets in, which requires accurate coupled solution of both the flow equations and the ionization kinetics. Two different numerical codes are being adapted for this purpose. Work is also underway on collisional radiative models of AI, AII and H in order to extract additional information from the measured excited state densities.

REFERENCES:

- (1) M. Martinez-Sanchez and D.J. Heimerdinger, "Two-Dimensional Analysis of an MPD Arcjet", AIAA paper 85-2040. 17th International Electric Propulsion Conference, Alexandria, VA, 1985.
- (2) M. Martinez-Sanchez, "The Structure of Self-Field Accelerated Plasma Flows", AIAA paper 87-1065. 19th International Electric Propulsion Conference, Colorado Springs, CO, 1987.

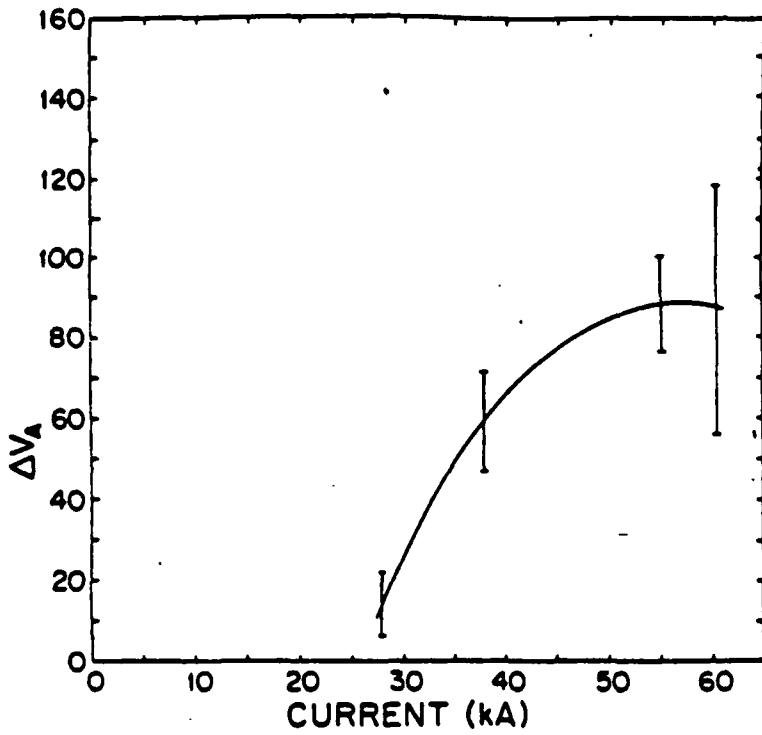


Figure 1 : Variation of the Voltage Drop from the Anode to a Point Two Millimeters from the Anode as a Function of Thrust Current in the Fully Flared Channel for an Argon Mass Flow Rate of 4 g/s

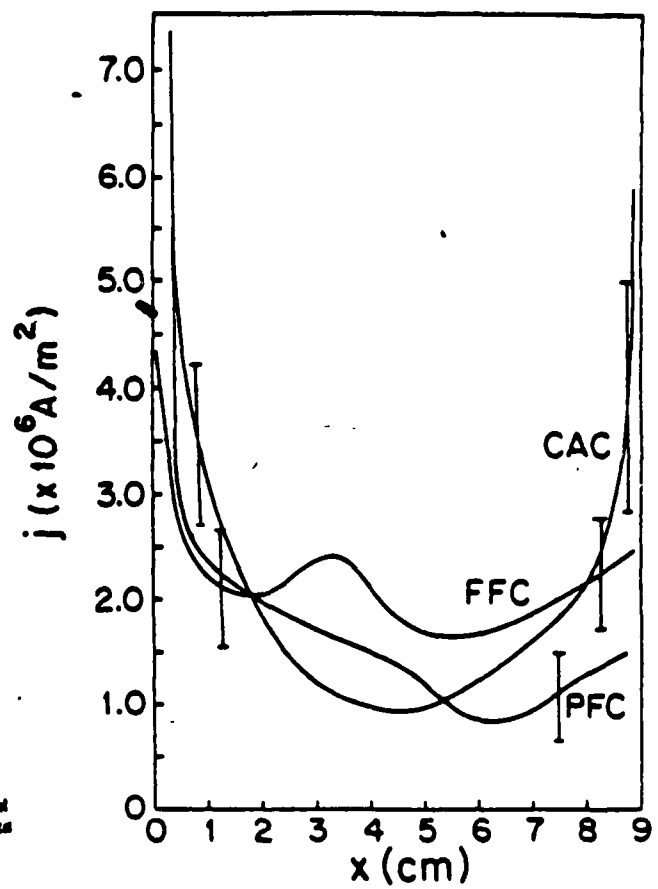


Figure 2 . Current Density Distribution on Each Cathode at 60 kA for an Argon Mass Flow Rate of 4 g/s

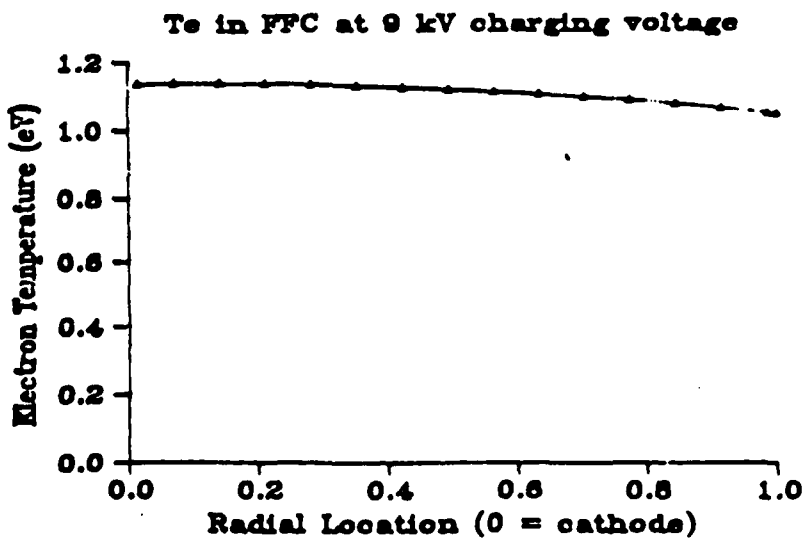


FIG. 3

FIG. 4

T_i for FFC at 9 kV charging voltage
(based on Argon FWHM)

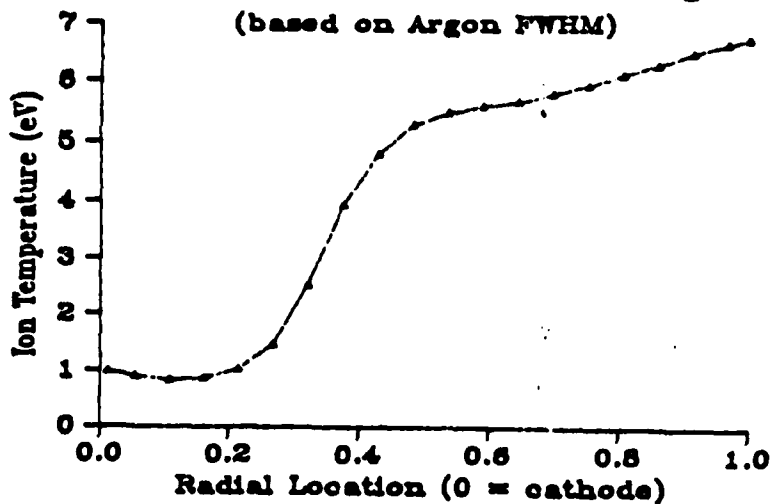
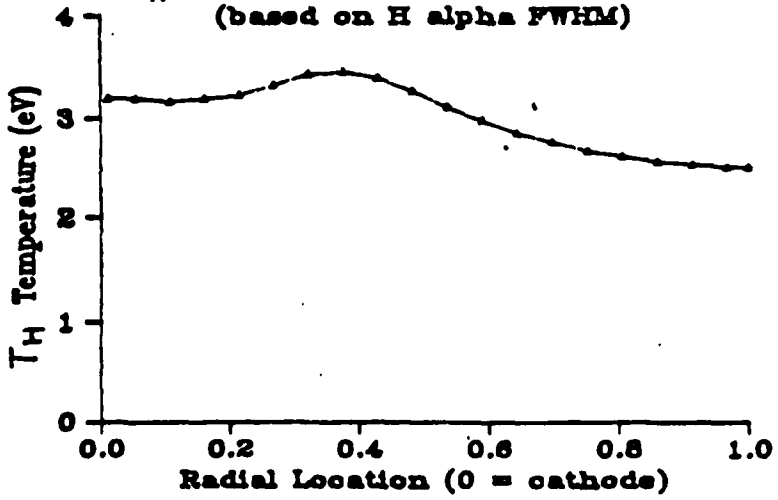


FIG. 5

T_H for FFC at 9 kV charging voltage
(based on H alpha FWHM)



MPD ARCJET THRUST CHAMBER FLOW DYNAMICS
(AFOSR Contract No. F49620-86-C-0117)

Principal Investigators: P.J. Turchi, J.F. Davis, III

R & D Associates
Washington Research Laboratory
301 S. West Street
Alexandria, VA 22314

SUMMARY/OVERVIEW:

The performance characteristics of MPD arcjets depend on proper matching of electromagnetic and fluid mechanical constraints within the thrust chamber. The present paper describes experimental measurements of flow conditions during MPD operation in an effort to guide development of flow models and to assess the validity of theoretical predictions. The parameters necessary to determine system performance include current, voltage, mass flow, interelectrode current and electric field distribution, electron density and temperature, ion density and temperature and ion velocity. The cylindrical two-dimensionality of the MPD flow field complicates comparison of experimental and theoretical results because simple solutions appropriate to the basic internal flow do not exist. Application of a two-dimensional MHD code (MACH 2) is in progress for comparison to experimental results with the goal of providing guidance in the design of improved MPD arcjets.

TECHNICAL DISCUSSION

Magnetic probes and floating electrostatic probes are used to map current contours and equipotential surfaces. Local measurements of the electron density and electron temperature are made using a swept Langmuir probe. Combination of a high resolution spectrograph with an intensified spectral and spatial data acquisition system provides digital output to a computer for analysis. Spatial distribution of electron temperature is inferred spectroscopically from observed argon line intensity ratios. The electron density distribution is inferred from line profile measurements of Stark broadened argon and hydrogen lines with corrections for contributions to the line profile due to thermal effects (Doppler broadening). These results are then compared to the Langmuir probe results. From knowledge of spatial electron density and temperature and by assumption of LTE or partial LTE the spatial plasma ion and neutral densities can be calculated. Spatial distribution of ion temperature is inferred from analysis of the emission line profiles of argon lines (which have little contribution to their profiles due to Stark effects).

Two MPD arcjet designs were used for the present experiments. The first device, studied extensively by Heimerdinger, et al., has a cathode center conductor diameter of 10.7 cm and an outer conductor inside diameter of 14.6 cm. Argon with 1.5 percent admixture of hydrogen by volume is used as

the propellant at a total flow rate of 4 g/sec. Current is delivered to the arcjet from an eight-stage PFN with a FWHM of 500 microseconds and peak current of 60 kA. Attempts have been made to characterize the argon ion axial flow velocity and ion temperature from measurements of the Doppler shift and emission profiles of ion spectral lines. Emission profile measurements were made of the Ar II 434.8 nm line at 0.5 and 15 cm axially downstream of the exit plane, viewed perpendicular to the arcjet centerline. Additionally, emission profile measurements were made looking axially upstream, parallel to the arcjet centerline and a slight angle (to avoid viewing the thrust chamber). These measurements indicate axial velocity components of up to 35 km/sec. At the arcjet exit plane, the inferred ion temperature varies from 3 eV near the cathode center conductor to 20 eV at the anode. At 15 cm axially downstream the observed emission profile is relatively uniform radially with radial velocity components (including thermal speed) of up to 13 km/sec. The interpretation of the data was difficult due to spatially-varying velocities and temperatures over the measurement line of sight.

In addition, local measurements of the electron density and electron temperature were made using a fast, optically-isolated, swept Langmuir probe with a temporal resolution of 200 nanoseconds. At the exit plane of the arcjet the electron density was $2 - 5 \times 10^{14} \text{ cm}^{-3}$ with an electron temperature of 1.5 to 7 eV. Temporal variations of the probe characteristic suggest that, for the conditions of operation, the MPD flow is not quasi-steady, but exhibits an early high density phase, followed by a lower density (possibly starved) phase and finally an approach to steady high density flow.

To avoid the complex temporal and spatial flow problems involved in the relatively large diameter/narrow annulus of the first device, a second MPD arcjet has been constructed with a brass outer anode 8.41 cm ID and a copper-tungsten alloy cathode 3.81 cm OD. The channel length is 5 cm from the boron nitride insulator backplate to the exit plane. Argon or argon-hydrogen mixtures are delivered to the arcjet through 16 choked orifices in the boron nitride backplate at the mid-radius of the channel gap. Current is delivered to the arcjet from the PFN with FWHM of 1 msec and peak current of 45 kA. The cylindrical two-dimensionality of the MPD flow field complicates comparison of experimental and theoretical results because simple solutions appropriate to the basic internal flow do not exist. Application of a two-dimensional MHD code (MACH 2) is in progress for comparison to experimental results with the goal of providing guidance in the design of improved MPD arcjets.

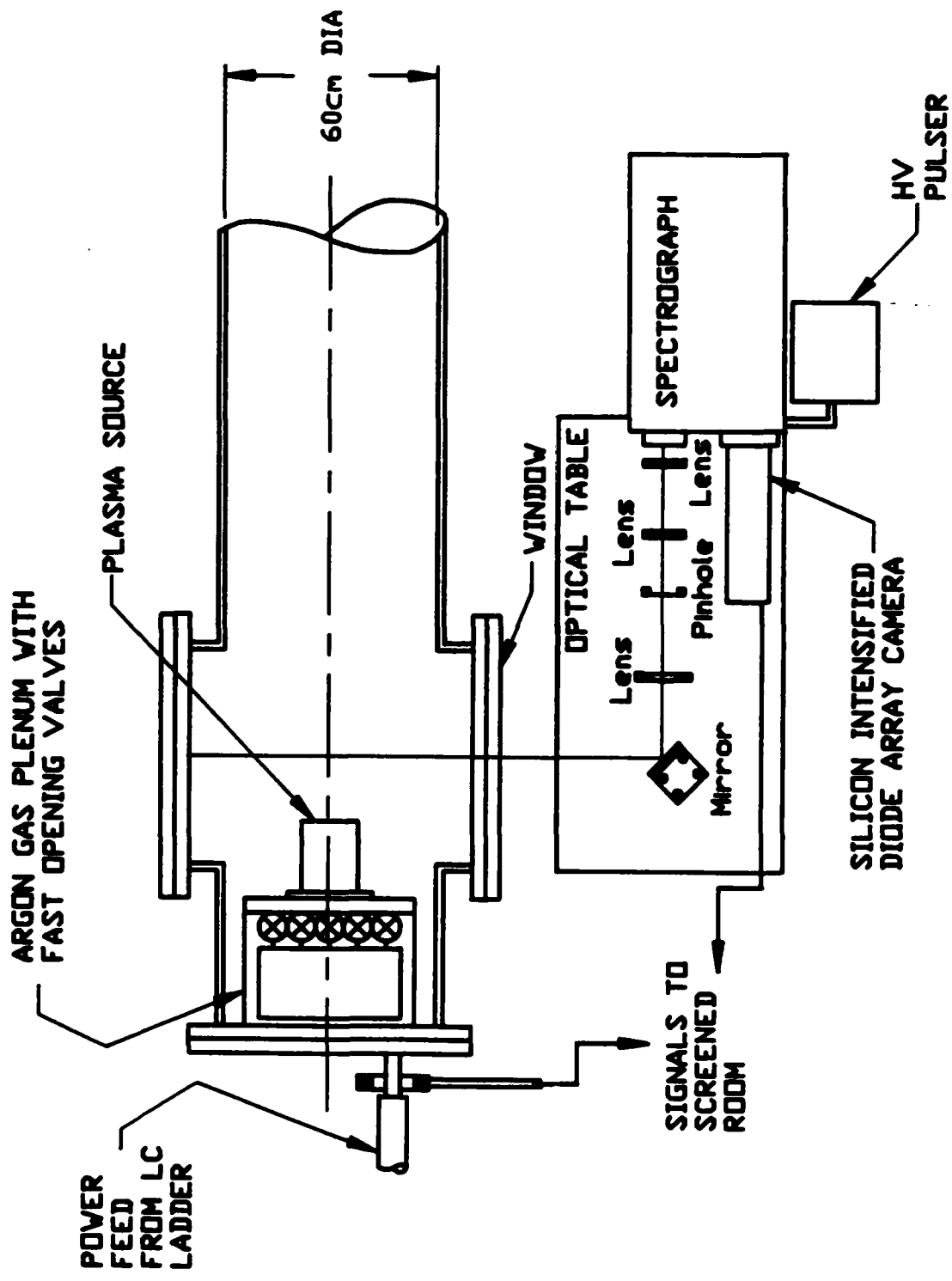


Figure 1. A quasi-steady MPD arcjet driven by an LC-ladder network is diagnosed using a time- and spatially-resolved spectrographic system and combinations of electrostatic and magnetic probes. The detailed data base thereby obtained allows comparison with theoretical models for MPD arcjet performance.

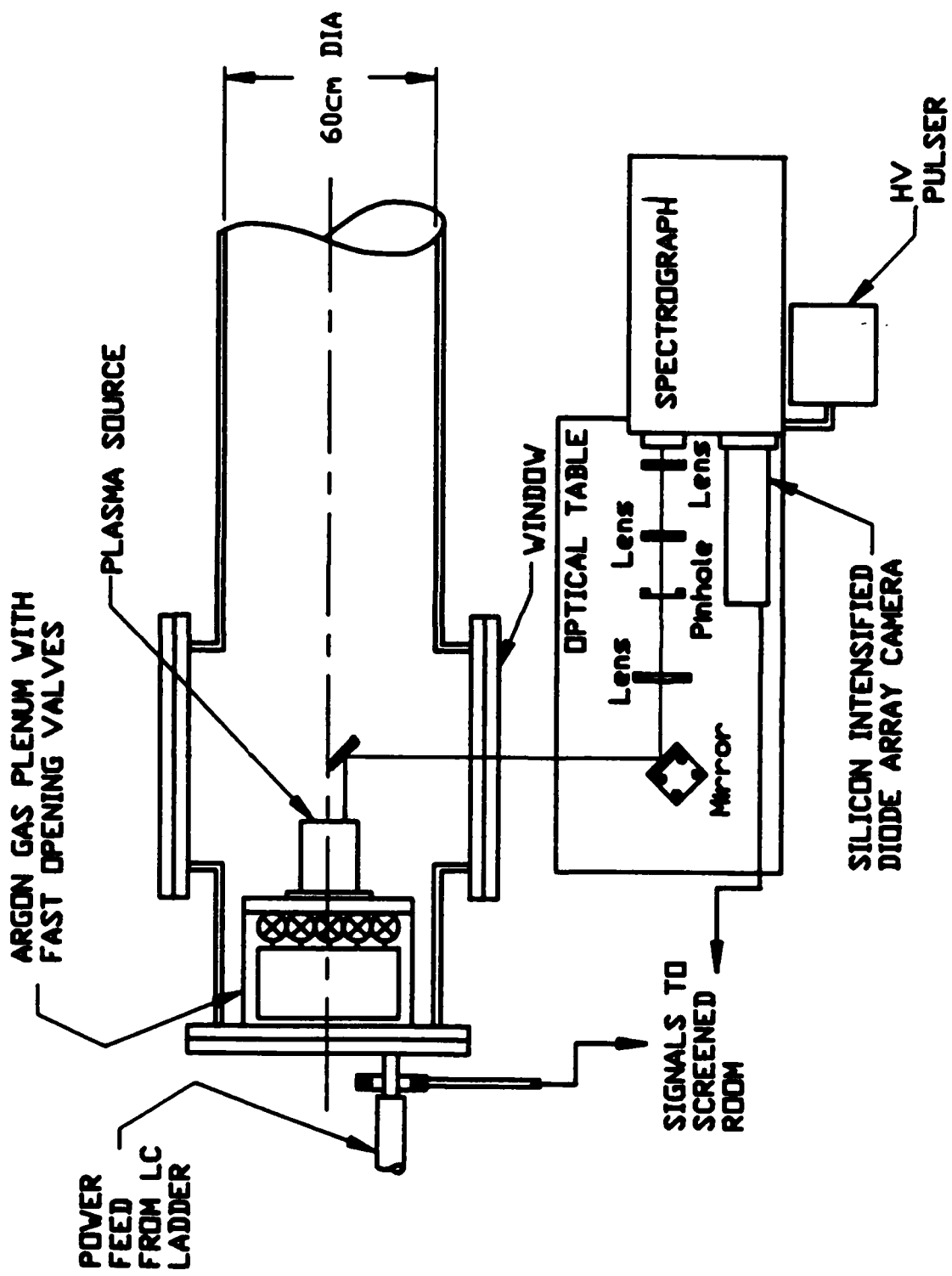


Figure 2. Spectroscopic measurement of line shape and displacement allows estimates of heavy particle speeds from Doppler broadening and Doppler shift.

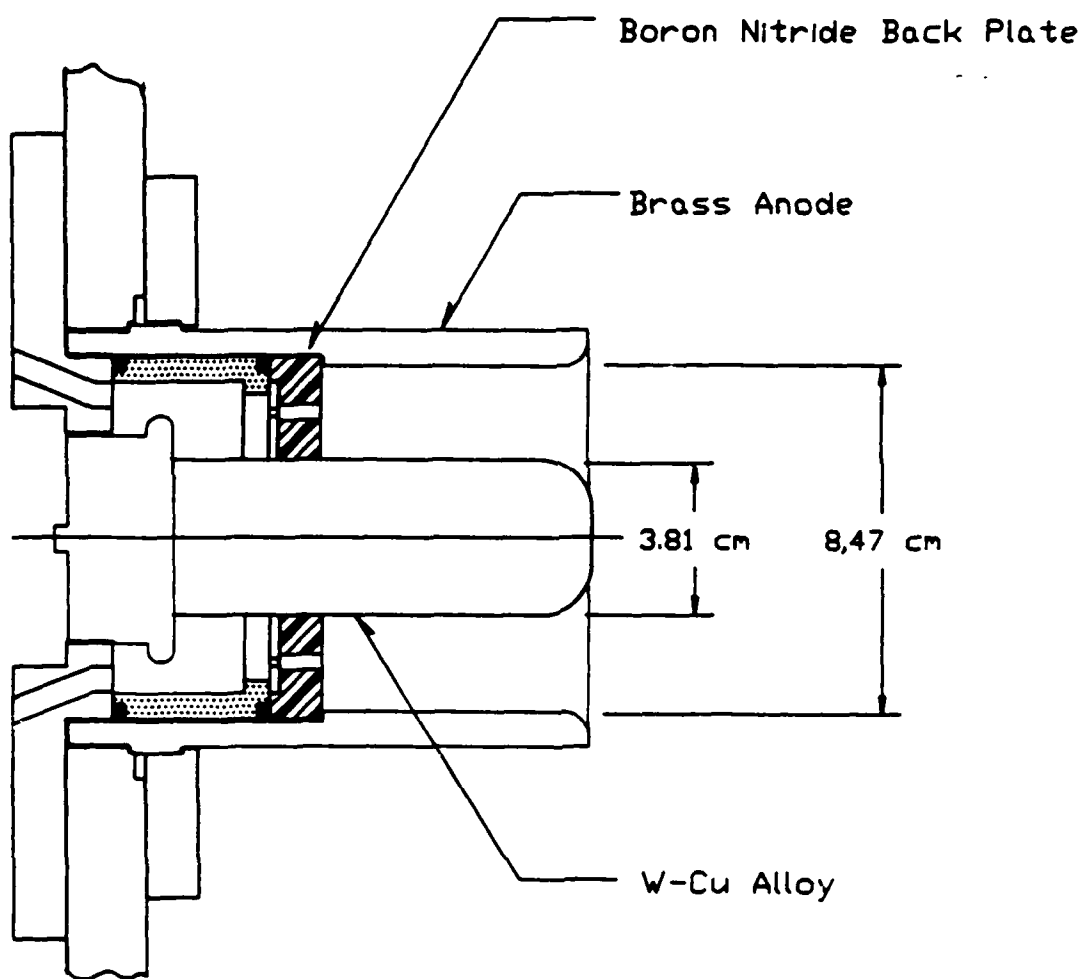


Figure 3. A new MPD arcjet device has been constructed and installed in order to provide quasi-steady MPD flow for comparison with numerical code calculations.

ELECTRON-CYCLOTRON-RESONANCE PLASMA ACCELERATION

Grant No. AFOSR-87-0205

F. E. C. Culick and J. C. Sercel

California Institute of Technology
Pasadena, California 91125

SUMMARY/OVERVIEW:

Electron-Cyclotron-Resonance (ECR) plasma acceleration is studied with the objective of developing a unified theory of this process. Analytical work has been concerned with cross field diffusion, plume divergence, ECR coupling of microwave power to plasma, and the effects of both elastic and inelastic electron-atom and electron-ion collision phenomena. Numerical calculations are in progress to unify the simple analytical models of the above effects into one computational model of ECR plasma acceleration which can be verified experimentally. An experimental apparatus has been developed with the unique capability of providing up to 20 kW of S-band microwave power for the scientific study of advanced microwave propulsion concepts. In initial tests, an argon ECR plasma has been initiated repeatably at power levels ranging from 0.3 to 7.0 kW. These tests confirm that the ECR coupling concept can be studied scientifically in the new apparatus.

TECHNICAL DISCUSSION

A collisionless model of ECR plasma acceleration first developed by Kosmahl¹ has been used to confirm that the shape of the plasma trajectory in separating from the magnetic field is independent of the ion mass and the magnitude of the assumed initial electron dipole moment (in the absence of the total accelerating energy), but is strongly dependent on the geometry of the applied diverging magnetic field and on the initial position of the plasma in the field. The conversion of the electron magnetic dipole energy into the directed energy of the ions is accomplished by an electrostatic potential supported by the dipole-moment force between the electron magnetic dipoles and the applied diverging magnetic field. The final azimuthal kinetic energy of the plasma particles was found to be negligibly small compared to the kinetic energy associated with their axial and radial motion.

Energy lost due to plume divergence in separating from the magnetic field can be expected to range from as low as 3 percent to as high as 10 percent of the total accelerating potential for simple field configurations of use in ECR plasma accelerators. Explicitly verifying this result was the first subject treated in the present analytical effort. Our results verify that even in the absence of collisions, the plasma can very efficiently be accelerated by, and separated from, a magnetic field of proportions useful for ECR plasma acceleration. We hope to extend this technique later in this program by relaxing the assumption of adiabatic invariability of the electron dipole moment through consideration of collisional effects.

In analyzing the effects of power lost to the walls of the accelerator due to diffusion of charged, energized species across magnetic field lines, it was found² that ECR plasma accelerators tested in the early 1960's operated under conditions for which the plasma would not be expected to move significantly down-stream before it diffused (by Bohm diffusion) across magnetic field lines. This observation explains the observed low thrust efficiencies of the early devices. Our quantitative analysis shows how to ensure, by design, that cross-field diffusion is not a dominant effect in

an ECR plasma accelerator; this design information has been incorporated into our laboratory apparatus.

Analysis of ion production and line radiation losses is being treated by the method of Dugan and Sovie.³ This method has been the standard approach to analyzing ion production costs in tenuous plasmas used in electric propulsion for the past two decades and is well understood. A unique aspect of the problem as applied to the ECR device is its somewhat higher electron energy as compared to, for example, ion thrusters. Calculations suggest that ion production costs in the ECR thruster should fall in the 30 to 50 eV/ion range.

Careful analysis of the electron energy distribution is closely linked to the problem of coupling microwave energy into the electron motion. We expect these linked problems to be the most challenging aspect of understanding ECR plasma acceleration. A meaningful solution will involve coupling the electron transport equations with the dynamical equations describing electron-cyclotron resonance, the electrostatic coupling of the electrons and ions through the space charge induced accelerating potential, and relevant collision phenomena, both elastic and inelastic.

As a first attempt to understand these problems, the elementary treatment of the propagation of right circularly polarized microwave radiation parallel to magnetic field lines was reviewed and applied to the ECR accelerator. This review showed that slightly upstream of the coupling region, very little microwave attenuation can be expected, as propagation occurs in the whistler mode. Further, since the applied magnetic field is near ECR throughout this plasma, reflection of the applied microwave power at the plasma frequency is minimized. A slightly more sophisticated treatment of the problem was then undertaken in which the electron energy distribution function was taken to be Maxwellian. This analysis suggested virtually 100 percent absorption of the applied microwave power in a region one to two centimeters thick with negligible reflection.

It is expected that the actual electron energy distribution will not be a simple Maxwellian. This expectation comes from review of the results of other resonance plasma heating schemes which invariably produce a small tail of higher energy runaway electrons in addition to the bulk Maxwellian distribution. The exact number, energy, and effect of these runaway electrons is not clear at this time, and will be an important subject of future years of this research effort.

The purpose of the numerical modeling in this program is to provide a means whereby the collective process of several individual effects can be analyzed. To accomplish this end, a one-dimensional computational model has been under development. The specific objectives being addressed by this one-dimensional model are to provide improved predictions of: i) the number densities of neutrals, singly ionized species, doubly ionized species, and ions of higher ionization states, ii) energy lost due to inelastic collisions, iii) effects of recombination reactions, iv) effects of ambipolar diffusion up-stream of the energizing region, and finally, v) the electron energy distribution. These predictions will than be compared against experimental results to test our understanding of ECR plasma acceleration.

As shown in Figure 1, several components are involved in the experimental aspect of this program. The microwave transmitter is based on a 20 kW output klystron tube with power provided from a power supply which uses the output of a three phase, 400 Hz motor-generator set. The transmitter is quite stable and produces single mode microwave power consistently at a frequency of 2.115 GHz at power levels between 20

watts and 20 kW. A water-cooled isolator is used to protect the transmitter from unexpected reflection of the microwave power. The 2-port circulator is a safety device which switches the microwave power into a water-cooled load in case the transmitter is inadvertently turned on when the laboratory is not correctly configured. The directional coupler allows both incident and reflected power to be measured to provide data on how much power the thruster is processing. The rectangular-to-circular waveguide transition with a Right Circular Polar (RCP) polarizer is required to provide the desired RCP microwave power to the accelerator. The argon flow meter and regulator can be used to control the flow of argon propellant into the accelerator at flow rates varying from zero to 50 sccm. The magnetic solenoid is a water-cooled copper coil with approximately 150 turns and a diameter of approximately 30 cm. To achieve a resonance field of 755 G the solenoid requires a D.C. current of 150 A.

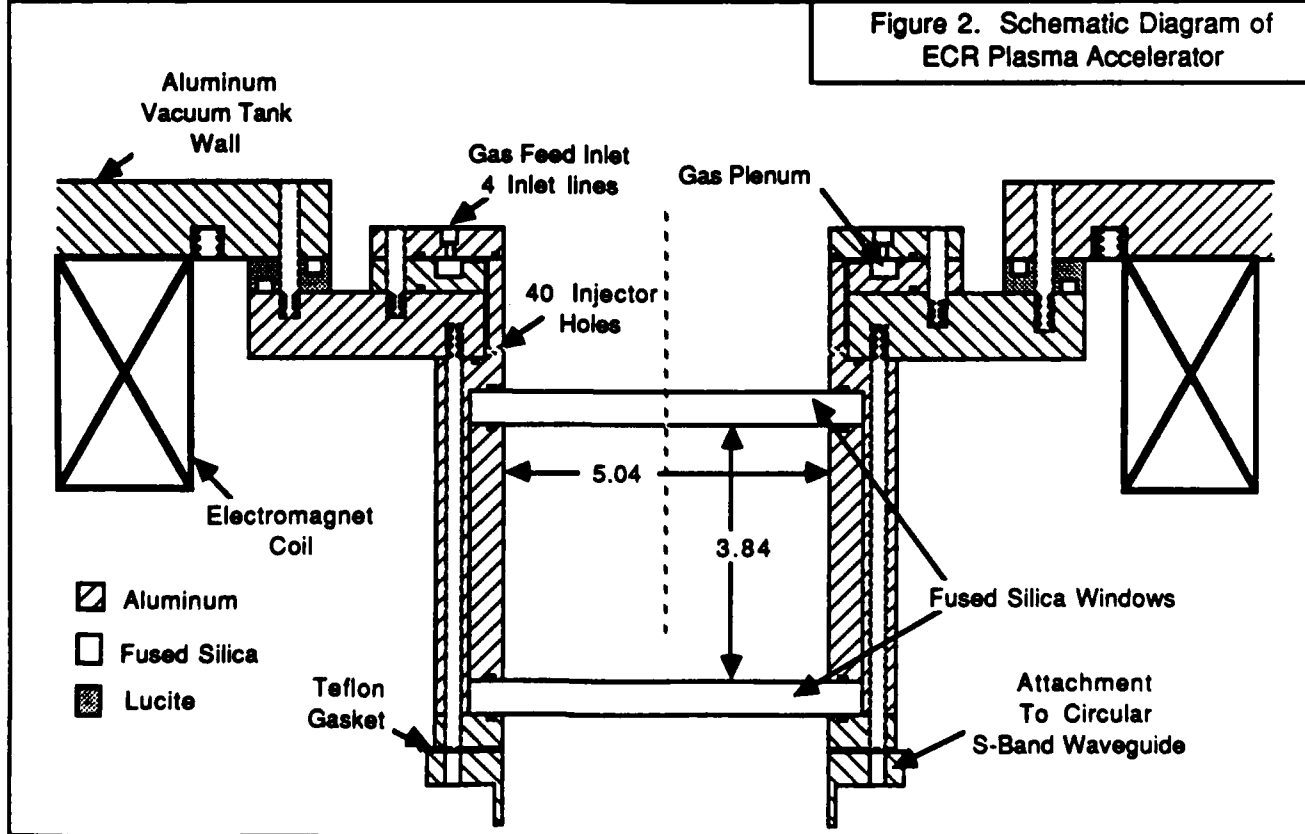
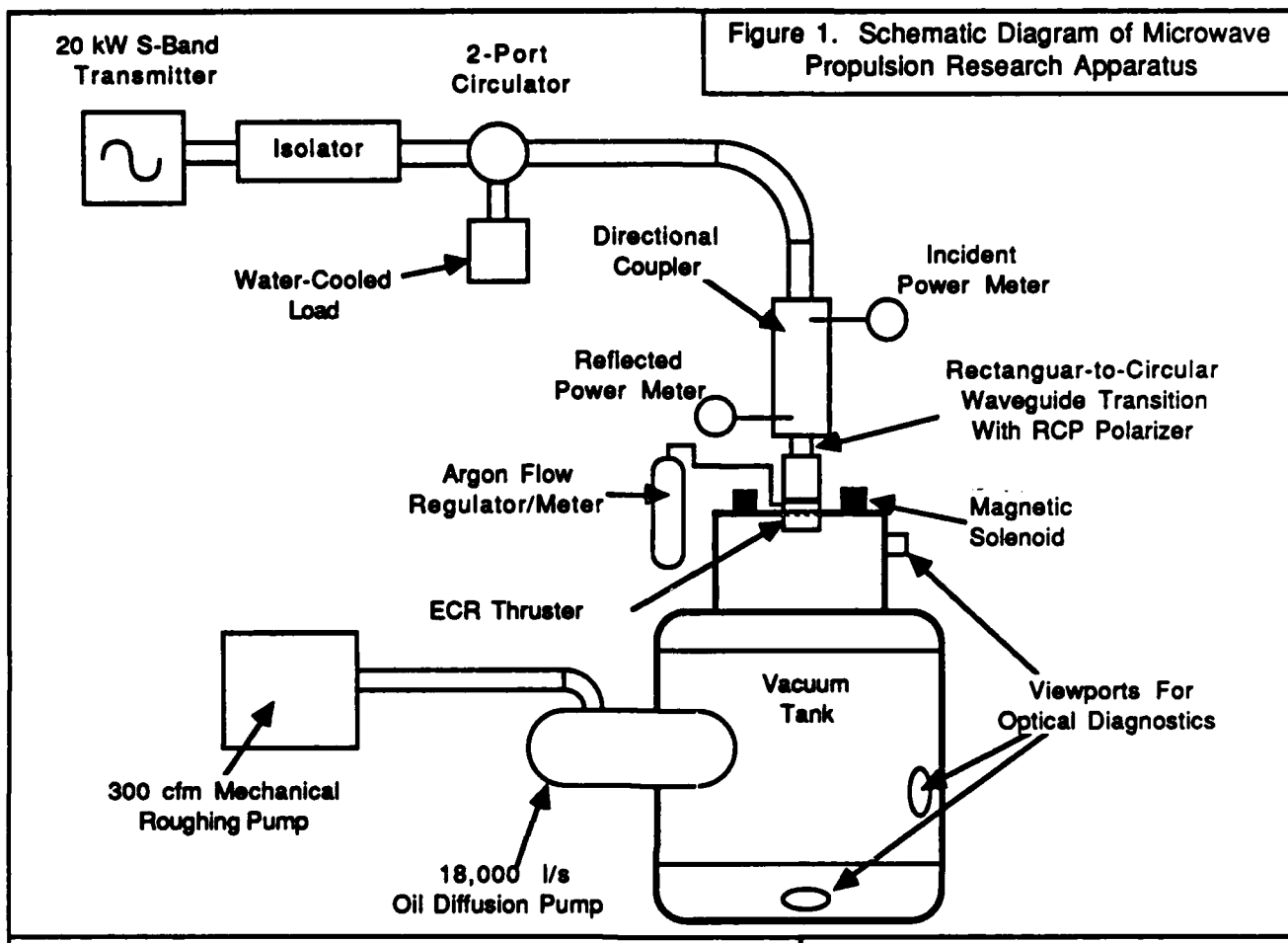
The vacuum system in this experiment consists of a stainless steel cylindrical vacuum tank with dimensions of approximately 2m x 2m. Pumping is accomplished by an 18,000 l/s oil diffusion pump backed up by a 300 cfm mechanical roughing pump. Entrainment of diffusion pump oil into the vacuum tank is limited by a baffle system that is cooled by a refrigerated convective liquid alcohol cooling loop.

The ECR plasma accelerator currently being tested is shown in Figure 2. Two fused silica windows are used to separate the vacuum from atmosphere and to allow microwave power into the accelerator. The use of two windows in place of a single window was decided upon to ensure redundancy for safety purposes in case of a window failure and to reduce window reflective losses. This window design was accomplished with the aid of an existing numerical model which suggested that at a separation distance of 3.84 inches, reflection from the first window would cancel reflection from the second window to enable maximum microwave power transmission. Actual reflective losses were measured to be 4 percent for this design at the design operating frequency of 2.115 GHz. At a slightly off-design frequency the reflection was found to be 0.2 percent, suggesting that the data used on the dielectric properties of fused silica was somewhat in error. In future accelerator designs we plan to adjust the separation distance accordingly and are confident that reflective losses can be minimized.

This accelerator has been tested using argon propellant at gas flow rates between 5 and 20 sccm and at input microwave power levels from 0.4 to 7.0 kW. The most significant qualitative observations made so far are: i) the plasma trajectory appears to have the predicted shape, ii) that the plasma is stable and easy to reproduce, and iii) that only a few percent of the applied microwave power is reflected by the plasma.

REFERENCES:

1. Kosmahl, H. G., "Three-Dimensional Plasma Acceleration Through Axisymmetric Diverging Magnetic Fields Based on Dipole Moment Approximation" NASA Technical Note, NASA TN D-3782, Lewis Research Center, January 1967.
2. Sercel, J. C., "Electron-Cyclotron-Resonance (ECR) Plasma Acceleration," AIAA-87-1407, presented at the AIAA 19th fluid Dynamics, Plasma Dynamics, and Lasers Conference, June 8-10, Honolulu, Hawaii.
3. Dugan, J. V. and Sovie, R. J., "Volume Ion Production Costs in Tenuous Plasmas: A General Atom Theory and Detailed Results for Helium, Argon, and Cesium," NASA TN D-4150, 1967.



PULSED INDUCTIVE THRUSTER

AFOSR Contract No. F49620-87-C-0059/P00003

Principal Investigator: Lee Dailey

TRW S&TG
1 Space Park
Redondo Beach, CA 90278
01/2270

SUMMARY/OVERVIEW:

The research objective is to investigate ionization and current sheet development in an impulsive, inductive discharge. This kind of discharge can be produced in a cold gas, without preionization, by discharging a capacitor bank into a low inductance flat, spiral coil. By means of small plasma probes measuring magnetic and electric fields and local current density it will be possible to determine the minimum electric field required for breakdown and the rate of current rise as functions of pressure.

TECHNICAL DISCUSSION

The experimental device, and its practical importance are summarized in Figure 1. A 24 strand, 1-turn, coil 67 cm in diameter is used to form a nearly radial magnetic field B_r close to the coil face. This is done by discharging the capacitor bank through a spark gap switch to produce a fast rising azimuthal electric field E_θ . Breakdown is observed to occur in about 20 nanoseconds with an applied E_θ of typically 100 V/cm in a layer of cold argon at about 150μ pressure.

In the thruster application, gas is supplied by a fast-acting valve that opens in 150μ sec and is closed in about 500μ sec. The capacitor bank is discharged at 1.2 m sec after valve opening. The gas pulse is directed toward the coil by the conical supersonic nozzle shown in Figure 2. The gas distribution at 1.2 m sec , measured by a fast ionization gage, is shown in the same figure.

The capacitor bank can be discharged in two modes: the clamped mode shown in Figure 1 where a diode clamp is used to prevent voltage reversal, and the ringdown mode with clamp removed. Since the first half-cycle of the discharge is the same for both modes, either one can be used to study the breakdown.

We have not yet been able to make systematic measurements over the plasma volume in front of the coil because of an on-going series of insulation failures involving both the spark gap and capacitor connections to the coaxial cables used to carry the circuit current. However, a limited amount of thrust balance measurements have been made for three capacitor bank configurations. One of these is a $17.4\mu\text{F}$ bank of 12 capacitors, shown in Figure 1, operated in the ringdown mode. The other two are clamped discharges, one with $6\mu\text{F}$ bank of 6 capacitors, the other with a $13.4\mu\text{F}$ bank of 10 capacitors. Efficiency versus I_{sp} data are shown in Figure 4. It is seen that the clamped mode gives more efficient performance than the ringdown mode. The most recent failure, involving the spark gap, is being repaired and probe measurements will be made soon.

Pulsed Inductive Thruster (PIT)

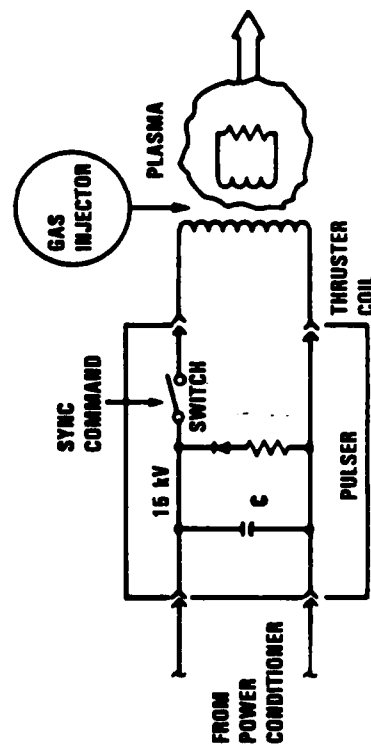
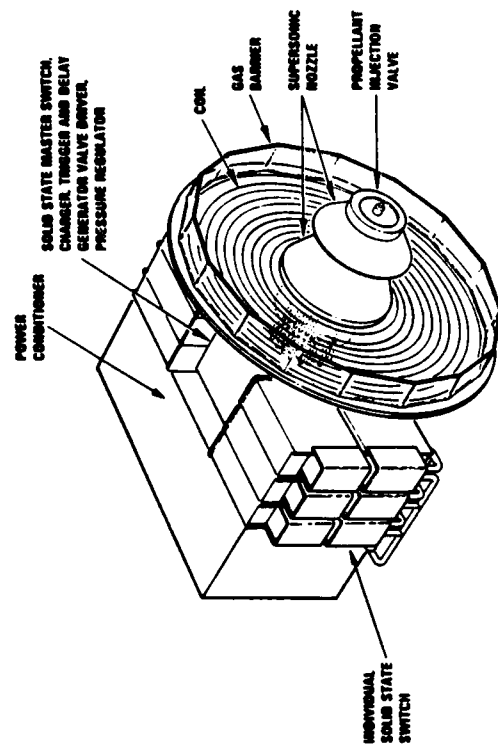
Pulsed Mode Operation

- Thrust control by changing pulse rate from single pulse to 1 kHz
- No electrodes (inductive discharge)
- No contamination
- Capable of design for indefinite life
- Multimegawatt capability
- Feasibility demonstrated
- Component technology development required (valve and switch)

Technology Status

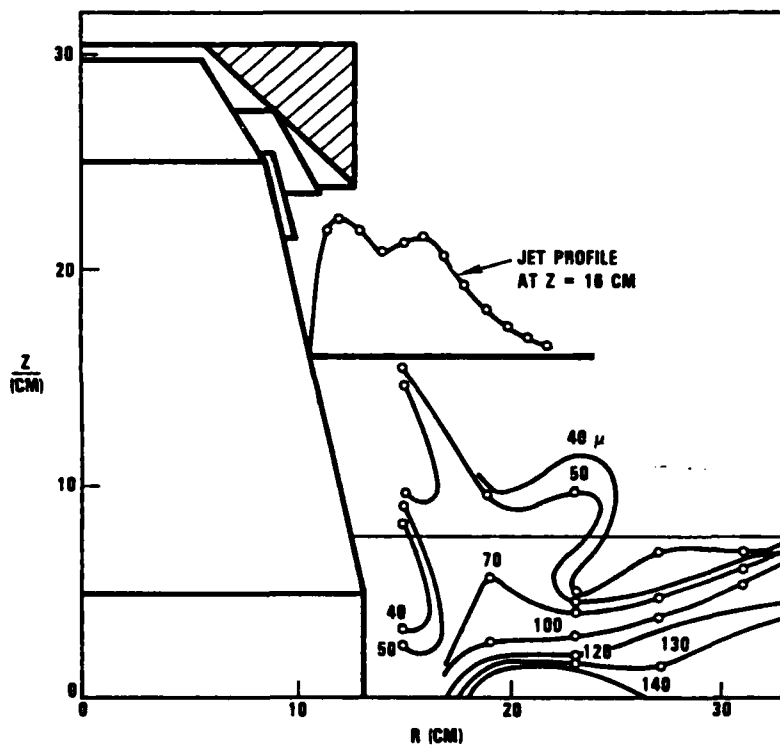
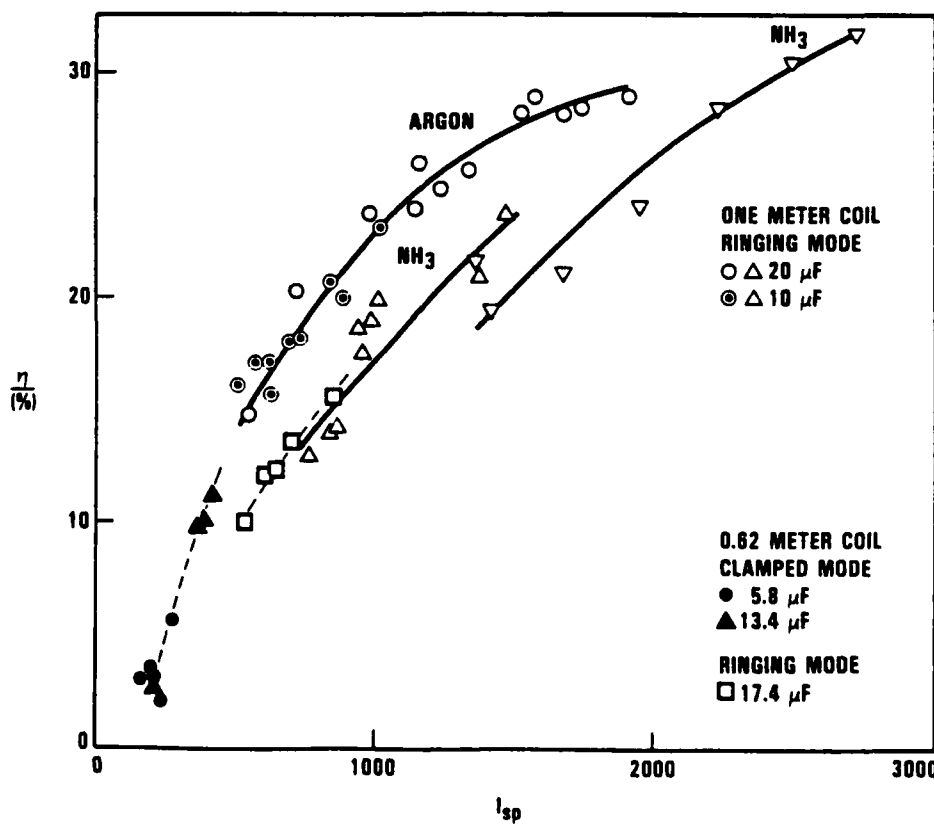
Applications

- Fast delivery of large payloads in Earth orbit transfer, lunar logistic support and planetary missions
- Example: Satellites comprising 90% of the HLV/STV cargo that is delivered to 500 NMi can be transferred to 2000 NMi in 8 days by a space based, 5 MW, Electric Orbit Transfer Vehicle (EOTV) using PIT (28 lbs thrust, one-meter diameter coil)



Coil Diameter	I_{sp}	η (%)	Pulse Rate (kHz)	Power (MW)
0.7	2000	30	1.0	0.5
1.0	3000	37	1.0	1.8
1.3	4000	40	0.9	5.0
1.7	5000	41	0.6	5.0
1.8	6000	42	0.2	5.0

FIG. 2 Argon Pressure Distribution at 1.2 ms

FIG. 3 Efficiency and I_{sp} for Different Coils and Capacitors

Numerical Modeling of the Hybrid Plume Rocket

AFOSR Grant No. AFOSR-84-0190

W. A. Krueger, L. R. Clegg, D. M. E. Yang

Plasma Fusion Center
 Massachusetts Institute of Technology
 Cambridge, Massachusetts 02139

Summary

Previous work has shown the viability of the hybrid plume rocket [1-3]. The interactions between the neutral gas jet and plasma have been demonstrated to form the transition region required to form the hybrid plume. The critical issue to address is the detailed flow dynamics of the hybrid plume concept. Specifically, whether the plasma flow will detach from the nozzle and produce usable thrust at high I_{sp} .

To address this issue, the computational model has been continuously improved. What started as a $1 - \frac{1}{2}D$, single fluid plasma, steady state code is currently a $2 - \frac{1}{2}D$, two fluid hybrid, time dependent code. The goal of the current development will be the ability to model the detailed behavior of the plasma/gas flow in a complex, time dependent magnetic field.

Technical Discussion

The previous code used a cylindrically symmetric duct with the plasma flowing axially and diffusing radially. This assumption was used to understand the principle mechanisms involved with the hybrid plume and to study the feasibility of the hybrid plume concept. The old code was not designed to specifically study the disconnection process. The magnetic field was assumed constant in time and essentially constant in space.

The current code is a zero-electron mass hybrid code. It is a time dependent code that is two dimensional in space, r and z , and three dimensional in \mathbf{V}_p , \mathbf{V}_n , \mathbf{B} , and \mathbf{E} . It has the ability to have arbitrary magnetic field configurations. It has been modified to include a neutral gas, \mathbf{V}_n . Also, various interactions between the neutral gas and the plasma needed to study the hybrid plume concept have been added. The minimum interactions required are electron impact ionization, charge exchange, and some type of recombination.

The time dependent code has many advantages over the previous steady state code. The most obvious benefit is the correct treatment of all the velocity components. (In the steady state code, V_r was modeled out of the problem.) This benefit is not a result of the code being time dependent, but of the different physical models utilized in each code. A direct benefit of the time-dependent process is the better demonstration of the complex dynamics involved in the interactions between the fluids. An unforeseen drawback of the time-dependent process lies in the disparate time-scales between the plasma and the neutral gas. The mean plasma velocity is significantly greater than the neutral fluid velocity, even with a hypersonic neutral gas jet. Being able to see this in the time-dependent code gives insight to the dynamic process of the plasma/gas interaction, but it places great demands on the numerical system implemented to solve the equations. Specifically, to see the interactions of interest, one must wait for many plasma transit times through the nozzle. This magnifies any slight perturbations that the plasma may excite when it crosses the *outflow* boundary at the exit of the nozzle. These random fluctuations can grow and dominate the solution, rendering it useless.

Our current effort has been to improve the computational robustness of the *outflow* boundary. It should be pointed out that this is not a simple hydrodynamic instability. The neutral gas solution is stable even at the outflow boundary. The plasma instability is a complex interaction between the fluid quantities and the electro-magnetic properties of the plasma.

Details of the equations and numerical techniques will be presented.

References

1. Chang, F.R., W.A. Krueger, T.F. Yang, "Numerical Modeling of the Hybrid Plume Plasma Rocket", AFOSR/AFRPL Chemical Rocket Research Meeting, paper 30, Lancaster, CA, Sept 86.
2. Chang, F.R., W. A. Krueger, T. F. Yang, AIAA DBLR JSASS Int. Electric Propulsion Conference, paper AIAA 85-2049, Alexandria, VA, Sept 85.
3. Chang, F. R., W. A. Krueger, T. F. Yang, J. L. Fisher, "Plasma-Gas Interaction Study in a Hybrid Plume Plasma Rocket", AFOSR-AFRPL Chemical Rocket Research Meeting, paper 51, Lancaster, CA, March 85.

The Construction of an Experimental Facility for Variable I_{sp} Propulsion Studies

Contract No. AFOSR-84-0190

T. F. Yang, F. R. Chang-Diaz*, Z. Yao, S. Y. Peng, W. A. Krueger, J. Urbahn

Plasma Fusion Center
Massachusetts Institute of Technology
Cambridge, Massachusetts 02139

Summary

This report will discuss the construction of an experimental facility for variable I_{sp} propulsion studies.

The facility consists of a compact tandem mirror magnetic plasma confinement device, RF power transmitters, diagnostics and data acquisition system. The major components of the tandem mirror device consist of 8 central cell coils, 4 mirror choke coils, 4 booster coils and vacuum chamber. These have been fabricated and tested. The vacuum chamber is made of seven sections which have been leak checked individually. The ultra high vacuum pumping system is being assembled. The component fabrication as well as the complete assembly will be presented.

Technical Discussion

The tandem mirror device is shown at the top of Figure 1. As previously reported [1,2,3], the tandem mirror magnetic confinement device will be used as a hot plasma source. A hybrid plume will be formed by surrounding the hot plasma exhaust from one end with an annular hypersonic coaxial gas jet. The resulting plasma-gas jet will be studied for its applications in high power, variable I_{sp} rocket propulsion.

The experimental set-up is shown at the bottom of Figure 1. The mirror coils, central cell coils and booster coils are all solenoidal. They are all contained in stainless steel casings. The magnetic force is transmitted through preloaded springs to the casing which is mounted on the test stand. The coils will be cooled by liquid nitrogen. The central

* Astronaut Office, NASA Johnson Space Center, Houston, Texas

cell coil casings will be thermally insulated by foam and super insulation. The mirror coil casings will be in a vacuum jacket. The coil construction and assembling methods are our unique design. The vacuum chamber is divided into the following sections: central cell spool section (for mounting mirror coils), choke region and exhaust. This design enables them to be separated for access to the interiors. The central cell coils are connected by stainless steel rods and with preloaded springs at the ends to allow for expansion and contraction of liquid nitrogen casings. The ultra high vacuum will be handled by turbo molecular pumping systems at both ends. The vacuum chamber and pumping system are being assembled. It will be leak-checked and cleaned by glow discharge and bake-out to achieve ultra high vacuum. The magnetic coils will be mounted and energized by the DC power supplies from the Tara tandem mirror experiment. High current cables are being laid from the Tara area to this device.

The system will be aligned with laser and electron beam. Cold hydrogen plasma will be created with microwaves. The ionization characteristics will be studied by both injecting the microwave at various locations, and by varying the gas feed. The plasma will be heated by three high-power RF transmitters, one in the central cell and two in the choke region. The design of RF antennae and impedance matching circuit is progress. The three high-power RF transmitters are on loan to us. Three smaller RF systems will be built before the expiration of the loan.

The initial diagnostic are diamagnetic loops, Langmuir probes, time sensitive magnetic probe and bolometers. The microwave interferometers, laser fluorescence, Thomson scattering and end-exhaust analyzer will be added gradually. We have permission to share the data acquisition system and computer with other fusion research projects.

The goal for the first year is to study various schemes for coupling RF power to the plasma, such as antenna shapes, locations, magnetic field variation and to learn the mechanisms for achieving high energy conversion efficiency.

References

1. Chang, F. R. , Fisher J. L. , Nuclear Fusion, **22**, No.8 (1982).
2. Chang, F. R. , Krueger, W. A., , Yang, T. F. , AIAA/DBLR/JSASS Int. Electric Propulsion Conference, paper AIAA-85-2049, Alexandria, VA, Sept. 1985.
3. Yang, T. F., Miller, R. H., Wenzel, K. W., Krueger, W. A., AIAA/DBLR/JSASS Int. Electric Propulsion Conference, paper AIAA-85-2054, Alexandria, VA, Sept. 1985.

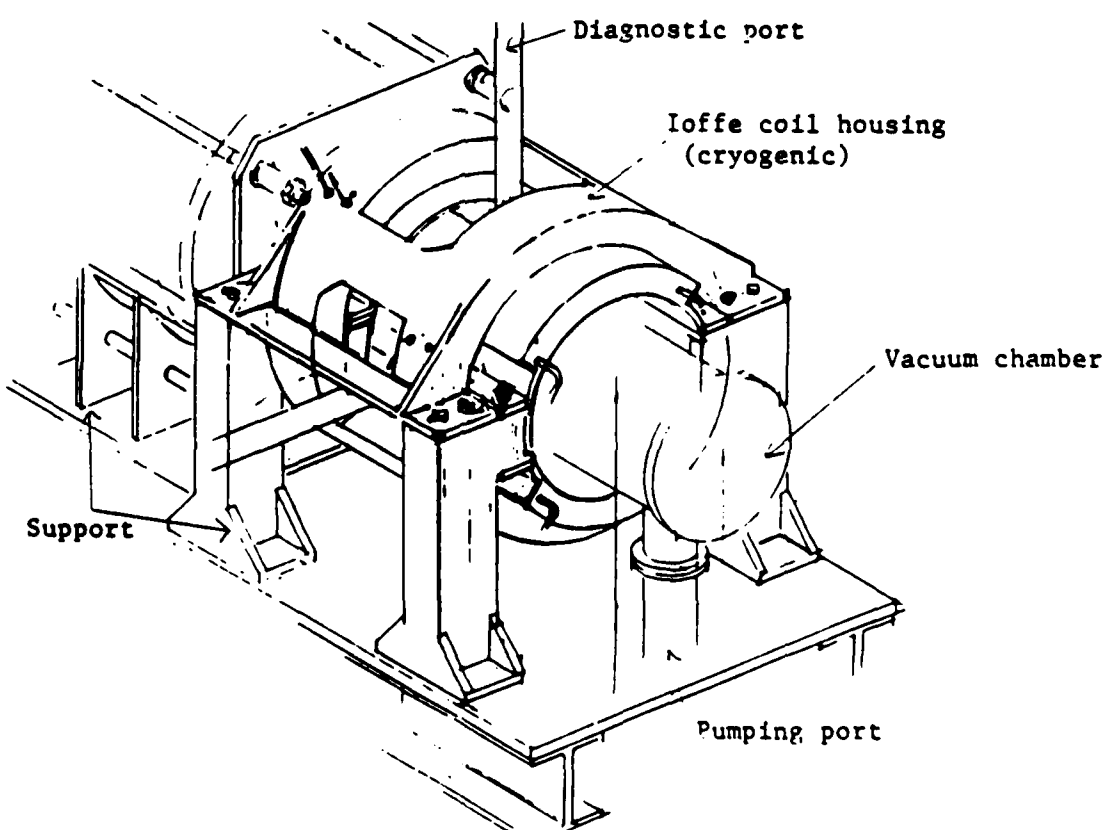
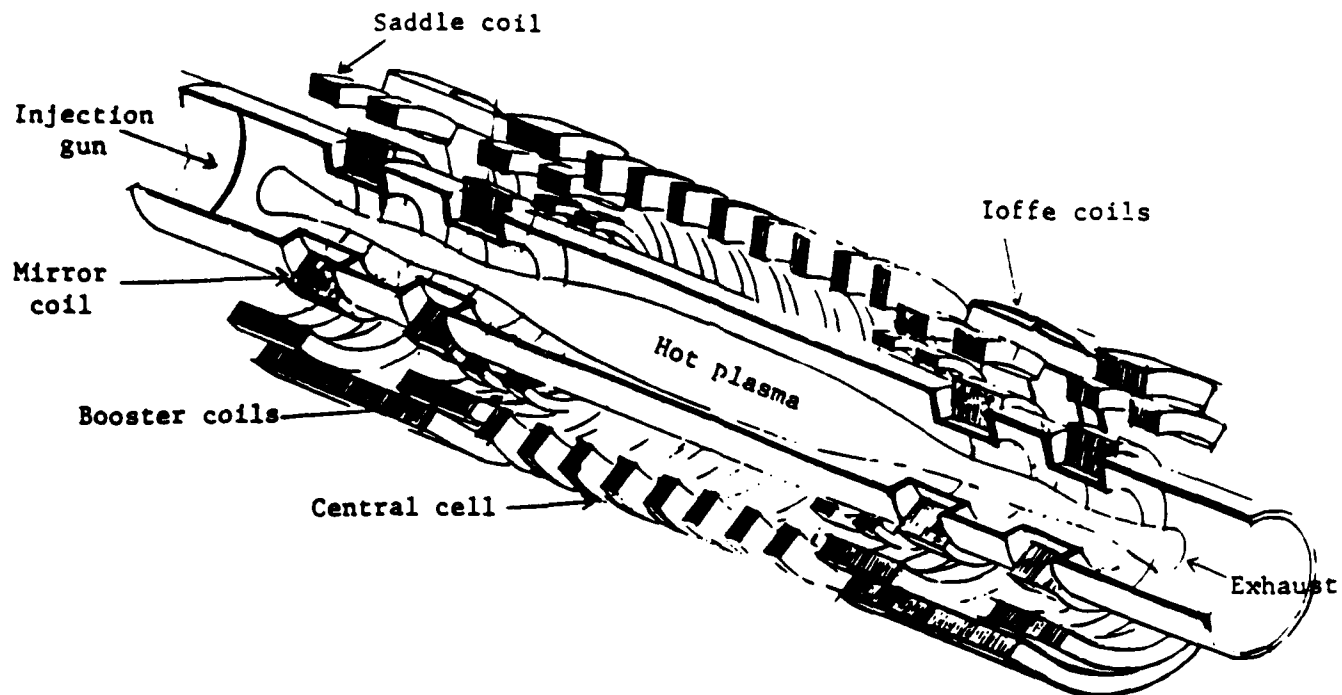


Figure 1 Tandem mirror assembly and experimental setup.

LASER THERMAL PROPULSION

AFOSR Grant No. AFOSR-86-0317

Principal Investigator: Dennis Keefer

Center for Laser Applications
University of Tennessee Space Institute
Tullahoma, TN 37388
615 455-0631

The objective of this research is to develop an understanding of the basic physical processes that control the interaction of plasmas sustained by laser beams in a flowing propellant gas. Previous experimental and theoretical studies have provided a reasonable understanding of these processes in flowing plasmas sustained by continuous lasers, and have shown that the absorption efficiency and radiation losses can be controlled through a combination of optical geometry, pressure and flow configuration. Practical beamed laser propulsion systems will require laser powers greater than one megawatt, and current laser development for other applications suggest that lasers capable of delivering average powers at these levels will be free electron lasers (FEL). The power from these free electron lasers will be pulsed, rather than continuous, and it is not currently known whether quasi-steady plasmas suitable for thermal propulsion can be sustained using these pulsed power formats. We are conducting experiments at our laboratory using excimer lasers and with the RF linac FEL at Los Alamos National Laboratory (LANL) to develop an understanding of the absorption and relaxation mechanisms in plasmas sustained with short pulses.

In a plasma sustained by the absorption of power from a continuous laser, the power is absorbed through inverse bremsstrahlung (free-free transitions in the electrons). The electrons are maintained in local thermodynamic equilibrium by electron-electron and electron-ion collisions, and the absorption coefficient can be accurately predicted using the Kramers-Uns 1d theory. In free electron lasers, the pulse duration may be as short as a few picoseconds; a time similar to the electron collision time. Under these conditions it is unlikely that the electrons will maintain a Maxwellian distribution, and the absorption predicted by the Kramers-Uns 1d theory will no longer apply. After the pulse terminates, the plasma will begin to decay from its nonequilibrium state through radiative and collision processes, approaching a local thermodynamic equilibrium prior to the arrival of the next pulse. If the time between pulses is sufficiently short, then subsequent pulses will be absorbed in the plasma remaining from the previous pulse, and a quasi-steady-state may be achieved, similar to plasmas sustained by continuous laser beams. However, it is unknown whether these plasmas will be as efficient in the absorption of laser power and whether the radiation lost from these plasmas will be comparable to their continuous counterparts.

Time-resolved spectra have been obtained from plasmas created from a focused pulsed excimer laser in one and two atmospheres of argon (Figures 1 and 2). These data clearly show the relaxation of the plasma from a highly ionized state as the plasma decays over times of the order of tens to hundreds of nanoseconds. It is clear from these data that there will be a significant

electron density remaining after tens of nanoseconds, and if the pulse separation is of this order, then it is reasonable to expect that a quasi-steady plasma will develop; similar to those sustained with continuous lasers. Experiments will be conducted using the FEL at Los Alamos to determine how this transition from a pulsed to quasi-steady plasma occurs, to obtain time-resolved photographs of the plasma and to measure the spectral emission from the plasma on microsecond, nanosecond and picosecond time scales.

The RF linac laser at LANL produces a burst of mode-locked pulses of approximately 10 ps duration at a wavelength of 10.6 micrometers. These micropulses are spaced 46 ns apart in a burst (macropulse) lasting for 100 to 300 microseconds. The macropulses occur at a rate of 1 Hz and the average power in the macropulse is approximately 10 kW. The wavelength and the average power are similar to those used for earlier experiments on continuous laser sustained plasmas, and provides a nearly ideal source for experiments that can be compared with this earlier work.

The peak power in the micropulse is approximately 50 MW and should be sufficient to cause the plasma to self-ignite, in contrast to the continuous plasmas which must be initiated by some auxiliary means. Thus, the plasma is expected to initiate near the focal point and then migrate up the beam toward the lens as power is absorbed from subsequent pulses. This transition will be observed using a Hadland 390 image converter streak and framing camera. This camera is capable of resolving phenomena of approximately 10 ns duration in the streak mode, and can acquire photographic images at a rate up to 20 million frames per second. These observations will be used to observe the evolution of the plasma shape and position from initiation throughout the duration of the macropulse (100-300 microseconds). A critical research issue is the rate of plasma decay between the micropulses, and an optical multichannel analyzer (OMA) will be used to observe the spectral emission of the plasma between pulses. Analysis of these spectral data will permit an estimate of the time required for relaxation to a state of local thermodynamic equilibrium, and estimates of the electron density and temperature in the plasma at the incidence of subsequent micropulses. Finally, a Hamamatsu streak camera with a time resolution of 2 ps will be used to observe the response of the plasma during the absorption of the micropulse. On this time scale the plasma is expected to be far from LTE, and this data may help to understand the plasma absorption mechanisms for ultrashort optical pulses.

The experiments using the LANL pulsed laser will be compared with additional experiments performed at UTSC using the same experimental chamber and optical geometry, but sustained using our continuous carbon dioxide laser. This will permit checkout of the diagnostic procedures prior to the experiments at LANL, and will provide a good database for comparison of the pulsed and continuous plasmas. The results of these experiments should provide a good understanding of the physical mechanisms that control plasmas sustained with a pulsed high-powered laser, and permit a realistic assessment of the potential for these lasers as a power source for future beamed energy propulsion systems.

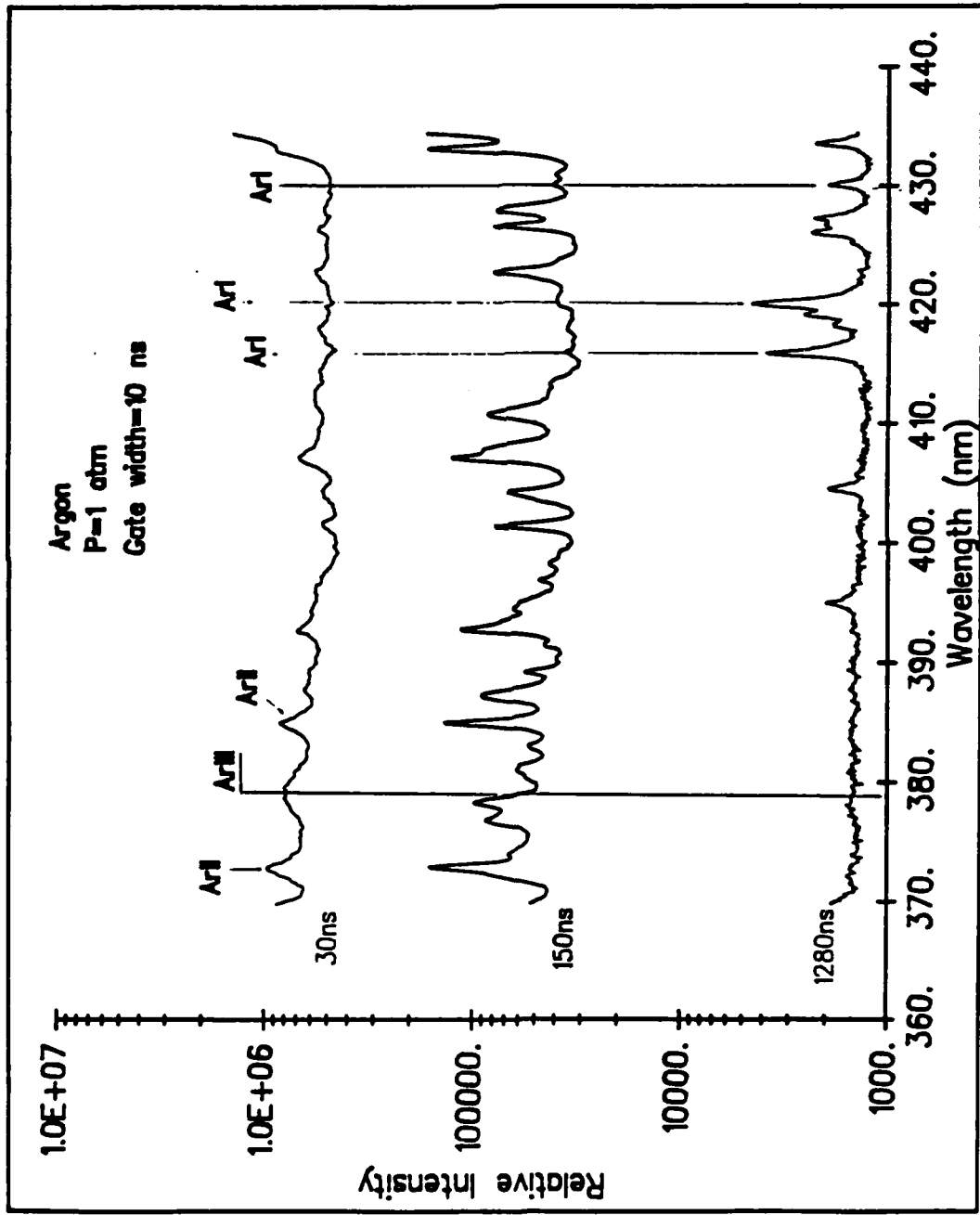


FIGURE 1. Spectral Emission During the Decay of a Pulsed Argon Plasma

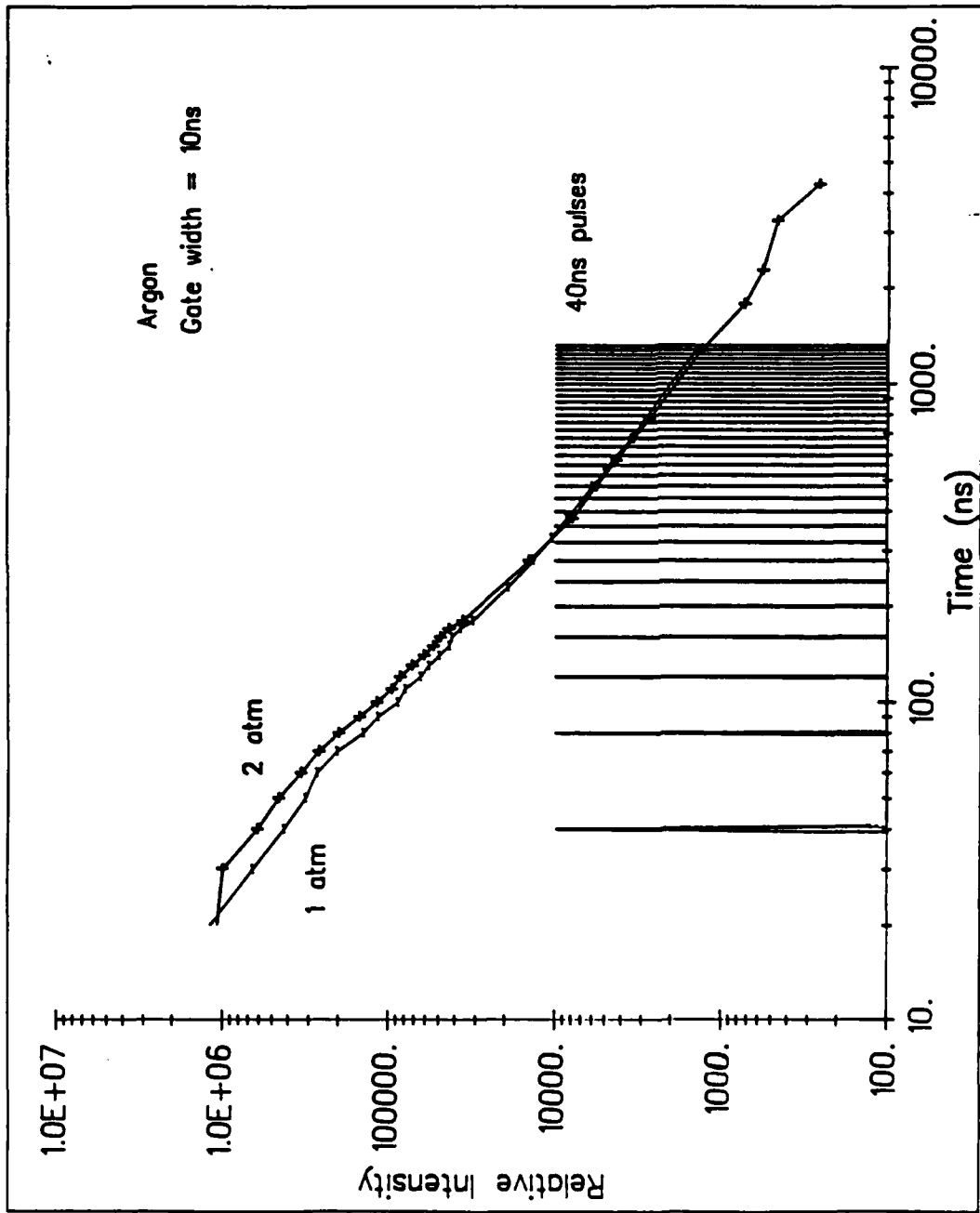


FIGURE 2. Decay of Continuum Emission
from Pulsed Argon Plasmas

Pulses Characteristic of RF Linac FEL

EFFECTS OF TURBULENCE ON STATIONARY AND NONSTATIONARY PROCESSES IN C-SYSTEMS

(AFOSR Grant No. 86-0319)

Principal Investigator: Robert A. Beddini

University of Illinois at Urbana-Champaign
Urbana, IL 61801-2997

OVERVIEW

While conventional chemical rockets provide large thrust levels at relatively low specific impulse, and electric propulsion systems provide low thrust levels at very high specific impulse, electrodeless plasma thrusters (implemented by various means) can provide an effective compromise on the I_{sp} versus thrust performance map. Concepts such as laser heated thrusters and microwave heated thrusters employ controlled and directable energy addition to achieve a desired plasma zone with temperatures of the order 10^4 K. The plasma is then mixed with the outer flow and expanded through a nozzle. Of particular interest in such flows are turbulent convective and radiative heat fluxes, which distribute the deposited energy, and their effects on the system enclosure for chamber cooling requirements and evaluation of system efficiency.

TECHNICAL DISCUSSION

Research efforts have focused on the analysis of radiative and gas dynamic interactions in beamed-energy propulsion chamber environments. Specific topics have included the development of turbulence, incident radiative transport and reradiative transport^{1,2}. The following is a brief summary of the methodology being employed at present.

Incident (I₀) radiation: A new transport equation for incident radiation was developed under this effort. Whereas prior analyses utilize ray-tracing techniques for the incident radiation, the new equation is of divergence form, and permits a strongly coupled solution with the hydrodynamic equations using contemporary finite volume techniques.

Plasma and chamber wall reradiation: The P1 (first-order spherical harmonics) method is being utilized. Initial work has solved the coupled one-dimensional (radial) radiative heat flux equation employing a gray gas absorption coefficient.

Numerical solution method: A flux-split, non-factored, implicit finite volume method has been implemented for the time-accurate solution of the axisymmetric Navier-Stokes equations and coupled incident radiation field.

Turbulence: Initial results have been obtained with an established second-order turbulence closure model. Further work will attempt a Large Eddy Simulation of turbulence in the flow.

SUMMARY OF PROGRESS

A flow with specified energy addition (intended to simulate a discharge in a microwave thruster), has been analyzed for both argon and hydrogen propellants (Figure 1). Flows with coolant injection through a porous chamber wall were also calculated.

The example case presented in Figures 2a-d, is the non-injected flow of argon through a constant area duct ($R = .05848m$) with inlet temperature and pressure of 2700 K and 1 atm

respectively. Energy addition to the flow is 50 kW and mass flow is 0.028585 kg/s. Figure 2a shows the temperature field for this flow, indicating a peak temperature of approximately 10,000 K slightly downstream of the region of peak energy addition. Figure 2b shows the axial velocity field; the inlet centerline velocity is 23.2 m/s and the flow is accelerated and diverted towards the wall region by the strong heat addition. The centerline exit velocity is approximately 38 m/s. Figure 2c shows the turbulence intensity field for the flow (normalized by the local axial velocity on the centerline), where it can be seen that initial turbulence decays and is no longer supported in the high temperature, low Reynolds number flow in the central region. Near the wall region, however, the turbulence begins to grow in an annular region just off the chamber surface, reaching approximately 6% at an axial distance downstream of 10 radii. In Figure 2d the radial radiative heat flux is shown. The peak radiative flux delivered to the wall is approximately 800,000 W/m², and the overall peak radiative flux occurs near the core region with a value of 1.4 MW/m².

A comparison of radiative and convective surface heat fluxes as a function of axial distance is shown in Figure 3 for cases involving: (1) argon, (2) argon with injection through the chamber wall (transpiration cooling), (3) hydrogen (non-injected), and (4) hydrogen injected. All cases have the same approximate chamber "thrust", and the dominance of radiative transfer in the region of energy addition is clearly seen.

Although turbulence fails to be supported due to low Reynolds numbers encountered in the high temperature regions, it can be produced transitionally in the cooling layer near the surface. The exit Reynolds numbers based on chamber diameter, axial mass flux, and centerline viscosity are on the order of 10³ for the conditions considered. However, Reynolds numbers near the edge of the plasma are on the order of 20,000 based on local flow properties and thickness of the coolant layer; such values would usually be expected to provide at least moderate levels of turbulence.

With respect to laser-gas dynamic interactions, the incident intensity field calculated with the third order finite difference method for a 60 radial by 80 horizontal point grid is shown in figure 4 for a non-absorbing medium. For this grid, approximately 6 radial and three axial points are retained within the 1 cm diameter of focal volume (large focal volumes are presently assumed while a stretched grid procedure is being implemented). Maximum relative errors of approximately 5% are obtained in this region when compared with an exact solution developed for this case (Figure 5).

PLANNED RESEARCH

The analytical results of this effort and other ongoing AFOSR programs have demonstrated the importance of radiative transport issues in the chamber (and, perhaps nozzle) environments of laser and microwave propulsion systems. Further research is required to address radiative-flowfield interactions which include losses from the plasma and transfer to and from the nozzle walls. Radiative transfer to the chamber surface does not provide a major impediment from a systems point of view, however, since cooling techniques have been analyzed which have the potential to accommodate significant chamber surface fluxes.

The present results indicate that for systems of a size (or Reynolds number) larger than traditional laboratory configurations, turbulence could form in the annular coolant layer adjacent to the chamber surface, and hence introduces the problem of a transitional or retransitional flow. A more adequate analytical representation of turbulence development should be pursued, and the formulation of a large-eddy simulation appropriate for these types of aerophysical environments is in progress. The effects of turbulence are not necessarily adverse, since the enhanced mixing that results could reduce peak chamber temperatures at a faster rate, thereby reducing radiative transfer and increasing thruster efficiency.

REFERENCES

1. Beddini, R. A., Owano, T. G. and Kuo, S.-L., "Analysis of Gas Dynamic Interactions with Intense Optical Beams," AIAA paper no. 87-1455, AIAA 19th Fluid Dynamics, Plasma Dynamics and Laser Conference, Honolulu, Hawaii, June 1987.
2. Beddini, R. A. and Owano, T. G. "Analysis of Turbulent Convective and Radiative Heat Transfer in High Temperature Rocket Chamber Flows," AIAA paper no. 87-1770.

ENERGY TRANSFER IN MICROWAVE THRUSTER CHAMBERS

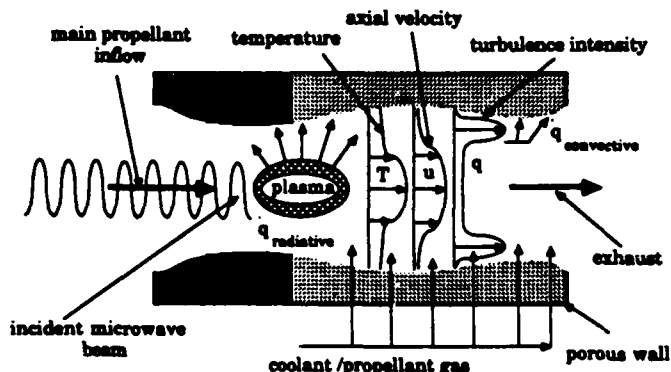


Figure 1.

Schematic diagram of the thrust chamber of a generic high-temperature plasma heated thruster, showing radiative heat fluxes to the chamber walls due to the high temperature ($> 10,000 \text{ K}$) core, as well as convective heat fluxes due to near wall turbulence.

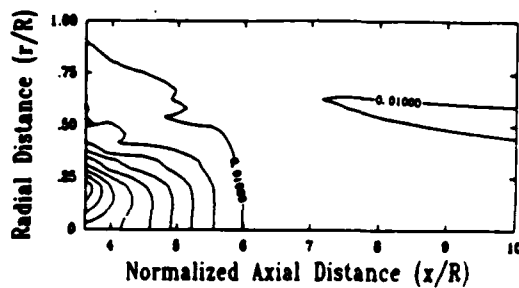


Figure 2a

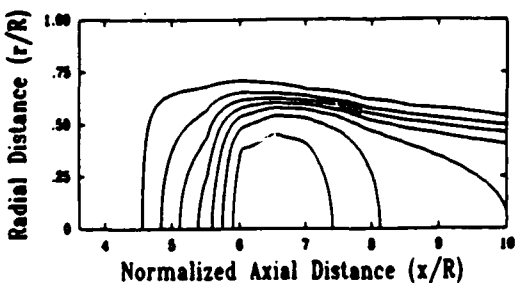


Figure 2b

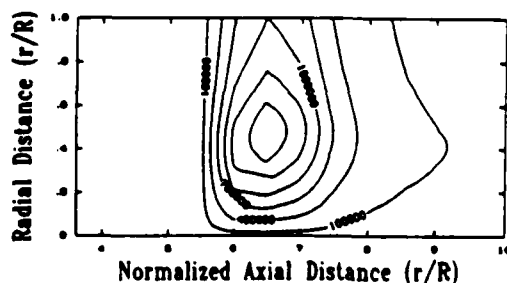


Figure 2c

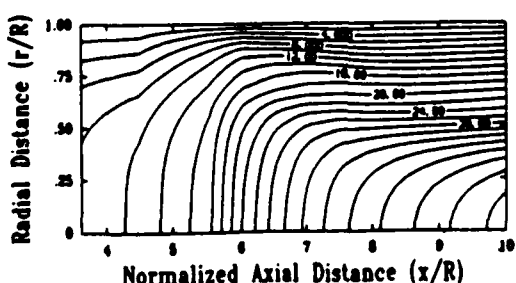


Figure 2d

- (a) Temperature field for a non-injected flow of argon gas through a constant area duct ($R = 0.5848 \text{ m}$). Inlet temperature and pressure are 2700 K and 1 atm respectively. Energy addition to the flow is 50 kW and mass flow is 0.026585 kg/s . contour increment is 10^3 K .
- (b) Corresponding axial velocity field.
- (c) Turbulence intensity field (normalized by the local axial velocity on the centerline) for the flow described previously.
- (d) Corresponding radial radiative heat flux field. Maximum heat flux levels approach $800,000 \text{ W/m}^2$; contour increment is $3 \times 10^5 \text{ W/m}^2$.

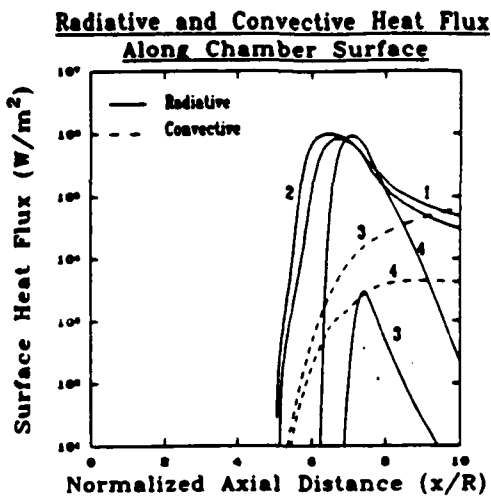


Figure 3

Figure 3. Comparison of the radiative and convective wall heat fluxes for the four flow cases

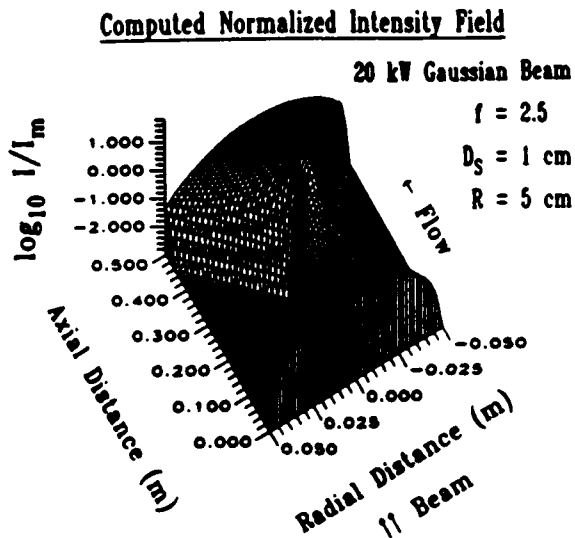


Figure 4.

Computed solution for the laser intensity distribution of a quasi-Gaussian beam (nonabsorbing gas). Intensity distribution calculated employing a finite volume third-order upwind method for a 60 radial by 60 axial point grid. Maximum relative error is approximately 5 percent compared with analytic solution.

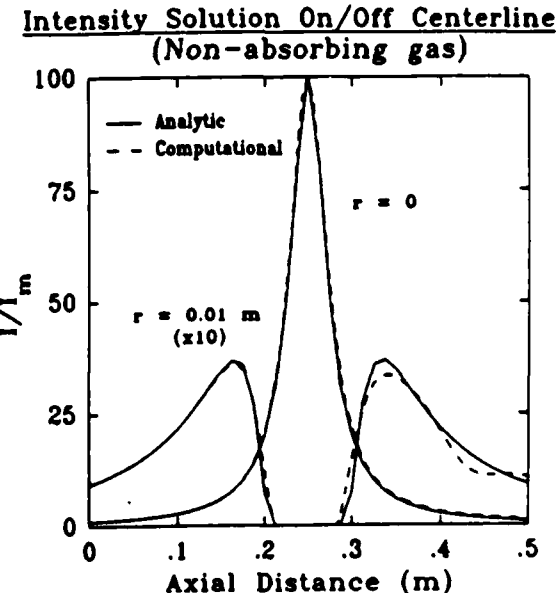


Figure 5.

A comparison of analytic and computational solutions for relative intensity as a function of axial distance along the centerline and at a radial position off the center line. Inlet beam profiles are quasi-Gaussian and focal spot size is 1 cm diameter.

ANALYTICAL MODELING OF DIRECT SOLAR ABSORPTION
IN A FLOWING GAS

(AFOSR Contract No. 84-0048)

Principal Investigator: Charles L. Merkle

The Pennsylvania State University
Departments of Mechanical Engineering
and Aerospace Engineering
University Park, PA 16802

The direct absorption of concentrated solar radiation in a flowing gas has potential utility in a number of engineering applications. The present research is concerned with evaluating the feasibility of direct absorption for solar thermal propulsion. The primary challenge in solar propulsion lies in finding a candidate working fluid that can absorb a significant fraction of the incoming energy in a reasonable length. The search for a candidate fluid involves two distinct issues. First, the absorptivity levels that are necessary for obtaining attractive rocket performance must be defined. Second, the absorptivity characteristics that can be achieved by acceptable working fluids must be identified. The present program deals with both of these issues.

The concept of solar thermal propulsion includes a concentrator to collect and focus the solar energy, an absorber that converts the radiant energy into thermal energy of a working fluid, and a nozzle to expand the fluid and produce thrust. A schematic of the concept is given in Fig. 1. A characteristic of solar radiation is its relatively low intensity even after concentration. Thermodynamic and practical limitations restrict concentration ratios to a factor of about 1000. It is this intensity restriction that limits absorption capability. In addition, the intensity limitation sets the physical size of the engine. The required thrust size dictates the energy level and both the collector size and the focussed spot size. The choking requirement at the throat then fixes the mass flow and the propagation velocity through the heating zone. The tentative working fluid of choice is a mixture of hydrogen with minor amounts of alkali metal vapors. The hydrogen provides low molecular weight to improve specific impulse, but remains essentially transparent at solar temperatures. The alkali metals provide reasonable broadband absorptivities over most of the solar spectrum at the temperatures of interest.

An estimate of the absorptivity of a H₂/Na/K/Cs mixture is given in Fig. 2. The alkali metals each provide atomic resonance absorption at specific lines, but these are augmented by photoionization and dimer bands and to a lesser extent by inverse bremsstrahlung. The composite curve in Fig. 2 was obtained by summing the individual mechanisms from the three alkali metals. In general, dimer absorption is effective at low temperatures (around 1000K) but decreases at higher temperatures because of dissociation. Photoionization becomes important around 2000K

for alkali metals while inverse bremsstrahlung is not effective until above 4000K. Additional absorption would be available from the metal hydrides that would be formed in the heated mixture, but their effect has been omitted here.

The total absorptivity of the gas mixture decreases with temperature over some parts of the solar spectrum while it increases with temperature in other regions as the results in Fig. 2 show. An understanding of the manner in which this complex absorptivity variation affects the coupling between the radiation and the gas dynamics requires a detailed calculation of the coupled phenomena. Another issue of importance is the necessity of maintaining the alkali vapors at a temperature above saturation. This implies the working fluid will have to be preheated before injecting it into the thruster. Such preheating is most effectively done regeneratively, thereby recapturing the reradiation loss to the walls.

Preliminary results of a coupled radiation-gasdynamic calculation for the absorption of solar energy are given on Fig. 3 for two different gas velocities, 15 and 150 mm/s. For both cases, the inlet temperature is 500K and the available solar power is 500 kW. Radiation losses which are handled by a Pl approximation are a significant factor at both velocities. At the lower speed, the radiation losses are more important and the heating region is large with a peak temperature of 3250K. At the higher speed, the heating zone is much smaller and the peak temperature is 3750K. A reduced density ray-trace used to simulate the uncollimated incoming radiation is given in Fig. 4.

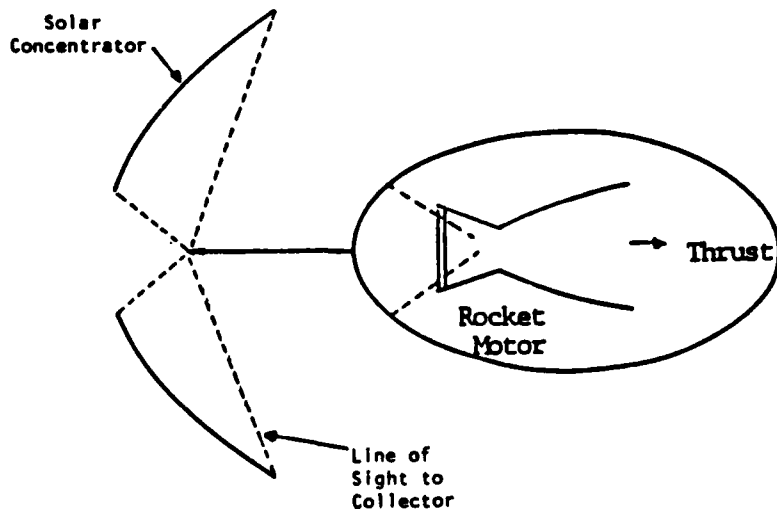


Fig. 1 The concept of solar thermal propulsion showing collector and rocket engine.

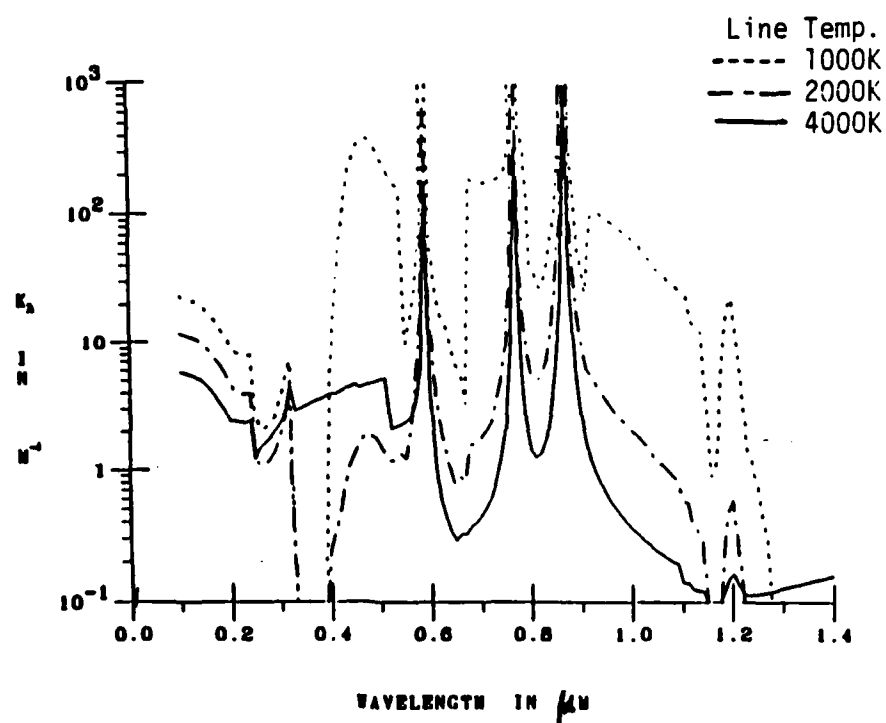


Fig. 2 Absorption coefficient of hydrogen/alkali metal vapor mixture containing 5% sodium, potassium and cesium.

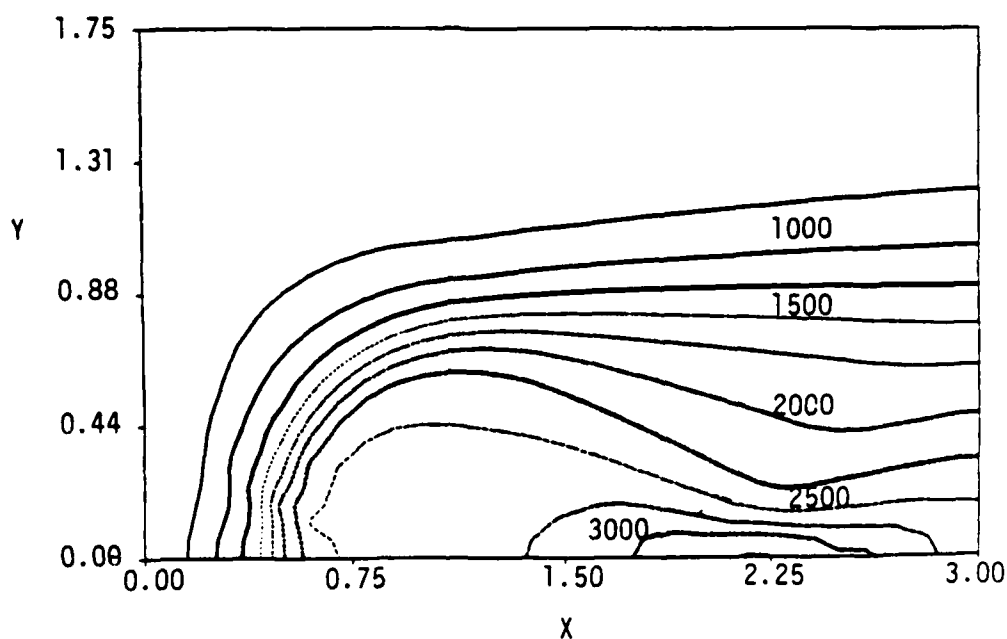
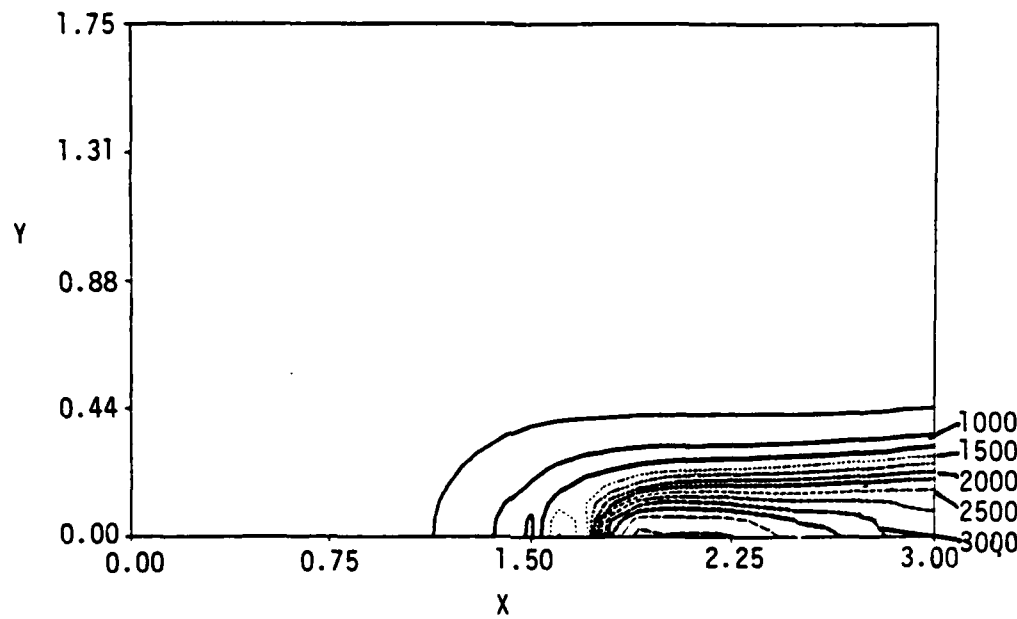


Fig. 3 Temperature contours for solar heating. $T_{in} = 300\text{K}$, solar power = 500 KW, (a) velocity 15 mm/s, power absorbed 200 KW;



(b) velocity 150 mm/s, power absorbed 360 KW.

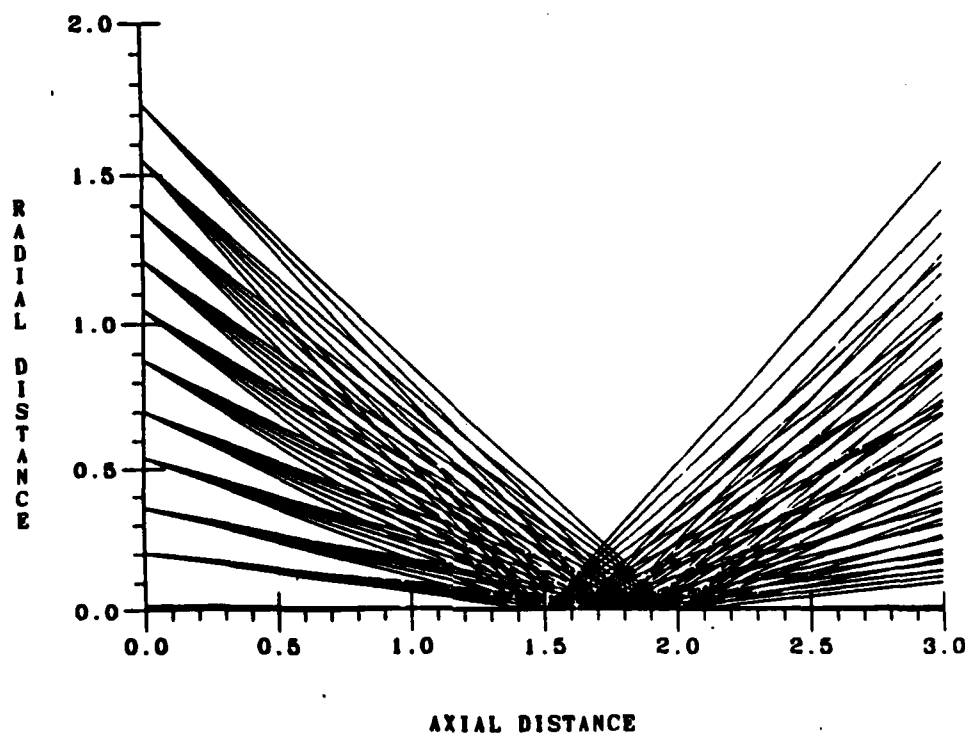


Fig. 4 Ray-trace of focussed solar beam. Number of rays shown here are one-fifth of those used in the calculations.

COUPLING BETWEEN GAS DYNAMICS AND MICROWAVE ENERGY ABSORPTION

AFOSR Grant No. AFOSR-84-0048

Principal Investigator: Dr. Michael M. Micci

The Pennsylvania State University
Department of Aerospace Engineering
University Park, PA

SUMMARY/OVERVIEW:

There is an understanding of the process of microwave energy addition to a high pressure gas for propulsive purposes for some of the available absorption modes but no unified comparison of all the modes in terms of absorption efficiency, maximum temperature, etc. Also there is little knowledge of the coupling of the absorbed energy to the gas dynamics required to obtain propulsive thrust. This research is the first experimental effort to examine and compare free floating filamentary and toroidal microwave absorbing plasmas and planar propagating plasmas in hydrogen gas as well as the first examination of the coupling of the energy absorption to the gas dynamics in order to convert internal thermal energy of the gas to directed kinetic energy by means of a nozzle expansion. The research will provide insight to the entire field of high temperature gas flows driven by radiation absorption.

TECHNICAL DISCUSSION:

Microwave equipment capable of generating up to 3 kW CW power at a frequency of 2.45 GHz has been interfaced to a microwave resonant cavity wherein both filamentary and toroidal plasmas can be produced. Free-floating spherical plasmas have been generated in stationary nitrogen and helium gas contained inside a spherical quartz vessel located within a cylindrical resonant cavity operated in the TM₀₁₂ mode. The plasmas are approximately two inches in diameter and are centered within the five inch ID quartz sphere. Power coupled to the plasma was measured as a function of nitrogen pressure and microwave power input to the cavity only for those combinations of pressure and power which resulted in the plasma being stabilized in the center of the quartz sphere away from adjacent walls. Figure 1 plots the coupling efficiency as a function of absolute pressure for several input power levels. The coupling efficiency is defined to be the percentage of input microwave power actually absorbed in the gas. It can be seen that the coupling efficiency rises with increased pressure but decreases with increased power. Higher input powers produced plasmas which moved to the wall of the resonant cavity threatening the destruction of the quartz vessel and were intentionally extinguished. This unstable behavior is believed to be related to asymmetries in the resonant cavity standing wave caused by the coupling probe which couples the microwave power from a coaxial cable into the cavity.

Maximum gas pressures which could sustain a stable plasma in nonflowing gas as a function of input power were measured for nitrogen and helium gas. Figure 2 shows that much higher gas pressures were achieved with helium than with nitrogen. This behavior is currently being investigated.

A 0.5 meter Spex scanning monochromator with a photomultiplier tube light sensor to measure gas temperatures as a function of spatial position has been interfaced with an IBM PC to allow the microcomputer to control both the scanning of the monochromator and the recording of the light intensity signal. Gas temperatures are currently being measured for helium plasmas.

A numerical model of the one-dimensional planar propagating microwave plasma in hydrogen, nitrogen or helium gas has been successfully formulated. This model numerically integrates the system of governing equations consisting of the one-dimensional steady energy equation

$$\rho u C_p \frac{dT}{dx} = \frac{d}{dx} \lambda \frac{dT}{dx} + \sigma \frac{E^2}{2} \quad (1)$$

where ρ is the gas density, u is the gas velocity, C_p is the specific heat, T is the gas temperature, λ is the thermal conductivity, σ is the electrical conductivity and E is the electric field vector; and Maxwell's equation describing the propagation of the microwave energy

$$\frac{d^2 E}{dx^2} = \sigma \mu \frac{\partial E}{\partial t} + \epsilon \mu \frac{\partial^2 E}{\partial t^2} \quad (2)$$

where ϵ is the permittivity and μ is the permeability. The specific heat, thermal conductivity and electrical conductivity are functions of temperature. The electromagnetic energy is absorbed by the plasma as the temperature rises with some microwave energy being reflected or transmitted. Due to thermal conduction to the cold gas ahead of it, the plasma propagates toward the microwave energy source at a velocity determined by the energy balance between the absorbed microwave power and the heated gas which is convected away downstream.

The two governing equations were numerically integrated using a fifth/sixth order variable step Runge-Kutta scheme. An iterative method was used to determine the propagation velocity eigenvalue, ρu , similar to the method used by Kemp and Root to solve for the propagating velocity of the laser heated plasma. The propagation velocity, maximum temperature and percent power absorbed were calculated as functions of the incident microwave power. The calculations show the propagation velocity increasing with higher incident power levels. A decreased velocity for higher gas pressure is primarily due to the increased gas density since ρu is the propagation eigenvalue. The maximum gas temperature was found to be constant for hydrogen and nitrogen because significant dissociation is occurring in this temperature range and is absorbing the additional absorbed power. The maximum gas temperature for helium, which is not dissociating, was seen to rise with increasing input power. The effects of radiation heat loss is currently being incorporated into the model. The results of this numerical model will be compared to experimentally measured values as they become available.

Coupling Efficiency Versus Absolute Pressure for Various Input Powers

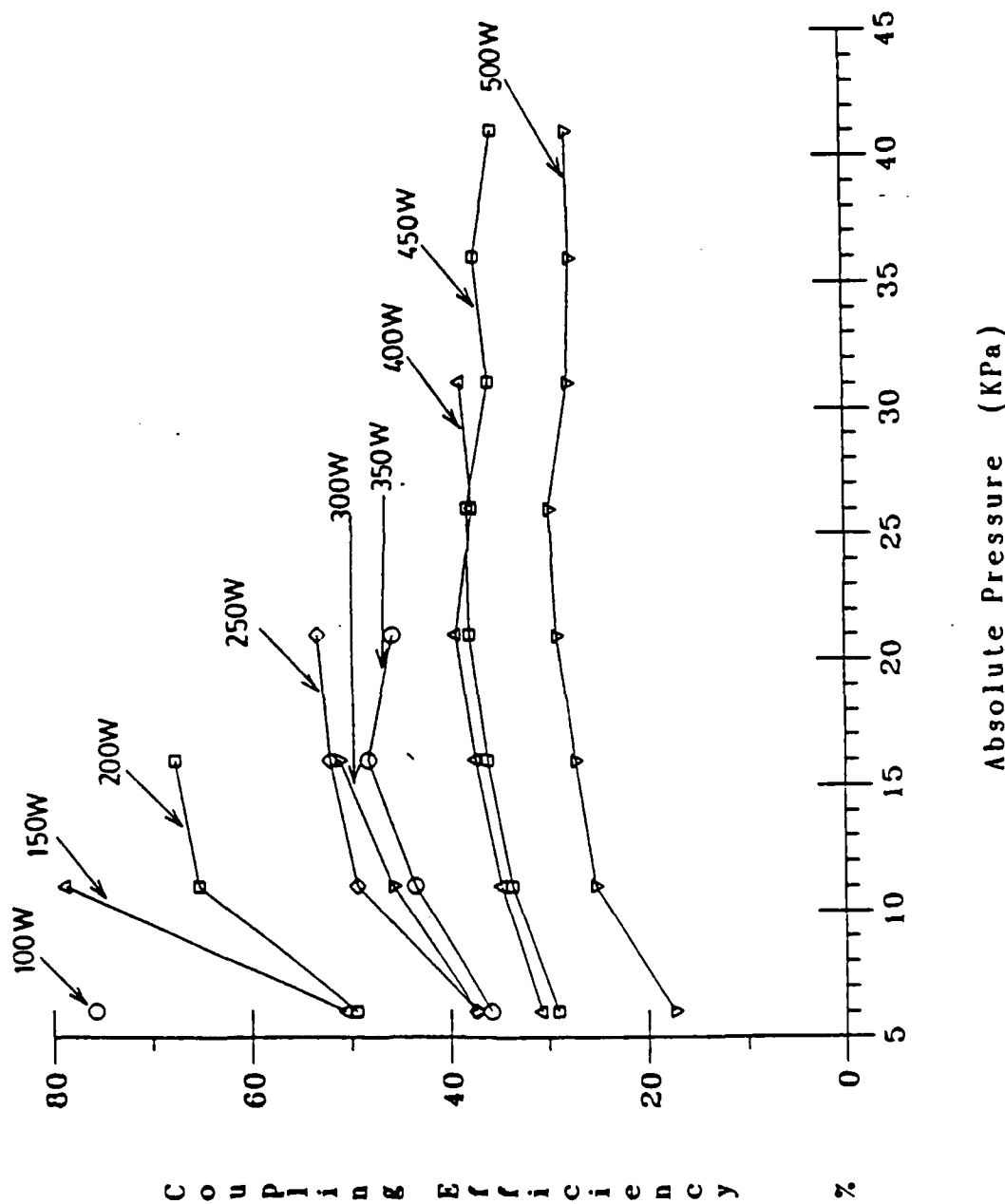


Fig. 1 Coupling efficiency of a free-floating spherical plasma in stationary nitrogen gas as a function of absolute pressure for several input microwave power levels.

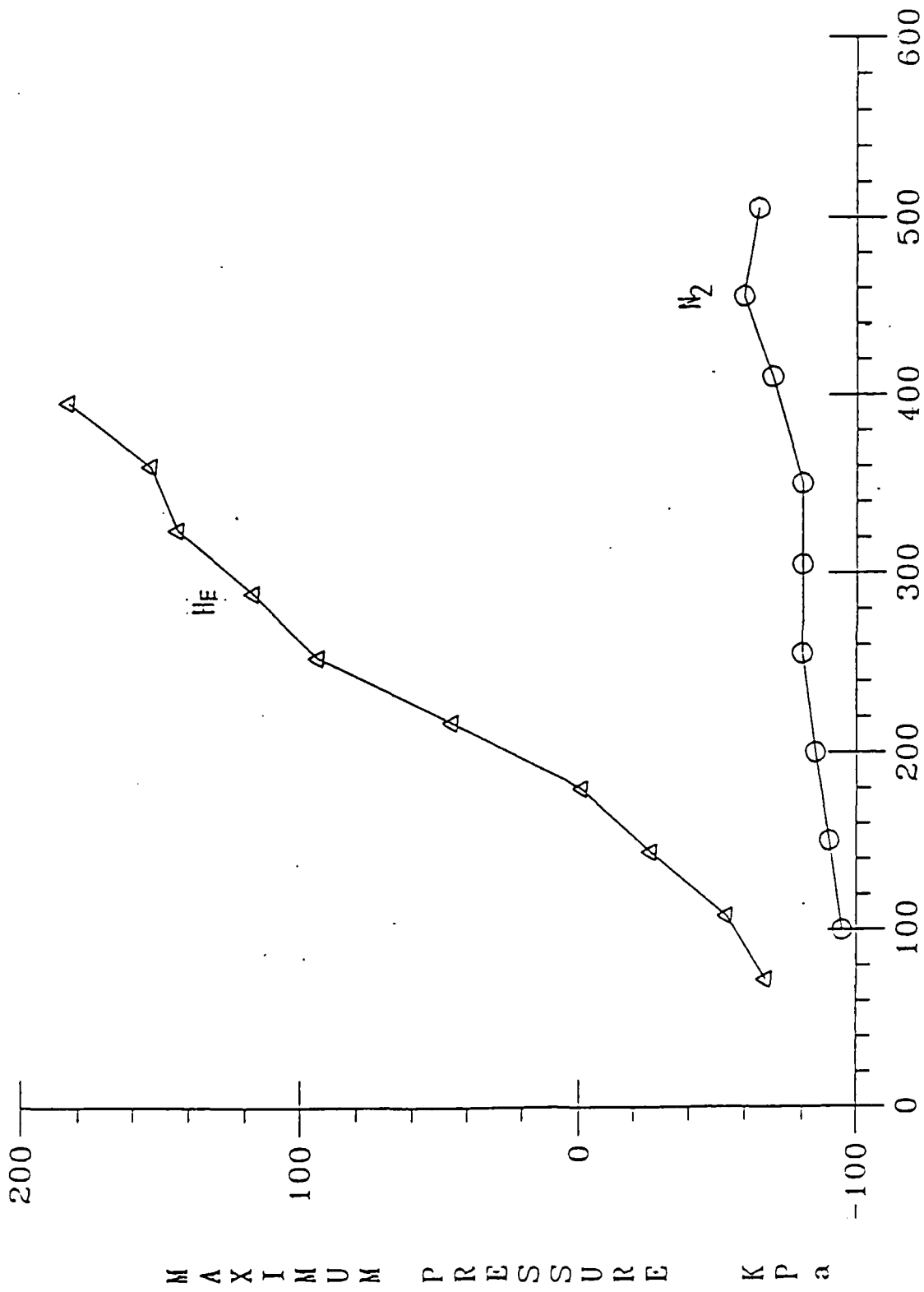


Fig. 2 Maximum gas pressure which can sustain a free floating TM_{01} plasma in nonflowing gas as a function of input power showing that helium can sustain much higher pressures than nitrogen.

HEATING OF A LIQUID/VAPOR MIXTURE
BY A PULSED ELECTRIC DISCHARGE

AFOSR Contract No. F49620-87-C-0061

Principal Investigator: Rodney L. Burton

GT-Devices, Inc.
5705A General Washington Drive
Alexandria, VA 22312

Overview

A liquid fuelled, pulsed electric discharge is being studied to identify the dominant energy exchange and mixing processes occurring between the liquid, vapor and plasma components. In this research, a water jet, injected into a small capillary tube, is subjected to a power pulse ~ 2 MW for 12 μ s. Spectroscopic techniques are being used to measure in detail the plasma density and temperature as functions of time under various discharge and liquid spray conditions.

Technical Discussion

Liquid-plasma discharges are of growing interest for the generation of high density, high enthalpy flows for rocket propulsion and wind tunnel testing. An electric propulsion device with an Isp of 1000-3000 seconds is the pulsed electrothermal (PET) thruster [1], which uses a high pressure ($\sim 10^2$ atm), modest temperature ($\sim 1-1.5$ eV) plasma generated in a capillary-confined electric discharge. In the PET scheme, liquid propellant (water) is injected into the capillary chamber through a small orifice at the cathode. A second device is a high enthalpy wind tunnel, which generates air at 2-7 km/sec for testing hypersonic aircraft.

Plasma generation in these devices proceeds with the application of a high current heating pulse from a capacitor PFN or similar source. Critical to the understanding of these discharges is an experimental and theoretical investigation into the interaction of a cold liquid/vapor mixture and hot

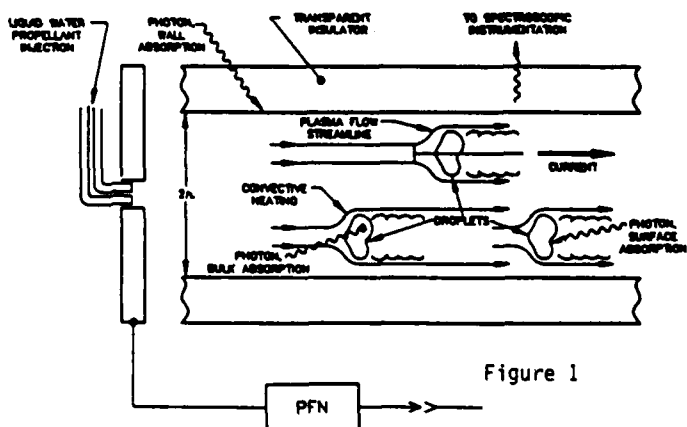
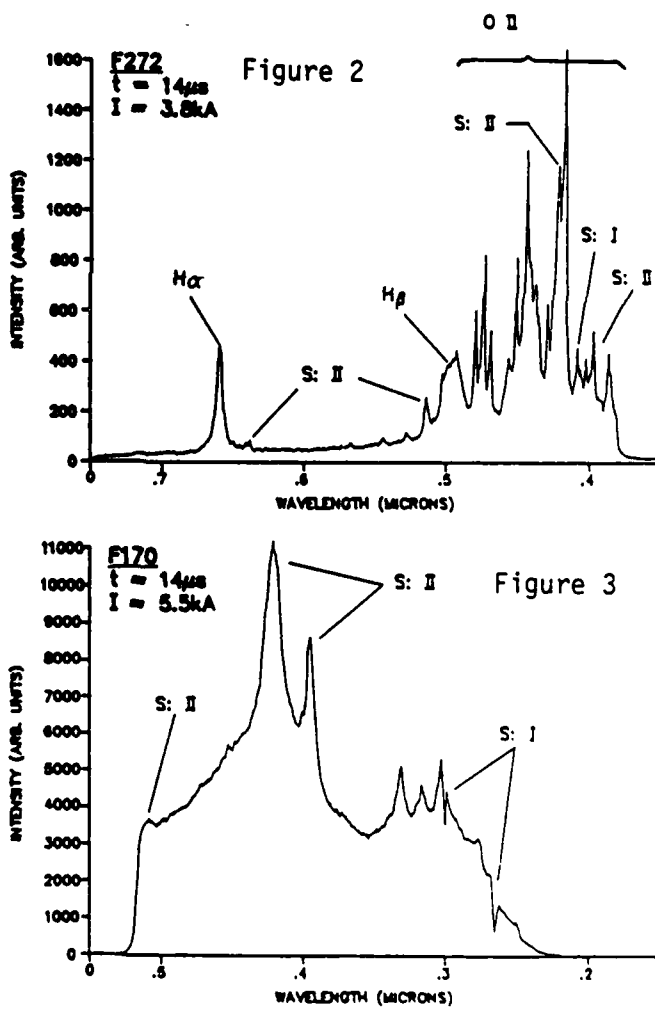


Figure 1

plasma present in the high power capillary environment.

A variety of complex, interdependent phenomena can participate in the energy transfer and mixing process (see Figure 1). Plasma radiation, thermal conduction and convection all play a role in contributing heat flux to both the surface and volume of the liquid. Vapor-plasma mixing can occur in the fast flow field as a steady surface erosion, or via instabilities leading to a more-or-less explosive event. The goal of this research is to identify the mechanisms dominating the liquid-vapor heating process by correlating models of the discharge dynamics with detailed spectroscopic measurements of the plasma parameters, namely temperature and density, as functions of time.

A transparent quartz tube (5 mm ID x 40 mm long) is used to provide direct visual access to the discharge. The expected high density, modest temperature plasma conditions may not generally be considered amenable to spectroscopic investigations. In particular one might expect a near pure blackbody radiator with temperature characteristic of a cool, dense boundary layer. However, because of the short pulse nature of the discharge (10-15 μ s current pulse) relative to typical flow time scales (e.g. $2r/cs \sim 1 \mu$ s, or $2l/cs \sim 10 \mu$ s) it should be possible to resolve and characterize the build-up to high density plasma conditions. The initial phase of this research attempts to assess the value of, and detail that can be



obtained with, time resolved spectroscopic measurement techniques.

Spectral data is obtained using a PAR-optical multichannel analyzer (OMA) and spectrograph system having a 700 channel intensified detector array, gateable to 20 ns time resolution. A low dispersion grating was used to survey the general nature and structure of the plasma emission spectrum. Time scans are taken on a shot-to-shot basis, though any given set of conditions is highly repeatable. A typical shot would have a water jet, 0.1-0.2 mm diameter, injected along the tube axis, with 20-50 joules delivered in a nominally square current pulse of $\sim 12 \mu\text{s}$ duration at 3-5 kA peak. Figures 2 and 3 sample the spectra observed near the end of the power pulse.

Strong emission lines are present during most of the pulse so that electron density is determined by their Stark broadened widths (primarily H_β) [2]. Spectroscopic techniques for measuring plasma temperature have proven more difficult. Conventional methods of using line intensity ratios or absolute continuum levels, though requiring considerable computational efforts, are being pursued. Rough indicators of a temperature near 2 eV is however indicated by the OII transitions (Figure 2) having upper level excitation potentials in the 20-30 eV range.

Figure 3 attempts to illustrate both the diagnostic power and pitfalls of these spectroscopic investigations. An overly energetic discharge produces severe wall ablation, accompanied by a dense, cold vapor layer. This is evidenced by the dominance and self-reversal in the silicon lines. However, the appearance of wall material in the plasma may give additional information on the heat flux environment of the propellant stream.

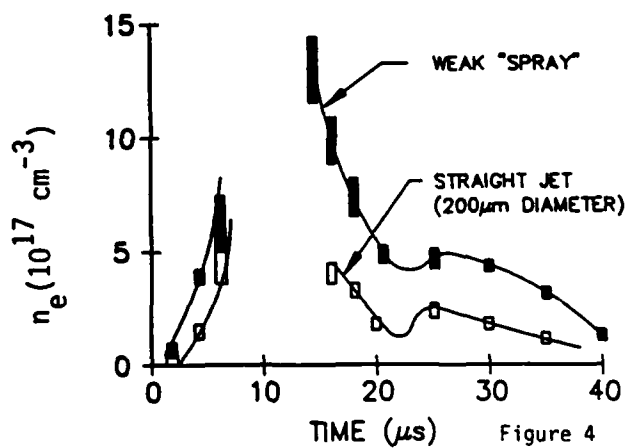


Figure 4

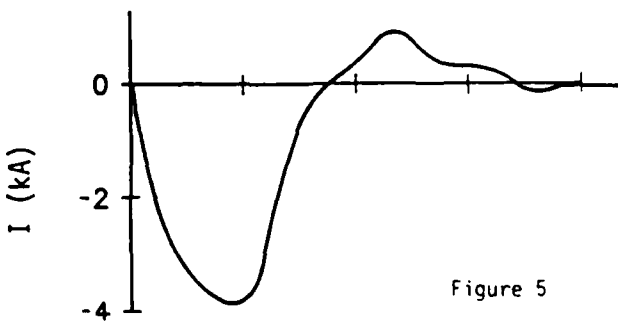


Figure 5

We are developing a so-called swirl generator to allow controlled break-up of the injected water jet into a spray. Preliminary data points towards the expected strong dependence of the plasma/liquid interactions on the liquid surface area. Figure 4 shows the electron density observed for a straight, solid cylindrical water jet, and a significantly higher density when a weak spray is used. Here, the weak spray condition has the droplet distribution confined to a full cone angle of $\sim 20^\circ$. Gaps in the data near peak n_e occur when overlapping OII lines severely distort the $H\beta$ line profile. Other, suitable, Stark broadened lines are being investigated to fill this gap and extend the measurement range to higher n_e .

The density build-up and decay is referenced to a typical current pulse (Figure 5). Peak density occurs basically near the end of the power pulse. The slight ring is current is mimicked in the residual plasma/vapor mixture. Clear resolution of the dynamical behavior in the early stages of the discharge will require some improvements in the measurement accuracy.

We have made extensive experimental investigations into the spectral composition of the plasma emission. This survey has illustrated the potential power of spectroscopic methods to provide detailed information on plasma conditions during the liquid/vapor heating process. The present diagnostics will be improved. In particular, the indicated temperature measurement techniques will be pursued with some priority. With the ability to modify and control the liquid injection, it will be important to quantify the spray structure in terms of droplet size and distribution prior to the discharge. A short exposure ($1 \mu s$), high magnification ($\times 16$) photographic system has been set-up for this purpose. The fan-out nature of the spray, along with a relatively long acoustic transit time, $2l/c_s \sim 10 \mu s$, suggests it would also be worthwhile exploring the discharge uniformity with respect to axial position.

With the experimental aspects reasonably well in hand, the primary emphasis in the second phase of this work will be towards developing a dynamical model of the liquid/vapor heating process.

[1] Investigation of a Repetitive Electrothermal Thruster R.L. Burton, et.al, Final Report GTD 86-5, CR-179464 NASA-Lewis.

[2] Spectral Line Broadening by Plasmas, H.R. Griem, Academic, NY (1974).

LASER-SUSTAINED ARGON PLASMAS AT ELEVATED MASS FLUX AND PRESSURE

AFOSR Grant No. 87-0169

Principal Investigators: Herman Krier and Jyoti Mazumder

Department of Mechanical and Industrial Engineering
University of Illinois at Urbana-Champaign

SUMMARY/OVERVIEW:

Laser propulsion is the production of high specific impulse rocket thrust using a high power laser as a remote energy source. Specific impulses in excess of 1000 seconds are achievable because propellant temperatures are very high and low molecular weight gases can be used. This investigation focuses on the energy conversion mechanisms of laser-sustained plasmas (LSP's) in flowing argon. Plasma thermal conversion efficiency and global absorption fraction are the key measured quantities. Improvements to the test apparatus have allowed plasma operating conditions never before possible, while we continue to utilize the University's 10 kW CW CO₂ laser. The results indicate that nearly all of the input laser power can be absorbed by a plasma, and thermal efficiencies as high as 35% have been recorded. Plasmas at elevated gas pressure have been tested, and preliminary results indicate that both efficiency and absorption decrease with increasing gas pressure. This indicates that the optimal operating conditions have yet to be determined for the available laser powers and gas pressures. Further experimentation at very high argon gas velocities (> 20 m/s) and alternative focusing geometries must be performed in order to completely characterize plasma behavior.

Fundamental research into the area of enhanced thermal mixing of the extremely high temperature gas with forced cold convection is called for. Multiple plasma testing also is required, as is the testing of low molecular weight gases. Non-intrusive laser induced fluorescence (LIF) diagnostic techniques are being pursued with efficiency measurement the key application. Two-dimensional plasma and flow chamber theoretical modeling is required to more accurately predict plasma behavior especially when confined to a small flow area geometry in which wall effects may become important.

TECHNICAL DISCUSSION:

Introduction

The key problem in the laser-sustained plasma rocket propulsion technique is the understanding and characterization of plasma energy conversion processes. These processes result in an increase in the thermal energy of the propellant gas. Various techniques are used to determine the fraction of the input laser energy absorbed by the plasma, how much is radiated to the plasma chamber environment, and finally how much is retained by the propellant gas as thermal energy. This gas thermal energy is the quantity used to determine thermal conversion efficiency by comparison to the input laser power.

Plasma temperatures are measured using a spectroscopic imaging system. With this system fractional laser absorption can be determined along with the amount of energy reradiated. The difference between these values is the energy retained by the gas. In addition laser absorption measurements are made with a water-cooled copper cone calorimeter, and gas

temperature measurements are made with conventional type K thermocouples downstream of the plasma. These measurements provide independent determinations of global absorption and thermal efficiency.

Much research has been done at our test facility involving the effects of varying flow velocity, laser power, and beam geometry. References 1-5 summarize much of our previous and ongoing work. Reference 6 is a paper on the quasi two-dimensional modelling of laser-sustained plasmas. Recent improvements to the laser beam quality and the dampening of inlet flow turbulence have led to our ability to perform plasma tests at over 9 m/s mean argon velocity at one atmosphere. Previously we were unable to test at velocities much over 1.25 m/s due to plasma instability. Elevated flow velocities are produced using a converging section placed inside the original 5 inch plasma chamber. This accelerates the flow with a decrease in flow area.

Experimental Procedure

A plasma will form if sufficient power is focused into a gaseous medium ($\sim 10^9$ W/cm²), or onto a metallic target ($\sim 10^5$ W/cm²). In our experiment the laser is focused onto a tungsten rod which releases electrons through thermionic emission. This leads to avalanche breakdown and plasma initiation. At this point the tungsten rod is removed from the beam focus.

Figure 1 is a schematic of our test stand, current optical arrangement, and plasma initiation and flow chamber. The annular laser beam first strikes the flat copper mirror in the upper right portion of the figure and is reflected 90 degrees downward. The beam is then reflected across the bottom of the test stand and up through a plano convex sodium chloride lens which focuses the beam through a zinc selenide window into the chamber. Figure 2 is a more detailed schematic of the chamber showing the side windows for spectroscopic access, the flow straightener used to dampen inlet turbulence, the converging section, downstream thermocouples, and the calorimeter. Temperature, pressure, and calorimeter data is monitored and recorded every 1.5 seconds by a Fluke datalogger system. Details of the experimental facility can be found in References 1, 3, and 5.

The spectroscopic system used is an EG&G PARC Optical Multichannel Analyzer (OMA) III. A simple lens images the plasma onto a vidicon detector through the horizontal slit of a 0.32 m Czerny-Turner spectrograph. The vidicon is a silicon intensified target with a UV scintillator applied for responses down to 200 nm. The OMA console is the CPU which configures the scanning sequence of the two-dimensional detector as well as the formatting and storage of data. The OMA CPU is also capable of limited data reduction functions. The monochromator and optics are mounted on an X-Z translation stage. Reference 2 summarizes the work of measuring plasma temperatures by emission spectroscopy. The line-of-sight intensity (W/cm²Sr), integrated over the various plasma annuli is then deconvoluted by an Abel inversion procedure to give plasma temperature profiles.

Efficiency and Absorption Measurements

The thermal efficiency of an LSP is defined as the ratio of the change in gas enthalpy flux to the laser power input to the plasma. Global absorption is the ratio of the total energy absorbed by the plasma to the input laser power. These quantities can be determined with both spectroscopic and conventional measurements.

Efficiencies presented in this abstract are based on bulk exhaust gas temperature measurements made with thermocouples in the chamber exhaust ports. The laser energy retained by the working gas is determined by calculating the change in enthalpy flux, ΔH , using $\Delta H = mC_p(T_e - T_i)$ where m is the measured mass flowrate, C_p is the specific heat of the gas, T_e is the measured bulk temperature of the exhaust gas, and T_i is that of the inlet gas.

Absorption percentages presented are based on calorimeter data. The calorimeter is mounted on top of the plasma chamber and collects the laser energy which is not absorbed by the plasma. The calorimeter is equipped with thermocouples which determine the difference in cooling water temperature as it absorbs the laser energy. This difference determines the amount of energy transmitted by the plasma and from this plasma absorption is calculated.

Figure 3 contains efficiency and absorption data from experiments at 2.5 kW and 5 kW input laser power. These tests were done at one atmosphere gas pressure and with f/7 focusing optics. Note that efficiency tends to increase with increasing mass flux. Efficiencies range from 16.4 % to 35.3 % for 2.5 kW plasmas and from 13.4 % to 30.3 % for 5 kW plasmas. It is thought that higher input powers have the potential to produce more efficient plasmas, but at much higher mass fluxes at which low power plasmas are not stable.

Absorption increases with increasing power at a given mass flux. It also appears that at this range of conditions there is a peak in the absorption curve, and that the peak occurs at a higher mass flux for higher input powers. The continued rise in efficiency even when absorption is decreasing indicates that the higher mass flux brings about a substantial decrease in plasma radiation. This trend has been confirmed for other operating conditions from the spectroscopic data referenced earlier.

Figure 4 contains data from experiments at elevated gas pressure. A comparison is made between the absorption and efficiency of a plasma at constant mass flux and two different gas pressures. The data indicates that both absorption and efficiency decrease with increasing pressure. It is thought that this trend may not exist at much higher mass fluxes because the higher pressure plasma will be better matched with its optimum operating condition. Reference 4 contains a complete summary of all current elevated mass flux and pressure research.

REFERENCES:

1. McMillin, B.K., Zerkle, D.K., Glumb, R.J., Mazumder, J., and Krier, H., "Energy Conversion in Laser Sustained Argon Plasmas for Application to Rocket Propulsion," AIAA paper 87-1459; Presented at the AIAA Fluid Dynamics, Plasma Dynamics, and Lasers Conference, June 1987.
2. Mazumder, J., Rockstroh, T.J., and Krier, H., "Spectroscopic Studies of Plasma During CW Laser Gas Heating in Flowing Argon," *Journal of Applied Physics*, Vol. 66, No. 2, pp. 4712-4718, December 1987.
3. Krier, H., Mazumder, J., Rockstroh, T.J., Bender, T.D., and Glumb, R.J., "Continuous Wave Laser Gas Heating by Sustained Plasmas in Flowing Argon," *AIAA Journal*, Vol. 24, No. 10, pp. 1656-1662, October 1986.
4. Krier, H., Mazumder, J., Zerkle, D.K., Mertogul, A., and Schwartz, S., "Energy Conversion Measurements in Laser Sustained Argon Plasmas for Application to Rocket Propulsion," Technical Report, Department of Mechanical and Industrial Engineering, University of Illinois at Urbana-Champaign, UILU-ENG-88-4006, April 1988.
5. Mazumder, J., Krier, H., Rockstroh, T.J., Glumb, R.J., McMillin, B.K., Zerkle, D.K., and Chen, X., "Laser Sustained Plasmas for Application to Rocket Propulsion," Technical Report, Department of Mechanical and Industrial Engineering, University of Illinois at Urbana-Champaign, UILU-ENG-87-4002, March 1987.
6. Glumb, R.J., and Krier, H., "Two-Dimensional Model of Laser Sustained Plasmas in Axisymmetric Flowfields," *AIAA Journal*, Vol. 24, No. 8, pp. 1331-1336, August 1986.

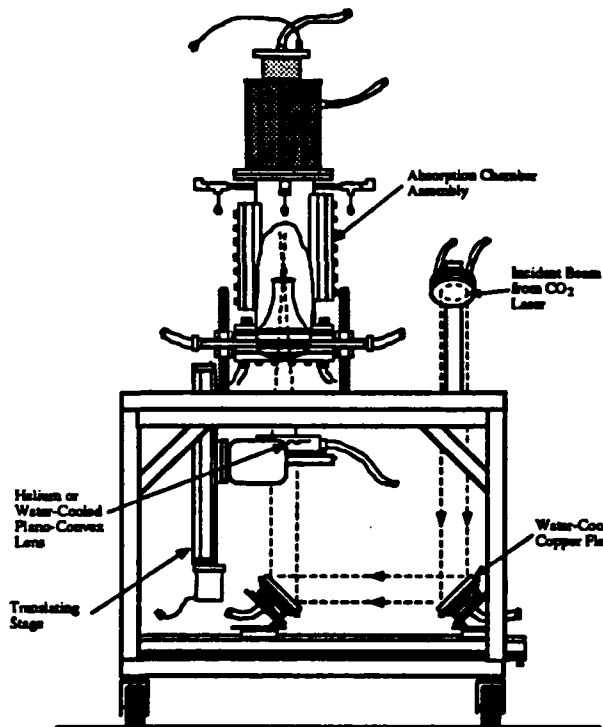


Figure 1 Schematic of the test stand used in the study of LSPs. An on-axis optical configuration is shown utilizing precision optical components and a lens translation stage.

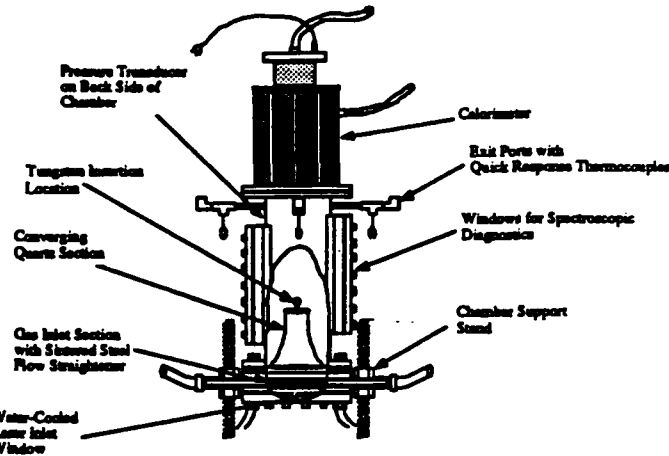


Figure 2 Schematic of the absorption chamber used in the study of LSPs. Note the flow straightener and quartz section in the cut-away view.

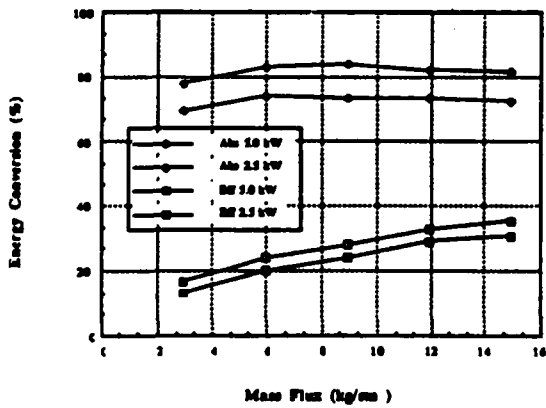


Figure 3 Comparison of efficiency and absorption for two laser powers versus mass flux at one atmosphere gas pressure.

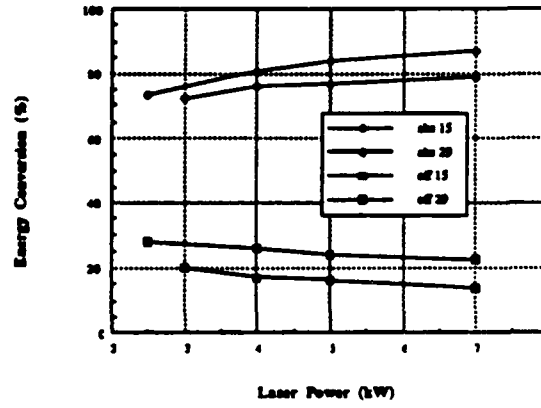


Figure 4 Comparison of efficiency and absorption for two gas pressures versus laser power at 8.95 kg/m² mass flux. Pressure is in psia.

FAST THERMOLYSIS OF ENERGETIC MATERIALS
AFOSR-87-NA-140

Principal Investigator: Thomas B. Brill

Department of Chemistry
University of Delaware
Newark, DE 19716

SUMMARY/OVERVIEW:

The thermal decomposition of energetic materials is being investigated at high heating rates and under pressures at or above atmospheric to identify the phenomena and chemical mechanisms that may be important in the decomposition and ignition of these materials. New techniques based on rapid-scan FTIR spectroscopy have been developed for these studies. With at least the order-of-magnitude higher heating rates and diagnostic data acquisition rates used here compared to what is more common for condensed phase studies, considerable new detail about the chemical and physical phenomena related to decomposition and ignition is being acquired. These results help define what is and is not important to consider about molecular behavior during the decomposition and ignition of an energetic material.

TECHNICAL DISCUSSION

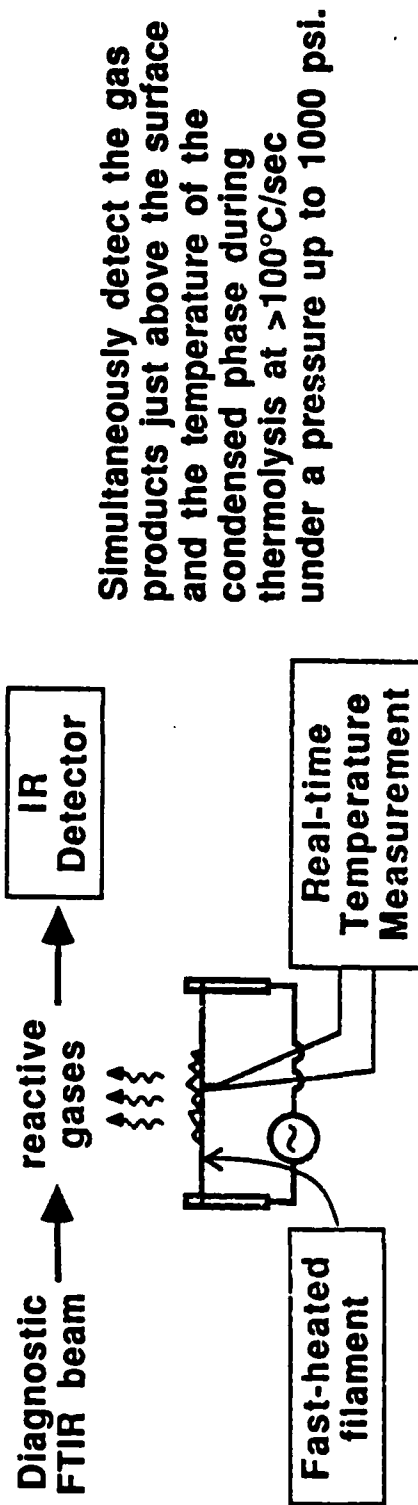
This presentation will give an overview of the decomposition/ignition/combustion process of propellants from the fundamental, molecular point of view. That is, what are the main considerations in describing the transition from the cool solid to the hot, combusted gas at the physicochemical level?

Following this introduction, one or more specific projects from our own research will be presented. Shown in Figure 1 is a simplified sketch of the experiment we employ to provide insight into the identity of the gas products ejected from the surface of a solid or liquid which has been rapidly heated. The temperature of the condensed phase is simultaneously measured so that endothermic and exothermic events can be correlated with the products generated. Figure 2 shows one result from the study of the fast-thermolysis of compounds containing the $-C(NO_2)_2N_3$ energetic functional group. This group decomposes by perhaps what is the most straightforward reaction of any non-trivial energetic site yet investigated. NO_2 and the organonitrile, RCN , are liberated. By inference, N_2 is also a product.

New techniques are currently under development that should give still further understanding of fast thermolysis. One of these experiments involves a "fast-heat-and-hold" technique to allow the decomposition to be studied at the temperature that it occurs rather than "on-the-fly" as is currently done. A second experiment is shown in Figure 3. With this device, the mass change, temperature change, and product species will be identified simultaneously while the sample experiences thermolysis at a high heating rate.

APPROACH

Simulation of the Condensed Phase Breakup During Decomposition/Ignition

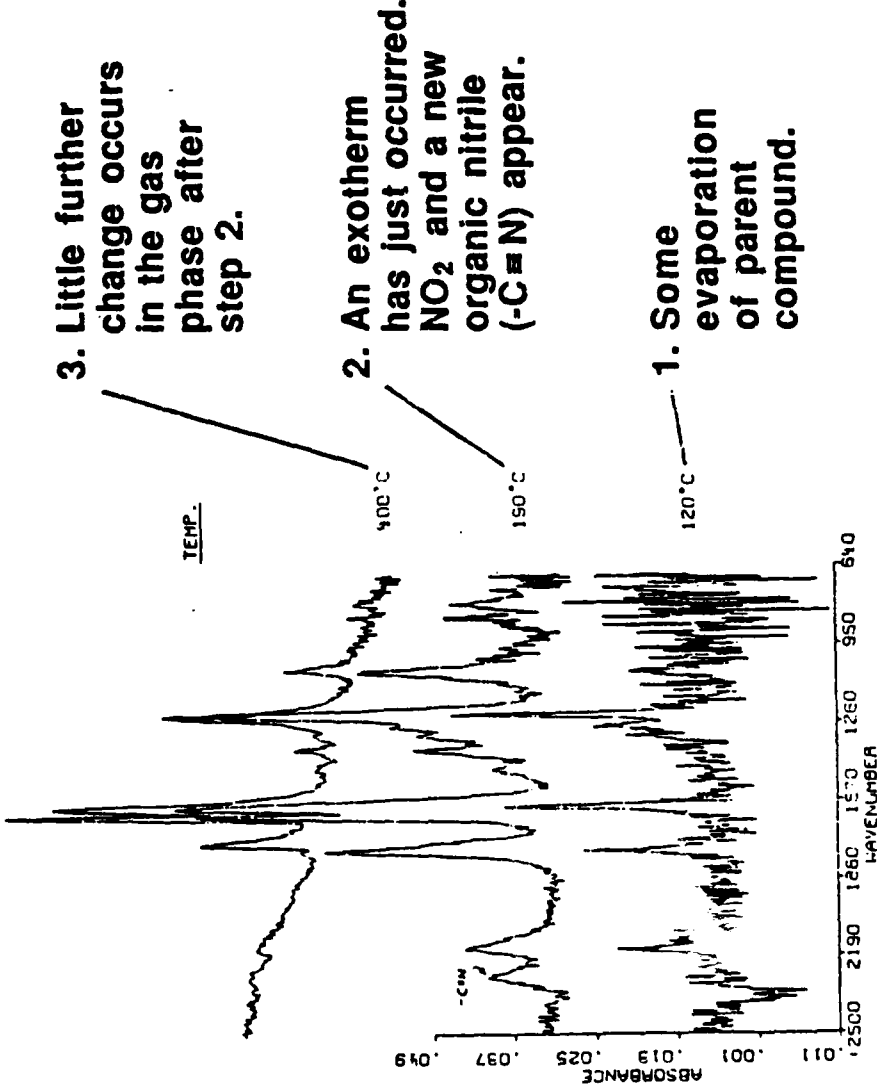


Research:

- Identify and characterize the reactive gases that feed a flame of an energetic material.
- Characterize dynamic physical phenomena, such as melting.
 - Define decomposition reaction mechanisms.
- Measure temperatures associated with chemical events in the condensed phase.

ONE OF THE ACCOMPLISHMENTS

The thermolysis of the $-\text{C}(\text{NO}_2)_2\text{N}_3$ functional group* is now better understood.



*Compounds synthesized by
M. Frankel and J. Weber (Rocketdyne).

CONCLUSION:

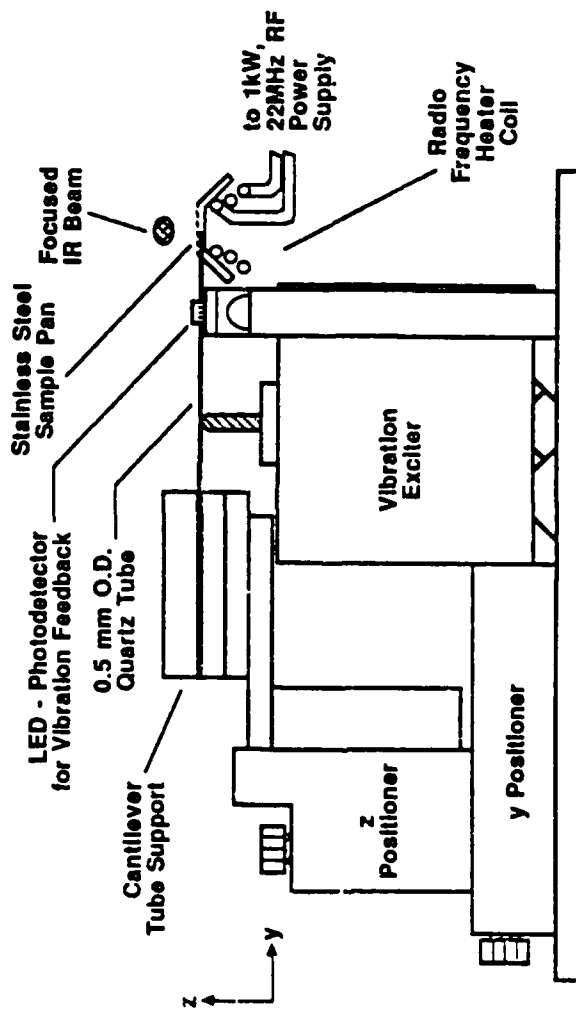
The results show that at about 180°C, this compound ignites/ explodes by the following reaction:

**Mid-infrared spectra of the gas phase above
 $\text{CH}_3\text{OC(O)CH}_2\text{C}(\text{NO}_2)_2\text{N}_3$ heated at 70°C/sec**



FUTURE PLANS

Construct a simultaneous Mass-loss, Temperature-change, product speciation Device for High Heating-rate Thermolysis studies.



Advantages:

This device will permit the amount of sample (mass loss) involved in each decomposition step to be correlated with the temperature of the event and the gas products released. The detailed description of decomposition related to combustion will be further advanced.

SOLID PROPELLANT COMBUSTION CHEMISTRY

AFOSR PROGRAM ELEMENT 2308M1

Principal Investigators: T. Edwards and D. P. Weaver

Air Force Astronautics Laboratory
AFAL/LSCC, Edwards AFB, CA 93523-5000

SUMMARY/OVERVIEW:

This research is designed to examine the structure and reaction mechanisms of high pressure solid propellant flames. Very little knowledge along these lines exists at present, with this lack of understanding limiting performance improvements of current solid propellants. The major experimental tools used in this research are laser-based combustion diagnostics such as laser-induced fluorescence. We anticipate that the experimental results, in the form of species and temperature profiles in a given solid propellant flame, will be quite useful in validating high pressure solid propellant flame chemistry models. These models will be useful in solving many chemistry-related solid propellant combustion problems of current interest.

TECHNICAL DISCUSSION

It is generally believed that improvements in the solid rocket performance will result from a better understanding of the chemistry and physics of solid propellant combustion. Many aspects of the structure and reactions of solid propellant flames are not well understood under rocket motor conditions (pressures on the order of 7 MPa), although enough is known that serviceable solid propellant combustion models have been created. These models tend to emphasize the heat transfer aspects of combustion at the expense of the chemistry. This allows much useful information to be derived from the models, although many situations that are directly chemistry related are not well handled. To improve the understanding of solid propellant combustion, much more detailed information is needed about propellant flames, preferably under high pressure combustion conditions. Laser-based combustion diagnostics have the potential to address many of the unknown aspects of propellant combustion, although the experimental difficulties are formidable. This presentation describes recent results obtained at AFAL in this area. Published results include studies of chemiluminescence and laser-induced fluorescence (LIF) in high pressure solid propellant flames [1-4]. Complementary work at the Naval Weapons Center is also underway [5].

Construction and verification of propellant combustion models incorporating detailed chemistry [6,7] requires species concentration and temperature information in the flames of interest. Radical species can be measured with LIF, major species and temperature measured with laser-Raman or CARS [8]. Temperature measurements can also be made with very fine thermocouples [9], although these are difficult measurements that are subject to possibly large errors.

Temperature measurements can also be made by atomic fluorescence techniques [10], which include surface temperature measurements [11]. The number of species needed to construct an adequate mechanism is difficult to determine a priori since model construction will require extensive interplay between experimental measurements and theoretical modeling efforts. For certain propellants, most notably double-base propellants, a one-dimensional flame chemistry model may suffice, while heterogeneous propellants (such as ammonium perchlorate propellants) will require more complex models. Two dimensional flame chemistry models exist, but are very computer-time intensive [12]. For complex propellants, the key to modeling efforts may be to discover the minimum number of reactions that will yield both adequate propellant flame properties and reasonable computational time.

References

1. Edwards, T., Weaver, D. P., Campbell, D. H., and Hulsizer, S., "A High Pressure Combustor for the Spectroscopic Study of Solid Propellant Combustion Chemistry," Review of Scientific Instruments, 56(11), 2131-2137 (1985).
2. Edwards, T., Weaver, D. P., Campbell, D. H., and Hulsizer, S., "Investigation of High Pressure Solid Propellant Combustion Chemistry using Emission Spectroscopy," Journal of Propulsion and Power, 2(3) 228-236 (1986).
3. Campbell, D. H., Hulsizer, S., Edwards, T. and Weaver, D. P., "High Pressure Solid Propellant Combustion Zone Structure from Analysis of Hydroxyl Radical Chemiluminescence," Journal of Propulsion and Power, 2(5), 414-422 (1986).
4. Edwards, T., Weaver, D. P., and Campbell, D. H., "Laser-Induced Fluorescence in High Pressure Solid Propellant Flames," Applied Optics 26(17): 3496-3509 (1987).
5. Parr, T., and Parr, D. M., "Temperature and Species Profiles in Propellant Ignition and Combustion," 24th JANNAF Combustion Meeting, CPIA Pub. 476, Volume I, 367-382 (1987).
6. Hatch, R. L., "Chemical Kinetics Modeling of HMX Combustion," 24th JANNAF Combustion Meeting, CPIA Publication 476, Volume I, pp. 383-391 (1987).
7. Melius, C., "Theoretical Studies of the Chemical Reactions Involved in the Ignition of Nitramines," 24th JANNAF Combustion Meeting, CPIA Publication 476, Volume I, pp. 359-366 (1987).
8. Eckbreth, A. C., Laser Diagnostics for Combustion Temperature and Species, Abacus Press (Cambridge, 1988).
9. Kubota, N., "Physicochemical Processes of HMX Propellant Combustion," 19th Symposium (Int'l) on Combustion, 777-785, Combustion Institute (Pittsburgh, 1983).
10. Winefordner, J. D., "Atomic and Molecular Gas Phase Spectrometry," AFOSR-TR-85-1034 (1985).
11. Goss, L. P., and Smith, A. A., "Application of Fluorescence to Measurement of Surface Temperature in Solid Propellants," Proceedings of 1986 AFOSR Contractors Meeting on Diagnostics of Reacting Flows, pp.61-64 (1986).
12. Hepler, W. A., Smith, O. I., "Numerical Simulation Study of a Hydrazine/Nitrogen Dioxide Diffusion Flame in a Burke-Schumann Burner," Combustion Institute Paper WSS/CI 87-23 (1987).

Table I - Propellants Studied

<u>Propellant</u>	<u>Composition</u>	<u>Reason for study</u>
AP1	87% AP, 13% inert binder ($r=8$ mm/s, $T_{fl}=2970$ K @ 35 atm)	Typical ammonium perchlorate composite propellant, complex time-dependent diffusion flame chemistry
HMX1	73% HMX, 27% energetic binder ($r=2.5$ mm/s, $T_{fl}=2620$ K @ 35 atm)	Typical HMX propellant, flame chemistry more premixed in character than AP
HMX2	80% HMX, 20% non-energetic binder ($r=1.5$ mm/s, $T_{fl}=2050$ K @ 35 atm)	Duplicate of one of Kubota's propellants; has "dark zone"
DB1	70% NG, 30% PEG ($r=4.4$ mm/s, $T_{fl}=2150$ K @ 35 atm)	"Double-base" propellant; homogeneous solid, has one-dimensional flame chemistry
AN1	67% AN, 33% energetic binder ($r=3.4$ mm/s @ 18 atm $T_{fl}=2140$ K @ 35 atm)	Ammonium nitrate of high Air Force interest; has poorly understood combustion behavior
AP2	68% AP, 16% Al, 16% inert binder ($r=7$ mm/s, $T_{fl}=3370$ K @ 35 atm)	Highly aluminized propellant, very difficult diagnostic environment

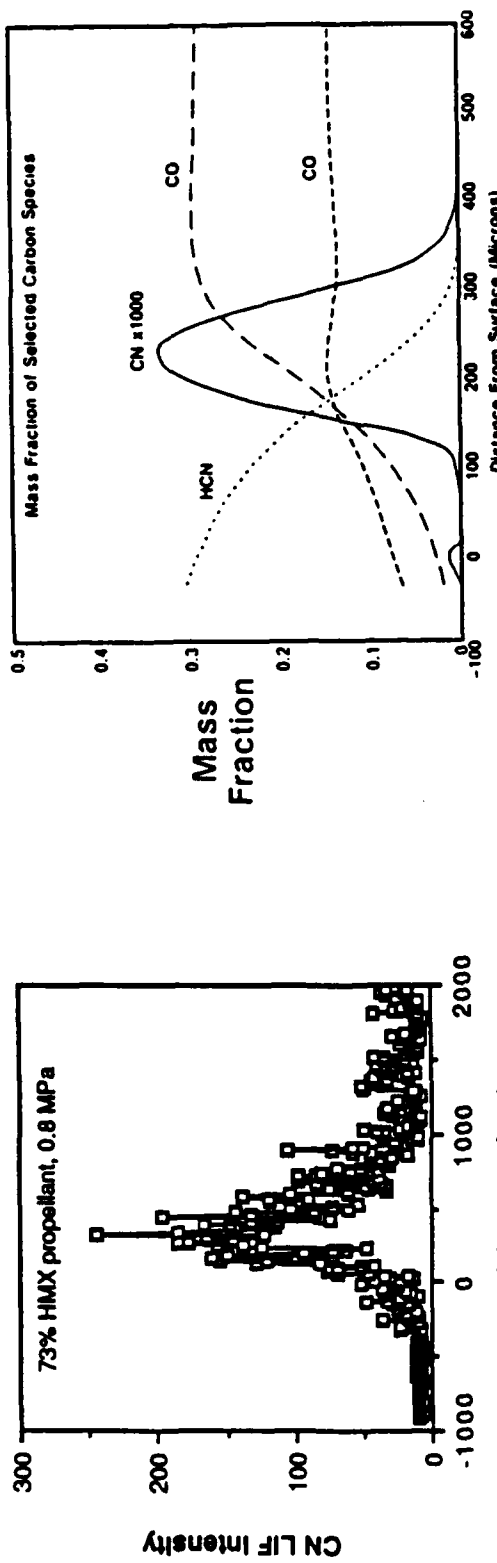
TABLE II - Results and Plans

Propellant	Pressure Range atm	LIF profiles		Emission profiles
		To date	Planned	
AP1	1-35	OH,CN,NH	NO,T	OH,CN,NH,CaCl,Na,K
HMX1	1-70	CN,OH,NH*	NO,T	OH,CN,NH,Na
HMX2	1-70	CN,NH*	NO,OH,T	--
DB1	1-35	CN*,NH*	NO,OH,T	Na
AN1	1-35	CN	NH,NO,OH,T	--
AP2	1-70	--	CN,OH,NO,T	CN,Al

*not yet successful

SOLID PROPELLANT COMBUSTION CHEMISTRY ACCOMPLISHMENT

70



EXPERIMENTAL RESULT
(73% HMX PROPELLANT)

MODEL RESULT (HATCH, THIOKOL,
100% HMX)

- FIRST WELL-RESOLVED SPECIES MEASUREMENTS OBTAINED IN HIGH PRESSURE PROPELLANT FLAMES

- COMPARISON WITH MODEL RESULTS SHOWS IMPORTANT INFLUENCE OF BINDER ON PROPELLANT FLAME STRUCTURE

CHEMICAL KINETICS OF NITRAMINE PROPELLANT COMBUSTION

AFOSR Grant Number AFOSR-84-0006

Melvyn C. Branch

Mechanical Engineering Department
University of Colorado
Boulder, Colorado 80309-0427

SUMMARY/OVERVIEW:

The decomposition of many solid rocket propellants and other energetic materials leads to the formation of gaseous hydrocarbons and oxides of nitrogen which react to form a flame above the surface of the solid. These flames can provide heat which is fed back to the surface and thereby influence the burning rate of the solid. The objective of the studies described here is to describe the characteristics of these flames experimentally and computationally in order to examine critical reaction paths and their influence on burning rate. In previous studies we have examined CH_4 and CH_2O burning with NO_2 and O_2 and found that the flames are slowed by the difficulty in reducing the NO formed from the NO_2 . The studies in progress and proposed for continuation of the research will consider the structure of fuel/ N_2O flames for comparison to the NO_2 flame data and will examine the effectiveness of several additives in generating radicals which can accelerate the decomposition of NO.

TECHNICAL DISCUSSION:

When they are heated, solid nitramines undergo phase changes before gaseous products are formed. The gas phase decomposition products include significant amounts of CH_2O , HCN, NO_2 , NO and N_2O which can react and form a gaseous flame above the surface of the propellant. The actual combustion of solid rocket propellants occurs at very high pressure and the reaction zones under these conditions are very thin and hence difficult to measure. The studies reported here are of low pressure flames which can be spatially resolved with considerable accuracy. No previous data have been reported on stable or unstable species concentration profiles in many fuel/NOx flames, particularly with formaldehyde as fuel. It is clear, however, that pressure effects will have a major effect on flames associated with burning propellants. Other research is addressing these pressure effects in propellant combustion chemistry.

The flames which were studied were stabilized on a 2 cm by 8 cm burner housed in an evacuated chamber maintained at 50 torr. The reactant gases, with the exception of formaldehyde, were supplied from gas cylinders and the flowrate controlled and measured by electronic mass flow controllers. Since formaldehyde cannot be stored as a monomeric gas at room temperature, a continuous flow, monomeric, gaseous formaldehyde generator was developed for use in these studies. Flame measurements were made of the concentration of stable species and selected intermediate species and of temperature through the reaction zone. Stable species were measured by probe sampling and gas chromatographic analysis, unstable species were measured by laser induced fluorescence (LIF) and temperature was measured by LIF and radiation corrected,

fine wire thermocouples.

Flame profiles have been measured for several $\text{CH}_4/\text{NO}_2/\text{O}_2$ and $\text{CH}_2\text{O}/\text{NO}_2/\text{O}_2$ flames and the kinetics discussed. Nitrogen dioxide is a poor oxidizer in relation to O_2 due to the chain propagating reaction of NO_2 with H atoms in contrast with the chain branching reaction of O_2 with H atoms. Therefore, NO_2 is converted relatively slowly to NO and much of the NO_2 remains as a diluent in the flames with the result that the flame temperature is well below the adiabatic flame temperature. In the methane flames some reduction of the NO to N_2 is possible because of the formation of C_2H and subsequent reaction of CH with NO. Since formaldehyde forms CHO rather than CH during its oxidation, the formation of molecular nitrogen is much more difficult in formaldehyde flames. The results suggest that the flame reaction rates may be significantly increased if additive radicals might be found which attack NO_2 and NO to increase the production of N_2 .

The studies planned for continuation of the research is to complete the characterization of fuel/NO_x flames with emphasis on more detailed chemical kinetic modeling. We plan first to study fuel/N₂O flames for direct comparison to the same flames with NO_x. We have already noted the difficulty which arises in reducing NO in many of these flames. We plan also to consider the effectiveness of amine species in promoting the decomposition of NO. The use of amines for NO reduction has been demonstrated at low concentration but not at the much higher concentrations encountered in propellant flames. These studies will be complemented by measurements of flame velocity of fuel/NO_x flames with and without additives designed to promote NO decomposition.

PUBLICATIONS:

M. Sadeqi and M.C. Branch, "A Continuous Flow, Gaseous Formaldehyde Generation System for Combustion Systems," *Combustion and Flame*, 71, pp. 325-29, 1988.

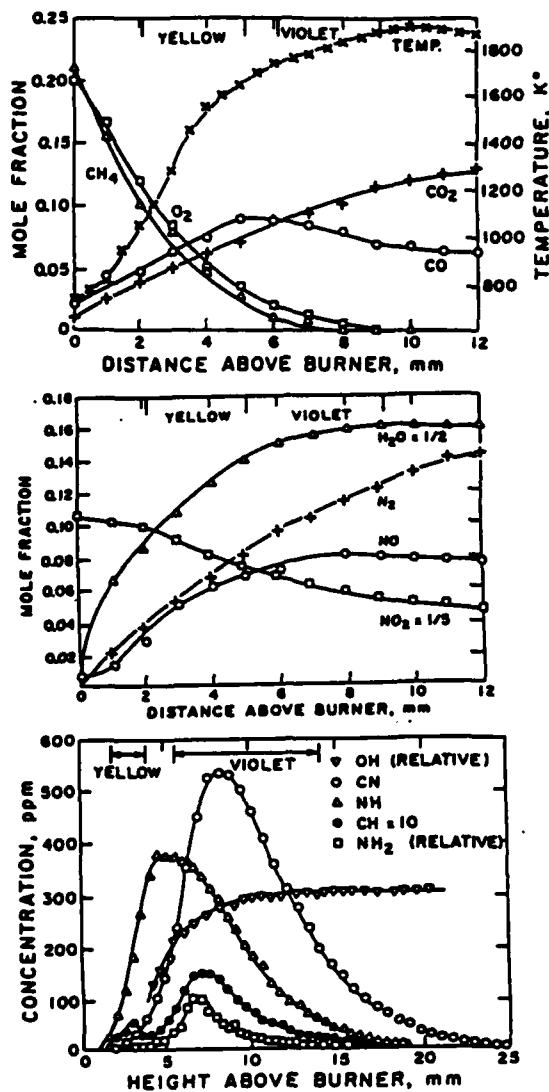
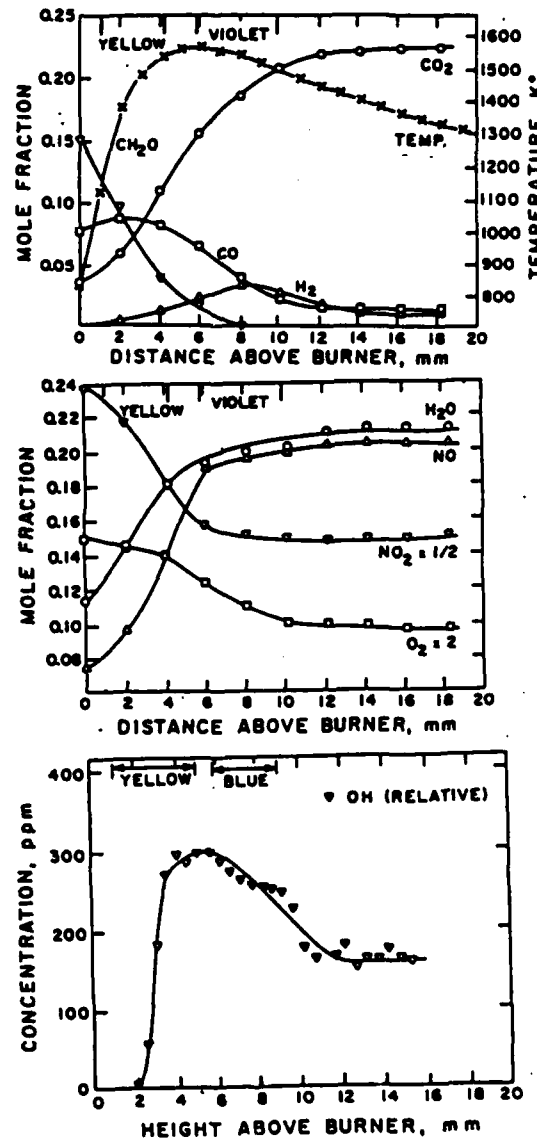
M.C. Branch, A. Alfarayedhi and M. Sadeqi, "Laser Induced Fluorescence Measurements of the Structure of $\text{CH}_4/\text{NO}_2/\text{O}_2$ Flames," *Proceedings of the 2nd ASME/JSME Thermal Engineering Conference*, 1, pp. 181-186, 1987.

M. Sadeqi and M.C. Branch, "Structure of Laminar Premixed Flames of $\text{CH}_2\text{O}/\text{NO}_2/\text{O}_2$ Mixtures," *Proceedings of the 24th JANNAF Combustion Meeting*, CPIA Pub. 426, 1, pp. 343-51, 1987.

M.C. Branch, A. Alfarayedhi and M. Sadeqi, "Flame Structure and Reaction Kinetics of $\text{CH}_4/\text{NO}_2/\text{O}_2$ and $\text{CH}_2\text{O}/\text{NO}_2/\text{O}_2$ Flames," *Combustion and Flame*, in preparation.

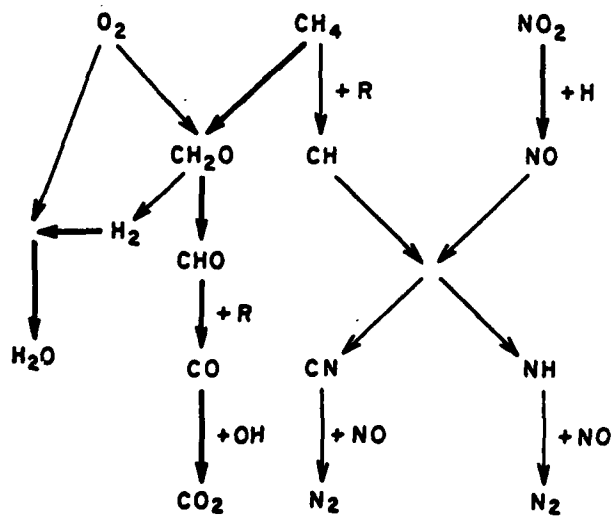
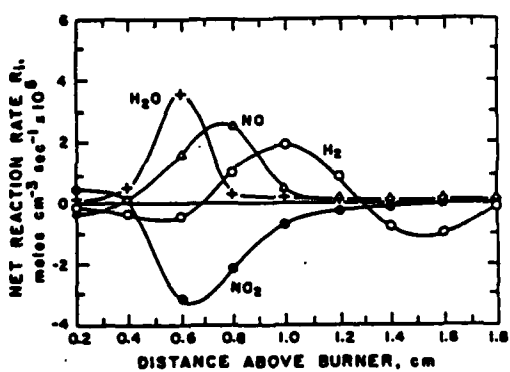
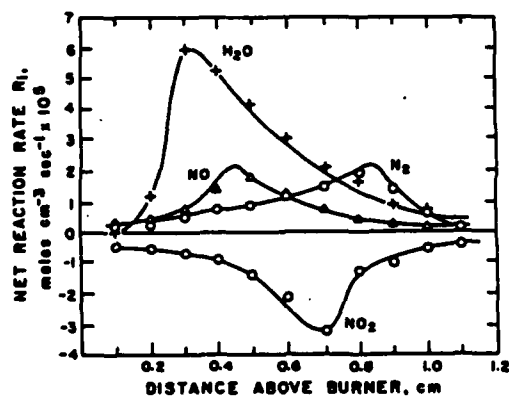
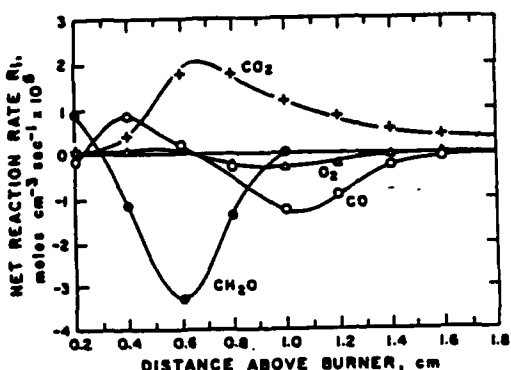
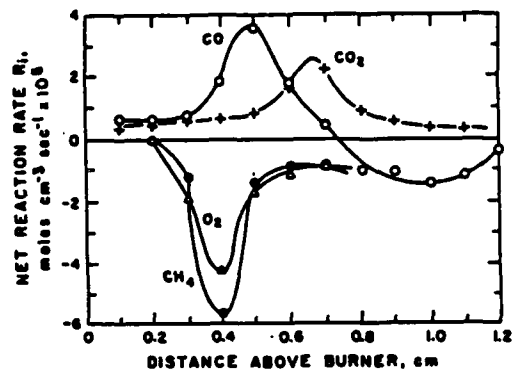
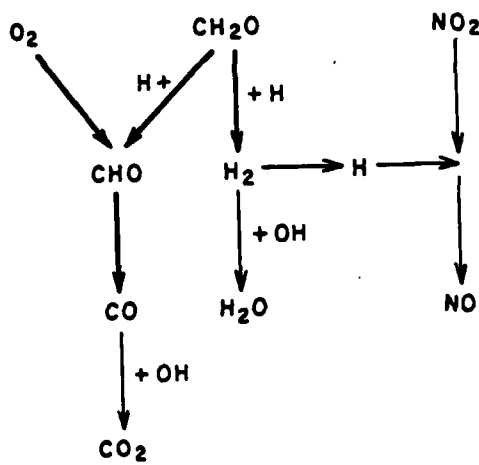
ACCOMPLISHMENTS I

FLAME STRUCTURE MEASURED FOR CH₄/NO₂/O₂ AND CH₂O/NO₂/O₂ LAMINAR PREMIXED FLAMES AT LOW PRESSURE. THIS REQUIRED DEVELOPING A RELIABLE FORMALDEHYDE GAS GENERATOR.

CH₄/NO₂/O₂CH₂O/NO₂/O₂

ACCOMPLISHMENTS II

FLAME PROFILES AND REACTION RATE CALCULATIONS HAVE SUGGESTED A REACTION MECHANISM FOR THE FLAME REACTIONS.

CH₄/NO₂/O₂CH₂O/NO₂/O₂

THE COMBUSTION OF HYDROGEN AND HYDROCARBONS IN FLUORINE

AFOSR 84-0196

Myron Kaufman

Department of Chemistry
Emory University
Atlanta, GA 30322

SUMMARY/OVERVIEW

Fluorine-supported flames are important to propulsion both directly in high specific impulse propulsion systems, and indirectly in what they can reveal about combustion in general. Light emission in F₂-hydrocarbon flames is studied by trace additions of C₂H to H₂-F₂ flames, a technique that keeps many flame parameters constant as the concentration of hydrocarbon radicals are varied. These studies indicate that the most likely mechanism for producing the blue emission from the A state of the CH radical is by combination of hydrogen and carbon atoms. Selected elementary reactions are studied in a flow reactor by observing their luminescence at long times, a method which provides kinetics and mechanistic information about the reaction and often permits titration of active species in gas-phase reactions.

TECHNICAL DISCUSSION

Besides the inherent interest of energetic fluorine-supported flames for propulsion systems, such systems are also important for what they can reveal about combustion processes in general. Fluorine-based combustion is related to oxygen-based combustion in that by studying the former we can learn much about the latter. Notwithstanding their high temperatures and burning velocity, fluorine flames are intrinsically simpler than oxygen flames. This is a result of fluorine being monovalent rather than divalent. There are no species analogous to peroxides and aldehydes to complicate fluorine-based combustion. Mechanisms for light emissions, non-steady behavior, etc. can be more easily established in fluorine than in oxygen supported combustion. Additionally, since there are no multiple bonds to fluorine, forming compounds with bond strengths comparable to CO, there are usually fewer energetically feasible routes for producing excited states in the fluorine systems. If the same chemiluminescence is observed in fluorine and oxygen systems, with sufficient similarity to suggest that they

result from identical mechanisms, it may be much easier to establish that mechanism in the fluorine system.

Two emissions that are observed in both F₂ and O₂ flames of hydrocarbons are those of CH and C₂. Decades of experiments on oxygen flames have not succeeded in establishing all the mechanisms producing these luminescences in hydrocarbon combustion. An additional prominent emission observed in fluorine-hydrocarbon flames is that of the CHF radical. We are interested in determining mechanisms for all these emissions, in order to use them as diagnostics for fluorine-supported flames, as well as to generally contribute to the advancement of combustion theory. As a supplement to our flame investigations, we also study the kinetics of selected reactions in flow reactors, in order to measure rate constants of interest and develop new methods for studying gaseous fluorine chemistry.

Studies of flames

A very revealing technique for studying mechanisms of phenomena observed in hydrocarbon-fluorine flames is the method of very dilute flames, whereby trace amounts of hydrocarbons are added to premixed H₂-F₂ flames. The trace additions at these very dilute levels do not appreciably change the basic flame parameters, such as flame temperature, burning velocity and the concentration of major hydrogen and fluorine species. They do, however, allow the dependence of flame phenomena, such as luminescence, to be studied as a function of the concentration of hydrocarbon and hydrocarbon-containing radicals. Similar experiments have been used to elucidate mechanisms in oxygen-supported combustion.¹ Using our low pressure flame burner, emissions of CH, C₂ and CHF are monitored as a function of added hydrocarbon for small additions of CH₄ and C₂H₂ to premixed H₂-F₂ flames. Flame structure and rotational distributions in HF emissions are employed to establish the range of additions that do not appreciably alter the flame. Selected experiments are performed with purified fluorine, containing very low concentrations of oxygen, to insure that the observed phenomena are not due to oxygen reactions.² An example of the type of data obtained in these experiments is shown in Figure 1. These preliminary results support a mechanism for formation of the A state of CH by combination of carbon and hydrogen atoms.

Studies of elementary reactions

We have found that a powerful method of exploring bimolecular chemical reactions is to study their long time behavior. At the stoichiometric ratio of reactants, the decay of reagent in such systems is second order and thus

inversely proportional to time. At any other concentration ratio of reactants, the reaction eventually becomes pseudo-first order, with the limiting reagent decaying exponentially. Since exponential decay is much faster than $1/t$ decay, at the stoichiometric ratio reaction persists for a longer time than at any other ratio of concentrations. Thus the rate of reaction at long times varies by many orders of magnitude for small variations around the stoichiometric ratio of concentrations.³

Analytic solutions for simple bimolecular reactions using the plug-flow approximation are shown in Figure 2. These indicate that measurements of chemiluminescent intensity as a function of the ratio of reactant concentration allows the determination of both the stoichiometric endpoint and rate constant of the reaction. However, it is necessary to include axial diffusion in the model in order to accurately measure rate constants by this method. Although the above results are interesting when applied to simple bimolecular reactions, we have by both analytic and numerical methods shown that similar results are obtained for more complicated mechanisms. Mechanisms consisting of reactions in series and in parallel have been considered.

This theoretical work has a number of applications to our studies of fluorine supported combustion. It provides an explanation of very "peaked" downstream emission that we previously have reported in studies of the F + H₂⁴ and F + CH₃OH⁵ reactions. We have been using the method with the F + NO and F₂ + NO reactions to verify the validity of our calculations. The experiment is most simply arranged in a flow reactor, with a chemiluminescence detector to measure the reaction rate positioned considerably downstream of the reagent mixing point. Persistent luminescence in the F + NO reaction provides a useful endpoint indicator for the measurement of fluorine atom concentrations in kinetic systems.

References

1. J. Peeters, J. F. Lambert, P. Hertoghe and A. Van Tiggelen, Thirteenth Symposium (International) on Combustion, p. 321 (1971)
2. D. Jones and M. Kaufman, Comb. Flame, 67, 217 (1987)
3. M. Kaufman, technical report, AFOSR 84-0196, Oct. 26, 1987
4. P. S. Ganguli, B. L. Hertzler and M. Kaufman, Chem. Phys. Lett., 37, 319 (1976)
5. D. J. Bogan, M. Kaufman, W. A. Sanders, C. W. Hand and H.-t Wang, Proc. of Eastern Section of Combustion Institute, Dec. 1982

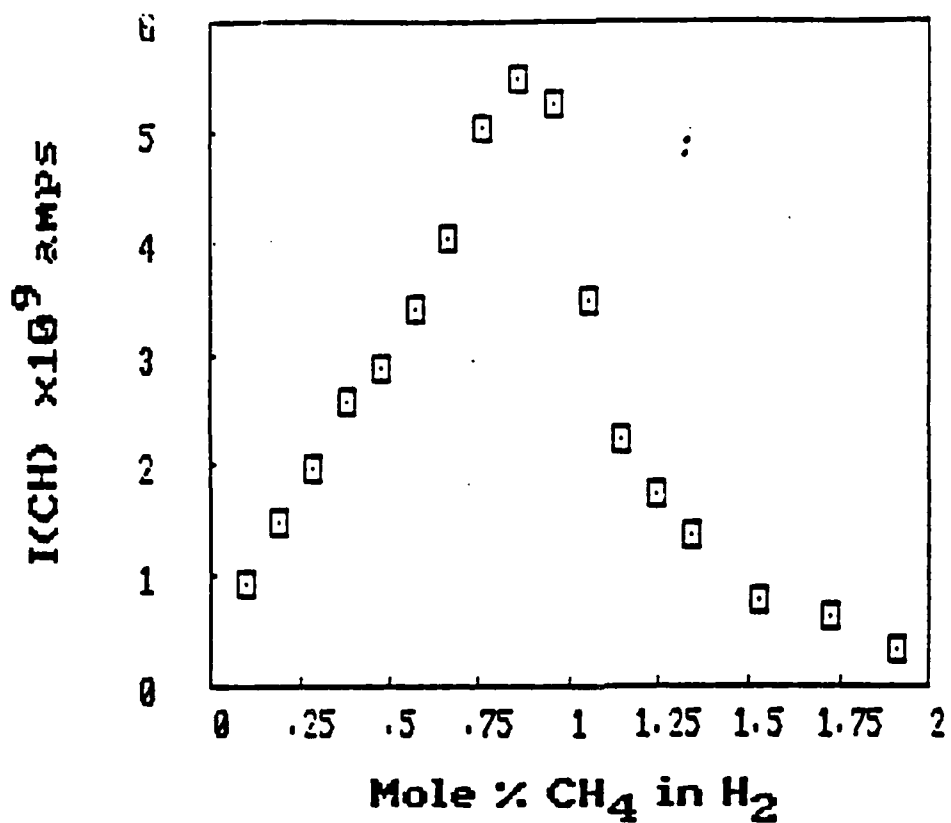


Figure 1. Intensity of CH(A state) emission with small additions of CH₄ to an near-stoichiometric H₂-F₂ flame

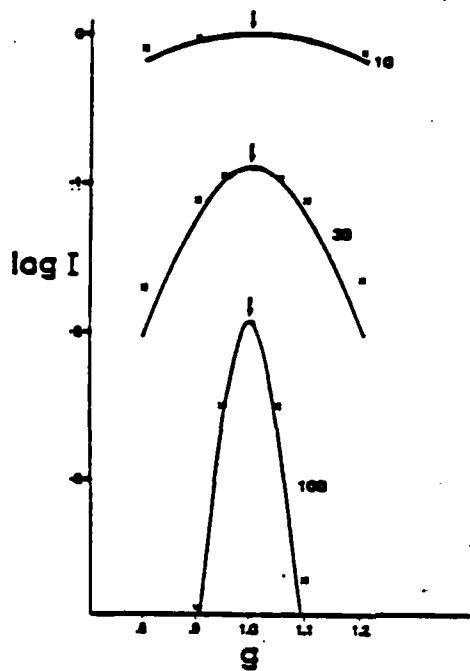


Figure 2. Chemiluminescent intensity as a function of stoichiometric ratio for different values of kt. Plug flow approx. Curves for elementary reaction. x, 2-step reaction

PHYSICS OF NOZZLE AND PLUME FLOW

Task Area 2308M2 - Plume Technology

David P. Weaver
Air Force Astronautics Laboratory
and
David H. Campbell
University of Dayton Research Institute
Edwards AFB, California 93523-5000

Summary: The objective of this research program is to understand the fundamental mechanisms controlling collisional energy exchanges in gas expansion flows that produce scattering of gas species upstream of a nozzle exit plane into the "backflow" region of spacecraft rocket nozzles and influence high altitude infrared and ultraviolet radiation produced by plume-atmospheric interactions.

Discussion: At present, no vacuum plume expansion flow model exists that accurately predicts observed backflow mass flux levels. Additionally, our understanding of the collisional processes (and specific chemical kinetic mechanisms) producing both infrared and ultraviolet radiation in the interaction of atmospheric and plume species at high altitude is almost nonexistent. As an example, no experimentally verified gas collisional model exists that can account for many of the important physical mechanisms that occur in plume gas flow, such as non-equilibrium gas dynamics or the influence of condensation. In fact, Monte-Carlo models for vacuum plume flows, coupled to Method-of-Characteristic technique predictions of the internal nozzle boundary layer structure, have been shown to miss experimentally measured backflow mass flux levels for pure, non-reacting gas flows by an order of magnitude or more. Clearly, a more fundamental knowledge of the physics and chemistry influencing nozzle flow must be developed before more accurate predictions for efficient design of spacecraft and their thrusters can be performed.

The shape of the nozzle lip may play an important role in determining the flux into the backflow and subsequently into the mixing region where plume species and atmospheric constituents interact. Using the Direct Simulation Monte Carlo Technique (DSMC) of G. A. Bird, Hueser, et al. (1) studied the detailed flow field around the nozzle lip for conditions simulating the IUS motor at 282 km altitude. They used a finite size nozzle lip shape, which was found to have a significant effect on the local flow field, but they used only one shape for

one set of initial flow conditions. Using the same DSMC technique, a detailed analysis of the effects of different nozzle lip thicknesses and shapes on the flow field around the lip and into the backflow region has been accomplished. Some of the results are shown in Figure 1. Shown in the figure is the total flux into the backflow region out to a radial distance of 8 mm from the outer wall of a 2 cm long tube flowing argon into vacuum for several tube lip shapes. The stagnation condition upstream of the tube entrance are $T=300$ K and $P=1$ kPa, and the Monte Carlo starting conditions at the tube entrance were obtained using a finite difference flow code calculation, and set to a uniform stream with a velocity of 240 m/sec. The reduction in backflow flux due to increased rarefaction and increased forward deflection of the flow as the wall thickness is increased and the marked influence of nozzle lip shape is apparent.

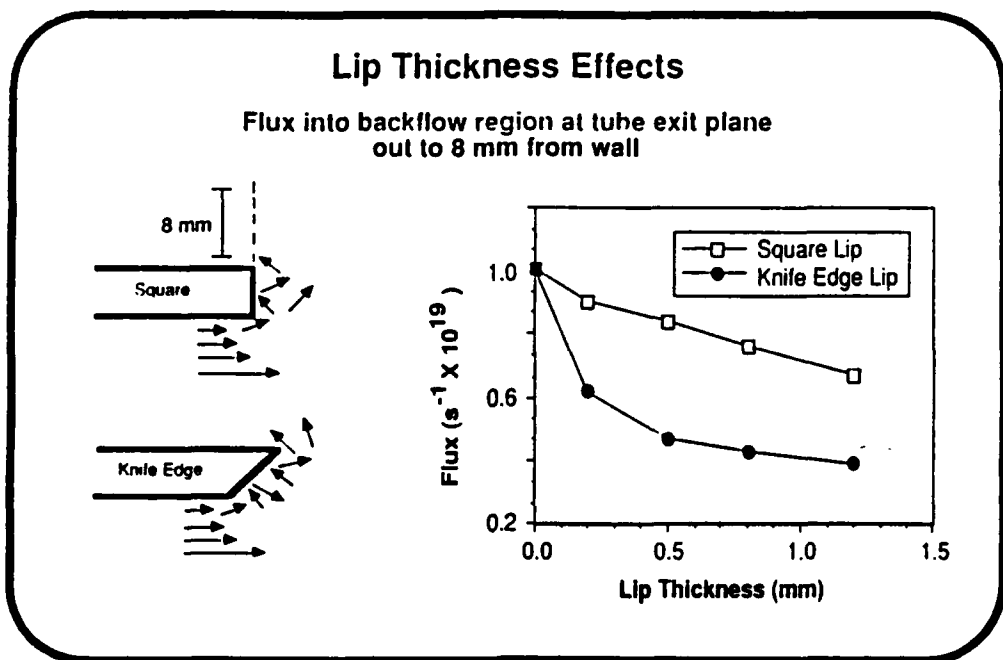
Experimentally, a sonic orifice/nozzle source is installed on a x-y-z translational table within a environmental chamber, Figure 2. The chamber is capable of supplying conventional and cryogenic pumping, including both liquid nitrogen and gaseous helium. Laser-based and electron beam diagnostic techniques are available to provide a spatial map of the molecular number density, rotational population distribution, and vibrational population distribution for molecules in the vacuum expansion near the source exit plane.

Additional experimental investigations of the chemical kinetic mechanisms for ultraviolet radiation production in flames of hydrazine and methylhydrazine with oxygen, nitric oxide, and nitrogen tetroxide in a low pressure diffusion burner operating between 0.1 and 1 atmospheres are underway. Figure 3 details some of the experimental approach for this part of the program.

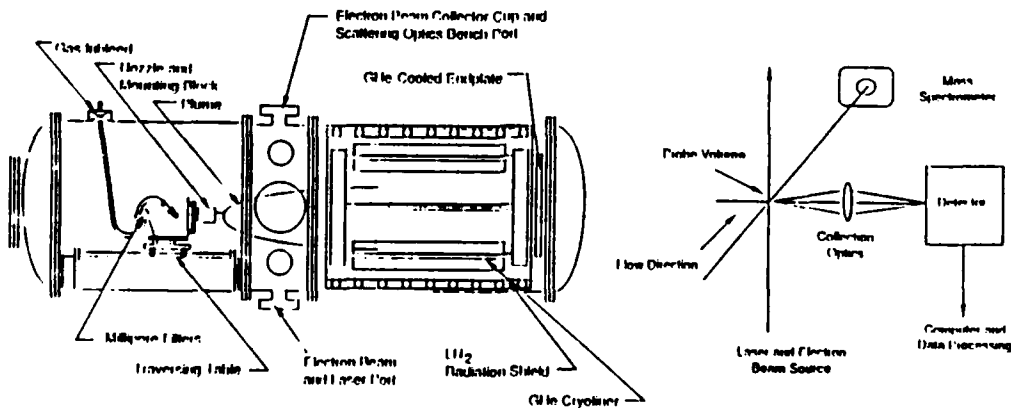
In addition to an accurate prediction of the plume flow field, an understanding of the collisional energy transfer mechanisms occurring in the plume-air interaction region is also required. In this part of the study, a stream of 5-25 eV oxygen atoms will be interacted with a molecular supersonic jet expansion to simulate processes occurring in high altitude plumes. Measurements of the vibrational populational distributions of the molecular collisional partners in the interaction zone of the two flows is made with laser and electron beam techniques. Time-resolved data is utilized to acquire information on the collisional and post-collisional processes which populate the specific vibrational levels from which subsequent UV and IR radiation originates. The atomic oxygen source employed uses the beam neutralization technique initiated by Mahadevan and Herr at The Aerospace Corporation (and developed further by Muntz at USC) but with significantly enhanced particle fluences. The beam neutralizer is a ring jet neutralizer and the ion source is a plasma discharge source as shown in Figure 4.

References

1. Hueser, J. E., L. T. Melfi, G. A. Bird, and F. J. Brock, "Rocket Nozzle Lip Flow by Direct Simulation Monte Carlo Method," AIAA Paper 85-0995 (June 1985).

**FIGURE 1**

Physics of Nozzle and Plume Flow Experimental Approach

**High Altitude Space Simulation**

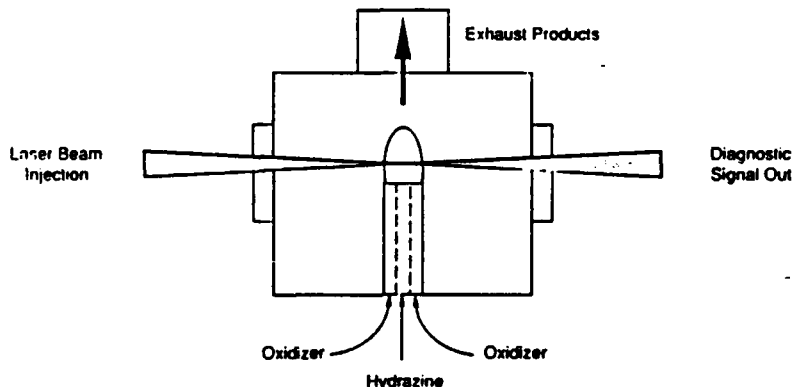
- Liquid Nitrogen and Gaseous Helium Cryogenic Pumping - Background Pressures to 10^{-6} Torr
- Electron Beam, Laser Scattering, and Mass Spectrometer Diagnostics - N(i), T(i), V(i)
- X - Y - Z Translation Mount for Source Flow - Spatial Map of Flow

FIGURE 2

UV Signatures in Hydrazine Flames - Approach

Experimental Approach

- Construct Model of Hydrazine Flame in the Laboratory
- Obtain Complete UV Signatures as a Function of Altitude (Pressure) and Reactants



Comparison With Experimental Results

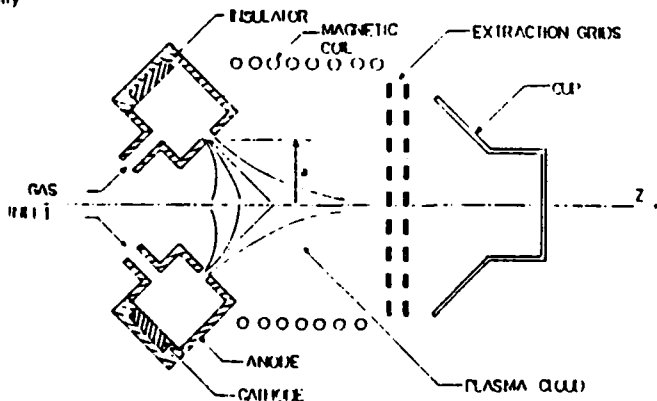
- Hydrazine Flame Model (22 Species, 151 Reactions)
- Perform Sensitivity Analysis on Reaction Mechanism
- Identify Key Chemical Kinetic Pathways

FIGURE 3

Atomic Oxygen Source

Source for High Speed Neutral Oxygen Atoms

- Energetic Source Beam : 5 - 25 eV
- Direct Excitation by Impact with O Atoms
- Secondary Collisional Processes in Transitional Flow
- Flame Chemistry



Source Characteristics

- Very Simple Design - Only Gas Pressure and Power Must be Varied for Optimizing Beam Performance
- Oxygen Ion Density Observed - $8 \times 10^{11} \text{ cm}^{-3}$; Degree of Ionization - 3%
- Source is Omnivorous - Both Nitrogen and Oxygen Can be Used

FIGURE 4

OVERVIEW OF COMBUSTION STABILITY EVALUATION METHODS**R. S. BROWN****UNITED TECHNOLOGIES / CHEMICAL SYSTEMS DIVISION
SAN JOSE, CA.****ABSTRACT**

Pressure oscillations have caused significant operations problems in solid propellant rocket motors for many years. These problems include excessive chamber pressures leading to case failures, excessive vibration levels on the motor case leading to failures of attached components, and thrust oscillations producing excessive loads on system components. Solving these problems has proved to be an expensive and time consuming process which have had substantial negative impacts on major motor development programs. Considerable effort has been directed to investigating the causes of these problems and to developing methods for anticipating and correcting these motor difficulties.

The combustion stability characteristics of a large number of motors have been predicted using the Standard Stability Prediction Program. Comparisons with actual motor behavior have demonstrated good agreement in some cases and the predictive methods have provided useful guidelines for reducing oscillatory pressures in motors. Unfortunately, a significant number of inconsistencies between predicted and observed stability have also found.

Analysis of these inconsistencies cast doubt on several aspects of the stability prediction process. Specifically, the results of these comparisons have been divided into three categories. The characteristics which can be predicted with reasonable confidence include the characteristic frequencies, the pressure coupled energy sources (using laboratory data for the combustion response), and the nozzle damping. Poorly characterized contributions include velocity coupling, flow turning, and energy from combustion distributed throughout the motor chamber. The accuracy of some contributions is difficult to determine, or is in transition. These contributions include the mean flow, particle damping, and periodic vortex shedding. Comments on each of these contributions are included in the paper. The principal conclusion is that the mean and oscillatory flow related processes are involved in many of the poorly characterized stability processes. Therefore significant improvements in the accuracy of motor stability predictions requires continuing research into these aspects of motor behavior.

Recent research has indicated that these conclusions are well founded and has also provided significant insight into methods for improving these prediction models. Studies on the mean flow field environment have shown that interpreting motor behavior by analogy to growing and/or fully developed turbulent boundary layers is not valid. The evolution of gas from the propellant surface causes the flow to be dominated by pressure forces and not by viscous

forces. The concept of a boundary layer is not valid for this class of flows and turbulence is important only towards the aft-end of the motor. When acoustic waves are imposed on these internal flows, the oscillatory heat transfer and vorticity show significant differences from the velocity coupling and flow turning models used in the stability prediction methods. This paper summarizes some of motor experience, motor stability prediction results, and research findings supporting these conclusions.

PARTICLE COMBUSTION IN SOLID PROPELLANTS

AFOSR Contract 83-0157

Principal Investigator: Merrill W. Beckstead

Brigham Young University, Provo, Utah 84602

APPROACH

Solid particles are commonly added to low smoke and smokeless propellants as acoustic suppressants. Suppressants work by one or more of three mechanisms: (1) energy loss due to viscous dissipation due to drag forces, (2) modification of the propellant combustion response function, or (3) energy interchange due to distributed combustion. The third mechanism considered is due to the effect of a particle burning as it traverses a relatively large portion of the system. As it does so, the interchange of energy between the burning particle and the acoustic environment can result in either a driving or damping contribution to the acoustics of the system. This third mechanism is the primary area of study of the current contract.

The principle objective of this work is to identify and develop an understanding of the mechanisms whereby acoustic suppressants modify an acoustic wave. Figure 1 is a graphic illustration of the approach. The experimental basis for the technical approach of this study is a Rijke burner which is a gas burner that generates acoustic oscillations. The burner has been modified to include a butterfly valve to control (stop and start) the oscillations. The unique advantage of this approach allows separation of the three mechanisms mentioned above by testing an additive independent of the propellant burning surface. Other advantages include avoiding use of solid propellants, and allowing for independent control of frequency, O/F ratio, temperature and particle addition.

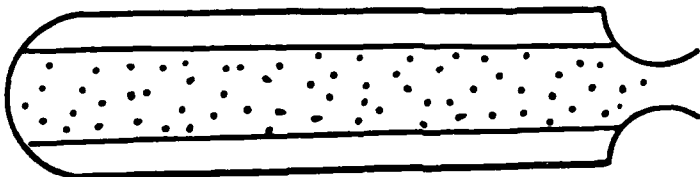
ACCOMPLISHMENTS

During the past year two major modifications have been made to the Rijke burner to facilitate obtaining more reproducible data. Digital mass flow meters have been installed on all the gas feed lines to improve the flow rate control, and a water bath was installed to control the temperature of the cooling water. These modifications have improved the reproducibility and quantitative nature of the data.

Last year acoustic growth rate data were obtained varying the mass flow rate, the oxidizer/fuel ratio, and the relative amount of nitrogen. In all cases, the growth rate increased as the energy release rate (or temperature) increased as shown in the accompanying figure. This year data have been obtained at constant temperature, varying the burner length (the frequency). The accompanying figure shows the growth rate changing as the frequency changes from a first mode to a second mode oscillation. The data are also compared to the previously developed model showing a reasonable degree of agreement between the data and the model. Future testing will involve different types of particles, typical of those used in solid propellants.

PARTICLE COMBUSTION IN SOLID PROPELLANTS

How Do Suppressants Work in Solid Propellant Rocket Motors?



Mechanisms Acoustic Suppressants:

- Viscous dissipation due to drag forces
- Modification of propellant response function
- Effect of distributed combustion

CURRENT PROGRAM:

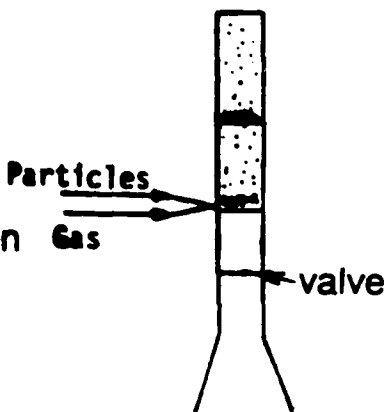
- Separate Effects of Different Mechanisms Using Unique Experiments

- The Modified Rijke burner

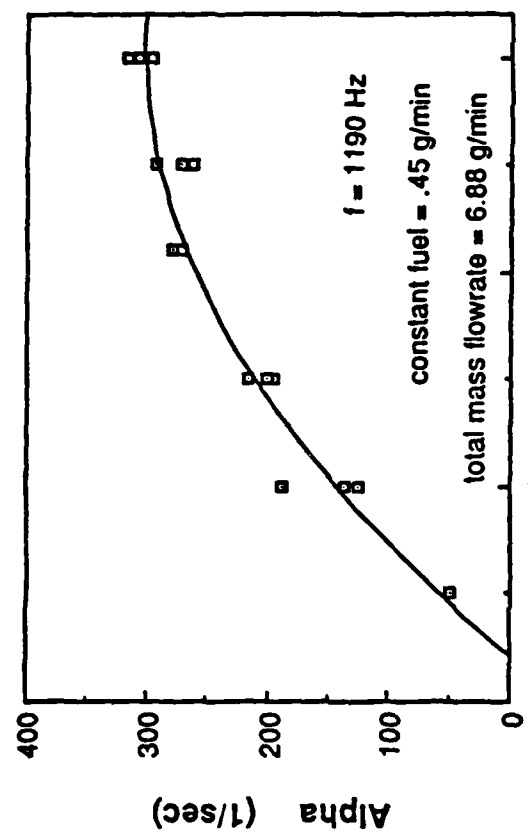
- Use gas (eliminate solid propellant)
- Evaluate acoustics w/o particles
- Can feed particles independently
- Vary particle type, size and concentration
- Evaluate reactive or inert particles
- Use paddle to control acoustic growth

- Results

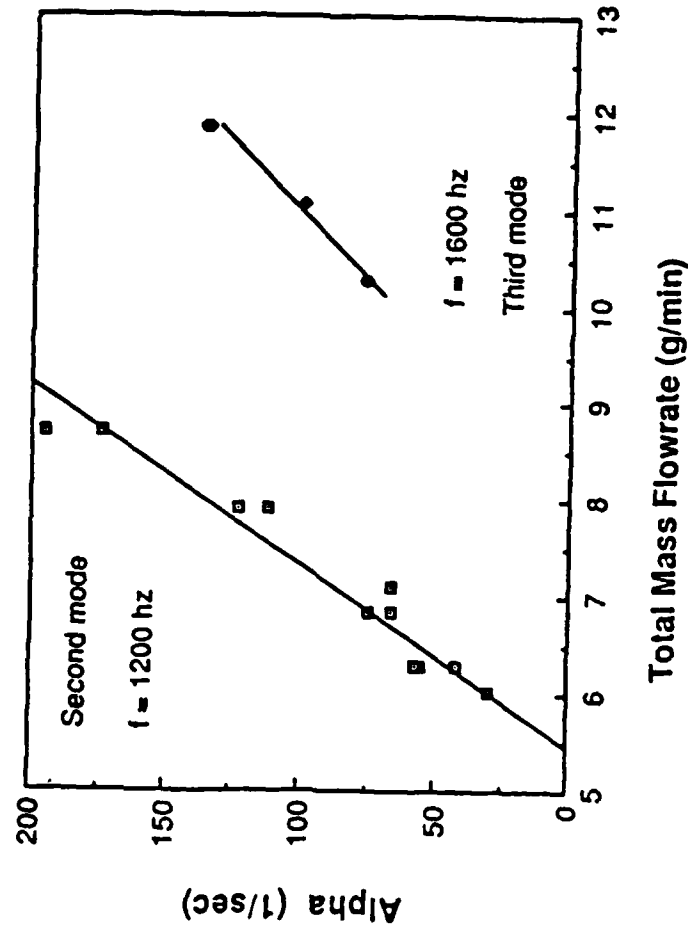
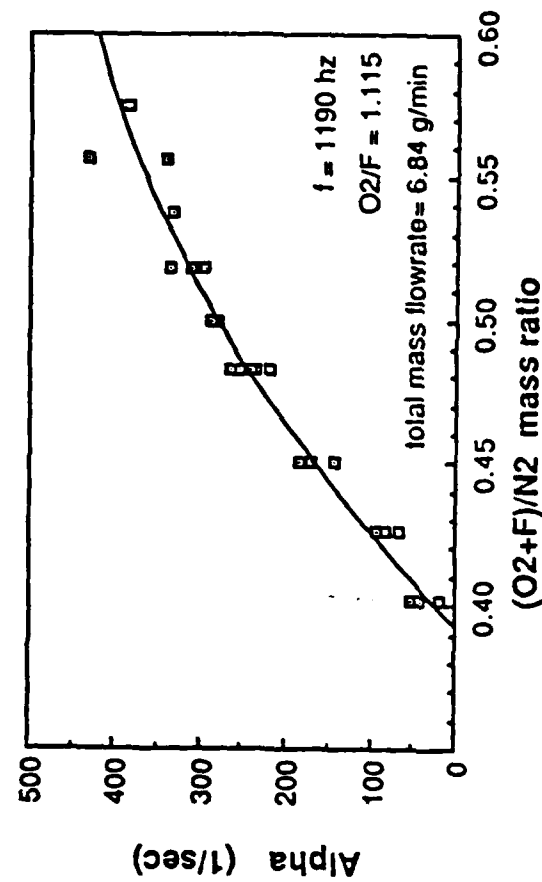
- Theoretical model for Rijke burner with variable properties
- Modify burner for quantitative reproducible data
- Install digital data acquisition system
- Control acoustic growth with sound absorption
- Characterize Rijke burner for varying test conditions
- Compare theory with experiment



ACOUSTIC GROWTH RATE DATA FROM THE RIJKE BURNER

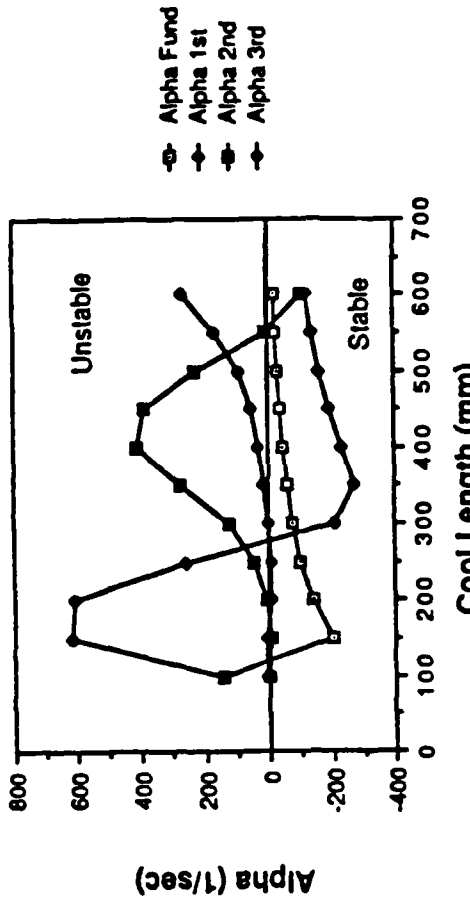


Stoichiometric O/F at Constant Total Mass

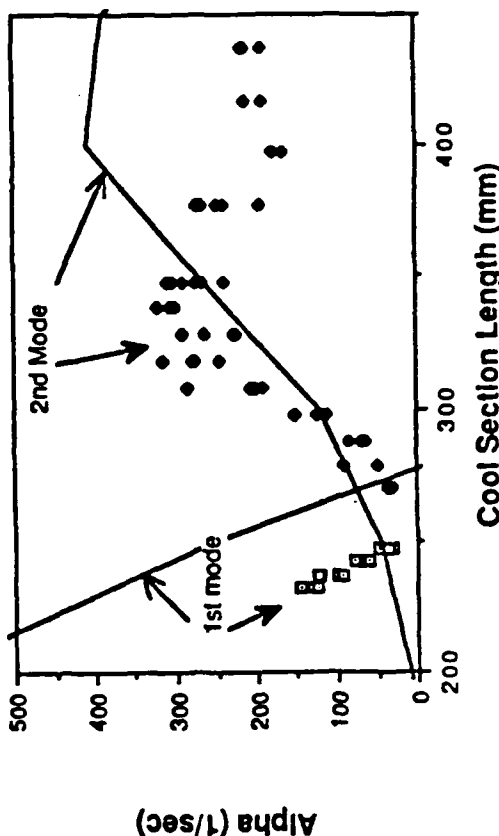


COMPARISON OF THEORY AND EXPERIMENT FOR RIJKE BURNER

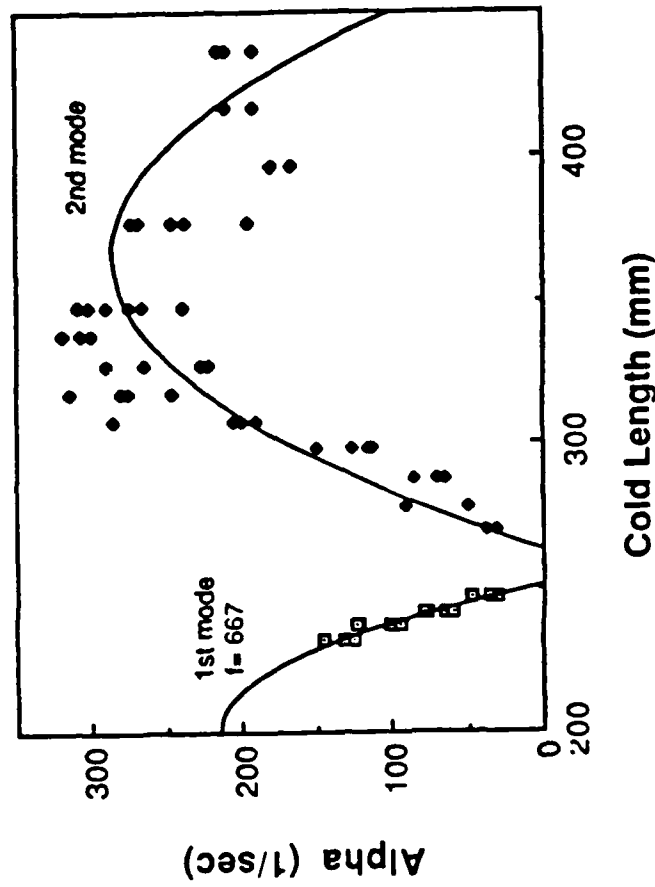
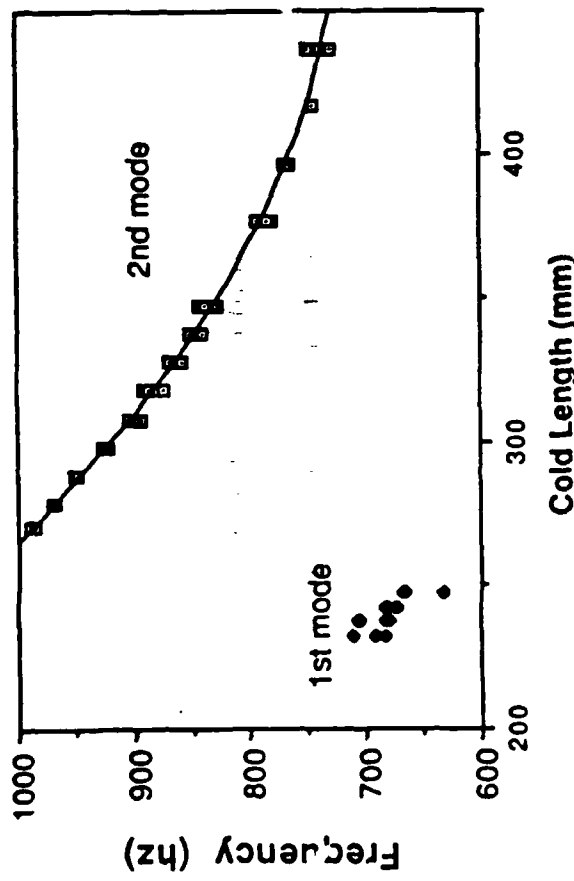
88



Predicted acoustic growth rates for the first 4 modes
vs cool section length.



Comparison of the calculated growth rates (lines)
with the experimental values (points) for the variable
cool section data set as a function of cool section
length.



EXPERIMENTAL DATA

ENERGY EXCHANGE MECHANISMS BETWEEN THE MEAN AND ACOUSTIC FIELDS IN SOLID ROCKET COMBUSTION CHAMBERS

Joseph D. Baum

Laboratory for Computational Physics and Fluid Dynamics

Naval Research Laboratory/ Code 4410

Washington, D.C. 20375-5000

The objective of this research effort is to enhance our understanding of the physical mechanisms by which energy is exchanged between the mean and the acoustic flow fields in resonant combustion chambers (in particular, solid rocket motors). As part of this investigation, research in the past year was directed at the numerical investigation of upstream wave propagation in a tube in which the mean flow was injected through the lateral boundary, simulating the flow in a solid propellant rocket motor. In addition, the dependence of these energy exchange mechanisms on the blowing rate through the lateral boundary and the frequency of the propagating wave, were also investigated.

The time-dependent compressible Navier-Stokes equations were solved utilizing a non-iterative Linearized Block Implicit scheme. Acoustic upstream traveling waves were initiated at the exit plane by perturbing the boundary conditions. These waves initially traversed the hard wall zone of the tube and then the injection zone. Results are compared to two previous studies,^{1,2} in which acoustic waves propagated downstream in the tube and downstream in a hard walled tube with a coexisting fully developed pipe flow. More details can be found in Ref. 3.

Acoustic refraction processes were strongly enhanced by the upstream propagation, for both acoustic wave propagation with and without wall injection. In either case, the radial distribution of the rms acoustic pressure was almost doubled for upstream wave propagation compared to the downstream wave propagation (Fig 1).

Complex wave evolution phenomena were demonstrated as the wave propagated upstream near the injection surface. When the axial acoustic velocity changed from negative to positive, the axial acoustic velocity near the injection wall led the axial acoustic velocity outside by approximately 90°. In comparison, the transition from a positive to a negative velocity near the injecting wall led the velocity transition outside the boundary layer by 45°. The phase lead for the downstream propagation was 60-70° when the acoustic velocity changed from positive to negative, and 35-50° when the wave transitioned from negative to positive. The axial acoustic velocity and acoustic pressure outside the acoustic boundary layer were 180° out of phase. Since the acoustic pressure inside the acoustic boundary layer suffered very little phase change, the axial acoustic velocity near the injection surface led the acoustic pressure by 35-90°, depending on the direction of wave propagation and the exact wave transition. The phase relation between the acoustic pressure and axial acoustic velocity has an important effect on the driving or damping of acoustic oscillations by the burning propellant, and thus on our ability to model solid propellant transient burn rate.

Acoustic boundary layer thickness (rms) was reduced by approximately 10% for wave

propagation upstream; 290 μm for upstream wave propagation over the injection wall compared with 330 μm for downstream propagation, and 160 μm for upstream propagation over the hard wall vs 180 μm for downstream propagation.

Acoustic streaming phenomena observed for the upstream propagation had significantly larger magnitudes than for the downstream propagation, resulting in larger mean acoustic pressure and velocity shifts. Excitation of mean flow by the acoustic wave was observed in three zones (as shown in Fig 2): upstream directed mean motion was excited over a zone from the centerline to about 1500 μm from the injection surface and inside the acoustic boundary layer; downstream directed mean flow was excited in between these rings. These streaming effects also resulted in the excitation of a mean vortex motion, with the maximum at the location of the maximum radial gradient of the excited mean velocity (Fig 3)

Larger streaming effects for upstream wave propagation near the injection surface resulted in increased distortion of the acoustic waveform. The axial velocity overshoots at the edge of the acoustic boundary layer had larger (absolute) minimum values than maximum values, with the wave minima located much closer to the injection surface. Thus, both vorticity and dissipation values had higher values for the wave minima than for the maxima. Higher dissipation and vorticity values were obtained for wave propagation upstream than downstream over the injection surface. Dissipation function calculations demonstrated that while the maximum values obtained for upstream wave propagation over the hard wall were higher than for wave propagation over the injection zone, the area over which they were observed was very small. Thus, total dissipation was higher for wave propagation over the injection zone. Time averaged dissipation for upstream propagation over the injection zone was approximately 10% higher than for the downstream propagating wave.

Finally, the time averaged axial energy flux values were integrated over radial planes to calculate axial dissipation of acoustic energy as the wave propagated in the tube. The results demonstrated higher energy dissipation rates for wave propagation over an injection zone than over a hard wall, and increased dissipation rates for upstream wave propagation relative to downstream propagation (Fig 4). Increased dissipation rates for upstream propagation resulted from enhanced acoustic energy dissipation due to viscous processes, and enhanced acoustic streaming effects. Similarly, increased energy dissipation for wave propagation over the injection zone resulted due to enhanced streaming effects within and near the acoustic boundary layer and within the axial velocity dc shift zone, and increased mechanical dissipation within the boundary layer.

REFERENCES

1. Baum, J.D. and Levine, J.N., "Numerical Study of Acoustic Refraction Phenomenon," AIAA J., Vol 25, No 12, Dec 1987, pp 1577-1586.
2. Baum J.D., "Acoustic Energy Exchange Through Flow Turning," AIAA Preprint 87-0217, Presented at the AIAA 25th Aerospace Sciences Meeting, Reno NV, Jan 12-15, 1987.
3. Baum J.D., "Investigation of Flow Turning Phenomenon; Effect of Upstream and Down-

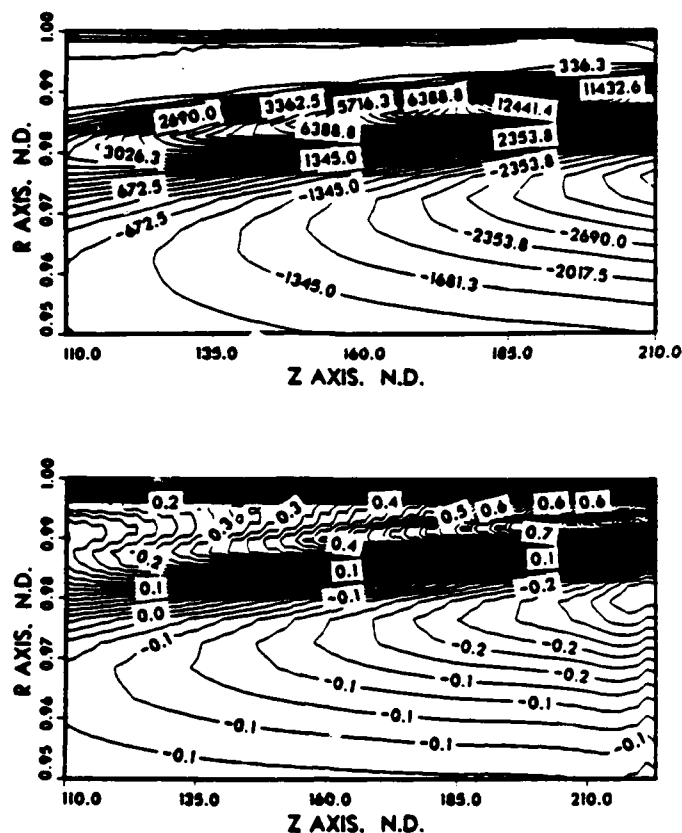


Fig 3. Comparison of Time Averaged Vorticity and Second Radial Derivative of the Steady Axial Velocity.

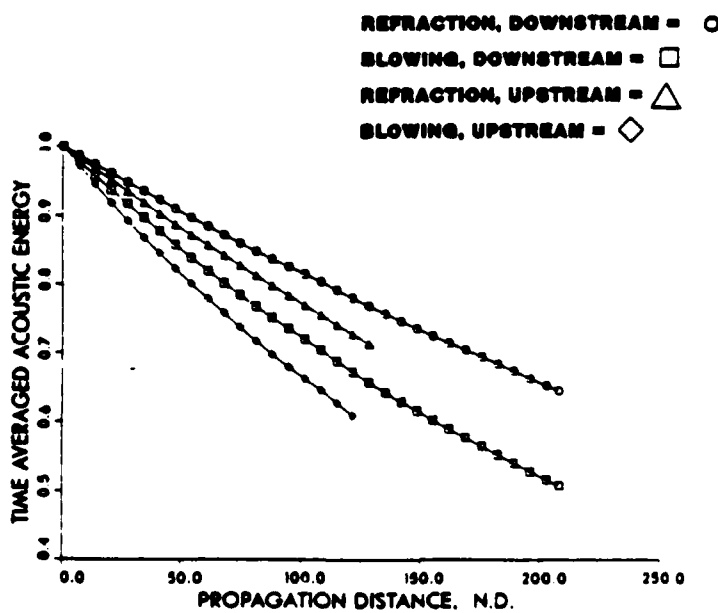


Fig 4. Comparison of the Axial Distribution of Time Averaged Acoustic Energy Flux.

stream Propagation," AIAA Preprint 88-0544, Presented at the AIAA 26th Aerospace Sciences Meeting, Reno NV, Jan 11-14, 1988.

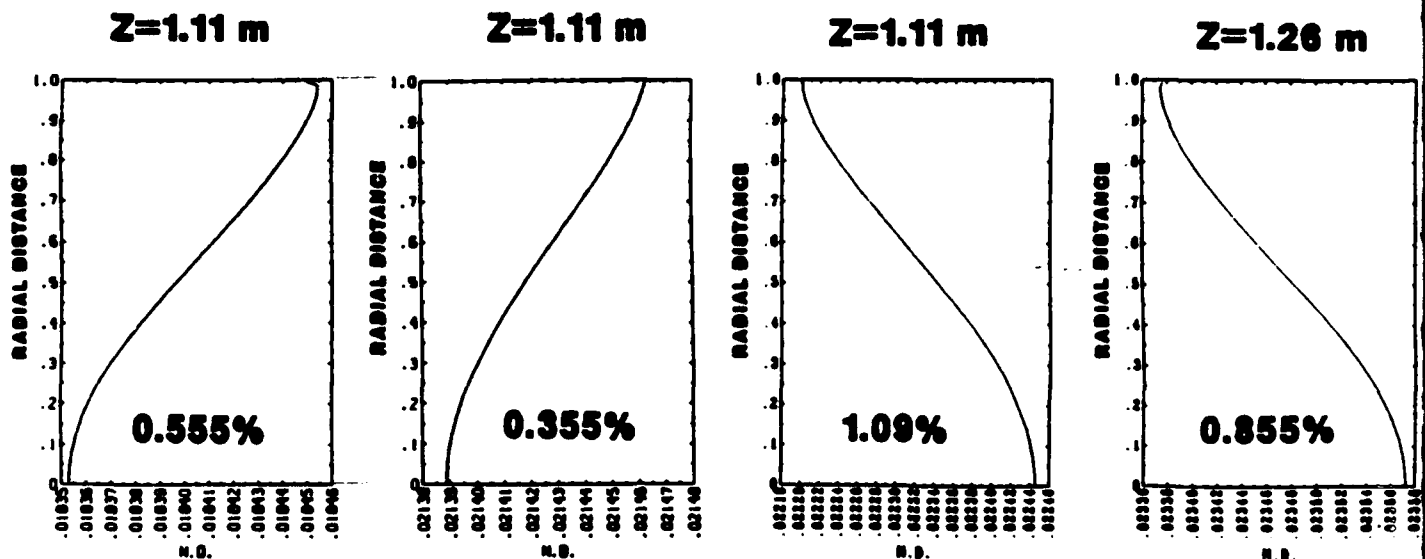


Fig 1. Radial Distribution of rms Acoustic Pressure: a) Flow Turning, Downstream, Z=1.11 m; b) Refraction, Downstream, Z=1.11 m; c) Flow Turning, Upstream, Z=1.11 m; d) Refraction, Upstream, Z=1.28 m;

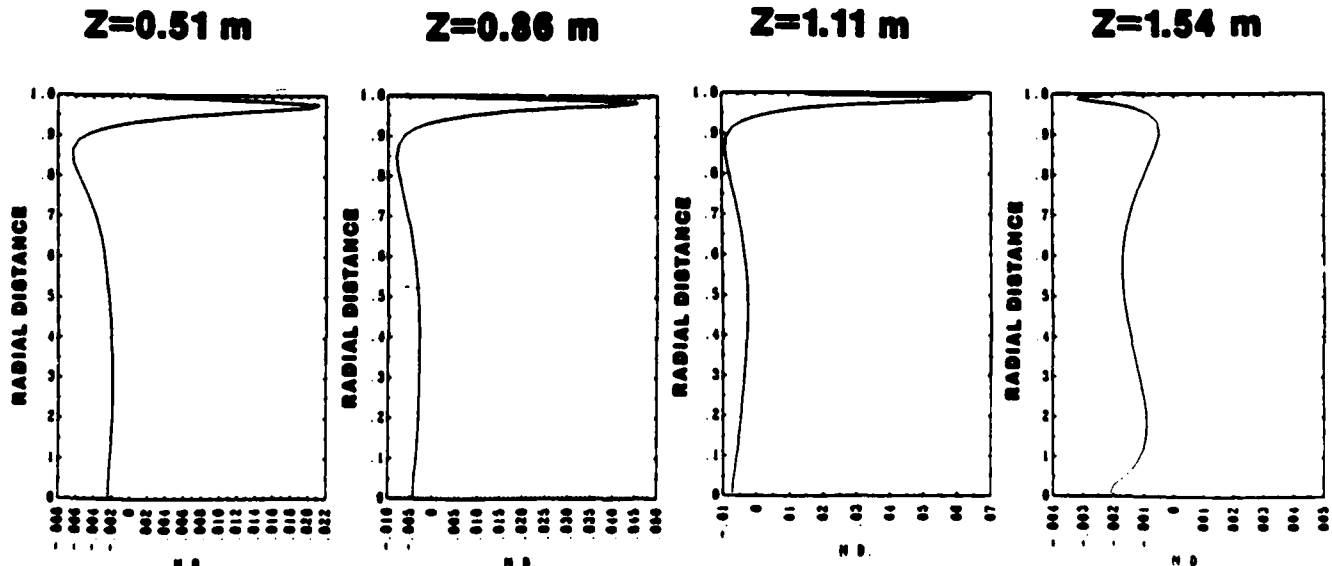


Fig 2. Radial Distribution of Time Averaged Axial Perturbation Velocity: a) Z=0.51 m; b) Z=0.86 m; c) Z=1.11 m; d) Z=1.64 m.

FLAME - ACOUSTIC WAVE INTERACTION DURING AXIAL
SOLID ROCKET INSTABILITIES

(AFOSR Grant/Contract No. AFOSR-84-0082)

Principal Investigators: B. T. Zinn, B. R. Daniel and U. G. Hegde

School of Aerospace Engineering
Georgia Institute of Technology
Atlanta, Georgia 30332

SUMMARY/OVERVIEW:

The objective of this study is to develop an understanding of the fundamental mechanisms through which flames stabilized on a side wall of a duct drive axial acoustic oscillations; a problem which has many similarities to the driving of axial instabilities in solid rockets. In the first phase of the program the response of a premixed flame stabilized on the side wall of a rectangular duct to imposed axial acoustic oscillations has been investigated theoretically and experimentally. These studies show that the flame driving is equivalent to that provided by a combination of a monopole and a dipole acoustic sources. This behavior is caused by the flame interaction with the acoustic field which produces flame oscillations normal to the duct side wall. In an actual rocket motor such oscillations will produce an unsteady heat transfer to the propellant surface. This, in turn, will result in an unsteady regression rate of the propellant which may sustain the instability. In the second phase of this program, currently underway, the response of diffusion flames stabilized on the duct side wall to axial acoustic oscillations is being studied. These investigations are expected to reveal the contributions of diffusion and mixing processes in the flame region to axial instabilities.

TECHNICAL DISCUSSION:

Solid propellant flames are extremely complex and they involve unsteady multidimensional chemical reactions, and heat, momentum and mass transfer processes which occur within an extremely thin region next to the solid-gas interface. The coupling between the unsteady combustion in this region, at the lateral boundaries of the rocket cavity, and the acoustic oscillations within the cavity drives the instabilities. The difficulties associated with performing direct diagnostics within the small dimensions of actual solid propellant flames necessitates the study of less complex flame configurations which preserve many important features of the solid propellant instability problem. Two such configurations, investigated under this program, are shown schematically in Figures 1 and 2 which depict, respectively, premixed and diffusion flames stabilized on a side wall of an acoustically driven rectangular duct.

In the first phase of the program the response of the sidewall stabilized premixed flame to an imposed acoustic field has been investigated to determine the mechanisms by which such flames drive axial oscillations.

Experimental efforts included high speed cinematography, optical CH radiation and temperature measurements, acoustic pressure measurements and LDV velocity measurements. These measurement systems were utilized to determine the time variations of the flame shapes and displacements, heat release rates and velocity field under a variety of excitation conditions. In addition, the predictions of a model of the investigated flame, developed earlier under the program¹, were compared with the measured data.

The measurements revealed that the investigated premixed flame position relative to the burner surface oscillates with the frequency of the excited acoustic wave. This, in turn, produces a spatial flame structure which exhibits a large and a small heat release regions upstream and downstream of the mean flame location, respectively². Measured and predicted spatial heat release rate distributions for a typical case are shown in Figures 3 and 4, respectively. Figure 3 shows that the heat release rate peaks on either side of the steady flame location are approximately 180° out of phase with each other. The space and time variations of the heat release rate describe the acoustic driving characteristics of the flame. Therefore, if the upstream peak is considered as the sum of two parts, one of magnitude equal to that of the downstream peak and the other equal to the difference between the two peaks, then the flame may be viewed as a combination of an acoustic dipole and an acoustic monopole. The acoustic dipole consists of the two equal magnitude upstream and downstream heat release rate peaks which oscillate out of phase and the monopole consists of the difference between the magnitudes of the two peaks. This newly uncovered mechanism is believed to play an important role in solid rocket instabilities where flame oscillations relative to the propellant surface undoubtedly occur. Such oscillations will result in an oscillatory surface regression rate capable of driving the instability.

In the second phase of this program, the interaction between the sidewall stabilized diffusion flames (Fig. 2) and axial acoustic waves is being investigated. These studies are expected to identify the contributions of diffusion and mixing processes in the flame region to axial instabilities. A theoretical model of the interaction has been formulated² and a computer program incorporating it is under development and testing. On the experimental side, a diffusion flame burner designed to simulate as many features as possible of actual solid propellant flames was fabricated and installed in the rectangular duct. High speed shadowgraphy and measurements of the oscillatory heat release rates from the developed diffusion flames have been carried out for several acoustic excitation conditions. Typical measured frequency dependence of the phase difference between the flame radiation and pressure oscillations at a pressure maximum for different frequencies in the range between 250 and 1000 Hz are presented in Fig. 5. A detailed analysis of these results is in progress.

References:

- 1) Hegde, U. G. and Zinn, B. T., "The Acoustic Boundary Layer in Porous Walled Ducts with a Reacting Flow", 21st Symposium (International) on Combustion, August 1986.
- 2) Zinn, B. T., Daniel, B. R. and Hegde U. G., "AFOSR Annual Technical Report on Grant No. AFOSR-84-0082", March 1988.

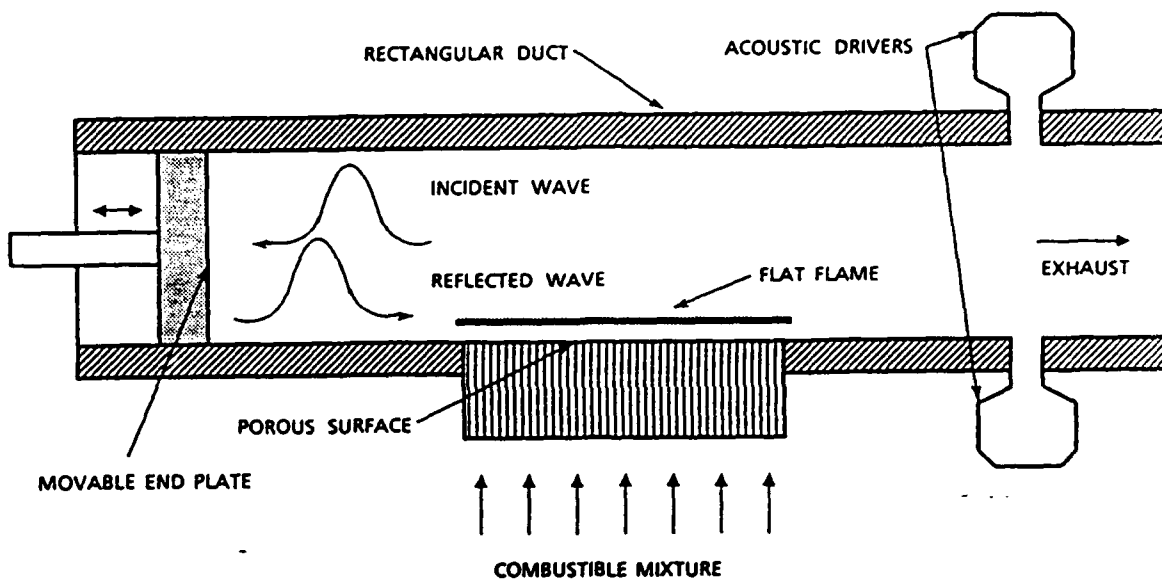


Fig. 1. A Schematic of the Experimental Setup Used to Investigate the Interaction between Gas Phase Premixed Flames and Longitudinal Acoustic Fields.

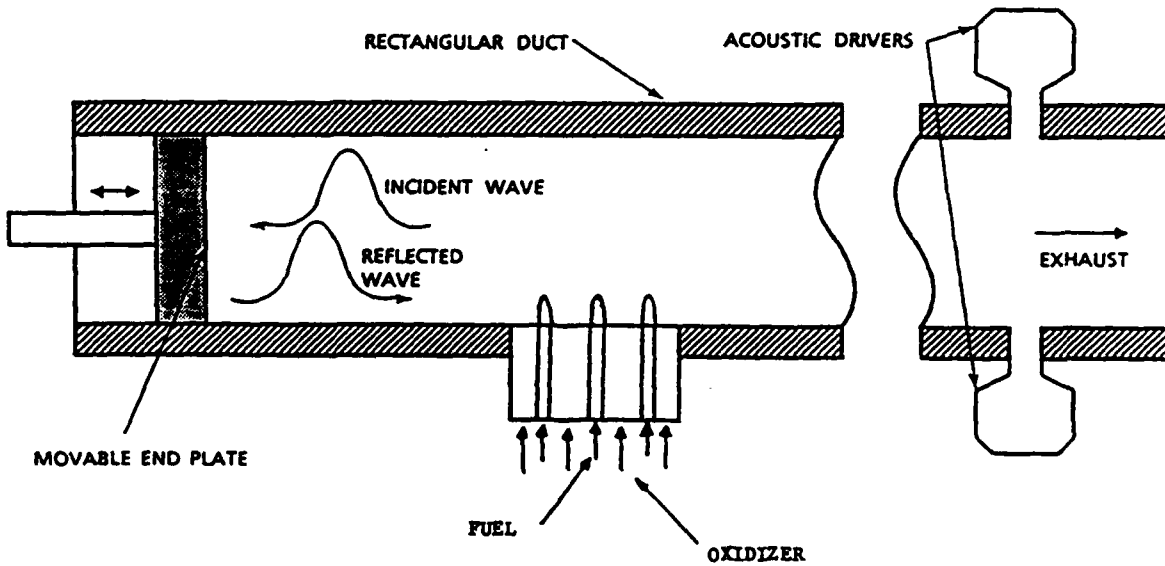


Fig. 2. A Schematic of the Experimental Setup Used to Investigate the Interaction between Gas Phase Diffusion Flames and Longitudinal Acoustic Fields.

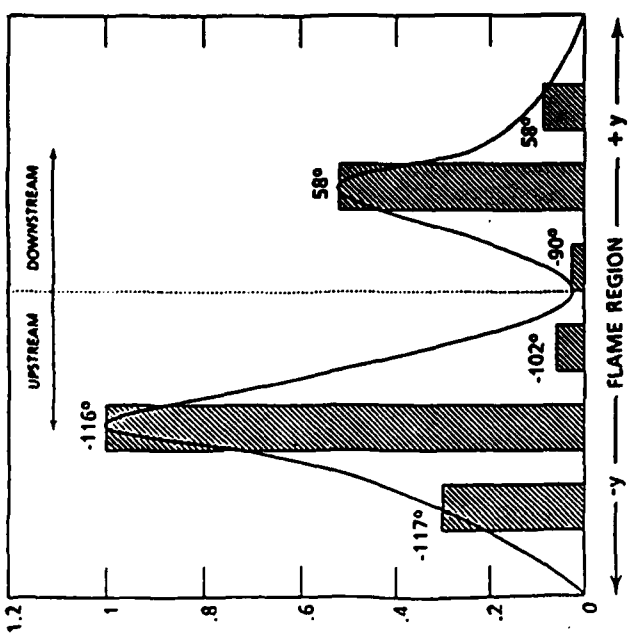


Fig. 3 Measured Distributions of the Magnitude and Phase of the Oscillatory Heat Release Rates Upstream and Downstream of the Investigated Steady Flame Location When Subjected to an 800 Hz Acoustic Oscillation.

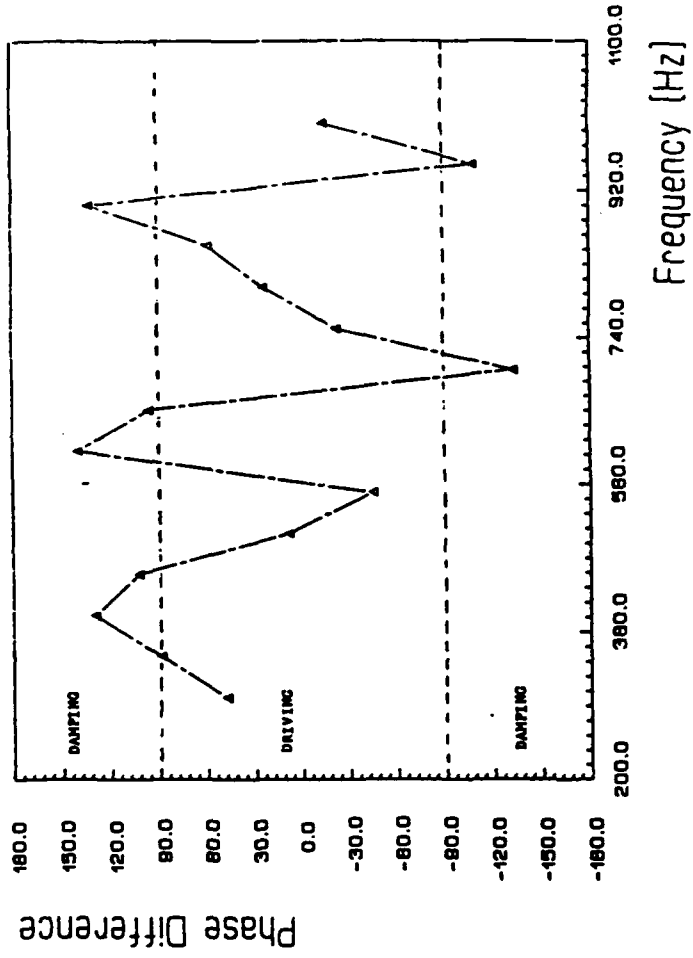
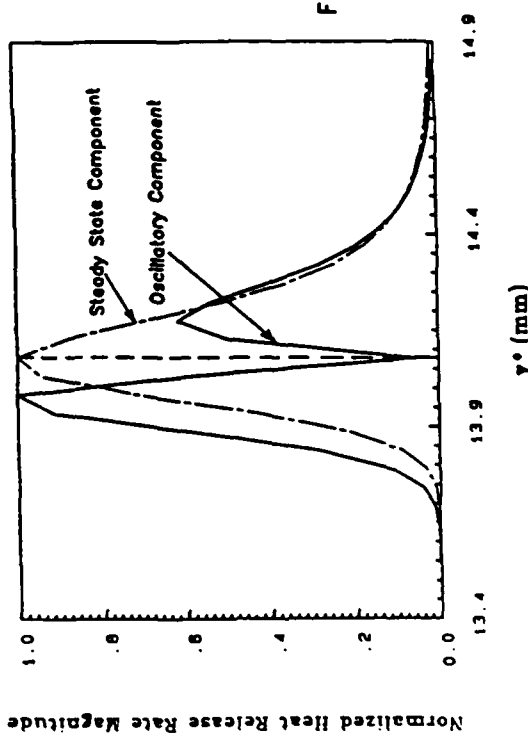


Fig. 5 Frequency Dependence of the Phase Difference Between the Diffusion Flame Radiation and Acoustic Pressure Oscillations Measured with the Flame at a Pressure Maximum. Frequencies at which the Flame Drives and Damps the Acoustic Oscillations have been Determined According to Rayleigh's Criterion.



SOLID FUEL COMBUSTION

(AFOSR Grant No. 85-0340)

Principal Investigator: J. S. T'ien
Other Professionals: S. T. Lee and N. Ait Messaoudene

Department of Mechanical and Aerospace Engineering
Case Western Reserve University
Cleveland, Ohio 44106

SUMMARY/OVERVIEW

The effects of gas-phase and surface radiation are being studied using a combustion model of a turbulent boundary layer adjacent to a solid fuel. Particular emphasis is placed upon the radiation from soots which are treated as a non-equilibrium species. In addition to those from soots, the absorption and radiation from fuel vapors are found to be important in determining the solid pyrolysis rate. This modeling work has been helpful in evaluating the relative importance of various mechanisms controlling solid fuel burning.

In a separate task, the soot distribution near the stagnation point induced by the thermophoretic motion is being investigated theoretically in a laminar flame. It has been found that Brownian diffusion, although small, becomes very important under certain conditions in the determination of the peak soot concentration level.

TECHNICAL DISCUSSION

Turbulent Boundary Layer Combustion Adjacent to a Solid Fuel

Introduction. The pyrolysis and combustion of solid fuel in a turbulent boundary layer are determined by the complex interaction of various transport and reaction processes. In order to access the relative importance of each component process, a comprehensive model has been established for a two-dimensional turbulent boundary layer. A low-Reynolds-number two-equation turbulence model [1] is used for flow transport. The treatment of turbulence and chemistry interaction follows the eddy-dissipation model of Magnussen et al. [2]. Radiative heat transfer is calculated by using a two-flux model. Since soot is an important radiation source in the gas phase, its concentration and distribution is important for radiation heat transfer prediction. Therefore, in the soot transport equation both the formation [3] and oxidation [4] terms are included in addition to the convective and diffusive contributions. Other contributors in gas-phase radiation and absorption, besides H_2O and CO_2 , include fuel vapors [5-7]. The solid fuel surface radiation, long known to be important, is also introduced.

Results and Discussion. Although rather simple expressions are given to the sub-model processes, the combined combustion model is rather complex. A careful evaluation and validation of the model prediction has to be made. Because the only existing experiment on solid fuel burning in turbulent flame with detailed measurements of radiative properties is in natural convection [8]. The comparison with experiments has been done mostly in this situation. The turbulent transport model was first tested in pure natural convection for a vertical heated plate. The results are in good agreement with the available

experimental data, and the model performance is just as good as those in Refs. 9 and 10.

The comparison with the vertical burning of a PMMA plate is shown in Fig. 1. All three theoretical curves contain surface radiation (a loss). Curve 3, with no gas-phase radiation, predicts a solid pyrolysis rate well below the experimental data. Curve 2, with radiation from soot and combustion products, improves the calculation, but still underpredicts. Curve 1, with the further addition of absorption/radiation from fuel vapor, passes through the data.

While the effect of soot radiation (from curve 3 to curve 2) is expected, the increase of solid burning rate with the introduction of fuel vapor absorption and radiation is somewhat of a surprise. We believe the interpretation is as follows. While the fuel vapor, being close to the solid surface, is a blocker of radiation from soot, it is also a blocker of radiative loss from the surface. Receiving radiation from both sides, the temperature of fuel vapor layer increases which produces a larger heat feedback to the solid through higher convective heating and re-radiation.

Soot Distribution Near the Stagnation Point Induced by Thermophoretic Motion

Introduction. In the combustion field, the study of particles transport is of particular importance to the sooting phenomenon. It is known that small particles suspended in a nonisothermal gas acquire a mean velocity relative to the gas in the direction opposite the temperature gradient. This phenomenon is known as thermophoresis. The customary approach to solid particles transport is to include this phenomenon and neglect the Brownian diffusion [11, 12]. This approximation is valid except close to the region where the velocity of the particles is nearly zero. Referring to Fig. 2, a jet containing soot particles is impinging onto a heated plate. Since the thermophoretic motion is opposed to the gas motion, a soot stagnation point is created at n^* . This situation also occurs in the more complicated configuration with flames. The behavior of soot transport in this region, which has not received proper attention, is the subject of this investigation.

Analysis. It is assumed that the particles are sufficiently small so that in the absence of thermophoresis they move with the gas. For the present, a uniform size distribution is assumed and the particles volume fraction is assumed to be very small. The expression for the thermophoretic velocity is

$$v_t = -A(\mu/\rho)\nabla T/T$$

where A is a coefficient depending on the regime of the flow, μ , ρ , and T are gas viscosity, density and temperature respectively.

Introducing the above expression into the soot transport equation, the following non-dimensional equation is obtained along the center line of the jet (Fig. 2):

$$(1/Sc)d^2Y/dn^2 + V(n)dY/dn + F(n)Y = -\dot{\omega} \quad (1)$$

where: $V(n) = f(n) + A\theta'/\theta$ is the particles velocity,

$$F(n) = A(\theta\theta'' - \theta')^2/\theta^2, \quad \dot{\omega} \text{ is the particle formation rate. } \theta \text{ and } f$$

(temperature and stream function) are computed from the energy and momentum equations.

The Schmidt number (Sc) for the soot particle is computed using the Brownian diffusion coefficient and is typically a very large number ($> 10^5$). Therefore, the first term in Eq. (1) is generally negligible. The simplified Eq. (1) can be solved readily. For a heated plate without particle formation ($\omega = 0$) and the particle is seeded at the free stream, the dotted lines in Fig. 3 gives the mass distribution of particles. Two cases can be distinguished. For $PrxA < 1$ [$F(n^*) < 0$], soot mass fraction falls to zero at the stagnation point, but for $PrxA > 1$ [$F(n^*) > 0$], soot mass fraction becomes unbounded. This singular behavior can be corrected by the inclusion of the diffusion term in Eq. (1). Since $1/Sc$ is such a small number which renders numerical solution difficult, a matched asymptotic expansion is used. In an inner region of the order of $\sqrt{\epsilon}$ around n^* , the coefficient V and F in Eq. (1) is linearized. The resulting equation can be solved in terms of parabolic cylindrical functions [13-17]. The inner solution is then matched with the outer solutions. The solid lines in Fig. 3 show that the introduction of Brownian diffusion, although very small, allows for a finite Y/Y_∞ at n^* to exist when $AxPr$ is greater than unity.

Status. Work is in progress to extend our analysis to a combustion situation with soot formation.

REFERENCES

1. Chien, K. Y., AIAA J., 20, 23 (1982)
2. Magnussen, B. F. and Hjetager, B. H., 16th Sym. on Comb., Comb. Inst., 719, (1977)
3. Galant, S. et al., 20th Sym. on Comb., Comb. Inst., 531 (1984)
4. Tesner, P. A. et al., Comb. & Flame, 17, 279 (1971)
5. Kashiwagi, T., Fire Safety J., 3, 185 (1981)
6. Modak, A. T., Fire Safety J., 3, 177 (1981)
7. Brosmer, M. A. and Tien, C. L., Comb. Sci. & Tech., 51, 21 (1987)
8. Orloff, L., Modak, A. T., and Alpert, R. L., 16th Symp. on Comb., 1345, Comb. Inst. (1977)
9. Plumb, O. A. and Kennedy, L. A., J. Heat Trans., 79 (1977)
10. Lin, S.-J. and Churchill, S. W., Num. Heat Trans., 1, 129 (1978)
11. Goren, S. L., J. of Coll. and Interf. Sci., 61, (1), 77 (1977)
12. Kennedy, I. M., Comb. and Fl., 68, 1-6 (1987)
13. O'Malley, R. E., SIAM J. Math Anal., 7 (4), 479 (1970)
14. Grassman, J., Ibid, 32 (3), 588 (1977)
15. Kreiss, H. O., Ibid, 5 (2), 230 (1974)
16. Pearson, C. E., J. of Math. & Phys., 47 (68), 134 (1968)
17. Abramowitz, M., "Handbook of Mathematical Functions," N.B.S. Appl. Math. Series 55, 686 (1964).

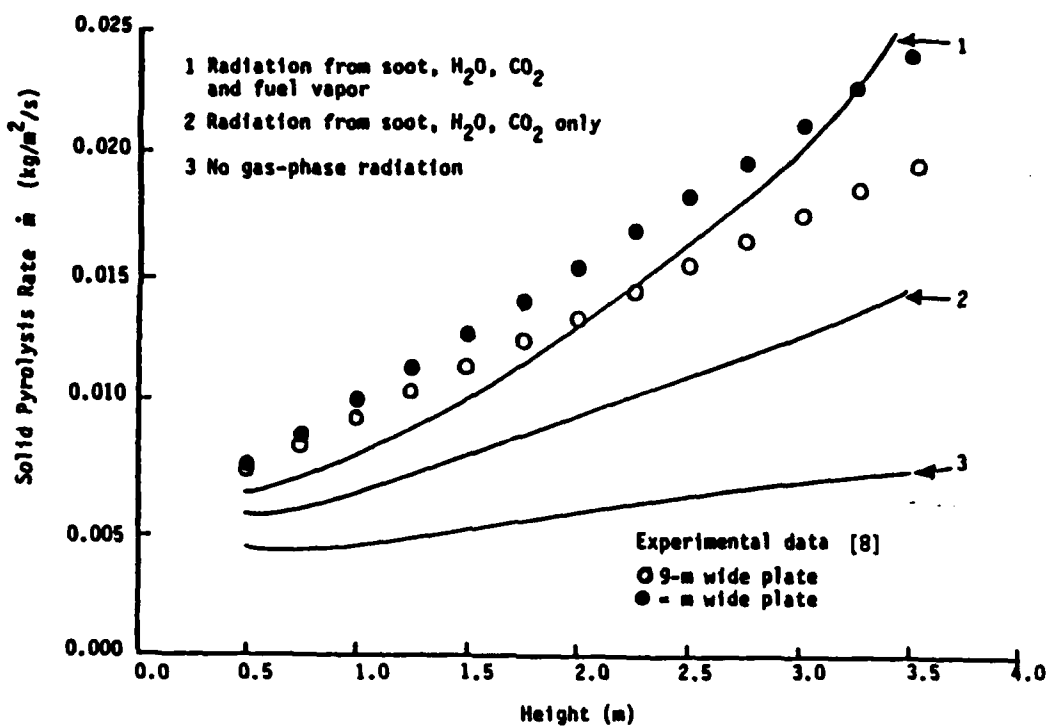


Fig. 1 Comparison of model calculation and experiment for vertical burning of PMMA in air

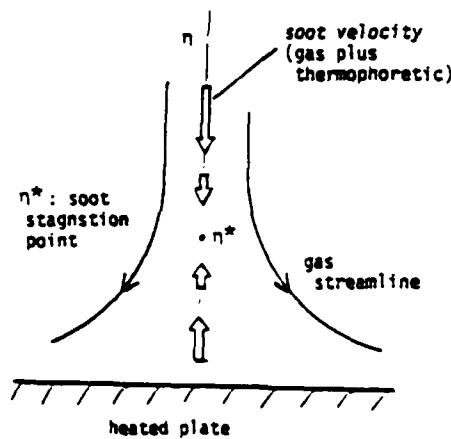
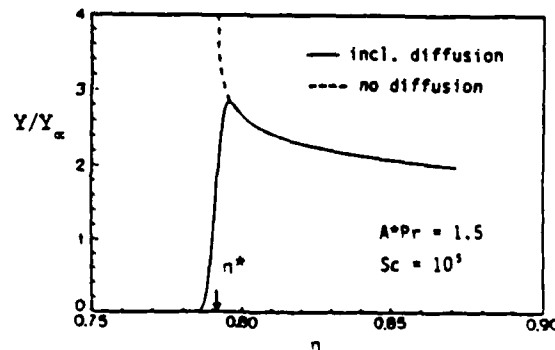
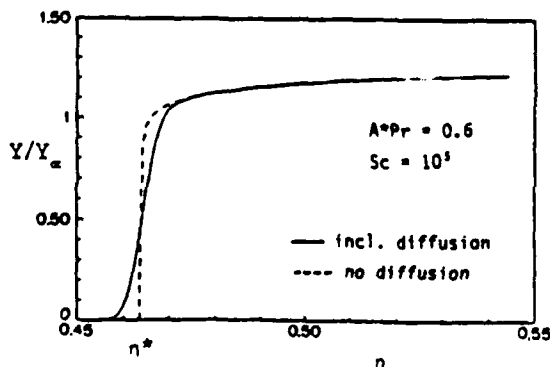


Fig. 2 Illustration of soot stagnation point induced by thermophoretic motion in an impinging jet onto a heated plate.

Fig. 3 Computed soot profiles near the stagnation point with and without Brownian diffusion. Heated plate case without combustion ($T_e/T = 2.33$). Soot particles are seeded in the freestream.



FRACTAL IMAGE COMPRESSION OF RAYLEIGH, RAMAN,
LIF AND LV DATA IN TURBULENT REACTING FLOWS

(AFOSR Contract No. 88-0001)

Principal Investigators: W. C. Strahle and J. I. Jagoda

School of Aerospace Engineering
Georgia Institute of Technology
Atlanta, GA 30332

SUMMARY/OVERVIEW:

It is the objective of this study to provide a data base for a complex reacting turbulent flow with recirculation and to investigate new methods of data analysis for short run times or limited data. Moreover, an analytical model has been developed for the flowfield and compared with the data as available. Diagnostics used have been laser velocimetry and Rayleigh scattering with concurrent development of Raman Spectroscopy. The flow is a two-dimensional backward facing step configuration with fuel injection from the floor behind the backward facing step. Fractal image compression techniques involving affine maps have been used for data compression. The purpose is to use certain fractal properties of turbulence data to aid in the data taking process.

TECHNICAL DISCUSSION

The work being undertaken under this contract can be divided into three, interrelated parts: 1) to generate a data base of velocity, concentration and temperature in the highly complex, turbulent reacting flow field behind a backward facing step with bleed of fuel through the porous floor behind the step, 2) to compare the obtained experimental data with the results of a modified $k-\epsilon$ model for this turbulent reacting flow and 3) to use fractal analysis to interpolate between a limited number of data points, relatively widely spaced in time.

The need for the first two objectives is self-evident. The flow field being investigated is one similar to that encountered in a solid fuel ramjet, whereby the pyrolysing solid fuel has been replaced by the injection of fuel through a porous plate. The acquisition of velocity, concentration and velocity-concentration covariance data and their comparison with results from the numerical model in the cold(i.e. non reacting) flow has been achieved during a previous contract. These measurements were carried out using a combined Laser Doppler Velocimetry (LDV) and Rayleigh scattering technique. The numerical code employed was a modified $k-\epsilon$ model. Good agreement was obtained between the theoretical and experimental results. The results of this work have been published in the open literature.

Under the current contract this work is being extended to the reacting flow. The distribution of the velocities and shear stresses are measured using LDV while local concentrations and temperatures are determined by Raman scattering. In this technique the concentration of a major species (e.g. nitrogen) is proportional to the intensity of its Stokes line, while the instantaneous vibrational temperature is determined from the ratio between the Stokes and Anti-Stokes lines. Furthermore, laser induced fluorescence (LIF) measurements of OH radical concentrations will be used to determine the degree of deviation from local chemical equilibrium in the turbulent reacting flow. At the same time, the modeling effort for the reacting flow is being completed. In this work both, infinite and finite reaction kinetics are being incorporated into the code.

The need for the third objective, i.e. the image compression work, arises when, for some physical reason, data can only be obtained at a finite rate for a limited period of time. This issue becomes critical when the time interval between data points exceeds the shortest characteristic time of the flow field. The problem is then further complicated if the treatment of joint properties of data is required. Such circumstances exist in the present investigation. The data rate in the Raman scattering experiment are limited by the repetition rate of the linear flash lamp pumped dye laser which is restricted to maximally 5 Hz. This data rate is further decreased if the LDV and Raman scattering measurements are carried out simultaneously since the flow can only be seeded lightly before Mie scattering by the seed particles interferes with the concentration measurements. In addition, the run times are limited to a few minutes after which the excessive temperature of the porous plate causes it to buckle. Nevertheless, a large number of data points are required at each location to fully characterize this highly turbulent flow field. A fractal reconstruction of the variation of the measured investigated properties with time from a limited number of measured data points would, therefore, be of great assistance in this work. Since covariances of different properties are required to fully describe the flow the problem lends itself to a full treatment of fractal reconstruction.

The fractal image compression technique is being developed using previously obtained Rayleigh scattering and hot wire anemometry data. These data were selected since they were acquired at a high data rate. The interpolation technique can, therefore, be applied to a set of selected data points and the results be checked against actually measured data. As a next step the technique will be extended to cover simultaneously measured LDV and Rayleigh data before being applied to the flow field under consideration here.

The reacting flow measurements of velocity, concentration and temperature are being carried out using hydrogen as a fuel. Hydrogen rather than methane was selected because it resulted in a smoother flame which is more two dimensional in nature. In addition, hydrogen flames produce a cleaner spectrum and are, therefore, more amenable to Raman spectroscopy. The vertical distributions of the axial velocity have been determined. The data rates in the reacting flow case were considerably lower than those in the cold flow. The distribution of axial velocities at three axial locations are shown in Fig. 1. Two of these locations lie in the recirculation zone while the third one is at reattachment. The observed results, as well as visual observations, do not agree with the model predictions. While the model

calculates a shortening of the recirculation zone for the flow with combustion as opposed to the cold flow, a lengthening of the recirculating zone upon heat addition is, in fact, observed. For this reason all measurements were carried out a number of times with good repeatability. In addition, axial velocities very close to the porous tunnel floor were measured along its center line. For these measurements the optical axis of the LDV was positioned parallel to the floor. While this blocked one of the beams required for the vertical velocity measurements it resulted in a much improved signal to noise ratio for the axial velocity determination. These measurements confirmed the lengthening of the recirculation zone upon heat addition.

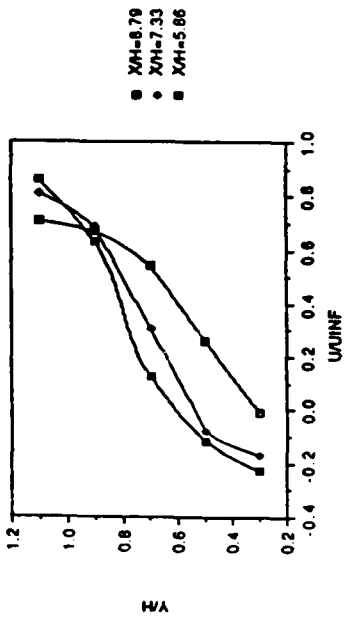
Currently, the Raman system is being tested in a non reacting flow. The linear relationship between the intensity of the Stokes line and the concentration of nitrogen are being confirmed and the noise level in the signal is being determined. Raman measurements in the reacting flow should have commenced by the time of the meeting.

Shown in Fig. 1 are the first attempts at fractal reconstruction of decimated data. A new visual data reduction technique of multifractal spectral analysis (not shown) has also been applied to the data and will be shown at the meeting. The objective is to use certain fractal properties of data traces in turbulent flows to circumvent usual probabilistic notions of data requirements. This is a high risk element of research, but one with great payoff if successful.

The modeling effort is now complete, with predicted reattachment lengths shown in Fig. 1. Finite rate kinetics calculations have also shown that, at least for H₂ injection, deviations from equilibrium should not be large. While excellent agreement between theory and experiment was attained in cold flow there is a discrepancy, mentioned above, in hot flow. Further data are required before the reason for this discrepancy can be resolved.

AIR FORCE BASIC RESEARCH ACHIEVEMENT

- DATA BASE



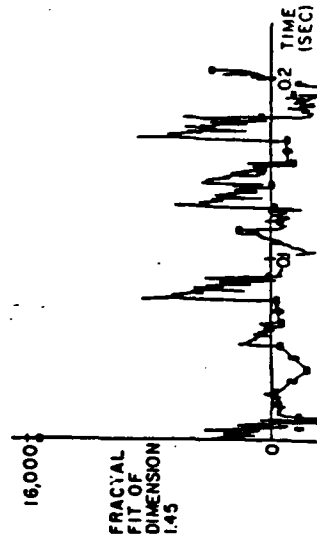
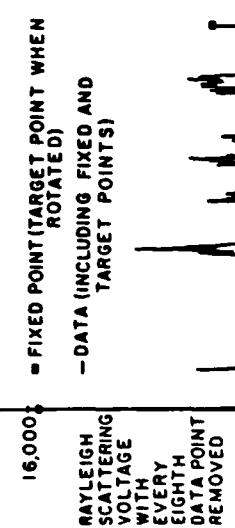
LDV-HOT

- THEORY

COLD FLOW		COMBUSTION			
HIGH REY. NO.	LOW REY. NO.	HIGH REY. NO.	LOW REY. NO.	COLD FLOW	COMBUSTION
MODEL	MODEL	MODEL	MODEL	FUEL	FUEL
INJ. VEL.	INJ. VEL.	INJ. VEL.	INJ. VEL.	INJ. VEL.	INJ. VEL.
0.0	0.0	0.57	—	—	—
M/SEC.	M/SEC.	7.50	—	—	—
0.0477	—	—	0.57	—	—
M/SEC.	M/SEC.	—	7.50	0.14	—
0.08	—	—	—	—	0.08
M/SEC.	M/SEC.	—	—	—	—

Reattachment Lengths for Various Test Cases

- NEW VISUAL TOOL FOR DATA INVESTIGATION-MULTIFRACTAL SPECTRUM
- FRACTAL IMAGE COMPRESSION ON TURBULENCE DATA



**THE PHYSICS OF POSITIVELY BIASED CONDUCTORS SURROUNDED BY
DIELECTRICS IN CONTACT WITH A PLASMA**

AFOSR Grant AFOSR-87-0340

D.E. Hastings

Dept of Aeronautics and Astronautics
MIT,Cambridge, MA 02139

Overview

The physics of a positively biased conductor surrounded by dielectrics in contact with plasma is investigated. It is shown that due to the presence of secondary emission from the surrounding dielectrics the voltage of the surfaces near the conductor can be bistable. One of the bistable solutions always has very low secondary emission while the other has high secondary emission. When the voltage on the dielectric undergoes a transition from one bistable solution to another this will be seen as a concomitant increase in the current collected to the conductor. This theory is applied to explain the "snapover" effect. The snapover effect is observed on high voltage solar arrays which involve the use of highly biased surfaces in contact with the space environment. It has been observed that when such surfaces are positively biased that the current undergoes an anomalous increase at a critical voltage.

1 Technical Discussion

As space systems become larger and more complex, the power required to run them has increased. Simple calculations show that the power lost in a transmission line expressed as a fraction of the power generated scales as the current carried in the line. It is also easy to show the mass of the transmission line scales as the square of the current. From these considerations space engineers

have tried to design high power systems to operate at high voltages rather than high currents since this minimizes the mass penalty. This has led to the development of high voltage solar arrays. The potential drop across these solar arrays may be several hundred volts. These solar arrays are typically designed with the solar cells connected by metallic interconnects which are exposed to the space environment. The reason for this is to reduce the mass of the solar array by removing the insulation from the connector and because it is observed that the insulation erodes under the impact of the low energy ions found in low earth orbit and also because small defects in the insulation render it useless. Maxwell's equations applied to the whole solar array demand that the net plasma current to the solar array must be zero for the system to be in equilibrium. In order for this to be true what is found is that some part of the array will take a positive potential with respect to the environment (and attract electrons to the interconnects) while the rest of the array will float negatively with respect to space and collect ions to the interconnects. One observation for these high voltage solar arrays is that the positively biased interconnects collect anomalously large currents above a critical voltage. This voltage has been termed the "snapover" voltage from the shape (an S shape) of the current voltage curve for the conductor. Negatively biased surfaces undergo arcing below a critical voltage. The two phenomena are connected when both occur on a solar array in that once the positively biased end of the array undergoes snapover the area of the negatively biased end of the array increases to maintain current balance. This exposes an increased area of the array to negative arcing damage.

We present an alternative theory which may account for the anomalously large current collected to a conductor surrounded by a dielectric. The basic idea is that the dielectric surface which must be in current balance can have more than one solution for its surface voltage. If the dielectric has a high enough secondary electron emission coefficient then it can achieve current balance(zero net current) in two possible ways. First by repelling most of the electrons so that the balance is between incoming ions and electrons and secondly by emitting secondary electrons so that the balance is between incoming primary and outgoing secondary electrons. Since the nearby conductor is always at a positive potential relative to the dielectric, secondary electrons which are emitted by the dielectric are collected by the conductor. The snapover is just the jump of the surface

potential and associated electron current from one means of achieving current balance to another. It therefore can show all the behaviour characteristic of such systems namely hysteresis behaviour and sensitivity to plasma fluctuations and the fact that the final state of the system will depend on the choice of the initial conditions.

In order to understand the interactions of the plasma with a surface a 2-dimensional PIC code [REPDW] was used to simulate the detailed physics over the surface of a high voltage system.

The PIC simulations were all performed for the following parameters. The system was taken to be a square of dimension 32 by 32 units. The spatial grid was also chosen as 32 by 32. The conductor was taken to have a length of 4 units and to have a dielectric on each side of 6 units. The simulations were always started with 1000 electrons and ions. The dielectric was modelled as having a capacitance of 64 units and the taken to have a maximum yield of 2.4 at an energy of 250 units. This gives it a first unity crossing of 28 units. All simulations were run to steady state.

In order to explore the effect of initial conditions all simulations were performed from two different initial conditions. The first was with the dielectric initially charged so that the voltage on the surface facing the plasma was zero voltage units. We shall refer to this as the charged case. The second initial condition was with the dielectric initially uncharged so that the voltage on its surface was the conductor voltage. This will be called the uncharged case.

In Fig. 1 we give the potential structure for the case where the conductor is biased to 40 voltage units and the initial condition was with the dielectric charged. In Fig. 2 we examine the potential for the same conditions except that the initial state of the dielectric was uncharged. The potential on the dielectric is now positive and sitting at about the first unity crossing. The dielectric is emitting secondary electrons in steady state.

These results show that the initial conditions are important and verify that the current voltage relationship will show hysteresis due to the dielectric allowing bistable solutions for its surface voltage.

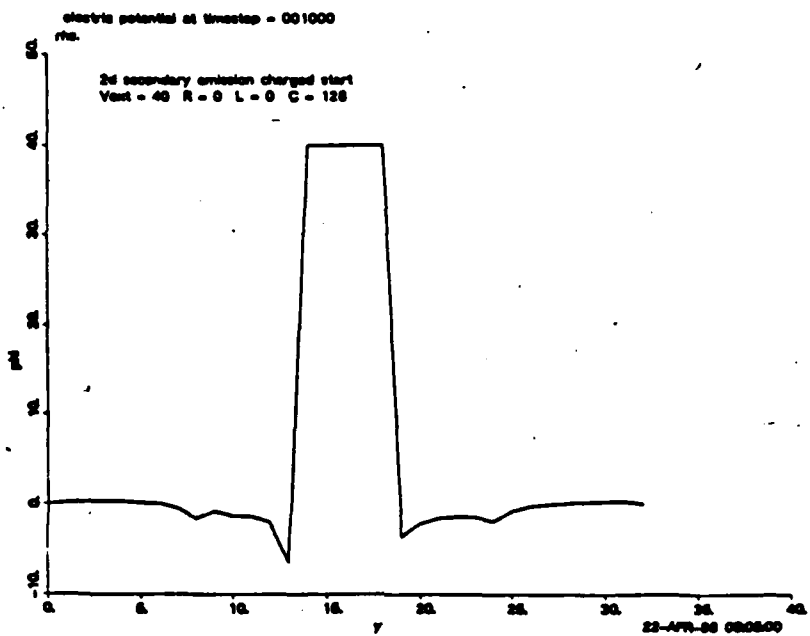


Figure 1: Potential structure along the conductor and dielectric, charged start, $\phi_c = 40$, $E_1 = 28$

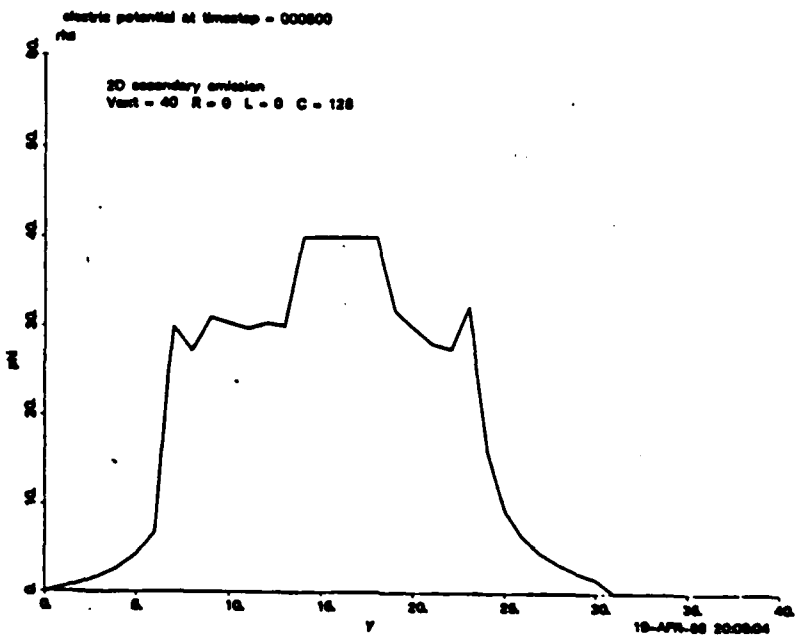


Figure 2: Potential structure along the conductor and dielectric, uncharged start, $\phi_c = 40$, $E_1 = 28$

ASYMPTOTIC METHODS APPLIED TO PLASMA OF KNUDSEN THERMIONIC CONVERTERS

AFOSR Grant 85-0375

Principal Investigator: Geoffrey L. Main

School Of Mechanical Engineering
Georgia Institute of Technology
Atlanta, Georgia 30332

SUMMARY/OVERVIEW:

A Knudsen thermionic converter is a thermionic converter in which the plasma filled gap between the emitter and collector is thin in the sense that the ion and electron mean free paths are of the same scale as the gap. Since the scales are the same, the plasma cannot be approximated as either collisionless or fully collisional. An asymptotic approximation is developed for Knudsen thermionic converter plasmas that shows what the voltage drop through the plasma gap should be for various Knudsen modes as a function of the gap to mean free path ratios.

TECHNICAL DISCUSSION

The theory for Knudsen thermionic converters developed here is broken down into two parts: first, for surface ionization Knudsen thermionic converters, and second, for trapped ion thermionic converters.

Surface Ionization Converters

Surface ionization thermionic converters maintain the plasma with positive ions from the emitter emitted according to the Saha-Langmuir equation,

$$J_{ion} = \frac{ep}{(2\pi mkT_E)^{1/2}(1 + \exp[(V_i - \phi_E)/kT_E])}, \quad (1)$$

where V_i is the ionization energy of the absorbate gas, ϕ_E is the emitter work function, T_E is the emitter temperature, p is the absorbate gas pressure, and e is the fundamental charge. Generally, the emitter temperature must be high (2200 K or more) so that sufficient ion current can be attained at the same time that a sufficient thermionic electron current is emitted. This is because thermionic electron emission is favored by low emitter work function while surface ionization is favored by high emitter work function. The expected behavior of the plasma in the surface ionization Knudsen thermionic converter is shown in figure 1. The quantities of interest in figure 1 are the plasma potential increase ϕ_p and the ratio of plasma density at the collector to the plasma density at the emitter n_C/n_E since these represent a limitation on the amount of current the thermionic convertor can carry without increased voltage loss.

The analysis of the plasma gap region is carried out by finding asymptotic solution to the Boltzmann equation and the Poisson equation simultaneously. It has been found that an asymptotic solution can be found by expanding the plasma potential as

$$\frac{e\phi}{kT_e} = -\ln(\xi) + \frac{a_1}{\xi^2} + \frac{a_2}{\xi^4} + \dots \quad (2)$$

where $\xi = 1 + \alpha z$ and where z is the distance across the plasma gap such that $z = -d$ is the emitter and $z = 0$ is the collector. The temperature T_e is the electron temperature which will be the same as the emitter temperature T_E in this case. The quantity α is of the order of $1/\lambda_i$ where λ_i is an ion mean free path and its precise value is determined as part of the solution. The ion distribution function in the gap also needs to be expanded and is given by

$$f(v, \xi) = \xi \exp(f_{-1}(v) + f_0(v)/\xi + f_1(v)/\xi^2 + \dots) \quad (3)$$

where v is the velocity space variable and where $f_{-1}(v)$ and so forth are determined as part of the solution.

The Boltzmann equation is written as

$$v \frac{\partial f}{\partial z} + \frac{1}{m} \frac{d(e\phi)}{dx} \frac{\partial f}{\partial v} = \frac{1}{\tau n_n} [f_n(v) \int_{-\infty}^{\infty} f(v, \xi) dv - n_n f(v, \xi)] \quad (4)$$

where the collision term assumes charge exchange collisions dominate. The quantity $n_n = \int_{-\infty}^{\infty} f_n(v) dv$ is the neutral density and $f_n(v)$ is the neutral distribution. The quantity m is the ion mass.

The Poisson equation simply becomes that the positive ion density is equal to the electron density because the Debye length is short compared to the mean free paths and the plasma gap. The electron density can be written as

$$n_e = n_C \exp(-e\phi/kT_e) \quad (5)$$

and is expanded in ξ accordingly.

The solution to this set of equation to the first order is

$$f(v, \xi) = \xi n_C \left(\frac{m}{2kT} \right)^{1/2} \exp\left(-\frac{mv^2}{2kT} - \frac{1}{\xi} \frac{\tau \alpha}{2} \left(1 + \frac{T_e}{T}\right) v\right) \quad (6)$$

and

$$\frac{e\phi_p}{kT_e} = \ln(1 - \alpha d) \quad (7)$$

Therefore the ion flux is

$$\Gamma_i = n_C \frac{\tau kT}{2m} \left(1 + \frac{T_e}{T}\right) \frac{1}{d} \left(\exp\left(\frac{e\phi_p}{kT_e}\right) - 1\right). \quad (8)$$

The ions at the collector sheath are not retained, therefore we have

$$1 = \frac{\Gamma_i}{n_C \sqrt{\frac{kT}{m}}} = \frac{\lambda_i}{d} \left(1 + \frac{T_e}{T}\right) \frac{1}{2} \left(\exp\left(\frac{e\phi_p}{kT_e}\right) - 1\right) \quad (9)$$

or

$$\frac{e\phi_p}{kT_e} = \ln\left(\frac{d}{\lambda_i} + 1\right) \quad (10)$$

where we have now assumed $T = T_e$.

The result of this analysis is that the net current through the converter is limited to

$$J_{limit} = J_{ion} \sqrt{\frac{m}{m_e}} \frac{1}{1 + \frac{d}{\lambda_i}} \quad (11)$$

where m_e is the electron mass. This implies that for currents below J_{limit} the electron collisions in the converter should make little difference, and that above J_{limit} significant resistance should be encountered. Since a typical Knudsen thermionic converter might have

$d/\lambda_i = 4$ the limit current would be only 20% of the collisionless value. The counterintuitive result of this analysis is that the ion collisions in the Knudsen thermionic converter should be minimized rather than the electron collisions.

Trapped Ion Converters

If there is insufficient surface ionization, the output voltage V_{out} may be reduced as shown in figure 2 so as to pull the potential in the plasma down toward the collector. The result is that the ions and electrons reverse roles with ions trapped. Equation (10) becomes

$$\frac{e\phi_p}{kT} = \ln\left(\frac{d}{\lambda_e} + 1\right) \quad (12)$$

and in this case the current through the converter is

$$\frac{J}{en_C \sqrt{\frac{kT_e}{m}}} = \frac{\lambda_e}{d} \left(1 + \frac{T}{T_e}\right) \frac{1}{2} \left(\exp\left(\frac{e\phi_p}{kT}\right) - 1\right). \quad (13)$$

Making the assumption that $T = T_e$ reduces (12) and (13) to

$$J = en_C \sqrt{\frac{kT}{m_e}} \frac{\lambda_e}{d} \left(\exp\left(\frac{e\phi_p}{kT}\right) - 1\right) \quad (14)$$

or to

$$J = en_E \sqrt{\frac{kT}{m_e}} \frac{\lambda_e}{d} \left(1 - \exp\left(-\frac{e\phi_p}{kT}\right)\right). \quad (15)$$

or approximately

$$J = en_E \sqrt{\frac{kT}{m_e}} \frac{\lambda_e}{d} \frac{e\phi_p}{kT}. \quad (16)$$

Thus in this case, it is desirable to reduce the electron collisions rather than ion collisions.

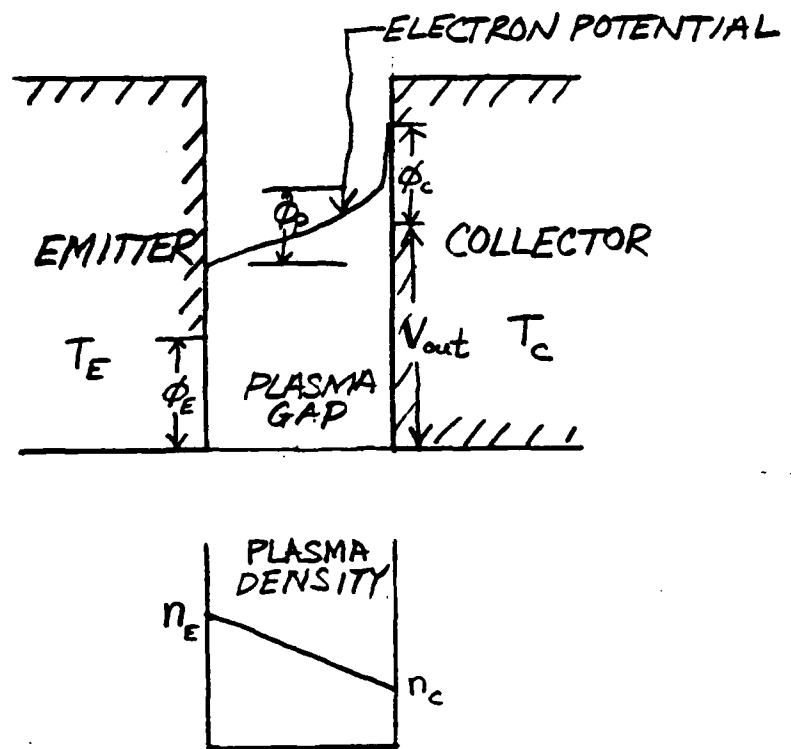


Figure 1. The Knudsen Thermionic Converter with Surface Ionization.

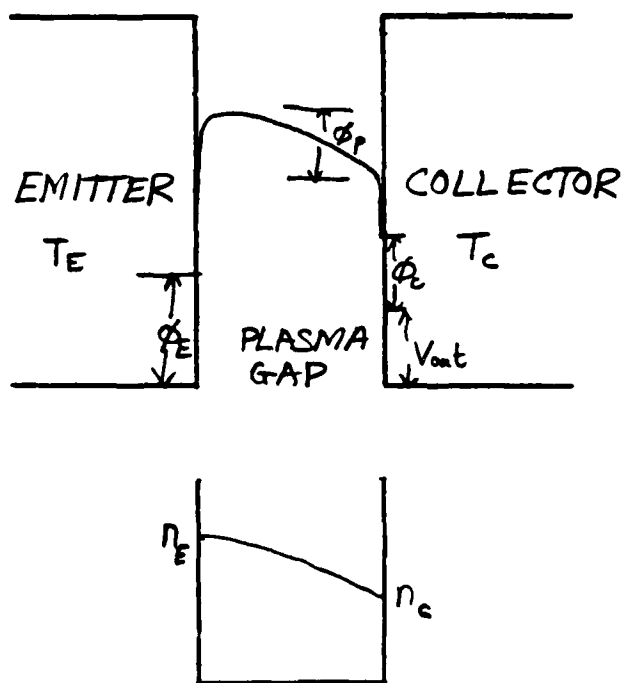


Figure 2. The Knudsen Thermionic Converter with Ion Trapping.

DIAGNOSTICS FOR INTELLIGENT ADAPTIVE CONTROL OF MPD ENGINES

(AFOSR Grant No. AFOSR-86-0278A)

Principal Investigators: Rahmat Shoureshi

School of Mechanical Engineering Purdue University West Lafayette, IN 47907

SUMMARY/OVERVIEW:

Formulation of an intelligent diagnostic system for MPD thrusters continues to be the focus of our research activities. This year's effort includes stabilizability and controllability analysis of distributed parameter systems which results in control strategies that guarantee stable operation of the MPD system. The resulting control scheme, in general, has a distributed nature which in most practical problems is not feasible to implement. Therefore, the study has focused on finding a finite order controller based on the distributed analysis of the system to guarantee a feasible stable closed loop characteristic. The extended Lyapunov stability theorem, using an equivalent norm of a Hilbert space of system state variables to form a functional, results in boundary and internal constraints which have to be satisfied. These conditions form the basis for stabilizability and controllability techniques of the distributed parameter systems.

TECHNICAL DISCUSSION

There are three major issues associated with system diagnostics: the required number of sensors that provide a relatively complete information about the system locally and instantaneously; the optimum locations for these sensors; and system accommodation in case of sensor failure, i.e. how the system should be commanded when it loses some of its sensors, without being pushed to the unstable mode of operation. Some of these issues are analyzed for linear systems described by a set of ordinary differential equations with constant coefficients. However, the field is open for extensive research on these issues when dealing with more realistic systems, namely those which are nonlinear and described by partial differential equations. The MPD engine is an example of such distributed parameter systems. In order to formulate an intelligent diagnostic system, which would automatically make decisions in regard to the above issues, the system has to be analyzed from stability, controllability, and observability points of view. These form the focal point of our research.

Modeling of equilibrium states and nonstationary states for the MPD thruster has been developed and shown to have the following state space representation [1,2].

$$\frac{\partial \mathbf{v}}{\partial t} = - \begin{bmatrix} u_e & \rho_e & 0 \\ \frac{RT_e}{\rho_e} & u_e & R \\ 0 & \frac{RT_e}{c_v} & u_e \end{bmatrix} \frac{\partial \mathbf{v}}{\partial x} - \begin{bmatrix} u'_e & -\frac{\rho_e}{u_e} u'_e & 0 \\ \frac{u_e}{\rho_e} u'_e + \frac{R}{\rho_e} T'_e & u'_e & -\frac{R}{u_e} u'_e \\ (\gamma-1) \frac{T_e}{\rho_e} u'_e + \frac{u_e}{\rho_e} T'_e & \frac{U_1}{\rho_e c_v} + T'_e & \frac{R}{c_v} u'_e \end{bmatrix} \mathbf{v}$$

(1)

$$\mathbf{v}(0, x) = \mathbf{v}_0(x), \quad \mathbf{v}(t, 0) = 0$$

where

$$\mathbf{v}_0(x) \in L^2(0, \ell), \quad \mathbf{v} = [\rho, u, T]^T$$

It is clear that $\mathbf{v} = 0$ (i.e., null solution) represents the condition where there is no variation from the equilibrium state. The parameters, ρ, u, T are perturbations of density, pressure, and temperature and the same parameters with index e denotes equilibrium values for these states variables.

The characteristic directions (eigenvalues) of this system of equations are:

$$\lambda_1 = u_e, \quad \lambda_2 = u_e + \sqrt{\gamma RT_e}, \quad \lambda_3 = u_e - \sqrt{\gamma RT_e},$$

Therefore, equation (1) represents a system of hyperbolic partial differential equations. For a general hyperbolic system of the form

$$\frac{\partial \mathbf{v}}{\partial t} = L \mathbf{v} \quad (2)$$

where

$$L \mathbf{v} = A \frac{\partial \mathbf{v}}{\partial x} + B \mathbf{v}, \quad (3)$$

it is possible to show that the system of equation (1) can be made into the form of equation (3) with a symmetric A matrix.

In order to derive stability conditions for the system of (3) an extended Lyapunov technique is used [1]. To construct a Lyapunov functional it is sufficient to select the functional as an equivalent norm in Hilbert space of transformed states [3,4], i.e., a bilinear form as following.

$$\mathcal{L} = \langle \mathbf{v}, \mathbf{v} \rangle_2 = \langle \mathbf{v}, S\mathbf{v} \rangle_1 = \int_0^\ell \mathbf{v}^T S(x) \mathbf{v} dx \quad (4)$$

It is shown [3,4] that the time derivative of this functional can be derived as

$$\frac{d\varphi}{dt} = -v^T S(x) A v + \int_0^t v^T \left\{ \frac{\partial S}{\partial x} A + \frac{S \partial A}{\partial x} - 2 S(x) B \right\} v dx \quad (5)$$

Based on this equation the following conditions for stability of the system can be derived.

i) Boundary constraint:

$$-v^T(t, \ell) S(\ell) A(\ell) v(t, \ell) + v^T(t, 0) S(0) A(0) v(t, 0) \leq 0 \quad (6)$$

ii) Interior constraint:

$$\left\{ \frac{\partial S}{\partial x} A + S(x) \frac{\partial A}{\partial x} - 2 S(x) B \right\} \text{ must be negative definite for } x \in (0, \ell) \quad (7)$$

If these conditions are not met, i.e., homogeneous system is not stable a control action can be amended to the system. Hence the controlled system would become

$$\dot{V} = -AV_x - BV - DU \quad (8)$$

A set of feedback control with the gain K can be proposed;

$$K = \begin{bmatrix} K_{11} & K_{12} & K_{13} \\ K_{21} & K_{22} & K_{23} \end{bmatrix}. \quad (9)$$

Hence (8) becomes

$$\dot{V} = -AV_x - BV + DKV \quad (10)$$

where

$$DK = \begin{bmatrix} 0 & 0 & 0 \\ \frac{K_{11}}{\rho_e \sqrt{RT_e}} & \frac{K_{12}}{\rho_e \sqrt{RT_e}} & \frac{K_{13}}{\rho_e \sqrt{RT_e}} \\ \left(\frac{K_{21} - u_e K_{11}}{c_v \sqrt{\gamma-1} \rho_e RT_e} \right) & \left(\frac{K_{22} - u_e K_{12}}{c_v \sqrt{\gamma-1} \rho_e RT_e} \right) & \left(\frac{K_{23} - u_e K_{13}}{c_v \sqrt{\gamma-1} \rho_e RT_e} \right) \end{bmatrix} \quad (11)$$

The elements of the feedback gain matrix, K, can be selected based on the negative definite condition of modified (ii) imposed on (10).

The controllability analysis of the system can be considered as stabilizability of the following system.

$$\dot{v} = \frac{1}{2} \left[\frac{\partial A}{\partial x} - 2B \right] v + DU \quad (12)$$

By application of the singular value decomposition of $\left[\frac{\partial A}{\partial x} - 2B \right]$, stabilization of

original problem with unbounded operations (i.e., $A \frac{\partial(\cdot)}{\partial x} - B$) can be imbedded into the stabilization of a problem with bounded operators. This technique results in the following controllability criteria.

$$W_c = \left\{ 2D \mid \left[\frac{\partial A}{\partial x} - 2B \right] (2D) \mid \left[\frac{\partial A}{\partial x} - 2B \right]^2 (2D) \mid \dots \mid \left[\frac{\partial A}{\partial x} - 2B \right]^{n-1} (2D) \right\}$$

must have full rank [4].

From the values of A , B , D for the MPD model in the previous section controllability matrix W_c can be constructed. This results in linear independence of D and $\left[\frac{\partial A}{\partial x} - 2B \right]$ provided $\frac{T'_e}{T_e}$ and $\frac{u'_e}{u_e}$ are nonzero, simultaneously. Namely, although there is not a formal input term influencing the density evolution equation (continuity equation), it is possible to control and stabilize density, velocity and temperature with the input terms appearing in the momentum and energy equations.

The condition $\frac{T'_e}{T_e} \neq 0$, $\frac{u'_e}{u_e} \neq 0$ depends on the equilibrium state which is investigated in [3], and accommodated by the proper choice of input fields to the equations of equilibrium states.

The controllability criteria discussed above, determines the condition whether there exists a distributed control input which stabilizes the system by a feedback law, $U = Kv$, i.e. the existence condition for feedback gain K . The stabilizing control, is distributed due to distributedness of the state vector v and gain K . However, in practical terms, distributed parameter systems must be controlled by a finite number of actuators and sensors. Therefore, there is a real need to find a technique where by application of finite controls an infinite order system can be stabilized. The basis for this technique is the controllability condition. If this condition is not satisfied over the spatial domain, then a finite order controller is not achievable. This emphasizes the significance of controllability analysis in the distributed system.

REFERENCES:

1. R. Shoureshi, F. Pourki, Stability Analysis of Electro-Magneto-Plasma Dynamics, accepted for publication in AIAA Journal of Guidance and Control.
2. R. Shoureshi, F. Pourki, Controllability Analysis of Nonlinear Distributed Parameter Systems, proceedings of the 1987 American Control Conference, pp. 880-885.
3. R. Shoureshi, F. Pourki, Stabilization of MPD Thrusters Via Pointwise Observation and Control, accepted for presentation at the 1988 ASME-WAM.
4. F. Pourki, R. Shoureshi, A Lyapunov Approach to Stability of Nonlinear Distributed Parameter Systems, accepted for presentation at the 1988 ASME-WAM.

AFOSR ROCKET PROPULSION CONTRACTORS MEETINGInvitees

Mr. Robert Acree
AFAL/DYCC
Edwards AFB CA 93523-5000
(805) 275-5598
AV525-5598

Dr George F. Adams
USA-BRL
AMXBR-I8D
Aberdeen Proving Gnd MD 21005-5006
(301) 278-6168
(301) 278-6783

Mr Ranney Adams
AFAL/PA
Edwards AFB CA 93523-5000
(805) 275-5465
AV525-5465

Dr. Horst Adolph
Synthesis and Formulations Br
Naval Surface Weapons Center
10901 New Hampshire Avenue
Silver Spring MD 20903-5000

Dr William S. Anderson
United Technologies/CSD
P.O. Box 50015
San Jose CA 95150-0015
(408) 778-4302

Mr W. C. Andreponi
P.O. Box 431
858 W. Jackman
Suite 111
Lancaster CA 93534
(805) 942-5098

Lt John L. Andreshak
AFAL/LKLR
Stop 24
Edwards AFB CA 93523-5000
(805) 275-5194
AV525-5194

Dr Ron Atkins
Naval Weapons Center
China Lake CA 93555-6001
(619) 939-1630
AV437-1630

Dr John Bahns
AFAL/LKCS
Stop 24
Edwards AFB CA 93523-5000

Dr William F Bailey
AFIT/ENP
Wright-Patterson AFB OH 45433-6583
(513) 255-4498
AV785-4498

Dr Joseph D. Baum
Naval Research Laboratory
Laboratory for Computational
Physics, Code 4410
Washington DC 20375
(202) 767-2556

Dr Roger J. Becker
KL-462
Research Institute
University of Dayton
Dayton OH 45469
(513) 229-3938

Mr Charles Beckman
AFAL/MKPA
Stop 24
Edwards AFB CA 93523-5000
(805) 275-5487
AV525-5487

Dr Merrill Beckstead
Dept of Chemical Engineering
Brigham Young University
Provo UT 84602
(801) 378-6239

Dr Robert Beddini
Univ of Illinois
AAE Department
104 South Mathews Avenue
Urbana IL 61801-2997
(217) 333-4239

Dr Clifford Bedford
SRI International
Chemistry Laboratory
Menlo Park CA 94025
(415) 859-4449

Dr S. J. Bennett
Adv Technology Projects Div
Morton Thiokol, Inc, Wasatch
Box 524
Brigham City UT 84302
(801) 863-2980

Dr Oscar Biblarz
Department of Aeronautics
Naval Post Graduate School
Monterey CA 93943-5100
(408) 646-2972
AV878-2972

Mr Robert A. Biggers
AFAL/XRX
Stop 24
Edwards AFB CA 93523-5000
(805) 275-5241
AV525-5341

Dr S Binkley
Combustion Research Facility
Sandia National Laboratories
Livermore CA 94550

Dr Mitat A Birkan
AFOSR/NA
Bolling AFB DC 20332-6448
(202) 767-4938
AV297-4938

Dr Arthur Bracut
ARDC
LCWSL
Dover NJ 07801
(201) 724-3788
AV880-3788

Dr Mel Branch
Mechanical Engineering Dept
University of Colorado
Boulder CO 80309-0427
(303) 492-6318
(303) 492-7151

Dr Tom Brill
University of Delaware
Department of Chemistry
Newark DE 19716
(302) 451-2466

Dr Bruce M. Broline
PO Box 3999
M/S 82-23
Boeing Aerospace
Seattle WA 98042
(206) 773-5846

Dr Robert S. Brown
United Technologies Corp
Chemical Systems Division
P. O. Box 49028
San Jose CA 95161-9028
(408) 778-4680

Dr James T. Bryant
Naval Weapons Center
China Lake CA 93555-6001
(619) 939-7206
AV437-7206

Dr Rodney L Burton
Director, Space Applications
GT Devices, Inc
5705A General Washington Drive
Alexandria VA 22312
(703) 642-8150

Mr David Byers
NASA Lewis Research Center
MS 500-219
21000 Brookpark Road
Cleveland OH 44135-3127
(216) 433-2447

Dr George Caledonia
Physical Sciences Inc
PO Box 3100
Andover MA 01810
(617) 475-9030

Dr David Campbell
AFAL/DYC
Stop 24
Edwards AFB CA 93523-5000

Dr Robert Cassel
Naval Sea Systems Command
Code 62D
Washington DC 20362
(202) 692-8635

Dr Robert J. Cattolica
Sandia National Laboratories
Division 9351
Livermore CA 94550

Dr Leonard Caveny
OSD/SDIO/IST
Pentagon
Washington DC 20301-7100
(202) 693-1530

Dr May Chan
Naval Weapons Center
China Lake CA 93555-6001
(619) 939-7519
AV437-7519

Dr Franklin R Chang-Diaz
Lyndon B Johnson Space Center
Code CB
Houston TX 77058
(713) 483-2321

Dr Robert Chapman
AFAL/LKLR
Stop 24
Edwards AFB CA 93523-5000
(805) 275-5416
AV525-5416

Dr Malcolm Chase
Center for Chemical Physics
National Bureau of Standards
Building 222, Room A158
Gaithersburg MD 20899
(301) 975-2526

Dr Won-Ho Choe
214 Nuclear Engineering Lab
University of Illinois
103 South Goodwin Avenue
Urbana IL 61801
(217) 333-2821

Dr Karl Christe
Rocketdyne Division
Rockwell International
6633 Canoga Ave
Canoga Park CA 91304
(818) 710-3268

Dr T. J. Chung
 University of Alabama
 Huntsville AL 35801
 (205)895-6394

Dr George M. Clark
 Aerojet Tactical Systems
 PO Box 13400
 Building 0525
 Sacramento CA 95813
 (916)988-6919

Dr William Clark
 Naval Weapons Center
 Code 3895
 China Lake CA 93555-6001

Dr Norman Cohen
 Aerospace Corporation
 PO Box 92957
 M/S 747
 Los Angeles CA 90045
 (213)648-7427

Dr Norman S. Cohen
 Professional Services
 141 Channing St
 Redlands CA 92373
 (714)792-8807

Dr Ronald Cohen
 The Aerospace Corporation
 PO Box 92957
 Mail Stop M5-754
 Los Angeles CA 90009
 (213)336-5946

Dr Cliff Coon
 Lawrence Livermore National
 Laboratories
 Livermore CA 94550
 (415)422-6311

Cpt Edward N. Coppola
 AFAL/MKPA
 Stop 24
 Edwards AFB CA 93523-5000
 (805)275-5534
 AV525-5534

Mr Robert Corley
 AFAL/DYC
 Stop 24
 Edwards AFB CA 93523-5000
 (805)275-5353
 AV525-5353

Dr L. Cottle
 RARDE, Fort Halstead
 Knockholt
 Matternrks Kent UK

Dr F E C Culick
 Engrg and Appl Sci Dept
 California Institute of
 Technology
 Pasadena CA 91125
 (818)356-4470

Dr C L Dailey
 TRW Space and Technology Group
 Applied Technology Division
 One Space Park
 Redondo Beach CA 90278
 (213)536-1874

Dr B R Daniel
 School of Aerospace Rnrg
 Georgia Institute of
 Technology
 Atlanta GA 30332

Mr S T Demetriades
 STD Research Corp
 P.O. Box C
 Arcadia CA 91006
 (818)357-2311

Dr. John O. Dimmock
AFOSR/CD
Bolling AFB DC 20332-6448
(202) 767-5018
AV297-5018

Col. Alan J. Driscoll
AFOSR/CC
Bolling AFB DC 20332-6448
(202) 767-5017
AV297-5017

Dr Joel Dubow
Materials Science
Univ of Utah
2008B Mechanical Engrg Bldg
Salt Lake City UT 84112
(801) 581-8388

Dr. J. T. Edwards
AFAL/DYCR
Stop 24
Edwards AFB CA 93523-5000
(805) 275-5656
AV525-5656

Dr John Eisch
Department of Chemistry
State University of New York
Binghamton NY 13901
(607) 798-3994

Dr John Fischer
Code 3853
Naval Weapons Center
China Lake CA 93555-6001
(619) 939-1641
AV437-1641

Dr J. E. Flanagan
Rocketdyne
6633 Canoga
Canoga Park CA 91304
(818) 710-2466

Dr Arthur Fontijn
Chemical Environmental
Engineering Department
Rensselaer Polytechnic Inst.
Troy NY 12180-3590
(518) 266-6508

Dr Milt Frankel
Rocketdyne
6633 Canoga Avenue
Canoga Park CA 91304
(818) 710-4803
(818) 710-5088

Dr Sheilah K. Fultz
Naval Weapons Center
China Lake CA 93555-6001
(619) 939-7521
AV437-7521

Mr Robert Geisler
AFAL/YS
Edwards AFB CA 93523-5000
(805) 275-5230
AV525-5230

Dr Eugene Gerber
Univ of Dayton Research
Institute
KL465
Dayton OH 45419
(513) 229-3221

Dr. Robert Ghirardelli
U.S. Army Research Office
P.O. Box 12211
Research Triangle Pk NC 27709-2211
(919) 549-0641
AV935-3331

Dr B. B. Goshgarian
AFAL/MKPB
Stop 24
Edwards AFB CA 93523-5000
(805) 275-5183
AV525-5183

Dr William H Graham
 Morton Thiokol, Inc
 Huntsville Division
 Huntsville AL 35807-7501
 (205) 882-8397

Dr Alten Grandt
 Department of Aeronautics
 and Astronautics
 Purdue University
 West Lafayette IN 47907

Dr John Guimont
 Chemistry Division
 United Technologies Corp
 P. O. Box 50015
 San Jose CA 95150-0015

Mr Eugene Haberman
 AFAL/MK
 Stop 24
 Edwards AFB CA 93523-5000
 (805) 275-5420
 AV525-5420

Dr Elmer Hansen
 Department of Mechanical
 Engineering
 University of Florida
 Gainesville FL 32611
 (904) 392-0802

Dr David Hastings
 Department of Aeronautics
 and Astronautics
 Massachusetts Inst of Tech
 Cambridge MA 02139

Dr Clark Hawk
 AFAL/LK
 Stop 24
 Edwards AFB CA 93523-5000
 (805) 275-6530
 AV525-6530

Dr Rich Hollins
 Naval Weapons Center
 China Lake CA 93555-6001
 (619) 939-1650
 AV437-1650

Maj E S Huston
 AFAL/LKC
 Edwards AFB CA 93523-5000
 (805) 275-5476
 AV525-5476

Dr J. I. Jagoda
 Aerospace Engineering Dept
 Georgia Institute of
 Technology
 Atlanta GA 30329
 (404) 894-3060

Dr Donald Jassowski
 Aerojet Technical Systems Co
 PO Box 13222
 Sacramento CA 95813
 (916) 355-2849

Dr Jay B. Jeffries
 Molecular Physics Lab
 SRI International
 333 Ravenswood Avenue
 Menlo Park CA 94025
 (415) 859-6341

Dr S M Jeng
 University of Tennessee
 Space Institute
 Tullahoma TN 37388

Mr Arch Johnston
 AFAL/DYC
 Stop 24
 Edwards AFB CA 93523-5000
 (805) 275-5441
 AV525-5441

Dr Jordin Kare
Building 197, Room 1020
Lawrence Livermore Nat'l Lab
P O Box 808
Livermore CA 94550
(415) 423-8300

Dr Myron Kaufman
Department of Chemistry
Emory University
Atlanta GA 30322
(404) 727-6619

Dr Dennis Keefer
University of Tennessee
Space Institute
Tullahoma TN 37388
(615) 455-0631

Dr Sue Kim
California State University
6000 J Street
Sacramento CA 95819
(916) 454-6712

Dr David King
Mail Stop 125-224
Jet Propulsion Laboratory
4800 Oak Grove Drive
Pasadena CA 91103
(818) 354-3315

Dr Merrill K. King
Atlantic Research Corp
5390 Cherokee Ave
Alexandria VA 22312
(703) 642-4217

Dr Kenneth Kolouko
Morton Thiokol
Wasatch Division
P.O. Box 524
Brigham City UT 84302
(801) 863-4220

Dr James J. Komar
Atlantic Research Corp
5390 Cherokee Avenue
Alexandria VA 23312
(703) 642-4473

Dr Herman Krier
Dept of Mechanical and
Industrial Engineering
University of Illinois
Urbana IL 61801
(217) 333-0529

Dr Warren A. Krueger
167 Alvana Street, NW16-160
Massachusetts Institute of
Technology
Cambridge MA 02139
(617) 253-0236

Dr Bill Larsen
AFAL/YSC
Edwards AFB CA 93523-5000
(805) 275-5657
AV525-5657

Dr Jack Lawless
Space Power, Inc.
1977 Concourse Drive
San Jose CA 95131
(408) 434-1671

Dr Miller Layton
AFAL/LKLR
Stop 24
Edwards AFB CA 93523-5000

Dr Ja H Lee
NASA Langley Research Center
M/S493
Hampton VA 23665
(804) 865-4332

Dr George A. Lo
 Lockheed Palo Alto Research
 Laboratory
 3251 Hanover St, 8204-93-50
 Palo Alto CA 94304
 (415) 424-2514

Dr Geoffrey Main
 School of Mechanical Engrg
 Georgia Institute of
 Technology
 Atlanta GA 30332-0420
 (404) 894-3242
 (404) 951-8058

Dr David M. Mann
 Army Research Office
 P.O. Box 12211
 Research Triangle Pk NC 27709-2211
 (919) 549-0641
 AV935-3331

Professor Alan P Marchand
 Dept of Chemistry
 North Texas State Univ
 NTSU Station, Box 13767
 Denton TX 76203-5068
 (817) 565-3823

Dr Stephen B Margolis
 Combustion Research Facility
 Sandia National Laboratories
 Livermore CA 94550
 (415) 294-

Dr Manuel Martinez-Sanchez
 Aeronautics and Astronautics
 Massachusetts Inst of Tech
 Building 37-401
 Cambridge MA 02139
 (617) 253-5613

Dr Peter Mattern
 Combustion Sciences
 Sandia National Laboratories
 Livermore CA 94550

Dr Anthony J. Matuszko
 AFOSR/NC
 Bolling AFB DC 20332-6448
 (202) 767-4963
 AV297-4963

Dr Jyotirmoy Mazumder
 Department of Mechanical and
 Industrial Engineering
 University of Illinois
 Urbana IL 61801
 (217) 333-1964

Dr Kenneth P. McCarty
 Hercules Inc
 Magna UT 84044
 (801) 250-5911
 ext 23360

Dr John McVey
 Rasor Associates, Inc
 253 Humboldt Court
 Sunnyvale CA 94086
 (408) 734-1622

Dr Franklin Mead
 AFAL/LK
 Edwards AFB CA 93523-5000
 (805) 275-5540
 AV525-5540

Dr Carl F. Melius
 Sandia National Laboratories
 Livermore CA 94550
 (415) 294-2650

Dr Charles L. Merkle
 205 ME
 Pennsylvania State University
 University Park PA 16802
 (814) 863-1501

Dr Claude Merrill
 AFAL/MKPL
 Stop 24
 Edwards AFB CA 93523-5000
 (805) 275-5169
 AV525-5169

Dr Michael M. Micci
 233 Hammond Building
 Pennsylvania State University
 University Park Pa 16802
 (814) 863-0043

Dr Richard S. Miller
 Office of Naval Research
 Mechanics Division, Code 432
 800 North Quincy Street
 Arlington VA 22217-5000
 (202) 696-4403

Dr. Robert Moriarty
 University of Illinois
 (Chicago Circle)
 Department of Chemistry
 Chicago IL 60680
 (312) 996-2364

Dr Marlow D. Moser
 AFAL/DYCC
 Stop 24
 Edwards AFB CA 93523-5000
 (805) 275-5442
 AV525-5442

Dr Kenneth G Moses
 Plasma Technology Division
 JAYCOR
 3547 Voyager Street, Suite 104
 Torrance CA 90503-1667
 (213) 542-3800

Dr Philip Muntz
 Dept. of Aerospace Engineering
 University of Southern
 California
 Los Angeles CA 90089

Dr S N B Murthy
 Dept of Mechanical Engineering
 Purdue University
 West Lafayette IN 47907
 (317) 494-1509
 (317) 494-5639

Dr Subhash Narang
 Chemistry Laboratory
 SRI International
 333 Ravenswood Avenue
 Menlo Park CA 94025

Dr Lori A. Newhouse
 AFAL/DYCC
 Stop 24
 Edwards AFB CA 93523-5000
 (805) 275-5305
 AV525-5305

Dr Arnold T. Nielsen
 Naval Weapons Center
 China Lake CA 93555-6001
 (619) 939-1614
 AV437-1614

Col James R Nunn
 AFAL/CC
 Edwards AFB CA 93523-5000

Dr Douglas B. Olson
 AeroChem Research Laboratories
 Inc.
 P. O. Box 12
 Princeton NJ 08542
 (609) 921-7070

Dr Tae-Woo Park
 AFAL/TODP
 Stop 24
 Edwards AFB CA 93523-5000
 (805) 275-5196
 AV525-5196

Dr Kenneth Philippart
 AFAL/DYCC
 Stop 24
 Edwards AFB CA 93523-5000
 (805) 275-5419
 AV525-5419

Lt Col Homer Presley
 AFAL/LK
 Edwards AFB CA 93523-5000
 (805) 275-6530
 AV525-5630

Dr Richard Priem
 Priem Consultants
 13533 Mohawk Trail
 Cleveland OH 44130
 (216) 845-1083

Dr Robert A. Rhein
 Naval Weapons Center
 China Lake CA 93555-6001
 (619) 939-7392
 AV437-7392

Dr Frank Roberto
 AFAL/MKP
 Stop 24
 Edwards AFB CA 93523-5000
 (805) 275-5430
 AV525-5430

Mr Wayne Roe
 AFAL/XRX
 Stop 24
 Edwards AFB CA 93523-5000
 (805) 275-5206
 AV525-5206

Dr S D Rosenberg
 P O Box 13222
 Sacramento CA 95813
 (916) 355-2609

Dr Leanne Pitchford
 GTE Laboratories
 40 Sylvan Road
 Waltham MA 02254
 (617) 466-2704

Dr Edward Price
 School of Aerospace Engrg
 Georgia Institute of
 Technology
 Atlanta GA 30332-0420
 (404) 894-3063

Dr Russell Reed
 Naval Weapons Center
 China Lake CA 93555-6001
 (619) 939-7296
 AV437-7296

Dr J W Rich
 Department of Mechanical
 Engineering
 The Ohio State University
 Columbus OH 43212-1194
 (614) 292-6309

Dr Stephen Rodgers
 AFAL/LKLR
 Stop 24
 Edwards AFB CA 93523-5000
 (805) 275-5416
 AV525-5416

Dr David Rosen
 Physical Sciences Inc.
 Dascom Research Park
 Andover MA 01810
 (617) 475-9030

Dr Kevin Rudolph
 Martin Marietta Corporation
 Mail Stop S8071
 PO Box 179
 Denver CO 80201
 (303) 977-3681

Dr. Michael J. Salkind
 AFOSR/NA
 Bolling AFB DC 20332-6448
 (202) 767-0467
 AV297-0467

Dr Robert Schmitt
 Chemistry Lab
 SRI International
 333 Ravenswood Avenue
 Menlo Park CA 94025
 (415) 859-5579

Dr Keith Schofield
 Quantum Institute
 University of California,
 Santa Barbara
 Santa Barbara CA 93106

Dr Herbert Schrade
 Institut Fur Raumfahrtantriebe
 Universitat Stuttgart
 Pfaffenwaldring 31
 D-7000 Stuttgart GE
 7116-852-383
 or 375

Dr Gary I. Sega
 Aerospace Corp
 P.O. Box 92957
 MS/747
 Los Angeles CA 90004
 (213) 648-6501

Dr Pam Sherrett
 Naval Weapons Center
 China Lake CA 93555-6001
 (619) 939-7392
 AV437-7392

Dr R Shoureshi
 School of Mechanical
 Engineering
 Purdue University
 West Lafayette IN 47907
 (317) 494-5639

Prof Jean'ne M. Shreeve
 Dept of Chemistry
 University of Idaho
 Moscow ID 83843
 (208) 885-6552

Lt Col LaRell Smith
 EQARD/LRC
 Box 14
 FPO NY 09510-0200
 AV235-4505

Dr Warren Strahle
 School of Aerospace Engrg
 Georgia Institute of
 Technology
 Atlanta GA 30332
 (404) 894-3032

Dr V V Subramaniam
 Department of Mechanical
 Engineering
 The Ohio State University
 Columbus OH 43212-1194
 (614) 292-6096

Dr. Mostafa Talukder
 AFAL/LKLR
 Edwards AFB CA 92397-5000
 (805) 275-5416
 AV525-5416

Dr James Tien
 Case Western Reserve
 University
 Glennan Building, Room 415
 Cleveland OH 44106
 (216) 368-4581

Professor William C Troglar
 Department of Chemistry
 University of California, San
 Diego
 LaJolla CA 92093
 (619) 452-6175

Dr Peter Turchi
 RD Associates
 301 S West Street
 Alexandria VA 22314
 (703) 684-0333

Mr Gary L. Vogt
 AFAL/DYCR
 Stop 24
 Edwards AFB CA 93523-5000
 (805) 275-5258
 AV525-5258

Dr Robert Vondra
 PO Box 596
 Wrightwood CA 92397
 (619) 249-3451

Dr Nzoo Vu
 Naval Weapons Center
 China Lake CA 93555-6001
 (916) 939-7392
 AV437-7392

Dr R H Woodrow Waesche
 Atlantic Research Corporation
 7511 Wellington Road
 Gainesville VA 22065

Dr Peter Wayner
 Dept of Chemical and
 Environmental Engineering
 Rensselaer Polytechnic Inst
 Troy NY 12180-3590
 (518) 266-6199

Dr David P Weaver
 AFAL/DYCR
 Edwards AFB CA 93523-5000
 (805) 275-5657
 AV525-5657

Dr Jim Weber
 Rocketdyne Division
 Rockwell International Corp.
 6633 Canoga Ave
 Canoga Park CA 91303
 (818) 710-5558

Dr Richard Weiss
 AFAL/CA
 Edwards AFB CA 93523-5000
 (805) 275-5622
 AV525-5622

Dr Rodney Willer
 Morton Thiokol Inc
 Elkton Division
 P.O. Box 241
 Elkton MD 21921
 (301) 398-3000
 (301) 398-4440

Dr D O Woolery
 Rocketdyne
 6633 Canoga Avenue
 Canoga Park CA 91304

Dr Ted F. Yang
 Massachusetts Institute of
 Technology
 167 Albany Street
 Cambridge MA 02139
 (617) 253-8453

Dr Vigor Yang
 Department of Mechanical
 Engineering
 Pennsylvania State University
 University Park PA 16802

Dr Tom York
 Department of Aeronautics and
 Astronautics
 The Ohio State University
 Columbus OH 43212
 (614) 292-7354

Dr Ben T. Zinn
School of Aerospace Engrg
Georgia Institute of
Technology
Atlanta GA 30332
(404)894-3033

Cpt Joseph Zirrolli
FJSRL/NC
United States Air Force
Academy
Colorado Springs CO 80840
(303)472-2655

AGENDA

1988 AFOSR CONTRACTORS MEETING ON DIAGNOSTICS OF REACTING FLOW

14-15 June 1988

Howard Johnson Plaza-Hotel
Monrovia, CA

Tuesday, 14 June

1:15	Welcome and Administrative Announcements
------	--

Session Topic:	Liquid/Solid Measurements
----------------	---------------------------

Chairman:	J. M. Tishkoff, AFOSR
-----------	-----------------------

1:30	Investigations of the Applications of Laser-Induced Exciplex Fluorescence to Fuel Spray and Single Droplet Vaporization L. A. Melton, University of Texas, Dallas	135
2:00	Nonlinear Spectroscopy of Multicomponent Droplets and Two- and Three-Dimensional Measurements in Flames R. K. Chang, Yale University	139
2:30	Multiple Scattering and the Inverse Fraunhofer Diffraction Particle Sizing Problem E. D. Hirleman, Arizona State University	143
3:00	BREAK	
3:30	Diagnostics for Research in Atomization and Turbulent Two-Phase Flow W. D. Bachalo, Aerometrics, Inc.	147
4:00	Air Force Spray Research A. S. Nejad and T. A. Jackson, AFWAL	Abstract Not Available
4:30	Surface Thermometry of Energetic Materials by Laser-Induced Fluorescence L. P. Goss, Systems Research Laboratories, Inc.	151
5:00	RECESS	

Wednesday, 15 June

8:15	Administrative Announcements
------	------------------------------

Session Topic:	Gas-Phase and Plasma Measurements
----------------	-----------------------------------

Chairman:	B. Ganguly, AFWAL
-----------	-------------------

8:30	Multiphoton Detection Techniques for F and F2 W. K. Bischel, SRI, International	155
9:00	Asynchronous Optical Sampling for Laser-Based Combustion Diagnostics in High-Pressure Flames G. B. King, N. M. Laurendeau and F. E. Lytle Purdue University	159
9:30	Nonlinear Spectroscopy of Multicomponent Droplets and Two- and Three-Dimensional Measurements in Flames M. B. Long, Yale University	163
10:00	BREAK	
10:20	Advanced Diagnostics for Reacting Flows R. K. Hanson, Stanford University	167
11:00	Laser Spectroscopy of Plasmas J. W. Daily, University of California, Berkeley	171
11:30	Measurement of Excitation Temperature and Electron Energy Relaxation Profiles B. Ganguly, AFWAL	175
12:00	LUNCH	
Administrative Session		
1:30	AFAL Research Interests R. R. Weiss, Chief Scientist, AFAL	
2:15	Dr. Michael J. Salkind, AFOSR/NA	
2:30	BREAK	
3:00	AFOSR Rocket Propulsion Interests M. A. Birkan, AFOSR/NA	
3:20	AFOSR Interests in Airbreathing Propulsion and Diagnostics of Reacting Flow J. M. Tishkoff, AFOSR/NA	193
3:40	Open Discussion of Government Support for Propulsion Research	
4:30	GENERAL ADJOURNMENT	

4:30 **Business Meeting**
 AFOSR Contractors Only

7:00 - ? **BANQUET**

QUANTITATIVE USE OF EXCIPLEX-BASED
VAPOR/LIQUID VISUALIZATION SYSTEMS

ARO Contract DAAL-87-K-0120

Principal Investigator:

Lynn A. Melton
Department of Chemistry
University of Texas at Dallas
P. O. Box 830688
Richardson, Texas 75083

SUMMARY/OVERVIEW

This report describes the development of a users manual for exciplex-based vapor/liquid visualization systems. The manual is intended to summarize all the photophysical functions and parameters specific to the exciplex system which will be needed by a user who is otherwise skilled with planar laser induced fluorescence. In addition, the major assumptions required for the derivations are identified, the experimental conditions under which near quantitative interpretation of the fluorescence is possible are stated,, and protocols for visualization experiments are recommended.

The best visualization systems developed so far are based on the exciplex formed between N,N,N',N'-tetramethyl-p-phenylene-diamine (TMFD) and 1-Methylnaphthalene or Naphthalene. For these systems, when used with n-tetradecane as the solvent (fuel), it should be possible to measure the liquid and vapor mass concentrations in a volume element of a fuel spray with absolute accuracies of approximately $\pm 25\%$, provided that oxygen is excluded. The functions and parameters given in the manual are those appropriate for these two systems.

TECHNICAL DISCUSSION

A. Basic Photophysics of Exciplex-Based Vapor/Liquid Visualization systems

All exciplex-based vapor/liquid visualization systems are based on the following reversible reaction



where M^* is the first excited singlet state of a fluorescent organic molecule, the monomer M , which is generally but not always an aromatic molecule, G is an appropriately chosen ground state reaction partner, and E^* is the exciplex. An

exciplex -- shortened from excited state complex -- is significantly bound in the excited state, with binding energies of 4-20 kcal/mole, but has no significant binding energy between the ground state molecules M and G. Thus, since E* is bound with respect to separated M* and G and emits to the same ground state, its emission is necessarily redshifted with respect to the M* emission, and this shift may be as much as 100-200 nm.

By setting the concentration of G in the liquid phase sufficiently high, it is possible to drive the equilibrium in equation (1) far to the right, i.e., the emission of E* from the liquid may be a hundred times that of M*. In the vapor, the relatively polar exciplex -- an excited state charge transfer complex -- is much less stable, and the concentrations are much lower; as a result, in the vapor the emission from M* may be a hundred times that of E*. These two facts taken together, distinct emissions from M* and E* and the identification of M* emission with the vapor phase and E* emission with the liquid phase, mean that a filter which isolates the M* emission enables one to photograph the vapor pattern, and a filter which isolates the E* emission enables one to photograph the liquid pattern. Thus the control of the monomer/exciplex equilibrium allows the separate two-dimensional, real-time, non-perturbative visualization of the vapor/liquid concentrations in a fuel spray.

B. Recommended Vapor/Liquid Visualization systems

Two exciplex-based vapor/liquid visualization systems are recommended in the manual; they are based upon the exciplex formed between N,N,N',N'-tetramethyl-p-phenylene-diamine (TMFD) and naphthalene (N) or 1-methylnaphthalene (1MN). The first system, 1 TMFD/10 N/89 T -- the notation means 1% TMFD, 10% N, 89% tetradecane (T) by weight -- is the exciplex with which we have the most experience. The second system, 1 TMFD/10 1MN/89 T, which uses 1MN to provide a better match of boiling points, is expected to be very similar photophysically to the first. Although much of the characterization of the first exciplex system has been done with hexadecane as the solvent, the substitution of tetradecane is not expected to alter the photophysical properties significantly. These compounds are all available commercially. These systems have also been tested in JP4, Jet-A, DF-2, as well as four experimental gas turbine fuels. In general they continue to work well, with the notable exceptions that TMFD does not track the evaporation of the very volatile JP4 and that DF-2 is optically thick at the appropriate excitation wavelengths.

C. Relation of Measured Fluorescence to Vapor and Liquid Concentrations

The equations which relate the incident laser intensity, $I(z_0, L_{ex})$, and the measured fluorescence intensity, $S_v(x, y, z_0, L, DL)$, are given below:

$$\begin{aligned} S_v(x, y, z_0, L_{ex}, DL) / I(z_0, L_{ex}) &= \\ B_l(L_{ex}) * M_l(x, y, z_0) + B_v(L_{ex}) * M_v(x, y, z_0) & \quad (2a) \end{aligned}$$

$$\begin{aligned} S_v(x, y, z_0, L_w, DL) / I(z_0, L_{ex}) &= \\ B_l(L_w) * M_l(x, y, z_0) + B_v(L_w) * M_v(x, y, z_0) & \quad (2b) \end{aligned}$$

where $B_l(L_{ex})$, $B_v(L_{ex})$, $B_l(L_w)$, and $B_v(L_w)$ are the specific emission strengths for the liquid or vapor (l or v) measured at the exciplex emission maximum (L_{ex}) or monomer emission maximum (L_w), respectively. $M_l(x, y, z_0)$ and $M_v(x, y, z_0)$ are the total liquid mass and the total vapor mass in the volume element centered at (x, y, z_0) , respectively.

The proposed visualization systems have been designed so that there exist wavelengths L_{ex} and L_w such that emission at L_{ex} is almost entirely from the liquid and emission at L_w is almost entirely from the vapor. Thus, at L_{ex} the first term in the sum in equation (2a) dominates the measured fluorescence signal, and at L_w the second term in equation (2b) dominates the signal.

Equation (2a) and (2b) implicitly include the following assumptions:

A1) The radial gradients of temperature and composition within droplets can be neglected.

A2) The droplet temperature and composition do not depend on the droplet size.

A3) Morphological resonances are negligible in both the absorption and fluorescence processes.

A4) The temperature dependence of the liquid phase density, absorptivities, and fluorescence quantum yields can be neglected.

A5) The liquid phase composition is independent of time, and the material evaporating from the droplets -- M, G, and Fuel -- does so at the composition of the droplet.

A6) The spray is optically thin, i.e., weakly absorbing and weakly scattering, so that the incident laser intensity is essentially constant across the spray.

The report includes calculations, estimations, and/or measurements for all the quantities required for the computation of the $B(L)$ coefficients in equation (2). It specifically addresses the following elements:

- 1) Calculation of the distribution of excited states inside a droplet, the calculation of the probability of emission into a specified lens aperture as a function of position in the droplet, and the convolution of these quantities to obtain the total liquid phase emission;
- 2) Presentation of fluorescence spectra, corrected for detector spectral response, which can be convoluted with a user's spectral response/filter function;
- 3) Measurements of the liquid phase quantum yield as a function of temperature and measurements of the vapor phase quenching of TMPD* by O₂, CO₂, and TMPD;
- 4) Choice of excitation and emission wavelengths; and
- 5) Estimation of degree to which the vapor phase composition bears a fixed and known relation to the initial liquid phase composition.

D. Recommended Experimental Protocols

Protocol 1: The use of the exciplex-based vapor/liquid visualization systems is recommended only for spray systems in which oxygen is excluded, both in the vapor and in the liquid.

Protocol 2: The quantitative interpretation of the intensities measured using the exciplex-based vapor/liquid visualization systems should only be attempted if the spray system is optically thin, i.e., the absorption and scattering are sufficiently weak that the laser beam is not significantly attenuated in crossing the spray.

Protocol 3: The chemicals described in the manual are commercially available, and may be probably be used as received. They have generally low toxicity.

Protocol 4: It is recommended that, where possible, users calibrate the sensitivity of their detection system using direct calibration methods instead of the relatively complex photophysical function/parameter methods described in the report.

ACKNOWLEDGEMENTS

The manual described in this report was prepared as a final report for ARO contract DAAL03-86-K-0082. It also incorporates results obtained under AFOSR grant 83-0307, ARO contract DAAG29-84-C-0010, and AFWAL contract F33615-85-C-2515. Dr. David Mann of ARO and Dr. Julian Tishkoff of AFOSR have provided continued encouragement during these projects.

NONLINEAR SPECTROSCOPY OF MULTICOMPONENT DROPLETS

AFOSR Grant No. 88-0100

Co-Principal Investigator: Richard K. Chang

Yale University
Section of Applied Physics and Center for Laser Diagnostics
New Haven, Connecticut 06520

SUMMARY/OVERVIEW

Nonintrusive in-situ optical diagnostic techniques of the chemical species and physical properties of multicomponent liquid droplets in a spray combustor require a fundamental understanding of linear and nonlinear optical interactions with individual droplets of various sizes and shapes. Our research is directed toward the understanding of nonlinear interactions with a high-intensity laser beam which leaves the droplet intact and provides information on its chemical content and physical characteristics. Further, our research is directed toward the understanding of laser-induced breakdown (LIB) mechanisms that lead to plasma formation, explosive vaporization, and droplet shattering.

TECHNICAL DISCUSSION

The spherical liquid-air interface of a droplet acts as a lens to concentrate the incident plane wave just within the droplet shadow face and to focus the incident wave just outside the droplet shadow face. The internal and external intensity distributions and the intensity enhancements have been calculated when the droplet circumference-to-wavelength ratio is not equal to a specific morphology-dependent resonance.¹ The internal high-intensity region greatly increases nonlinear optical interactions of the liquid while the internal and external high-intensity regions greatly decrease the LIB threshold of the liquid and/or the surrounding gas. The internal high-intensity region gives rise to a large gradient of the intensity (∇I) and thus causes laser-induced electrostriction. Figure 1 shows the effect of such electrostriction on a CCl₄ droplet irradiated by a flashlamp pumped dye laser beam. The laser-induced electrostrictive force opposes the surface tension force and causes the droplet to bulge at the shadow face. The surface tension and the bulk viscosity of the droplet can be deduced from the bulge amplitude and the subsequent droplet shape oscillation frequency.

The spherical liquid-air interface of a droplet also acts as an optical cavity for the internally generated radiation, such as Raman scattering, Brillouin scattering, and fluorescence. We have measured the lifetime of photons trapped within the droplet using mode-locked laser pulses of 100 psec and a streak camera with 1 psec resolution. The measured lifetime (as long as several nanoseconds) was found to be input-intensity dependent, implying that photons within the droplet have two decay mechanisms:²

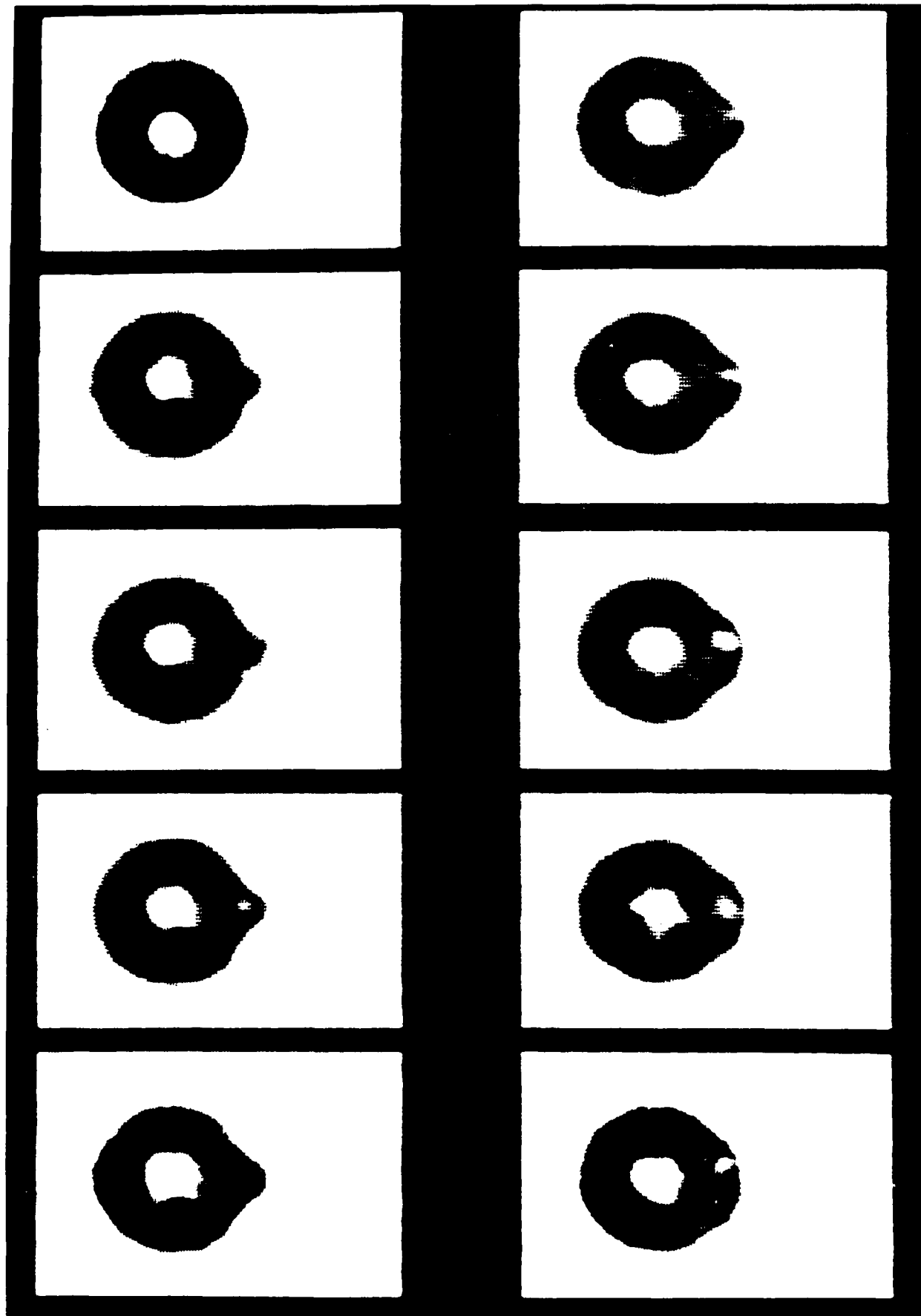


Fig. 1. Shadowgraphs of a CCl_4 droplet ($a \approx 50 \mu\text{m}$) irradiated by a flashlamp pumped dye laser beam traveling from left to right ($\lambda = 620 \text{ nm}$, 400 ns pulse duration, and 20 mJ intercepted by the droplet).

(1) leakage from the droplet, depending on the Q factor of the morphology-dependent resonance and (2) depletion of the photons with frequency ω_1 via nonlinear optical conversion to ω_2 . Another manifestation of the droplet cavity effect is the delay time between the buildup of the stimulated Raman scattering and the incident pump laser pulse. A time delay was observed only between the first-Stokes pulse and the input laser pulse, while no time delay was noted between the higher-order Stokes and the first-Stokes pulses.³ Such time delays can be explained by the standard four-wave-mixing theory that is accepted for liquids contained in a large optical cell. As the internally trapped radiation makes many full trips around the droplet rim, four-wave mixing can also lead to time-varying-index modulation, i. e., through the intensity-dependent index of refraction effect, $n = n_0 + n_2 I(t)$. The presence of a time-varying-index modulation was confirmed by noting that the increased linewidth of the stimulated Raman scattering spectrum was intensity dependent.⁴

The lens effect of the droplet greatly lowers the LIB intensity threshold, e. g., by as much as three orders of magnitude compared to the LIB intensity threshold of clean air without any droplets. The LIB intensity threshold in nonabsorbing liquid droplets sets an upper limit on the amount of laser intensity that can be used for laser diagnostics of sprays in a combustor. An experimental research program was set up to further our understanding of LIB mechanisms.

Using a spatially resolved plasma emission spectroscopic technique (consisting of a spectrograph and a two-dimensional detector at its exit plane), we determined the following properties of the LIB plasma: (1) the location of LIB initiation which can be inside the shadow face in the liquid or outside the shadow face in the surrounding gas;⁵ and (2) the time-averaged electron density and atomic temperature of the plasma plumes ejected from the shadow and illuminated faces.⁶ Using a novel spatially and time-resolved plasma emission detection technique, we determined the propagation velocity of the plasma front traveling toward the laser either within the droplet from the shadow face or outside the droplet from the illuminated face.^{7,8} The droplet and the emerging vapor were photographed with a framing camera after the droplet was irradiated by a high-intensity laser beam which caused LIB.⁹

Based on all our experimental results on the plasma created by the LIB process, we conclude that the most plausible LIB process consists of (1) multiphoton ionization, which produces the few initial electrons and (2) cascade multiplication, which produces many electrons and, therefore, a dense plasma. Depending on the droplet size and the LIB threshold of the liquid and surrounding gas, LIB can be initiated within the droplet or outside it. Once the LIB threshold is reached within the droplet, the resultant plasma transforms the original transparent droplet into an absorbing droplet, initially at the shadow face region and then in other regions toward the illuminated face. The expanding plasma continues to absorb the laser radiation, causing the plasma to be sustained and to propagate as an optical detonation wave. After the laser pulse is shut off, the plasma continues to propagate toward the laser as a shock wave that decays rapidly. A summary of our LIB results will be published in the June 15th issue of Applied Optics.¹⁰

REFERENCES

1. D.S. Benincasa, P.W. Barber, J.-Z. Zhang, W.-F. Hsieh, and R.K. Chang, "Spatial Distribution of the Internal and Near-Field Intensities of Large Cylindrical and Spherical Scatterers," *Appl. Opt.* 26, 1348 (1987).
2. J.-Z. Zhang, D.H. Leach, and R.K. Chang, "Photon Lifetime within a Droplet: Temporal Determination of Elastic and Stimulated Raman Scattering," *Opt. Lett.*, 13, 270 (1988).
3. W.-F. Hsieh, J.-B. Zheng, and R.K. Chang, "Time Dependence of Multiorder Stimulated Raman Scattering from Single Droplets," *Opt. Lett.*, in press.
4. S.-X. Qian and R.K. Chang, "Phase-Modulation-Broadened Line Shapes from Micrometer-Size CS₂ Droplets," *Opt. Lett.* 11, 371 (1986).
5. W.-F. Hsieh, J.H. Eickmans, and R.K. Chang, "Internal and External Laser-Induced Avalanche Breakdown of Single Droplets in an Argon Atmosphere," *J. Opt. Soc. Am. B* 4, 1816 (1987).
6. J.H. Eickmans, W.-F. Hsieh, and R.K. Chang, "Plasma Spectroscopy of H, Li, and Na in Plumes Resulting from Laser-Induced Droplet Explosion," *Appl. Opt.* 26, 3721 (1987).
7. W.-F. Hsieh, J.-B. Zheng, C.F. Wood, B.T. Chu, and R.K. Chang, "Propagation Velocities of Laser-Induced Plasma inside and outside a Transparent Droplet," *Opt. Lett.* 12, 576 (1987).
8. J.-B. Zheng, W.-F. Hsieh, S.-C. Chen, and R. K. Chang, "Temporally and Spatially Resolved Spectroscopy of Laser-Induced Plasma from a Droplet," *Opt. Lett.*, in press.
9. J.-Z. Zhang, J.K. Lam, C.F. Wood, B.T. Chu, and R.K. Chang, "Explosive Vaporization of a Large Transparent Droplet Irradiated by a High Intensity Laser," *Appl. Opt.* 26, 4731 (1987).
10. R.K. Chang, J.H. Eickmans, W.-F. Hsieh, C.F. Wood, J.-Z. Zhang, and J.-B. Zheng, "Laser-Induced Breakdown in Large Transparent Water Droplets," *Appl. Opt.*, in press.

MULTIPLE SCATTERING AND THE INVERSE FRAUNHOFER DIFFRACTION PARTICLE SIZING PROBLEM

AFOSR Grant No. 84-0187

Principal Investigator: E. Dan Hirleman

Mechanical and Aerospace Engineering Department
Arizona State University
Tempe, AZ 85287

SUMMARY/OVERVIEW:

The phenomenon of multiple scattering significantly complicates the analysis of radiation transfer through particulate-laden media. Nonintrusive diagnostics for reacting flows depend on an understanding of light scattering and propagation, and for that reason have often been limited to measurements in optically thin media. Unfortunately, many important measurement applications are in optically dense media, for example in fuel sprays very near the nozzle exit. Similarly, intelligent particle sizing sensors for autonomous operation in next-generation combustion systems will obviously need to at least *detect* the presence of significant multiple scattering which would generally introduce large systematic errors into the measurements. The research proposed here has the much more challenging objective of advancing the scientific understanding of the process to a point where *on-line correction* of the resulting bias errors would be possible, i.e. so that particle size measurements by optical scattering in optically thick media would be feasible.

TECHNICAL DISCUSSION:

One of the most difficult problem areas for future work in optical diagnostics involves measurements in optically thick media. The overall objective of this research is to develop methods to perform inverse scattering measurements of particle size distributions under conditions where multiple scattering is significant. The research involves work in the following four areas: development of an experimental facility for multiple scattering research; verification of a new multiple scattering scaling law; research on inverse multiple scattering algorithms; and research on strategies for "active interrogation" of multiple scattering media.

To develop an understanding of the inverse scattering problem for optically thick media we take the single scattering problem as a baseline and consider the changes in the mathematical formulation of the problem as the optical depth b increases. Intuitively, one would expect that the amount of useful particle size information which can be obtained from an inverse scattering (remote sensing) scheme would be a continuous function of optical depth. Our recent work [1,2] addressed the inverse problem from an information theory point-of-view by consideration of issues such as (1) the maximum amount of useful information about particle populations which can be extracted from forward scattering measurements, and (2) the optimal number and locations of the scattering sensors for the most efficient extraction of this available information. In previous work [2] the optimal scaling of the inverse Fraunhofer problem was derived, and we are using an analogous approach here. To develop this argument, assume that n unique pieces of information (i.e. an estimate of the particle population in n discrete size classes) can be obtained under ideal single scattering conditions. Then as the optical depth is increased, the characteristic single scattering signature which uniquely determines these n data values (degrees of freedom) becomes distorted or blurred since many of the single scattered photons are rescattered into

various directions before reaching the detector. Now the degree to which the single scattering information is garbled should monotonically increase with the probability that photons are multiple scattered before leaving the medium. In other words, as the optical depth is increased the number of unique pieces of information (or degrees of freedom) in the size distribution would gradually decrease from n to $n-1$, then $n-2$, etc.

To develop a theoretical basis to quantify this effect we use the derivations provided in previous stages of this work. Recall that the single scattering inverse problem can be written after Koo [1] and Hirleman [2]:

$$S = K \cdot N \quad (1)$$

where S is the scattering signature over the detectors, N is the unknown size distribution vector, and K is a the scattering matrix such that the element K_{ij} indicates the amount of energy that a single particle representative of the j th size class would scatter into the i th detector assuming single scattering. We next recall the multiple scattering redistribution matrix H defined previously in this work by Hirleman [3] whereby H_{ik} represents the probability that a photon incident on a multiple scattering medium at an angle representative of the k th detector would leave the medium in a direction corresponding to the i th detector. Note that H depends on the detector geometry and the scattering characteristics of the medium which include the optical depth and the unknown particle size distribution. Since the scattering characteristics of the medium are not known ahead of time, it is H which must be measured on-line using the "active interrogation" schemes proposed and discussed below. The successive-order multiple scattering model of Hirleman [3] gave the equation:

$$S_m = \exp(-b) \cdot \exp(afb \cdot H) \cdot S_1 \quad (2)$$

where S_m is the scattering signature for a general medium and S_1 is the signature of single-scattered photons (S_1 would therefore be identical to the scattering signature for an optically thin medium). Figure 1 shows plots of S_m calculated via Eq. (2) for two quasi-monodisperse size distributions for two values of optical depth b . The plots for the lower value of b (optically thin media) show significant contrast in the oscillations of the data, indicating a high degree of information content. However, as the optical depth increases to 5.0 the contrast is significantly decreased (blurred), suggesting that it would be much more difficult to distinguish between 40 and 55 μm particles at greater optical depths.

If we would like to formulate the inverse multiple scattering problem as a linear system of the form:

$$S_m = K_m \cdot N \quad (3)$$

we must define (and determine) K_m as the scattering coefficient matrix which applies for a multiple scattering medium. The inverse multiple scattering problem could then be formulated as:

$$N = K_m^{-1} \cdot S_m \quad (4)$$

Here K_m^{-1} is the inverse of the matrix K_m (recognizing of course that the inverse operation may be ill-conditioned) where K_m is given after consideration of Eq. (2) by:

$$K_m = \exp(-b) \cdot \exp(afb \cdot H) \cdot K \quad (5)$$

A measure of the potential for extracting size distribution information from a multiple scattering medium is related to the condition of K_m . Figure 2 plots the inverse of the condition number of K_m against the optical depth b . The expected dependence is observed, whereby the "stability"

measure decreases with increasing optical depth as qualitatively suggested by Fig. 1. The condition number of K_m is a measure of the sensitivity of the solution vector N in Eq. (4) to uncertainties in K_m and/or S_m . Another perspective of the data in Fig. 2 involves the fact that the stability of the inverse *single scattering* problem for 12 degrees of freedom is equivalent to that of the multiple scattering problem with only 8 degrees of freedom at an optical depth of about 6 (99.8% extinction). This new formulation of the inverse problem can provide both an estimate of both the size distribution and the number of unique degrees of freedom that can be justified.

As discussed above it will be necessary to determine the matrix H on-line to implement the inversion scheme from Eq. (4) using K_m determined from Eq. (5). Measurement of H requires interrogation of the particle field with a series of incident beams at discrete angles corresponding to the detectors. In other words, a series of hollow cones of light must be directed through the medium, with the cone angles corresponding to the scattering angles of the detectors, and the redistribution of the energy by the medium over the all detectors must be measured. Each column of H corresponds to the redistribution signature from one input cone of light. The interrogation (conical) beams can be experimentally created using the Fraunhofer optical system in reverse, by placing a ring of light of radius r at the input focal plane. This produces an axisymmetric cone (half-angle θ) of light on the output side of the lens as governed by the equation $r = f\theta$. Again this must be done on-line, and we have demonstrated this ability using a transmission-mode spatial light modulator. This device is basically an programmable array of optical shutters, and results obtained with such a device are reported by Dellenback and Hirleman [4,5].

If the optical shutter array is used at the Fourier transform plane of a Fraunhofer instrument, this technology allows the detector configuration to be programmable, i.e. adjusted in real-time to an optimal configuration (adaptive control) [4,5]. The multiple scattering scaling laws derived here [3] significantly compress the data required to configure the inversion software, making feasible the storage of a wide range of instrument scattering matrices K_m in a reasonable amount of memory.

REFERENCES:

1. J. H. Koo, "Particle Size Analysis using integral transform techniques on Fraunhofer diffraction patterns", Ph.D. dissertation, George Washington University and Arizona State University, 1987.
2. E. D. Hirleman, "Optimal Scaling for Fraunhofer Diffraction Particle Sizing Instruments," *J. Part. Char.*, V. 4, pp. 128-133 (1988).
3. E. D. Hirleman, "Modeling of Multiple Scattering Effects in Fraunhofer Diffraction Particle Size Analysis," *Optical Particle Sizing: Theory and Practice*, Plenum Publishing Co., First International Conference on Particle Sizing, Rouen, France. Accepted for publication in *J. Part. Char.*.
4. E. D. Hirleman and P. A. Dellenback, "Faraday-effect Light Valve Arrays for Adaptive Optical Instruments", Invited Review Paper presented at the Seventh International Congress on Lasers and Electro-optics, San Diego, CA, November, 1987, published in *Optical Methods in Flow and Particle Diagnostics*, Vol. 63, pp. 6-11, Laser Institute of America, 1988.
5. Dellenback, P. A. and Hirleman, E. D. "Adaptive Fraunhofer Diffraction Particle Sizing Instrument Using a Spatial Light Modulator", Proceedings, OSA Meeting on Spatial Light Modulators, Lake Tahoe, NV, June, 1988. To be published in a special issue of *Applied Optics*.

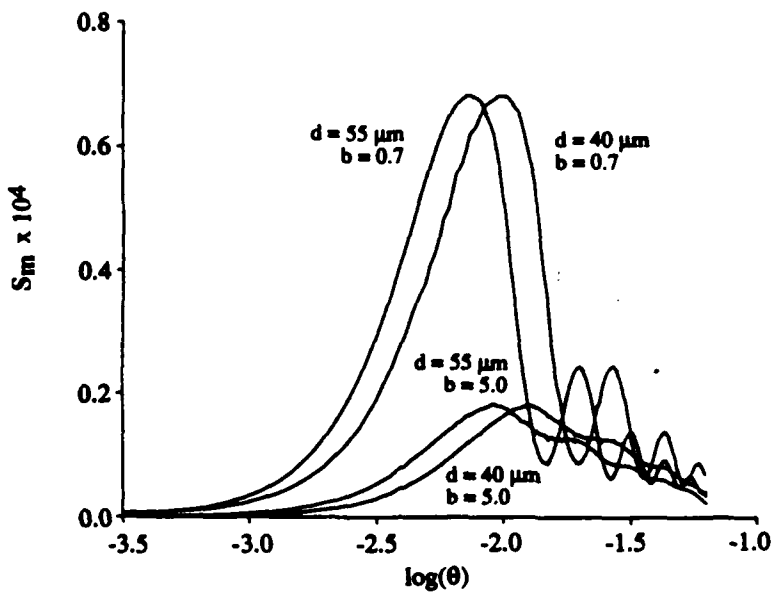


Figure 1. Plot of multiple scattering signatures S_m as a function of scattering angle θ for monodisperse particle fields of 40 and 55 μm diameter for two values of optical depth b . Note the decrease in total scattered energy reaching the detectors and the blurring of the scattering pattern structure (loss of information) as b increases.

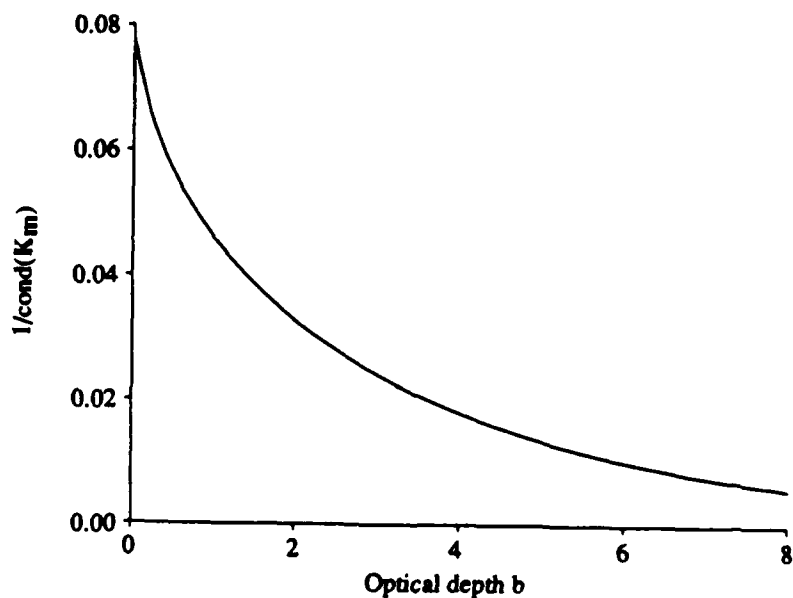


Figure 2. Plot of the inverse of the condition number (which is a measure of stability of the inversion) of the multiple scattering matrix K_m vs. optical depth b . The fraction optical (unscattered) transmission can be found from $T = \exp(-b)$. The data apply for a ring detector with 8 degrees of freedom in an optimally-scaled [2] inverse Fraunhofer formulation for a Rosin-Rammier size distribution with $X=26.0 \mu\text{m}$ and $N=2.9$.

**DIAGNOSTICS FOR RESEARCH IN ATOMIZATION AND TURBULENT
TWO-PHASE FLOWS**
(AFOSR Contract no. F49620-86-C-0078)

Principal Investigator: William D. Bachalo

Aerometrics, Inc.
Sunnyvale Technology Center
894 Ross Drive Unit 105
Sunnyvale, CA 94089

SUMMARY / OVERVIEW:

Advances have been made in the light scattering interferometry theory for particles larger than the light wavelength. The present theory incorporates the effects of nonuniform particle illumination by a Gaussian beam and describes the variations in the fringe pattern that occur as a function of time due to the particle motion. In an effort to provide an acceptable means to measure the size and velocity of irregularly-shaped particles moving at high speeds, a new method using confocal beams and a novel analysis to eliminate ambiguity associated with particle trajectory is being investigated. For advanced studies of particle dynamics in turbulent two-phase flows, an additional method has been derived to measure particle velocities in a Lagrangian reference frame.

TECHNICAL DISCUSSION:

Research on the diagnostics include three methods: the phase Doppler method for simultaneous drop size, velocity, number density, and volume flux measurements, the ratiometric method that allows the measurement of irregular-shaped particles from submicron to relatively large sizes, and the Lagrangian frame method for evaluating the behavior of individual particles as they move within a turbulent two-phase flow.

Phase Doppler Analysis:

Recent calculations by others^{1,2} of the light scattering interferometry using the Mie theory have shown contradictory results. Therefore, we have enhanced our theoretical analysis to clearly explain these differences. In an effort to extend the method to higher number density sprays, the laser beam is generally focused to diameters that are on the order of the drops to be measured. This leads to a violation of an important Mie theory boundary condition which requires uniform particle illumination. Because of the change in sign of the phase for the various scattering components, the fringe patterns also change as a function of time. Furthermore, the amplitude and phase of the scattered light must be calculated for a sufficiently fine grid over the receiver aperture for each time step. Even for a uniformly illuminated particle, the computation time for a range of particle sizes can become large using the Mie theory. Because of the computation time, only a few points were used in the above-cited references and the existence of the nonuniform illumination and time variation were not recognized.

Our approach is to use the geometrical optics theory and include all of the scattering components to describe the amplitude and phase of the scattered light. It is well-known that this theory is an asymptotic solution of the scattering of electromagnetic waves by spheres for which the Mie theory is the exact solution.

under the appropriate boundary conditions. The computations allow the evaluations of such parameters as the drop to beam diameter ratio, trajectory through the beam, and the size and location of the receiver.

The following equation provides a generalized expression for describing the scattering for the beam at one polarization:

$$S_{ip}(\theta_s) = \frac{a}{r} \cdot \sqrt{I(\theta_{ip})} \cdot |\Psi(\theta_{ip})| \cdot \sqrt{G(\theta_{ip}, \theta_s)} \quad i=1,2 \quad p=1,2$$

The interference relationships were written to include each of the scattering components which resulted in the superposition of six interference patterns given in generalized terms as :

$$E_{ip}(m, \theta, d, t) = S_{ip}(m, \theta, d) \cdot \exp(-jk\rho + j\omega t)$$

and

$$I_n(m, \theta, d, t) = |E_{ip}|^2 + |E_{qp}|^2 + 2|E_{ip}||E_{qp}| \cos(\Delta_n + \omega_D t) \quad n=1,6 \quad q=1,2$$

Figure 1 shows representative interference fringe patterns superimposed over the receiver lens. These fringe patterns were calculated for the scattered light by particles passing through the center of the beam (a) and the edge (b). The secondary interference pattern that can be seen along the primary fringe pattern is due to the interference between reflection and refraction. In figure 1b the shape of the fringe pattern has changed since for this trajectory, the amplitude of the unwanted reflection component is significant. Figure 2 shows the calculated instrument response function with and without integration over the receiver aperture. Serious oscillations seen here are similar to those found using the Mie theory without integration over the lens. Considering the local fringe intensity variations seen in figure 1, it is easy to see how erroneous conclusions could be made when the integration is neglected. Integration over the aperture removes the effects of the local variations in the pattern to produce a linear response function.

Ratiometric Method

Light scattering intensity measurement is a well-known means to obtain particle size. However, the incident intensity on the particles is uncertain when using Gaussian beams. This problem can be overcome by using confocal beams (Bachalo, U.S. Patent 4,329,054, 1980). In the original concept, beams with a diameter ratio of 7 to 10 were needed to insure accurate measurements. With the present approach, a simple two-equation solution has been derived allowing the use of a beam diameter ratio of 3 which will significantly improve the performance of the method.

The problem of determining the particle path through the Gaussian beam and hence, establishing the incident intensity can be solved using two confocal beams of different diameters and the general expressions for the light scattered by particles passing through these beams:

$$I_{sca1} = I_{01} Q_1(d) \exp\left[\frac{-2x_p^2}{b_1^2}\right]$$

$$I_{sca2} = I_{02} Q_2(d) \exp\left[\frac{-2x_p^2}{b_2^2}\right]$$

where I_{01} and I_{02} are the incident beam intensities, $Q_1(d)$ and $Q_2(d)$ are the scattering coefficients, b_1 and b_2 are the beam diameters, and x_p is the particle path measured from the center of the beam. Taking the ratio of the scattered light intensities yields:

$$\frac{I_{\text{sca}1}}{I_{\text{sca}2}} = \frac{I_{01} Q_1(d)}{I_{02} Q_2(d)} \exp \left[-2x_p^2 \left(\frac{1}{b_1^2} + \frac{1}{b_2^2} \right) \right]$$

Solving for x_p results in the following:

$$x_p = \left\{ \frac{1}{2} \cdot \left(\frac{b_1^2 b_2^2}{b_1^2 + b_2^2} \right) \ln \left[\left(\frac{I_{\text{sca}1}}{I_{\text{sca}2}} \right) \left(\frac{I_{02}}{I_{01}} \right) \left(\frac{Q_2(d)}{Q_1(d)} \right) \right] \right\}^{\frac{1}{2}}$$

Figure 3 shows the intensity distributions of the confocal beams and the particle path. Knowing x_p , the incident intensity on the particle can be determined and hence, its size from the measured scattering intensity. Direct measurement of the beam radius and size for each particle crossing the beams can be used to form a statistical distribution of the beam radii for each particle size class. This information is needed to correct the sampling statistics for probe volume bias and to determine the sampling cross section. The particle path length and the measured transit time can be used to obtain the speed.

Lagrangian Frame Particle Analyzer

This system is intended to track the course of individual drops as they move within a turbulent two-phase flow. Trace particles will be tagged with a fluorescent dye. The method will consist of a beam scanning system and a pair of array detectors, figure 4. Both a single beam and a parallel beam system are being considered. The two-beam system will allow good resolution of velocity at high particle speeds. Rotating polygons have been selected that provide sweep rates to 10,000 per second with good stability.

Two orthogonally oriented linear array detectors with cylindrical lenses are needed to determine the two components of velocity in the plane of the sweep. There is the potential of stepping the scans normal to the path of the sweep to obtain an indication of the third component of velocity. Available CCD's with 2048 pixels and read rates of 20 MHz will accommodate the beam sweep. A position sensor may also be used to provide a more direct reading. The breadboard system is currently being assembled.

1. S.A.M. Al-Chalabi, Y. Hardalupas, A.R. Jones, and A.M.K.P. Taylor, Proceedings of the International Symposium on Optical Particle Sizing 12-15 May 1987, I.N.S.A. de Rouen, France

2. K. Bauckhage, H.H. Floegl, U. Fritsching, and R. Hiller, International Conference on Laser Anemometry: Advances and Applications, Glasgow, Scotland 21-23 September, 1987.

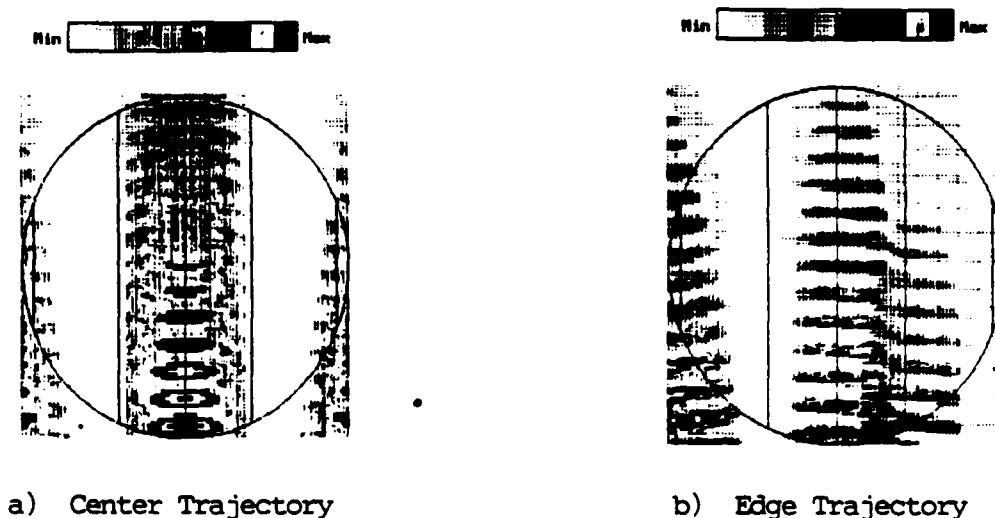


Fig. 1. Interference Fringe Patterns Overlayed on Lens

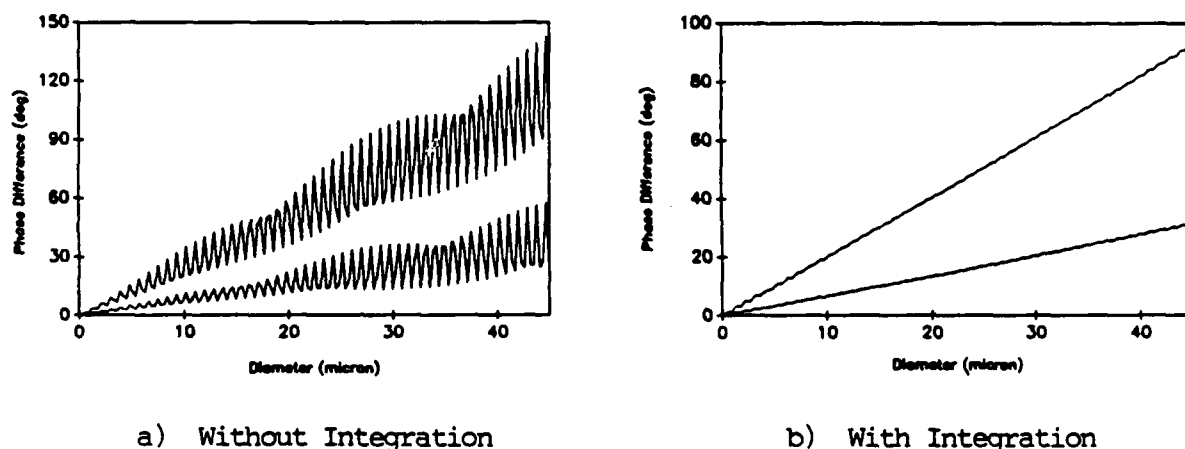


Fig. 2. Instrument Response Function

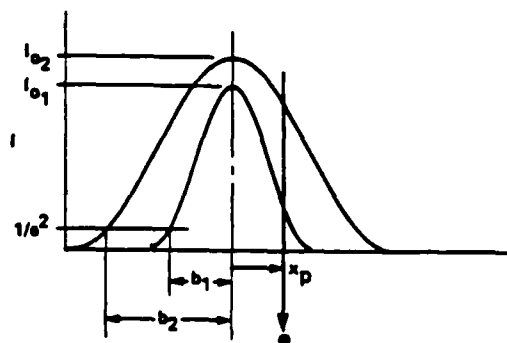


Fig. 3. Beam Intensity Profiles

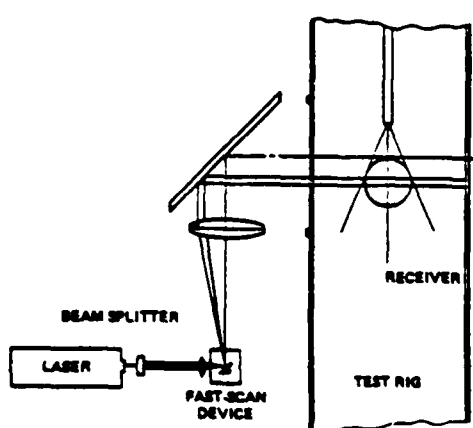


Fig. 4. Schematic of Lagrangian Frame System

SURFACE THERMOMETRY OF ENERGETIC MATERIALS BY LASER-INDUCED FLUORESCENCE

AFOSR Grant/Contract No. F49620-87-C-0040

Principal Investigators: Larry P. Goss and Michael E. Post

Systems Research Laboratories
A Division of Arvin/Calspan
2800 Indian Ripple Road
Dayton, OH 45440-3696

SUMMARY/OVERVIEW: The objective of this research is to develop and apply the technique of Laser-Induced Fluorescence (LIF) of thermal phosphors to the measurement of temperature on reacting surfaces. The goals were 1) to extend the LIF technique from point measurements to line and two-dimensional surface-thermometry mapping, 2) to develop a thermal depth profiler for reacting materials based on the LIF technique, and 3) to demonstrate the application of the LIF technique to the study of nonmetallic materials such as ceramic composites.

TECHNICAL DISCUSSION

Efforts during the first year of this program were directed toward the development of the hardware and software required for both thermal surface mapping and the thermal depth profiler. The temperature-measurement technique utilized in this work was LIF of thermographic phosphors. This technique involves embedding small 10 - 100 μm sized temperature-sensitive phosphor crystals in the surface to be studied. The LIF emission from the phosphors can be used to determine the temperature of the crystal and, thus, of the surrounding surface. An ideal crystal for this purpose was determined to be Dy:YAG. The temperature sensitivity of Dy:YAG results from a "thermalization" process in which the population of two adjacent energy levels (F and G) of the Dy^{+3} ion varies with temperature according to the energy separation of the levels, which is $\sim 1000 \text{ cm}^{-1}$. As the population of the levels changes, the resulting fluorescence intensity changes, which allows the temperature of the phosphor to be monitored. The ratio of the F to G fluorescence levels located at 496 and 467 nm, respectively, is displayed in Fig. 1. Because the 496-nm line is relatively insensitive to temperature, it can be used as an internal calibration, allowing the temperature determination to be reduced to a relative measurement rather than a more-difficult absolute measurement.

One of the major advantages of employing LIF is the possibility of extending this technique to multi-dimensional measurements through the use of line and/or two-dimensional detectors (cameras). The experimental arrangement employed for thermographic imaging is shown in Fig. 2. The main component of the system is an intensified camera--either linear diode array or two-dimensional CCD array--which records the fluorescence from the surface under study. The fluorescence from the phosphors is excited by the tripled output of a Nd:YAG laser. The intensified detector is gated with a 10- μs pulse which is an aid in discriminating against unwanted background radiation from the surface. The

fluorescence from the surface is collimated by an f/6 lens, split into two paths, and directed through 496- and 467-nm filters corresponding to the F- and G-fluorescence levels, respectively. The two paths are then imaged side by side on the linear or CCD camera. Image analysis consists of ratioing the two fluorescence signals and converting the resulting relative intensity to a temperature with the aid of a calibration curve established using a platinum-coiled oven.

An example of thermal mapping with a linear array is shown in Fig. 3. The temperature contour map displays the temperature along a line as a function of time from the surface of a plastic material doped with the Dy:YAG crystals as it is being heated by a CO₂ laser of ~ 30 W. The figure depicts both the laser heating of the surface and the cooling of the surface after the laser excitation is extinguished.

The effort with the two-dimensional camera was expended mainly in the development of the software and hardware required to synchronize the camera and the firing of the Nd:YAG laser. The acquisition and analysis software was written in FORTH, and a custom-designed interface was developed for downloading the image to a small main-frame computer for image analysis. Preliminary measurements have been made with the CCD camera on a nonreacting, doped ceramic surface. The target consisted of a cylindrical piece of ceramic with two parallel Nichrome wires suspended above its surface. The Nichrome wires were coated with a ceramic adhesive and doped with Dy:YAG crystals. Current was allowed to flow through the wires to produce a local heat source which was monitored by the thermographic phosphors. The two-dimensional image of the surface at the peak of the temperature buildup is shown in Fig. 4. One-half of this figure corresponds to the 467-nm fluorescence, while the second half corresponds to the 496-nm signal. As the temperature of the wires increases due to the electrical heating, the intensity of the 467-nm signal increases. By ratioing the 467-nm and the 496-nm signals, the spatial temperature distribution along the wires can be determined.

Future effort on this program will be directed toward applying the LIF technique to the study of reacting materials as well as nonmetallic materials which are employed in diverse high-temperature environments.

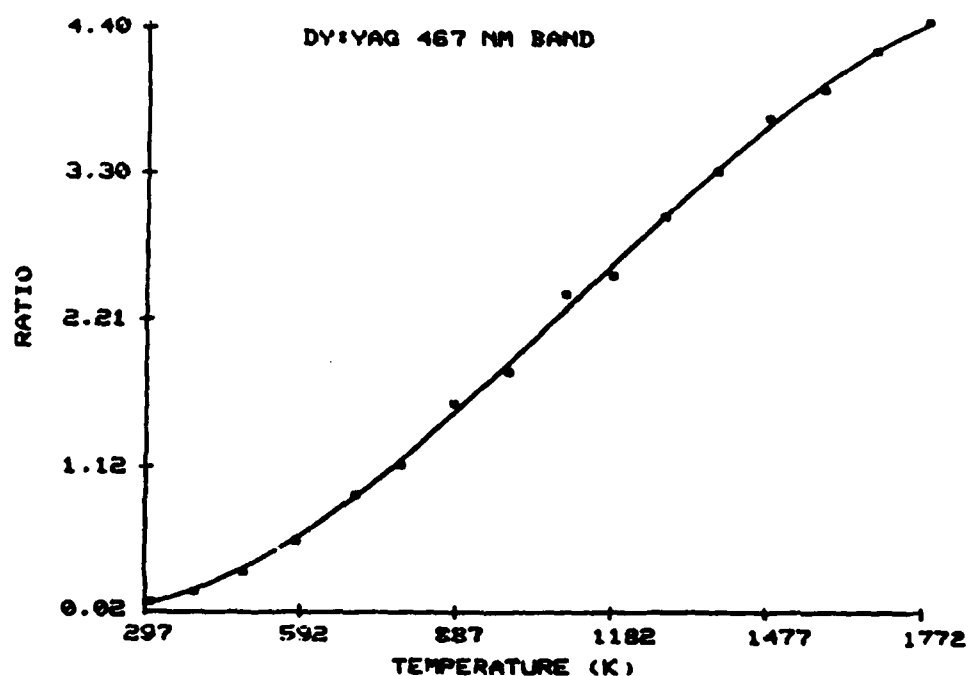


Figure 1. Variation of Relative Intensity of 467-nm G-Level Stark Component to 496-nm F-Level of Dy:YAG as Function of Temperature.

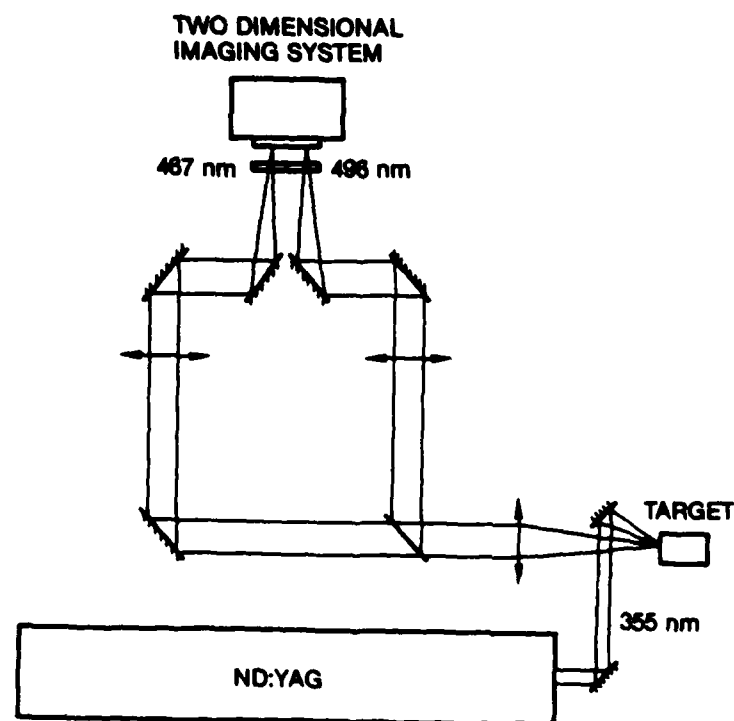


Figure 2. Experimental Arrangement Employed for Surface Thermographic Imaging.

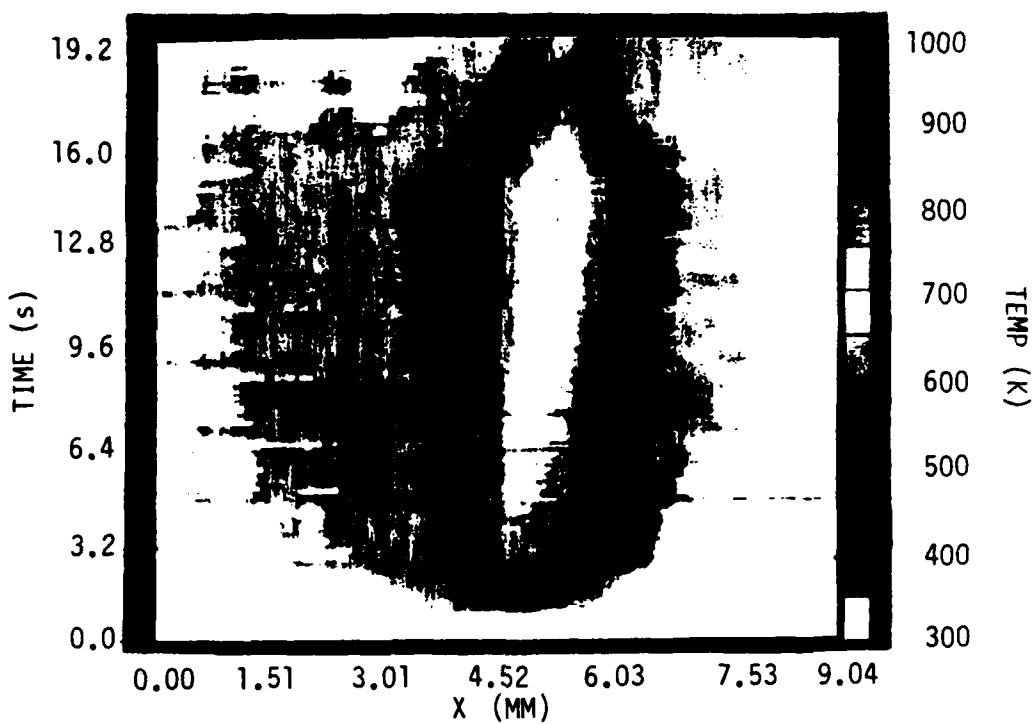


Figure 3. Temperature Contour Map Showing Results of Heating Plastic Surface with CO₂ Laser.



Figure 4. Fluorescence Image of Nichrome Wires at Peak of Heat Cycle (Left - 496-nm Signal; Right - 467-nm Signal).

MULTIPHOTON DETECTION TECHNIQUES FOR F AND F₂

(AFOSR Contract No. F49620-88-K-0003)

Principle Investigator: William K. Bischel

Collaborating Staff: Gregory W. Faris and Roberta P. Saxon

SRI International
Chemical Physics Laboratory
333 Ravenswood Ave.
Menlo Park, CA 94025

SUMMARY/OVERVIEW:

New quantitative remote detection techniques for atomic and molecular fluorine that have high sensitivity, coupled with good temporal and spatial resolution, are needed for such diverse applications as semiconductor manufacturing and laser development. The goal of this project is to develop quantitative detection techniques based on two-photon excitation of atomic or molecular states followed by the detection of fluorescence or ionization. In this paper we review the recently developed two-photon detection technique for atomic fluorine and report the first two-photon resonant, three-photon ionization spectroscopy of molecular fluorine.

TECHNICAL DISCUSSION

At the 1987 AFOSR Contractor Meeting we reported two photon excited fluorescence detection of atomic fluorine.¹ The $^2D_J^0$ state at approximately 118,000 cm⁻¹ was excited with two 170 nm photons. The resulting fluorescence at 776 nm to the 2P_J state was detected. The 170 nm light was produced by Raman-shifting the doubled output of a Nd:YAG pumped dye laser to the sixth anti-Stokes, yielding an energy of 10 μ J. Because the efficiency of the two photon excitation is proportional to the square of the laser intensity, the detection sensitivity may be improved by using a two color excitation. The relatively high intensity output from a F₂ laser can provide photons at 157 nm for one step, while anti-Stokes shifted tunable light at 185 nm provides the other step. Work is in progress on demonstrating this technique for increasing the F atom detection sensitivity.

This research program is also directed toward the sensitive detection of molecular fluorine. We have previously reported resonantly enhanced multiple photon ionization (REMPI) detection of molecular fluorine using the H $^1\Sigma_u$ and h $^3\Sigma_u$ states.² This was a three photon resonant photon excitation using -280 nm light. It is anticipated that a two photon resonant REMPI detection scheme would have better sensitivity. We have recently observed two photon

resonant REMPI detection of fluorine from the $F^1\Pi_g$ and $f^3\Pi_g$ states with -210 nm light. The spectra obtained are the highest resolution measurements of these states to our knowledge. The $f^3\Pi_g$ signal is weak because it is a spin forbidden transition from the ground state. However, it is of interest because it is believed to be the upper level of the F_2 laser, which is the brightest laser source in the VUV. Understanding the mechanism of this laser might lead to extension of laser sources further into the VUV and XUV regions. In a recent theoretical paper Sakai *et al.*³ concluded that they could not conclusively assign the F_2 laser transition. Observation of fluorescence from the two photon excited $f^3\Pi_g$ state and lifetime measurements would be a significant contribution to the understanding of the F_2 laser transition, as well as provide a sensitive remote detection technique for F_2 .

The experimental arrangement for the two photon resonant MPI detection of molecular fluorine is shown in Figure 1. The doubled light from a Nd:YAG pumped dye laser is focused through a H_2 -filled Raman cell. The third anti-Stokes line is separated with a Pellin-Broca prism and focused through a cell containing 10% F_2 in He. This gas mixture is flowed slowly through the cell, while maintaining a pressure of about 120 torr. The ionization signal is collected by a biased pair of electrodes and amplified with a charge amplifier. After passing through the F_2 cell the UV light is focused through a second cell containing nitric oxide. The energy of the pulses reflected from the entrance window to the nitric oxide cell is measured with a pyroelectric energy meter. The single photon resonant NO MPI signal and the signal from the energy meter are digitized and recorded on a VAX computer simultaneously with the F_2 MPI signal. These are used to monitor the excitation wavelength and intensity.

An MPI signal for the $f^3\Pi_g$ state is shown in Figure 2. The signal has been divided by the cube of the recorded laser intensity to reduce noise due to laser intensity fluctuations. The NO spectrum has been assigned and used to give an accurate wavelength scale.

The next experiment will be to excite this transition in F_2 with a higher laser intensity and try to observe the 157 nm laser transition in the VUV using a solar blind photomultiplier tube. If this experiment is successful, new data for the spectroscopy of the F_2 laser transition will be obtained as well as demonstrating a remote fluorescence based detection technique for F_2 .

REFERENCES

- 1.G. C. Herring, M. J. Dyer, L. Jusinski, and W. K. Bischel, Opt. Lett. 13, 360 (1988).
- 2.W. K. Bischel and L. E. Jusinski, Chem. Phys. Lett. 120, 337 (1985).
- 3.T. Sakai, K. Tanaka, A. Murakami, H. Iwaki, H. Terashima, and T. Shoda, J. Phys. B 21, 229 (1988).

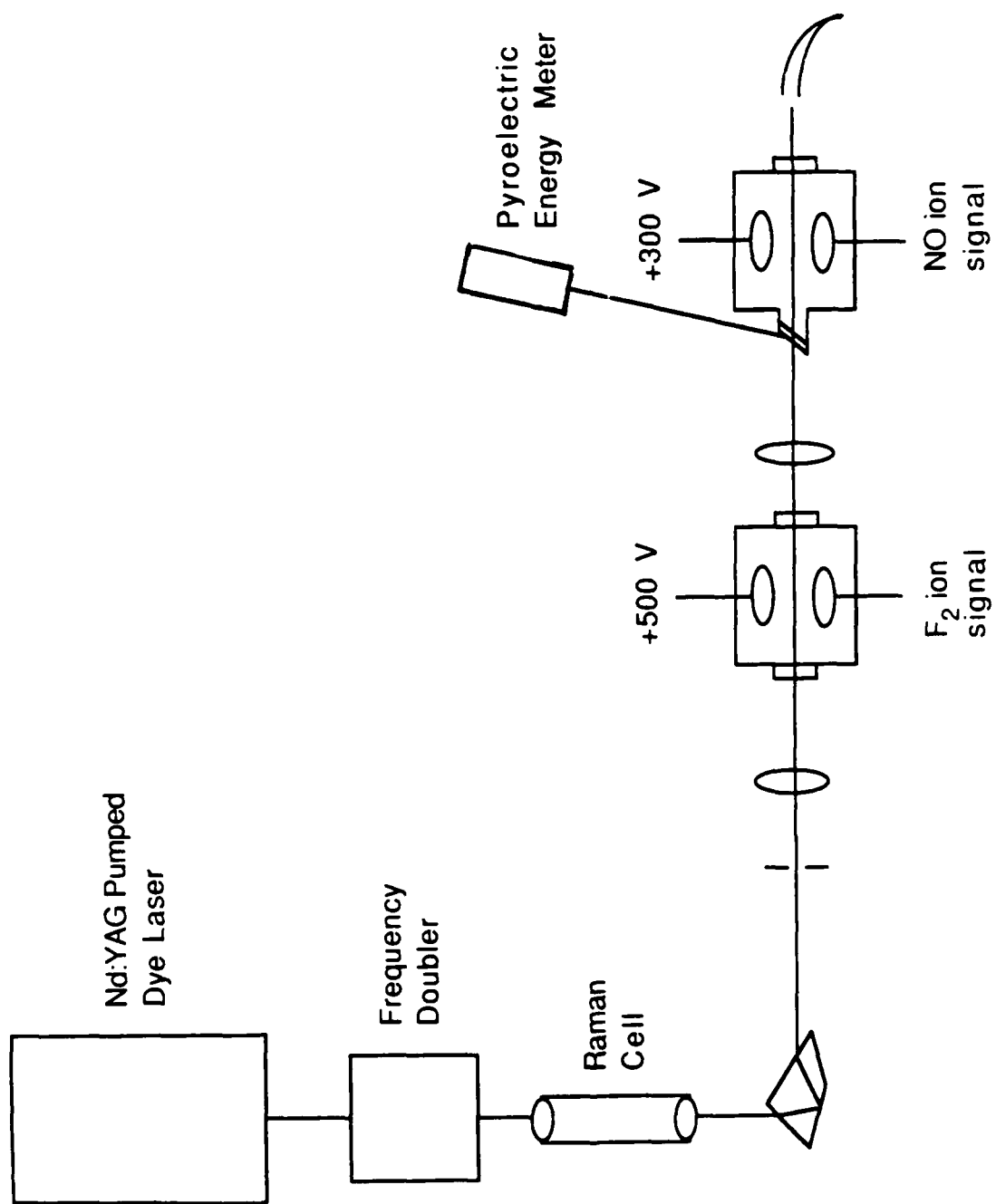


Figure 1. Experimental arrangement for two photon resonant ionization spectroscopy of the $F_{1\pi g}^1$ and $f_{3\pi g}^3$ states in molecular fluorine.

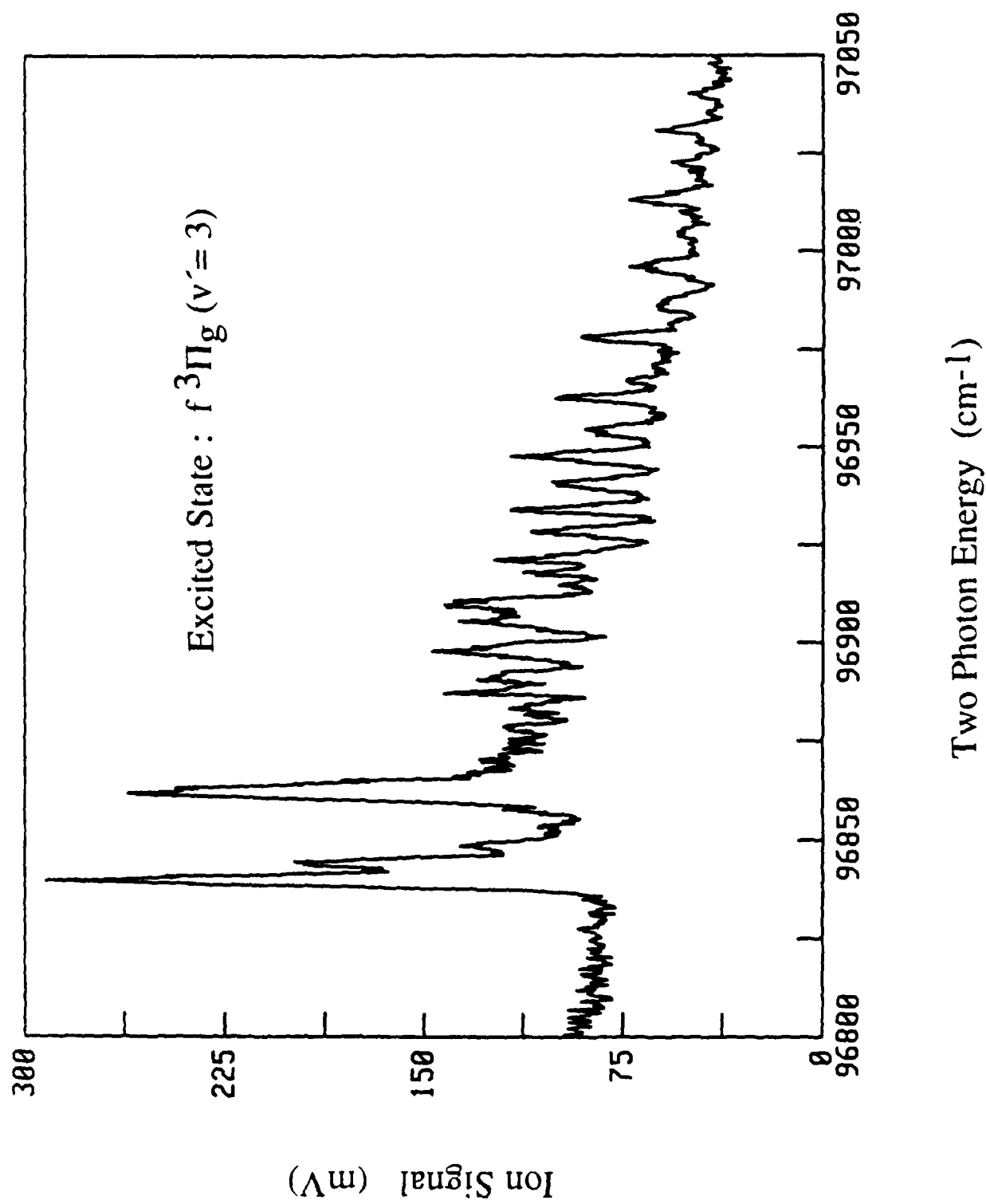


Figure 2. Ionization signal for the $f^3\Pi_g$ ($v'=3$) state in molecular fluorine.

ASYNCHRONOUS OPTICAL SAMPLING FOR LASER-BASED COMBUSTION DIAGNOSTICS IN HIGH PRESSURE FLAMES

AFOSR Grant No. AFOSR-84-0323

Galen B. King

Normand M. Laurendeau

Fred E. Lytle

Flame Diagnostics Laboratory
School of Mechanical Engineering
Purdue University
West Lafayette, IN 47907

SUMMARY/OVERVIEW:

This research is concerned with the development and subsequent testing of a new laser-based combustion diagnostic for the quantitative measurement of both major and minor species concentrations in high-pressure flames. The technique, called Asynchronous Optical Sampling (ASOPS), is a state-of-the-art improvement in picosecond laser spectroscopy. ASOPS is a pump/probe method which will allow determination of both electronic quenching and state-to-state relaxation rates. Such information is necessary for quantitative application of both laser-induced and laser-saturated fluorescence at high-pressure. The specific goal of the project is to develop and prove the viability of the ASOPS technique as a practical, quenching independent diagnostic. This will be achieved through measurements of atomic sodium and the hydroxyl radical in simple flames.

TECHNICAL DISCUSSION

Pump/probe methods are commonly employed to measure subnanosecond excited state processes in liquid and gas phase systems.^{1,2} Asynchronous Optical Sampling (ASOPS) is a newly-developed pump/probe method that will potentially allow the determination of number densities and relaxation rates in turbulent, high-pressure flames. In addition, ASOPS should yield a signal-to-noise ratio comparable to that for laser-induced fluorescence in practical combustion environments. The ASOPS method utilizes a coherent, signal-carrying beam and thus requires no more optical access than LDV measurements.

In conventional pump/probe instruments the pump and probe lasers operate at identical repetition rates, and an optical delay line is used to control the relative timing between pulses from the two lasers. Moreover, some type of mechanical or electro-optical chopping scheme is generally employed to induce an amplitude modulation on the signal which facilitates the use of

¹ G. R. Fleming, *Adv. Chem. Phys.* **49**, 1 (1982).

² F. E. Lytle, R. M. Parrish, and W. T. Barnes, *Appl. Spectrosc.* **39**, 444 (1985).

synchronous detection.^{3,4,5,6} In contrast, the ASOPS instrument employs pump and probe lasers operating at slightly different repetition rates. This induces a repetitive phase walk-out between the pump and probe pulse trains.

The ASOPS process is illustrated in Fig. 1a, which shows the excited state population produced by several pump pulses over which the temporal positions of several probe pulses have been superimposed. Each successive probe pulse is delayed in time relative to the pump pulse train by a constantly increasing duration which is determined by the beat frequency of the system. Thus each probe pulse samples the excited-state population at a slightly later time than the immediately preceding pump pulse. This is equivalent to varying the optical delay in a conventional pump/probe instrument. The entire process of Fig. 1a repeats itself when the cumulative delay equals the period of the pump laser. Hence any modulation of the probe beam, resulting from the creation and subsequent decay of the excited state, repeats at the beat frequency of the system. Therefore, in contrast to a conventional pump/probe instrument, there is no need to amplitude modulate either beam to employ synchronous detection.

Figure 1b illustrates the change in probe intensity which occurs owing to stimulated emission from the excited-state population shown in Fig. 1a. The net effect of the ASOPS technique is that a small amplitude waveform, which is directly related to the fluorescence decay of the species under study, is impressed onto the probe laser intensity. In essence, a temporal transformation of the excited-state decay is performed with the time scaled by the factor $[(f_{\text{pump}}/(f_{\text{pump}} - f_{\text{probe}}))]$, where f is the repetition rate of the two lasers. The ASOPS technique is thus an optical analog of the sampling oscilloscope.

Since the wavelengths of both the pump and probe lasers can be independently controlled, specific electronic quenching rates and state-to-state relaxation rates for a variety of atomic and molecular species can ultimately be determined. This assertion is valid because the stimulated emission (absorption) appears as a gain (loss) in the probe laser intensity; therefore, only those states which are directly connected by the probe laser wavelength are sampled. The gain/loss in the probe laser beam provides information on the rate at which the depopulated lower level gains population from neighboring levels within the ground electronic state or the rate at which the populated upper level transfers population to its neighboring levels within the excited electronic state. In other words, the ASOPS technique can yield information about state-to-state relaxation rates within both the upper and lower rovibronic manifolds for molecular species.

A block diagram of the basic ASOPS instrument is shown in Fig. 2. The pump and the probe beams are derived from dye lasers, which are synchronously-pumped by frequency-doubled, mode-locked Nd:YAG lasers. The mode-locking frequencies are generated by two frequency synthesizers operated in a master-slave (i.e. phase-locked) configuration to minimize drift in the beat frequency of the system. The probe beam intensity is monitored by a photodiode the output of which is amplified and directed to the signal processing system.

³ G. J. Blanchard, and M. J. Wirth, *Anal. Chem.* **58**, 532 (1986).

⁴ E. L. Quitevis, E. F. Gudgin Templeton, G. A. Kenney-Wallace, *Appl. Opt.* **24**, 318 (1985).

⁵ L. Andor, A. Lorincz, J. Siemion, D. D. Smith, and S. A. Rice, *Rev. Sci. Instrum.* **55**, 64 (1984).

⁶ P. Bado, S. B. Wilson, and K. R. Wilson, *Rev. Sci. Instrum.* **53**, 706 (1982).

In previous papers,^{7,8} we reported initial ASOPS studies of Rhodamine B in methanol. We have now extended the ASOPS technique to measurement of the relative number density of atomic sodium in an atmospheric CH₄/O₂/N₂ flame. For this study, the pump and the probe beams passed colinearly through the flame to maximize the available signal-to-noise ratio in these first flame studies. Polarization elements were used to first combine and then to separate the pump and the probe beams before and after the flame. The reconstruction of a fluorescence decay by excitation and detection of the sodium D₂ transition (589.0 nm), as shown in Fig. 3, can be used to determine the decay time of atomic sodium under flame conditions. Based on a least squares fit, the equivalent decay time is 8.9 μ sec. This corresponds to an actual lifetime of the excited state of 1.1 nsec; this value is consistent with previous decay times (~1 nsec) reported in the literature.^{9,10}

To demonstrate the viability of ASOPS as a combustion diagnostic, both ASOPS and laser-induced fluorescence (LIF) have been used to measure relative concentration profiles (Fig. 4) and saturation curves (Fig. 5). As shown in Fig. 4, the relative concentration profiles obtained using each method are nearly identical. Furthermore, the signal-to-noise ratio (SNR) for ASOPS was of the same order-of-magnitude as that for LIF. The ASOPS method yielded an inverse relative standard deviation of 34, while the LIF method yielded a value of 44. We believe that a considerable portion of the noise in the ASOPS signal can be attributed to impedance mismatches at the trigger photodiodes and at the double balanced mixer. Corrections are currently being made in these devices to improve the SNR. Furthermore, suitable upgrades are possible with respect to the performance of both the Nd:YAG laser systems and the detection electronics. The saturation studies also show that the ASOPS measurements correspond closely with the LIF measurements.

We thus conclude that the ASOPS method has great potential for use in high-pressure, turbulent flames. Although visible pump and probe beams are used in the above experiments, the ASOPS technique can eventually be extended to ultraviolet wavelengths to monitor molecular species such as the OH radical.

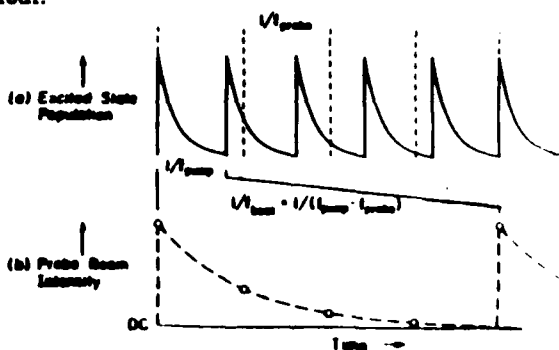


Figure 1. ASOPS timing diagram showing (a) excited state population and (b) probe beam intensity. The vertical dashed lines in (a) represent probe pulses.

⁷ P. A. Elzinga, F. E. Lytle, Y. Jiang, G. B. King, and N. M. Laurendeau, *Appl. Spectrosc.* **41**, 2 (1987).

⁸ P. A. Elzinga, R. J. Kneisler, F. E. Lytle, Y. Jiang, G. B. King, and N. M. Laurendeau, *Appl. Opt.* **26**, 4303 (1987).

⁹ C. Th. J. Alkemade, Tj. Hollander, W. Snellemen, and P. J. Th. Zeegers, *Metal Vapours in Flames*, Pergamon Press, 1981.

¹⁰ Y. Takubo, T. Okamoto, and M. Yamamoto, *Appl. Opt.* **25**, 740 (1986).

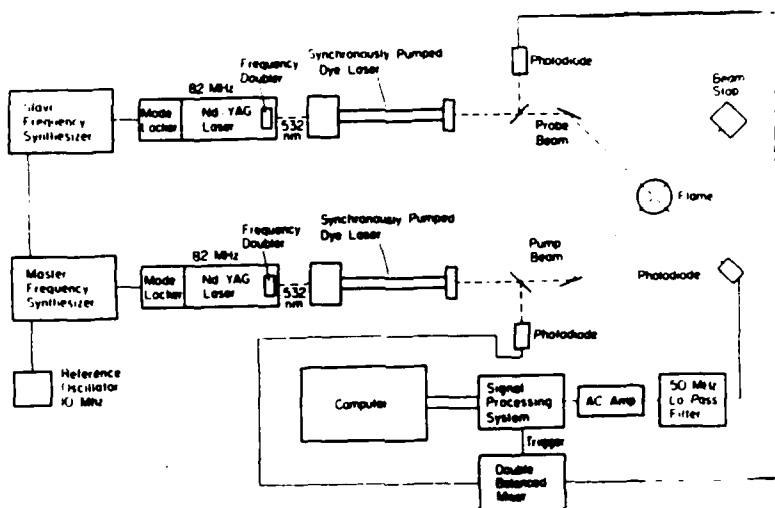


Figure 2. Block diagram of the basic ASOPS instrument.

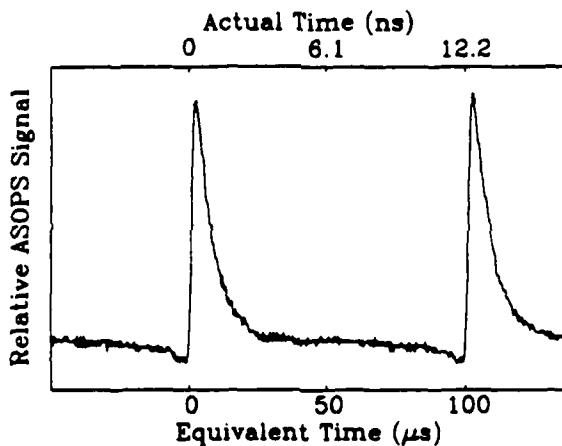


Figure 3. Temporal decay for atomic sodium obtained with both the pump and probe beams tuned to the D_2 transition (589.0 nm).

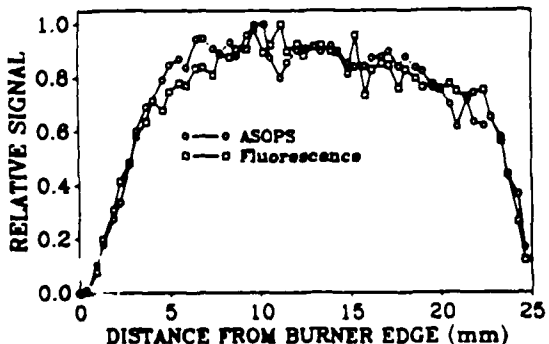


Figure 4. ASOPS and LIF horizontal relative concentration profiles.

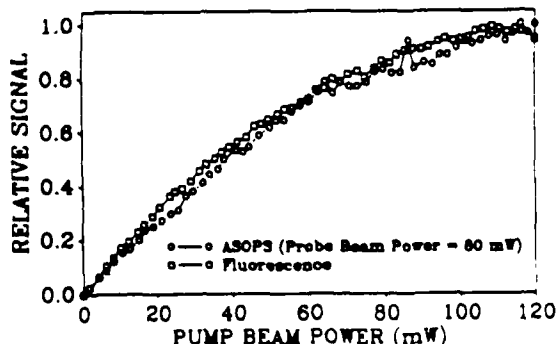


Figure 5. ASOPS and LIF pump-beam saturation curves.

TWO- AND THREE- DIMENSIONAL MEASUREMENTS IN FLAMES

(AFOSR Grant/Contract No. AFOSR-88-0100)

Principal Investigator: Marshall B. Long

Department of Mechanical Engineering and Center for Laser Diagnostics
Yale University, New Haven, Connecticut 06520-2157

SUMMARY/OVERVIEW:

Laser diagnostic techniques are being developed that can provide quantitative data on scalar quantities from many points in reacting and nonreacting flows. The capabilities of previously developed imaging techniques are being extended in two ways. First, new detectors are being used to allow imaging at higher speeds in order to follow the temporal development of structures in the flows. Second, techniques are being developed to obtain information on the three-dimensional character of the large-scale flow structures.

TECHNICAL DISCUSSION

As an example of this work, Fig. 1 shows a series of images of the flame front in the central plane of a turbulent premixed jet flame. A stoichiometric hydrogen/air mixture was uniformly seeded with submicron-sized aerosol particles. The aerosols were removed from the flow at the reaction front, and their presence was used to map the interface between the reacted and unreacted fuel/air mixture. An Ar⁺ laser was used to form the illumination sheet that intersected the flame along the jet axis. The Lorenz-Mie scattering from the aerosols in the unburned mixture was recorded in two dimensions at 48,000 frames/sec using an electronic framing camera. Because of the high framing rate available with this detector, the motion of the flame front could be followed by observing the sequence of images. The convection velocity was computed from the motion of centroids of unburned gas packets. Using this information, the burning velocity was then determined by comparing successive realizations in a convecting frame of reference.

Another goal of the current research effort is to develop techniques capable of providing information on the three-dimensional character of structures in turbulent flames. One means of extending the two-dimensional measurement approach to obtain three-dimensional information is to use two closely-spaced parallel laser sheets and detect the scattered light from each sheet separately. From this measurement, all three components of the scalar gradient can be calculated at points within a two-dimensional plane. Two components of the gradient can be determined from within one of the sheets, and by considering the same location in both sheets, the third gradient component can be obtained. From the full three-dimensional scalar gradient, the scalar dissipation can be determined. Figure 2 shows data derived from measurements using two parallel light sheets. In Fig. 2(a), the Freon mixture fraction (as determined from Rayleigh scattering) in an ambient temperature Freon jet mixing with air is shown. Figure 2(b) shows the scalar dissipation calculated by considering the three-dimensional gradients at each point in the plane. If a large number of independent instantaneous image pairs are recorded, statistics

on the flow can be compiled. Of particular interest is the probability density function of the scalar and the scalar dissipation.

Although the technique using two sheets provides three-dimensional gradient information and statistical characterization of the flow, it cannot provide a good visualization of the topology of the flow structures. One way in which a three-dimensional flow measurement can be realized is to make two-dimensional measurements at many closely spaced sheets. To accomplish this, a laser illumination sheet is rapidly swept through the flow and the scattered light from this scanning sheet is recorded by a high-speed electronic framing camera. The framing camera produces a series of images (corresponding to different sheet locations) on a phosphor screen and this intensity distribution is recorded electronically or on film. By combining the high speed framing camera with a flashlamp-pumped dye laser available at Sandia National Laboratories, instantaneous ($0.6 \mu\text{sec}$) three-dimensional measurements from molecular scattering were recorded. Figure 3 shows an instantaneous measurement of the nozzle gas concentration from a turbulent premixed methane flame as obtained with fluorescence from biacetyl.



Figure 1. Consecutive images of the reactant distribution in a premixed hydrogen/air flame recorded at a rate of 48,000 frames/sec.

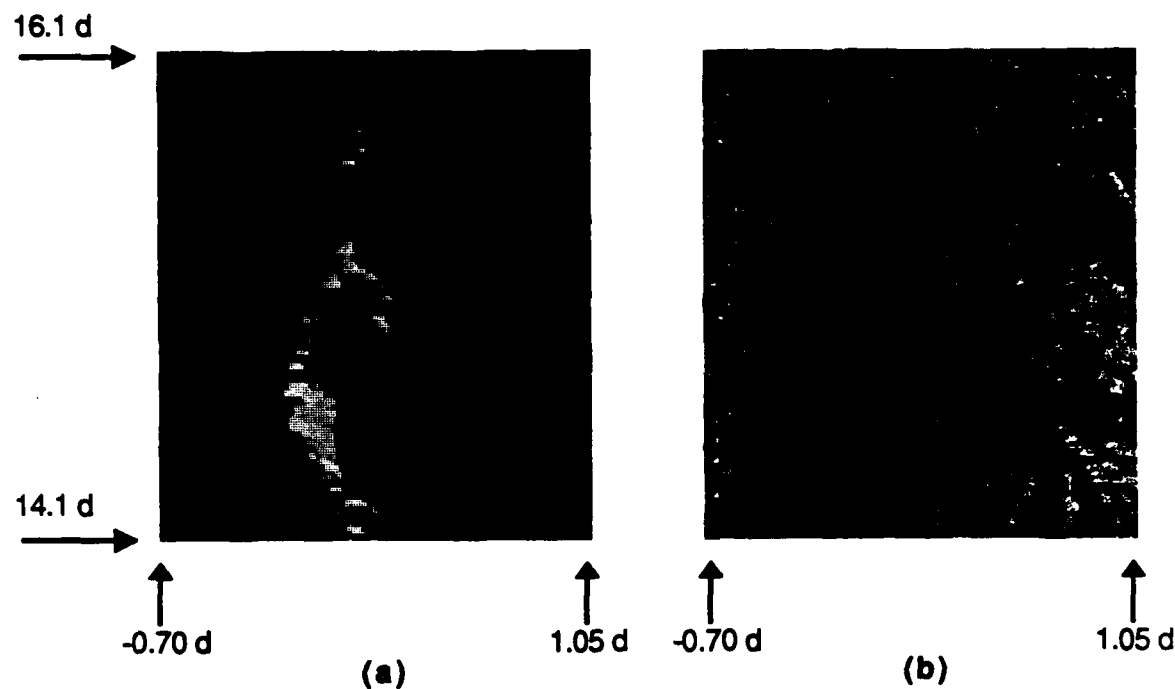


Figure 2: Instantaneous mixture fraction (a) and corresponding mixture fraction dissipation (b) in a Freon jet.

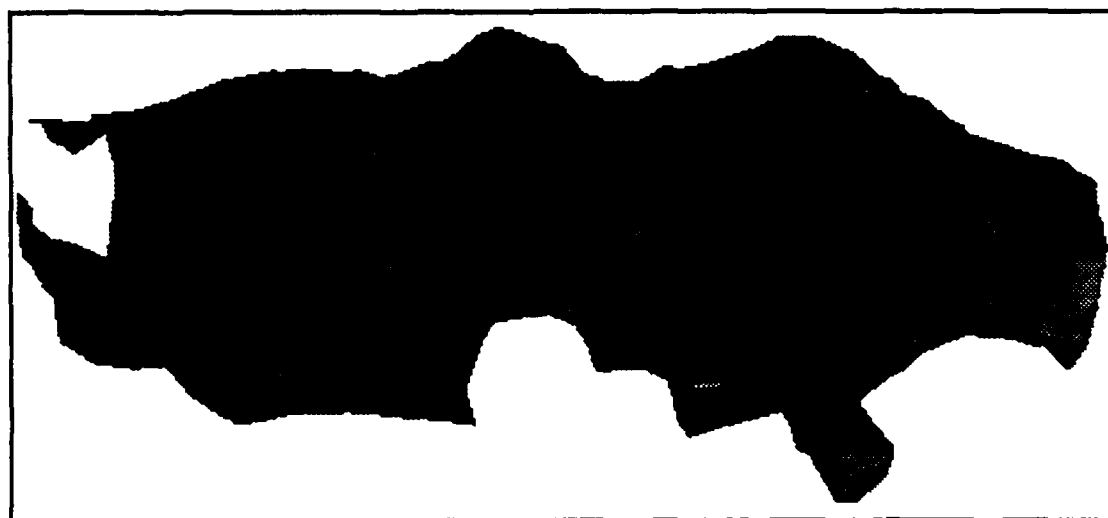


Figure 3. Isoconcentration surface in a premixed methane-air flame seeded with biacetyl vapor as a fluorescent marker.

ADVANCED DIAGNOSTICS FOR REACTING FLOWS

AFOSR-87-0057

Ronald K. Hanson

High Temperature Gasdynamics Laboratory
Mechanical Engineering Department
Stanford University, Stanford, CA

SUMMARY/OVERVIEW:

This research is directed toward innovation of advanced diagnostic techniques applicable to combustion and plasma flows. Emphasis is placed on laser-induced fluorescence methods suitable for digital 2-d and 3-d imaging of species concentrations, electron density, mass density, temperature, velocity and pressure. This approach can provide non-invasive, simultaneous measurements at 10^4 - 10^6 points, useful for studies of propulsion, aerothermodynamics, and combustion sciences. Other research topics include: laser-wavelength modulation techniques, digital imaging of Mie scattering for determining particle-size distributions, laser photolysis in shock-heated gases for kinetics/spectroscopy studies, laser ignition of combustion gases, and advanced diagnostics for hypersonic flows.

TECHNICAL DISCUSSION

In the following paragraphs we highlight our primary activities during the past year.

Plasma Diagnostics

Two new plasma facilities are now operational for research on plasma diagnostics: a 3 kW RF-powered plasma torch suitable for benchtop studies of diagnostic concepts, and a 50 kW RF-powered torch which yields higher enthalpies and allows study of practical plasmodynamic behavior. Both torches operate at atmospheric pressure on a range of gases. An example of work in progress is illustrated in Fig. 1 which indicates the approach being taken to apply planar laser-induced fluorescence (PLIF) to the measurement of atomic species in plasma flows. In addition to PLIF we are exploring laser wavelength modulation concepts for absorption and fluorescence measurements of concentrations, temperature and velocity.

Development and Application of Solid-State Cameras

A critical element in our PLIF imaging research is the continued development of solid-state cameras. Progress on two separate camera systems can be reported here. The first system is an intensified CCD array with high spatial resolution (244 x 610 pixels); previously, large CCD arrays were available only without intensification. As an example of current research aimed at refining the camera and investigating PLIF strategies for supersonic flows we have successfully recorded high-quality images of both NO and I₂ seeded at low levels in an underexpanded jet. The two important conclusions are: (1) the camera performance is quite good and allows flexible, video-compatible real-time displays at 30 Hz; and (2) instantaneous PLIF images are able to reveal details of flow structure in supersonic flows that are masked in any scheme which averages in either space (e.g., schlieren) or time.

Our second camera project is aimed at providing a combination of high spatial resolution and high signal dynamic range, needed for example in imaging turbulent flows. The camera utilized to achieve these goals is an unintensified CCD array (384 x 576 pixels). Fig. 2 shows an instantaneous PLIF image of jet mixture fraction in the central plane of a biacetyl-seeded N₂ jet.

(Also see Ref. 1.) Although information is lost here in the use of a gray-scale display, it is clear that such images provide important new capability for imaging turbulent flow structures. A related activity is our work to develop interactive methods for processing high-resolution PLIF images using a Pixar Image Computer; this system enables high-speed processing of 2-d and 3-d images and provides a flexible work environment for investigating issues associated with intelligent use of PLIF image data.

Velocity Imaging

A major objective in our research is the development of imaging schemes suitable for recording gaseous velocities without the use of particulates. During the past year we published the conclusions of a study which used a narrow-linewidth cw laser source to simultaneously probe velocity (2 components) and pressure in an I₂-seeded supersonic jet (see Ref. 2). The physical basis of the measurement is the Doppler-shift which results from the relative motion of the gas and incident laser light. Recently we have been investigating an alternative scheme which would allow use of pulsed lasers; such an approach offers hope of obtaining instantaneous velocity images and for extending velocity imaging to species which absorb outside of the visible spectrum. The basic concept under study is illustrated in Fig. 3. Here the correspondence between imaging a broad absorption line with a narrow laser line, and imaging a narrow absorption line with a broad laser, is indicated. This correspondence suggests that pulsed lasers may provide an elegantly simple alternative to the use of spectrally narrow lasers for velocity imaging. Initial results will be presented at the contractors' meeting.

Laser Photolysis Shock Tube

During the past year we have completed assembly of a new shock tube which seeks to combine gasdynamic heating with laser photolysis as a means of generating controlled levels of free radical species at elevated temperatures. Such a device will provide important new capability for fundamental studies of reaction kinetics and spectroscopy in species of interest in combustion and plasma sciences. A schematic of the facility is shown in Fig. 4. In this case the photolysis source is an excimer laser (ArF) emitting at 193 nm, the photolyzed gas is NH₃, and the species probed is NH using cw narrow-line absorption.

Flow Facility Development

New flow facilities under development include: a new square shock tube to be used for research on PLIF imaging of shock-heated gases; a shock tunnel extension of the square shock tube, to be used in research on hypersonic flow diagnostics; a small-scale supersonic combustor for use in investigating PLIF techniques suitable for supersonic reacting flows; and a supersonic test section to be added to the 50 kW plasma torch to provide a steady, high-enthalpy supersonic air flow for use in studying diagnostics of species in high-temperature air (O₂, O, NO, NO⁺).

Other Projects

Other research projects currently underway include: (1) quantitative imaging of Mie scattering from sheet-illuminated sprays to obtain instantaneous particle size distributions; (2) development of detailed absorption/fluorescence spectroscopy codes for O₂ and NO; (3) laser ignition of combustion gases; (4) two-photon PLIF imaging; and (5) research on laser-wavelength modulation techniques for diagnostics of combustion and plasma flows.

REFERENCES

1. G. Kychakoff, P. H. Paul, I. van Cruyningen and R. K. Hanson, App. Opt. 16, 2498 (1987).
2. B. Hiller and R. K. Hanson, App. Opt. 27, 33 (1988).

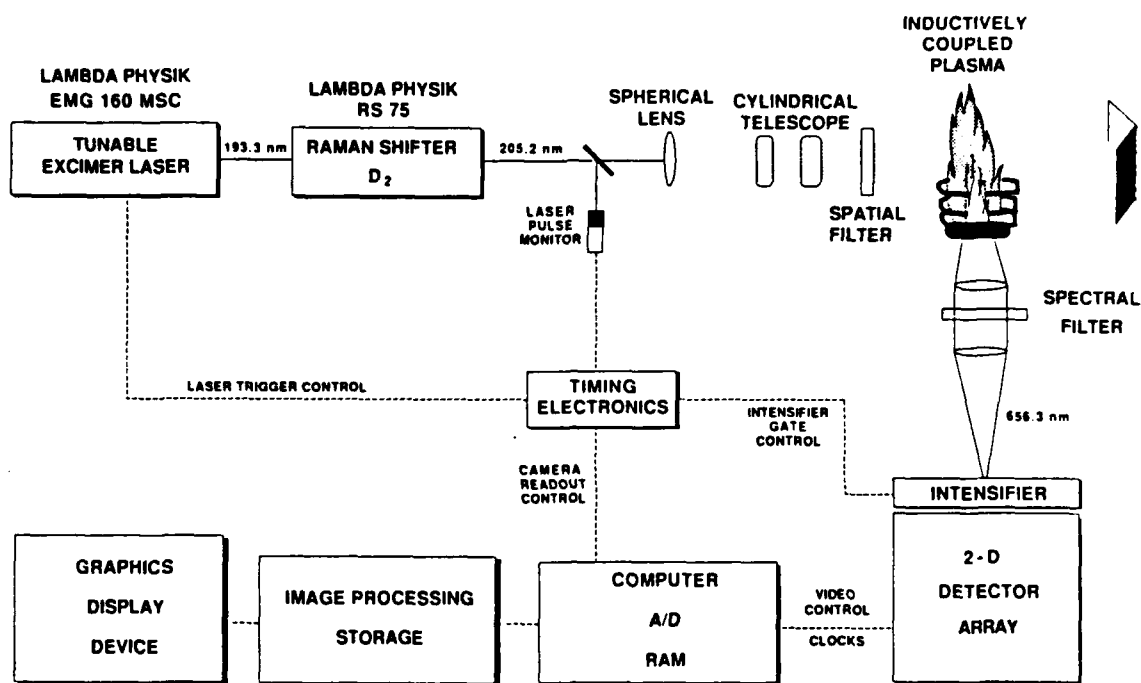
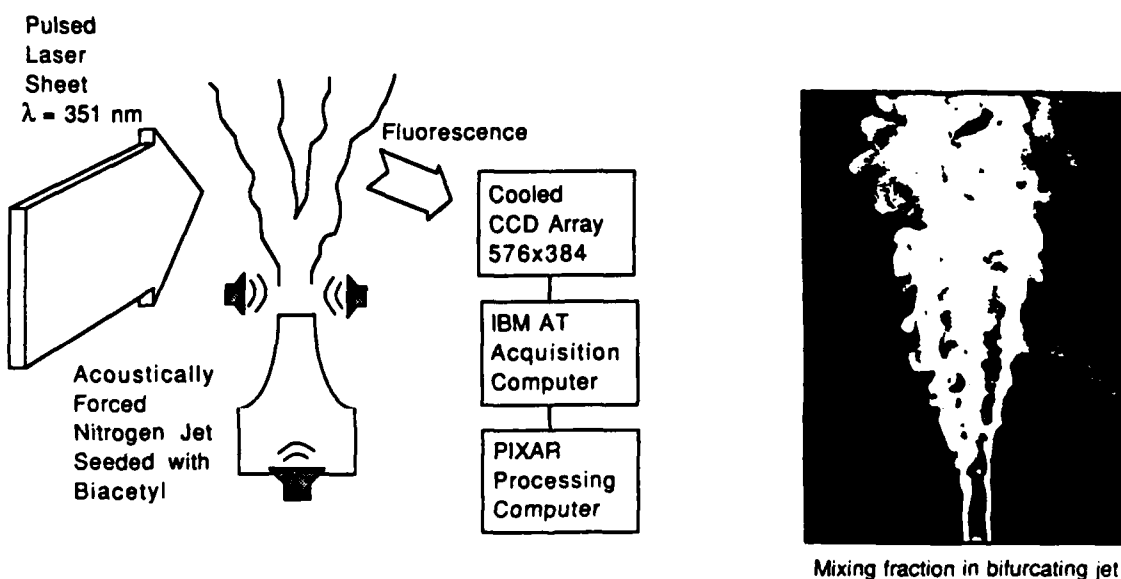


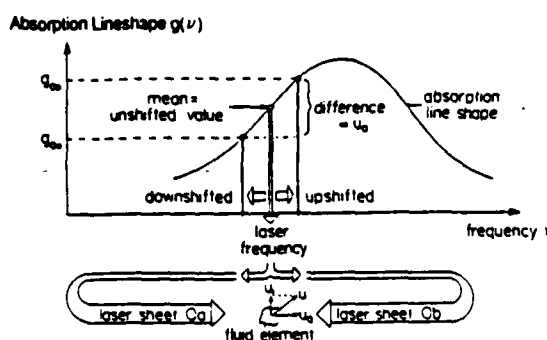
Figure 1. Schematic diagram of two-photon PLIF imaging of H in a plasma torch.



- Use of 221,184 Pixel Array Allows Fine Structure To Be Observed
- Factor of 5 Improvement in Spatial Resolution and >100 in Dynamic Range Over Previous Digital Imaging

Figure 2. High-Resolution PLIF imaging of turbulence flow structure.

Narrowband Laser Scheme



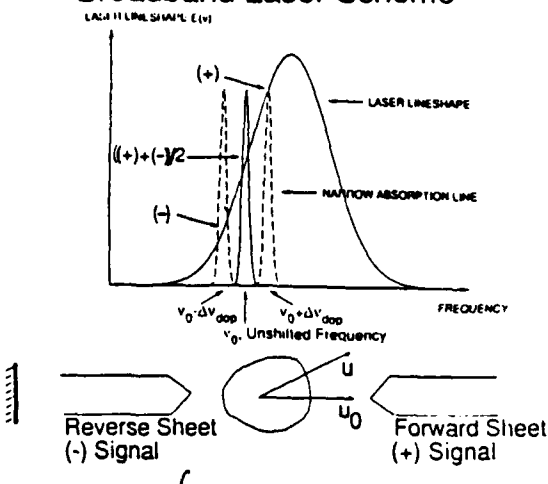
Effect of Doppler-Shift on Absorption Lineshape Function: Single Frequency

$$u_0 = \frac{c}{\nu} \Delta \nu_{\text{dop}} = \lambda \Delta \nu_{\text{dop}}$$

$$\frac{(+) - (-)}{(+) + (-)} = (\Delta \nu_{\text{dop}}) = \frac{u_0}{\lambda} \quad [\text{slope of laser line} = dE(\nu)/d\nu]$$

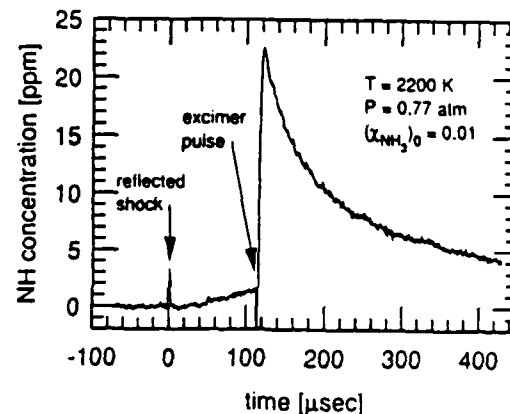
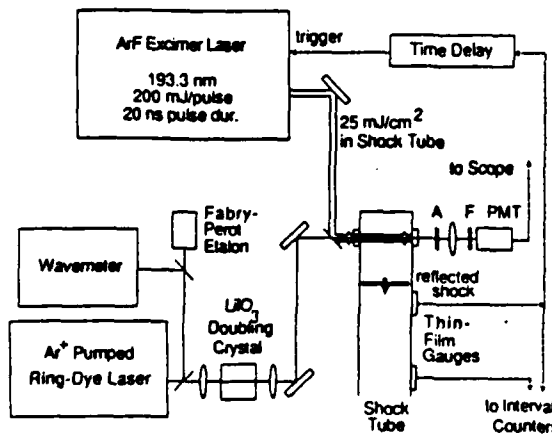
- Broadband concept allows use of pulsed lasers for instantaneous measurements
- Concept applicable over broad ranges of density, temperature and velocity
- No particle seeding required

Broadband Laser Scheme



$$\text{Signal} = \int E(\nu) g(\nu) d\nu = E(\nu)$$

Figure 3. Correspondence between narrow and broadband laser schemes for velocity imaging.



- EXCIMER PHOTOLYSIS PROVIDES CONTROLLED POOL OF RADICALS IN SHOCK-HEATED GASES
- PROVIDES FIRST-TIME ACCESS TO MANY CRITICAL COMBUSTION SPECIES
- ENABLES FUNDAMENTAL SPECTROSCOPIC STUDIES OF RADICALS AT HIGH TEMPERATURES
- ENABLES FUNDAMENTAL KINETICS STUDIES OF RADICALS AT HIGH TEMPERATURES

Figure 4. Laser photolysis shock tube for fundamental studies of combustion radicals.

LASER SPECTROSCOPY OF PLASMAS

AFOSR Grant 86-0067

John W. Daily

Department of Mechanical Engineering
University of California at Berkeley
Berkeley, CA 94720

SUMMARY

The purpose of our work has been to develop advanced laser spectroscopy methods to diagnose partially ionized plasmas. We have focused on methods that are based on observing the Doppler shift in ionic spectra due to the presence of an ion drift velocity. Two particular methods we are working with are Velocity Modulated Laser Spectroscopy (VMLS) and Two Beam Doppler Shift Laser Spectroscopy (TBDSLS).

TECHNICAL DISCUSSION

The scientific goal of our work is to increase understanding of the role of flow non-uniformities and plasma/wall interactions in plasma devices by making in-situ measurements of electric field strength, ion mobilities, concentrations and temperatures in a non-intrusive fashion that allows point, one, and two dimensional imaging.

The scientific approach is to use conventional laser spectroscopic methods such as Rayleigh scattering, Raman scattering, or fluorescence, to probe ion absorption line profiles. If there is an electric field present, the ions will experience a net force and undergo drift, resulting in a shift in the position of the line profile. If the ion mobility is known, then the electric field component along the probe direction can be calculated. If the electric field driving the plasma is modulated, one will observe an oscillating shift in the line profile that arises because of the oscillating force imposed on the ions. The shift may be related to the ion mobility, thus conductivity.

Temperature and concentration may be recovered by conventional laser spectroscopic means. The methods are species and state selective, allowing one to make measurements on more than one species and to study the effect of internal mode nonequilibrium.

The merit of the methods lies in their ability to provide simultaneous measurements of important parameters in plasmas. The methods are well suited to multi-dimensional imaging. One may use an array detector to image lines and planes in addition to the more conventional point configuration.

During the first year of the program, the theoretical basis of the method was developed and our experimental facility modified for the purpose of demonstrating its effectiveness. During the past year we have worked mostly on understanding the plasma environment that we have chosen to use in the demonstration experiments. The next few months will be spent obtaining laser data.

THEORETICAL BASIS

The basis of Doppler shift methods is Coulomb's law which states that the force felt by a charged particle is directly proportional to the imposed electric field

$$\vec{F} = q \vec{E}$$

where \vec{E} is the electric field, q the charge, and \vec{F} the force. For a collisionally dominated, partially ionized plasma, the net Doppler shift for D.C. and A.C. fields respectively is

$$\frac{dv}{v_0} = \frac{\mu_i E}{c}$$

or

$$\frac{dv}{v_0} = \left\{ \frac{\left(\frac{\mu_i E}{c} \right)}{[1 + i(\omega/v_c)]} \right\} E_0 \exp(i\omega t)$$

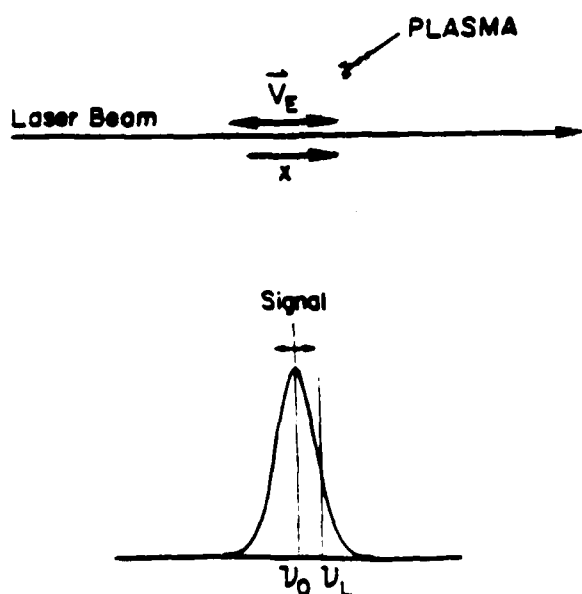
For a Doppler broadened line, the modulation depth (peak depth for an A.C. field) is

$$\frac{dv}{dv_D} = \left(\frac{\pi q}{8Q\sqrt{\ln 2}} \right) \left(\frac{E}{P} \right)$$

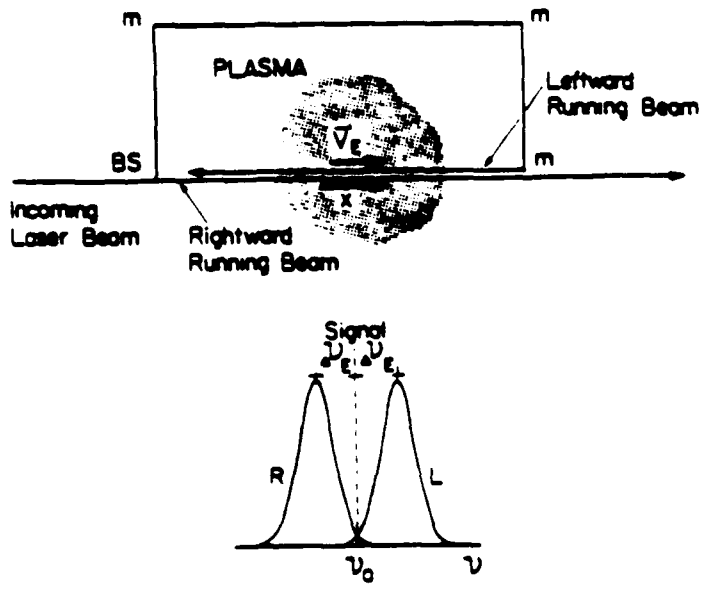
The coefficient of E/P is of order unity in typical plasmas for electric field in volts/meters and Pressure in Pascals. Thus one can obtain significant modulation depths at moderate values of E .

MEASUREMENT CONFIGURATIONS

Velocity Modulated



Two Beam Doppler Shift



PLASMA THEORY

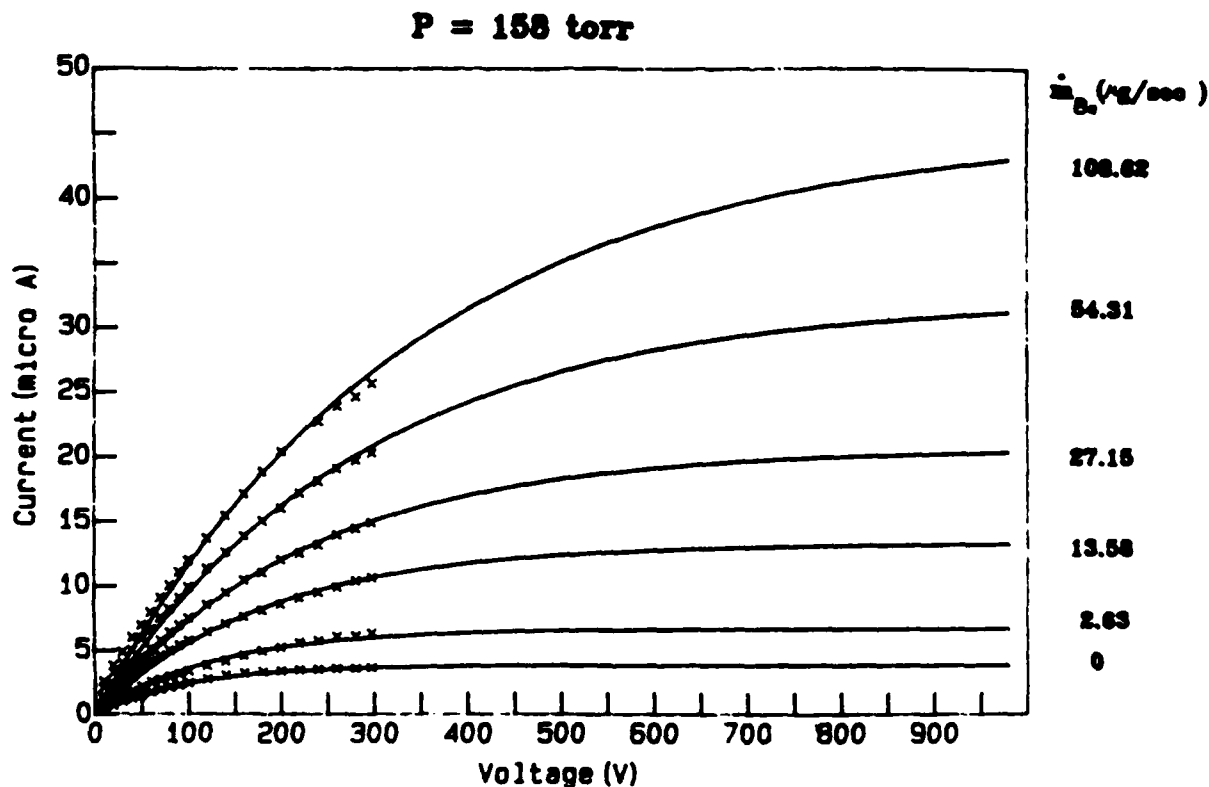
The advantage of utilizing a collisionally dominated plasma is that the theoretical description of the plasma is simplified considerably. Such a simplified description has been formulated by Lawton and Weinberg expressly for flames. Our approach has been to use their theory in conjunction with experiments to ensure that we have a reasonable understanding of the plasma conditions.

The Lawton and Weinberg theory is based on the assumption that diffusion of ions and electrons can be neglected in comparison with drift. Under this assumption and assuming that the plasma is one-dimensional with uniform properties, the governing equations display simple limiting solutions. These are the zero field limit, the saturation limit, and the sub-saturation limit. The current-voltage relationship takes on the form

$$\frac{I}{I_s} = 1 - \exp\left(-\alpha \frac{V}{V_s}\right)$$

where the subscript s indicate saturation conditions, and α is a constant whose value depends on the definition of the saturation condition.

We have conducted experiments to determine whether the theory is adequate for our purposes. The figure below shows that the theory fit the data extremely well.



MEASUREMENT OF ELECTRON EXCITATION TEMPERATURE
AND ELECTRON ENERGY RELAXATION PROFILES

AFOSR PROGRAM ELEMENT 2308S9

Principal Investigator: B. N. Ganguly
AFWAL/APL
Wright-Patterson AFB OH 45433-6563

SUMMARY/OVERVIEW:

Investigate the applicability of several optical diagnostic techniques for electron temperature, ion density and electric field profiles measurement with spatial and temporal resolution in non-equilibrium volume plasmas and boundary demarcated plasmas. The specific goal of this task is to develop, validate and apply optical measurement techniques for energy conversion device diagnostics.

TECHNICAL DISCUSSION:

a. Electron Excitation Temperature Measurement: The plasmas of thermionic energy converters (TEC), operating with no external load, have been shown¹ to exhibit Maxwellian electron energy distribution. However the plasma properties of dc as well as inductively coupled thermionic converter when operating with external load are expected to approach quasi-equilibrium or non-equilibrium behavior due to the formation of increased sheath voltage drops. The energy conversion efficiency of the TEC device is inversely proportional to the sheath voltage drop and, therefore, measurement techniques that can characterize the transition of electron energy distribution from Maxwellian to non-Maxwellian plasma behavior can be a useful diagnostic tool for TEC device. Electron excitation temperature measurement of neutrals and ions or two neutral species with widely different excitation energy levels can be used to determine the non-Maxwellian behavior of the electron energy distribution. The purpose of the present study is to apply plasma induced emission measurement as a means to determine the electron excitation temperature in a low pressure argon-cesium plasma. Electron excitation temperature can be obtained by measuring the spectral line intensities. The electron excitation temperature dependence of the line intensity I can be expressed as

$$I = N \left(\frac{16m}{\pi K T_e} \right)^{1/2} n_i n_e h c \left(\frac{E_i}{Q_{max}(E_{max}-E_i)} \right) \times \frac{\Lambda_i}{\lambda_i \sum \Lambda_n} e^{-E_i / K T_e} \quad (1)$$

Equation (1) can be rearranged as

$$-\frac{E_i}{KT_c} = \ln \left[\frac{I_i \lambda_i \sum A_i}{A_i B_i} \right] + C(n, l.) = G(E) + C(n_e, t_e) \quad (2)$$

where $B_i = \frac{Q_{\max}(E_{\max}-E_i)}{E_i}$, $C(n, l.) = \ln \left[\Lambda \left(\frac{16m}{\pi K T_c} \right)^{1/2} n_e n_i \hbar c \right]$

and $G(E) = \ln \left[\frac{I_i \lambda_i \sum A_i}{A_i B_i} \right]$

At a given spatial location within the plasma, n_e and t_e will be constant and thus equation (2) becomes a linear equation in which the slope of E_i versus $G(E)$ will be inversely proportional to the electron excitation temperature.

A planar diode configuration discharge with variable cathode temperature (500 to 1000K) has been used for this measurement at 0.5 to 0.9 torr argon and 0.04 torr cesium pressure. The argon and cesium visible and near uv emission spectra have been measured at several locations within the discharge volume starting at 3mm up to 13mm from the cathode. The electron excitation temperature of cesium has been obtained by measuring 6F-nD and 6P-nS transitions. Figure 1 (a) shows a plot of $G(E)$ versus E_i at 3.18mm from the cathode. The slope yields excitation temperature value of 2800 ± 400 K. The corresponding electron excitation temperature from argon spectral lines is 12700 ± 1900 K. Figure 1(b) shows the plot of $G(E)$ versus E_i for argon at the same location. The electron excitation temperature values for both argon and cesium were found to be approximately constant over the measured discharge region. Two significantly different electron excitation temperature values for argon and cesium indicates highly non-equilibrium nature of the low pressure argon-cesium plasma.

Population Inversion in Atomic Cesium: Population inversion in high principal quantum number states of cesium have been observed for high current density pulsed discharge. The population inversion is caused by the recombination process in the high electron density and low electron temperature pulsed discharge. In argon-cesium plasmas, we have observed population inversion for states $n > 10$ in low pressure low current dc

discharge. The negative temperature slope of high n $6P^{1/2}$ to $nD^{3/2}$ transitions of cesium is shown in figure 2. Population inversion in cesium seems to be caused by collisional and optical pumping from argon emission at 805.3 nm which is resonant with the 5D to 6G transition in cesium.

References:

1. D.T. Shaw and S.H. Margolis, J. Appl. Phys., 40, 4377 (1969)
2. P.E. Oettinger, J. Appl. Phys., 55, 3411 (1984)

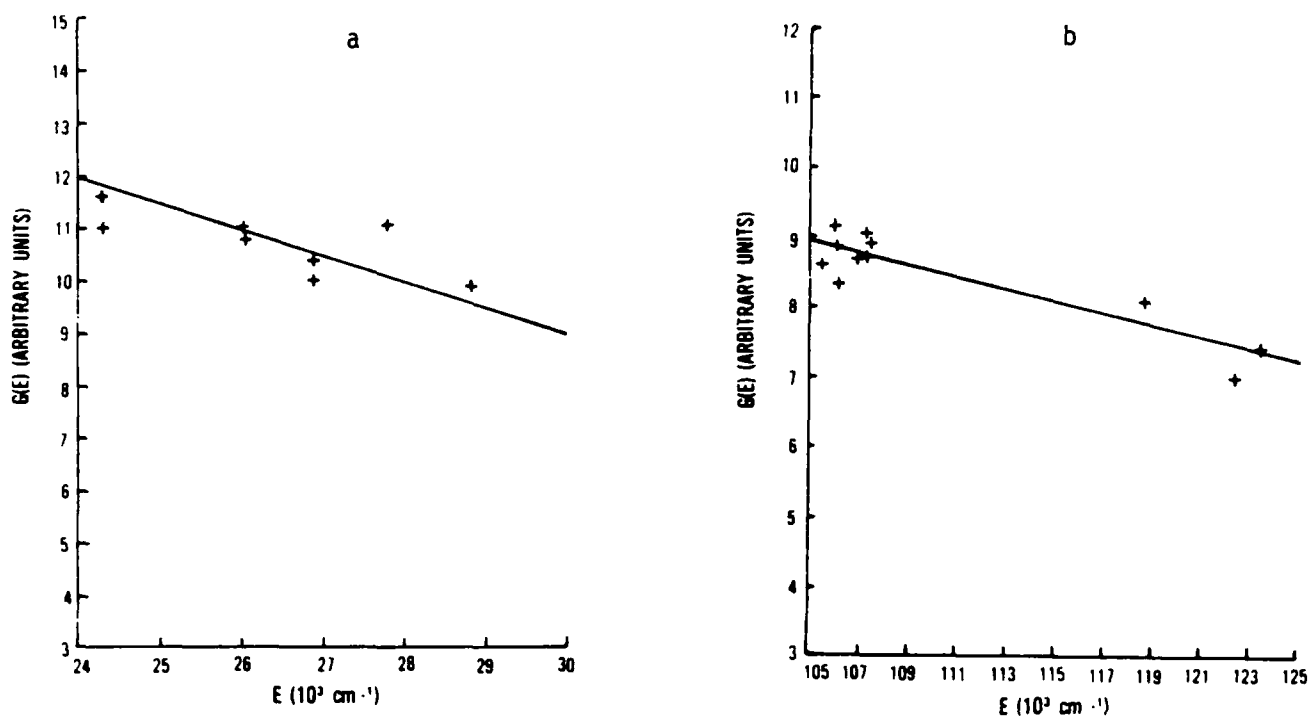


FIGURE 1 Electron excitation temperature of (a) cesium and (b) argon in argon-cesium plasma.

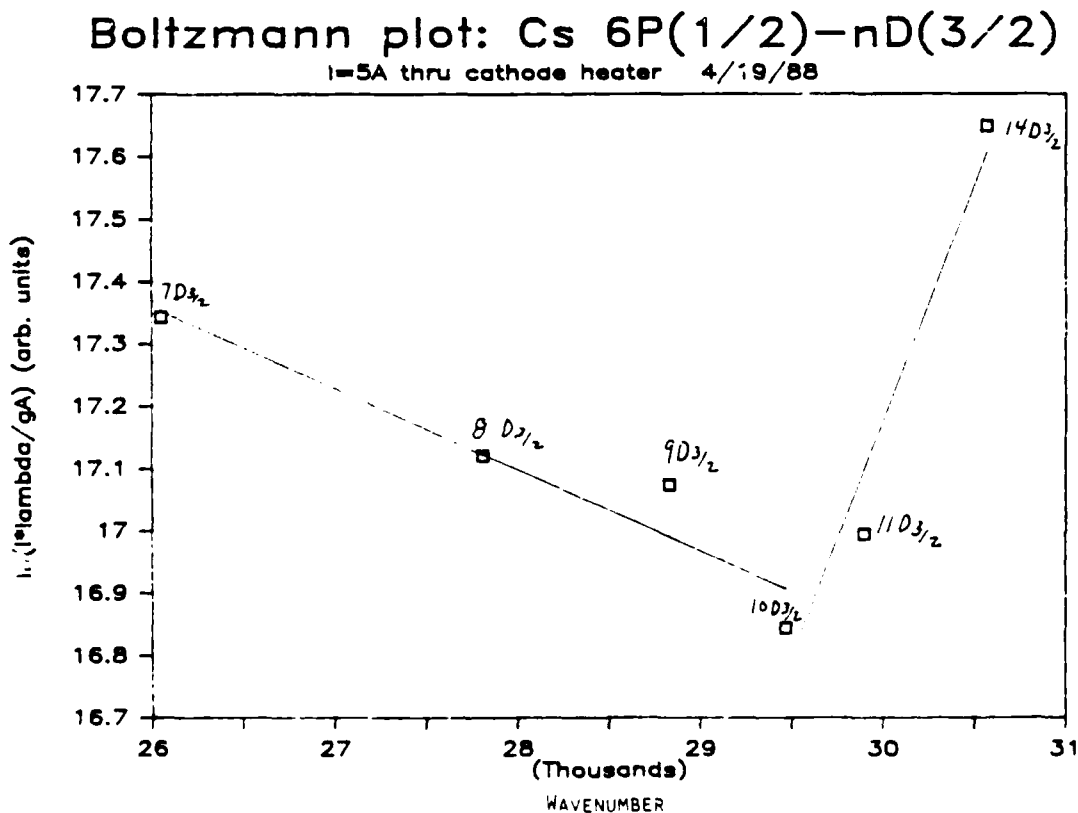


FIGURE 2 Population inversion of high n states of cesium.

AFOSR SPONSORED RESEARCH IN DIAGNOSTICS OF REACTING FLOW

PROGRAM MANAGER: JULIAN M. TISHKOFF

AFOSR/NA
BOLLING AFB DC 20332-6448

SUMMARY/OVERVIEW: The Air Force Office of Scientific Research (AFOSR) program in diagnostics of reacting flow currently is focused on five areas of study: gas-phase measurements; thermochemical and geometric characterization of solid surfaces; particle and droplet measurements; plasmas; and sensors for adaptive feedback control of propulsion systems. An assessment of major research needs in each of these areas is presented.

TECHNICAL DISCUSSION

AFOSR is the single manager for Air Force fundamental research, including programs based on external proposals and in-house work at Air Force laboratories. The diagnostics of reacting flows task is assigned to the AFOSR Directorate of Aerospace Sciences along with programs in rocket propulsion, airbreathing combustion, fluid and solid mechanics, and civil engineering.

Interests of the AFOSR diagnostics of reacting flow program are given in the SUMMARY section above. This program, now in its seventh year, has produced many "first-ever" laser-based measurements. The instrumentation with which these measurements were made is becoming commonly available for laboratory and bench test utilization. Measurements range from microscopic to macroscopic scales with relevance to: plasma acceleration; combustion aerothermochemistry; the behavior and synthesis of advanced energetic materials; characterization of exhaust plume formation and radiation; and dynamic control of propulsion, weapon and power generation systems.

Decisions on support for research proposals are based on scientific opportunities and technology needs. Current AFOSR perceptions of scientific opportunities appear in Figure 1. Technology needs have been defined by the results of the Forecast II exercise which the Air Force completed recently.

Included in Forecast II are four technology areas which are relevant to the AFOSR diagnostics of reacting flow task: combined cycle engines, high performance turbine engines, safe compact nuclear rockets and space-based reusable orbital transfer vehicle. The first area would provide the propulsion system for the aerospace plane. As indicated by

the orientation of the arrows in Figure 1, the task areas with the greatest growth potential are gas-phase measurements relevant to supersonic combustion and plasmas.

The purpose of this abstract has been to communicate AFOSR perceptions of research trends to the university and industrial research communities. However, communication from those communities back to AFOSR also is desirable and essential for creating new research opportunities. Therefore, all proposals and inquiries for fundamental research are encouraged even if the content does not fall within the areas of emphasis described herein. Comments and criticisms of current AFOSR programs also are welcome.

Air Force Basic Research

Aerospace Sciences

Diagnostics of Reacting Flow

Science Area	Trend	Increase
Gas - Phase Measurements	↗	Supersonic Flows. Oxygen Imaging, Flame
Solid Surface Characterizations	↗	
Particle/Droplet Measurements	↘	Multidisciplinary Sprays. High Particle Velocities
Plasmas	↗	Quantitative Images
Adaptive Control Sensors	↗	

AFOSR CONTRACTORS MEETING ON DIAGNOSTICS OF REACTING FLOWInvitees

Mr. Leonard Angello
 Electric Power Research
 Institute
 3412 Hillview Avenue
 Palo Alto CA 94303
 (415) 855-2873

Dr. W. D. Bachalo
 Aerometrics, Inc.
 P. O. Box 308
 Mountain View CA 94042
 (415) 965-8887

Dr. William K. Bischel
 SRI International
 333 Ravenswood Avenue
 Menlo Park CA 94025
 (415) 326-6200

Dr. Richard K. Chang
 Electrical Engineering Dept.
 P. O. Box 2157, Yale Station
 Yale University
 New Haven CT 06520
 (203) 432-4272

Dr. Wai K. Cheng
 Department of Mechanical
 Engineering
 MIT
 Cambridge MA 02139
 (617) 253-4531

Dr. David R. Crosley
 Molecular Physics Department
 SRI International
 333 Ravenswood Avenue
 Menlo Park CA 94025-3696
 (415) 326-6200

Dr. John W. Daily
 Department of Mechanical
 Engineering
 University of California
 Berkeley CA 94720
 (415) 642-0238

Dr. Gregory Dobbs
 United Technologies Research
 Center - Mail Stop 90
 Silver Lane
 East Hartford CT 06108
 (203) 727-7145

Dr. Joel Dubow
 Materials Science Department
 University of Utah
 2008B Mechanical Engrg. Bldg.
 Salt Lake City UT 84112
 (801) 581-8388

Dr. A. C. Eckbreth
 United Technologies Research
 Center
 Silver Lane
 East Hartford CT 06108
 (203) 727-7269

Dr. Richard Field
 U. S. Army Armament RD Center
 DRSMC-LCA-G(D)
 Building 382-S
 Dover NJ 07801
 (201) 724-5844
 (201) 724-5682

Dr. Bish Ganguly
 AFWAL/POOC-3
 Wright-Patterson AFB OH 45433-6563
 (513) 255-2923
 AV785-2923

Dr. Alan Garscadden
 AFWAL/POOC-3
 Wright-Patterson AFB OH 45433-6563
 (513) 255-2923
 AV785-2923

Dr. Larry P. Goss
 Research Applications Division
 Systems Research Labs, Inc.
 2800 Indian Ripple Road
 Dayton OH 45440-3696
 (513) 252-2706

Dr Robert Goulard
 National Science Foundation
 Chemical and Process Eng. Div.
 1800 G Street, N. W.
 Washington DC 20550
 (202) 357-9606

Dr. R. K. Hanson
 Department of Mechanical
 Engineering
 Stanford University
 Stanford CA 94305-3032
 (415) 723-1745

Dr. D. L. Hartley
 Combustion Sciences
 Sandia National Laboratories
 Livermore CA 94550

Dr. L. Hesselink
 Department of Aeronautics and
 Astronautics
 Stanford University
 Stanford CA 94305-3032
 (415) 723-3466

Dr. E. D. Hirleman
 Department of Mechanical and
 Aerospace Engineering
 Arizona State University
 Tempe AZ 85287
 (602) 965-3895

Dr. Donald J. Holve
 Insitec
 28 Bobbie Court
 Danville CA 94526
 (415) 837-1330

Dr. Roman Kuc
 Department of Electrical
 Engineering
 Yale University
 New Haven CT 06520
 (203) 432-4891

Dr. Marshall B. Long
 Department of Mechanical
 Engineering
 Yale University
 New Haven CT 06520
 (203) 432-4229

Dr. Bruce G. MacDonald
 Research Applications Division
 Systems Research Labs, Inc.
 2800 Indian Ripple Road
 Dayton OH 45440-3696
 (513) 252-2706

Dr. Timothy Parr
 Naval Weapons Center
 Code 3893
 China Lake CA 93555
 (619) 939-2521

Dr. S. S. Penner
 Dept. Of. Appl. Mech. and
 Engrg. Sci.
 University of California
 La Jolla CA 92093
 (619) 534-4284

Dr Emil Pfender
 Department of Mechanical Engrg
 125 Mechanical Engineering
 The University of Minnesota
 Minneapolis MN 55455

Dr. John P. Renie
Department of Mechanical and
Industrial Engineering
University of Illinois
Urbana IL 61801
(217) 333-6199

Dr Gregory P Smith
Department of Chem Kinetics
SRI International
333 Ravenswood Avenue
Menlo Park CA 94025
(415) 859-3496

Dr. James D. Trolinger
Spectron Development Labs. Inc
3535 Hyland Avenue
Suite 102
Costa Mesa CA 92626-1439
(714) 549-8477

Dr. James F. Verdieck
Rockwell International
Rocketdyne Div, M/S FA26
6633 Canoga Avenue
Canoga Park CA 91303
(818) 700-4709

Dr Won B Roh
Department of Engrg Physics
Air Force Institute of
Technology
Wright-Patterson AFB OH 45433-6583

Dr. Alan C. Stanton
Southwest Sciences, Inc.
1570 Pacheco Street
Suite E-11
Santa Fe NM 87501
(505) 984-1322

Dr. John A. Vanderhoff
Ballistic Research Laboratory
DRSMC-BLI (A)
Aberdeen Proving Ground MD 21005
(301) 278-6642

Dr. Joda Wormhoudt
Aerodyne Research, Inc.
45 Manning Road
Manning Park Research Center
Billerica MA 01821
(617) 663-9500

AGENDA

1988 AFOSR/ONR CONTRACTORS MEETING ON COMBUSTION

15-17 June 1988

Howard Johnson Plaza-Hotel
Monrovia CA

Wednesday, 15 June

Administrative Session

1:30	AFAL Research Interests R. R. Weiss, Chief Scientist, AFAL	
2:15	Dr. Michael J. Salkind, AFOSR/NA	
2:30	BREAK	
3:00	AFOSR Rocket Propulsion Interests M. A. Birkan, AFOSR/NA	
3:20	AFOSR Interests in Airbreathing Propulsion and Diagnostics of Reacting Flow J. M. Tishkoff, AFOSR/NA	193
3:40	Open Discussion of Government Support for Propulsion Research	
4:30	GENERAL ADJOURNMENT	
4:30	Business Meeting AFOSR Contractors Only	
7:00 - ?	BANQUET	

Thursday, 16 June

8:15	Welcome and Administrative Announcements	
Session Topic:	Boron Fuel Combustion	
Chairman:	J. Bellan, Jet Propulsion Laboratory	
8:30	Transport Phenomena and Interfacial Kinetics in Multiphase Combustion Processes D. E. Rosner, Yale University	197
9:00	Charged Slurry Droplet Research A. J. Kelly, Princeton University	203

9:30	Fuels Combustion Research F. A. Williams, Princeton University	207
10:00	BREAK	
10:30	Fuels Combustion Research F. L. Dryer, Princeton University	211
11:00	Ignition and Combustion Processes of Boron-Based Solid Fuels K. K. Kuo, T. A. Litzinger and V. Yang, Pennsylvania State University	215
11:30	Advanced B and Al Combustion Kinetics Studies Over Wide Temperature Ranges A. Fontijn, Rensselaer Polytechnic Institute	219
12:00	LUNCH	
Note: The 16 June afternoon session on boron chemistry will be conducted concurrently with workshops on topics given below.		
1:30 - 5:00	WORKSHOPS (Locations To Be Announced)	
	Supersonic Combustion	
	Reacting Flow Experiments	
	Reacting Flow Predictions	
Session Topic: Boron Chemistry		
Chairman:	Maj. Larry P. Davis, AFOSR/NC	
1:30	Boron-Assisted Hydrocarbon Combustion: Sensitivity Analysis R. A. Yetter, S. Y. Cho, H. Rabitz and F. L. Dryer Princeton University R. C. Brown, K. Annen and C. E. Kolb Aerodyne Research, Inc.	223
2:00	Boron-Assisted Hydrocarbon Combustion: Sensitivity Analysis R. A. Yetter, S. Y. Cho, H. Rabitz and F. L. Dryer Princeton University R. C. Brown, K. Annen and C. E. Kolb Aerodyne Research, Inc.	227
2:30	NRL Boron Propellants Combustion Program H. Nelson, Naval Research Laboratory	231
3:00	BREAK	

3:30 Cluster Beam Studies of Boron Combustion 233
 S. L. Anderson, State University of New York,
 Stony Brook

4:00 Open Discussion - Future Directions for Boron Combustion Research

5:00 RECESS

Friday, 17 June

8:00 Administrative Announcements

Session Topic: Sprays
 Chairman: T. A. Jackson, AFWAL/POSF

8:15 The Modeling of Drop Containing Turbulent Eddies 237
 J. Bellan, Jet Propulsion Laboratory

8:45 Fundamental Studies on Spray Combustion and Turbulent Combustion 241
 W. A. Sirignano and G. S. Samuelsen, University of California, Irvine

9:15 Dense Spray Structure and Phenomena 245
 G. M. Faeth, University of Michigan

9:45 Coalescence and Break-Up of Droplets In Binary Collisions 249
 U. S. Rohatgi and C. R. Krishna, Brookhaven National Laboratory

10:15 BREAK

Session Topic: Ignition and Combustion Enhancement
 Chairman: R. Goulard, National Science Foundation

10:35 Initiation and Modification of Reaction by Energy Additions: Kinetic and Transport Phenomena 253
 F. E. Fendell and M-S Chou, TRW Space and Technology Group

11:05 Ignition and Combustion Enhancement by Multiphoton Photochemical Means 257
 A. W. Mizolek, U. S. Army Ballistic Research Laboratory

11:35 Combustion Enhancement by High Energy Electron Impact Processes 261
 R. B. Peterson, Oregon State University

12:05	LUNCH	
Session Topic:	Soot	
Chairman:	Maj. Paul Kerch, AFESC/RDV	
1:30	The Determination of Rate-Limiting Steps During Soot Formation M. B. Colket III, United Technologies Research Center	265
2:00	Fuels Combustion Research I. Glassman, Princeton University	269
2:30	Computer Modeling of Soot Formation Comparing Free Radical and Ionic Mechanisms H. F. Calcote, AeroChem Research Laboratories M. Frenklach, Pennsylvania State University	273
3:00	BREAK	
3:30	Fuel Structure and Pressure Effects on the Formation of Soot Particles in Diffusion Flames R. J. Santoro, Pennsylvania State University	277
4:00	Investigation of Fuel Additive Effects on Sooting Flames P. A. Bonczyk, United Technologies Research Center	281
4:30	Lumped Model Generation and Evaluation: Sensitivity and Lie Algebra Techniques With Application to Combustion F. L. Dryer and H. Rabitz, Princeton University	285
5:00	ADJOURN	

ABSTRACTS OF RESEARCH NOT
PRESENTED

- Time-Dependent Simulation of Turbulent Combustion 289
H. R. Baum, R. G. Rehm
National Bureau of Standards
- Turbulent Mixing in Exponential Transverse Jets 293
R. E. Breidenthal
University of Washington
- An Experimental Investigation of Flow Structure, 297
Mixing and Chemical Reaction in Combusting
Turbulent Flows
B. J. Cantwell
Stanford University
- Carbon Monoxide and Turbulence-Chemistry 301
Interactions: Blowoff and Extinction of
Turbulent Diffusion Flames
S. M. Correa, A. Gulati
General Electric Corporate Research and
Development Center
- Chemical Reactions in Turbulent Mixing Flows 305
P. E. Dimotakis, J. E. Broadwell, A. Leonard
California Institute of Technology
- Numerical Simulation of Turbulent Combustion 311
Using Vortex Methods
A. F. Ghoniem
Massachusetts Institute of Technology
- Aerodynamic and Kinetic Processes in Flames 315
C. K. Law
University of California, Davis
- Research on Mixing Control in a Supersonic 319
Shear Layer
D. K. McLaughlin, P. J. Morris, G. S. Settles
Penn State University
- Investigation of Combustion in Large Vortices 323
F. E. Marble, E. E. Zukoski
California Institute of Technology
- The Effects of Compressibility on a Supersonic Mixing 327
Layer
D. Nixon
Nielsen Engineering & Research, Inc.

Numerical Investigation of Turbulent Flame Sheets S. B. Pope Cornell University	331
Premixed Turbulent Flame Propagation D. A. Santavicca The Pennsylvania State University	333
Experimental Investigation of Opposed Jet Turbulent Diffusion Flames L. Talbot University of California, Berkeley	337
Thermal and Flow Structures of Turbulent V-Flames at Low Damköhler's Numbers T-Y Toong Massachusetts Institute of Technology	341

AFOSR SPONSORED RESEARCH IN AIRBREATHING COMBUSTION

PROGRAM MANAGER: JULIAN M. TISHKOFF

AFOSR/NA
BOLLING AFB DC 20332-6448

SUMMARY/OVERVIEW: The Air Force Office of Scientific Research (AFOSR) program in airbreathing combustion currently is focused on seven areas of study: reacting flow, soot, sprays, methods, boron slurries, ignition/combustion enhancement and supersonic combustion. An assessment of major research needs in each of these areas is presented.

TECHNICAL DISCUSSION

AFOSR is the single manager for Air Force fundamental research, including programs based on external proposals and in-house work at Air Force laboratories. Airbreathing combustion is assigned to the AFOSR Directorate of Aerospace Sciences along with programs in rocket propulsion, diagnostics of reacting flow, fluid and solid mechanics, and civil engineering.

Interests of the AFOSR airbreathing combustion program are given in the SUMMARY section above. Many achievements can be cited for these interests, yet imposing fundamental research challenges remain. The objective of the program is publications in the refereed scientific literature describing significant new understanding of multiphase turbulent reacting flow. Incremental improvements to existing scientific approaches, hardware development and computer codes fall outside the scope of this objective.

Decisions on support for research proposals are based on scientific opportunities and technology needs. Current AFOSR perceptions of scientific opportunities appear in Figure 1, and areas of emphasis are indicated by arrows with positive slopes. Technology needs have been defined by the results of the Forecast II exercise which the Air Force completed recently.

Included in Forecast II are two technology areas which are relevant to the AFOSR airbreathing combustion task: combined cycle engines and high performance gas turbines. The former area would provide the propulsion system for the National Aero Space Plane, and related research proposals will receive primary consideration for available support. The combined cycle engine concept has motivated significant research interest in supersonic combustion. In fiscal year 1986 (FY86) substantial research activity was initiated to study mixing and chemical reaction under supersonic flow

conditions. In FY87 new research efforts were directed at novel means for achieving ignition, combustion enhancement and low-loss flameholding in supersonic combustion. FY89 will see new research opportunities in interactive control of fluid transport processes. These opportunities reflect a generic interest in interdisciplinary efforts between researchers in control theory and fluid transport behavior. For the combined cycle engine a particular focus of interactive flow control will be the investigation of means to overcome the suppression of mixing which high Mach number flows experience in relation to subsonic flows.

The physical behavior of boron slurry fuels is another research area with high technological benefit. An AFOSR organizational change has transferred responsibility for the chemical aspects of boron fuel utilization to the AFOSR Directorate of Chemical and Atmospheric Sciences.

The behavior of single fuel droplets has been the subject of renewed research activity. Both computational and experimental capabilities appear to be poised to expand studies of spray combustion to spatial dimensions smaller than those of the droplets themselves. A particular focus of this research activity will be the interactions between droplets and gas-phase turbulent transport processes.

The purpose of this abstract has been to communicate AFOSR perceptions of research trends to the university and industrial research communities. However, communication from those communities back to AFOSR also is desirable and essential for creating new research opportunities. Therefore, all proposals and inquiries for fundamental research are encouraged even if the content does not fall within the areas of emphasis described herein. Comments and criticisms of current AFOSR programs also are welcome.

Air Force Basic Research Aerospace Sciences

Airbreathing Combustion

Science Area	Trend	Decrease	Increase
Reacting Flow	↑		
Soot	↑		
Sprays		→	
Boron Slurries	↑		
Supersonic Combustion		↑	
Methods		↑	
Ignition / Combustion Enhancement		↑	
			Atomization, Nondilute Sprays, Turbulence Interactions, Drop Transport Processes
			Chemistry (To AFOSR/NC)
			Shear Layer Mixing, Flow Control
			Plasmas, Detailed Photochemistry, Flow Interactions

**TRANSPORT PHENOMENA AND INTERFACIAL CHEMICAL KINETICS
IN MULTIPHASE COMBUSTION SYSTEMS***



Grant No. AFOSR-84-0034

Principal Investigator[†] : Daniel E. Rosner

High Temperature Chemical Reaction Engineering Laboratory
Yale University, P.O. Box 2159 YS, New Haven, CT 06520 U.S.A.

SUMMARY/OVERVIEW:

The performance of ramjets burning slurry fuels (leading to condensed oxide aerosols and liquid film deposits), gas turbine engines in dusty atmospheres, or when using fuels from non-traditional sources (e.g., shale-, or coal-derived), depends upon the formation and transport of small particles across non-isothermal combustion gas boundary layers (BLs). Even airbreathing engines burning "clean" hydrocarbon fuels can experience soot formation/deposition problems (e.g., combustor liner burnout, accelerated turbine blade erosion and "hot" corrosion). Moreover, particle formation and transport are important in many chemical reactors used to synthesize or process aerospace materials (turbine blade coatings, optical waveguides, ...). Accordingly, our research is directed toward providing chemical propulsion systems engineers and materials-oriented engineers with new techniques and quantitative information on important particle- and vapor-mass transport mechanisms and rates.

An interactive experimental/theoretical approach is being used to gain understanding of performance-limiting chemical-, and mass/energy transfer phenomena at or near interfaces. This includes the development and exploitation of seeded laboratory flat flame burners (see, e.g., Figs. 1,7), flow-reactors (Fig.8), and new optical diagnostic/spectroscopic techniques. Resulting experimental rate data, together with the predictions of asymptotic theories (Section 2), are then used as the basis for proposing and verifying simple viewpoints and effective engineering correlations for future design/optimization studies.

TECHNICAL DISCUSSION

1. Seeded Flame Experiments on Vapor and Submicron Particulate Transport Rates

We are using seeded, atmospheric pressure flat flame burner techniques (1,10,14,20) combined with laser optical probing of chemically inert, reflective targets (e.g., Pt ribbons) and diffusion boundary layers (see Fig. 1) to study rates of chemical vapor deposition (14), submicron particle deposition (1,4,5) and condensate evaporation (e.g., $B_2O_3(1)$ (14), $Na_2SO_4+K_2SO_4(1)$ (10)) under well-characterized conditions amenable to theoretical investigation (Section 2) and systematic physicochemical model development (10,22). This includes the formation and detection of dispersed condensates ("mists") in thermal boundary layers (21), the scavenging of supersaturated vapors by dispersed particulate matter (12,22), and the use of seeded laboratory counterflow burners (Fig. 6) to infer particle thermophoretic diffusivities in combustion products (Section 2 and Fig.7).

2. Transport Theory (13, 29, 32): Chemical Reaction, Phase Change, and Thermophoretic Effects on Boundary Layer Convective Mass Transport

We have begun to exploit and extend a 'limiting case' (asymptotic)-approach in which we compare CVD-rates in the two interesting extremes of vapor phase chemical kinetics (24), viz. local thermo

* AFOSR/QNR Contractors Meeting on Combustion, Monrovia, CA, 13-17 June, 1988

† For research program collaborators consult the REFERENCES.

chemical equilibrium (LTCE) everywhere along the diffusion path (29), and no chemical reactions ("chemically frozen" (CF)) (except at the deposition surface, where LTCE is assumed due to heterogeneous reactions). Laminar boundary layer theory predictions (24) for the illustrative case of sodium sulfate salt deposition (Fig.2) revealed a remarkable insensitivity to vapor phase chemical kinetics — a fortunate circumstance in view of the great mechanistic complexity and associated uncertainties in the relevant vapor phase kinetics in this (and other) important CVD case(s). In view of the possibility of departures from LTCE at/near the "cold boundary", we have also developed a systematic scheme for testing which species are likely to depart from LTCE first (29), and have begun develop a geometry-insensitive 'sublayer' theory to predict deposition rates in such circumstances (29).

Regarding particle transport, we have extended our previous solutions and correlations of thermophoretically modified submicron particle mass transport across laminar ELs (3,7,8) and turbulent ELs (6,8) into the domain of high particle mass loading (16,23), a situation encountered in numerous materials-processing applications (See Fig.3, pertaining to our model calculations of the deposition of doped SiO_2 in optical waveguide fabrication), and, locally, in two-phase (e.g., droplet/gas) flows of chemical propulsion interest. High mass loading is predicted to have an appreciable effect on thermophoretically dominated mass transfer coefficients (see our laminar EL results, Fig.2). Moreover, since coagulation is likely to be important in highly loaded 'aerosol' systems (27), and may alter the structure of the resulting ('quasi')solid deposits, we have developed methods to predict the particle size distribution at the deposition site (Fig.5), as well as dopant incorporation levels (23). Another interesting phenomenon recently investigated (8, 25, 31) is the absence of particles adjacent to a hot solid surface (or diffusion 'flame sheet', as in Fig.7). This 'phase separation', caused by the thermophoretic repulsion of particles near a hot surface, could be exploited in gas/ particle separation devices even at high mass loading (25), and used to protect semiconductor surfaces from damaging dust (31). Using a lightly seeded opposed-jet laminar diffusion flame apparatus (Fig.7) we are now exploiting this phase-separation phenomenon to estimate the thermophoretic diffusivity of submicron metal oxide particles (See Fig.7 and Ref. 26) at combustion gas temperatures.

Because of increasing interest in the Soret diffusion of large, highly nonspherical molecules (e.g., polycyclic aromatic soot precursors and large metal-organic vapors used to deposit thin films with useful optical properties) and the thermophoretic transport of nonspherical submicron particles (e.g., long soot aggregates) we have recently predicted the shape dependence of their (orientation-averaged) thermal diffusion velocities (15) and will experimentally test some of these predictions, and their EL-consequences, in the future. Of course, particle size and shape also affect Brownian diffusivities, and we have begun developing useful engineering methods for predicting total mass deposition rates from 'coagulation-aged' distributions of particles — including 'fractal' agglomerates (30).

3. Gasification Kinetics of Solid Boron (28)

To make (i) rapid-response gas/solid reaction rate measurements over a large temperature range, and (ii) surface mass balances necessary for mechanistic understanding of high temperature gas/solid reactions (18), we have recently been exploiting a sensitive emission spectroscopic technique. In this technique, a low pressure microwave-induced plasma (MIP) is used to excite characteristic emission from atoms in the gaseous product species of a gas/solid reaction in a low pressure flow reactor.

We are now employing a modified version of our transonic, vacuum flow reactors (Fig.8) developed earlier under AFOSR-support (18) for studying important gas reactions with solid boron (28). The reaction product vapor species are dissociated and photon emission from the resulting boron atoms is produced in the products of a microwave discharge plasma before leaving the reactor. Evaporation and gasification reactions are studied by measuring the emission intensity from this discharge, via a 0.5m Jarrell-Ash monochromator. The skimmer and the inner co-axial tube (Fig.8) were installed so that the system detects only reaction products from the central, uniform-temperature region of the CVD boron filament.

This microwave-induced plasma emission spectroscopy (MIPES) technique is now being applied to the oxidation of high temperature solid boron by $\text{OBO}_2(\text{g})$, (28), a system of considerable interest to the chemical propulsion community. The $\text{B}_2\text{O}_3(\text{g})$ is generated from an upstream electrically heated folded metal "boat" source. Our preliminary results for the inferred reaction probability over the broad surface temperature range from ca. 1300K to 2050K are displayed in Fig.9. Note that above about 1400K (at the stated reactant pressure level) this gas/solid chemical reaction is remarkably efficient — more

so than boron gasification by $O_2(g)$, $O(g)$, or $CO_2(g)$. Also of considerable interest is the location of the "break" in the Arrhenius diagram — i.e. the surface temperature below which the kinetics reveals oxide-layer 'protective' behavior at the prevailing oxidizer partial pressure (18). Our recent experimental results for this locus are displayed in Fig.10. We are now exploring this locus in the simultaneous presence of hydrogen-containing vapor species.

CONCLUSIONS, FUTURE RESEARCH

In the OSR-sponsored research briefly described here we have shown that new laser-based methods and emission spectroscopy for rapidly measuring vapor- and particle-mass transfer rates (1,5,14,20,29), combined with recent advances convective mass transfer theories (2,3,6-9,13,19,23,25,27,29), are providing useful means to incorporate these phenomena in many propulsion engineering and materials engineering design/optimization calculations. We are now extending work on the potentially important effects of high local particle mass loading (16,23,25,27), polydispersed aerosols (27,30), non-negligible particle inertia, and highly nonspherical particles, aggregates (or molecules) (15,19). To shed light on boron particle ignition, quasi-steady combustion and extinction, our current research on the kinetics of solid boron gasification using MIFES (28) has been extended to examine the remarkably efficient $B_2O_3(g)/B(s)$ reaction in the broad temperature interval: 1300K-2050K. In the near future, we plan to supplement these gasification kinetic studies with theoretical studies of their implications for boron particle combustion, and embark on experimental/theoretical studies of the nucleation kinetics of $B_2O_3(g)$.

REFERENCES

1. Rosner, D.E. and Kim, S.S., "Optical Experiments on Thermophoretically Augmented Submicron Particle Deposition from 'Dusty' High Temperature Gas Flows," The Chem. Engrg. J. 29, No. 3, 147-157 (1984).
2. Gokoglu, S.A. and Rosner, D.E., "Correlation of Thermophoretically-Modified Small Particle Diffusional Deposition Rates in Forced Convection Systems with Variable Properties, Transpiration Cooling and/or Viscous Dissipation," Int. J. Heat & Mass Transfer 27, 639-645 (1984).
3. Gokoglu, S.A. and Rosner, D.E., "Thermophoretically-Augmented Forced Convection Mass Transfer Rates to Solid Walls Across Non-Isothermal Laminar Boundary Layers," AIAA J. 24, No. 1, 172-179 (1986).
4. Eisner, A.D. and Rosner, D.E., "Experimental Studies of Soot Particle Thermophoresis in Non-Isothermal Combustion Gases Using Thermocouple Response Techniques," Combustion & Flame 61, 153-166 (1985).
5. Eisner, A.D. and Rosner, D.E., "Experimental and Theoretical Studies of Submicron Particle Thermophoresis in Combustion Gases," J. PhysicoChemical Hydrodynamics (Pergamon) 7, 91-100 (1986).
6. Gokoglu, S.A. and Rosner, D.E., "Thermophoretically Enhanced Mass Transport Rates to Solid and Transpiration-Cooled Walls Across Turbulent (Law-of-the-Wall) Boundary Layers," I/EC Fundamentals 24, No. 2, 208-214 (1985).
7. Gokoglu, S.A. and Rosner, D.E., "Viscous Dissipation Effects on Thermophoretically-Augmented Particle Transport Across Laminar Boundary Layers," Int. J. Heat & Fluid Flow 6, No. 4, 293-297 (1985).
8. Gokoglu, S.A. and Rosner, D.E., "Prediction and Rational Correlation of Thermophoretically Reduced Particle Mass Transfer to Hot Surfaces Across Laminar or Turbulent Forced-Convection Gas Boundary Layers," ChE Communications, 44, 107-119 (1986).
9. Gokoglu, S.A. and Rosner, D.E., "Effect of Particulate Thermophoresis in Reducing the Fouling Rate Advantages of Effusion-Cooling," Int. J. Heat & Fluid Flow 5, No. 1, 37-41 (1984).
10. Rosner, D.E. and Liang, B., "Laboratory Studies of the Deposition of Alkali Sulfate Vapors from Combustion Gases Using a Flash-Evaporation Technique," ChE Communications 42, 171-196 (1986); see also Liang, B., and Rosner, D.E., "Laboratory Studies of Binary Salt CVD in Combustion Gas Environments," AIChE J. 33, No. 12, 1937-1948 (1987).
11. Santoro, G.J., Gokoglu, S.A., Kohl, F.J., Stearns, C.A. and Rosner, D.E., "Deposition of Na_2SO_4 from Salt-Seeded Combustion Gases of a High Velocity Burner Rig," NASA TM 83751 (1984).
12. Castillo, J.L. and Rosner, D.E., "Nonequilibrium Theory of Surface Deposition from Particle-Laden, Dilute Condensable Vapor-Containing Streams, Allowing for Particle Thermophoresis and Vapor Scavenging Within the Laminar Boundary Layer," Int. J. Multiphase Flow 14, No. 1, 99-120 (1988).

13. Rosner, D.E., Transport Processes in Chemically Reacting Flow Systems, Butterworths, Stoneham, MA (June, 1986); (Second printing, 1988).
14. Seshadri, K. and Rosner, D.E., "Optical Methods and Results of Dewpoint and Deposition Rate Measurements in Salt/Ash-Containing Combustion Gases — $B_2O_3(1)$ Deposition Rates by Interference Methods and Comparisons with Theory" Amer. Inst. Chem. Engrg. J. 30, No.2, 187-196 (1984); see, also: "Polarization (Ellipsometric) Measurement of Condensate Deposition and Evaporation Rates and Dew Points in Salt/Ash Containing Combustion Gases," Combustion & Flame 61, 251-260 (1985).
15. Garcia-Ybarra, P., and Rosner, D.E., "Thermophoretic Properties of Small Nonspherical Particles and Large Nonspherical Molecules," AIChE J., (in press, 1988).
16. Rosner, D.E. and Park, H.M., "Thermophoretically Augmented Mass, Momentum and Energy Transfer Rates in High Particle Mass-Loaded Laminar Forced Convection Systems," ChE Science (in press, 1988).
17. Rosner, D.E., Gunes, D. and Nazih-Anous, N., "Aerodynamically-Driven Condensate Layer Thickness Distributions on Iso-Thermal Cylindrical Surfaces," ChE Communications 24, 275-287 (1983); see also Rosner, D.E. and Nagarajan, R., "Vapor Deposition and Condensate Flow on Combustion Turbine Blades: Theoretical Model to Predict/Understand Some Corrosion Rate Consequences of Molten Alkali Sulfate Deposition in the Field or Laboratory," Int. J. Turbo/Jet Engines (in press, 1988).
18. Rosner, D.E., "High Temperature Gas-Solid Reactions," in Annual Review of Mat. Sci. 2, Annual Reviews, Inc., 573-606 (1972).
19. Rosner, D.E., "Mass Transfer Across Combustion Gas Thermal Boundary Layers — Power Production and Materials Processing Implications," in Heat Transfer in Fire and Combustion Systems, HED 45, C.K. Law, Y. Jaluria, W.W. Yuen and K. Miyasaka, Eds., ASME, NY, 3-8 (1985).
20. Rosner, D.E., "Experimental and Theoretical Studies of the Deposition of Inorganic Compounds from Combustion Gases", Yale HTCRE Laboratory (May 1987).
21. Liang, B., Gomez, A., Castillo, J.L., and Rosner, D.E., "Experimental Studies of Nucleation Phenomena within Thermal Boundary Layers — Influence on Chemical Vapor Deposition Rate Processes", AIChE J. (submitted, 1988); Paper A5A, 1987 Annual Mtg. of the Amer. Assoc. Aerosol Research.
22. Rosner, D.E., and Liang, B. "Experimental Studies of Deposition Rates in the Presence of Alkali Sulfate Vapor Scavenging by Submicron Particles in Combustion Gas Boundary Layer", Chem. Engrg. Communications 64, 27-46 (1988).
23. Park, H.M., and Rosner, D.E., "Dopant Redistribution Across Aerosol-Laden Laminar Non-Isothermal Boundary Layers", Chem. Engrg. Sci. (in press, 1988).
24. Rosner, D.E., Nagarajan, R., Kori, M., and Gokoglu, S.A., "Maximum Effect of Vapor Phase Chemical Reactions on CVD-Rates and Deposition Onset Conditions in the Absence of Interfacial Chemical Kinetic Barriers", Proc. 10th Int. Conference on Chemical Vapor Deposition, Electrochemical Society.
25. Park, H.M., and Rosner, D.E., "Thermophoretically Induced Phase-Separation in Highly Mass-Loaded 'Dusty' Gas Mixtures", Yale HTCRE Lab. (March 1987).
26. Gomez, A., and Rosner, D.E., "Counterflow Diffusion Flame: A New Tool for Estimating Fine Particle Thermophoretic Diffusivities", paper #26f presented at the 1987 Annual Mtg. of the AIChE, NY.C and at the 11/87 Eastern States Comb. Inst. Mtg., Gaithersburg, MD.
27. Park, H.M., and Rosner, D.E., "Effect of Coagulation in the Boundary Layer on the Size Distribution of Thermophoretically Deposited Particles", Chem. Engrg. Sci. (in press, 1988).
28. Gomez, A., Zvuloni, R., and Rosner, D.E., "Flow Reactor Studies of Boron Vaporization and Kinetically-Controlled Oxidation Using Microwave-Induced Plasma Emission Spectroscopy: Preliminary Results", presented at the 1986 Technical Meeting - The Combustion Inst.-Eastern Section, Dec. 12, 1986, San Juan, Puerto Rico; and at the Joint Meeting of the French and Italian Section of the Combustion Institute, June 16-19, 1987 Amalfi, Italy; see also Rosner, D.E., Gomez, A., and Zvuloni, R. "Recent Developments in Microwave Discharge-Low Pressure Flow Reactors for Kinetic Studies of Rapid Gas/Solid Etching Reactions — Use of Surface Temperature Modulation and Microwave-Induced Plasma Spectroscopy to Monitor Reaction Rates", presented at the Engineering Research Foundation Conference on Chemical Reaction Engrg., Santa Barbara, CA, March 6-13, 1987.
29. Rosner, D.E., "Transport Processes and Chemical Kinetics in High Temperature Lamp Modeling", (invited paper) in Proc. Symposium on High Temperature Lamp Chemistry, Vol. 88-4, 111-138, 173rd Electrochemical Society Meeting, Atlanta, GA, (May 17, 1988)
30. Rosner, D.E., "Rapid Estimation of Total Mass Deposition Rates by Convective-Diffusion from Poly-dispersed' Aerosols"; AIChE J. (Submitted, April 1988)

31. Friedlander, S.K., Fernandez de la Mora, J., and Gokoglu, S.A. "Diffusive Leakage of Small Particles across the Dust-Free Layer near a Hot Wall". J. Colloid Interface Sci. (in press, 1988)

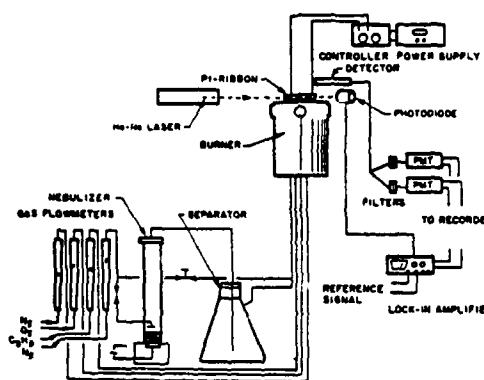


Figure 1. Experimental arrangement (schematic) for laboratory studies of mixed alkali sulfate deposition rate processes using the 'flash-evaporation' technique (Roemer and Liang, 1986, 1987).

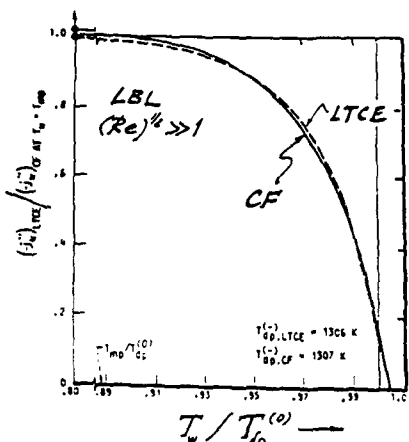


Figure 2. Laminar boundary layer (LBL) theory-predicted deposition rates of Na_2CO_3 in the asymptotic extremes of infinite (LTCE) and vanishing ('chemically frozen') homogeneous reaction kinetics; dependence on normalized surface temperature $T_w/T_w^{(0)}$ when $T_w = 1936 \text{ K}$, $T_w^{(0)} = 1301 \text{ K}$, $T_w^{(0)} = 1157 \text{ K}$ (after Gokoglu, 1988; and Roemer, Negarajah, Gokoglu and Kori, 1987).

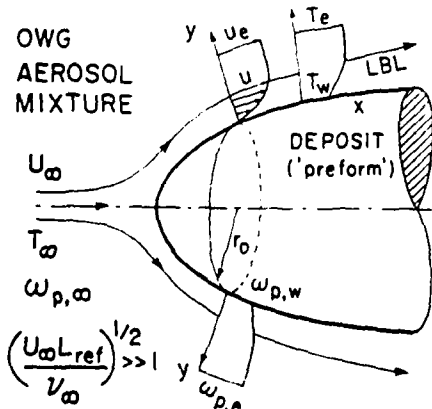


Figure 3. Viscous flow configuration for optical waveguide glass preform deposition. Body-oriented boundary layer (BL) coordinate system and nomenclature: axisymmetric case shown (after Roemer and Park, 1988 (18)).

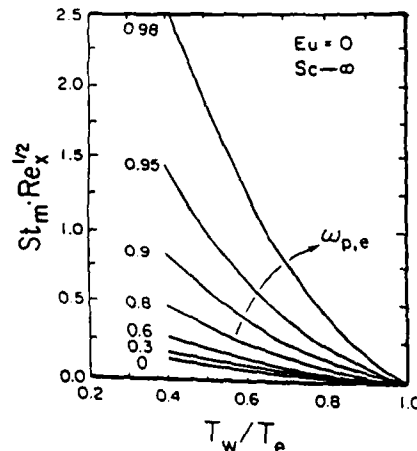


Figure 4. Dependence of thermophoretically dominated dimensionless particle wall diffusion flux, on wall temperature ratio T_w/T_e at several particle mass loadings; laminar flat plate boundary layer (after Roemer and Park, 1988 (18)).

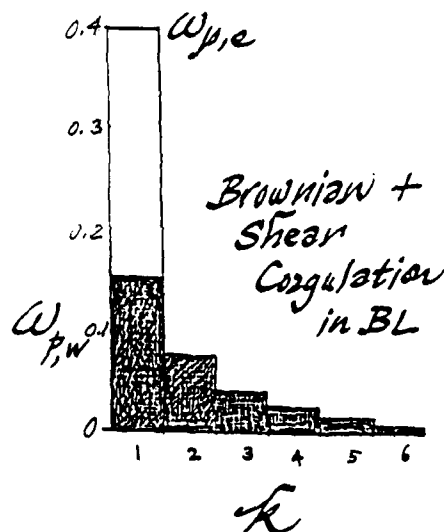


Figure 5. Predicted (mass) distribution of the size of thermophoretically depositing particles (of 'initial' diameter 0.2 μm at the outer edge of the laminar boundary layer with $\omega_{p,e} = 0.4$; $T_w/T_e = 0.6$; $U_w = 200 \text{ cm/s}$; $T_w = 0$); combined Brownian and shear coagulation (after Park and Roemer, 1988 (27)).

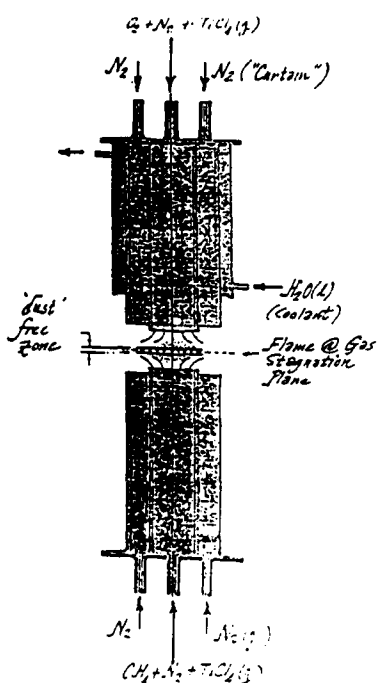


Figure 6. Seeded opposed-jet laminar diffusion flame burner configuration for experimental determinations of the thermophoretic diffusivity of submicron particles (Gomes and Roemer, 1987).

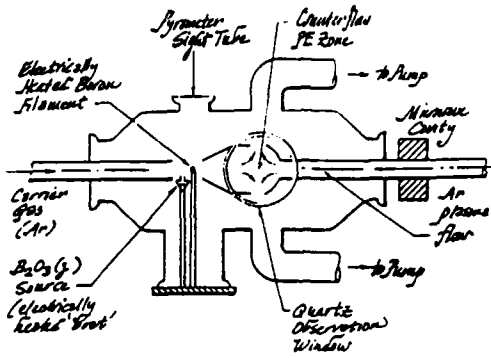


Figure 8. Flow reactor configuration for kinetic studies of gas/solid reactions using product detection via microwave-induced plasma emission spectroscopy (MIPES) (Gomes, Zvuloni and Roemer, 1986; 1987).

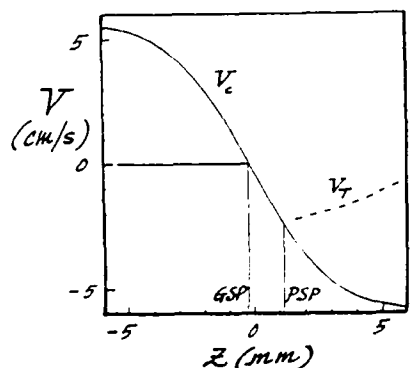


Figure 7. Convective axial velocity and aerosol particle thermophoretic velocity versus axial coordinate (after Gomes, Roemer, 1987, (26)).

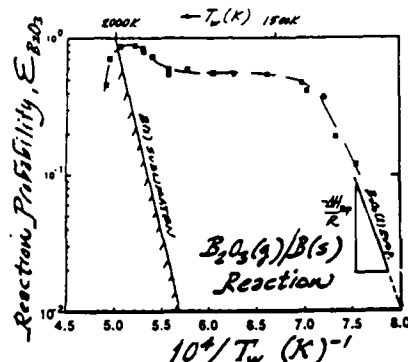


Figure 9. Experimental results (Arrhenius diagram) for the inferred reaction probability for gasification of solid boron by OBOBO(g) at a reaction partial pressure of ca. 10^{-3} atm (after Zvuloni, Gomes and Roemer, 1988); shown for comparison, are corresponding boron sublimation rate and slope of the expected B2O3(c) evaporation rate.

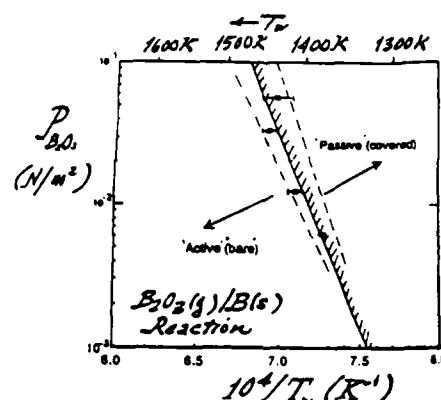


Figure 10. Experimentally determined 'active'-to-'passive' transition locus defining the conditions under which solid boron gasification by OBOBO(g) occurs in the absence or presence of a 'protective' B2O3(c)-layer (after Zvuloni, Gomes and Roemer, 1988).



CHARGED SLURRY DROPLET RESEARCH

(AFOSR Grant No. 86-0013)

Principal Investigators:

Dr. Arnold J. Kelly
School of Engineering/Applied Science
Mechanical and Aerospace Engineering Department
Princeton University, Princeton, NJ 08544

Professor Robert G. Jahn
School of Engineering/Applied Science
Mechanical and Aerospace Engineering Department
Princeton University, Princeton, NJ 08544

SUMMARY/OVERVIEW

Over and above the unique self-dispersive behavior of charged sprays, the individual droplets are subject to electrostatic surface forces that produce "Rayleigh Bursting" and the electrostatic deagglomeration of residual particulate clusters from evaporatively dried droplets. Both Rayleigh Bursting and the deagglomeration process, while beneficial to atomization and combustion, are inadequately documented, poorly understood and involve the rapid dispersal of small ($\sim 10 \mu\text{m}$) charged particulates. Two new research instruments have been developed to study these processes: a levitated droplet apparatus for imaging the disruption of isolated droplets/agglomerates and a high mass (10^{14} AMU) quadrupole mass spectrometer/high speed electrometer (QMS/HSE) to measure both the charge and the mass of the post disruption debris. The QMS/HSE experiment has produced evidence that the surface charge on droplets in the size range of interest is in a "frozen," "crystalline" state. These data are consistent with, and provide an explanation for, the assumption of limited surface mobility that has had to be invoked in order to obtain a realistic description of the Rayleigh bursting process.

TECHNICAL DISCUSSION

No quantitative data exist concerning the most elemental features of either Rayleigh bursting or the deagglomeration processes. In fact the temporal development of the disruption, the number of particles generated and their mass, charge, velocity and spatial distribution have yet to be observed. This research effort has been directed to answering these questions and thereby to address the larger concern of whether charged sprays can benefit slurry fuel combustion. The charged particle levitator has been specifically designed to provide direct quantitative information concerning both the behavior preceding disruption and a quantitative measure of the number of siblings produced. Sibling charge and mass are measured using a high mass (10^{14} AMU) quadrupole mass spectrometer/high speed electrometer instrument that also has been expressly designed for this investigation.

The charged droplet levitator apparatus, depicted in the schematic diagram of figure 1, is an extensively refined variant of the design first described by Rhim, et al^(1,2). A Compaq 386 microcomputer is used to control all aspects of particulate levitation, positioning and imaging. Imaging now involves an

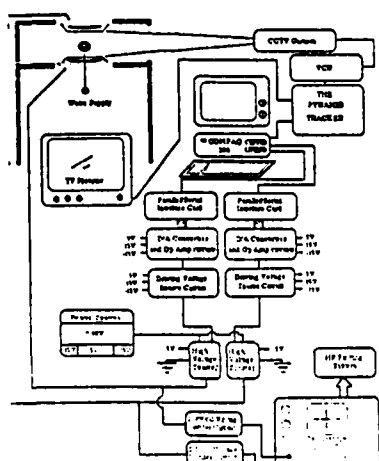


Figure 1 Charged Particle Levitation Experiment System Schematic

image processing computer the "Pyramid Tracker" that has recently been developed^(3,4) by the David Sarnoff Research Laboratories of SRI.

During operation the Compaq computer issues a droplet launch command sequence that controls the application of high voltage to the levitator electrodes. Once launched the droplet is automatically tracked and stabilized for observation within the field of view of the CCD camera optics. Stabilization and observation of the evaporating particulate occurs by the "real time frame grabber" capability of the Pyramid Tracker computer. This proprietary circuitry is programmed to automatically analyze visual data at any of six resolution levels ranging from level 1 consisting of 7x8 pixels to

maximum resolution level 6 having the full 240x256 pixel image. By automatically adjusting the image resolution the Pyramid Tracker can rapidly process the visual data to generate droplet position control signals. This is typically accomplished using low resolution level 1 imaging. Once stabilized the droplet/agglomerate is then imaged at level 6 in anticipation of the disruption process. In this way it is possible to use the same system to position the particle and to capture the disruption process. All of the necessary software has been written and all of the D/A interface electronics for levitation is now operational. Particulates are now being levitated on a routine basis.

The QMS/HSE has been calibrated for particle charge density levels from ~ 100 to $\sim 3000 \text{ C/m}^3$ corresponding to droplet, and particulate radii of from about 0.7 to about 3 microns. Figure 2 displays a comparison of mean Octoil spray droplet data obtained with this instrument with those observed independently by Hendricks⁽⁵⁾. The good correlation indicates that the QMS/HSE is capable of providing quantitatively accurate data for the charge and mass of droplets/particulates in the size range of interest to this study.

Droplet spectra obtained using the QMS/HSE operated at a fixed droplet charge to mass ratio when compared to the statistical equilibrium model of electrostatic spraying⁽⁶⁾, as illustrated in figure 3, permits the extraction of fundamental spray and droplet property parameters in the vicinity of the droplet charging discontinuity. One parameter of particular interest is the droplet surface limiting electric field strength E_s . Table 1 summarizes the E_s values for Octoil. Droplets smaller than the discontinuity (smaller than 0.87 microns radius,) are on branch A larger, and more highly charged droplets are on branch B. These data confirm the very preliminary results reported in the last abstract; the effective electric field differs by almost a factor of two depending upon whether the droplet is larger or smaller than the discontinuity.

It is difficult to ascribe physical meaning to this approximately 2:1 variation of limiting electric field strength since it is anticipated to be an intrinsic and immutable feature of the droplet surface. The only physically

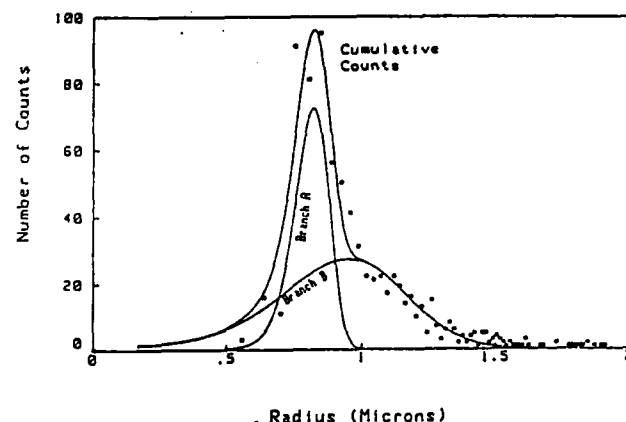
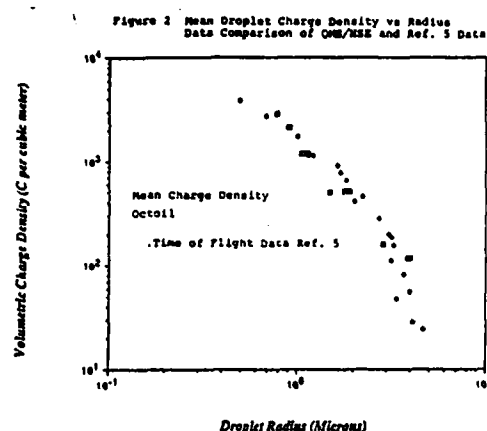


Figure 3 Q/M/XSE size data for 1.23 C/kg Octoil droplets showing the contribution of droplets smaller than the discontinuity (Branch A) and larger than the discontinuity (Branch B)

meaningful way to interpret these data is to consider them to be a reflection of shifts in the permittivity, a parameter that is always multiplicatively associated with E . If E is taken to have an immutable value of ~ 6.5 GV/m the average value obtained from spray data, the relative permittivity ϵ/ϵ_0 on branch B is unity or slightly above. This is constant with a vapor cloud surrounding the droplet whereas the fractional value for this ratio on branch A would signal the presence of a plasma state. In other words the large droplet branch B corresponds to a cold, frozen electron state whereas the small droplets of branch A are surrounded by a hot electron plasma. This description is⁽⁷⁾ consistent with what is known concerning electron crystallization. Data⁽⁷⁾ indicate that electron crystallization occurs when the ratio of electrostatic to thermal energy for the electrons exceeds about 137. As noted in figure 4, this condition is amply satisfied by the droplets on branch B, but not on branch A. This concept of a crystalline electron layer provides a natural explanation for why it was necessary to assume limited surface mobility in order⁽⁸⁾ to obtain a physically realistic description of the Rayleigh Bursting process⁽⁸⁾. The data support the view that Rayleigh Bursting involves the shattering of electron crystals.

<u>Q/M</u> (C/kg)	<u>E</u> <u>sA</u> (GV/m)	<u>E</u> <u>sB</u> GV/m
0.118	2.83	4.6
0.118	2.81	4.7
0.162	4.21	4.58
0.513	3.77	5.77
0.53	3.99	6.71
1.23	5.14	9.04
2.198	4.97	8.89
2.198	5.36	8.40

Table 1

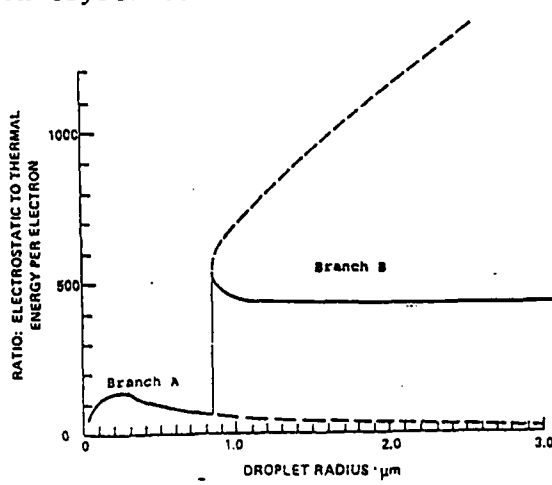


Figure 4 Theoretical plot of the ratio of surface charge electrostatic to thermal energy per electron to droplet radius for Octoil

REFERENCES

1. Rhim, W-K, Chung, S. K., Trinh, E., Hyson, M. T., Ellemann, D. D. "Large Charged Drop Levitated Against Gravity," IEEE-CH 2272, 1383 (1986).
2. Rhim, W-K, Saffren, M. M., Ellemann, D. D., "Development of an Electrostatic Positioner for Space Material Processing." Rev. Sci. Inst. 56, 1, 307 (1985).
3. Trevor, D., Kwangyoen, W., "Calculating Depth from Focus using a Pyramid Architecture", Grasp Laboratory, Department of Computer and Information Science, University of Pennsylvania, (1987).
4. Burt, P. J., Adelson, E. H., "The Laplacian Pyramid as a Compact Image Code," IEEE Trans. Communication, vol., COM 31, pp. 532, (1983).
5. Hendricks, Jr., C. D., "Charged Droplet Experiments," J. Colloid Sci. 17, 249, (1962).
6. Kelly, A. J., "Low Charge Density Electrostatic Atomization", IEEE Trans. Industrial Applications, IA-20, 2, 267, (1984).
7. Brinkman, W. F., Fisher, D. S., Moncton, D. E., "Melting of Two-Dimensional Solids," Science 217, 693, (1982).
8. Roth, D. G., Kelly, A. J. "Analysis of the Distribution of Evaporating Charged Droplets," IEEE Trans. Industry Applications, IA-19, 5, 771 (1983).

FUELS COMBUSTION RESEARCH

Boron Suspension Combustion

(AFOSR Contract No. F49620-86-C-0006)

F.A. Williams

Department of Mechanical and Aerospace Engineering
PRINCETON UNIVERSITY
Engineering Quadrangle
Princeton, New Jersey 08544

SUMMARY/OVERVIEW

Thermochemical calculations demonstrate appreciable advantages associated with the addition of boron to fuels for air-breathing propulsion, but realization of improved performance is contingent upon efficient combustion of boron. Problems in combustion of boron clouds are addressed here by both theory and experiment. Limiting factors are the finite-rate chemistry of the ignition and combustion of fine boron particles. The research is focused on mechanisms of ignition and combustion in the regime of chemical-kinetic control. Ignition times are measured, and theories of the ignition process are developed to explain the observations. Through improved understanding of the combustion, the results may suggest practical methods for increasing performance by reducing burning times.

TECHNICAL DISCUSSION

Earlier in this program, studies of transient processes occurring in slurry droplets during vaporization and combustion were completed [1-4]. The current work, pursued now for two years, concerns the combustion of suspensions of fine boron particles. In particular, experimental work has been performed on boron suspension combustion in the hot reaction products of a flat-flame burner. Associated theoretical analyses enabled ignition times to be extracted from the results. The research is progressing toward establishment of ignition conditions and combustion times of boron particles 0.1 μ to 5 μ in diameter.

An apparatus for boron suspension combustion was constructed and includes a flat-flame burner employing methane-oxygen-nitrogen mixtures (see Fig. 1). The flame temperature and oxygen concentration in the product gas can be varied independently by adjusting flow rates of the reactants. A particle feed system was designed and constructed for transporting particle suspensions in a nitrogen stream upward through a narrow tube in the center of the burner. The boron particles, placed in a cylindrical chamber, are agitated by a rotating blade driven by an electric motor, and the nitrogen carrier stream is split into two parts, one of which enters the chamber near the bottom, and the other of which passes by the conically tapered top of the chamber (see Fig. 1). The independent controls are the total nitrogen flow rate, the bypass ratio, and the speed of the electric motor. These controls can be adjusted to vary the boron particle

loading at any fixed nitrogen flow rate.

The suspension, fed through the central tube into the products of the flat-flame burner, mixes and spreads as an axisymmetric laminar jet. The conservation equations for axisymmetric jet flow were employed as a basis for describing boron particle histories in the experiment. For the region in which a similarity solution applies for the flow field, the calculation of particle histories is easiest. Similarity profiles were obtained, and it was found that, theoretically, the optimum location for boron ignition in the jet occurs at the edge of the jet near the jet exit. This is consistent with the flame types seen; as the flat-flame temperature was increased, the green luminosity of the boric-acid fluctuation bands appeared first at the lower edge of the jet and gradually spread to surround the entire jet. Beside the green there is a yellow region surrounding a colorless core (Fig. 1). The yellow region is mainly that of boron particle ignition, and the sharp yellow-green boundary marks the end of the ignition process.

The height of the yellow region (see Fig. 1) was measured as a function of the flat-flame temperature for different jet velocities (see Fig. 2) and was found to increase with increasing jet velocity and to decrease with increasing flame temperature, as would be predicted from the expected corresponding variations in temperature-time histories of the particles. The strength of the dependence on flame temperature decreases with increasing flame temperature, and above 2000 K, there is no further discernable decrease in yellow height with increasing temperature. These yellow heights were found to be independent of the oxygen concentration in the product gas within experimental accuracy. The jet theory was applied to obtain centerline velocity and temperature profiles for interpretation of the results for the yellow height. Calculated temperature histories are shown in Fig. 3, from which it is seen that in these experiments the ignition process is completed at local ignition temperatures ranging from about 1690 K to 1980 K.

An Arrhenius ignition theory was developed and applied to the ignition data, using the jet theory, to extract overall rate information from the measurements. The results, shown in Fig. 4, indicate that for ignition temperatures between 1690 K and 1820 K the overall activation energy of $E=50$ kcal/mol with a prefactor of $A=6.1 \times 10^8 s^{-1}$ is consistent with the data. At higher temperatures the activation energy is lower, and at lower temperatures it is higher, with a cutoff suggested in the vicinity of 1670 K. This behavior can be interpreted by assuming that $B+B_2O_3 \rightleftharpoons 3BO$ occurs in equilibrium at the inner edge of the oxide layer, while the rate processes $B_2O_3(l)+H_2O(g) \rightarrow 2HOBO(g)$ (endothermic) and $4BO(l)+2H_2O(g)+O_2(g) \rightarrow 4HOBO(g)$ (exothermic) occur at the outer edge, the latter resulting from $BO+H_2O \rightarrow HBO+OH$, $HBO \rightarrow BO+H$, $H+O_2 \rightarrow OH+O$, $O+H_2O \rightarrow 2OH$, $OH+BO \rightarrow HOBO$. If the first step is controlling then E is the activation energy of that step, while if the second step is most important, E reflects a combination of the equilibrium constant for the boron dissolution and the rate of the $BO + H_2O$ step. This research is reported in [5,6].

Work in progress includes applying the ignition theory to results of earlier experiments of others, measurement and analysis of ignition times for larger boron particles, and measurement of particle-size histories in the yellow region by laser scattering. Based on the light-scattering theory, the ratio of the

light scattering intensity at one direction, $i(\theta_1)$, to that at another direction $i(\theta_2)$ in the boron particle flame has been calculated. The results have shown that the ratio $i(110^\circ)/i(20^\circ)$ decreases very rapidly and monotonically as the boron particle diameter increases up to 0.3μ . Since the boron particle diameter is in the range of 0.04μ to 0.15μ in our present experiment, it is possible to measure the particle size in the boron-particle flame by measuring $i(110^\circ)/i(20^\circ)$ (Mie scattering). An optical set-up has been constructed. The 488nm line of an argon-ion laser is employed as a light source, with maximum power 1.3W. The light-scattering signals, detected by two photomultipliers, are sent to a digital oscilloscope. The measured results at flat-flame temperatures of 2200 K have shown that the ratio $i(110^\circ)/i(20^\circ)$ is almost constant throughout the colorless and yellow regions. The light-scattering intensity in the green region is very weak, suggesting that the combustion stage is short compared with the ignition stage, as estimated from theory. Thus, the change in the particle size during the ignition stage seems to be negligible and that during the combustion stage rapid.

Future plans include completing corresponding yellow-height and scattering-intensity measurements for particles in different size ranges, up to 5μ . Particle-size classification equipment has been acquired, set up in the laboratory, and tested so that samples in the size ranges of interest can be obtained. The ignition theory that is being developed will be employed to predict the results of the experiments with particles of different sizes, and comparison between theory and experiment will serve to test the correctness of the theory.

REFERENCE

1. Antaki, P., "Transient Processes in a Rigid Slurry Droplet During Liquid Vaporization and Combustion," *Combustion Science Technology* 46, 113 (1985).
2. Antaki, P., "Studies of Slurry Droplet Combustion and Boron Particle Ignition," Ph.D. Thesis, Department of Mechanical and Aerospace Engineering, Princeton University, Princeton, NJ (1985).
3. Antaki, P. and Williams, F.A., "Transient Processes in a Nonrigid Slurry Droplet During Liquid Vaporization and Combustion," *Combustion Science and Technology* 49, 289 (1986).
4. Antaki, P. and Williams, F.A., "Observations on the Combustion of Boron Slurry Droplets in Air," *Combustion and Flame* 67, 1 (1987).
5. Li, S.C., Williams, F.A., and Takahashi, F., "Ignition and Combustion of Boron Suspensions of Very Fine Particles", MAE Rept. No. 1818, Princeton University, Princeton, NJ, 1988.
6. Li, S.C., Williams, F.A., and Takahashi, F., "An Investigation of the Combustion of Boron Suspensions", Twenty-Second Symposium (International) on Combustion, The Combustion Institute, Pittsburgh, to appear, 1988.

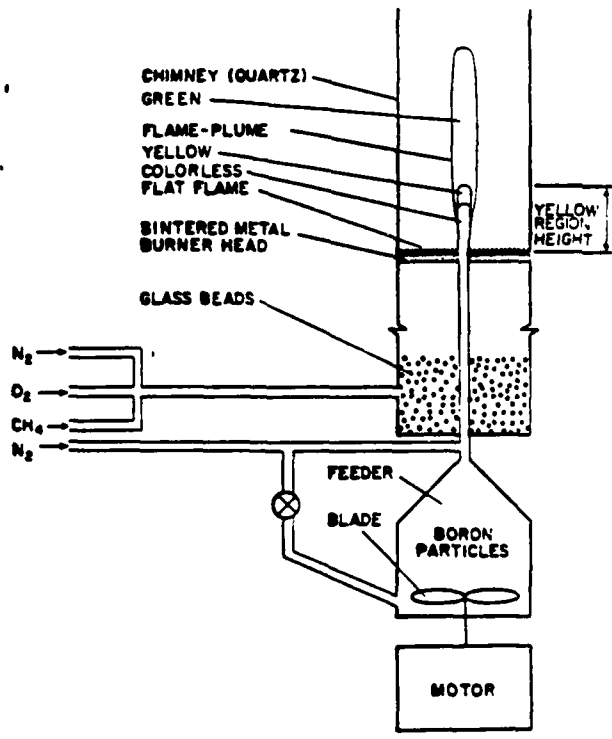


Fig. 1: Schematic diagram of the experimental arrangement, and the appearance of boron flame plume.

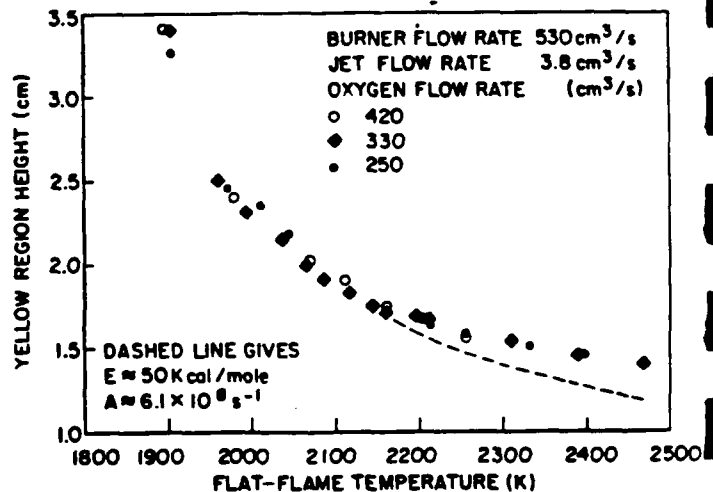


Fig. 2: Measured dependence of the height of the bright-yellow region on the flat-flame temperature for three concentrations of oxygen at a total burner flow rate of $530 \text{ cm}^3/\text{s}$ and a jet flow rate of $3.8 \text{ cm}^3/\text{s}$.

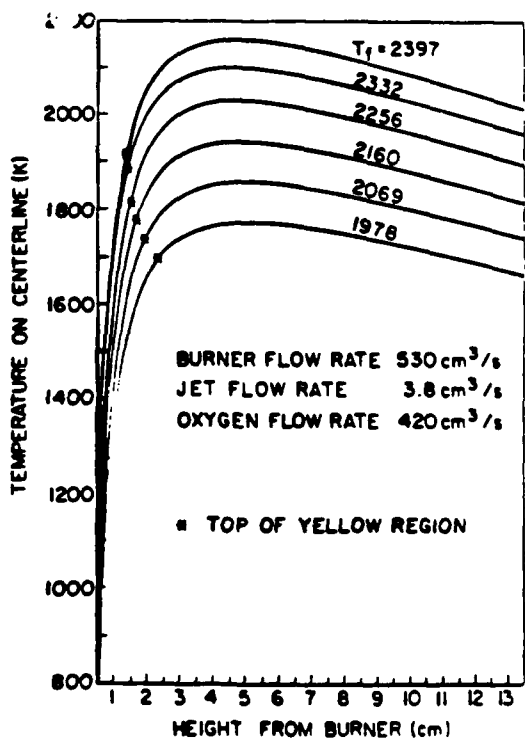


Fig. 3: The centerline temperature as a function of height, calculated from the jet theory, for various flat-flame temperatures, at a total burner flow rate of $530 \text{ cm}^3/\text{s}$ and a jet flow rate of $3.8 \text{ cm}^3/\text{s}$; the stars identify the observed heights of the bright-yellow region.

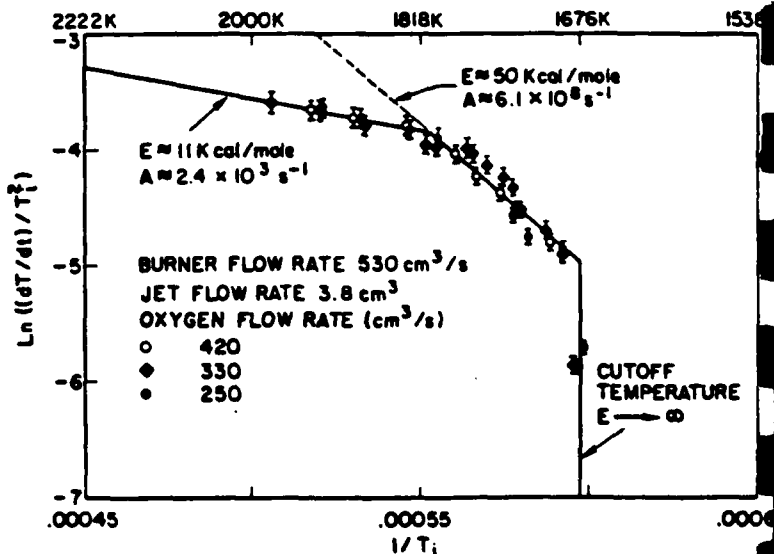


Fig. 4: An arrhenius graph constructed from the yellow-height data by use of the ignition theory; here identify estimated uncertainties from measurement and data reduction, solid lines are linear-squares fits over different temperature ranges, and the dashed extension of the lower-temperature fit corresponds to the dashed curve in Fig. 2.

FUELS COMBUSTION RESEARCH

(AFOSR Contract No. F49620-86-C-0006)

Principal Investigators: I. Glassman, F.L. Dryer, and F.A. Williams

PROGRAM SUBSECTION

Combustion Behavior of Free Boron Slurry Droplets

Principal Investigator: F.L. Dryer

Other Professionals: F. Takahashi, S.Y. Cho, and I.J. Heilweil

Department of Mechanical and Aerospace Engineering

Princeton University

Princeton, New Jersey 08544

SUMMARY/OVERVIEW

In order to realize the potential advantages of boron slurries as high-energy-density fuels for air-breathing propulsion systems, efficient atomization of the slurry, proper dispersion of boron particles into the oxidizing atmosphere, and subsequent ignition and efficient combustion of the boron are the essential requirements. The disruptive burning phenomena of free slurry droplets has major implications in achieving the requirements. Additional experiments on the shell agglomerate formed during combustion of boron/JP-10 slurries have been performed and physical and mathematical models of the disruptive burning mechanism have been developed.

TECHNICAL DISCUSSION

A stream of free monodisperse droplets of boron/JP-10 slurry was projected downward into a high-temperature, atmospheric-pressure, oxidizing gas stream [1-4]. A water-cooled, premixed, flat-flame burner, operated with fuel-lean methane/oxygen/nitrogen mixtures, was used to generate the hot oxidizing gas. All results reported in this paper were obtained for the oxygen mole fraction of $X_{O_2} = 0.39$ (gas mix. no. 1 [1-4]).

Two types of in-house boron slurries, one with a surfactant and another one without surfactant, were used in addition to a commercially available product (SunTech). Amorphous boron particles (H.C. Starck, 95/97% purity, 0.20-0.32 average diameter) were mixed with pure JP-10. A small amount (2 wt.%) of a sorbitan fatty acid ester-type surfactant (ICI Americas, SPAN85, sorbitan trioleate) was used to stabilize the slurries of the initial boron mass fractions of $Y_{B,0} = 0.1$ and 0.3.

Figure 1 shows direct photographs of the boron agglomerates, collected from the combustion chimney, and Figure 2 shows back-lit micrographs of a thin-sliced cross-sectional portion of the agglomerates. Figures 1a and 2a are for the in-house slurry with no surfactant ($Y_{B,0} = 0.3$), for which only a weak gaseous puffing occurred at substantially delayed times, close to the end of the vapor phase combustion (see [3]). No indication of the boron ignition was observed. The agglomerates are essentially hollow spheres with no blowholes. The surface

layers of some agglomerates are scaled off, indicating the result of the puffing and the weak sporadic disruption observed [3]. By contrast, as shown in Figs. 1b and 2b, the boron agglomerates from the in-house slurry with the surfactant ($Y_{B,0} = 0.3$) are fragmented as a result of the violet disruption (see [3]). Among the fragments, quasi-spherical shells with a large blowhole are seen, indicating the eruption of the slurry in the interior. Notice that these shells have a glossy outer surface, in contrast to the coarser textured spheres in Fig. 1a. These observations lend experimental support to the physical model [4] of the formation of an impermeable shell, and subsequent internal vaporization promoting pressure buildup, which eventually leads to the disruption.

The mathematical model is divided into two parts, i.e., (1) the initial vaporization stage in which the d-square law applies and (2) the shell formation stage in which the drop diameter remains constant. The formulations of the vaporization stage, experimentally observed for low $Y_{B,0}$ (~0.1)[2,4], was derived in a conventional manner by assuming quasi-steady state, spherical symmetry, constant properties, and a unit Lewis number for the gas phase, and no droplet heating. The slurry was treated mathematically as a boron/JP-10 binary mixture with low diffusivity, and only the species conservation equations were solved in the droplet interior. In the shell formation stage the liquid surface is assumed to regress into the interior of the droplet leaving behind a rigid porous shell, and the heat and mass conservation equations within the drop were added. The model simulation was performed for $Y_{B,0} = 0.1$, as described below.

Figure 3 shows the theoretical prediction of diameter (d)-squared vs. time (t) in the vaporization stage as well as the experimental results for both the diluted SunTech slurries and pure JP-10 [2,4]. The prediction is in good agreement with the experiment. Figure 4 shows the calculated boron mass fraction at the surface ($Y_{B,s}$) for various diffusion coefficients (D_f), which correspond to the Lewis numbers of 5-25. $Y_{B,s}$ increases from 0.1 to between 0.3-0.4 in 60 ms, during which the d-square law regime was experimentally observed [2,4]. Figure 5 is the radial distribution of the boron mass fraction (Y_B). A marked increase in Y_B in the thin layer near the droplet surface ($r = 0.23$ mm) is observed.

The calculation scheme was then switched to the shell formation stage at $t = 60$ ms. Figure 6 shows the estimated shell thickness (δ), defined as the thickness of the layer between the droplet surface and the liquid regression surface. At $t = 110$ ms, i.e. when the disruption was experimentally observed, the shell thickness was ~20 μm , which is in reasonable agreement with the experiment (5-15 μm [3]). Figure 7 shows the estimated temperature difference (ΔT) between the shell surface and the liquid regression surface, which was assumed to be at the boiling point of JP-10 (455 K), for a wide range of thermal conductivity of the shell (λ_{eff}). For $\lambda_{\text{eff}} = 1 \times 10^{-4}$ cal/cm \cdot s \cdot K, the temperature difference was ~60 K, resulting in the shell surface temperature of ~520 K, which appears to be in a temperature range in which the pyrolysis of surfactants is initiated. The refinements of the mathematical model itself as well as the property evaluating procedures (particularly for λ_{eff} and D_f) are currently under way.

REFERENCES

1. Takahashi, F., Dryer, F.L., and Williams, F.A., AFOSR TR-85-0559 (1985).
2. Takahashi, F., Dryer, F.L., and Williams, F.A., Fall Eastern States Section Meeting/The Combustion Institute, November 1985.
3. Takahashi, F. and Dryer, F.L., AFOSR/ONR Contractors Meeting, June 1987.
4. Takahashi, F., Dryer, F.L., and Williams, F.A., Twenty-First Symposium (International) on Combustion, p. 1983 (1988).

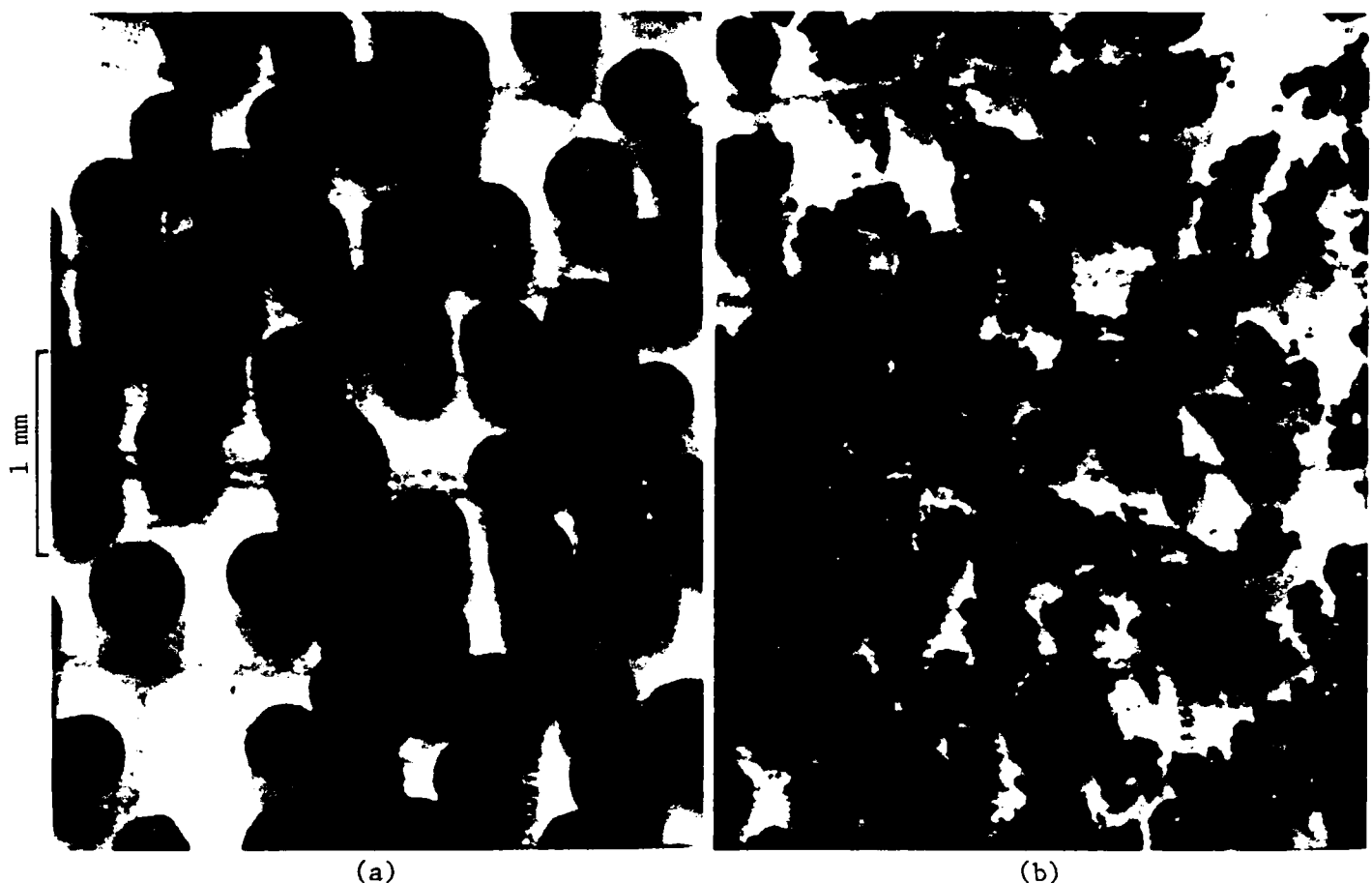


Fig.1 Direct photographs of boron agglomerates. (a)No surfactant, (b)with surfactant.

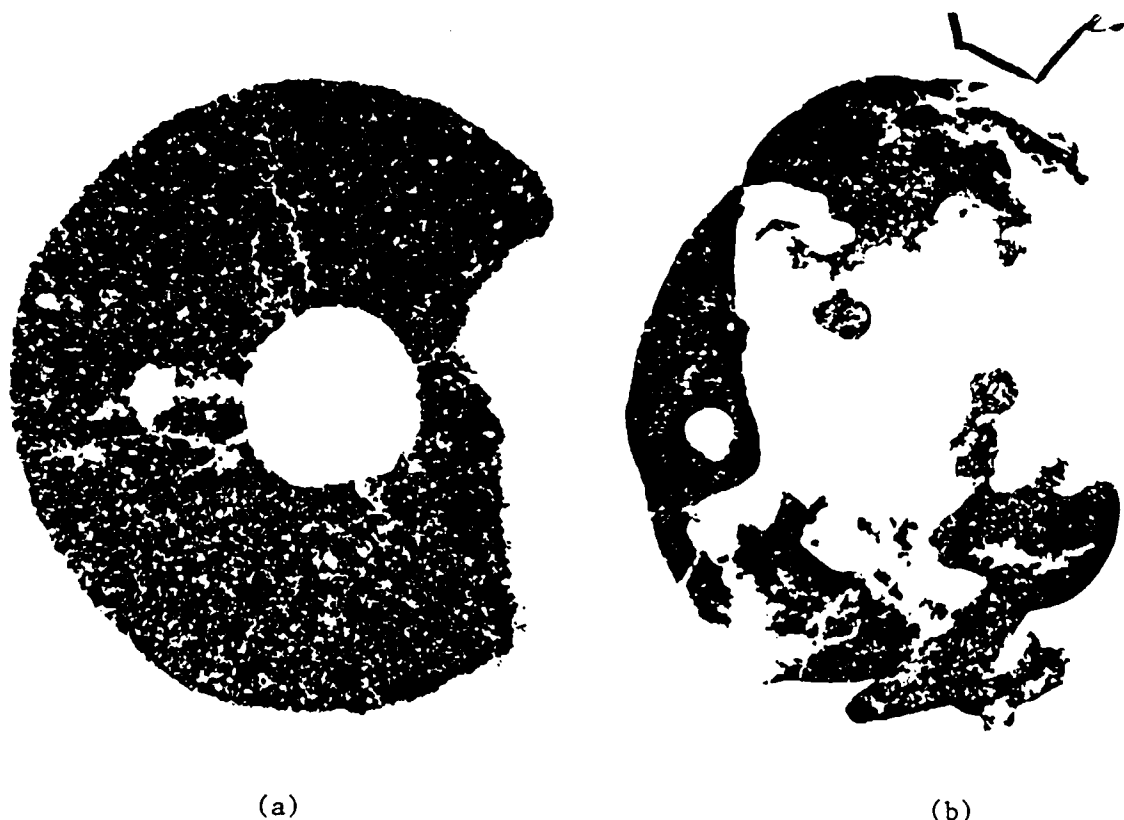
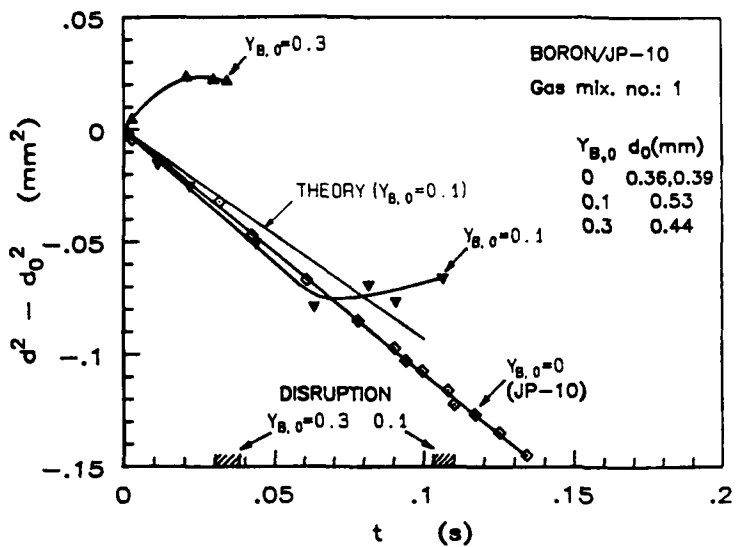
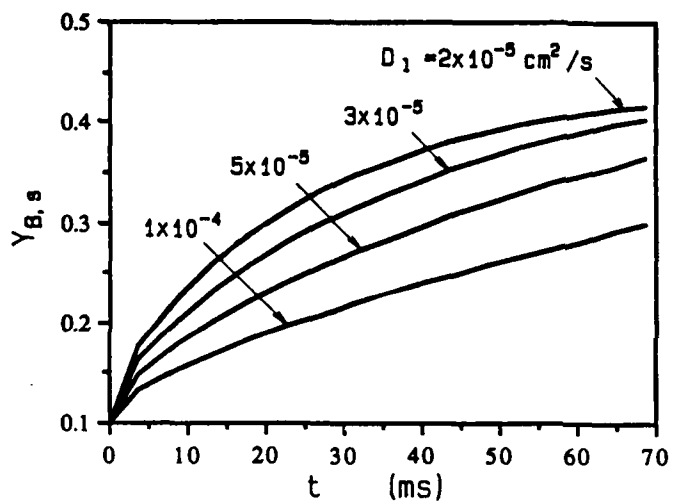
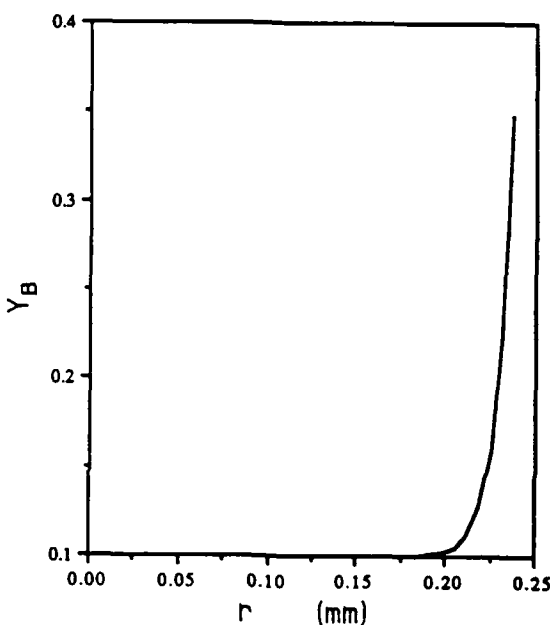
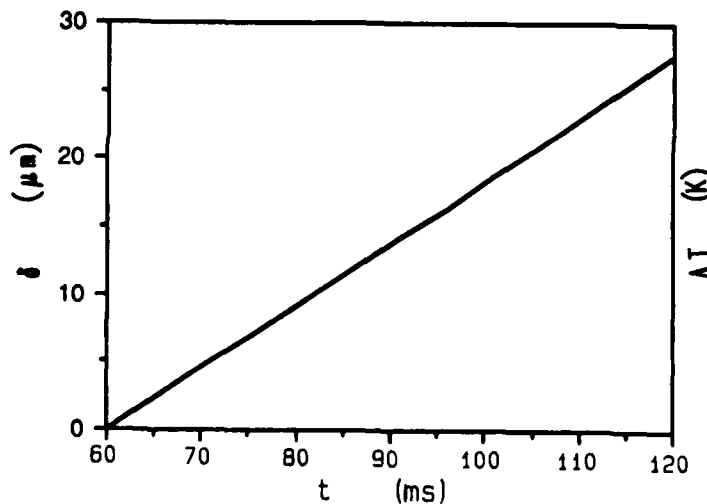
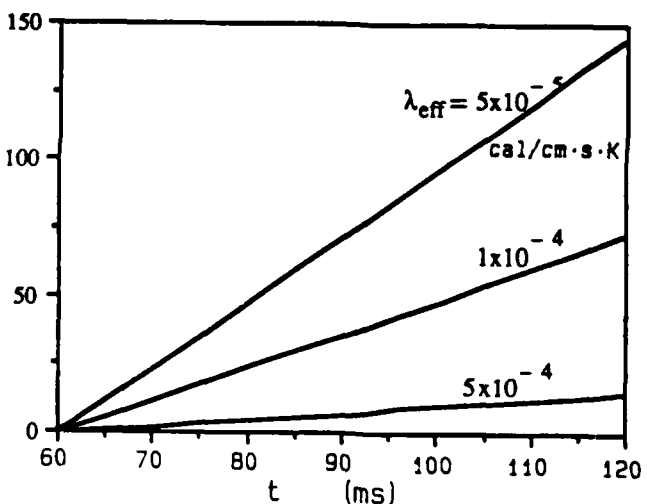


Fig.2 Crossectional micrographs of agglomerates. (a)No surfactant, (b)with surfactant.

Fig.3 The d -square plot.Fig.4 Temporal variations of $Y_{B,s}$.Fig.5 Radial profile of Y_B .
 $D_1 = 5 \times 10^{-5} \text{ cm}^2/\text{s}$, $t = 60 \text{ ms}$.Fig.6 Temporal variation of δ .Fig.7 Temporal variations of ΔT .

FUNDAMENTAL COMBUSTION PROCESSES OF PARTICLE-LADEN
SHEAR FLOWS IN SOLID FUEL RAMJETS
(ONR Contract No. N00014-86-K-0468)

Principal Investigators: K. K. Kuo, T. A. Litzinger, and V. Yang

Department of Mechanical Engineering
The Pennsylvania State University
University Park, PA 16802

Solid fuels can be used in ramjet propulsion and various military applications. Three major unresolved areas regarding combustion of solid fuels under stagnant and cross-flow conditions are: 1) ignition and combustion characteristics of high energy boron-based solid fuels and magnesium-based pyrotechnic materials are not well understood; 2) kinetic parameters and thermophysical properties of the above materials are not well characterized; and 3) the effects of chemical compositions and ambient flow conditions on the infrared radiation output is not fully established.

The purpose of this research project is to help answer some of the fundamental questions involved in the three areas listed above. The specific program objectives are:

1. to acquire a basic understanding of physical and chemical mechanisms involved in the combustion of solid fuels under strong cross-flow conditions for both supersonic and subsonic modes;
2. to conduct detailed flow measurements and visualization of the particle-laden boundary-layer flows;
3. to construct a comprehensive theoretical model for describing the two-phase fluid dynamic phenomena and combustion processes of solid fuels under ramjet environments; and
4. to characterize the thermal degradation, pyrolysis, and ignition phenomena of the specially formulated solid-fuel samples used in this project.

Significant results obtained in the past year are summarized below.

I. Combustion of Solid Fuels under Strong Cross-Flow Conditions

To study both subsonic and supersonic combustion processes of high-energy metalized solid fuels, a blowdown wind tunnel facility has been designed and constructed to simulate ramjet environments. The facility is capable of simulating a broad range of flight Mach numbers and altitudes. The flow Mach number selected for supersonic combustion tests is 2.0, with a maximum mass flow rate of 9 Kg/s and a test duration of 340 seconds.

The test section design allows detailed measurement of particle-laden turbulent reacting boundary-layer flows above burning solid-fuel samples. Advanced nonintrusive diagnostic instruments (including a real-time X-ray

radiography and image analyzer system, a fast wavelength tracking Smeets-George interferometer, and a multi-channel laser Doppler velocimeter) have been set up for flow measurements and visualization. Boron-based solid-fuel samples have been fabricated and acquired from Aerojet, UT/CSD and NWCS for this research study.

While the operation of the blowdown wind tunnel facility is being tested, initial tests of the combustion processes of solid fuels under strong cross-flow conditions have been conducted using a kerosene burning test rig. These tests serve as a guide for determining the basic flow structures, calibrating the firing control and data acquisition systems, and selecting appropriate solid-fuel samples for improved combustion performance. In this setup, the air is heated in a kerosene burner to provide high stagnation-temperature flows through the test section. A slab of solid fuel is placed just below the two-dimensional exit of the burner with a small recirculation zone in the upstream region of the sample. The chemically reacting turbulent boundary-layer flows and the instantaneous surface motion of the regressing solid-fuel samples are observed using high-speed movie and video cameras.

Figure 1 shows a direct photograph of the flow field above a burning solid-fuel sample with 30% boron particles and 70% HTPB. The luminous region encompasses the diffusion flame from the burning fuel. The bright streaklines are caused by burning particles being ejected from the surface region. Figure 2 shows the recovered sample with the downstream portion regressed more than the upstream portion. This is attributed to the lower convective heat transfer in the front region caused by a lower flow velocity in the recirculation zone. The surface and subsurface layers exhibit porous structures, allowing for the tunneling of air and subsequent burning in these regions.

II. Pyrolysis and Ignition of Solid Fuels

Experiments are being conducted to obtain fundamental information on the physical and chemical processes involved in the pyrolysis and ignition of candidate solid fuels for ramjets and other applications. This work is being performed using a CO₂ laser as the heat source. The diagnostics used include near-infrared photodiodes, high-speed visible and Schlieren video movies, microthermocouple probes and gas chromatography/mass spectrometry. The materials studied over the past year include HTPB containing boron, HTPB/boron fuels with additives (Mg, Mg/Al, LiF and CeF₃), BAMO/NMMO, BAMO/NMMO with boron, polytetrafluoroethylene (PTFE) and Mg/PTFE. Among the important experimental variables were heat flux, pressure, and ambient gas composition.

In order to establish the effect of changing the composition of the HTPB/boron fuels on ignition behavior, four different materials were blended into a base fuel of 70% HTPB/30% boron by weight. The blended materials studied were Mg, Mg/Al, LiF and CeF₃; they were all added at a level of ten percent by weight. Figure 3 shows the effect of these materials on the ignition delay time compared to the baseline fuel. Clearly, at low heat fluxes where ignition was most difficult to achieve, the CeF₃ showed the greatest reduction in delay time. The LiF showed almost no change from the baseline fuel, while both Mg and Mg/Al showed an

intermediate level of reduction. At higher heat fluxes, the times for ignition of the Mg, Mg/Al and CeF₃ appear to converge. Thus, only at low heat fluxes is the CeF₃ superior to the Mg/Al and Mg containing fuels.

Another set of experiments involved a comparison of HTPB and an energetic binder, BAMO/NMMO provided by Dr. Gerry Manser of Aerojet. Tests were conducted with and without boron in the fuel. The high-speed, Schlieren videos of the laser heating of the BAMO/NMMO show very distinctive features compared to those of pure HTPB. During laser heating, the gaseous products evolved from the BAMO/NMMO have a much higher velocity than the HTPB case; in fact the velocities are so high that the jet is turbulent. Unlike all other fuels tested, the pure BAMO/NMMO has poor repeatability in ignition times; from test to test, the ignition delay times may vary by a factor of two. However, with boron combined with the BAMO/NMMO, the fuel shows typical repeatability in the delay times. An explanation for this behavior is being pursued at present. The most significant finding of the comparison of the BAMO/NMMO-boron fuel to the HTPB/boron fuel is that the fuels with the energetic binder have shorter delay times by approximately a factor of two over the entire heat flux range from 150 to 850 W/cm².

In the studies of the Mg/PTFE fuels, the effects of heat flux, pressure, and oxygen concentration have been investigated. Figure 4 illustrates the effect of heat flux on the ignition delay time for heating in air at one and one-tenth atmosphere pressures. Interestingly, at the lower pressure, the ignition times are shorter; this could be due to lower pressure or to lower oxygen concentration. To investigate which factor was responsible, tests were performed at atmospheric pressure using nitrogen/oxygen mixtures with varying oxygen concentration. The results of these tests indicate that the oxygen concentration is the critical factor in reducing the ignition time. This effect of oxygen on ignition time suggests that the presence of oxygen is inhibiting the ignition process, most likely, through some chemical means. Finally, in order to obtain fundamental information on the composition of the gaseous species generated by the PTFE during combustion, pure PTFE was heated in nitrogen to suppress reactions between the products and oxygen. The analysis of the products show a wide range of saturated and unsaturated fluorocarbon compounds; the most common compounds detected by the GC/MSD analysis were C₂F₄, C₂F₆, C₃F₆, C₄F₈. Knowledge of the most common products formed is critical to the modeling of the chemical processes during the combustion of Mg/PTFE.

III. Burning Rate Measurements under Strand Burner Conditions

In addition to the studies of pyrolysis and ignition, the burning rate of the Mg/PTFE fuels have been studied in a strand burner apparatus. Although the Mg/PTFE sample is fuel rich, it can burn almost completely in air under atmospheric pressure. Burning rate data obtained from this study can provide a reference case for the burning of the material under cross-flow conditions. To date, tests have been conducted to measure the burning rate of the sample in air and pure nitrogen over pressures from 40 to 700 kPa. From the burning rate data, the burning-rate exponent and pre-exponential coefficient used in Saint Robert's law were deduced to relate the strand burning rates to pressures. Residues were collected after the test for X-ray diffraction analysis to determine their chemical

compositions. Results of X-ray diffraction analysis indicate that the major compounds found in the residue are MgO, together with MgF₂ and some noticeable amount of unburned carbon for the sample burned in air. However, while the sample burns in N₂, the major compound of residue is MgF₂; next to that is MgO, and some solid carbon and magnesium also appear among them.

For a number of strand-burner tests, microthermocouple probes were imbedded within the fuel sample to measure the sample temperature and the gas-phase temperature as the surface regresses. The temperature traces provide an estimate of the surface temperature which is needed for the derivation of kinetic parameters. Also, the complete trace can be used to calculate the thermal diffusivity of the Mg/PTFE through the use of a simple heat transfer calculation. The diffusivity is a critical element in the modeling of ignition and combustion processes of these materials, and is therefore determined by several different means to establish its reliable, functional dependence on temperature.



Fig. 1 Photograph of Burning Sample



Fig. 2 Recovered Samples (HTPB/B, 70/30)

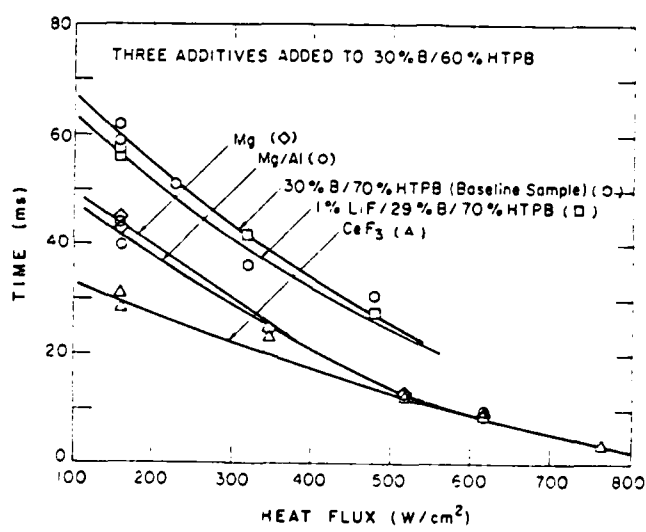


Fig. 3 Delay Time vs. Heat Flux

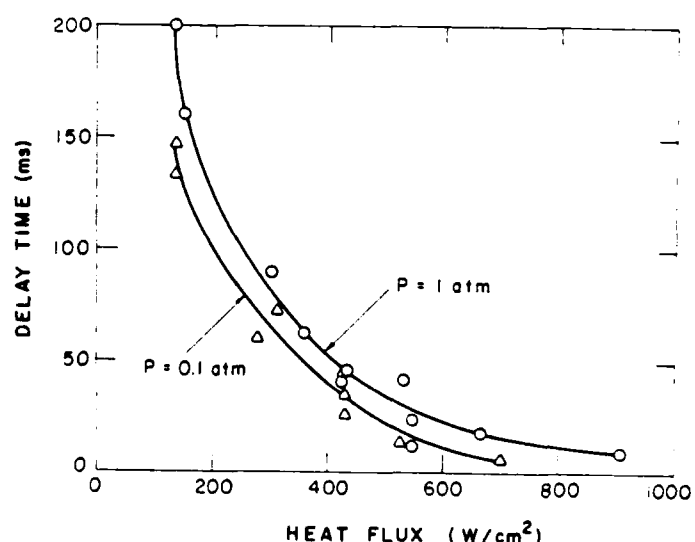


Fig. 4 Ignition Delay Characteristics of Mg/PTFE Sample

ADVANCED B AND Al COMBUSTION KINETICS STUDIES OVER WIDE TEMPERATURE RANGES

AFOSR Grant No. 86-0019

Principal Investigator: Arthur Fontijn

Research Collaborators: Donald F. Rogowski, Aleksander G. Slavejkov and
Dr. P. Marshall

High-Temperature Reaction Kinetics Laboratory
Department of Chemical Engineering
Rensselaer Polytechnic Institute
Troy, NY 12180-3590

SUMMARY

Current ability to model rocket and plume combustion in advanced propulsion systems is hampered by a lack of understanding and knowledge of individual B and Al species reactions and the ways by which temperature affects their rate coefficients. The Arrhenius equation $k(T) = A \exp(-E_A/RT)$ has over limited temperature ranges been of great value. However, over large temperature ranges order of magnitude errors can be made by extrapolations based on it, particularly for exothermic and slightly endothermic reactions. The goal of the present program is to provide, through accurate measurements, insight into the kinetic behavior of B and Al atom, halide and oxide species oxidation reactions, as influenced by temperature. The measurements are made by the HTFFR (high-temperature fast-flow reactor) technique. Current theory has been found to be inadequate to either predict or describe the observations, which should stimulate the development of theories applicable to reactions of metallic propellant species.

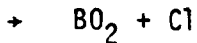
TECHNICAL DISCUSSION

Technique

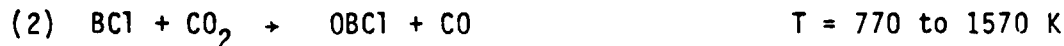
HTFFR is a unique method, which can provide accurate kinetic measurements on reactions of refractory species, such as B and Al, over the 300 to 1900 K temperature range. The elementary reactions are studied in isolation in a heat bath. With traditional high-temperature techniques such isolation is usually impossible to achieve; as a result, data on any given reaction depend on the knowledge of other reactions occurring simultaneously, leading to large uncertainties. In the HTFFR shown in Fig. 1, B_2H_6 and Cl_2 in Ar bath gas are passed through a microwave discharge to produce BCl . These radicals are mixed with an oxidant, e.g., O_2 , CO_2 . The relative BCl concentration is measured by laser-induced fluorescence, LIF, as a function of oxidant concentration for several pressures, reaction times and average gas velocities to yield a rate coefficient k . Plots of $\ln k(T)$ vs. T^{-1} are then obtained from similar measurements at various temperatures. The reactions reported here are all pressure-independent.

Results and Discussion

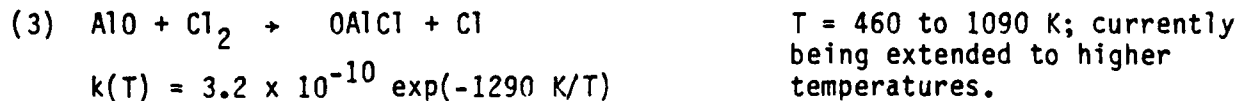
Over the past year we have made a series of measurements on reactions of BC₁ and AlO. The following k(T) data, in cm³ molecule⁻¹ s⁻¹, have been obtained:



$$k(T) = 2.2 \times 10^{-11} \exp(-4620 \text{ K}/T)$$



$$k(T) = 6.7 \times 10^{-13} \exp(-4500 \text{ K}/T)$$



Reaction (3) is studied as part of our ongoing effort to measure all reactions leading to di- and tri-atomics in the Al/O/Cl reaction system, see Fig. 2. That particular effort is to be completed by the study of AlO + HCl → OAlCl + H. The work on reactions (1) and (2) is the beginning of the study of a series of reactions to characterize the B/O/Cl system in a manner similar to the Al/O/Cl system and to compare B to Al reactivities, cf. Figs. 3 and 4.

Figure 3 shows that while the AlCl + O₂ reaction has a sharply curved Arrhenius plot above ~1000 K, the BC₁ + O₂ reaction displays no noticeable deviation from linear ln k vs. T⁻¹ (normal Arrhenius) behavior. We have speculated that the AlCl plot indicates a transition from dominance of the AlO₂ + Cl product channel at lower temperatures to OAlCl + H at higher temperatures. The straight line for BC₁ + O₂ suggests that only one channel is operative (one type of product is formed). If this were OBCl, the equivalent of the postulated high-temperature Al product, the shape of the two plots would suggest that they may cross, i.e., that at very high temperatures the AlCl reaction could be faster than the BC₁ reaction. However, if the BC₁ product is BO₂, the equivalent of the lower temperature Al product, a very fast BC₁ + O₂ reaction may be indicated at high temperatures as sharp upward curvature in the BC₁ + O₂ plot, similar to that of AlCl + O₂, would then be a reasonable expectation.

In Fig. 4 the BC₁ + CO₂ + OBCl + CO and AlCl + CO₂ + OAlCl + CO reactions are compared. The products as written represent the only possible paths, based on thermochemical considerations. While the AlCl reaction is the slower at the measured temperatures, extrapolation would suggest that above 2300 K it could be the faster.

For several of the reactions of Figs. 2-4, the products can be established unambiguously by thermochemical and spin-correlation considerations. However, as discussed, this is not possible for BC₁ + O₂ and AlCl + O₂, as well as for AlO + O₂, and AlO + CO₂. Apart from BO₂, the potential products of these reac-

tions have no identified uv-visible optical transitions. The LIF-HTFFR could therefore not be used to identify the product channels and their relative importance as a function of temperature. To allow direct observation, we have commenced experiments with an HTFFR equipped with a mass spectrometer. The long term goal of that work is to study the kinetics of the steps leading to the ultimate combustion products B_2O_3 and Al_2O_3 .

CUMULATIVE LIST OF PUBLICATIONS RESULTING FROM THIS GRANT

1. D.F. Rogowski and A. Fontijn, "An HTFFR Kinetics Study of the Reaction Between $AlCl$ and O_2 from 490 to 1750 K," Twenty-first Symposium (International) on Combustion (1986/1988), p. 943.
2. D.F. Rogowski and A. Fontijn, "An HTFFR Kinetics Study of the Reaction Between $AlCl$ and CO_2 from 1175 to 1775 K," Chemical Physics Letters, 132, 413 (1986).
3. D.F. Rogowski and A. Fontijn, "The Radiative Lifetime of $AlCl\ A^1_{II}$," Chemical Physics Letters, 137, 219 (1987).
4. A.G. Slavejkov, D.F. Rogowski and A. Fontijn, "An HTRRF Kinetics Study of the Reaction Between BCl and O_2 from 540 to 1070 K," Chemical Physics Letters, 143, 26 (1988).
5. D.F. Rogowski, P. Marshall and A. Fontijn, "High-Temperature Fast-Flow Reactor Kinetics Studies of the Reactions of Al with Cl_2 , Al with HCl and $AlCl$ with Cl_2 Over Wide Temperature Ranges," The Journal of Physical Chemistry, submitted.
6. D.F. Rogowski, Ph.D. thesis, Rensselaer Polytechnic Institute, Feb./May 1988.

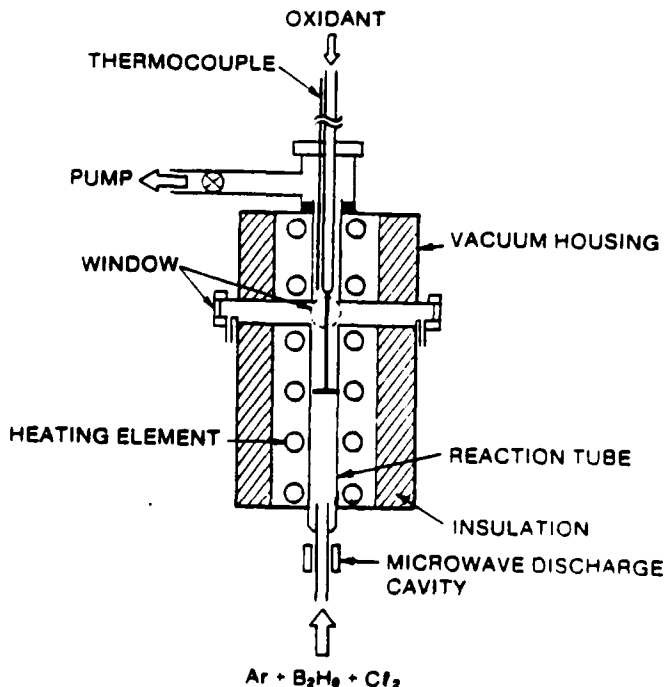


Figure 1. Schematic of an HTFFR

T, K

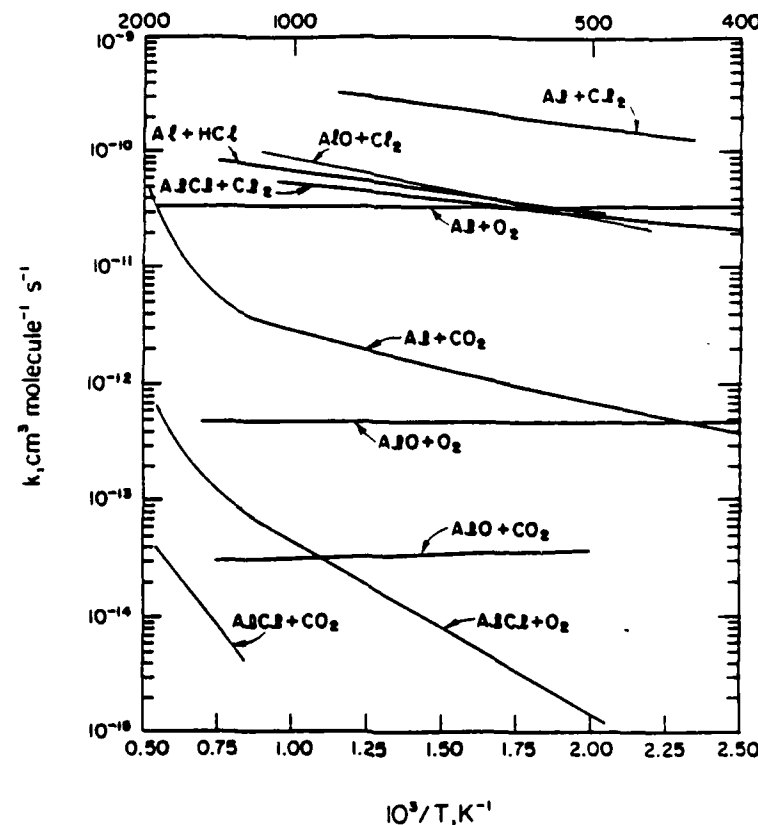


Figure 2. Summary of HTFFR Rate Coefficient Measurements for Al/O/Cl Reactions

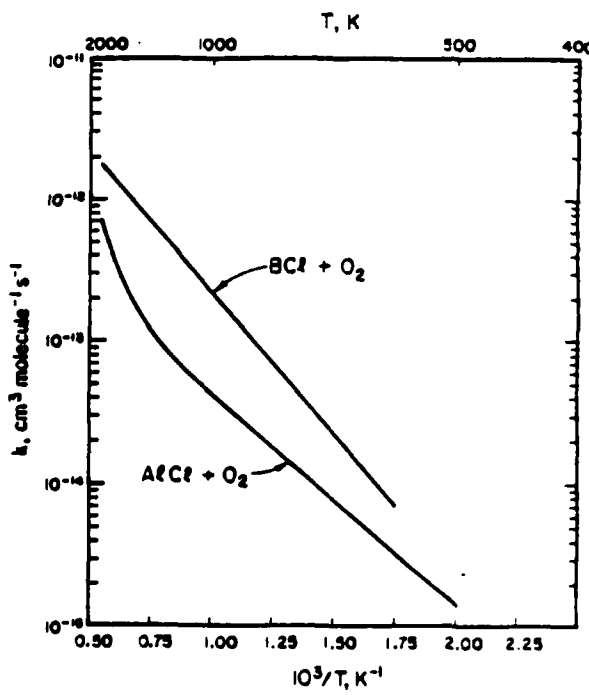


Figure 3. Comparison of $\text{BC}_1 + \text{O}_2$ and $\text{AlCl}_1 + \text{O}_2$ Rate Coefficients

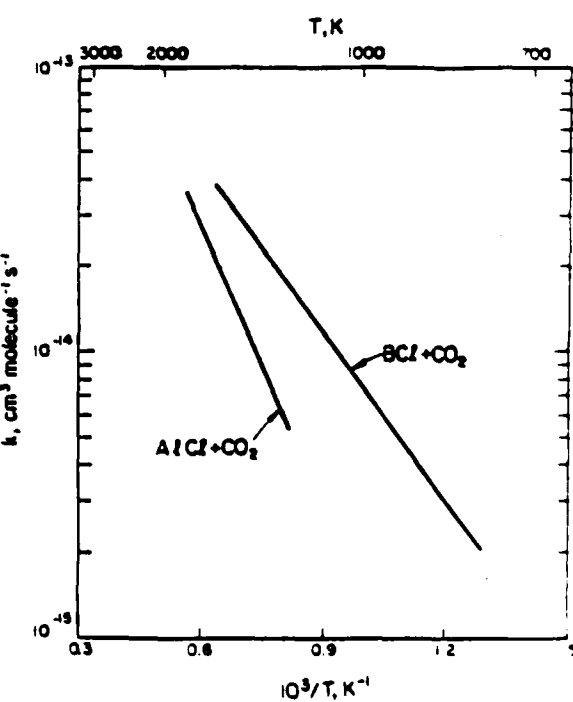


Figure 4. Comparison of $\text{BC}_1 + \text{CO}_2$ and $\text{AlCl}_1 + \text{CO}_2$ Rate Coefficients

CHEMICAL KINETIC MODELING AND SENSITIVITY ANALYSIS
FOR BORON ASSISTED HYDROCARBON COMBUSTION I

(AFOSR Contract No. F49620-88-C-0040)

Principal Investigator: C.E. Kolb

Other Professionals: R.C. Brown, K. Annen and H. Rabitz

Aerodyne Research, Inc.
Billerica, MA 01821

ARI Subcontract No. ARI-3462

Principal Investigators: F.L. Dryer and R.A. Yetter

Other Professionals: S.Y. Cho

Department of Mechanical and Aerospace Engineering
Princeton University
Princeton, NJ 08544

SUMMARY/OVERVIEW

This paper and the companion paper¹ that follows briefly describe the current status of an Air Force sponsored program to develop a microscopic model for all phases of boron assisted hydrocarbon combustion. This work uses gradient sensitivity analysis to identify the critical chemical and physical parameters which control the boron combustion process. However, unlike other combustion modeling studies, in which the framework of the model is well defined, considerable uncertainty exists not only in the input parameters, but also in the formulations of the boron combustion model itself. Hence, the philosophy and utility of sensitivity analysis in this work is unique. We rely heavily on sensitivity analysis for the formulation of alternate reaction mechanisms as well as eventual evaluation of the proposed models. Furthermore, by utilizing sensitivity analysis techniques, we will maximize the use of combined modeling and experimental efforts to identify the most probable model (or eliminate improbable models) and to pinpoint the more crucial steps of that model.

The general goal of this program is to obtain a better fundamental understanding of boron combustion, and ultimately, to produce a model for predictive applications. However, the immediate goal is to help focus ongoing research by identifying key thermochemical and kinetic parameters for subsequent experimental/theoretical evaluation.

TECHNICAL DISCUSSION

The combustion of solid boron particles with an oxygen based oxidizer is a complex process involving both heterogeneous (gas/solid) and homogeneous (gas/gas) chemical kinetics. The overall process is currently viewed as including an initial heterogeneous phase of particle oxidation, ignition and volatilization of partially oxidized boron. Volatilized boron species undergo further homogeneous gas phase oxidation to form a mixture of gaseous boron oxides and oxyhydrides (primarily HBO and HOBO). Finally, as

the combustion gas cools, this complex B/O/H mixture must condense to liquid or solid B_2O_3 in a third heterogeneous combustion phase to achieve the full theoretically predicted heat release. Since the following paper³ summarizes the results of our work on the homogeneous oxidation phase of boron combustion, the present paper will focus exclusively on preliminary efforts to model the heterogeneous ignition phase.

Experimental work indicates that the initial oxidation, ignition and volatilization phase of boron combustion is a two stage process.² For temperatures below approximately 1800-2000°K, oxidation of the boron particle produces an oxide coating which may, if sufficiently thick, inhibit further combustion. At higher temperatures, vaporization of the oxide coating results in a second combustion stage in which a relatively clean boron particle burns vigorously in the hydrocarbon/air environment. Removal of the oxide layer can be enhanced by reaction with hydrogen containing species (i.e., H_2O , OH, etc.) to yield boron oxyhydrides.

On the basis of this experimental work, in addition to earlier modeling efforts, qualitative descriptions of the low and high temperature oxidation of particulate boron are shown in Figures 1a and 1b. From these qualitative models, specific nonelementary reactions can be written to describe the chemical kinetics. For example, Table I lists a sampling of several reactions for the high temperature reactions at the B(s)/gas interface. Similar reactions can be written for the low temperature chemistry.

Reactions listed in Table I could be used in a first cut model for the oxidation kinetics. However, several key features may be missing which require mechanisms based on more elementary reactions. For example, reactions between gas phase species and/or weakly physisorbed species on the surface with other adsorbed species are clearly missing. In addition, highly endothermic reactions in which all products are in the gas phase may actually proceed via a mechanism in which strongly chemisorbed species remain on the surface long enough to undergo further heterogeneous reactions. Consequently, ongoing work is focusing on developing mechanisms in which the elementary reactions include adsorption on the surface, reactions between adsorbed species and gas phase or mobile physisorbed species, and dissociation of adsorbed complexes.

REFERENCES

1. "Chemical Kinetic Modeling and Sensitivity Analysis for Boron Assisted Hydrocarbon Combustion II," Yetter, R.A., Cho, S.Y., Rabitz, H.E., Dryer, F.L., Brown, R.C., Annen, K., and Kolb, C.E.
2. Faeth, G.M., "Status of Boron Combustion Research," Air Force Office of Scientific Research (October 1984) also partially presented under the same title at the 21st JANNAF Combustion Meeting, Laurel, MD (October, 1984).

FIGURE 1A. LOW TEMPERATURE BORON OXIDATION, IGNITION AND COMBUSTION MODEL

PHASE:	SOLID	LIQUID	GAS
SPECIATION:	$B(s)$	$B_2O_3(\epsilon)$	AIR
		DISSOLVED SUBOXIDES DISSOLVED OXYHYDRIDES $O, H, OH, O_2, H_2, H_2O, CO, CO_2$	B_xO_y $H_xB_yO_z$ $BO, BO_2, B_2O, B_2O_2, B_2O_3$
DIFFUSION GRADIENTS:		LOWER O/B SUBOXIDES	0, O ₂ , H, OH, ETC. LARGER O/B OXIDES
REACTIONS AT INTERFACE:		DIFFUSION CONTROLLED ¹ OXIDATION OF $B(s)$ VIA REACTION WITH O ₂ , H ₂ O, ETC.	OXIDATION/REDUCTION OF OXIDES OXIDE REDUCTION TO OXYHYDRIDES VAPORIZATION

¹REACTIONS MAY BE KINETICALLY LIMITED FOR INITIALLY CLEAN BORON PARTICLES AND/OR FOR VERY THIN OXIDE LAYERS.

FIGURE 1B. HIGH TEMPERATURE BORON OXIDATION, IGNITION AND COMBUSTION MODEL

PHASE:	SOLID / LIQUID	GAS
SPECIATION:	$B(s)/B(\epsilon)$	AIR BORON OXIDES AND OXYHYDRIDES HYDROCARBON COMBUSTION PRODUCTS
DIFFUSION GRADIENTS:	BORON OXIDATION/REDUCTION PRODUCTS	0, O ₂ , OH, H, H ₂ , H ₂ O, CO, CO ₂ OXIDES + OXYHYDRIDES
REACTIONS AT INTERFACE:	HETEROGENEOUS (SURFACE BURNING) REACTIONS	GAS PHASE HOMOGENEOUS OXIDATION KINETICS

Table I. High Temperature Reaction List for Heterogeneous Combustion
Boron Kinetics

Reaction	$\Delta H_f, 298$ (Kcal/mole)	
B(s) + O(g) → BO(g)	-59. ± 2.05	R1
B(s) + 2O(g) → BO ₂ (g)	-186. ± 2.1	R2
2B(s) + O(g) → B ₂ O(g)	-36. ± 25.05	R3
B(s) + O(g) → 1/2 B ₂ O ₂ (g)	-168. ± 2.05	R4
2B(s) + 3O(g) → B ₂ O ₃ (g)	-376.8 ± 1.15	R5
B(s) + 1/2O ₂ (g) → BO(g)	0. ± 2	R6
B(s) + O ₂ (g) → BO ₂ (g)	-68. ± 2.0	R7
2B(s) + 1/2O ₂ (g) → B ₂ O(g)	23. ± 25	R8
2B(s) + O ₂ (g) → B ₂ O ₂ (g)	-109. ± 2.0	R9
2B(s) + 3/2O ₂ (g) → B ₂ O ₃ (g)	-199.8 ± 1.0	R10
B(s) + OH(g) → HBO(g)	-107.2 ± 3.9	R11
B(s) + OH(g) → BO(g) + H(g)	42.2 ± 0.6	R12
B(s) + 1/2H ₂ (g) → 1/2O ₂ (g) → HBO(g)	-47.2 ± 3	R13
B(s) + 1/2H ₂ (g) + O ₂ (g) → HOBO(g)	-134.0 ± 1	R14
B(s) + H ₂ O(g) → BO(g) + H ₂ (g)	-57.795	R15
B(s) + H ₂ O(g) → BO(g) + 2H(g)	162.498	R16
B(s) + H ₂ O(g) → HBO(g) + H(g)	62.498	R17
B(s) + 2H ₂ O(g) → BO ₂ (g) + 2H ₂ (g)	47.59	R18
B(s) + 2H ₂ O(g) → B(OH) ₂ (g) + H ₂ (g)	1.59	R19
B(s) + BO(g) → B ₂ O(g)	23.0 ± 27	R20
B(s) + BO ₂ (g) → 2BO(g)	111.0 ± 6.7	R21
B(s) + B ₂ O ₂ (g) → B ₂ O(g) + BO(g)	132.0 ± 29	R22
B(s) + HOBO(g) → B ₂ O(g) + OH(g)	166. ± 26	R23
B(s) + HOBO(g) → BO(g) + HBO(g)	86. ± 6	R24
B(s) + CO ₂ (g) → BO(g) + CO(g)	68.6 ± 2.56	R25

Chemical Kinetic Modeling and Sensitivity Analyses
for Boron Assisted Hydrocarbon Combustion II

(AFOSR Contract No. F49620-88-C-0048)

Principal Investigator: C.E. Kolb
Other Professionals: R.C. Brown, K. Annen, and H. Rabitz

Aerodyne Research, Inc.
Billerica, MA 01821

ARI SUBCONTRACT NO. ARI-3462

Principal Investigators: F.L. Dryer and R.A. Yetter
Other Professional: S.Y. Cho

Department of Mechanical and Aerospace Engineering
Princeton University
Princeton, NJ 08544

SUMMARY/OVERVIEW

The use of elemental boron as a fuel in conjunction with traditional hydrocarbon fuels has the thermochemical potential to greatly enhance the volumetric efficiency of air breathing combustors. However, achieving this potential has been difficult due to inadequate ignition characteristics and poor combustion efficiencies.

The objectives of the present program are to model boron particle ignition, oxidation and vaporization, homogeneous boron combustion kinetics, and boron oxide condensation in a hydrocarbon combustion environment [1]. Gradient methods of kinetic sensitivity analysis are being extended and integrated into the boron combustion model to help identify the most probable reaction pathways and to select individual model inputs, including reaction rate constants, thermochemical parameters, and heat and mass transfer processes which most require accurate assessment in dedicated theoretical or experimental programs.

TECHNICAL DISCUSSION

As part of this program, a gas-phase kinetic model of homogeneous combustion chemistry for B/O/H/C systems has been developed and can be used to study a number of energetic and propulsion systems. The reaction model includes 19 chemical species and 59 forward and reverse elementary reactions. When possible, reaction rate constants and mechanisms were chosen from an evaluation of published experimental data. However, most boron species reaction mechanisms and rate parameters had to be estimated from data for analogous species or from transition state theory.

The reaction model has been studied, thus far, for homogeneously reacting, adiabatic and isothermal mixtures over a temperature range from 1800 K to 3000 K [2,3]. The results include the effects of mixture temperature, pressure, oxygen content, hydrogen content, and carbon content on the reaction dynamics of B, BO, BO₂, B₂O₂, B₂O₃, HBO, and HBO₂. For example, hydrogen addition is observed to

accelerate both the oxidation of intermediates and the heat release rate, as well as to alter the dominant suboxides and reaction products. From the sensitivity analysis calculations, a group of 19 key boron-containing reactions are identified and suggested for future elementary reaction studies. To date, only one of these reactions has been studied experimentally.

Figure 1 is an example of the reaction kinetics for a mixture in which the initial conditions were derived from equilibrium calculations of a fuel-rich B(s)/air mixture. The overall reaction for complete heat release requires about 100 μ s. The temperature profile is separated into two regimes; the first regime is associated with the formation of BO₂, and the second is associated with formation of B₂O₃. Both BO and BO₂ are observed to be major reaction intermediates.

In comparison, Fig. 2 shows the results of a mixture in which the initial conditions were derived from equilibrium calculations of a fuel-rich JP4/B(s)/air mixture. In this case, the reaction time for complete heat release is approximately 10 μ s; however, the time for complete formation of B₂O₃ is again approximately 100 μ s. Here, a significant portion of the energy release is controlled by radical recombination. Hence, as the pressure of this system is increased, the heat release eventually becomes controlled by HBO₂ formation. Since the final equilibrium process is nearly isothermal, it is evident that hydrogen addition to boron chemistry significantly enhances the rate of heat release, in addition to altering the dominant suboxides and reaction products.

A general examination of the reaction fluxes and sensitivities indicates the following sequence of reaction: first, the initial stable suboxides and/or suboxyhydrides are reduced to BO; the BO is then oxidized to BO₂; and finally, the BO₂ is reduced to either HBO₂ or B₂O₃. The final equilibrium species distribution between HBO₂ and B₂O₃ is determined to a large extent by the equilibrium relationship of $2\text{HBO}_2 \rightarrow \text{B}_2\text{O}_3 + \text{H}_2\text{O}$, for which the equilibrium constant can be expressed as $2.52 \exp(-12,640/RT)$.

Tables I and II list the reactions found important to homogeneous, gas-phase kinetics of -/O/H/C mixtures. The order of listing in each set of brackets represents the general trend of effectiveness of various reactants as estimated from the sensitivity analysis.

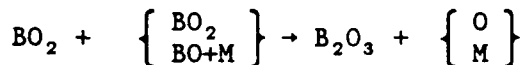
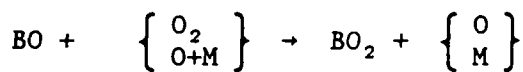
In addition to the elemental kinetic results, several important conclusions can be surmised about the combustion process of particulate boron from the present calculations. For example, the current homogeneous calculations have shown that the sensitivity of the species concentration profiles to the chosen initial species speciation (for a fixed number of moles of each element) is nearly independent of this speciation for reaction times greater than a few micro-seconds, suggesting that the identity of the species evolving from a reacting boron particle is not critical to the surrounding gas-phase combustion process. Furthermore, as noted above, hydrogen containing species have a significant impact on accelerating the gas-phase combustion. However, larger quantities of hydrogen promote the formation of HBO₂, which is thermodynamically favored over gaseous B₂O₃ as the temperature is lowered. Consequently, if the product condensation stage of boron combustion must proceed via simple nucleation to achieve high combustion efficiencies, hydrogen addition, although beneficial to the gas phase kinetics, may have an adverse affect on the condensation process.

Steady-state and unsteady one-dimensional codes with sensitivity analysis are currently being developed to include the gas-phase kinetics described here and the heterogeneous processes described previously [1].

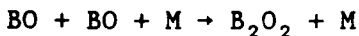
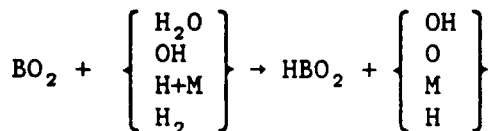
REFERENCES

1. Kolb, C.E., Brown, R.C., Annen, K., Dryer, F.L., Yetter, R.H., Rabitz, H., and Cho, S.Y., Chemical Kinetic Modeling and Sensitivity Analyses for Boron Assisted Hydrocarbon Combustion I, Abstracts from the 1988 AFOSR/ONR Contractors Meeting on Combustion.
2. Yetter, R.A., Rabitz, H., Dryer, F.L., Brown, R.C., and Kolb, C.E., Kinetics of High Temperature B/O/H/C Chemistry, submitted to Combustion and Flame, Feb. 1988.
3. Yetter, R.A., Cho, S.Y., Rabitz, H., Dryer, F.L., Brown, R.C., and Kolb, C.E., Chemical Kinetic Modeling and Sensitivity Analyses for Boron Assisted Hydrocarbon Combustion, Twenty-Second Symposium (Int'l.) on Combustion, The Combustion Institute, accepted for presentation, Aug. 1988.

Table I. Important Reactions to the High Temperature Oxidation of Boron Monoxide

B/O Chemistry

Fuel-Rich

B/O/H Chemistry

Fuel-Rich

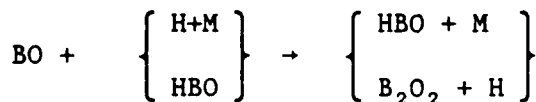
B/O/C Chemistry

Table II. Important Reactions to the High Temperature Oxidation of B_2O_2 and HBO

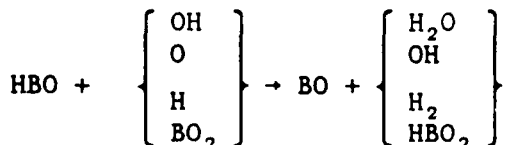


FIGURE CAPTIONS

Figure 1. Species mole fraction and temperature profiles of a B/O mixture reacting adiabatically and at constant pressure. Initial Conditions: $X_{B_2O_2} = 0.164$, $X_{BO} = 0.018$, $X_{O_2} = 0.172$, $X_{N_2} = 0.646$, $T = 1800$ K, $P = 8$ atm.

Figure 2a. Species mole fraction and temperature profiles of a B/O/H/C mixture reacting adiabatically and at constant pressure. Initial Conditions: $X_{B_2O_2} = 0.035$, $X_{BO} = 0.003$, $X_{HBO} = 0.072$, $X_{O_2} = 0.163$, $X_{N_2} = 0.617$, $X_{H_2} = 0.055$, $X_{CO} = 0.055$, $T = 1800$ K, $P = 8$ atm.

Figure 2b. Mole fraction profiles from the B/O/H/C mixture of Fig. 2a for species of the CO/H₂/O₂ sub-mechanism which react simultaneously with the boron compounds shown in Fig. 2a.

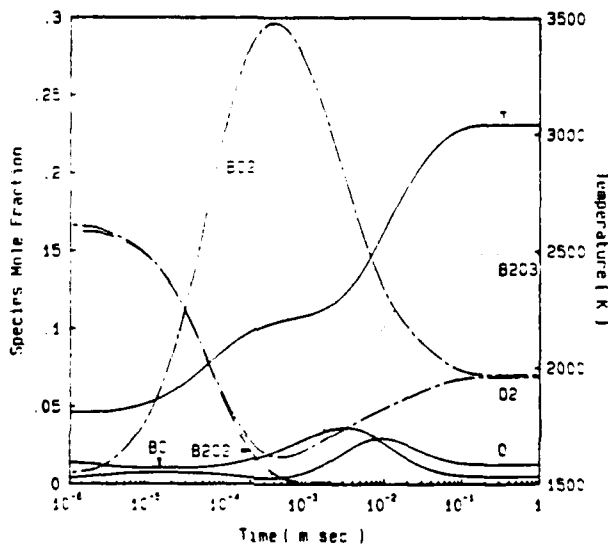


Figure 1

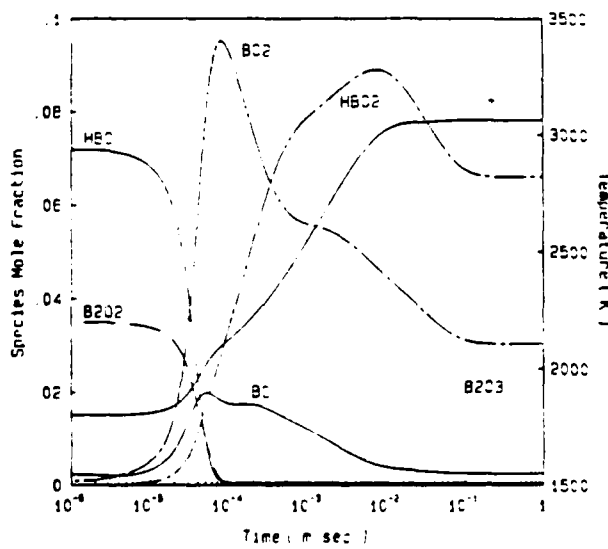


Figure 2a

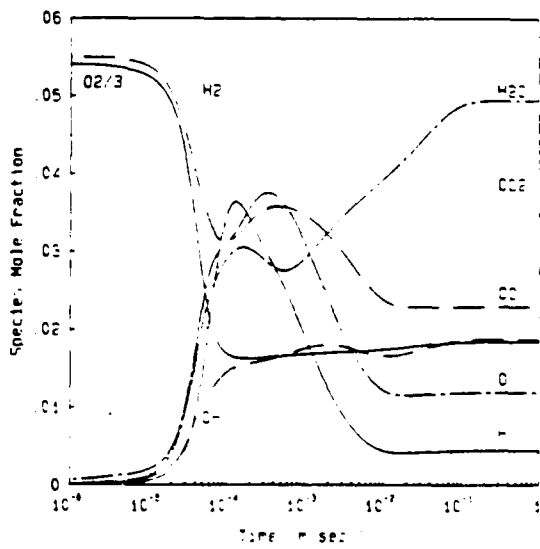


Figure 2b

NRL BORON PROPELLANTS COMBUSTION PROGRAM

H.H. Nelson
Chemistry Division/Code 6110
Naval Research Laboratory
Washington, DC 20375-5000

SUMMARY/OVERVIEW:

The NRL program on High-Energy Propellant Chemistry includes work in three project areas. The first of these is a mass spectrometry based study of the oxide layer formed at the surface of elemental boron. The second involves the study of chemical mechanisms of homogeneous boron combustion. This work has focussed on boron hydrides in the past year but is expanding to cover boron oxyhydrides. The third area is a theoretical investigation of important intermediates in boron combustion. Structures, thermodynamics and reaction pathways are being studied. All three projects are oriented to assist in the understanding and control of heterogeneous and homogeneous combustion of boron and boron-doped fuels.

TECHNICAL DISCUSSION:

The oxide coating that forms rapidly on boron (B_2O_3)_n has been investigated by fast-atom bombardment mass spectrometry. Bombardment of the glassy surface of oxidized boron by high energy xenon atoms yielded twenty-two gas-phase boron oxide ions that were heretofore unknown.[1,2] Collisional activation of these ions has revealed structural elements that are common to the most stable boron oxide ions. These ions exist with boron limited to two- or three-coordination with oxygen and are thus built upon integral BO_2 triangles and terminal -B=O units.

We have studied the reactions of BH_3 [3] and BH with various oxidants and hydrocarbons. The BH_3 radical is produced by 193nm photolysis of B_2H_6 and monitored by infrared diode laser absorption near 1140 cm^{-1} . The BH is produced by BH_3CO photolysis and probed by UV lif near 430 nm. We have measured rate constants for the reactions of BH_3 with CO, NO and C_2H_4 and upper limits to the rate constants for reaction with O_2 and H_2O . Rate constants for reaction of BH with NO, H_2O , O_2 , CO_2 , C_2H_4 , TME, CO and H_2 have also been measured and will be discussed in the presentation.

Finally, we have been performing ab-initio quantum chemical calculations of potential energy surfaces for species important to boron combustion. Efforts have focussed on the theoretical prediction of heats of formation for small boron hydrides and a few oxygen containing species and on kinetic studies involving critical species.

We have recently completed a theoretical study of the reaction $H_2 + BO \rightarrow H + HBO$. Our calculations predict this reaction to have a zero point corrected barrier of 9.5 kcal/mole and an exoergicity of 6.4 kcal/mole. The calculated rate constant is well represented over a wide temperature range by the three parameter expression:

$$k(T) = 2.96 \times 10^{-22} T^{3.29} e^{-4.40/RT}$$

We are currently performing a study of the reaction between BO and water. The potential energy

surface calculations are done using multiconfiguration SCF and multireference CI techniques. The rates are computed using conventional or variational transition state theory with quantum corrections along the reaction coordinate. Also underway is the calculation of the regions of the BH_3 potential energy surface important to the unimolecular dissociation to BH and molecular hydrogen.

REFERENCES

1. Doyle, R.J., Jr., Anal. Chem. 1987, 59, 537-539.
2. Doyle, R.J., Jr., J. Am. Chem. Soc. In Press, June 1988 publication.
3. L. Pasternack, R.J. Balla and H.H. Nelson, J. Phys. Chem. 92, 1200 (1988).

Cluster Beam Studies of Boron Combustion

ONR Contract N00014-85-K-0678

Principle Investigator:

Scott L. Anderson
Chemistry Department
State University of New York at Stony Brook
Stony Brook, NY 11794-3400

SUMMARY/OVERVIEW

We have developed two instruments for studying the physical and chemical properties of boron and other metal/semiconductor cluster ions ranging in size from 1 to ~200 atoms. The clusters are used as well characterized experimental "models" for boron surfaces under chemical attack. We obtain thermochemical and mechanistic information on reactions important in the combustion of boron, and rate constants can be derived from the cross section data. Reaction of the clusters with oxygen will be presented as an example of the technique.

TECHNICAL DISCUSSION

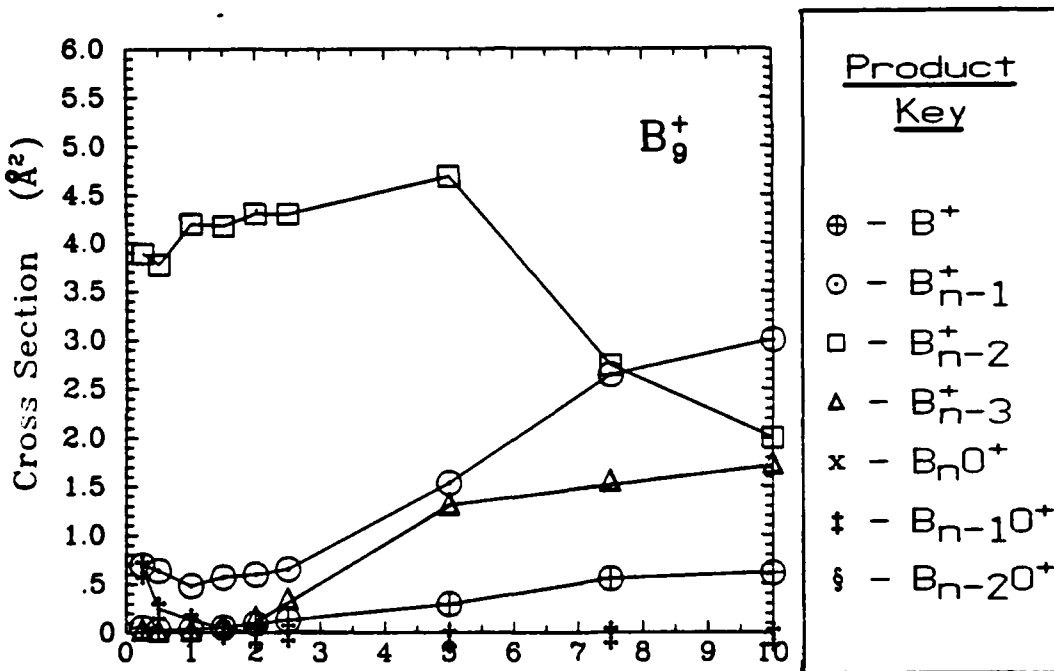
One of the problems in understanding and modeling the chemistry involved in boron and metal containing fuels is lack of information regarding the heterogeneous processes involved. Few of the detailed mechanisms or rate constants that might be important in boron volatilization or in condensation of the oxide products are known, and conventional kinetics or surface science techniques are hard to apply to these problems. We have developed techniques for producing boron and metal/semiconductor cluster ions ranging from atomic size to several hundred atoms¹⁻⁵. Using mass spectrometry techniques we can isolate particular size and composition clusters, and study their properties and chemistry over a wide range of collision energies (8-10 eV, corresponding to "temperatures" from room temperature to 100,000K)⁵⁻¹⁰. The idea is to use the clusters to study the surface chemistry of interest under well controlled experimental conditions.

Boron cluster ions are generated by one of several techniques. Most of our work to date has been done using a laser ablation source developed in our lab^{5,8}. This can produce boron cluster ions containing up to ~100 atoms with useable intensities. After production, the clusters are stored in helium^{1,4} buffer gas for ~25 msec to thermalize their internal degrees of freedom^{1,4}. A second source using laser vaporization inside the throat of a supersonic nozzle is under development. The thermalized cluster ions pass through a mass filter which allows us to select the desired size and composition for study. We are able to produce clusters of pure boron, and boron oxides, nitrides, hydroxides, ... of varying composition. The energy of the reagent cluster ion beam is then set to give the desired collision energy, and the clusters are

passed through a gas cell containing a reactant gas. Products are collected and analyzed by guided beam mass spectrometry.

Several types of experiments have been performed. For any given cluster composition, we first use collision-induced-dissociation (CID) to characterize the geometric and bonding structure of the clusters^{4,5,6}. This information is necessary in working out the thermochemistry and mechanisms for chemical reactions. For boron, we have also performed high level (SCF-CI) quantum chemistry calculations to aid understanding of the rather unique bonding properties of boron.

Reaction of the clusters with oxygen⁹ and water have been studied. In both cases, we see oxidation of the clusters, yielding B_9O^+ or B_9OH^+ species, as well as "volatilization" in which small $B_nH_{x,y,z}^+$ species are ejected from the cluster surface. Cross sections for the various product channels for a typical small cluster are plotted as a function of collision energy in Fig. 1. From the thresholds observed for some reactions, together with our CID data, we can derive bond energies and reaction thermochemistry. The product branching as a function of reaction conditions gives us insight into the reaction mechanisms. As an adjunct to the oxidation studies we have examined the bond energies and chemisorption dynamics of hydrogen on small boron cluster ions¹⁰.



We are currently extending the work in two ways. First is simply to study more types of chemistry related to combustion of boron containing fuels. We will be looking at reactions of boron and boron oxide cluster ions with nitrogen, small hydrocarbons, fluorinated species, and nitro-compounds. We will also carry out a systematic study of B-B, B-O, and B-OH bonding in small

clusters. This thermochemical data is relevant to understanding the condensation/dehydrogenation process which is a major bottleneck in efficient boron combustion.

In addition, we are completing a new instrument capable of working with much larger size cluster ions. Larger clusters are more representative of the macroscopic fuel grains of interest in combustion applications. The new instrument is unique in its ability to handle heavy cluster ions over a wide range of collision conditions.

References

1. "Chemistry and Cooling of Transition Metal Cluster Ions", Luke Hanley and Scott L. Anderson, *Chem. Phys. Lett.* 122 (1985) 410.
2. "Reactions of Bare Aluminum Cluster Ions", Luke Hanley and Scott L. Anderson, *Chem. Phys. Lett.* 129 (1986) 429.
3. "Chemistry of Small Metal Cluster Ions", Luke Hanley, Stephen Ruatta, and Scott Anderson, in The Physics and Chemistry of Small Clusters, Jena and Rao eds., Plenum, New York (1986).
4. "Collision Induced Dissociation of Aluminum Cluster Ions: Fragmentation Patterns, Bond Energies, and Structures for $\text{Al}^+ - \text{Al}_7^+$ ", Luke Hanley, Stephen A. Ruatta, and Scott L. Anderson, *J. Chem. Phys.* 87 (1987) 260.
5. "Size Dependent Barriers for Reaction of Aluminum Cluster Ions with Oxygen", Stephen A. Ruatta, Luke Hanley, and Scott L. Anderson, *Chem. Phys. Lett.* 137 (1987) 5.
6. "Production and Collision-Induced-Dissociation of Small Boron Cluster Ions", Luke Hanley and Scott L. Anderson, *J. Phys. Chem.* 91 (1987) 5161.
7. "Reaction of Aluminum Cluster Ions with Oxygen and Nitrous Oxide: Energetics and Dynamics of Cluster Oxidation", Stephen A. Ruatta, Luke Hanley, and Scott L. Anderson, *J. Chem. Phys.* (in press)
8. "Collision Induced Dissociation and *Ab Initio* Studies of Boron Cluster Ions: Determination of Structures and Stabilities", Luke Hanley, Jerry L. Whitten, Scott L. Anderson, (in press).
9. "Oxidation of Small Boron Cluster Ions (B_{1-13}^+ by Oxygen". Luke Hanley and Scott L. Anderson, *J. Chem. Phys.* (submitted).
10. "Dynamics of Hydrogen Chemisorption on Boron Cluster Ions", Stephen A. Ruatta, Luke Hanley, and Scott L. Anderson, (in preparation).

THE MODELING OF DROP-CONTAINING TURBULENT EDDIES

(AFOSR Contract No. NASA 7-918 Task Order RE182 Amendment 480)

Principal Investigator:

J. Bellan
Jet Propulsion Laboratory
California Institute of Technology
4800 Oak Grove Drive,
MS 125/214
Pasadena, CA 91109

SUMMARY/OVERVIEW:

The development of a mathematical model describing the behavior of a drop-containing turbulent eddy is proposed with the goal of initiating a theory describing the interactions of several drop-containing eddies during evaporation, ignition and combustion of liquid fuels injected into combustors. Specifically, the approach taken here is that it is reasonable to take a first step towards such a description by formulating the description of the behavior of a cluster of single component fuel, monodisperse, uniformly-distributed drops contained in a turbulent eddy. Since this model is thought to be utilized as a subscale or subgrid model in more elaborate calculations, the interest is focussed on the global rather than the detailed aspects of behavior. These global aspects are in many cases sufficient to characterize regimes of specific behavior and also to identify the parameters that control various phenomena in each particular regime.

TECHNICAL DISCUSSION:

In this study we seek to develop a subgrid model that is general enough to be useful both close to the atomizer and further downstream from the atomizer. For this reason it is important that the formulation be valid for both dense and dilute clusters of drops.

This study is to be accomplished in two steps. First, it is important to understand the influence of turbulent transport from the ambient to the eddy. It is this transfer of mass, momentum, species and heat through the surface of the cluster and the transfer from the cluster to the ambient that provides the coupling between the subgrid model and the macroscale. Second, it is crucial to understand the interaction between the drops and the vortical motion of the gas inside the eddy. What is described below is the study of the transport process between the cluster and the ambient. The interest is focussed on global, rather than detailed aspect of behavior as the information obtained is expected to yield a qualitative understanding.

The initial model of droplet evaporation in a cluster and the interactions between cluster and ambient are described in recent publications [1,2]. Basically, a monodisperse, uniformly distributed collection of single component liquid spherical drops evaporates in a spherical cluster. The pressure in the

cluster is the same as in the ambient and constant. All drops move at the same velocity with regard to the ambient.

Transfer from the surroundings to the cluster was modeled using, consistently with the treatment of convective drop evaporation[1], a convective correction to a diffusive model. As a first step, two ad-hoc turbulence models were used in order to determine the importance of turbulence upon drop evaporation. In the first model turbulence is not present initially but rather builds up with time if the cluster "porosity" (i.e. the relative axial velocity between drops and gas) diminishes significantly. In contrast, in the second model turbulence is present initially. The details of the formulation are given in Ref. 2.

Because of the global aspect of the model in which all drops are assumed to behave identically, the transport from the cluster to surroundings was modeled using a "trapping factor". Basically, the "trapping factor" is a weighing factor which allows the modeling of intermediary situations between those of dilute clusters where evaporated mass was assumed to be trapped in the cluster and that of dense clusters where evaporated mass was assumed to escape to ambient.

The most important conclusion of the above formulation was that whereas in the dilute regime turbulence is not a controlling parameter, in the dense regime it becomes the crucial control parameter. Since the transport processes between the cluster and its surroundings were found to be so important in the case of dense clusters, it was thought very important to improve the description of the transport of heat, mass and species from the cluster to its surroundings.

The new model preserves most of the aspects of the initial model, however, in contrast to our previous formulation [2], the radial motion of the drops is assumed to be self-similar. Thus, a typical drop inside the cluster is located at a distance $\tilde{r} = \xi R$ with ξ fixed (\tilde{r} is the radial coordinate; R is the cluster radius). Here ξ is a similarity parameter assuming values between zero and unity. More precisely, whereas in our initial model, for example, the drops and gas moved with respective relative velocities u_d and u_g in the axial direction, now there is additionally a radial velocity component, respectively $\xi \frac{dr}{dt}$ (for the drops) and ξu_g (for the gas). Momentum exchange between the phases is associated with drop evaporation rate, the drop drag coefficient and a cluster drag coefficient in the same manner as previously [1]. Unlike in the previous formulation [1,2], the new similarity parameters, ξ , now appears in the drop momentum equation. In the spirit of still keeping the global formulation, an averaged momentum equation is obtained by integrating over ξ . By doing so, we neglect the tendency of nonlinear drag to destroy the self-similar radial motion. This assumption seems reasonable in the case of strong evaporation.

The results of this model were presented in Ref. 3 where a comparison with the results of our initial model was made as well. Figure 1 shows the results of one such comparison. The figure shows that the discrepancy between the four sets of results (two turbulence models and two axial drop motion models) is small in the dilute regime. This is because in this regime transport processes are not important in determining the evaporation time due to the fact that the drops are far apart and enough heat is available for evaporation. As the initial mixture becomes rich the discrepancy between the "trapping factor" and similarity models becomes larger. Although the qualitative predictions are the

same (evaporation time peaks in the dense regime), reliable quantitative predictions should be expected only when results of global models can be compared with experimental observations. The present results indicate that only measurements of evaporation times in the dense regime (where the sensitivity is highest) will be able to decide the matter.

Additional results presented in Ref. 3 show that transport processes are more important for smaller clusters of drops in the dense regime. Results obtained with the more sophisticated cluster model have also shown that the ratio of the fuel lost from the cluster to the initial amount of fuel available in the cluster depends strongly on cluster size and turbulence model whereas the total mass loss is nearly insensitive to turbulence except in the case of small clusters. It has also been suggested that the necessary experimental data that could bridge the gap between qualitative and quantitative behavior include evaporation times, dynamics of cluster drop size during evaporation in terms of ratio of growth or decay, total mass ratio and fuel ratio lost /gained in various conditions, all to be obtained in the dense regime.

Nomenclature

n^o	- initial drop number density
R^o	- initial drop radius
\tilde{R}^o	- initial cluster radius
R^o_2	- initial nondimensional radius of the sphere of influence of each drop, a/R^o
T^o_{ga}	- initial temperature of the ambient
T^o_{gs}	- initial temperature of the drop
t	- time
u^o_r	- initial relative velocity between drop and gas
Y^o_{Fva}	- initial mass factor of fuel vapor in the ambient

REFERENCES

1. Bellan J. and Harstad, K. "The Details of the Convective Evaporation of Dense and Dilute Clusters of Drops," Int. J. Heat Mass Transfer, 30, 6, 1083-1093, 1987
2. Bellan, J. and Harstad, K., "Turbulence Effects During Evaporation of Drops in Clusters," Int. J. Heat Mass Transfer, in press
3. Bellan, J. and Harstad, K., "Transport-Related Phenomena for Clusters of Drops", to be presented as the ICLASS 1988 Meeting, Sendai, Japan

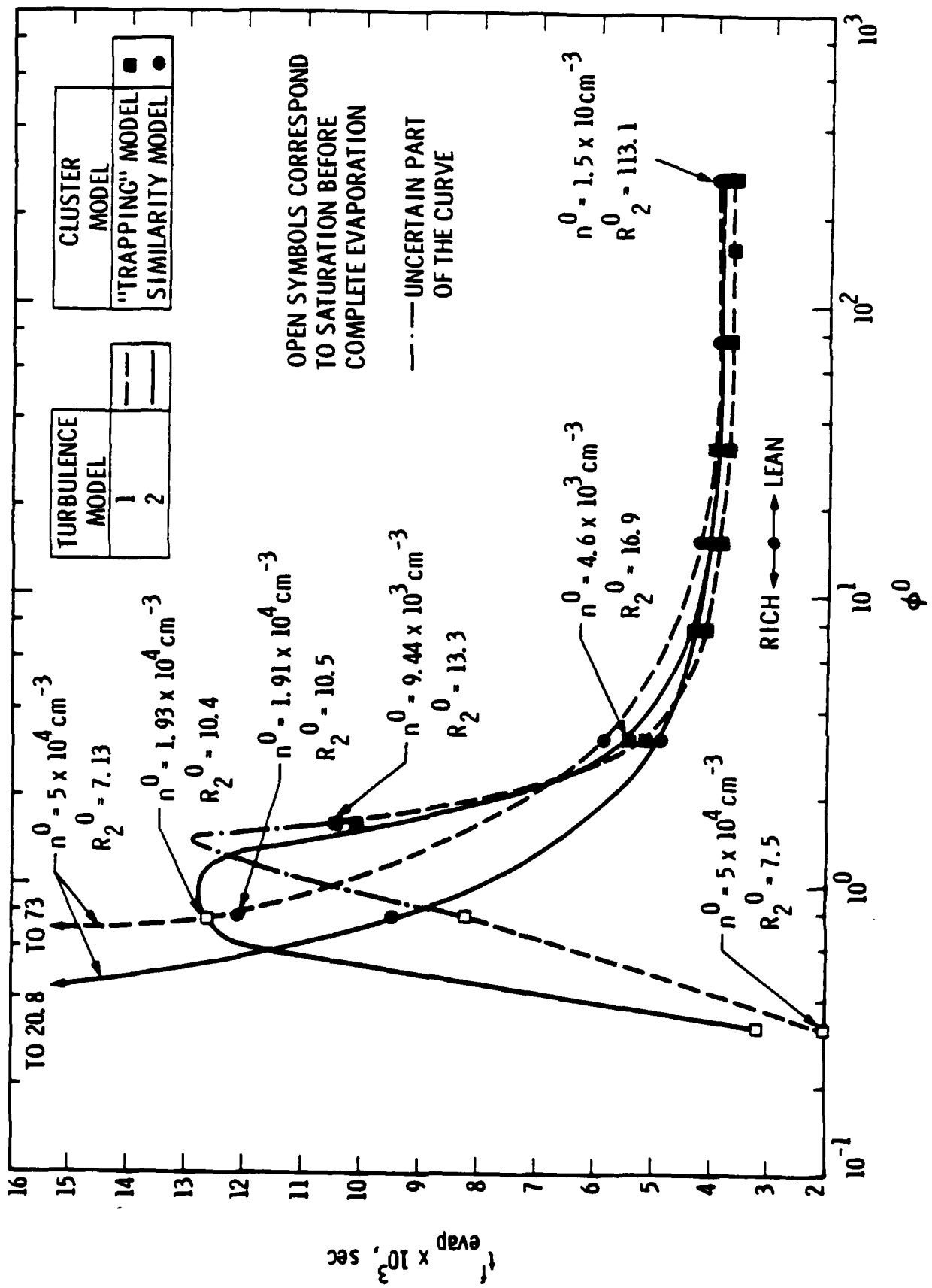


Fig. 1 Evaporation Time versus Initial Air/Fuel Mass Ratio.
 $T_{0a} = 10000K$, $T_{0f} = 3500K$, $y_{0u} = 0.0$, $y_{0d} = 0.0$

FUNDAMENTAL STUDIES IN SPRAY COMBUSTION AND TURBULENT COMBUSTION

AFOSR Grant 86-0016

Principal Investigators: W.A. Sirignano
G.S. Samuelsen

Department of Mechanical Engineering
University of California
Irvine, California 92717

SUMMARY

Experimental development and theoretical analysis on liquid-fuel-sheet distortion and break-up are underway. Vertical structures balanced by surface-tension restraints determine the primary distortion; a bifurcation occurs in Weber number space so that vertical roll occurs only in part of the space. Variable transport properties have been considered in recent droplet vaporization calculations. Drag coefficients, transfer numbers, and Nusselt numbers are shown to depend upon transport property models and liquid heating models. The Renksizbulut-Haywood correlation does not apply at high transfer number.

TECHNICAL DISCUSSION

The AFOSR program at UCI has four major tasks. The task on turbulent reacting flows was presented last year and will not be discussed this year. The spray work is emphasized herein.

During the present reporting period, the experimental fixture for the atomization experiment was fabricated, tested, and modified to more easily produce the sprayed liquid sheet. The modifications included (1) improving clearances within the nozzle to reduce pressure drop prior to the nozzle tip, and (2) the provision of supports to maintain the gap thickness of the nozzle outlet constant. After the modifications, the fixture ("Prototype I") was evaluated with consistent and encouraging results. A second nozzle, Prototype II, has been designed with the information gained from Prototype I (see Figure 1). The breakup of the sheet will be characterized by varying the initial sheet thickness, the velocity of the liquid, and the velocity of the shear air on either side of the liquid sheet. The initial tests will evaluate the size and shape of the ligaments occurring at the point of sheet breakup, along with the distance from the nozzle tip to breakup of the sheet. Correlations of the ligament formation with the test parameters will be developed, along with studies relating the contribution of ligaments to atomization resulting in spherical droplets. The effects of surface roughness, nozzle tip geometry (see Figure 2), and liquid surface tension on ligament formation will be addressed. Data for the aforementioned tests will be obtained using the flow visualization system presented in Figure 2.

The objective of the liquid-sheet theoretical study is to extend the model (Rangel and Sirignano, 1988) to simulate the behavior of a finite-thickness liquid sheet in contact with a stream of air on each side of it. We

first consider cases in which the air streams on either side of the liquid sheet move with the same velocity. Symmetric waves and asymmetric or, more properly, shifted-symmetric waves are considered. Linear theory shows that the second class is more unstable and, for such a case, it predicts a cutoff wavenumber that divides the spectrum into a region of stable waves and a region of exponentially growing waves. Our non-linear investigation is based on the vortex discretization method. It is described in detail by Rangel and Sirignano (1988). Figure 3 shows the growth of a disturbance at a dimensionless time of one for three different values of h/λ . These values are, from top to bottom, 1.0, 0.25, and 0.1. In all cases the density ratio is one and surface tension is neglected. (Note that the vertical scale is different in each of the plots.) Other cases with surface-tension and density differences are under study. Extension to the case of the two air streams moving with different velocities should follow. By studying the non-linear evolution of these disturbances, some inferences will be made on the dependences of the ligament sizes to the various parameters.

The Navier-Stokes equations are solved for two distinct droplet flow configurations. The interaction between two droplets in an intermediate-Reynolds-number-flow over a wide range of initial conditions has been studied and the results describing the dramatic changes in the drag coefficient and Nusselt number due to interaction effects are summarized in Raju and Sirignano (1987, 1988) and Sirignano (1987). The other configuration involves the isolated droplet behavior in a hot and convective environment where the earlier work of Patnaik et al. (1986) and Patnaik and Sirignano (1986) is extended to include the effect of variable transport properties.

The results of an isolated droplet behavior with variable transport properties are presented in Figures 4 and 5. Figure 4 shows the variation of the drag coefficient vs instantaneous Reynolds number, the isolated solid sphere standard drag coefficient, and the variation of the drag coefficient for the case in which the temperature behavior of the liquid phase is taken into account by the simplified infinite conductivity model (Sirignano (1983)). The drag coefficient does not simply increase as Reynolds number decreases with time and the solid sphere correlations can be grossly inaccurate. The significant reduction in the drag during the final period of our calculations results from a decrease in the skin friction drag caused by an increase in the blowing velocity. The increase in the transfer number is primarily caused by a reduction in the heat entering the liquid phase as the droplet surface temperature rises with time. In the high transfer number regime, the reduction in the drag is observed to be much higher than the previous results in which the effect of variable transport properties has been neglected (Patnaik, et al. (1986) and Patnaik and Sirignano (1986)). The effect of finite conductivity on the variation of transfer number with time is found to be significant and the importance of liquid-phase temperature behavior on the drag and Nusselt number variation can be seen from Figures 4 and 5. Figure 5 also shows that the applicability of the Renksizbulut-Haywood correlation is limited to rather low transfer numbers and the correlation for high transfer numbers needs further investigation.

REFERENCES

- Rangel, R.H. and Sirignano, W.A. (1986). "Non-Linear Growth of Kelvin-Helmholtz Instability: Effect of Surface Tension and Density Ratio," to appear in The Physics of Fluids.

Raju, M.S. and Sirignano, W.A., AIAA-87-0300, AIAA 25th Aerospace Sciences Meeting, Reno, Nevada, January 12-15, 1987.

Raju, M.S. and sirignano, W.A., submitted to the Physics of Fluids (1988).

Sirignano, W.A., AFOSR-Annual Technical Report, 1987.

Patnaik, G., Sirignano, W.A., Dwyer, H.A., and Sanders, B.R., Prog. in Astronautics and Aeronautics, Vol. 105, 1986.

Patnaik, G., and Sirignano, W.A., Western States Section/The Combustion Institute Spring Technical Meeting, Banff, Canada, 1986.

Sirignano, W.A., Prog. Energy Combust. Sci., Vol. 9, 1983.

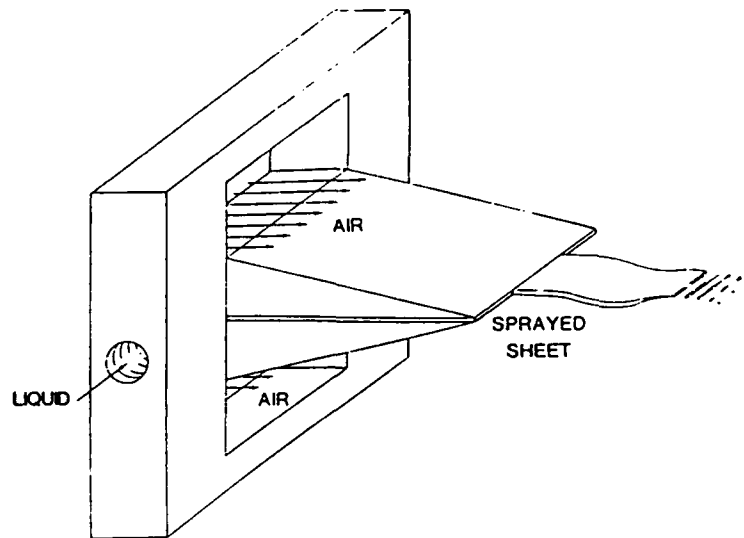


Figure 1. Injector design.

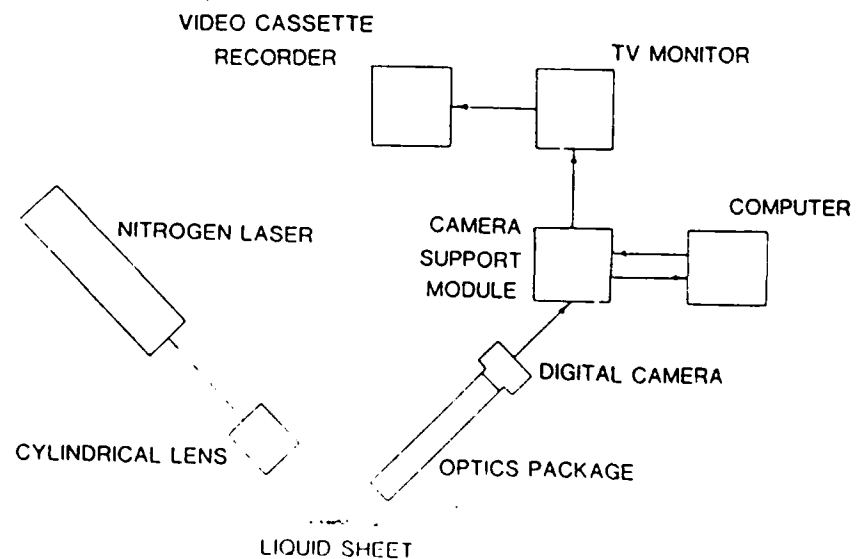


Figure 2. Flow visualization system.

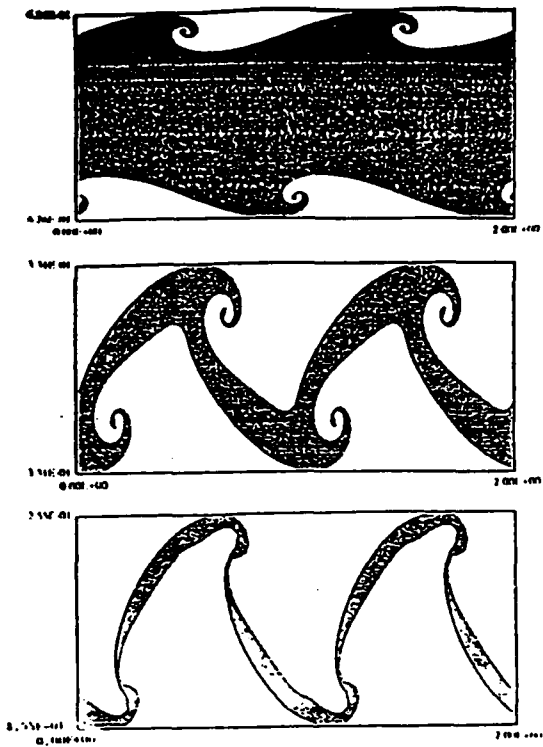


Figure 3. Sheet distortion at a dimensionless time of 1 for thickness-to-wavelength ratios of 1.0, 0.25, and 0.1. Density ratio = 1. Surface tension = 0.

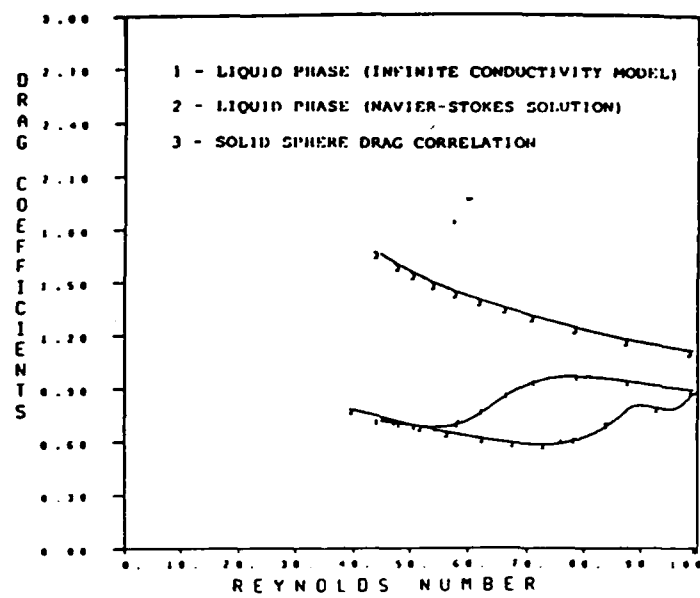


Figure 4. Drag coefficient vs. instantaneous Reynolds number.

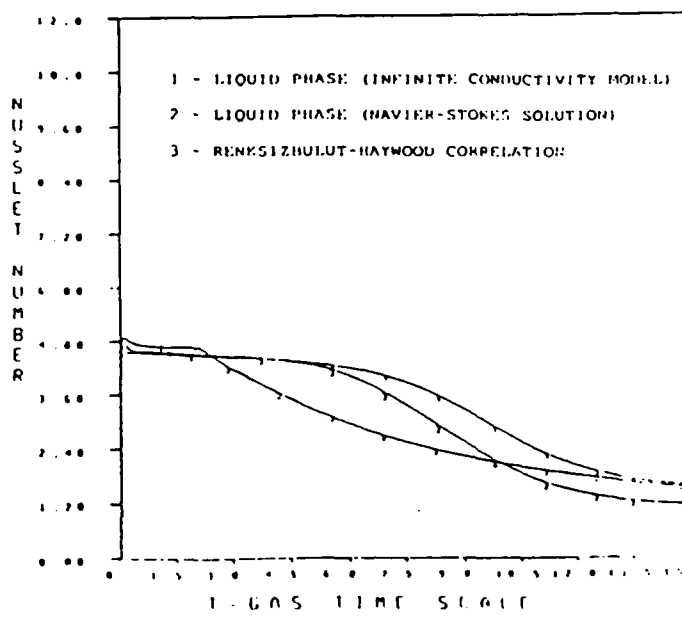


Figure 5. Nusselt number vs. nondimensional time.

DENSE-SPRAY STRUCTURE AND PHENOMENA

(AFOSR Grant No. 85-0244)

Principal Investigator: G.M. Faeth

217 Aerospace Engineering Building
The University of Michigan
Ann Arbor, Michigan 48109-2140

SUMMARY/OVERVIEW

Aspects of dense sprays are being investigated both theoretically and experimentally. The study has two major objectives: (1) to study the modification of continuous-phase turbulence properties by the presence and motion of the dispersed phase (which is called turbulence modulation); and (2) to study the structure of the near-injector dense-spray region of pressure-atomized sprays. Results include: first measurements of properties of turbulence generated entirely by the motion of dispersed phases; proof of the importance of jet exit turbulence properties on the structure of dense sprays; and better understanding of the limitations of the locally homogeneous flow approximation which is often used to analyze dense sprays.

TECHNICAL DISCUSSION

Introduction. Compared to dilute sprays, the near-injector dense spray region is not well understood (Faeth, 1987a). This hampers understanding of spray processes, since the dense spray region controls initial conditions for the rest of the flow. The present investigation is considering aspects of dense sprays using two novel experiments. One involves particle-laden flows which highlight effects of dispersed phases on continuous-phase turbulence properties, a key issue for dense sprays, in an environment which permits reliable measurements. The other involves large-scale (10 and 20 mm diameter) pressure-atomized jets which mitigate spatial resolution difficulties of conventional dense sprays. Analysis is also being developed to assist interpretation of the measurements. Methods and accomplishments for both phases of the study are described in the following.

Particle-Laden Flows. This phase of the study is considering the modification of continuous phase turbulence properties by the presence and motion of the dispersed phase, denoted turbulence modulation. The first part of the study involved measurements and analysis of dilute particle-laden water jets in water (Parthasarathy and Faeth, 1987a,b). Existing methods for analyzing dilute sprays yielded encouraging predictions, however, a deficiency of predictions highlighted the potential for studying turbulence modulation in dilute flows which is being pursued. It was observed that turbulence intensities became much greater than predictions which ignored turbulence modulation far from the injector where relative particle velocities begin to exceed mean flow velocities. This was attributed to conventional turbulence mechanisms becoming small in comparison to turbulence modulation effects resulting from the finite relative velocities of the particles.

To begin study of turbulence modulation along these lines we are considering a uniform flux of nearly monodisperse glass particles falling in a stagnant water bath. The particles quickly reach terminal velocities in the bath, providing an extensive region where the continuous phase is a homogeneous turbulent flow produced entirely by a turbulence modulation mechanism. Measurements include: motion-picture shadowgraphs for particle trajectories, Mie scattering for particle fluxes, and a two-point phase-discriminating laser-Doppler anemometry for phase velocities.

Flow properties are being predicted using a stochastic analysis, assuming linear superposition of wakes distributed uniformly in the crossstream direction and randomly (Poisson statistics) in time. Turbulent wake properties are used, since the wakes relaminarize when velocity defects are too small to be measured for present conditions. Thus far, we have limited predictions to streamwise velocities and only considered mean velocities in the wakes. For present flows both mean and fluctuating velocities in the wakes become part of the turbulent field since particle motion is random. As a result, the dissipation rate of turbulence kinetic energy is known immediately since it is equal to the rate of loss of potential energy of the particles per unit volume.

The analysis implies that turbulent fluctuations should be proportional to the square root of the dissipation rate of turbulence kinetic energy and relatively independent of particle size. Measurements of streamwise and crosstream velocity fluctuations and turbulence kinetic energy illustrated in Fig. 1 support these trends as well as quantitative predictions of streamwise velocity fluctuations for the two particle sizes considered thus far.

Predictions and measurements of the temporal spectra of streamwise velocity fluctuations are illustrated in Fig. 2. A remarkable feature of these results is the large frequency range of the spectra even though initial wake Reynolds numbers are relatively low (ca. 10^2). The theory indicates that temporal spectra should be independent of particle loading (or the overall rate of dissipation) for a particular particle size: a trend which is clearly satisfied by the measurements. The low-frequency portion of the spectrum is also predicted quite well, including the shift in frequencies for different particle sizes. Roughly half-way down the spectra, however, there is a plateau region followed by subsequent decay parallel to the predictions: this enhancement of the high frequency end of the measured spectra is due to wake turbulence itself. Thus, the large spectral range of the particle turbulence field is due to combined effects of mean and fluctuating velocities in the particle wakes, since mean wake velocities cannot be separated from conventional wake turbulence when wake arrival times are random.

Measurements to find two-point correlations and to study effects of particle and continuous phase properties must still be completed. The theory must also be extended to consider effects of wake turbulence and to find other measured properties of the flows. Finally, the experimental and theoretical description of the turbulence field of the particles will be used to develop stochastic analysis to find mean and fluctuating particle velocities and the turbulent dispersion of particles.

Large-Scale Jets. This phase of the study is considering the structure and mixing properties of dense sprays directly, using large-scale pressure-atomized sprays to minimize spatial resolution difficulties. Measurements include: mean liquid volume fractions using gamma-ray absorption; jet exit and entrainment velocities, using laser-Doppler anemometry; and drop sizes and phase velocities, using double-flash holography.

The flows are analyzed using the locally-homogeneous flow (LHF) approximation, which implies that interphase transport rates are infinitely fast. An objective of the theory is to help resolve controversy concerning the effectiveness of LHF analysis for dense sprays (Faeth, 1987a,b). Initial results of the study are reported by Ruff et al. (1987,1988).

Typical results are illustrated in Figs. 3 and 4. Figure 3 is a plot of mean liquid volume fractions in the near-injector region for fully-developed flow and atomization breakup. The LHF predictions are reasonably effective when liquid volume fractions are high, but begin to overestimate mixing rates far from the injector as the dilute spray region is entered: this agrees with earlier observations of the performance of LHF analysis in dilute sprays (Faeth, 1987a).

Predicted and measured entrainment rates for a variety of test conditions are illustrated in Fig. 4 - LHF predictions being only influenced by the degree of flow development at the jet exit for these conditions. Use of the LHF approximation invariably causes entrainment rates to be overestimated, since entrainment is strongly influenced by dilute spray properties near the edge of the flow where the LHF approximation is less effective. Furthermore, LHF predictions provide no warning of vastly reduced mixing rates in regimes other than atomization breakup regime. Thus, present work involves use of

multiflash holography to penetrate the dense-spray region and provide drop sizes and velocities as well as the properties of irregular liquid elements like ligaments. A variety of jet exit conditions and breakup regimes are being considered.

REFERENCES

- Faeth, G. M. (1987a) Mixing, transport and combustion in sprays. Prog. Energy Combust. Sci. 13, 293-345.
- Faeth, G. M. (1987b) Turbulent multiphase flows. Proceedings of U.S.-France Workshop on Turbulent Reactive Flows (S.N.B. Murthy and R. Borghi, ed.), Springer-Verlag, Berlin, in press.
- Parthasarathy, R. N. and Faeth, G. M. (1987a) Structure of turbulent particle-laden jets having comparable phase densities. Proceedings of 1987 Spring Technical Meeting, Central States Section of the Combustion Institute, Pittsburgh, pp. 470-475.
- Ruff, G.A., Sagar, A. D. and Faeth, G. M. (1987) Structure of large-scale pressure-atomized sprays. First Annual Conference of ILASS-Americas, Madison, WI.
- Ruff, G. A., Sagar, A. D. and Faeth, G. M. (1988) Structure and mixing properties of pressure-atomized sprays. AIAA Paper No. 88-0237; also, AIAA J., in press.

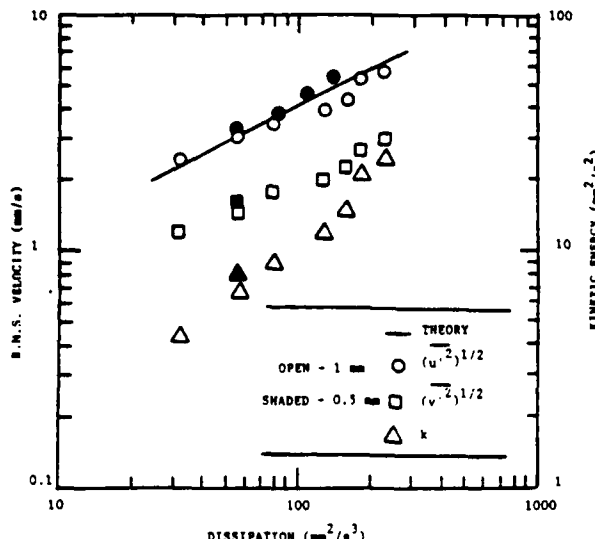


Fig. 1 Velocity fluctuations and turbulence kinetic energy due to turbulence modulation.

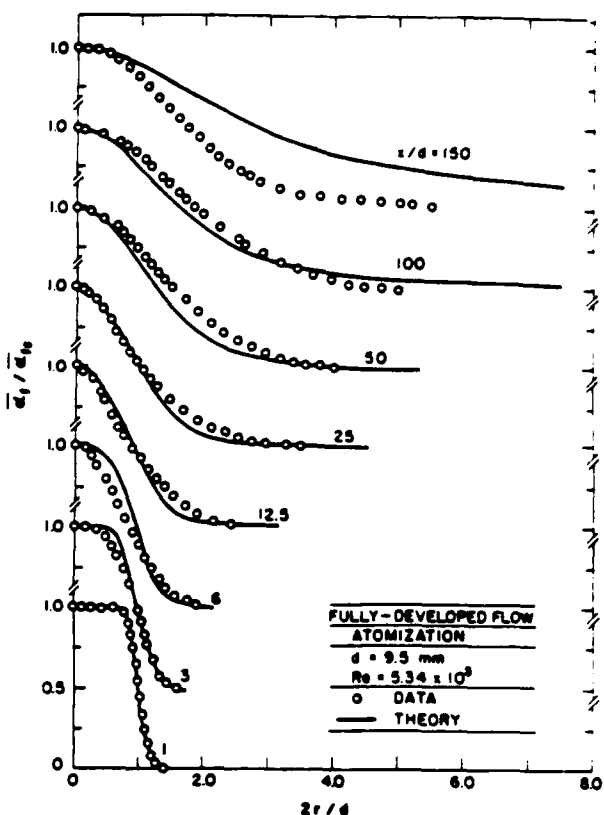


Fig. 3 Liquid volume fractions in dense sprays.

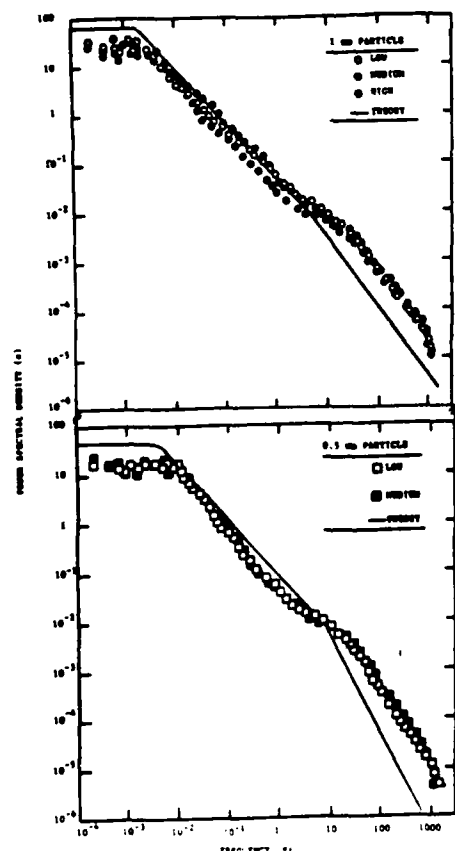


Fig. 2 Streamwise power spectra due to turbulence modulation.

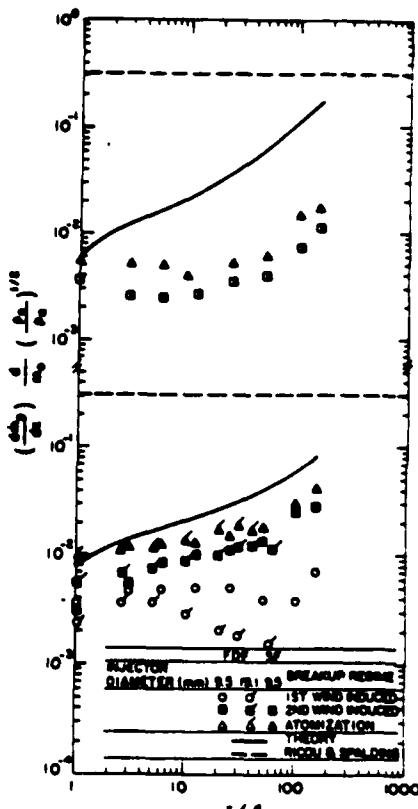


Fig. 4 Entrainment of dense sprays.

PHENOMENA OF COALESCENCE IN BINARY DROP COLLISIONS

(AFOSR Grant/Contract No. ISSA 87-0010)

Principal Investigators: U. S. Rohatgi
C. R. Krishna

Brookhaven National Laboratory
Upton, New York 11973

SUMMARY/OVERVIEW:

Droplet-air interfacial area is very important in the vaporization and subsequent combustion of fuel sprays. In the case of dense and intersecting sprays, the droplets are physically close and are likely to collide. The study being conducted in binary collisions have shown that: droplet collisions and coalescence do take place in the sprays and the combined droplet in fuel sprays are stable and there is a lower limit of Weber number based on relative velocity ($\rho_1 V^2 R / \sigma$) below which drops will bounce off.

TECHNICAL DISCUSSION

1.0 BACKGROUND

The droplets encountered in fuel sprays and of interest in this work are below 150 μm in diameter and with relative velocity of the order of 1m/sec. Thus collision Weber numbers are low (i.e., 2.5 or less). The current models (O'Rourke, 1981; Andersen et al., 1982; etc.) of the dynamics of fuel sprays need empirical expressions to account for the outcome of drop collisions. The possible observed outcome of such collisions are (Brazier-Smith et al., 1972; Adam et al., 1968): (a) coalescence, (b) bouncing, and (c) formation of satellite droplets. The spray models will require a knowledge of the probability of these three outcomes, and the size and velocity distributions of the resulting droplets. This information is particularly crucial for modeling sprays where droplet collisions are likely to occur.

Much of the previous work has been motivated by the need to understand rain formation. Figures 1 and 2 show a comparison of critical impact parameter (X/D) or coalescence efficiency ($E = X^2/D^2$) obtained by various researchers (Adam et al. 1968; Brazier-Smith et al., 1972; Arkhipov et al., 1978). These curves indicate that in the high Weber number range the coalescence efficiency is governed by the stability of the combined drop and decreases with the increase in Weber number. There is also lack of data at low Weber numbers where bouncing is more important. Jayaratne et al. (1964) have shown the importance of air film separating the drops. Hence, models developed from large Weber number data may be inappropriate for fuel sprays.

2.0 EXPERIMENTAL RESULTS

In the experimental work collision results from streams of drops and from intersecting sprays are being studied. Some results from the spray work are

shown in Figures 3 and 4.

In the figures, Nozzle 1 represents the main atomizer, the spray from which is intersected by the spray from a much smaller flow Nozzle 2, the result being given by the data for Nozzle 1 + 2. The data in Figure 3 are for the case when the sprays were more nearly collinear than in Figure 4. It can be seen that there is significant increase in the percentage of small drops ($<30 \mu\text{m}$) in the latter case. The contribution of Nozzle 2 to the total mass is very small even though its spray has a larger fraction of small drops than the spray from Nozzle 1. Therefore, the redistributions in size fractions must come from interaction of the drops (coalescence, break-up, etc.). An interpretation of this and other data with sprays is being developed.

3.0 ANALYTICAL RESULTS

A binary droplet collision will lead to coalescence or at least to surface contact if the droplets have sufficient momentum to drain the intervening air/vapor film. Droplets nearing collision have been observed to deform at the leading edge a dimpled surface. After contact, the combined drop will either stabilize or break up. The drop breakup can be due to two very different mechanisms. For head-on collisions, that is with an impact parameter of zero, the kinetic energy can deform the drops and result in shattering of the combined drop. When the impact parameter is large, the combined drop may have significant angular momentum and can develop instability (Chandrasekhar, 1965) leading to break up. Brazier-Smith et al., (1972) have used the stability analysis of Chandrasekhar (1965) to derive the following stability criterion for coalesced drop in terms of normalized angular momentum Ω_n .

$$\Omega_n = 4\pi\rho_g V X R_1^3 R_2^3 / (3(R_1^3 + R_2^3)^{13/6} (\rho\sigma)^{1/2}) < 5.0 \quad (1)$$

Here V is the relative velocity between drops of sizes R_1 and R_2 , ρ and σ are the liquid density and surface tension respectively and X is the impact parameter. For droplets of fuel sprays ($R \sim 100 \mu\text{m}$, $V \sim 1 \text{ m/s}$), the highest normalized angular momentum can be 1.55 which is much less than 5.0, implying that the coalesced drop (low relative Weber number, $We = \rho_g V^2 R_1 / \sigma$) will remain stable independent of impact parameter.

In the low Weber number region, the flow dynamics of the intervening film controls the process of coalescence. This film flow depends upon the droplet velocities ($We_1 = \rho_g V_1 R_1 / \sigma$), direction of motion (X), and air viscosity (Reg). An analytical model consisting of mass and momentum balances for the droplets and the air film was developed. A schematic of a collision shown in Figure 5. The initial droplet deformation was obtained from Fasel et al. (1983). It was observed that for grazing collisions the component of the relative velocity in the direction of line joining two centers controls the coalescence. The relative Weber number (We) at which coalescence occurred for grazing collisions can be estimated from the relative Weber number for head-on collision

$$We = We(X=0) / (1 - (X/(R_1 + R_2))^2) \quad (2)$$

Figure 6 shows the boundary between coalescence and bouncing as predicted

by the analysis for various droplet Weber numbers (We_1) and stability curve (Brazier-Smith et al., 1972). The droplets with large Weber number (We_1) have large dimples and will require large relative velocity (We) to coalesce. Furthermore, for the same droplet Weber number, the relative velocity (We) needed for coalescence increases with impact parameter (X).

4.0 CONCLUSION

A shift in the size distribution towards larger sizes was observed in the interaction of two sprays confirming the probability of coalescence of droplets. An analysis based on energy considerations indicated that the coalesced drop resulting from two small droplets will not break up. Results from the analytical model indicate that there is a region of low Weber numbers where droplets bounce and this region is strongly dependent on droplet Weber number.

ACKNOWLEDGEMENTS

This work was supported by the Air Force Office of Scientific Research (AFORS ISSA 87-0010) and administered by Dr. Julian Tishkoff. The Authors would like to thank Dr. James Guppy and Dr. James Wegrzyn for suggestions and Mrs. Linda Hanlon for the fine typing.

REFERENCES

1. Adam, J. R., Lindblad, N. R., and Hendricks, C. D., "The Collision, Coalescence, and Description of Water Droplets," *Journal of Applied Physics*, V. 39, No. 11, October 1968.
2. Anderson, O. L., Chiapetta, L. ., Edwards, D. E., and McVey, J. B., "Analytical Modeling of Operating Characteristics of Premixing-Prevaporizing Fuel-Air Mixing Passages, V. 1 Analyses and Results," NASA CR-167990, February 1982.
3. Arkhipov, V. A., Vasenin, I. M., and Trofimov, V. F., "Experimental Study of the Stability of Viscous Drops at Collisions." *Fizicheskaya hydrodinamika i teploobmen*, Novosibirsk, pp. 91-95, 1978
4. Brazier-Smith, P. R., Jennings, S. G., and Latham, J., "The Interaction of Falling Water Drops: Coalescence," *Proc. of Royal Society of London, A* 326, 1972, pp. 393-408.
5. Chandrasekhar, S., "The Stability of a Rotating Liquid Drop," *Proc. R. Soc. Lond. A286*, pp. 1-26, 1965.
6. Frankel, I., and Weihs, D., "Shape and Stability of a Liquid Drop Moving at Low Weber Number," *Applied Scientific Research (Hague)*, Vol. 40, No. 3, 1983, pp. 279-299.
7. Jayaratne, O. W. and Mason, B. J., "The Coalescence and Bouncing of Water Drops at an Air/Water Interface," *Proc. R. Soc. London, A280*, 545, 1964.
8. O'Rourke, P. J., "Collective Drop Effects on Vaporizing Liquid Sprays," Ph.D. Thesis, August 1981, Princeton University.

SPRAYS INTERACTION

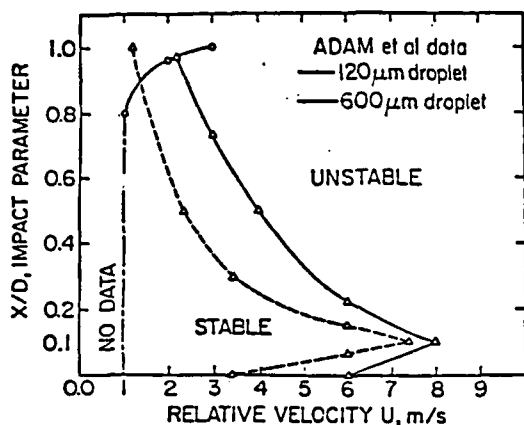


Figure 1 Impact parameter as function of relative velocity for Adam et al. (1968) data

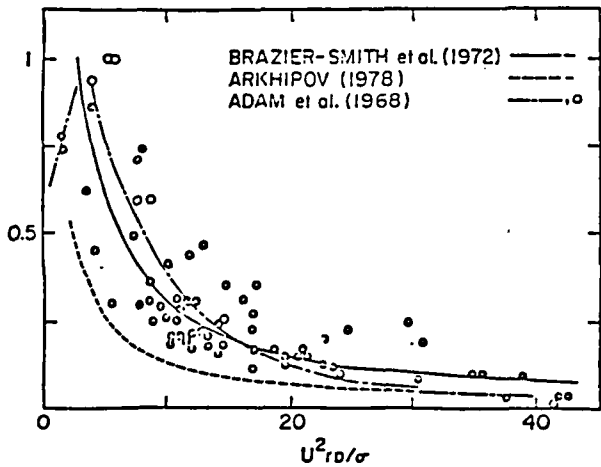


Figure 2 Coalescence efficiency as function of Weber number for different data sets

SPRAYS INTERACTION

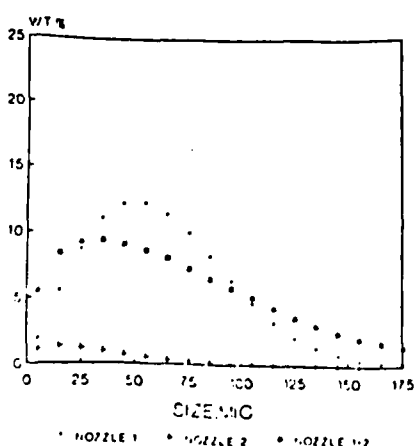


Figure 3 Small angle interaction of sprays

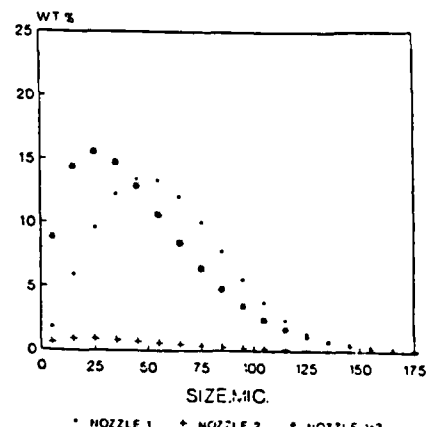


Figure 4 Large angle interaction of sprays

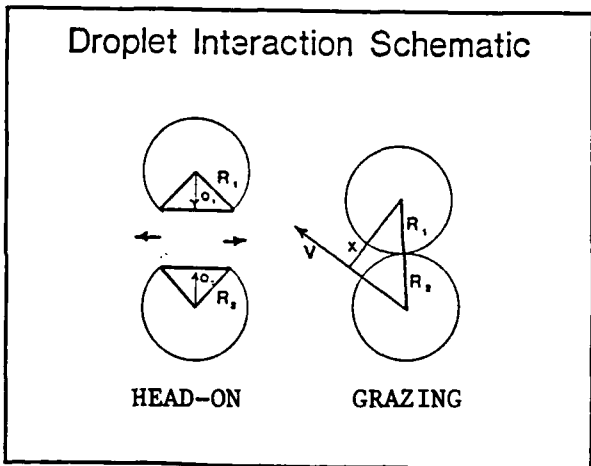


Figure 5 Schematic of two types of collisions

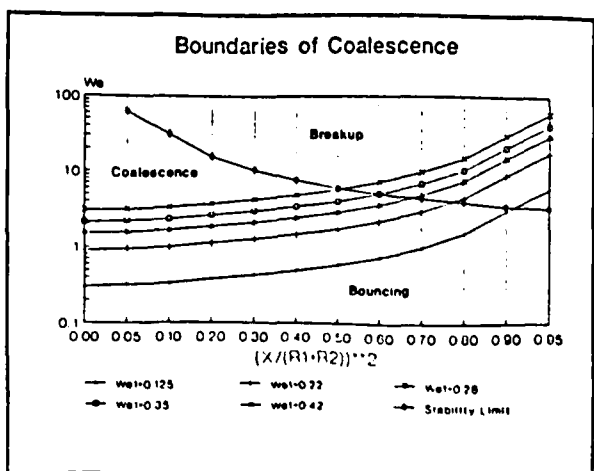


Figure 6 Predicted region of stable coalescence

IGNITION AND MODIFICATION OF REACTION BY ADDITION:
KINETIC AND TRANSPORT PHENOMENA

AFROSR Contract No. F49620-87-C-0081

Principal Investigators: Francis E. Fendell, Mau-Song Chou and
Tmitri J. Zukowski

Engineering Sciences Laboratory, TRW Space and Technology Group
One Space Park, Redondo Beach, CA 90278

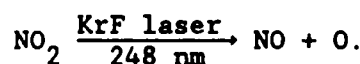
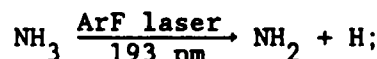
SUMMARY/OVERVIEW

Increased activity in high-speed air-breathing combustion systems puts a premium on the complete release of chemical energy during the relatively brief residence time of reactants within combustors of practical length: mixing, ignition, and chemical reaction must be achieved in a relatively short time. We address, from a fundamental chemical-dynamics and fluid-transport point of view, the use of both alternative, photochemical ignition (by laser irradiation) and ignition-promoting additives, in order to alter chemical-reaction pathways to achieve rapid ignition and enhanced combustion rate. We plan ultimately to address the influence of mixture inhomogeneity, and of departure from stoichiometric proportion in fuel/air mixtures, on the processes of ignition, flame development, and flame propagation. Chemical systems of particular interest include hydrogen/air and methane/air, often with trace amounts of carefully selected sensitizers. We seek to identify optimal circumstances [minimal input energy, minimal amount of sensitizer(s), etc.] for achieving ignition and burnup with currently available optical sources by irradiating premixtures flowing faster than the adiabatic flame speed, and by carrying out supporting approximate analyses of these experiments.

TECHNICAL DISCUSSION

Experiment

The early phase of the experimental program is to use a combination of initiation and probe lasers to study the chemical mechanisms of ignition. A flat-flame burner will be used to provide a homogeneous premixture of fuel and oxidizer. The initial active species will be prepared by photolysis of appropriately doped precursors; the photolysis will be carried out by use of a pulsed excimer laser. NH₃ and NO₂ have been identified to be suitable precursors to generate atomic hydrogen and atomic oxygen, respectively, via the following photodissociative processes:



The photon yields of H atoms and O atoms are known to be nearly unity for 193 nm and 248 nm, respectively. On the basis of the known absorption coefficients of NH₃ and NO₂, one should be able to prepare an initial uniform known concentration of the active species (H or O atoms), by

adjusting the density of the precursor and the energy of the incident excimer laser. Furthermore, the initial active-species density also can be derived on the basis of the excimer-laser energy transmitted through the flowing gaseous medium.

The ignition time will be derived by monitoring, in the aftermath of the initiation pulse, the visible/UV emission from the premixture. We also shall monitor the temporal growth of the OH radicals by means of a CW ring dye laser. The ring dye laser will be used to probe near the center of the volume uniformly excited by the excimer laser. Probing in this region minimizes any complication encountered because of radical diffusion. Furthermore, the ring dye laser will be tuned to various OH vibronic lines of the $A^2\Sigma^+ \rightarrow X^2\Pi(0,0)$ transition near 308 nm. The variation of the OH rotation distribution based on the absorption of several OH rotation lines will allow us to derive an OH rotational temperature as a function of time. The OH rotational temperature should be approximately equal to the thermal temperature of the mixture because of the rapid equilibration between the rotational and translational temperatures near the one-atmosphere-pressure condition at which our experiment is conducted. The temporal growth of the profiles of the OH radical and the temperature history are taken to be two of the most important parameters of the ignition process, for purposes of adequately modeling the ignition chemistry. In particular, we wish to address several significant issues, including (1) what is the critical reaction path in terms of the minimal active-species concentrations (H and OH) and temperature required for ignition; (2) is there a controlling reaction step (or steps) for ignition; (3) can the initially prepared H atoms or O atoms lead to alternative, rapid reaction pathways relative to the pathways associated with thermal processes; and (4) how do the pathways for enhanced reactivity vary with the stoichiometric ratio.

We shall also discuss briefly our research plans for experimentally studying the ignition process in nonuniform (ie., imperfect) premixtures of gaseous fuel and oxidizer.

Analysis

The initial experimental activity concentrates entirely on the nonintrusive, intermittent addition (via pulsed laser) of a small amount of energy in an optimal mode into a small volume of a homogeneous gaseous premixture (that is flowing at a speed in excess of the adiabatic flame speed to preclude flashback). This way, without the pressure losses and flow disturbances associated with intrusive solid surfaces, photoselective chemical processes initiate reactivity in a small amount of the volumetric flow, with the aim of achieving complete burning in the entire flux of premixture. The first goal set for the analysis is to proceed through a tractable set of fundamental combustion investigations to indicate why this "blob" experiment is precisely the appropriate choice of experiment. In fact, at the outset, we believe that it is the only experiment that need be pursued to answer questions about ignition and flame development and flame propagation. The point is that tractable aerothermochemical analysis can provide, to an accuracy satisfactory for practical purposes, the answers to the key questions about subsequent events in the aftermath of a rapid (photochemical) conversion of a small fraction of the contents of a single "blob" of reactive gases to product gases.

One helpful sequence of analytical studies to complement the "blob" experiment is to proceed as follows. Consider the steady uniform streaming at supercritical speed (i.e., at a speed in excess of the adiabatic flame speed) of a homogeneous premixture, characterized by large Arrhenius activation energy. If one formed a flame in such a premixture, it would be blown off, because upwind diffusion of heat and radicals is ineffective for bringing fresh mixture to the reactive temperature. One may stabilize a flame in such a premixture by the continuous nonintrusive deposition of energy; in effect, this is a "continuous ignition" achieved by nonintrusive energy addition. For a planar concentrated source (say, a Dirac delta function), one finds (by treatment of a modified version of the classical steady one-dimensional formulation of laminar flame propagation) that a relatively broad, convective-diffusive preheating zone precedes a thin reactive-diffusive zone, and that this two-zone flame structure lies upwind of the site of the energy deposition. Incidentally, the burned-gas temperature is the sum of the adiabatic flame temperature plus the temperature equivalent of the radiatively added enthalpy. (Nonintrusive conductive addition of enthalpy does not succeed in flame stabilization in supercritical flow. Of course, conductive extraction of enthalpy upwind of the flame structure is the means by which a subcritically flowing premixture is stabilized against flashback, as for a heat-sink-type burner.) This supercritical-flame-stabilization problem is tractable for monopropellant decomposition and bipropellant reactions at general Lewis-Semenov number. What one finds is that the energy-deposition requirement is appreciable because the entire preheating must be furnished by the continuous nonintrusive source.

However, it is informative to postulate a continuous cylindrical or point source of intrusive energy in a uniform supercritical stream of premixture, in order to define the "downwind-bent" configuration of the flame locus. For asymptotically large lateral distances from the plane or axis of symmetry (on which the source is situated), the flame locus becomes a parabola (in two dimensions) or cone (in three dimensions), with the flame locus so situated that the component of the freestream velocity normal to the flame locus is the adiabatic flame speed. Closer to the axis of symmetry, heat from the source modifies the asymptotic configuration, which is based on the flame exothermicity only; in fact, on the axis of symmetry, the previously discussed, one-dimensional (planar) problem assures that the flame locus lies at a finite distance upwind of the heat source.

For more modest enthalpy-addition requirements of the nonintrusive source, one turns to the intermittent irradiation of spherical "blobs" within the supercritically flowing premixture. One could vary the geometry of the irradiated volumes, but this seems of perturbational consequence; if ignition is achieved, two successive downwind-translating blobs will spawn outwardly propagating, mutually approaching flames that will eventually consume all the intervening nonirradiated premixture within a domain suggested by the above-discussed, continuous-point-source solution. The crucial advantage of the pulsed source is that one conceptually need add only enough energy to convert quickly a small fraction of this throughflux, because the exothermicity evolved from this quick conversion on an alternate chemical path can then spawn a conventional, outwardly propagating flame.

Thus, by subtracting out the convection, the classical hot-blob-ignition problem (in which relaxation by radial diffusion of heat from the hot spot competes in time with the release rate for chemical exothermicity, to determine whether a flame develops) should be rephrased as follows in the pulsed-irradiation context. Over a given finite volume, with a given modest supplemental thermal heating, what fraction of the premixture need be converted effectively instantaneously for a flame to evolve in a brief time (from consumption of the remaining reactant within the volume and of the entirely unconverted reactant outside the volume). A few isolated cases of this revised hot-spot-ignition problem have been calculated in specific contexts, but we seek a general tractable approximation to display parametric dependence. Incidentally, we have isolated the effects associated with convective motion (expansion of the hot burned gas) and with weak pressure waves propagating into the undisturbed unburned premixture, so that only a simple time-dependence/diffusion/reaction balance need be included in the revised hot-spot-ignition problem.

When these tasks are completed, attention may be turned to the effects of mixture inhomogeneity and of off-stoichiometry, and ultimately to augmenting insight into the selective photochemistry.

IGNITION AND COMBUSTION ENHANCEMENT BY MULTIPHOTON PHOTOCHEMICAL MEANS

AFOSR Contract No. 88-0013

Andrzej W. Mizolek
Brad E. Forch

U. S. Army Ballistic Research Laboratory
Aberdeen Proving Ground, MD 21005-5066

SUMMARY/OVERVIEW:

Our research effort is aimed at applying uv laser multiphoton photochemistry for the purpose of enhancing the ignition and combustion characteristics of chemical systems relevant to air-breathing and rocket propulsion. Our approach has been to investigate the underlying physical phenomena which govern the ignition of reactive gases using focussed uv laser radiation, as well as to study the actual photochemical mechanisms of the pertinent individual molecules irradiated by intense uv laser radiation. Our attention is currently focussed on reactive systems relevant to the National Aerospace Plane (NASP) effort, i.e. H₂/O₂ and H₂/air. In spite of considerable progress, a number of important technical issues still remain to be addressed. These include the spectroscopic and photochemical characterization of highly electronically excited molecular states that are populated by multiphoton absorption as well as the study of the effect of collisions on their behavior.

TECHNICAL DISCUSSION**A. Ignition Studies (H₂/O₂)**

Last year we reported on the extension of our ignition\microplasma formation wavelength dependencies from the oxygen atom system at 225.6 nm to the hydrogen and carbon atom systems at 243 and 193 nm, respectively. In order to further characterize the hydrogen system, we compared room temperature D₂ gas behavior with that of H₂ gas. Figure 1 shows the wavelength dependence for microplasma formation in both gases at 70 torr. In both cases we were monitoring the H/D atom emission at 656 nm (n=3 --> n=2). A well-defined isotopic shift is clearly evident with a wavelength separation corresponding to about 22 cm⁻¹. This is exactly the energy spacing difference given in energy level tables for the n=2 upper level involved in the two-photon excitation of H and D atoms (n=1 --> n=2). We also observe the same isotopic shift at atmospheric pressure with the only difference being broader excitation spectral widths. We believe that these substantial widths observed in ignition/microplasma formation are due to the finite absorption in the "wings" of the atomic transitions. This isotopic shift behavior further substantiates our interpretation of the microplasma formation mechanism, i.e. multiphoton photolysis of parent molecules to form atoms, resonant multiphoton ionization of these atoms, followed by microplasma formation in the laser focal volume using free electrons liberated in the previous step.

One of the most important considerations in making this laser igniter practical for in-flight use is the laser itself. A tunable laser system, such as is required for O-atom excitation at 225.6 nm, is not likely to be used in a supersonic aircraft. However, a much more simple device, such as an excimer laser, can be envisioned as being made flight worthy. In view of this, we conducted a number of laser ignition experiments using the ArF (193 nm) excimer laser which was focussed into a jet of a premixed H₂/O₂ flow at room temperature. Figure 2 shows the dependence of the incident laser energy (ILE) on the equivalence ratio. The laser was run in the unstable resonator mode which yields a much less divergent beam as compared to the stable resonator, and thus much better focussing ability. The minimum of the curve shows that this approach is indeed very efficient, with less than 1 mJ pulse energy required to cause ignition. The specific mechanisms for microplasma formation include at least two possibilities; (1) a 1+1 multiphoton ionization (MPI) of O₂ going through the Schumann-Runge bands and (2) the 2+1 MPI of H₂ going through the E,F electronically excited states (see next section).

We also conducted another study relevant to the O-atom system with particular emphasis on the collisional dynamics involved in the two-photon excitation process which populates the 3p ³P state.¹ The specific technical issue that is being addressed here is the delineation of the excited-state quenching mechanisms which affect directly the ability to make the seed electrons needed to promote microplasma growth. What was found is that spin-exchanging collisions were significant but minor (few percent) channels in the total quenching process. Figure 3 shows the temporally-resolved atomic emissions at 844.8 nm (Fig. 3a) and 777.5 nm (Fig. 3b). This latter emission exhibits an initial slow growth due to spin-exchanging collisions which populate the ⁵P state followed by radiative decay. In a theoretical study, a collision dynamic model was proposed and calculations were conducted for this O-atom case.²

B. Photochemical Mechanisms (H₂)

Recently we completed a study on the photochemical mechanisms involved in ArF laser photolysis of small carbon-containing molecules.³ Subsequent research comprised of similar studies (although now looking at the ion pathways) of molecules relevant to the NASP program. Figure 4 shows the time-of-flight mass spectra (TOF-MS) generated during the irradiation of a molecular beam of H₂ by an ArF (193 nm) excimer laser. Our interpretation of this data is that under our collisionless conditions, the H₂ first ionizes via a 2+1 process involving the E and F states,⁴ and then subsequently the molecular ion is photolyzed to produce H ions. If the same experiment is repeated using the laser set at the peak of the two-photon excitation at 243 nm (see Fig. 1), then there is no signal from either of these ionic species. Similarly, with the laser set at 225.6 nm (O-atom two-photon transition) we did not detect either the molecular or atomic oxygen ions. This data clearly indicates the importance of collisions in inducing photofragmentation. Studies are currently underway to better understand the importance of collisions on these pathways.

1. P.J. Dagdigian, B.E. Forch and A.W. Mizolek, Chem. Phys. Lett. (in press).
2. M.H. Alexander, J. Chem. Phys., (submitted).
3. R.C. Sausa, A.J. Alfano, and A.W. Mizolek, Appl. Opt., 26, 3588 (1987).
4. E.E. Marinero, C.T. Rettner, and R.N. Zare, Phys. Rev. Lett., 48, 1323 (1982).

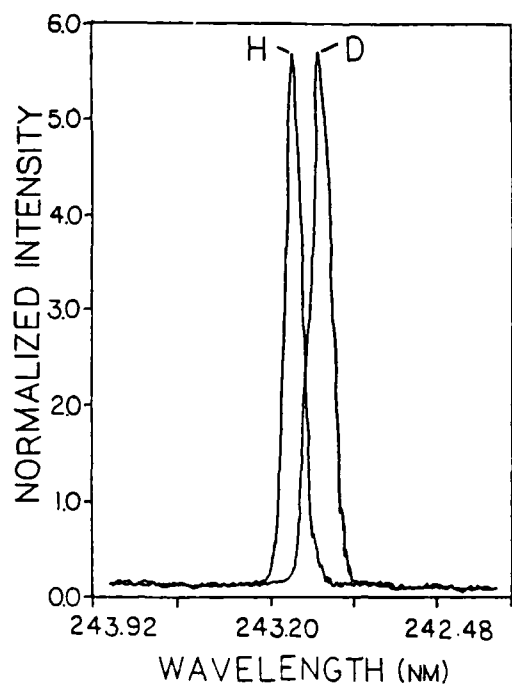


Figure 1. Excitation Spectrum for Microplasma Formation in H_2 and D_2 at 70 torr and Room Temperature. Emission Monitored at 656 nm.

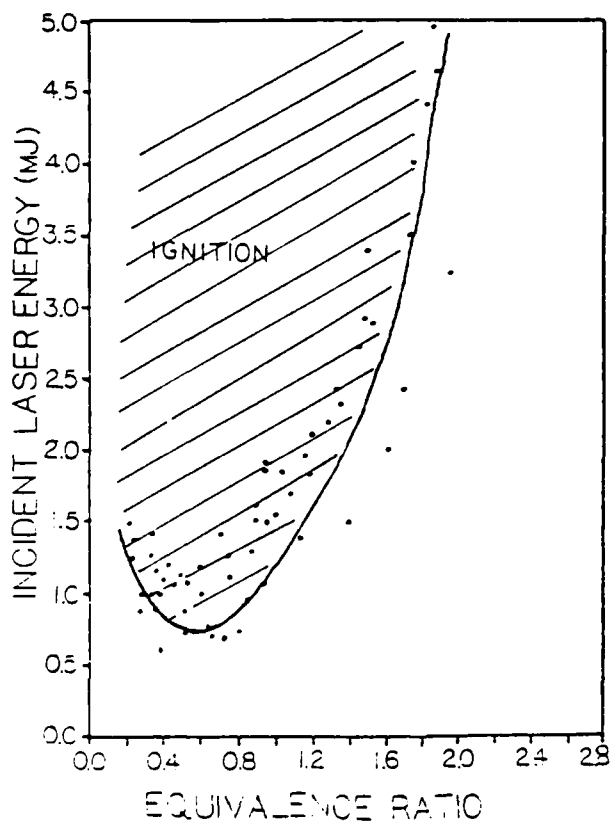


Figure 2. Dependence of ILE on Equivalence Ratio for H_2/O_2 Premixed Flows Using ArF Laser (193 nm) (Unstable Resonator).

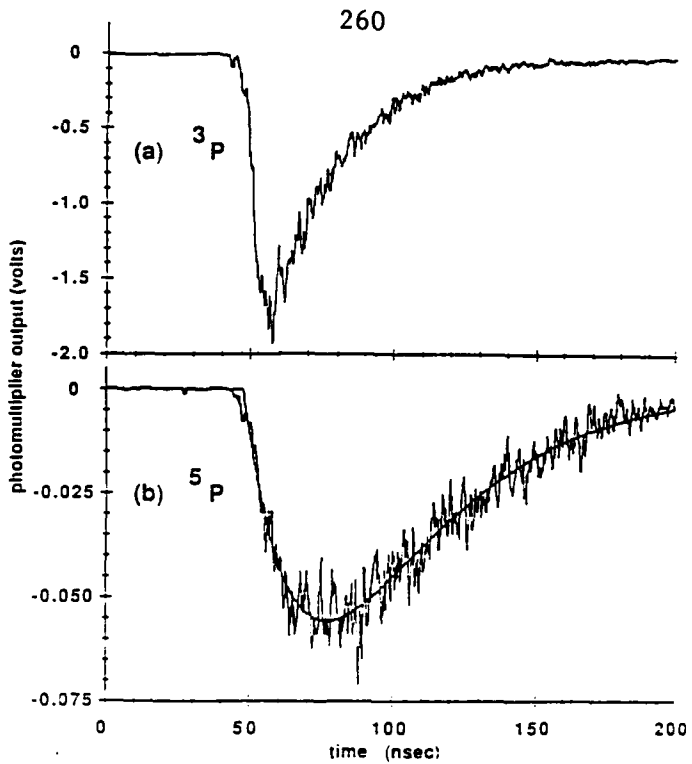


Figure 3. Waveforms for (a) the $^3P \rightarrow ^3S$ and (b) the $^5P \rightarrow ^5S$ Fluorescence Emission Upon Two-Photon Excitation of the $3P^3P$ state. Pressures: 1.47 torr He and 0.30 torr O₂.

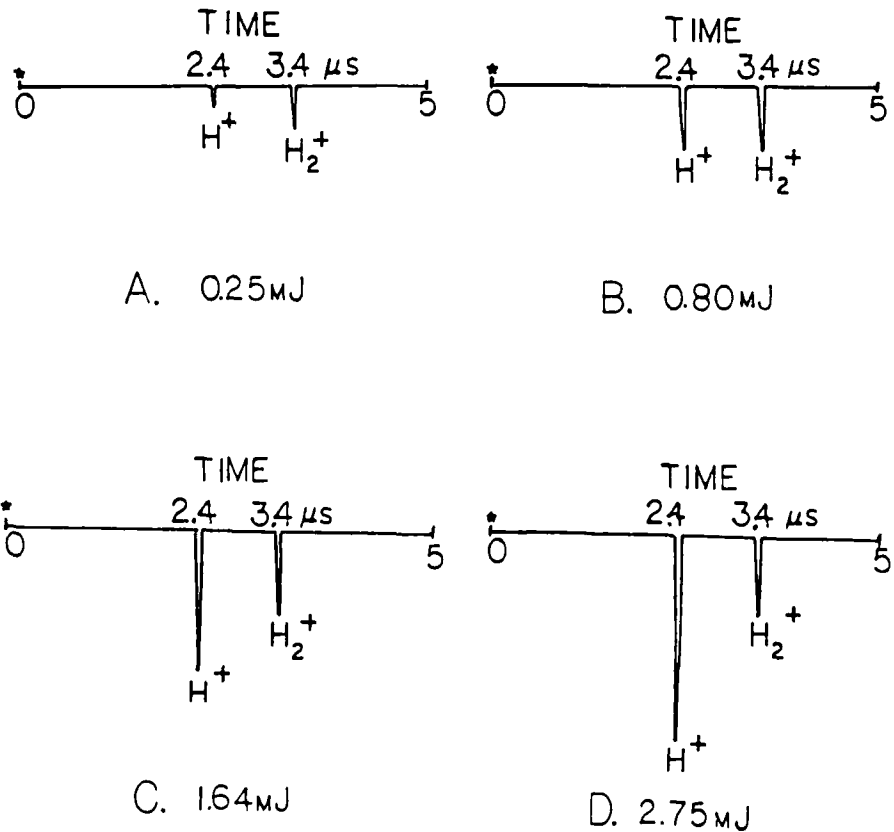


Figure 4. Time-of-Flight Mass Spectra for MPI of H₂ Molecular Beams Using an ArF Excimer Laser (Unstable Resonator). Focusing Lens f.l.=150 mm.

COMBUSTION ENHANCEMENT BY HIGH ENERGY ELECTRON IMPACT PROCESSES**NSF Grant No. CBT-8713328****Principal Investigator: Richard B. Peterson**

**Department of Mechanical Engineering
Oregon State University
Corvallis, Oregon 97331**

SUMMARY/OVERVIEW:

Combustion enhancement is an area of research having great importance in the development of advanced SCRAMJET engines. Many techniques have been proposed for accomplishing this enhancement with the salient feature of each being the creation of free radicals for the purpose of initiating and promoting the characteristic reactions of combustion. This project is concerned with the investigation of a new technique for accomplishing radical generation in the gas phase. It involves the use of high energy electrons to ionize and dissociate molecules typically found in the H₂/air and CH₄/air combustion systems to produce free radicals such as H, O, and N atoms. Once these species are formed, they can go on to participate in the chain branching reactions leading to ignition of the reactant mixture. This research is expected to provide a greater understanding of the various processes associated with combustion enhancement. The experimental plan and work accomplished to date are described below.

TECHNICAL DISCUSSION:

A three part approach is being taken in this research project: (1) design, construction, and use of a 1 kW electron beam facility with integral burner assembly, (2) development of diagnostics for the detection of free radicals such as H, O, and N atoms, and (3) modeling of the experiment. Much progress has been made on the first of these over the last 6 months -- a description of this progress is provided below. The diagnostic aspect of this project is also advancing with the development of an intrusive, direct sampling technique sensitive to atomic free radicals. This part of the project will also be described below. The topic of modeling will be deferred to a later time.

A schematic diagram of the electron beam facility now under construction is shown in Fig. 1. It consists of an electron gun chamber, lens and drift tube, and a vacuum/air interface chamber. The first of these, the electron gun chamber, is a 6 inch elbow section providing ports for the various connection necessary for gun operation. One opening of the elbow, as shown in the figure, provides for the pumping of the chamber by a 150 l/s turbo-molecular pump. Another access port is for the electrical feed-through that powers the filament isolation transformer residing inside the vacuum chamber. An auxiliary 2 inch vacuum line is attached to the bottom of the elbow section and is used to connect the high voltage power supply to the electron gun.

Inside the chamber a simple diode-type, electron gun is used to generate the electron beam. Specifications of the gun include an accelerating potential of 100 kV, maximum current capability of 10 mamps, and a focussed spot size of 2 mm. The electron source is a heated tungsten filament powered through an isolation transformer. We have developed this transformer to provide the necessary isolation from ground while supplying enough current to heat the filament to incandescent temperatures.

High energy electrons are directed into the atmosphere through a vacuum/air interface chamber. The principle of operation here is to send the 1 kW electron beam through a "free air" aperture -- any material window that may be considered for isolating the vacuum chamber from the atmosphere would be destroyed by the power density of the beam. The gas flow downstream of the aperture is a jet expansion from a source pressure of one atmosphere. The gas load on the first stage of the vacuum system necessitates the use of a high volume (350 cfm) Roots-type pump. With the background pressure lowered to the range between 1 and 10 Torr, the initial jet overexpands to a density less than that of the gas inside the chamber. At this point, the flow is skimmed to provide a limited amount of isolation between the first and second vacuum stages. Since the jet is skimmed in the overexpanded region of flow, the gas load on the second stage is much reduced. A 250 l/s oil diffusion pump is used to provide pumping in the second stage. With this type of arrangement, a focussed electron beam can pass through the skimmer aperture, then pass through the free air aperture and into the laboratory atmosphere to participate in experiments. We plan to use helium as the gas surrounding the "free air" aperture to increase the range of the electrons as they travel to the experiment.

With the building and testing of the electron beam facility, we also plan to develop two burners for the experiment. The first will be based on the flat flame geometry and will operate at atmospheric pressure. High flow rates will be used thus requiring electron beam stabilized combustion in the region above the burner. Initial experiments planned are flammability studies where the energy input by the electron beam and the equivalence ratio are the variable parameters. Later, when our diagnostic apparatus has been developed, we will study the evolution of various species found in the reaction zone of the experiment. The second type of burner that will be used in this study is based on the Perfectly Stirred Reactor (PSR) concept. This type of combustion system will be well suited for a study of the combustion enhancing effects of radicals since a simple model exists employing detailed kinetics. This part of the project will be developed once the electron beam apparatus is completed.

The last topic discussed here is the diagnostics for the project. For our purposes, it will be important to detect the species generated by the electron beam and follow their evolution as they react in the bulk mixture. Although many species are of interest here, initially we will concentrate on the atomic free radicals H, O, and N. The technique we have chosen for this task involves intrusively extracting a gas sample using a quartz probe, expanding the gas into a vacuum chamber, and then using Atomic Resonance Absorption Spectroscopy (ARAS) to detect the species of interest. This is shown in Fig. 2. We have constructed a specially designed lamp for this purpose and are now testing it on our direct sampling apparatus. Using a freely propagating hydrogen/air flame as a transient source of hydrogen atoms, detection is accomplished by recording a decrease in light transmission at 121.6 nm from the lamp. We have observed such a decrease in our experiments at two locations in the recorded data. The first has been attributed to H atoms generated by the flame. The second appears to be interference from H₂O also generated in the flame, but at a later time. We are currently refining our sampling process to better discriminate between H and H₂O.

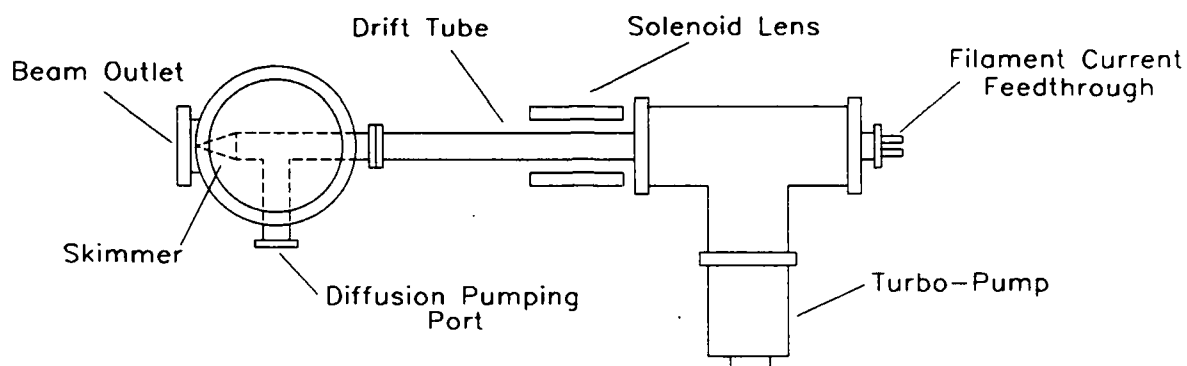
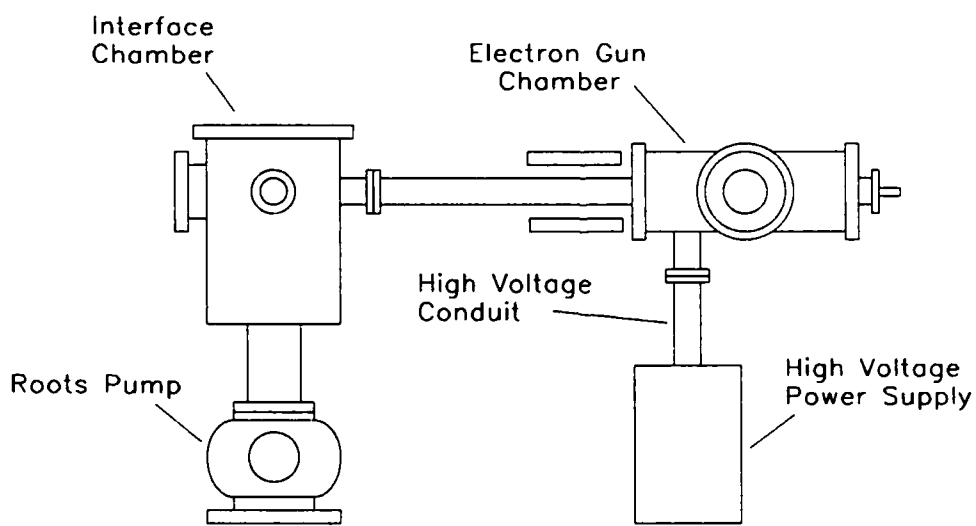
TOP VIEWSIDE VIEW

FIGURE 1: ELECTRON BEAM APPARATUS

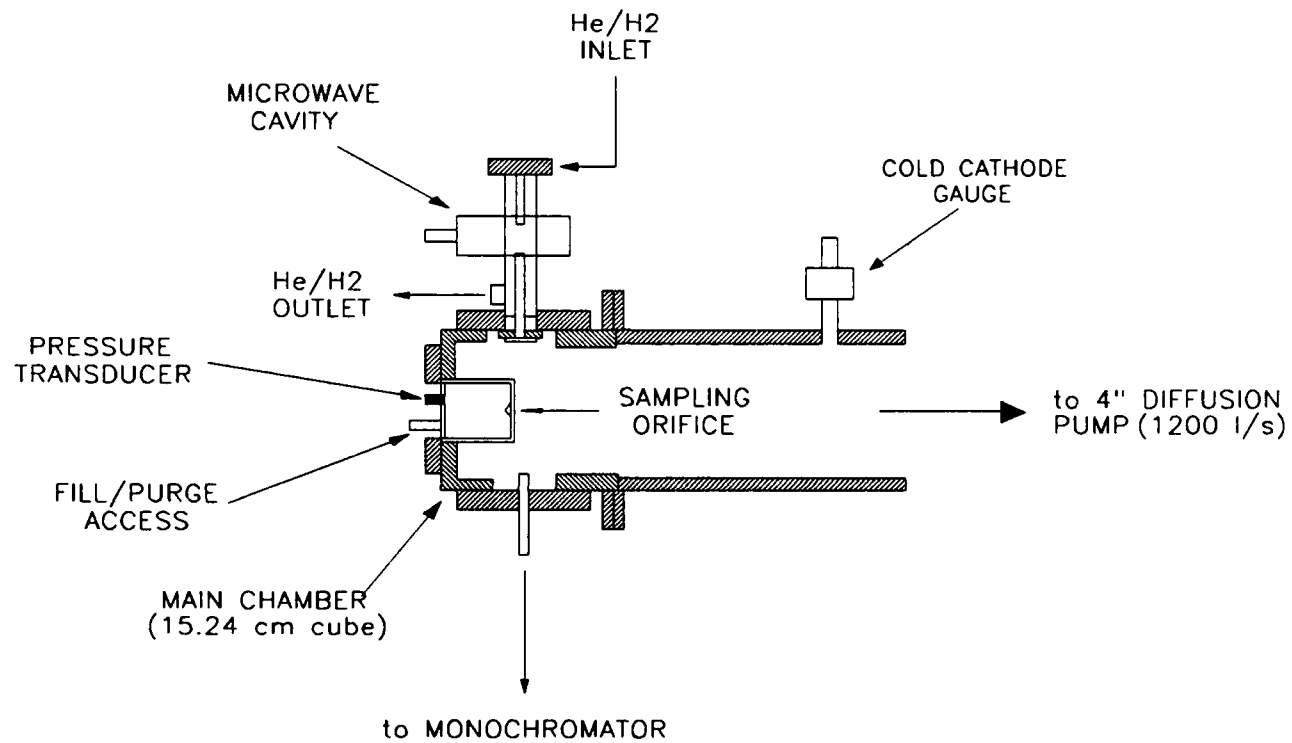


FIGURE 2: ATOMIC RESONANCE ABSORPTION APPARATUS

DETERMINATION OF RATE-LIMITING STEPS DURING SOOT FORMATION

AFOSR Contract No. F49620-88-C-0051
F49620-85-C-0012

Principal Investigator: Meredith B. Colket, III

United Technologies Research Center
E. Hartford, CT 006108

SUMMARY/OVERVIEW:

A variety of hydrocarbons are being pyrolyzed and/or oxidized in a single-pulse shock tube. End gases are being collected and then analyzed using capillary gas chromatography. Real time data will be collected using a time-of-flight mass spectrometer directly coupled to the end wall of the shock tube. Data will be used to identify rate-limiting steps during soot formation and to assist in the development and/or verification of chemical models describing formation of products and soot-precursors. A focus of the work is to obtain time-dependent data and to collect and analyze multi-ringed species (C₁₀-C₁₆ hydrocarbons) which are believed to be pre-cursors of soot. Chemical kinetic modeling has focused on the pyrolysis of acetylene due to its importance in all aspects of soot formation and growth.

TECHNICAL DISCUSSION

Twenty-seven separate series of single-pulse shock tube experiments have been completed. For each series, a single hydrocarbon, a mixture of hydrocarbons, or a mixture of a hydrocarbon and oxygen were shock-heated in argon over an approximate temperature range of 1100K to 2300K. Total pressures were about five to ten atmospheres and dwell times were 500 to 700 microseconds. Gas samples were collected automatically at the end wall of the shock tube and then were analyzed using gas chromatography. Final concentrations of hydrocarbons were determined quantitatively using a CP Sil 5 CB fused silica capillary column and flame ionization detection. Hydrogen and oxygen were analyzed using a silica gel packed column and a thermal conductivity detector and carbon oxides were measured using a Carbosieve S-II column with the column effluent passing through a hydrogenation catalyst prior to flame ionization detection. Hydrocarbons pyrolyzed (or oxidatively pyrolyzed) include acetylene, ethylene, vinylacetylene, 3-penten-1-yne, 1,3,5-hexatriene, benzene, and styrene.

Based on experimental data on acetylene, vinylacetylene, and benzene pyrolyses, a detailed chemical kinetic model (Ref. 1-2) has been constructed which adequately describes the formation and the destruction of aromatic rings. Due to the ability to predict profiles of product species during the pyrolysis of these three hydrocarbons and comparison to other proposed mechanisms, there is a high level of confidence for the proposed chemical mechanisms (and rate constants) which describe the formation of the first aromatic ring. This fact is significant since benzene formation has been

correlated with the production of soot during the pyrolysis of hydrocarbons (Ref. 3).

The acetylene model has been extended in an attempt to explain the formation of polycyclic aromatic hydrocarbons (Ref. 4). Although model results for ring growth were interesting, they differed from other proposals; yet there is no adequate way of proving any of these concepts due to an inadequate base of experimental data. Present experimental modifications have been directed towards detecting the presence of high molecular weight species (>128 grams/mole). First, the gas sampling system has been modified (new valves, heating tapes, etc.) to operate at temperatures of 100 to 150°C. Secondly, modifications have been made so that the gas sample can be frozen in liquid nitrogen in order to condense and concentrate high molecular weight species in a one cc sample injection loop. The first of these techniques is now being tested. Shock-heated mixtures of toluene and methanol have been analyzed recently and as many as twenty peaks have been observed with elution times longer than naphthalene. This work is continuing. The condensation technique is believed to be most useful when only small fractions of the hydrocarbon are converted to heavy species (as much as 70% of toluene (Ref. 5) can be lost to heavy species during pyrolysis). Nitrogen must be used as the carrier gas during shocks, since argon freezes well above liquid nitrogen temperatures. The use of nitrogen in turn effects the character of the shock, required shock strengths and the tailoring of the single-pulse shock tube.

Other new experimental efforts include the coupling of a time-of-flight mass spectrometer to the end wall of the shock tube for measurement of species profiles in real-time. Data obtained from this facility will reduce some ambiguities regarding species whose concentrations peak during the shock or are effected by finite quenching in the rarefaction wave.

Examples of the type of experimental data obtained from the shock tube are shown in Figs. 1-3. Profiles of aromatics produced during the pyrolysis of ethylene and the oxidative pyrolysis of ethylene (0%, 0.5%, and 2.0% O₂ with ~ 3.5% ethylene in argon) are shown as a function of initial post-shock temperature. It is clear that as the oxygen concentration increases aromatic production (benzene, styrene and phenylacetylene) occurs at lower and lower temperatures. The primary explanation is that oxygen simply enhances kinetic rates so that the chemistry occurs at lower temperatures. The main mechanism for ring formation is not believed to be altered. There is some evidence that small concentrations of oxygen may slightly enhance the production of styrene (see Fig. 3).

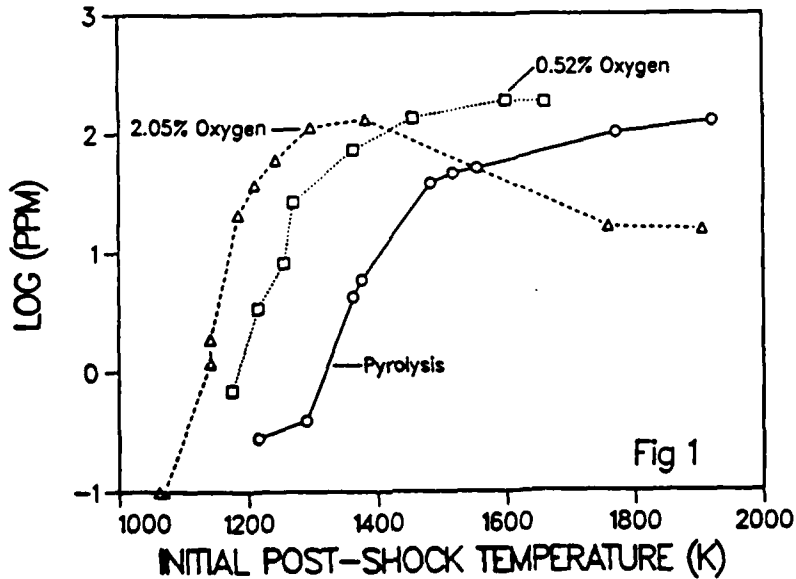
Detailed chemical kinetic modeling of acetylene pyrolysis has continued in an attempt to describe the early flow reactor data. The motivation behind this effort has been the fact that recently several authors have advocated a mechanism drastically different from the chain mechanism used in the present study. The alternative mechanism involves a predominant role of vinylidene, a diradical. This mechanism is supported by some convincing arguments and some rate constants from this work are being used to assist in describing species profiles in flames. Furthermore, related mechanisms are being proposed to describe acetylene addition to ring compounds. Consequently, two very different mechanisms have been proposed to describe ring formation. To investigate the relative importance of the two mechanisms, the basic

assumptions and mechanisms of acetylene pyrolysis were re-examined. One of the main arguments against the radical chain mechanism as used in this study is the lack of a sufficiently fast initiation step. It has now been shown (Ref. 6) that impurities of acetone at levels of 1000 ppm in acetylene are likely the source of the radicals. Profiles of all the major species and most of the minor species can now be described using rate constants and reaction mechanisms which are now considered to be well established. Thus support for the chain mechanism is confirmed.

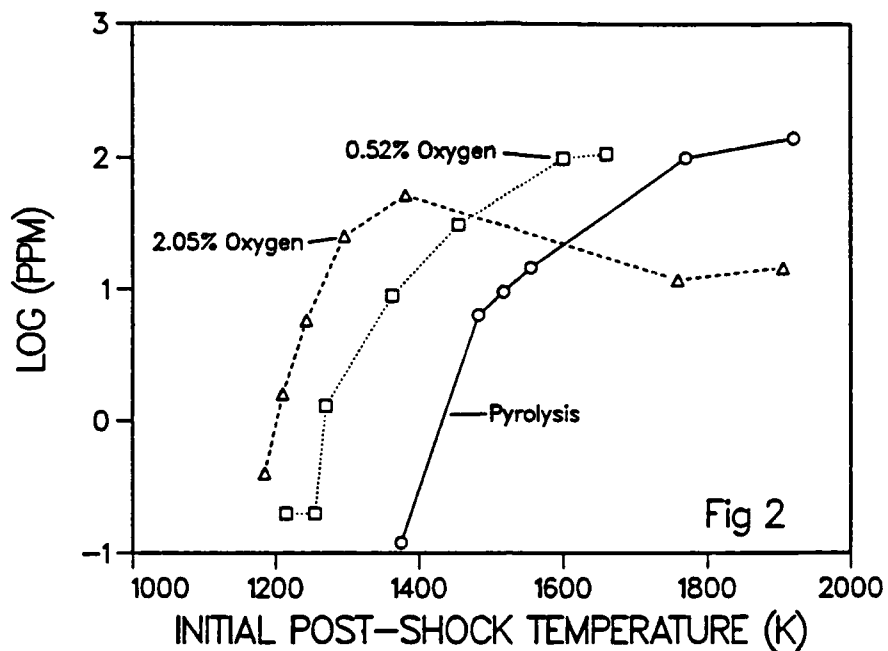
REFERENCES

1. "The Pyrolysis of Acetylene and Vinylacetylene in a Single-Pulse Shock Tube" by M. B. Colket, Twenty-First Symposium (International) on Combustion, The Combustion Institute, p. 851 (1988).
2. "Pyrolysis of C₂H₆" by M. B. Colket, Division of Fuel Chemistry Preprints, American Chemical Society 31(2), p. 98 (1986).
3. "Some Thoughts on Pre-Particle Chemistry" by M. B. Colket, Eastern Section of the Combustion Institute, November 2-6, 1987.
4. "Kinetic Mechanism for Pyrolysis of Acetylene Near 1000K", by M. B. Colket, Division of Fuel Chemistry Preprints, 32(3), p. 417 (1987).
5. "Pyrolysis of Toluene in a Single-Pulse Shock Tube", by M. B. Colket, Eastern Section of the Combustion Institute, December 8-10, 1982.
6. "The Pyrolysis of Acetylene Initiated by Acetone", by M. B. Colket, H. B. Palmer and D. J. Seery. To be published by Combustion and Flame, 1988.

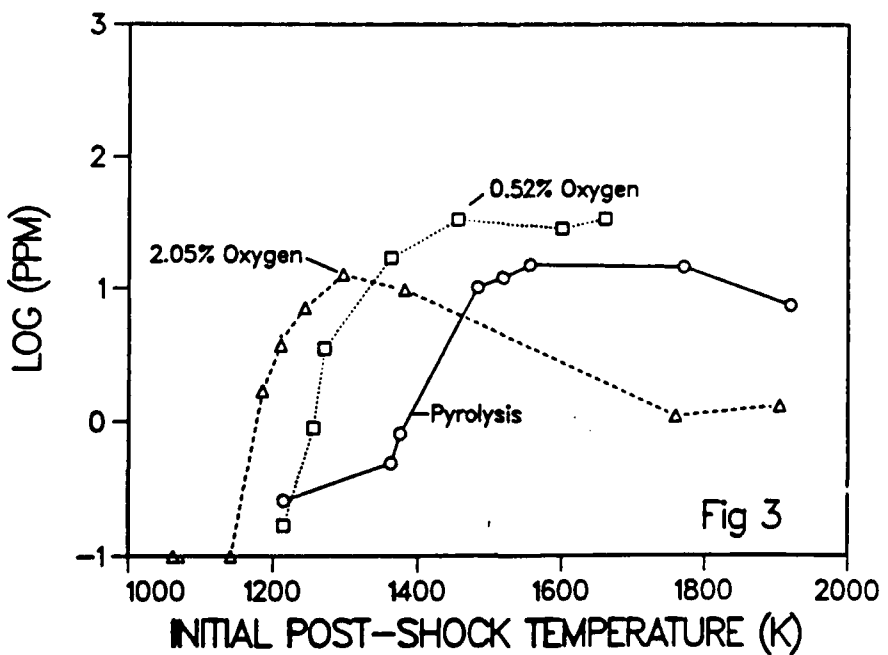
BENZENE FORMATION 3.5% Ethene



PHENYLACETYLENE FORMATION
3.5% Ethene



STYRENE FORMATION
3.5% Ethene



FUELS COMBUSTION RESEARCH

(AFOSR Contract No. F49620-86-C-0006)

Principal Investigators: I. Glassman, F.L. Dryer, and F.A. Williams

Department of Mechanical and Aerospace Engineering
Princeton University
Princeton, New Jersey 08544

PROGRAM SUBSECTION

Soot Formation and Aromatic Reaction Processes

Principal Investigator: I. Glassman
Other Professional: K. Brezinsky

SUMMARY/OVERVIEW

Little had been known about the processes which control the formation of soot in combustion systems and the effect of fuel type, particularly aromatics. By use of pre-mixed and both co-flow and counter-flow diffusion flame systems in which temperatures are controlled, it has been possible to determine the relative effects of flame temperature, equivalence ratio, and C/H ratio in premixed systems and temperature, additives (particularly O₂) and fuel structure in diffusion controlled systems. Corresponding studies of the high temperature oxidation and pyrolysis mechanisms of aromatic, naphthenic and paraffinic fuels using the Princeton turbulent flow reactor are not only providing important kinetic data and mechanisms for those modeling combustion, but also fundamental information necessary to understand the controlling processes in soot formation.

TECHNICAL DISCUSSION

Past results [1] in the soot formation aspect of the program established that: (1) the combustion system temperatures must be controlled in order to understand the relative tendency of a fuel to soot; (2) in premixed flames, the higher the flame temperature, the less is the tendency of a fuel to soot; (3) in premixed flames, the critical sooting equivalence ratio correlates with the fuel's number of C-C bonds, which is an indirect measure of the fuel's pyrolysis rate and C/H ratio (which determines the OH concentration), and thus fuel structure plays no fundamental role in a fuel's tendency to soot; and (4) in diffusion flames, the higher the flame temperature, the greater is the tendency to soot and fuel structure plays a significant role in sooting tendency.

Recent efforts were directed at determining what the important precursors to soot were and what effect small amounts of oxygen in the fuel jet of a diffusion flame had on the soot formation process. In order to attack these problems, extensive experiments were performed with normal and inverse [2] and counterflow diffusion flames [3,4].

In order to examine what the important chemical species were prior to soot nucleation; chemical samples were withdrawn from near and slightly sooting normal (NDF) and inverse (IDF) diffusion flames. Obtaining stable inverse diffusion

flames and analyzing the variation of the height of these and normal diffusion flames were an accomplishment in their own right and the details of this effort are given in Ref. 2. The sampling results reveal that the initial number density of soot particles which form scales with the aromatic content just prior to soot inception. These results were found to correlate as well with the extensive smoke height test results of normal diffusion flames. Shown in Fig. 1 is a histogram of sample species versus concentration. For sample species, the results of a particular fuel are shown as different bars in the figure. Note, as well, in the figure that there is no correlation with species such as acetylene or diacetylene with the known sooting tendency of the various fuels.

Many have shown [5,6] that addition of small amounts of oxygen to a fuel jet increased the sooting tendency of ethene, but slightly decreased that of the alkanes. In order to eliminate the possible effect of oxygen leakage from the outer air stream across the jet rim in the co-flow diffusion flame studies, experimentation was begun with a counter-flow (opposed jet) diffusion flame in which particle number density, volume fraction and average particle size were measured [3,4] as a function of oxygen addition to the fuel. These results revealed the same oxygen trends as the earlier qualitative experiments. The explanation of this trend is that concentrations of the order of 10% oxygen in fuel affect the pyrolysis of tightly bound fuels such as ethene, ethyne and benzene at modest temperature ranges, but only affect the pyrolysis of the alkanes at very low temperatures. Detailed chemical kinetic computations [3] showed that the addition of small amounts of oxygen had a large effect on the radical concentrations (particularly H atoms) of ethene and acetylene pyrolysis in the 1200-1400 K range and had no such effect on propane pyrolysis. In the sooting temperature range the relative ease of breaking a carbon-carbon bond leads rapidly to a large radical pool in alkanes, so that oxygen addition has no affect on this pool or the fuel pyrolysis rate.

In the first experiments of their type, the opposed jet diffusion flame studies were extended [4] to examine the sooting propensity of ethene and propane under conditions in which the fuel side was varied from an equivalence ratio (ϕ) of infinity (pure diffusion flame) to about 2.5 (premixed flames within the flammability limit). The results are shown in Fig. 2. The propensity to soot of ethene rises with decreasing ϕ (small oxygen addition). As ϕ decreases further there is chemical reaction and energy release altering the temperature profile and increasing the sooting tendency further until a maximum is reached at which point the conditions approach that of a premixed flame. The sooting tendency then decreases with decreasing ϕ and vanishes at a value near the critical sooting equivalence ratio determined by conventional methods. The same trends hold for propane except that initially the oxygen acts as a diluent and lowers the soot production until sufficient reaction is initiated to raise the overall thermal level.

That element of the program studying the oxidation of the aromatic components of jet engine residual fuels continued with the study of di-alkylated benzene species after completion of the work on mono-alkylated compounds (7-13). The major current effort has concentrated on p-xylene. The numerous experiments performed indicated that stoichiometry did not affect the oxidation mechanism, consequently most data taken were for stoichiometric conditions. As reported previously, the major species detected during the experiments were toluene, benzene, p-tolualdehyde, p-ethyltoluene, CO, and fuel. The major aliphatic found was methane. The concentration of CO increased throughout the oxidation, hence no CO₂ was formed and the experiments were essentially isothermal. The fuel concentration appears to decay linearly and the rate thus indicates a zero order decomposition. This result is contrary to the suggested mechanism in which the fuel is oxidized primarily through

abstraction of a side chain hydrogen by a quasi-steady state concentration of radicals leading to a first order exponential decay [8]. The discrepancy is believed to be caused by the resulting p-methylbenzyl radical ($\text{CH}_3\text{C}_6\text{H}_4\text{CH}_2$). The intermediates formed during the oxidation indicate that this radical could be present in large amounts due to resonant stability. The mechanism postulated from analysis of the p-xylene data involves the oxidation of one side chain at a time before the ring is broken - in a manner not unlike the oxidation of the single side chain species toluene. During the present period work was directed toward the explicit determination of the concentration of the methylbenzyl radical to explain and clarify the linear fuel decay observed. The p-xylene decay rate is due to abstraction of an H by a radical to form the p-methylbenzyl radical, displacement of a methyl group by an H to form toluene or homolysis to again form a p-methylbenzyl radical and an H atom. Detailed experimentation has revealed that in the temperature range of operation abstraction accounts for about 75% of the xylene decay, displacement about 20% and homolysis about 5%. These results are now being used to detail the overall p-xylene oxidation mechanisms.

REFERENCES

1. Glassman, I., "Soot Formation in Combustion Processes", invited paper, Twenty-Second Symp. (Int'l.) on Combustion, 1988.
2. Sidebotham, G., "An Inverse Co-Flow Approach to Sooting Laminar Diffusion Flames", Princeton University, Dept. of Mech. and Aero. Eng. Ph.D. Thesis, 1988.
3. Hura, H. and Glassman, I., "Fuel Oxygen Effect on Soot Formation in Counter-flow Diffusion Flames", Comb. Sci. and Tech. 53, 1 (1987).
4. Hura, H. and Glassman, I., "Soot Formation in Diffusion Flames of Fuel-Oxygen Mixtures", paper accepted for presentation at Twenty-Second Symp. (Int'l.) on Combustion, 1988.
5. Chakraborty, B.B. and Long, R., "The Formation of Soot and Polycyclic Hydrocarbons in Diffusion Flames. III: Effects of Oxygen to Ethylene and Ethane Respectively as Fuels", Comb. and Flame 12, 469 (1968).
6. Wright, F.J., "Effect of Oxygen in the Carbon-Forming Tendencies of Diffusion Flames", Fuel 53, 232 (1974).
7. Brezinsky, K., Litzinger, T.A., and Glassman, I., "The High Temperature Oxidation of the Methyl Side Chain of Toluene," Int. Jour. Chem. Kin. 16, 1053 (1984).
8. Litzinger, T.A., Brezinsky, K., and Glassman, I., "The Oxidation of Ethyl benzene Near 1060 K," Combust. Flame 63, 251 (1986).
9. Litzinger, T.A., Brezinsky, K., and Glassman, I., "Reactions of n-Propylbenzene During Gas Phase Oxidation," Combust. Sci. Tech. 50, 117 (1986).
10. Brezinsky, K., "The High Temperature Oxidation of Aromatic Hydrocarbons," Prog. in Energy Combust. Sci. 12, 1 (1986).
11. Litzinger, T.A., Brezinsky, K., and Glassman, I., "Gas Phase Oxidation of Isopropylbenzene at High Temperature," J. Phys. Chem. 90, 508 (1986).
12. Brezinsky, K., Linteris, G.T., Litzinger, T.A., and Glassman, I., "High Temperature Oxidation of n-Alkyl Benzenes," accepted for publication, 21st Symp. (Int'l.) on Combustion.
13. Venkat, C., Brezinsky, K., and Glassman, I., "High Temperature Oxidation of Aromatic Hydrocarbons," 19th Symp. (Int'l.) on Comb., The Combustion Institute, Pittsburgh, 1982, p. 143.

FIGURE CAPTIONS

- Fig.1. Intermediates in near sooting and smoke point conditions of normal and inverse diffusion flames.
- Fig.2. Peak extinction coefficient (l/cm), a measure of soot volume fraction, vs. equivalence ratio of the fuel/oxygen mixture in propane and ethene CFDF's.

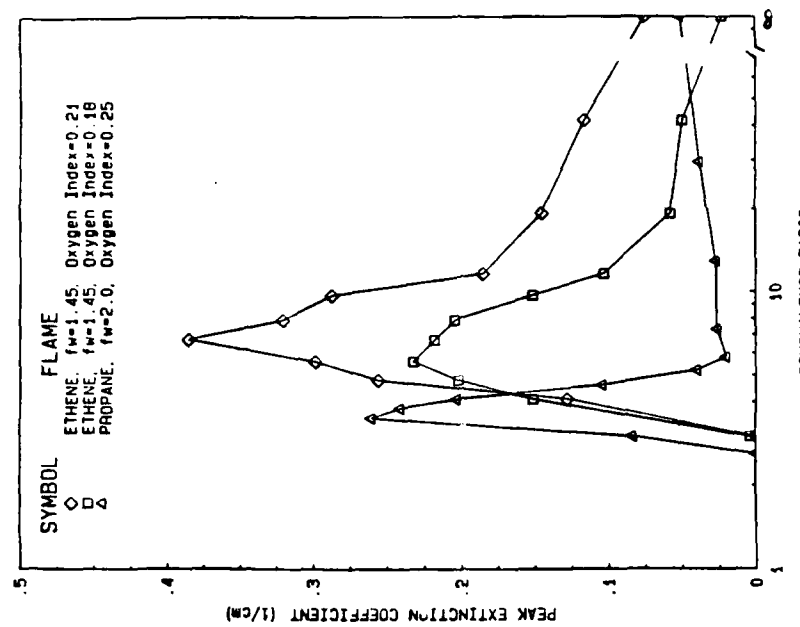


Figure 2

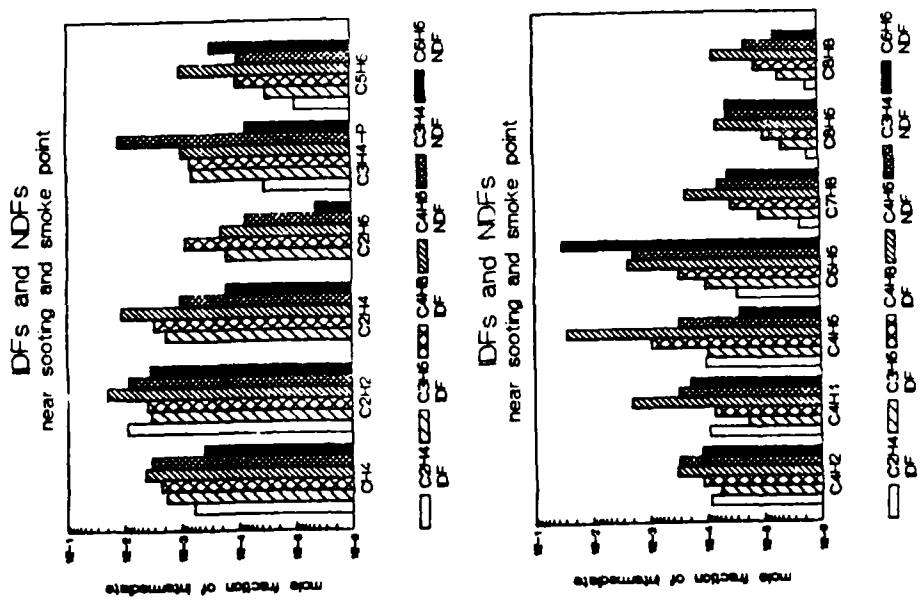


Figure 1

COMPUTER MODELING OF SOOT FORMATION
COMPARING FREE RADICAL AND IONIC MECHANISMS

AFOSR Contract No. F49620-88-C-0007
and Grant No. AFOSR 88-0072

Principal Investigators: H. F. Calcote and M. Frenklach

AeroChem Research Laboratories, Inc
P.O. Box 12,
Princeton, NJ 08542
and
Fuel Science Program
Department of Materials Science and Engineering
The Pennsylvania State University
University Park, PA 16802

SUMMARY/OVERVIEW:

A joint project has been initiated at AeroChem and Penn State to compare the free radical mechanism developed by Frenklach and associates and the ionic mechanism of soot formation using computer simulations. The ionic mechanism reaction kinetics are being developed to add to the free radical mechanism currently in the model. Several well-studied sooting flames will be modeled. The objectives are to determine the relative importance of the two mechanisms in forming soot and to determine where additional work is required to better define the mechanism of soot formation.

TECHNICAL DISCUSSION

The thermodynamic quantities, C_p° and S° for hydrocarbon ions, were calculated following Benson's thermochemical methods. For a few cases, such as for the cyclopropenyl ion, $C_3H_3^+$, there was sufficient experimental information to employ the more accurate statistical mechanics methods. Enthalpies of formation at 298 K, were obtained either directly from the literature or calculated from experimental proton affinities and the corresponding neutral molecule's enthalpy of formation. However, there are several molecules for which the thermodynamics are poorly known and this uncertainty will be manifest in the flame simulations when rates for reverse chemical reactions are calculated from thermodynamics and forward reaction rate coefficients.

A set of reactions and rate coefficients, which will be added to the neutral mechanism of Frenklach's program to accommodate the ionic mechanism, is being assembled from the literature by estimation where data are not available. Some preliminary reactions and reaction rate coefficients are presented in Table I along with the free energy of reaction at 2000 K.

The small species, C_2H_3 , C_2H_4 , C_3H , C_3H_2 , C_3H_3 , C_3H_4 , and C_3H_5 , which are prominent in fuel rich and sooting flames, are all candidate building blocks for adding to ions. Reliable kinetic data on these species are mostly unavailable. In developing this mechanism, only ions which have been observed in flames have been included. In choosing product channels for the large ion-electron recombination reactions, only molecules observed by Bockhorn et al. have been assumed as products. Rate coefficients for ion-electron reactions are not strongly temperature dependent but increase with the size of the ion.

There are several excellent sources of ion-molecule rate coefficients, including some of the reactions in this mechanism. Kinetic values from these sources are generally consistent with Langevin theory and correlations have been developed to estimate rate coefficients of ion-molecule reactions. We have not yet applied these techniques to this set of reactions in the ion-molecule mechanism; the differences in rate coefficients in Table I represent measured values. The temperature effect on ion-molecule reactions is not understood although some theoretical considerations are available. Experimental measurements over a reasonable temperature range for the reaction types in which we are interested are not available. The temperature dependence is generally considered to be negative; thus for the initial tests we have assumed $n = -0.5$; this assumption will be improved in the future.

The only pathway for producing ions has been assumed to be Reaction (18). We have neglected other possible sources such as: $CH^* + C_2H_2 \rightarrow C_3H_3^+$ based on recent modeling of fuel rich flames by Brown. The rate of formation of CH^* is not well known; there are some reactions in the basic Frenklach et al. mechanism and we have included another, Reaction (17). The next problem arises with the rate of isomerization between the propargyl ion, $C_3H_3(l)^+$ and the cyclopropenyl ion, $C_3H_3(c)^+$, which is important because the linear isomer reacts more rapidly in most reactions than the cyclic isomer. This rate coefficient (Reaction 28) has been estimated from the neutral isomerization rate of cyclopropane to propene. We have assumed that only the linear structure is formed and reacts; all reactions of the cyclic structure are neglected; it only serves as a pool for the reactive linear isomer.

Propyne, $C_3H_4(p)$, and allene, $C_3H_4(a)$, are both expected to be present at 2000 K; however, to simplify the initial simulations, we have considered only propyne in the ion-molecule reactions. $C_6H_5^+$ is assumed to be linear and cyclization is assumed to occur at the first seven carbon atom species.

The present capabilities of the state-of-the-art premixed laminar flame codes that take transport properties into account correctly are limited, by physically realistic constraints on computer time and memory, to about 50 chemical species and a couple of hundred chemical reactions. In dealing with PAH and soot formation, significantly larger mechanisms must be considered, since it is unclear at present which part of the reaction set will be dominant at flame conditions. Another difficulty is that there are no flame codes available that incorporate or are suitable for an easy implementation of chemical lumping required to properly model PAH growth and soot formation. Our solution to these problems is: first, the reaction mechanism will be reduced in size in such a way that it still describes faithfully the flame structure. To accomplish this in a systematic way we are developing a technique in which the formation of PAH and soot will be computed with the full reaction mechanism using a simple kinetic code in which the flame environment (temperature

and critical species profiles computed with the reduced mechanism) will be imposed. The testing of this concept is in progress.

Clearly much work remains to be done.

TABLE I

PRELIMINARY IONIC REACTION MECHANISM FOR SOOT FORMATION

Only reactions in addition to those in
Frenklach et al. (CS&T 50, 79 (1986))

$k = AT^n \exp(-E/RT)$; units are $\text{cm}^3, \text{K}, \text{kJ}, \text{mol}, \text{s}$

	REACTION	ΔG (2000 K)	A	n	E
1	$\text{C}_2\text{H} + \text{H} \rightarrow \text{C}_2 + \text{H}_2$		1.00E+12		96
2	$\text{C}_2\text{H}_2 + \text{CH} \rightarrow \text{C}_3\text{H}_3$	-530	3.00E+13		
3	$\text{C}_2\text{H}_2 + \text{CH}_2 \rightarrow \text{C}_3\text{H}_3 + \text{H}$	-335	1.80E+12		15
4	$\text{C}_3\text{H}_2 + \text{H} \rightarrow \text{C}_3\text{H}_3$	-100	6.00E+12		
5	$\text{C}_3\text{H}_2 + \text{O} \rightarrow \text{C}_2\text{H} + \text{HCO}$	-224	6.80E+13		
6	$\text{C}_3\text{H}_2 + \text{OH} \rightarrow \text{C}_2\text{H}_2 + \text{HCO}$	109	6.80E+13		
7	$\text{C}_3\text{H}_3 + \text{H} \rightarrow \text{C}_3\text{H}_4(\text{p})$	-109	2.00E+13		
8	$\text{C}_3\text{H}_3 + \text{O} \rightarrow \text{C}_3\text{H}_2 + \text{OH}$	-119	3.20E+12		
9	$\text{C}_3\text{H}_3 + \text{O}_2 \rightarrow \text{CH}_2\text{CO} + \text{HCO}$	-359	3.00E+10		12
10	$\text{C}_3\text{H}_4(\text{p}) + \text{H} \rightarrow \text{CH}_3 + \text{C}_2\text{H}_2$	238	2.00E+13		10
11	$\text{C}_3\text{H}_4(\text{p}) + \text{H}_2 \rightarrow \text{C}_3\text{H}_5 + \text{H}$	173	1.00E+13		167
12	$\text{C}_3\text{H}_4(\text{p}) + \text{OH} \rightarrow \text{C}_3\text{H}_3 + \text{H}_2\text{O}$	-143	5.00E+12		5
13	$\text{C}_3\text{H}_4(\text{p}) \rightarrow \text{C}_3\text{H}_4(\text{a})$	15.6	7.76E+11		230
14	$\text{C}_3\text{H}_4(\text{a}) + \text{H} \rightarrow \text{C}_3\text{H}_5$	-55.8	1.20E+13		9
15	$\text{C}_3\text{H}_4(\text{a}) + \text{OH} \rightarrow \text{C}_3\text{H}_3 + \text{H}_2\text{O}$	-158.0	2.70E+11		
16	$\text{C}_4\text{H}_2 + \text{O} \rightarrow \text{C}_3\text{H}_2 + \text{CO}$	-377.0	2.70E+13		7
17	$\text{C}_2 + \text{OH} \rightarrow \text{CH}^* + \text{CO}$	-96.6	3.40E+12		
18	$\text{CH}^* + \text{O} \rightarrow \text{HCO}^+ + \text{e}$	-77.5	4.81E+14		
19	$\text{HCO}^+ + \text{C}_2\text{H}_2 \rightarrow \text{C}_2\text{H}_3(1)^+ + \text{CO}$	-401	1.46E+16		-0.5
20	$\text{HCO}^+ + \text{C}_3\text{H}_2 \rightarrow \text{C}_3\text{H}_3(1)^+ + \text{CO}$	-222	1.26E+16		-0.5
21	$\text{HCO}^+ + \text{C}_3\text{H}_4(\text{p}) \rightarrow \text{C}_3\text{H}_3(1)^+ + \text{H}_2 + \text{CO}$	-227	1.21E+16		-0.5
22	$\text{HCO}^+ + \text{CH}_2 \rightarrow \text{CH}_3^+ + \text{CO}$	-196	1.23E+16		-0.5
23	$\text{HCO}^+ + \text{H}_2\text{O} \rightarrow \text{H}_3\text{O}^+ + \text{CO}$	-105	3.29E+16		-0.5
24	$\text{H}_3\text{O}^+ + \text{C}_3\text{H}_2 \rightarrow \text{C}_3\text{H}_3(1)^+ + \text{H}_2\text{O}$	-117	1.48E+16		-0.5
25	$\text{CH}_3^+ + \text{C}_2\text{H}_2 \rightarrow \text{C}_3\text{H}_3(1)^+ + \text{H}_2$	-474	1.35E+15		-0.5
26	$\text{CH}_3^+ + \text{C}_4\text{H}_2 \rightarrow \text{C}_5\text{H}_3^+ + \text{H}_2$	-246	1.35E+15		-0.5
27	$\text{C}_2\text{H}_3^+ + \text{C}_2\text{H}_2 \rightarrow \text{C}_4\text{H}_3^+ + \text{H}_2$	-427	5.22E+15		-0.5
28	$\text{C}_3\text{H}_3(\text{c})^+ \rightarrow \text{C}_3\text{H}_3(1)^+$	57	3.20E+15		274
29	$\text{C}_3\text{H}_3(1)^+ + \text{C}_2\text{H}_2 \rightarrow \text{C}_5\text{H}_3^+ + \text{H}_2$	-408	5.22E+15		-0.5
30	$\text{C}_3\text{H}_3(1)^+ + \text{C}_3\text{H}_4(\text{p}) \rightarrow \text{C}_4\text{H}_5^+ + \text{C}_2\text{H}_2$	205	1.29E+16		-0.5
31	$\text{C}_3\text{H}_3(1)^+ + \text{C}_3\text{H}_4(\text{p}) \rightarrow \text{C}_6\text{H}_5(1)^+ + \text{H}_2$	-155	1.15E+16		-0.5
32	$\text{C}_3\text{H}_3(1)^+ + \text{C}_3\text{H}_4(\text{p}) \rightarrow \text{C}_4\text{H}_3^+ + \text{C}_2\text{H}_4$	-79	1.15E+16		-0.5
33	$\text{C}_3\text{H}_3(1)^+ + \text{C}_4\text{H}_2 \rightarrow \text{C}_7\text{H}_5^+$	44	1.04E+16		-0.5
34	$\text{C}_4\text{H}_3^+ + \text{C}_3\text{H}_4(\text{p}) \rightarrow \text{C}_7\text{H}_5^+ + \text{H}_2$	9	1.04E+16		-0.5

	REACTION	ΔG (2000 K)	A	n	E
35	$C_4H_5^+ + C_2H_2 \rightarrow C_6H_5(l)^+ + H_2$	-360	$1.04E+16$	-0.5	
36	$C_4H_5^+ + C_4H_2 \rightarrow C_8H_7^+$	-36	$1.04E+16$	-0.5	
37	$C_6H_5(l)^+ + C_3H_4(p) \rightarrow C_7H_7^+ + C_2H_2$	164	$1.12E+16$	-0.5	
38	$C_7H_7^+ + C_3H_4 \rightarrow C_8H_7^+ + C_2H_2$	125	$1.04E+16$	-0.5	
39	$C_7H_7^+ + C_2H_2 \rightarrow C_9H_7^+ + H_2$	-203	$1.04E+16$	-0.5	
40	$C_8H_7^+ + C_2H_2 \rightarrow C_{10}H_9^+$	-329	$1.04E+16$	-0.5	
41	$C_8H_7^+ + C_3H_4(p) \rightarrow C_{11}H_9^+ + H_2$	25.7	$1.04E+16$	-0.5	
42	$C_9H_7^+ + C_2H_2 \rightarrow C_{11}H_9^+$	-247	$1.04E+16$	-0.5	
43	$C_{10}H_9^+ + C_2H_2 \rightarrow C_{12}H_9^+ + H_2$	-325	$1.04E+16$	-0.5	
44	$C_{11}H_9^+ + C_2H_2 \rightarrow C_{13}H_9^+ + H_2$	-232	$1.04E+16$	-0.5	
45	$C_{11}H_9^+ + C_3H_4(p) \rightarrow C_{14}H_{11}^+ + H_2$	105	$1.04E+16$	-0.5	
46	$C_{12}H_9^+ + C_2H_2 \rightarrow C_{14}H_{11}^+$	22.5	$1.04E+16$	-0.5	
47	$C_{12}H_9^+ + C_3H_4(p) \rightarrow C_{15}H_{11}^+ + H_2$	118	$1.04E+16$	-0.5	
48	$C_{13}H_9^+ + C_2H_2 \rightarrow C_{15}H_{11}^+$	329	$1.04E+16$	-0.5	
49	$C_{13}H_9^+ + C_3H_4(p) \rightarrow C_{16}H_{11}^+ + H_2$	-547	$1.04E+16$	-0.5	
50	$C_{14}H_{11}^+ + C_2H_2 \rightarrow C_{16}H_{11}^+ + H_2$	-884	$1.04E+16$	-0.5	
51	$C_{14}H_{11}^+ + C_4H_2 \rightarrow C_{16}H_{11}^+ + C_2H_2$	-248	$1.04E+16$	-0.5	
52	$C_{15}H_{11}^+ + C_2H_2 \rightarrow C_{17}H_{11}^+ + H_2$	-489	$1.04E+16$	-0.5	
53	$C_{15}H_{11}^+ + C_4H_2 \rightarrow C_{17}H_{11}^+ + C_2H_2$	147	$1.04E+16$	-0.5	
54	$C_{16}H_{11}^+ + C_2H_2 \rightarrow C_{18}H_{11}^+ + H_2$	-6	$1.04E+16$	-0.5	
55	$C_{16}H_{11}^+ + C_4H_2 \rightarrow C_{20}H_{11}^+ + H_2$	192	$1.04E+16$	-0.5	
56	$C_{17}H_{11}^+ + C_2H_2 \rightarrow C_{19}H_{11}^+ + H_2$	-537	$1.04E+16$	-0.5	
57	$C_{17}H_{11}^+ + C_4H_2 \rightarrow C_{21}H_{11}^+ + H_2$	-270	$1.04E+16$	-0.5	
58	$HC_0^+ + e \rightarrow CO + H$	-873	$1.20E+17$		
59	$H_3O^+ + e \rightarrow H_2O + H$	-768	$1.20E+17$		
60	$CH_3^+ + e \rightarrow CH + H_2$	-696	$1.20E+17$		
61	$C_2H_3^+ + e \rightarrow C_2H + H_2$	-799	$1.20E+17$		
62	$C_3H_3^+ + e \rightarrow C_2H_2 + CH$	-222	$1.20E+17$		
63	$C_4H_3^+ + e \rightarrow C_2H_2 + C_2H$	-372	$1.20E+17$		
64	$C_5H_3^+ + e \rightarrow C_2H + C_3H_2$	-571	$1.20E+17$		
65	$C_6H_5^+ + e \rightarrow C_4H_4 + C_2H$	-592	$1.20E+17$		
66	$C_7H_5^+ + e \rightarrow C_4H_2 + C_3H_3$	-796	$1.20E+17$		
67	$C_7H_7^+ + e \rightarrow C_6H_4 + CH_3$		$1.20E+17$		
68	$C_8H_7^+ + e \rightarrow C_6H_6 + C_2H$		$1.20E+17$		
69	$C_9H_7^+ + e \rightarrow C_6H_6 + CH$		$1.20E+17$		
70	$C_{10}H_9^+ + e \rightarrow C_{10}H_8 + H$		$1.20E+17$		
71	$C_{11}H_9^+ + e \rightarrow C_{10}H_8 + CH$		$1.20E+17$		
72	$C_{12}H_9^+ + e \rightarrow C_{12}H_8 + H$		$1.20E+17$		

FUEL STRUCTURE AND PRESSURE EFFECTS ON THE FORMATION OF SOOT PARTICLES IN DIFFUSION FLAMES

(AFOSR Contract No. AFOSR-87-0145)

Principal Investigator: Robert J. Santoro

Department of Mechanical Engineering
The Pennsylvania State University
University Park, PA 16802

SUMMARY/OVERVIEW:

The next generation of gas turbine engines will operate on broader specification fuels at higher operating pressures. These conditions will lead to increased soot formation and radiation transfer which represents a serious challenge to gas turbine performance. Unfortunately, the present understanding of the fundamental processes leading to soot particle formation, growth and subsequent oxidation is insufficient to allow an evaluation of the potential impact that these processes are likely to have on engine technology. In order to gain a better understanding of this problem, a fundamental study of the formation, growth and oxidation of soot particles is being undertaken in laminar diffusion flames. These studies are focused on the effects of fuel structure and operating pressure on the soot formation process. Detailed measurements of the soot particle, velocity and temperature fields are used to examine the evolution of the soot particle field. The objective of the work is to provide a fundamental understanding of the effects of fuel structure and operating pressure on the formation of soot particles under conditions which are characteristic of practical combustion systems. A primary goal of these studies is to provide the quantitative basis needed to model soot formation phenomena.

TECHNICAL DISCUSSION

The objective of the present study is to provide an understanding of the effects of fuel molecular structure and operating pressure on the formation of soot particles in combustion systems. These studies are carried out in a series of laminar diffusion flames and require extensive characterization of the particle, velocity and temperature fields present in these flames. Studies are conducted at both atmospheric and elevated pressures in order to examine the effect of pressure on both the formation and oxidation of soot particles. A coannular diffusion flame apparatus is used to study the soot formation processes in these gaseous flames. The coannular burner has been selected as the experimental burner because of its demonstrated capability to produce stable flames over a wide range of operating conditions [1]. High pressure flame studies are carried out in a flame facility assembled for this work which has the capability to operate at pressures as high as twenty atmospheres.

The effect of fuel structure is studied by the addition of aliphatic hydrocarbons (e.g., butane, butene, butadiene) and aromatics (e.g., alkylated benzenes, naphthalenes and naphthenes) in various proportions to well characterized diffusion flames. Effects of such characteristic compounds are examined using previously well characterized ethene and methane diffusion flames. The measurement approaches stress the use of non-intrusive optical diagnostic techniques, such as laser light scattering and laser anemometry, to measure the soot particle and velocity fields.

A brief summary of the accomplishments and current status of the present effort is given below. This summary is followed by a more detailed presentation of the progress achieved to date. Over the past year, our research efforts have concentrated on assembly of the required apparatus as well as initiation of the soot formation studies. The following tasks have been accomplished:

- (1) The atmospheric and high pressure flame facilities, along with the laser light scattering apparatus, have been designed, constructed and tested.
- (2) A series of baseline studies have been completed for methane and ethene atmospheric diffusion flames. The results of the ethene flames have been compared to previous studies to assure that proper operation of the experimental facilities has been achieved. These flames have also been used as baseline comparison flames for a series of fuel addition studies.
- (3) Fuel addition studies have been undertaken for methane, ethene, propene, butane, butene and butadiene fuel species. These studies have been used to examine the degree of conversion of fuel carbon to soot as a function of fuel flow rate and molecular structure. Additionally, comparisons between the methane and ethene baseline flames have provided a basis for examining potential synergism between the baseline fuel and the fuel species added to the flame.
- (4) Previously completed studies of ethene, propene, butene and toluene fuel addition studies have been further analyzed. Specific attention has been given to fuel structure effects on the surface growth process. These results indicate that the specific surface growth rate coefficients are similar in magnitude for all the fuels studied, even though the available surface area varies strongly with fuel species. The magnitude of the specific surface growth rate coefficient is comparable to that observed in premixed flames.

Atmospheric and High Pressure Diffusion Flame Facilities

The atmospheric diffusion flame facility consists of a coannular diffusion flame burner, chimney, positioning system and gas metering system. The burner consists of a 1.1 cm fuel tube surrounded by a 10 cm air annulus. The fuel flow can consist of up to three gases, each metered with a separate rotameter. This allows for mixtures of fuels as well as nitrogen dilution of the fuel for temperature control. To protect the flame from room disturbances, a metal chimney has been incorporated into the burner facility. This chimney translates horizontally with the burner which slides vertically within the chimney. Slots machined in the chimney provide for optical access. The burner is mounted on a pair of computer controlled motorized translating stages which are used to traverse the burner through the laser beam to obtain measurements over the cross section of the flame.

In order to provide for studies at elevated pressure, a high pressure diffusion flame facility has also been constructed. This facility is composed of a coannular burner, pressure vessel, positioning system and gas metering apparatus. A burner, identical to that used in the atmospheric facility, is mounted on a motorized translation stage located internal to the pressure vessel. Electrical connections are made through the base of the pressure vessel allowing external computer control of the vertical position of the burner. To provide horizontal movement, the pressure vessel is attached to a precision ball bearing stage which is connected to a computer controlled motorized translation stage.

To accommodate this approach, the pressure vessel has been constructed in two separate sections. Figure 1 shows a schematic of the present apparatus. The lower section of the vessel houses the vertical translation and burner mounting system. The upper section provides for optical access to the flame region using four large diameter windows which allow a 2" clear aperture for the laser scattering and laser velocimetry measurements. The operating pressure in the vessel is adjusted using manual valves located in the exhaust line. Control and measurement of the fuel and air flow rates are accomplished using mass flow controllers and allow up to three fuels to be metered independently. The high pressure diffusion flame facility is presently operational with flame studies now underway.

Fuel Molecular Structure Effects on Soot Surface Growth Processes

A number of studies have been undertaken to investigate the effects of fuel molecular structure on soot formation processes. These studies have focused on the particle inception, percent fuel

conversion to soot, and surface growth rate effects. In light of recent work in premixed flames [2], particular emphasis has been given to the study of surface growth processes in diffusion flames [3].

The surface growth process has been studied using a fuel addition approach. These studies were conducted using a well characterized ethene/air diffusion flame as the baseline flame. Different fuel species were added to the baseline fuel, such that the carbon flow rate is held constant. In addition, the flame size and shape remains similar for all the flames studied, thus minimizing changes in burner heat loss or particle transport in the flame. An ethene fuel flow rate of 3.85 cc/s was selected for the baseline flame since this diffusion flame has been extensively studied. Results obtained for ethene, propene, butene, and toluene will be discussed.

Using the previously obtained detailed information on the particle paths for the ethene flame, comparisons between the different fuel mixtures can be made. Figure 2 shows the time evolution of the soot volume fraction, f_v , along the particle path which traverses the annular region of the flame where the maximum f_v is observed. The fuel mixtures shown include three alkenes (ethene, propene and butene) and an aromatic (toluene) fuel. The calculated adiabatic flame temperatures for these fuel mixtures vary by less than 10K. Thus, the temperature fields characterizing these flames should be similar allowing a direct comparison between the flames.

Figure 3 shows the particle surface area calculated from the particle diameter and number density measurements along the same particle path. For each of the fuel mixtures studied, the surface area is observed to increase with time and fuel mixtures which exhibit larger f_v also display greater surface area available for growth. Harris and co-workers in their studies of premixed ethene flames [2] have described the surface growth by

$$\frac{dM}{dt} = k S[C_2H_2]$$

where M is the mass of soot in g/cm^3 , k is a growth rate constant ($\text{g}/\text{cm}^2 \text{ s atm}$), S is the surface area (cm^2) and the last term is the concentration of acetylene [atm]. In the present experiments, measurements of the acetylene concentration are not available. However, a comparison of the specific surface growth rate ($1/S dM/dt$) can be obtained and is shown in Figure 4. For these calculations, the density of soot was chosen to be $1.8 \text{ g}/\text{cm}^3$. Shown also on this figure are the data for an ethene premixed flame studied by Harris, et al. with a C/O ratio of 0.94. The data of Harris, et al. have been offset 15 ms to allow presentation in a proper time frame for these diffusion flame studies. The resulting specific surface growth rates calculated in this manner are very similar for each of the fuel mixtures studied. Furthermore, the comparison between the diffusion flame and premixed flame studies is quite reasonable. Considering the differences in the flame environments, this agreement is very encouraging and indicates the surface growth processes in both flame systems are quite similar. It is also of interest that for the propene, butene and toluene mixtures that slightly larger rate constants are observed at the earliest times. These results emphasize the need for further study of the particle inception process which may well be controlling the evolution of the soot particle field.

REFERENCES

1. Santoro, R. J., Yeh, T. T., Horvath, J. J and Semerjian, H. G., Combustion Science and Technology, 53, p. 89 (1987).
2. Harris, S. J. and Weiner, A. M., Combustion Science and Technology, 31, 155 (1983).
3. Santoro, R. J., "Fuel Molecular Structure Effects on Soot Particle Growth in Diffusion Flames," Twentieth Fall Technical Meeting of the Eastern Section of the Combustion Institute, Gaithersburg, MD, Nov. 2-5, 1987.

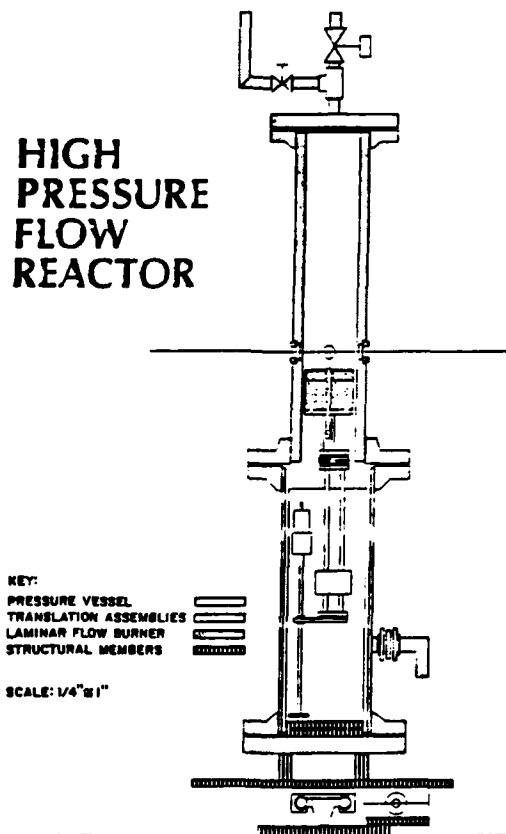


Figure 1. Schematic diagram of high pressure diffusion flame facility.

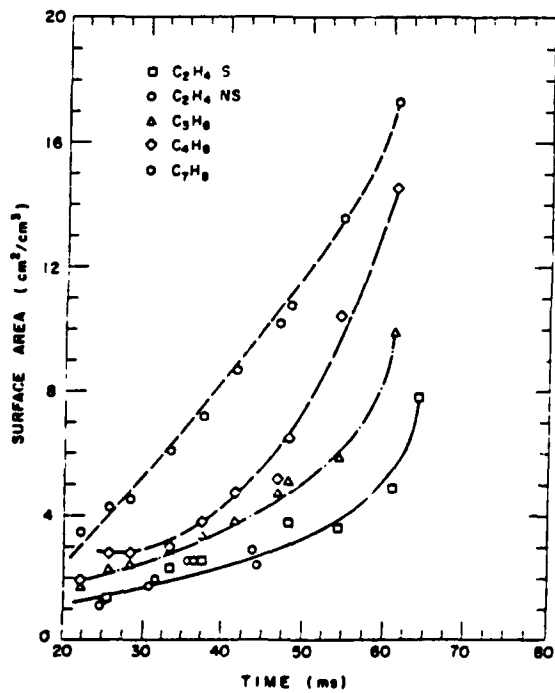


Figure 3. Soot particle surface area along the particle path exhibiting the maximum soot volume fraction for fuel mixtures containing ethene (S - $4.9 \text{ cm}^3/\text{s}$ and NS - 3.85 cm^3 fuel flowrate), propene, butene, and toluene.

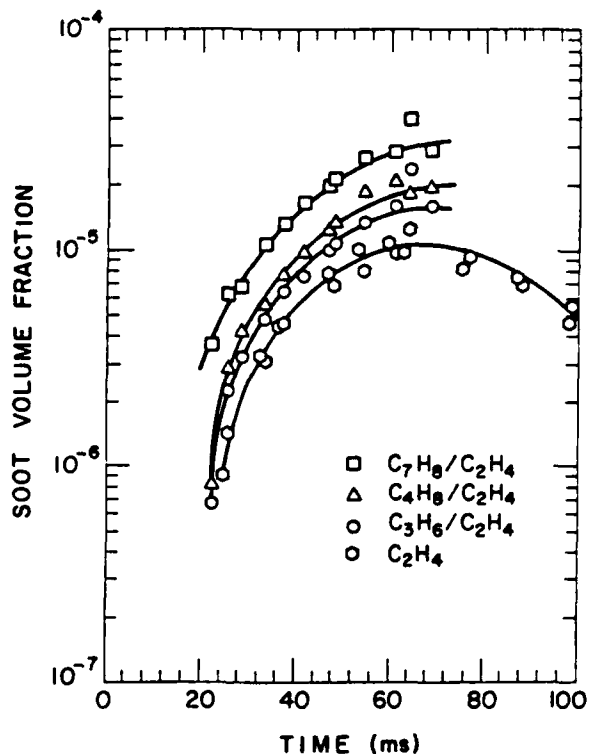


Figure 2. Comparison of the soot volume fraction along the particle path exhibiting the maximum soot volume fraction for fuel mixtures containing ethene, propene, butene, or toluene.

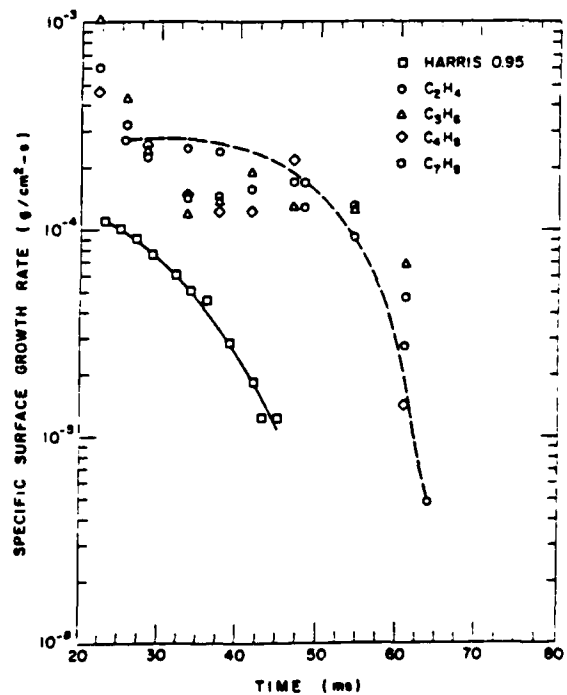


Figure 4. Specific surface growth rate along the particle path exhibiting the maximum soot volume fraction. The dashed line (---) is a best faired curve through the ethene flame results.

FUEL ADDITIVE EFFECTS IN SOOTING FLAMES

(AFOSR Contract No. F49620-86-C-0054)

Principal Investigator: P. A. Bonczyk

United Technologies Research Center
East Hartford, CT 06108

SUMMARY/OVERVIEW

Fuel additives have been used in the past to suppress soot formation in both laboratory and practical flames. Since, however, the mechanism of suppression has not been established as yet, there are no criteria for additive selection and evaluation. The purpose of this research is to clarify the nature of additive behavior in relation to soot control. Emphasis is placed on metal compounds since they have been shown to be very effective soot suppressants. Specifically, organo-iron compounds as well as inorganic alkali and alkaline-earth salts are the principal additives used. The metals are introduced into small laboratory-scale laminar flames. One of the objectives is to establish the one or more soot formation stages at which the additive intervenes. This is not an easy task since its execution requires the measurement of a significant number of gaseous and particulate species. To this end, both in-situ laser as well as sampling probe measurements are relied on. The laser is used to characterize soot particulates, whereas the sampling probe and related chromatographic analysis is used to characterize soot precursor and intermediate species. Post flame soot collection on cooled surfaces followed by small spot ESCA analysis has been done as well.

TECHNICAL DISCUSSION

For several years now, a considerable effort has been made by us to document the sooting behavior of an axi-symmetric prevaporized iso-octane/air diffusion flame with and without ferrocene present. The flame has proven to be very difficult to interrogate by optical or other means. Our persistence has been motivated by a desire to understand the very strong soot suppressing properties of ferrocene. Until recently, our emphasis has been on in-situ particulate characterization, from which we have demonstrated that soot size, number density and volume fraction are all reduced by ferrocene at late combustion stages. During the past year, two other important areas have been addressed. In one case, post flame particulates have been collected from a seeded flame and subjected to Auger/ESCA (Electron Spectroscopy for Chemical Analysis) analysis for the purpose of detecting any occlusion of ferrocene combustion products such as Fe or Fe_xO_y by the soot particulates. Secondly, a quartz sample probe and chromatographic analysis have been used to compare the more important molecular species concentrations in the flame with and without ferrocene present. Both of these efforts are outlined briefly below.

Quartz Measurements

Quartz probes have been used to collect gaseous hydrocarbon and other species at various points along the vertical axis of an axisymmetric diffusion flame. Two different flames were studied. One was fueled by prevaporized (135°C) iso-octane mixed with air, while the other differed from the first in that it had a 0.3% (by wght.) ferrocene additive present in the starting liquid fuel. The unseeded flame operated above its smoke point, whereas for the second flame the ferrocene seed caused the soot plume to disappear entirely. Most of the measurements were made with an uncooled probe having a 0.17 mm diam. aperture, with sampling at or near 1-3 Torr. This low pressure was chosen in order to effect a rapid reduction in static pressure (and temperature) and thereby quench species altering chemical reactions occurring within the probe or transfer line. Typically, the probe was inserted into the flame for a 1-2 min sampling period, following which the collection vessel was transferred to a neighboring facility for chromatographic analysis.

Sampling of the flames was done successfully, but not without certain difficulties and limitations. Under the best conditions, sampling could be done for 1-2 min after which condensates plugged the probe aperture. In some cases, condensation was so heavy and rapid that sampling was not possible at all. The principal condensates were soot and ferric oxide for the unseeded and seeded flames, respectively. The most significant consequence of condensation is that species sampling could be done for $z \leq 15$ mm, or for vertical positions up to but not including those of peak pcah and soot concentration. An attempt was made to collect pcah (at liquid nitrogen temperature) at $z = 15$ mm with and without ferrocene, but the permissible sampling period was too short for adequate sample collection.

Despite the limitations outlined above, a reasonably large number of species was detected in the range $0 < z \leq 15$ mm. Table I lists all of the species observed at $z = 15$ mm. With the exception of naphthalene (C_{10}H_8), as indicated by the large error, all the measured mole fractions were very repeatable. Generally, Table I indicates that ferrocene is not very perturbing of the species mole fractions. The exceptions are C_2H_2 , H_2 and CO. Figs. 1 and 2 give the representative behavior of a few species concentrations as a function of vertical position. In contrast with the absence of any perturbation of C_6H_6 , ferrocene appears to decrease C_2H_2 systematically and increase H_2 dramatically, or to enhance C_2H_2 oxidation. Although an increase in CO was observed only at $z = 15$ mm, the increase is consistent with the foregoing hypothesis. Since our existing particulate measurements have demonstrated ferrocene activity at late combustion stages as well, it may not be possible to formulate additive behavior in terms of a single mechanism.

Auger/ESCA Particulate Analysis

In premixed ethylene flames seeded with ferrocene, Ritrievi et al. (Combust. Flame 70, 17) have presented evidence that the ferrocene combustion products (Fe and/or Fe_xO_y) are occluded by the soot particulates, and that under favorable conditions the additive species may diffuse to the surface of the particulate and enhance soot oxidation. Experiments were performed to look for this occlusion in our flame. An aluminum collection

disk was placed in the effluent stream of the seeded flame for some tens-of-minutes, and a visible condensate was allowed to form. The sample was then subjected to chemical analysis versus depth using Auger/ESCA analysis. For a 0.3% ferrocene seed, only trace amounts of carbon could be detected. The red-orange condensate was identified as Fe_2O_3 , with no measurable Fe/O % variation with depth. For very slight ferrocene seeding (smoke plume still visible), the condensate was principally carbon with, however, detectable quantities of iron present. The chemical state of the additive was elemental iron (Fe), and the results of the depth profile were inverse to that expected for occlusion.

ACKNOWLEDGMENTS

I am grateful to Dr. Meredith B. Colket, III for guiding me through the probe measurements, and to Dr. Bruce L. Laube for doing the Auger/ESCA sample analysis.

TABLE I

Species mole fractions at 15 mm height
with and without ferrocene. Measurement
uncertainties are given in parentheses.

<u>Species</u>	<u>Mole %</u> <u>without</u> <u>Ferrocene</u>	<u>Mole %</u> <u>with</u> <u>Ferrocene</u>
CH_4	3.12 (18)	3.35 (23)
C_2H_2	2.19 (22)	1.75 (40)
C_2H_4	1.44 (8)	1.43 (8)
C_2H_6	0.14 (2)	0.11 (5)
C_3H_4	0.58 (8)	0.46 (12)
C_3H_6	0.33 (8)	0.35 (12)
C_4H_6	0.09 (3)	0.08 (2)
isobutene	0.14 (5)	0.15 (9)
C_6H_6	0.54 (2)	0.52 (7)
C_7H_8	0.10 (3)	0.13 (5)
phenylacetylene	0.08 (2)	0.06 (4)
styrene	0.11 (3)	0.10 (4)
C_9H_8	0.10 (5)	0.05 (3)
C_{10}H_8	0.31 (28)	0.37 (41)
H_2	3.98 (60)	7.60 (219)
CO	4.90 (21)	6.32 (33)
CO_2	7.41 (30)	7.83 (72)

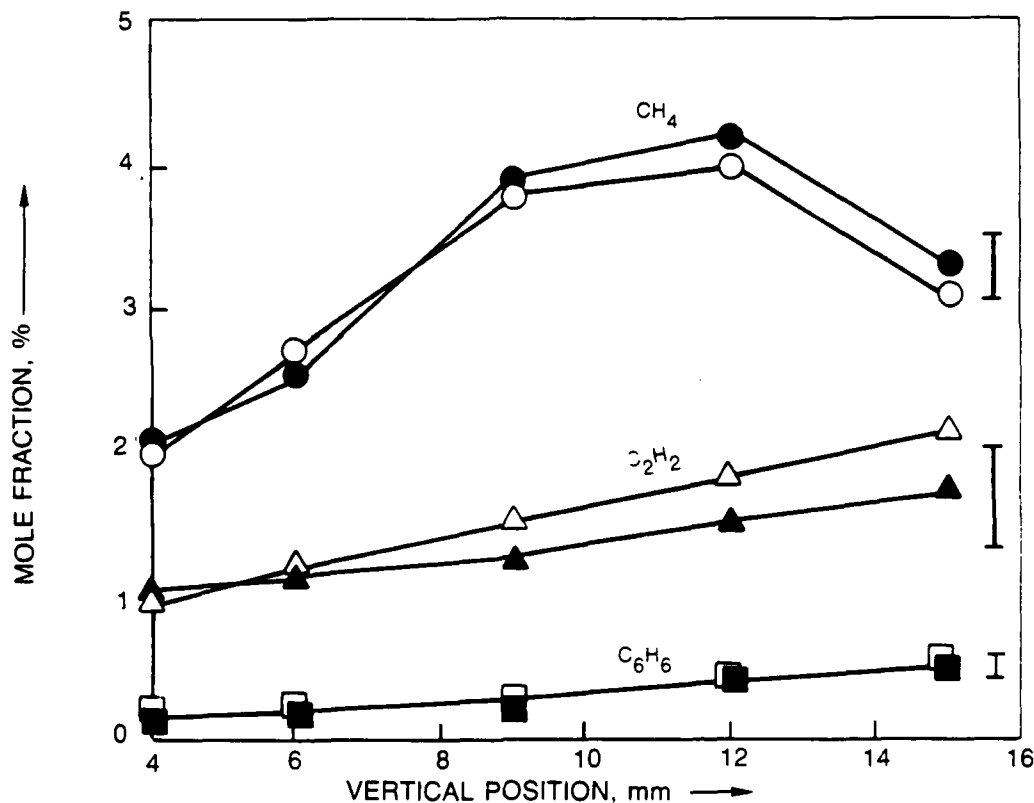


Fig. 1 CH_4 , C_2H_2 and C_6H_6 concentrations with (\bullet , \blacktriangle , \blacksquare) and without (\circ , \triangle , \square) ferrocene.

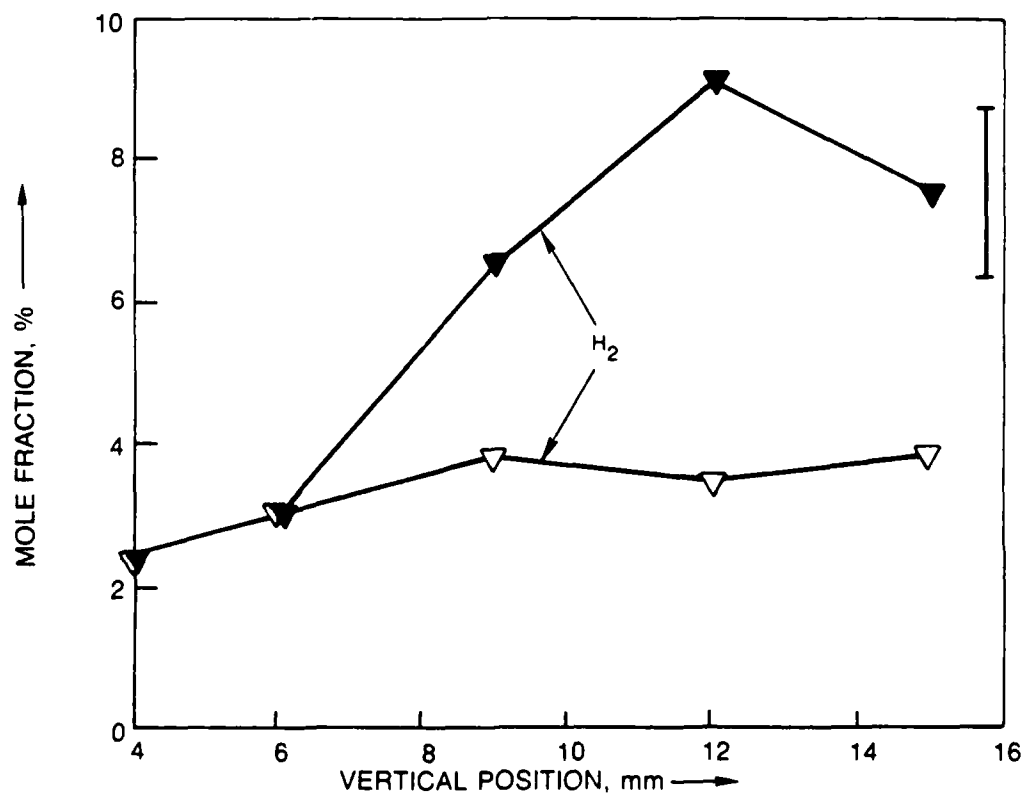


Fig. 2 H_2 concentration with (\blacktriangledown) and without (\triangledown) ferrocene.

LUMPED MODEL GENERATION AND EVALUATION: SENSITIVITY
AND LIE ALGEBRA TECHNIQUES WITH APPLICATIONS TO COMBUSTION

Grant No. AFOSR-85-0346

Principal Investigators:

Fredrick L. Dryer
Department of Mechanical
and Aerospace Engineering

Herschel Rabitz
Department of Chemistry

Princeton University
Princeton, NJ 08544

SUMMARY

This research is concerned with the development and application of new techniques to systematically simplify combustion models. Particular emphasis is placed on the role of complex chemistry with the effort directed towards both reducing the number of chemical species by lumping techniques and reducing the effective number of kinetic steps to a physically acceptable minimum. In general terms, the key new contribution in this research is its emphasis on the use of rigorously founded systematic techniques to achieve these goals. In particular, tools from sensitivity analysis, lumped system reduction, and Lie groups are being utilized.

TECHNICAL DISCUSSION

This research consists of three main components as outlined below. Each activity has its own goal, with the general connection being through the objective of combustion system reduction. The research involves the close collaboration between the principal investigators and Professor Carl Wulfman, University of the Pacific, and Dr. Richard Yetter, Research Staff Member, Princeton University.

A. Scaling and Self Similarity Behavior: An Indicator of Combustion System Reduction

Sensitivity coefficients provide the quantitative means to assess the relationship between combustion system parameters and the observable dependent variables. For example, one may routinely calculate the system sensitivity coefficients of the type $\delta c_i / \delta k_j$ which provide the response of the i -th chemical species concentration with respect to the significance of the j -th system rate constant or $\delta c_i / \delta J_n$ which provides the response of the i -th chemical species to the introduction of an infinitesimal flux δJ_n of the n -th chemical species. Similarly, the focus here is upon the information content in these various types of coefficients with regard to combustion system simplification. First, a calculation and careful examination of the coefficients in any particular system can provide valuable insight regarding

identification of the important as well as unimportant portions of a model. However, most significantly, this line of research has lead to the identification of systematic self similarity and scaling behavior among sensitivity coefficients in strongly coupled systems as often found in combustion. This behavior manifests itself in a collapse of the independent system response such that large blocks of sensitivity coefficients typically have the same temporal and/or spatial structure. The thrust of the research along these lines is two-fold. First, we desire a fundamental understanding of the conditions or origin of the behavior; second, we desire to exploit its presence for system lumping as well as kinetic parameter reduction. The existence of a high degree of exothermicity and significant mass transport appears to enhance the likelihood of finding the scaling and self similarity behavior.

B. System Lumping by Linear Transformations

This line of research is based on seeking a systematic linear transformation $\hat{c} = Mc$ where M is a $n \times n$ nonsquare lumping matrix transforming the original n -vector of chemical species c to the lumped \hat{n} -vector \hat{c} with $\hat{n} < n$. The possibility of finding such transformations had been raised some years ago for linear as well as certain classes of nonlinear systems in chemical engineering. Our research has extended these concepts to chemically important broader classes of nonlinear systems including the prospects for exact as well as approximate system lumping. The context of these goals may be understood by considering the simple example of a nominal set of coupled kinetic equations $\dot{c} = f(c)$ where f is generally a nonlinear function of the system concentrations (or other dependent variables). The corresponding reduced set of lumped equations has the form

$$\dot{\hat{c}} = \hat{f}(\hat{c})$$

In this case, the goal is to find the lumped mechanism function \hat{f} . Our research in this general area has followed two lines. First, by analyzing the Jacobian of the original system it is possible to identify the necessary and sufficient conditions for exact lumping to exist. The presence of exact lumping would imply the existence of hidden symmetries in the kinetic equations, but this circumstance is not likely to be found in many realistic cases. Therefore, a second line of research is being pursued to use the identified criteria for exact lumping as a basis to seek approximate transformation matrices M such that lumping can be achieved in a practical way. For example, it is possible to show that \hat{f} may be identified as

$$\hat{f}(\hat{c}) \approx Mf(\bar{M}\hat{c})$$

where \bar{M} is a generalized inverse of M . This line of research should also have significant applications to similar problems arising in other fundamental and applied areas where lumping is desired.

C. System Reduction and Lumping by Nonlinear Transformations

This approach to system reduction is based on the use of nonlinear transformations produced by Lie groups. The Lie generators giving rise to these transformations correspond to the generalized symmetry properties in the hyperspace of chemical species and parameters for a combustion system. The transformations may be used in a nonlinear fashion to investigate the effects of wide-ranging changes in the rate constants and input/output fluxes upon chemical reactions. Every Lie group corresponds to either exactly or approximately converting a solution of a set of combustion rate equations into corresponding solutions of a family of altered rate equations. Most importantly, all of these solutions have topologically equivalent equilibrium points and phase trajectories in the space of concentration variables. The concepts and techniques behind this technique are quite general, and thusfar our research has focused on establishing the tools as well as illustrating them on simple systems. Current research is being focused on a systematic extension of the methodology to produce an algorithmic procedure which may be carried forth on a wide variety of combustion kinetic problems. The general techniques as well as simple illustrations have already shown that the Lie transformations may be used to shift concentrations as a means to study changes in input/output fluxes as well as change rate constants over wide ranges. Other mappings can be used to create lumped concentration variables for both linear as well as nonlinear kinetic equations. Another application of these transformations is to the approximate linearization of nonlinear kinetics valid in regions larger than those obtained by the usual power series expansions. It is ultimately expected that the Lie group transformations will be able to take explicit advantage of the presence of scaling and self similarity as identified in part A of the research.

TIME-DEPENDENT SIMULATION OF TURBULENT COMBUSTION

AFOSR Contract No. AFOSR ISSA - 88-0026

Howard R. Baum and Ronald G. Rehm

National Bureau of Standards
Gaithersburg, MD 20899**SUMMARY:**

A mathematical model for diffusion controlled combustion in a turbulent eddy is presented. The model is intended as a computational "molecule" to be imbedded in a larger scale reacting flow simulation. Two parallel developments have been pursued, one involving a simplified two-dimensional model, a generalization of the Marble problem, on which the computational methodology can be developed, and the other a three-dimensional model on which more general issues can be examined. Methodology for including finite rates for more realistic chemical reactions is being developed in conjunction with J. deRis.

TECHNICAL DISCUSSION:

Turbulent combustion is difficult to analyze because it is highly nonlinear, transient and involves a wide range of length and time scales. When the Reynolds number is large, experiments indicate that the length and time scales associated with different physical phenomena become disparate. Away from boundaries, the large scale is essentially nondissipative and is related to the geometry defining the flow configuration. Combustion, on the other hand, takes place on the small scale associated with the diffusion and reaction; this scale establishes the rate at which the reactants disappear and heat is released. An outline of a general approach for studying the problem of turbulent reacting flows, based on these observations, has been given earlier by the authors. The approach is to analyze large-scale flow fields separately from the small-scale mixing and reaction but in a way that will allow the phenomena to be coupled through analytical and computational techniques.

Emphasis has been on the development of a model for the small-scale combustion phenomena. Two parallel developments have been pursued, one involving a simplified two-dimensional model on which the computational methodology can be developed, and the other involving a three-dimensional model on which more general issues can be examined. A description of each of these efforts is briefly reported.

The two-dimensional model consists of a constant-density diffusion-controlled reaction with finite reaction-rate chemistry. Earlier the authors noted that when the chemical reaction rate is large and the flame-sheet approximation is made, this problem, which was originally formulated by F. Marble, admits an exact analytical/numerical solution. They solved this problem by noting that a Lagrangian coordinate system eliminates the convection-diffusion competition, that the equation admits a global similarity solution, that the linearity allows the mixture fraction to be Fourier-analyzed

in angle, and finally that the resulting ordinary differential equations for the Fourier amplitudes of the mixture fraction can be solved to arbitrary accuracy by a combination of asymptotic and numerical techniques.

Recently, we have formulated and begun to analyze a generalization of that work to include finite-rate chemistry. Consider the configuration in which there is fuel in the left half-plane and oxidizer in the right half-plane initially. These half-spaces are brought into contact and simultaneously a line vortex with axis at the origin is imposed. The vortex induces a convective mixing of the interface between the two species, increasing the area of the separating surface in the neighborhood of the origin and enhancing the diffusion of the species into each other. The chemical reaction is assumed to take place at constant density and all diffusion coefficients are assumed to be constant. With the assumptions described above, the equations for species and energy are decoupled from momentum conservation and continuity; they are equations representing a balance between convection, diffusion and reaction. The reaction rate, which is quadratic in concentration and assumed independent of temperature, can be eliminated from one equation by working with the mixture fraction or Shvab-Zeldovich variable. The solution for the mixture fraction, obtained earlier, is used together with one of the species equations in the complete convection, diffusion, reaction problem for the fuel and oxidizer. The single resulting nonlinear problem is also analyzed in a Lagrangian coordinate system. This transformation eliminates the need to resolve small-scale transition layers which may arise especially when the Reynolds number is large. The change of variables reduces the convection-diffusion equation to a complicated diffusion equation, which can then be analyzed by both asymptotic and numerical methods.

When the Schmidt number and reaction rate are large, asymptotic methods allow one to determine an analytical solution from which the character of the problem for large Reynolds number can be determined. For a stoichiometric mixture, there are two reaction regions. In the outer region there is a flame sheet, which remains close to the convectively mixed interface in the absence of diffusion. For moderately large radius, this interface is very close to the initial interface in the Lagrangian coordinate system. In the inner region, there is a burnt core in which both fuel and oxidizer are depleted. Important quantities of interest from this analysis are the global rates of species consumption and of heat release; it is desired to calculate these quantities as functions of the Reynolds number, Schmidt number, kinetics rate and initial concentrations of fuel and oxidizer.

The second analysis is directed toward the development of a general mathematical model of diffusion controlled gas phase combustion appropriate for use in a large eddy simulation of turbulent reacting flows. The basic idea is that while the large eddy simulation of necessity is highly dependent upon the geometrical and physical boundary conditions prescribed by the macroscopic problem of interest, the combustion phenomena are influenced by local conditions near the fuel/oxidizer interface. The

combustion process resolved on the scale of an individual fuel parcel contains three essential ingredients. First, the molecular mixing of fuel and oxidizer and consequent release of heat; second, a local flow field on the scale of the fuel parcel characteristic of turbulence; finally, a mechanism whereby the flow is modified by the combustion process.

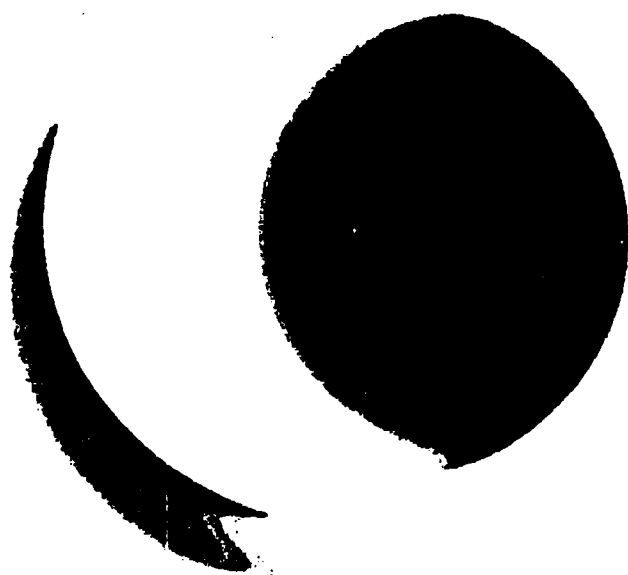
To address the first point we consider a highly idealized reaction in which fuel and oxidizer react instantly. We further assume that all species diffuse according to Fick's law with equal diffusivities, and that the Lewis number of the mixture is unity. These assumptions together with the equation of state allow all species mass fractions and thermodynamic variables to be uniquely related to a single mixture fraction variable. The variable obeys a diffusion-convection equation subject to initial values of unity in the fuel parcel and zero elsewhere.

Next, we consider an appropriate description of the local flow field. In a frame of reference moving with the large scale fluid motion, it is always possible to express the local velocity as the sum of a solenoidal (vortex-induced) flow and a potential flow. The solenoidal velocity field is assumed to be a transient vortex stretched by an imposed strain field. This geometry is known to be characteristic of the velocity field in an individual turbulent eddy. In fact, it can be shown that the smallest length scale in this model emerges naturally as the Kolmogoroff scale. The velocity field employed is an exact solution of the constant property Navier-Stokes equations.

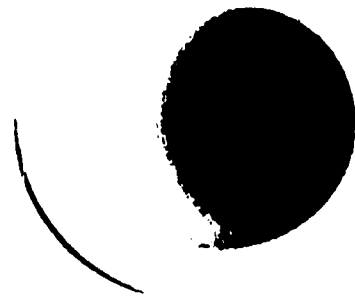
Finally, the feedback of the energy release on the local flow field is determined by the potential flow. The mass conservation equation relates the potential field to the local density changes. These changes, which are generated by the heat addition, lead to a nonlinear relationship between the velocity potential and the mixture fraction. Thus, the final form of the combustion model is a nonlinear three-dimensional time-dependent equation for the mixture fraction variable. The solution is obtained analytically by employing a generalization of the Cole-Hopf transformation to obtain a linear equation for a psuedo-mixture fraction variable. This equation, which has the form of a constant-property diffusion-convection model studied earlier, is solved using Fourier and asymptotic methods in Lagrangian coordinates. Bit mapped graphics displays of the evolution in time of an initially spherical fuel blob in an oxidizing atmosphere have been produced; two are shown on the following page. They show, at two times in the evolution, the mixture fraction on a plane cross section through the blob as it is consumed by combustion and mixed by a cylindrical vortex whose axis is one half the radius from the center of the sphere.

Within a quasisteady approximation, using a single-step reaction, the effects of finite-rate chemistry are being included in this model using an analysis described by F. Williams. A general methodology for including finite rates for more realistic chemical reactions is being developed in conjunction with Dr. John deRis of Factory Mutual Research Corporation.

$\varepsilon = .002$ $\Omega = 2.$ TIME=1.0



$\varepsilon = .002$ $\Omega = 2.$ TIME=2.0



**TITLE: TURBULENT MIXING IN EXPONENTIAL TRANSVERSE
JETS**

(AFOSR Grant No.: AFOSR - 87 - 0366)

Principal Investigator:

Robert E. Breidenthal, Associate Professor
Department of Aeronautics and Astronautics
University of Washington, FS-10
Seattle, Washington 98195
(Telephone: 206-545-1098)

SUMMARY/OVERVIEW:

Effects of spatial acceleration on turbulent mixing are being investigated experimentally in a new flow visualization water tunnel facility. For this purpose, an array of discrete nozzles with exponentially increasing cross-sectional area and injection speed has been designed. Photographs of a fast chemical reaction, between the transversely injected fluid through these nozzles and the freestream, will reveal mixing characteristics of this flow. It is expected that unsteady effects due to exponential acceleration will inhibit mixing significantly in the near field of injection. Measured trajectories and mixing lengths will be compared to those of a single transverse jet of equal momentum flux.

TECHNICAL DISCUSSION

For unforced free shear flows, vorticity associated with each vortex is inversely proportional to its own lagrangian age. Global vorticity is diluted as pure irrotational fluid from the freestream is entrained into the vortex. Vortices grow significantly in size as they move downstream and mixing occurs rapidly.

Contrary to this, it is proposed that, under forcing, global vorticity of a particular vortex can be made constant with time. If this can be accomplished, then the vortex does not entrain ambient

fluid, and mixing is inhibited as long as forcing is present. A particularly simple way of obtaining such a flow pattern is injecting one stream into another one of uniform velocity, through an array of transverse nozzles with exponentially increasing size and injection speed.

Current experiments are designed to test the validity of this hypothesis using flow visualization techniques in a water tunnel. Under the current grant, construction of the water tunnel has been completed. A simple drawing of the tunnel is given in figure 1. Test section dimensions are 70cm X 70cm X 300cm, and maximum flow speed in the test section is 70 cm/sec. The tunnel is capable of handling a variety of chemicals as it is constructed with a stainless steel diffuser, settling chamber, contraction section, screen, and perforated plates ; glass test section windows; and PVC return pipeline. Flow speed can be regulated via a variable frequency drive unit that controls frequency input of a 30 HP electric motor powering a centrifugal recirculation pump. A remote control for variable frequency drive is mounted close to the test section for convenience.

A bottom view of the array of nozzles is shown in figure 2. In this configuration there are 10 discrete nozzles, machined from clear plexiglas and separated by thin stainless steel sheets. Nozzle width increases exponentially from 0.6 cm to 12.05 cm with an e-folding distance of 8.0 cm. Nozzle injection speed also increases exponentially from 3 cm/sec for the first nozzle to 60 cm/sec for the last one, with the same e-folding distance as for the nozzle size.

The water tunnel will be filled with an acidic solution of sulphuric acid. An alkaline solution containing a pH indicator will be injected through the transverse array of nozzles into the freestream. The mixing of the two streams will be visible with the pH indicator. To obtain a cross sectional view, a three watt argon ion laser will illuminate a transverse plane, exciting a fluorescent pH indicator, sodium fluorescein. Mixing length and trajectory information will be obtained from the visible injected fluid in the freestream. Results obtained will be compared with the results of a single transverse jet of equivalent momentum flux.

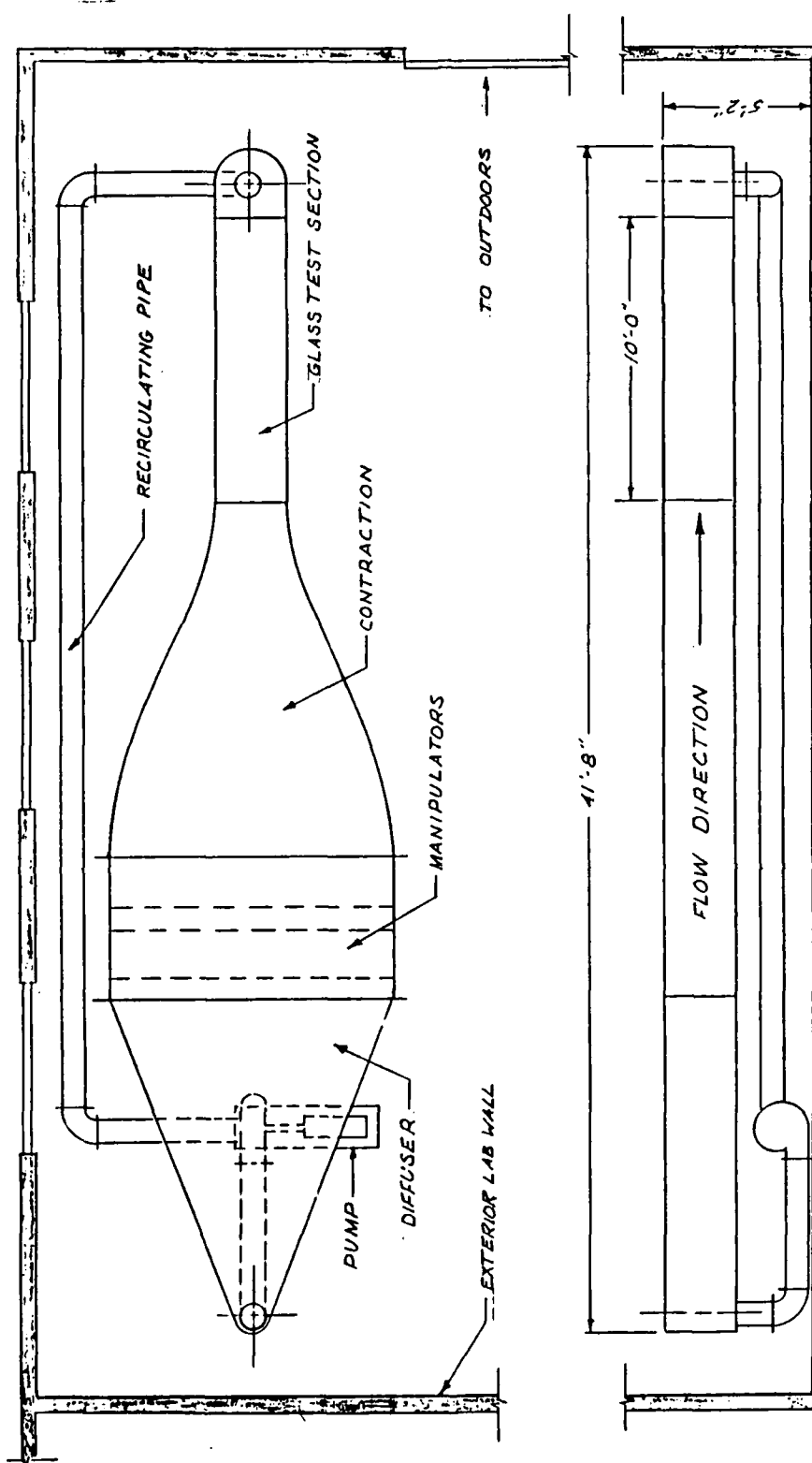


Fig. 1. Recirculating type flow visualization water tunnel facility.

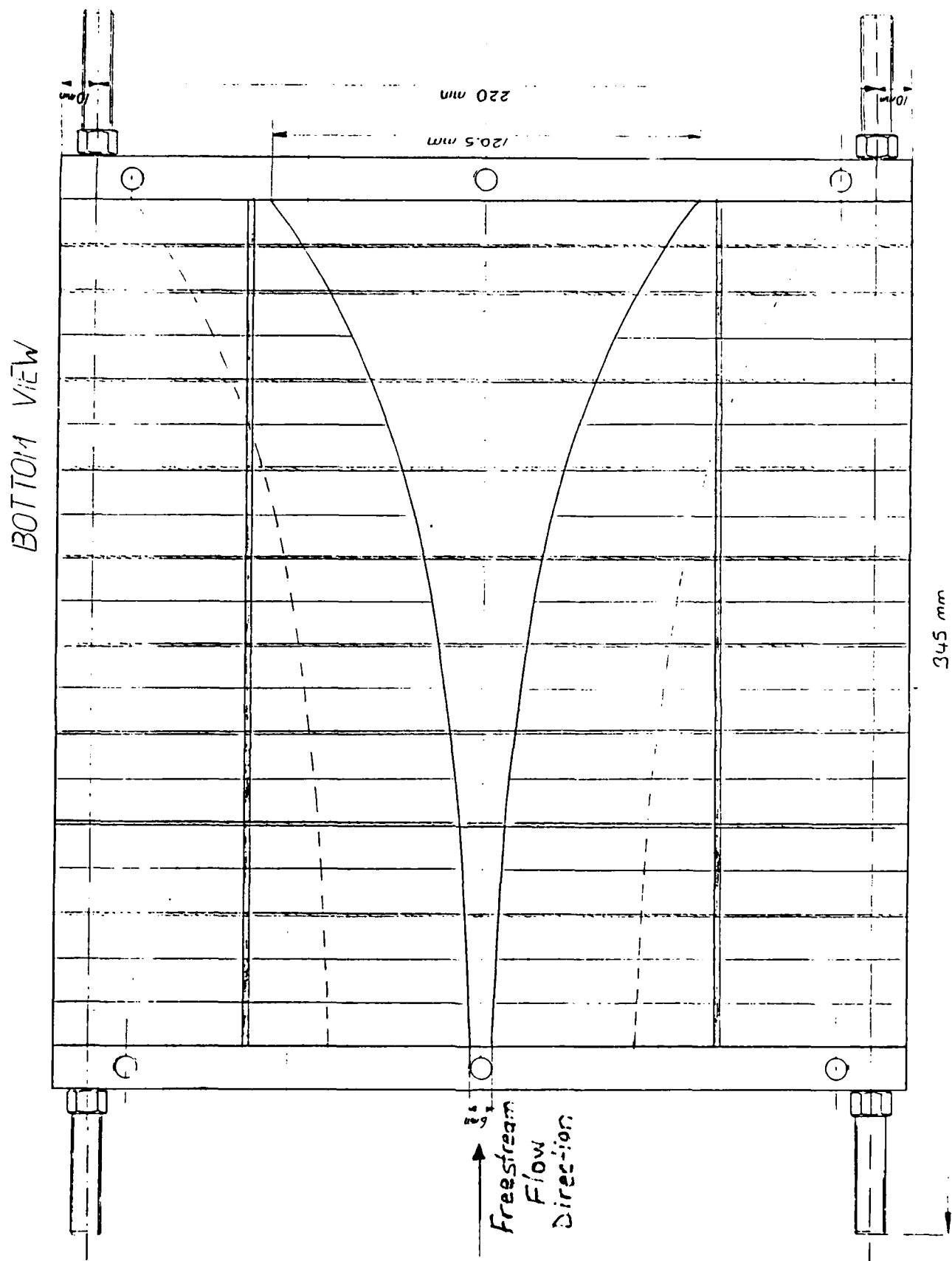


Fig. 2. Bottom view of array of exponential jets.

AN EXPERIMENTAL INVESTIGATION OF FLOW STRUCTURE, MIXING AND CHEMICAL REACTION IN COMBUSTING TURBULENT FLOWS

AFOSR Grant Number 84-0373

Brian J. Cantwell

Department of Aeronautics and Astronautics
Stanford University, Stanford, California 94305

SUMMARY / OVERVIEW

An experimental investigation of the relationship between flow structure and chemical reaction structure in a combusting turbulent flow is being carried out. The objective is to study the coupling between the unsteady velocity field and the unsteady reaction field. The method of approach involves the use of laser techniques to measure velocity and the concentration of minor species which are present only in the reaction zone. A particle tracking technique has been developed to facilitate acquisition of velocity field data and is presently being used to map planar velocity fields in the flame. This data is overlaid on the reaction field data to produce a picture of the mixing and reaction process. The work will lead to an improved understanding of the sequence of flow events involving entrainment, mixing and reaction of free stream reactants in unsteady flames. Information of this type should contribute to improved models of combustion.

TECHNICAL DISCUSSION

The configuration investigated is a co-flowing, non-premixed jet flame with methane in the core flow and air in the surrounding flow. The methane passes through a small chamber containing a loud speaker which can be used to add a velocity perturbation to the core flow at various frequencies and amplitudes. By forcing the fuel jet in a narrow range of frequencies, a very periodic and controllable flow suitable for making conditionally sampled measurements of the velocity and reaction fields can be produced. Visualization of the periodic flame structure has been accomplished using several visualization techniques. The density gradient field is recorded by high-speed schlieren photography. Flame front location is determined from images of the OH concentration field using planar laser-induced fluorescence. The inner flame structure is obtained from photographs of soot luminosity. Fluid motion inside the flame front is determined from planar images of laser light scattered by TiO_2 seed particles in the fuel jet, which are formed by reacting $TiCl_4$ with water vapor. Velocity vector fields are measured using particle

tracking velocimetry.

Images of the velocity vector field and flame luminosity at two successive phase angles of the excitation (45 and 90 degrees) are shown in Figure 1. The vectors are plotted with respect to a frame of reference which moves with the flamelet. These images indicate a large stagnant region inside the flame and a large toroidal vortex ring at the base of the flame which entrains ambient fluid into the flame. Near the flame tip at the top of the image, the flow pattern, seen in a moving frame, consists of a pair of saddle points (stagnation points) on either side of the centerline with upward flow on the centerline. The flow is axisymmetric and so the pair of stagnation points are, in fact, part of a circular stagnation line which surrounds the flame tip. The flow pattern near the base of the flame has a saddle point on the centerline which feeds entrained fluid into a large toroidal vortex which surrounds the flame stem. Within the flame the velocities are too low to permit the flow pattern to be fully resolved everywhere; however, the only pattern which is consistent with the topology of the surrounding flow is for the flame interior to be regarded as an effective volume source. This is a consequence of the volumetric expansion associated with heat release at the flame front.

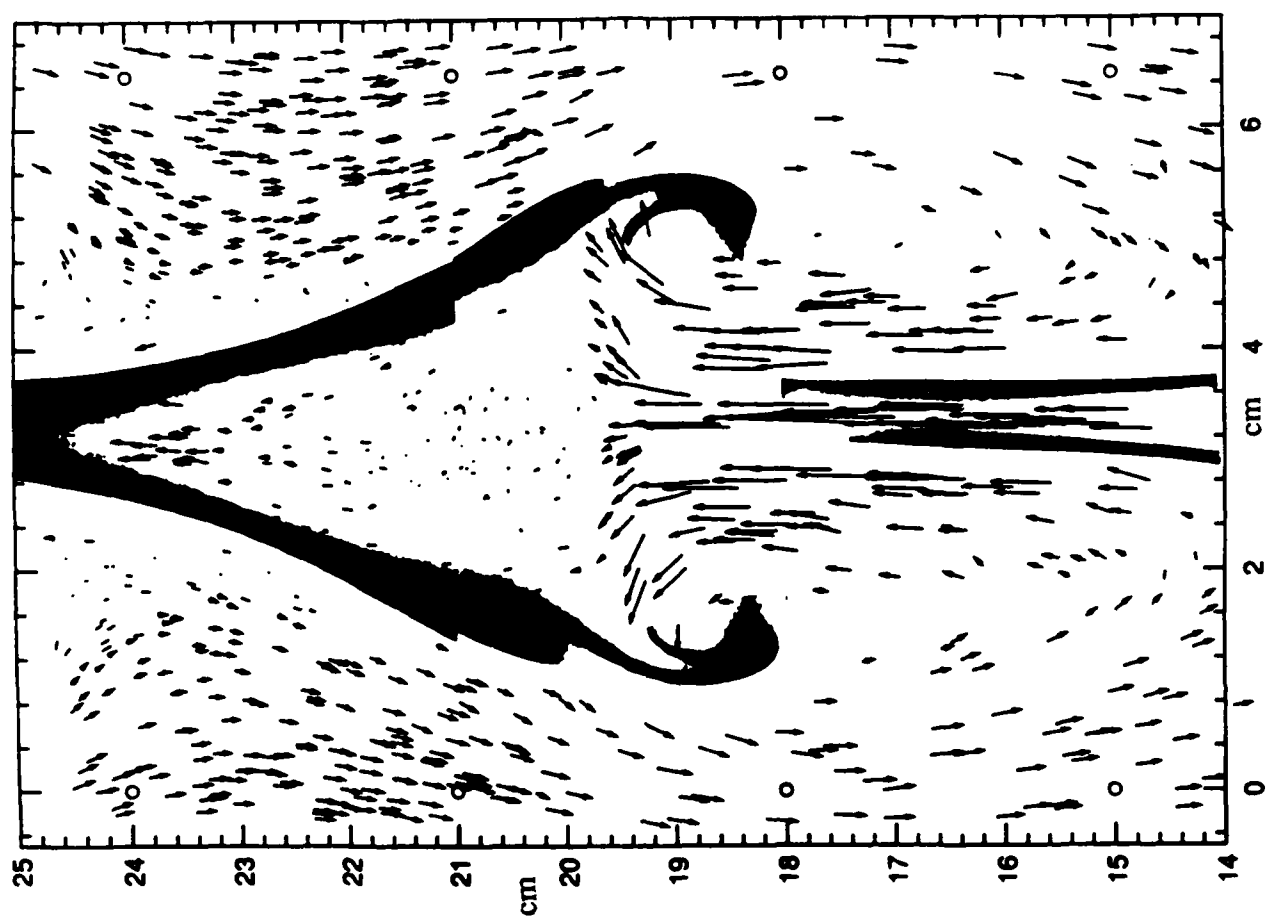
The measurements show a high strain rate at the base of the flame. The absolute value of the peak strain rate increases from 304 sec^{-1} at the 0° phase angle to 402 sec^{-1} at the 45° angle then decreases slightly to 383 sec^{-1} at the 90° angle. Measurements of the OH concentration field indicate that flame extinction occurs near the base of the flame on the flow centerline between these two phases. This is consistent with the loss of flame luminosity which occurs in the same region as can be seen in Figure 1b. As the flame evolves, the region of high strain pushes into the flame and decreases the size of the stagnant region. Studies have indicated that the extinction limit for a strained, steady, laminar methane-air diffusion flame at the stagnation point of a porous cylinder occurs at strain rate levels of about $330\text{-}410 \text{ sec}^{-1}$. This is consistent with the values of strain observed at the base of the present flame where OH images reveal flame extinction along the centerline.

The results of the present study indicate that topological methods may be usefully employed to characterize the structure of such a complex reacting flow. When viewed in a frame of reference moving with the flamelet, the flow structure becomes apparent as a pattern of elementary flow features such as saddles and nodes which have been previously observed in non-reacting flows. The interior of the flame is seen to be nearly stagnant, and the primary fluid mechanical role of

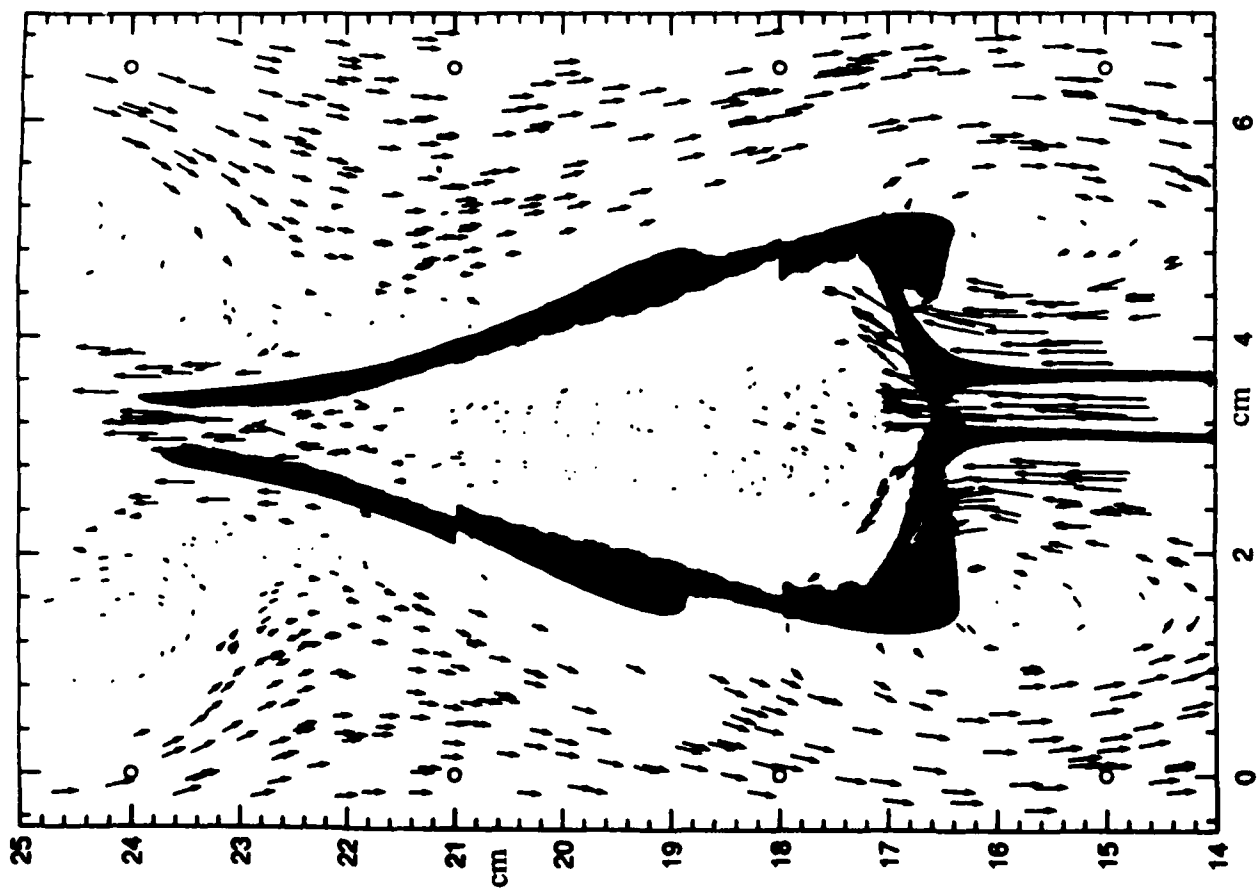
the flame is that of a volume source. Relatively high local strain rates, produced by the vortical motion, are found in a region where flame extinction occurs. These observations suggest that effects of flame extinction and volumetric expansion associated with heat release should be included in models of flame-vortex interactions.

PUBLICATIONS

- (1) Strawa, A. W. and B. J. Cantwell , "Visualization of the Structure of a Pulsed Methane-air Diffusion Flame", Physics of Fluids **28** : 2317-2320, 1985.
- (2) Strawa, A.W., "An Experimental Investigation of the Structure of an Acoustically Excited Diffusion Flame", PhD thesis and Stanford University Dept of Aero/Astro report 558, August 1986.
- (3) Lewis, G.S., B.J. Cantwell and A. Lecuona, "The Use of Particle Tracking to Obtain Planar Velocity Measurements in an Unsteady Laminar Diffusion Flame", paper 87-35, Western States Combustion Institute Meeting, April 1987.
- (4) Strawa, A. W., B. J. Cantwell, "Investigation of an Excited Jet Diffusion Flame at Elevated Pressure", J. Fluid Mech (to appear), 1988.
- (5) Lewis, G. S., B. J. Cantwell, U. Vandsburger and C. T. Bowman, "An Investigation of the Structure of a Laminar Non-premixed Flame in an Unsteady Vortical Flow", accepted for the 22nd Symposium (International) on Combustion, The Combustion Institute, Pittsburgh, 1988.



(b)



(a)

Figure 1

CARBON MONOXIDE AND TURBULENCE-CHEMISTRY INTERACTIONS:

BLOWOFF AND EXTINCTION OF TURBULENT DIFFUSION FLAMES

AFOSR Contract No.: F-49620-85-C-0035

Principal Investigators: S.M. Correa and A. Gulati

General Electric Corporate Research and Development Center

Schenectady, New York 12301

SUMMARY

The goal of this program is to understand the physical phenomena responsible for localized extinction in non-premixed flames due to intense turbulence. We use a non-premixed 40% CO/10% H₂/50% N₂ Re = 15,000 jet flame burner in co-flowing air stabilized with a coannular premixed pilot. The large amount of carbon present called for modification of the Raman system used for laser-based spectroscopic data on major species and temperature. The data show significant temperature decrements due to finite-rate chemistry but no evidence of localized extinction. A computational model for a jet flame under such conditions has been developed. In the model, combustion chemistry is represented by two-body shuffle reactions and three-body recombination reactions. The scalar dissipation field is examined for critical values below which the two-body reactions are assumed to be in partial equilibrium and above which they are assumed to be frozen and the gas therefore unburned. The kinetics of the recombination reactions are activated for the former fraction of the gas. This approach has been implemented in a shear-layer finite-volume averaged Navier-Stokes model with k-ε/assumed shape pdf sub-models for turbulence. The model is useful for moderate to high Reynolds number turbulent flames.

THEORY

The flamelet approach¹ has been advanced to account for finite-rate chemistry in turbulent flames. An important shortcoming of traditional flamelet models is that in practice laminar flames are not necessarily thin compared with turbulent scales. In H₂ and CO/H₂ flames, there are two distinct scales associated with the chemistry, that corresponding to two-body chain-branching or propagating (shuffle) reactions and that corresponding to three-body radical recombination reactions. In flames below about 10 atm., the former reactions are fast compared with the latter and with fluid mechanical mixing processes. This disparity implies that in turbulence the two-body reaction zones would remain comparatively thin while the three-body zones would overlap, leading to distributed reaction zones which are incompatible with the laminar flamelet analysis.

The significance of the difference between the rates of the two-body and the three-body reactions is apparent from comparisons of data with the partial equilibrium model for CO/H₂ in an Re = 8500 (cold jet) flame.² The data indicated negligible or no local extinction - i.e., none of the Raman data showed low temperature in flammable gas - but large amounts of superequilibrium OH, up to factors of 5. The model agreed well with these data. One may conclude that the time-scales of turbulence in such flames are short enough to interfere with three-body recombination chemistry, i.e., a Damköhler number based on the recombination reactions is of O(1). The time-scales are still too long to disturb the two-body reactions ($D_{2\text{-body}} > > 1$) and so there is little or no local extinction. This behavior is consistent with the notion that the abrupt transitions in a stretched flamelet are characteristic of high-activation energy (shuffle) reactions while well-distributed reaction zones are characteristic of low or zero activation-energy (recombination) reactions. Here it is proposed to retain the partial equilibrium model, successful for radicals and thermal NO_x^{2,3,4}, but with the quenched flamelet approach to the two-body reaction zone to account for extinction as well.

The partial equilibrium model for CO-H₂-air systems has been described previously.² CO/H₂ mixtures are used as the fuel because they are intermediates in hydrocarbon combustion and have simpler chemistry. These mixtures are also important as synthetic fuels. The model has been used in conjunction with both k-ε/ assumed shape probability density function (pdf)⁴ and full velocity-scalar joint pdf/Monte-Carlo models,^{4,5} with good success on velocity, temperature, major species and OH in a Re = 8500, jet flame of medium BTU gas (40% CO, 30% H₂, 30% N₂) in air. The partial equilibrium model is here applied to LHC gas (Low Hydrogen Content, 40% CO/10% H₂/50% N₂) and accounts for ten species (O₂, H₂, N₂, CO, CO₂, H₂O, O, OH, H, HO₂), temperature and density in terms of the mixture fraction (ξ) and radical pool reaction progress variable (η). As in the case of medium BTU gas², the temperature decreases as η decreases below the equilibrium value of unity while OH has the expected superequilibrium peak. The degree of superequilibrium in stoichiometric gas [$(OH)_{max}/(OH)_{eq}$] is approximately 6, larger than that in the medium BTU gas.²

Since the mean scalar dissipation rate decreases as the jet fluid flows downstream, the region of intense stretch experiences a transition through the critical strain rate. The two-body reactions are assumed to be co-located with this region and are further assumed to immediately reach partial equilibrium. This is analogous to the approach used by Liew et al.⁶ who assumed a burnt flamelet state for the flamelets which were below a critical scalar dissipation rate. In the present case only the 2-body reactions are assumed to reach (partial) equilibrium; the recombination reactions commence and drive the system towards full chemical equilibrium. Thus this model has both flamelet features and partial equilibrium features. The argument by which the local pdf of scalar dissipation rate is obtained has been described previously.⁶

The model is easily explained in one dimension. If the pdf's for local strain X at an upstream and downstream location are denoted by P_u(X) and P_d(X), respectively, and the probabilities of 2-body reaction equilibration are P_u(X < X_{cr}) and P_d(X < X_{cr}), then it follows that the probability that the recombination reactions "just" started is P_d(X < X_{cr}) - P_u(X < X_{cr}). The gas which undergoes this transition is added to the gas described by the reactedness transport equation with an initial value of $\tilde{\eta} = 0$. The increments are calculated by evaluating the differential change in the probability P(X < X_{cr}) along the mean streamlines.

For the fraction of gas which is burning, the joint pdf for the occurrence of values of the two thermochemical variables is needed. Here occurrences of the two variables are assumed to be uncorrelated, and so the joint pdf may be assumed to be separable.² The shear-layer equations are solved numerically in axial distance-stream function coordinates. They consist of the axial velocity, turbulence kinetic energy k, dissipation rate ε, mean and variance of mixture fraction and mean reaction progress variable. Boundary conditions on the variables correspond to fully-developed turbulent fuel flow with appropriate assumed intensity and length scale of turbulence.

EXPERIMENTAL SETUP

The subsonic, low turbulence jet diffusion flame combustor has been used extensively for experimental studies of laminar, transitional and turbulent H₂ diffusion flames in the past. The fuel in this study consists of LHC gas defined above. To stabilize the high Reynolds number flame (Re = 15,000, jet exit velocity = 80 m/s), the burner was modified to include a co-axial annular premixed pilot flame.

The turbulent flame provides a fluctuating strain field which can cause local extinction when the critical strain rate is exceeded locally. Extensive regions of such localized extinction spots can result in eventual liftoff or blowoff of the flame. The pilot-stabilized burner (Fig. 1) is designed to provide a stable flame in the region of large strain near the exit yet devoid of gross unsteady features. The pilot flame consists of a stoichiometric mixture of the LHC gas and air ($\xi_p = 0.43$), which simplifies modeling by reducing the mixing to a two-stream problem. The premixed annular burner has an open area five times that of the main jet. The exit velocity of the premixed products is estimated to be 20 m/s based on an estimated post-flame temperature of 2000 K. The co-flowing air velocity in the tunnel was 5 m/s. The fuel mixture is chosen to maximize the probability of local extinction. The value of α_c , the critical strain as determined in a counterflow diffusion flame burner, increases from 400 s⁻¹ corresponding to 2% H₂ to 1350 s⁻¹ corresponding to 15% H₂, and is 950 s⁻¹ for the LHC fuel used here. This value is much lower than the estimate (12,000 s⁻¹) for H₂ and the estimate (greater than 2000 s⁻¹) for medium BTU gas (40% CO, 30% H₂, 30% N₂) and is of the same order as α_c for methane flames ($\approx 400\text{s}^{-1}$). Thus the fuel chosen should yield a turbulent flame in which the probability of extinction is significant.

The Raman diagnostic system used here is similar to that used for previous studies with modifications appropriate for the more luminous LHC gas. Because of increased chemiluminescence due to $\text{CO} + \text{O} \rightarrow \text{CO}_2$, two photomultiplier tubes were added to monitor the chemiluminescence from the flame. The flame luminescence was found to be very broad-banded throughout the visible region. A polarization filter was used in the collection optics system to reduce flame luminescence. The polarization vector was aligned to pass the horizontally polarized Raman and Rayleigh scattered light. Typically, 200 measurements were made at each station although 2000 shots were recorded at some locations for statistical purposes. The system was calibrated extensively using 100% pure gases and well-characterized premixed porous plug burners.

The instantaneous temperature at every shot was determined using three independent methods. The Stokes-anti-Stokes (SAS) ratio method based on the nitrogen element yields the value of the temperature directly. The second method is based on an iteration scheme in which an initial temperature is guessed, from which the mole fractions of all major species are calculated using their measured vibrational intensities. The mole fractions are then corrected using high temperature correction factors. This process is repeated until the sum of the mole fractions is unity, and converges in two to three iterations because the correction factors are relatively weak functions of the temperature. Since the N_2 channel is affected most by the luminosity of the flame, the SAS measurements were susceptible; hence, Rayleigh scattering was used to obtain another measurement of temperature. Changes in the Rayleigh cross-section of the mixture were obtained from the Raman data for the major species.

DISCUSSION

Since the region of maximum strain rates is within the first twenty diameters, comparisons between predictions and the data have been conducted at the axial planes $x/d = 10$ and 20 (d = fuel tube diameter). The temperatures measured by the three methods (N_2 SAS ratio, sum of mole fractions, Rayleigh) agree well. The mean temperature at $x/d = 10$ is predicted well (Fig. 2) except for the cool fuel-rich core of the flame, where partial equilibrium is expected to break down.² The comparisons at $x/d = 20$ are very similar. Indirect evidence of the probability of two-body equilibration (combustion) is available from mixture-fraction vs. temperature scattergrams constructed from the Raman data (Figs. 3,4). The large variations of the temperature data from the adiabatic equilibrium curve indicate that local temperature-decreasing mechanisms are active. Figure 3 bears no evidence of local extinction, however, even at this location ($x/d = 10$) where the strain rates are high; extinction would have manifested itself in low temperatures in the flammable range of samples. The temperature scatter is apparently caused by the slowness of recombination reactions, a contention which is supported by non-unity values of the computed mean radical pool reaction progress variable. [A possible explanation of why hydrocarbon flames exhibit localized extinction effects may be the propensity of alkyl species to consume radicals and terminate the oxyhydrogen chain.] The model is expected to be useful over a range of turbulence-chemistry interactions extending from moderate (superequilibrium radicals, moderate temperature decrement, enhanced thermal NO_x) to strong (large temperature decrement, local extinction). Velocity and initial conditions will be measured next, and higher speed flames will be studied.

REFERENCES

- [1] Peters, N.: *Prog. Energy. Combust. Sci.* 10, 319 (1984)
- [2] Correa, S.M., Drake, M.C., Pitz, R.W. and Shyy, W.: *Twentieth Symposium (International) on Combustion*, The Combustion Institute, 1984, p. 337.
- [3] Drake, M.C., Correa, S.M., Pitz, R.W., Shyy, W., and Fenimore, C.P.: *Combust. Flame* 69, 347 (1985).
- [4] Correa, S.M., Gulati, A. and Pope, S.B.: "Assessment of Partial-Equilibrium Model for Turbulent Syngas Flames," to appear in *Combustion and Flame*, (1988).
- [5] Pope, S.B. and Correa, S.M.: *Twenty-first International Symposium on Combustion*, The Combustion Institute, 1986, p. 1341.
- [6] Liew, S.K., Bray, K.N.C. and Moss, J.B.: *Combust. Flame* 56, 199 (1984).

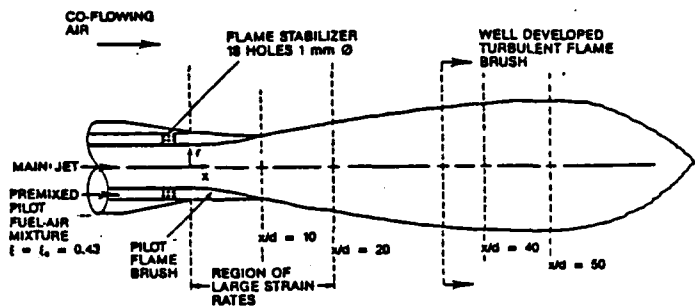


Figure 1. Pilot-stabilized non-premixed turbulent CO/H_2 flame.

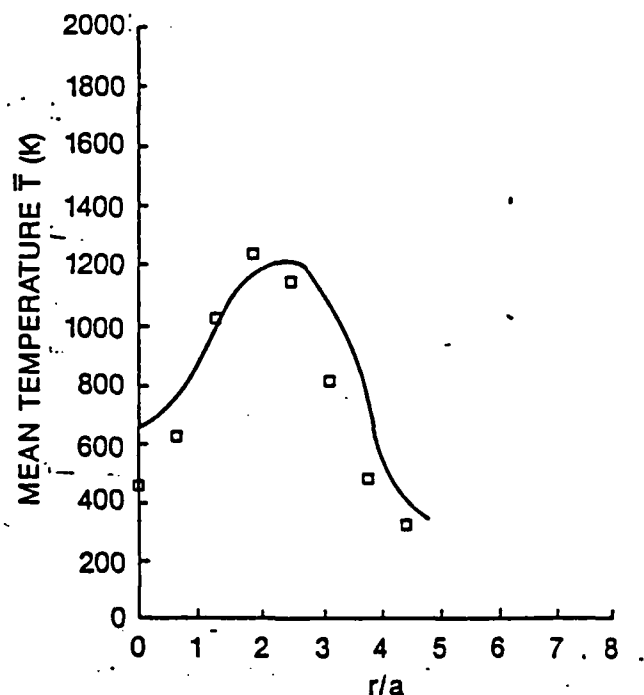


Figure 2. Comparison of prediction and data on mean temperature at $x/d = 10$ ($a = d/2$).

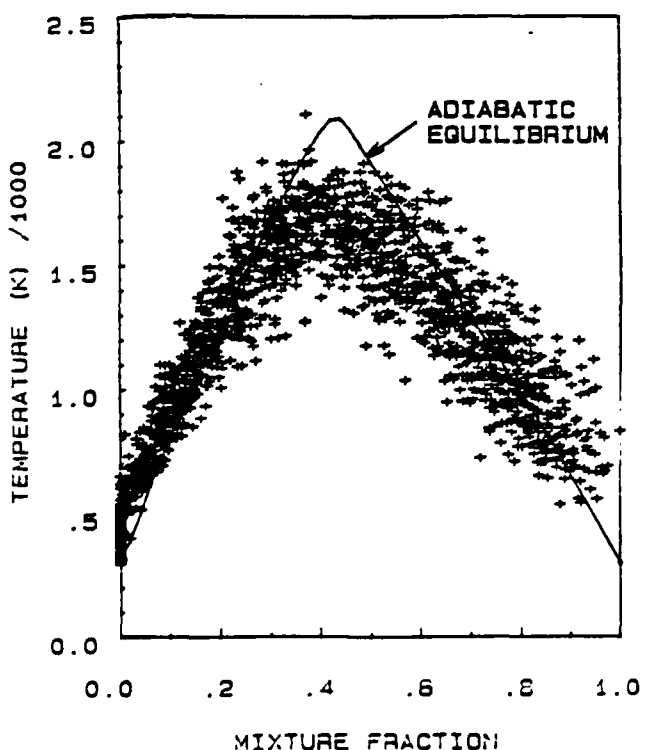


Figure 4. Temperature-mixture fraction scattergram at $x/d = 20$.

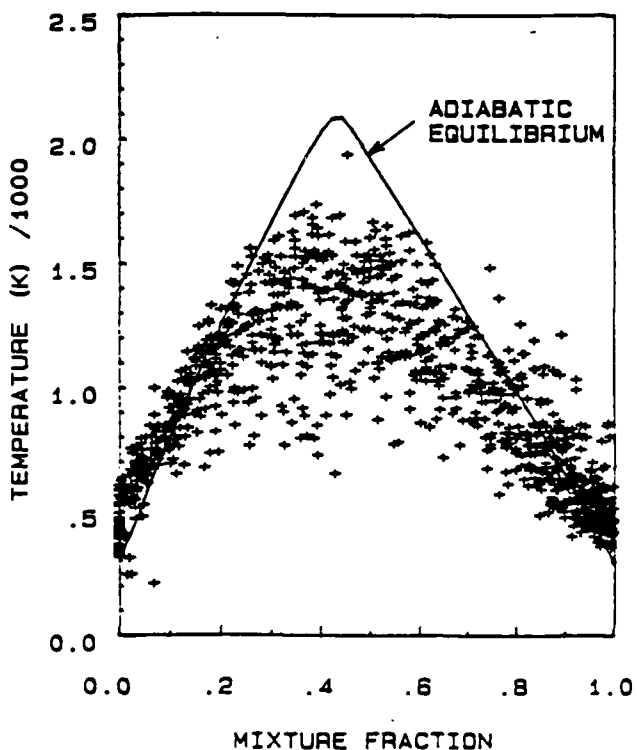


Figure 3. Temperature-mixture fraction scattergram at $x/d = 10$.

CHEMICAL REACTIONS in TURBULENT MIXING FLOWS

AFOSR Grant 83-0213 and 88-0155

P. E. Dimotakis, J. E. Broadwell and A. Leonard

*Graduate Aeronautical Laboratories
California Institute of Technology
Pasadena, California 91125*

Summary/Overview

The purpose of this research is to conduct fundamental investigations of turbulent mixing, chemical reaction and combustion processes in turbulent, subsonic and supersonic flows. Progress in this effort thus far has uncovered *important deficiencies in conventional modeling of these phenomena, primarily in subsonic turbulent flow, and offered alternative suggestions and formulations to address some of these deficiencies.* While continuing with our efforts in subsonic, incompressible turbulence, we are extending our work to supersonic (compressible) turbulent mixing investigations, where *virtually no modeling schemes exist that can accommodate the effects of compressibility on the mixing and combustion/flow coupling processes.* This program is comprised of an experimental effort, an analytical modeling effort, a computational effort, and a diagnostics development and data-acquisition effort, the latter as dictated by specific needs of our experiments.

Our approach is to carry out a series of detailed theoretical and experimental studies primarily in two well-defined, fundamentally important flow fields: free shear layers and axisymmetric jets. To elucidate molecular transport effects, experiments and theory concern themselves with both liquids and gases.

Technical discussion

Our experimental investigations of the effects of free stream density ratio in gas phase, subsonic shear layers are nearing completion. The first phase of our findings, will be reported at the 1st National Fluid Dynamics Congress (NFDC), this coming July (Frieler & Dimotakis 1988). In the course of these investigations, which were conducted using H_2 , NO and F_2 as reactants, in mixtures of diluent gases as required to produce the desired density ratios, we have discovered *important new phenomena in the coupling of differential diffusion and finite chemical kinetics effects, that cannot be explained by either process alone.* This arises because H_2 possesses a significantly higher diffusivity than the other reactant/diluent species, coupled with the fact that the $H_2 + F_2$ reaction is catalyzed by the presence of NO (which is premixed with but diffuses slower than H_2). This complication could also play a possibly important role in the modeling of $H_2 + air$ systems, as would be required in hypersonic RAMJET propulsion, for example. In particular, in the limit of fast but finite chemical rate, the chemical product is formed at strained interfaces, across which the chemical species composition cannot be described by a conserved scalar. We are making progress in solving the unsteady, strained interface diffusion problem, coupled with a full finite chemical kinetics calculation for the $(H_2 + NO + diluent_1) + (F_2 + diluent_2)$ system, with an eye to incorporating the solutions in the shear layer turbulent mixing model by Dimotakis (1987).

In our efforts to extend these experimental studies to supersonic flow¹, we have almost completed the design of the new supersonic $H_2 + F_2$ combustion, shear layer facility (Hall, Dimotakis, Papamoschou & Frieler 1987) and have begun taking delivery of some of the facility components. In particular, delivery of the 100 Atm, 600 K pressure vessel is expected shortly. It was decided to design and fabricate the fast throttling valve for the ≈ 3 sec run time of the blow-down facility in house (presently in fabrication). The remainder of the preliminary design is complete with orders to outside vendors, detailed design of the various components for in-house fabrication, or actual fabrication, in progress. We note here that we have taken some care in the new design so as not to preclude subsonic flow operation, even though the new facility is primarily designed for bi-sonic shear layer, i.e. $1.5 \leq M_1 \leq 3$, $M_2 \leq 0.3$, in its next phase of operation². At this writing, we expect to.

June-July 1988: begin dismantling the subsonic facility,

next 6 months: fabrication, delivery, assembly and integration.

March-April 1989: testing and calibration, first supersonic cold (non-reacting) runs.

June-July of 1989: first supersonic hot (combusting) runs.

We are excited by progress in this part of the effort and are looking forward to the realization of this time-table.

We have completed the first part of our compressible flow, shear layer (linear) hydrodynamic stability calculations. In this part of the effort, an attempt was made to investigate whether the unifying ideas of Papamoschou & Roshko (1986) and Papamoschou (1986). These authors found that the convective Mach number represents the relevant scaling parameter gauging the effects of compressibility in the shear layer growth rate. This is defined with respect to each stream as

$$M_{c1} = \frac{U_1 - U_c}{a_1}, \quad \text{and} \quad M_{c2} = \frac{U_c - U_2}{a_2}, \quad (1)$$

respectively. The quantity U_c represents the convective velocity of the large scale structures and was estimated as \tilde{U}_c by Papamoschou & Roshko assuming that the dynamic pressures match at stagnation points in the flow (Coles 1981, Dimotakis 1986) and computed assuming that the flow along the respective paths from each stream can be approximated as isentropic, i.e.

$$\left[1 + \frac{\gamma_1 - 1}{2} \left(\frac{U_1 - \tilde{U}_c}{a_1} \right)^2 \right]^{\gamma_1 / (\gamma_1 - 1)} = \left[1 + \frac{\gamma_2 - 1}{2} \left(\frac{\tilde{U}_c - U_2}{a_2} \right)^2 \right]^{\gamma_2 / (\gamma_2 - 1)}. \quad (2)$$

Using a hyperbolic tangent as an approximation to the velocity profile, we have investigated the maximum amplification rate for several velocity ratios and temperature ratios of the same gas across the shear layer. Our calculations confirm the Papamoschou & Roshko findings, namely that the convective Mach number scales the effects of compressibility. In these calculations, the convective velocity is estimated as $\tilde{U}_c = c_r$, where c_r represents the

¹ Co-sponsored by AFOSR (URI) Contract F49620-86-0113

² Future extensions in Mach number have also not been precluded.

(real part) of the unstable mode convective velocity. This is found to be very close to \tilde{U}_c , as given implicitly by Eq. (2), for $M_c \leq 1$, but not so for $M_c > 1$. As opposed to the Papamoschou & Roshko findings, however, the growth rate in these calculations decreases to zero as $M_c \gg 1$. These results are being reported (Zhuang, Kubota & Dimotakis 1988) at the 1st NFDCC. In calculations since, we are finding that a finite growth rate for large M_c does result from a more complicated velocity and/or density profile, as in fact was the case in the Papamoschou & Roshko experiments.

Our gas phase, matched density, low to moderate Reynolds number turbulent jet mixing experimental studies, using high time/space resolution laser Rayleigh scattering diagnostics, have been completed (Dowling 1988). In our preliminary investigations, which will also be reported at the 1st NFDCC (Dowling & Dimotakis 1988), we discovered that the actual molecular diffusion scales are not as small as our original conservative calculations had suggested they might be. This serendipity, coupled with the use of a new, low-noise, solid state photodetection system developed for the purpose (Dowling, Lang & Dimotakis 1988), permitted the investigations to be carried out at Reynolds numbers we had not initially imagined would have been attainable under our strict resolution specifications. Several important conclusions can be drawn from this work.

- At each Reynolds number, the far field ($x/d > 20$) jet flow and ensuing turbulent mixing can be described by a *strict similarity along rays that extends throughout the spectrum of scales at the Reynolds number of the flow*.
- The local mixing (molecular diffusion) rate is found to span roughly *three orders of magnitude*, a fact that has to be contended with in modeling mixing and combustion in turbulent jet mixing flows.
- The probability density function (PDF) of the jet fluid concentration, *when scaled by the local mean*, is found to be very nearly Reynolds number independent. The local mean, however, *does not*. Consequently, the absolute PDF shows interesting Reynolds number effects, which suggest a possible revision of some of the tenets in turbulent jet flow descriptions.
- Using the measured jet centerline PDFs, flame length calculations were performed and compared with the (liquid phase) flame length measurements of Dahm & Dimotakis (1985) and Dahm (1985). The resulting values are close, but differ by an amount that may not be attributable to possible experimental difficulties, or the manner in which the calculations were performed. This raises the possibility that Schmidt number effects may play a role in turbulent jet mixing.

We will attempt to extend these measurements to the limits of the Reynolds number capability of the experiment in the near future.

These investigations, as well as earlier investigations in shear layer mixing and combustion studies, suggested that subtle Reynolds number effects characterize these phenomena. To extend the dynamic range of Reynolds number, a second facility to study Reynolds number, Damköhler number, heat release, buoyancy and density ratio effects in gas phase, chemically reacting turbulent jets is nearing completion³. It is a 0.1 *Atm* to 10 *Atm* combus-

³ Co-sponsored by the Gas Research Institute

tion facility, capable of handling reactant gases like H_2 , F_2 , NO , as well more conventional oxidizer/fuel pairs. Depending on the specifications of the experiments in each case, a Reynolds number range as high as three orders of magnitude may be achievable in this new facility. Cold flow shadowgraphs have been obtained, using different jet and reservoir gases. Hot flow experiments are expected to begin this summer.

Models for chemical reactions in turbulent shear layers and axisymmetric jets have been under development for some time. The basic ideas for an important part of this effort are described in Broadwell & Breadenthal (1982) for the shear layer and Broadwell (1987) for the jet. A generalization of the shear layer model to the case of finite chemical reaction rates is described in Broadwell & Mungal (1986) and will be presented at the 22nd International Combustion Symposium in August 1988. The recently completed work on jet mixing, described above (Dowling 1988), provides new evidence in support of these models. In particular, a critical idea underlying both of these models leads to a mixing rate that is the sum of two terms: one independent of Reynolds number Re and the Schmidt number Sc , and the other dependent on the product ($Re Sc$). Dowling finds a centerline PDF, which when scaled by the local mean, is independent of Re , for his limited Re range, and in addition notes that his (local mean scaled) PDFs agree quantitatively with those measured by Dahm (1985) at a much higher product of Sc and Re . In contrast, at radial positions near the edge of the jet, the mean-mixed fluid composition is higher in liquids ($Sc = 600$, Dahm 1985), than it is in the present experiments conducted in a gas. Interpreted in terms of the model, the fluid at, and near, the centerline is a homogeneous mixture with a composition independent of Re and Sc , while the fluid near the edges is in three states:

1. pure reservoir fluid.
2. the homogeneous mixture, and
3. flame sheets, the volume fraction of the latter depending on $(Re Sc)^{-1/2}$.

Additional support for this interpretation comes from noting that pure reservoir fluid is found only near the jet edge and recalling the flame sheets lie between jet and pure reservoir fluid.

In the computational part of this program, our efforts to increase the efficiency of vortex element calculations have continued. Using hierarchical clustering techniques, targeted reductions from $O(N^2)$ to $O(N \log N)$ have in fact achieved $O(N)$ in the computational effort, where N is the number of vortex computational elements. In a second part of this program, non-linear dynamical systems methods have been used to analyse the entrainment and mixing of a vortex line pair in an unsteady strain field in two-dimensional flow. The results (Rom-Kedar, Leonard & Wiggins 1988) represent the first time, to our knowledge, dynamical systems theory has been used to obtain a quantitative measure of this behavior.

References

BROADWELL, J. E. [1987] "A model for reactions in turbulent jets: Effects of Reynolds, Schmidt and Damköhler numbers". US-France Workshop on Turbulent Reactive Flows, 7-10 July 1987 (Rouen, France).

BROADWELL, J. E. and MUNGAL, M. G. [1986] "The effects of Damköhler number in a turbulent shear layer", GALCIT Report FM86-01.

BROADWELL, J. E. and BREIDENTHAL, R. E. [1982] "A Simple Model of Mixing and Chemical Reaction in a Turbulent Shear Layer". *J. Fluid Mech.* 125, 397-410.

COLES, D. [1981] "Prospects for Useful Research on Coherent Structure in Turbulent Shear Flow", *Proc. Indian Acad. Sc.* 42(2), 111-127.

DAHM, W. J. A. [1985] "Experiments on Entrainment, Mixing and Chemical Reactions in Turbulent Jets at Large Schmidt Numbers", Ph. D. thesis, California Institute of Technology.

DAHM, W. J. A. and DIMOTAKIS, P. E. [1985] "Measurements of Entrainment and Mixing in Turbulent Jets". *AIAA 23rd Aerospace Sciences Meeting*, 14-17 January 1985 (Reno, Nevada), AIAA Paper No. 85-0056.

DIMOTAKIS, P. E. [1986] "Two-Dimensional Shear-Layer Entrainment", *AIAA J.* 24(11), 1791-1796.

DIMOTAKIS, P. E. [1987] "Turbulent shear layer mixing with fast chemical reactions", US-France Workshop on Turbulent Reactive Flows, 7-10 July 1987 (Rouen, France), GALCIT Report FM87-01.

DOWLING, D. R. [1988] "Mixing in gas phase turbulent jets", Ph. D. thesis, California Institute of Technology.

DOWLING, D. R. and DIMOTAKIS, P. E. [1988] "On mixing and structure of the concentration field of turbulent jets", *First National Fluid Dynamics Congress*, 24-28 July 1988 (Cinc., Ohio),

DOWLING, D. R., LANG, D. B. and DIMOTAKIS, P. E. [1988] "A New Laser-Rayleigh Scattering photodetection system", submitted to *Exp. in Fluids* (15-May-1988).

FRIELER, C. E. and DIMOTAKIS, P. E. [1988] "Mixing and Reaction at Low Heat Release in the Non-Homogeneous Shear Layer", *First National Fluid Dynamics Congress*, 24-28 July 1988 (Cinc., Ohio),

HALL, J., DIMOTAKIS, P., PAPAMOSCHOU, D. and FRIELER, C. [1987] "Design Overview of the Supersonic Hydrogen-Fluorine Facility", V1.1, GALCIT Internal Report (30 September 1987).

PAPAMOSCHOU, D. [1986] "Experimental Investigation of Heterogeneous Compressible Shear Layers", Ph. D. thesis, California Institute of Technology.

PAPAMOSCHOU, D. and ROSHKO, A. [1986] "Observations of Supersonic Free Shear Layers", *AIAA 24th Aerospace Sciences Meeting* (Reno, Nevada), AIAA Paper 86-0162.

ROM-KEDAR, V., LEONARD, A. and WIGGINS, S. [1988] "An Analytical Study of Transport, Mixing and Chaos in an Unsteady Vortical Flow", submitted to the *J. Fluid. Mech.*

ZHUANG, M., KUBOTA, T. and DIMOTAKIS, P. E. [1987] "On the stability of inviscid, compressible free shear layers". *First National Fluid Dynamics Congress*, 24-28 July 1988 (Cinc., Ohio).

NUMERICAL SIMULATION OF TURBULENT COMBUSTION USING VORTEX METHODS

(AFOSR Grant No. 84-0356)

Principal Investigator:

Ahmed F. Ghoniem

Department of Mechanical Engineering
Massachusetts Institute of Technology
Cambridge, MA 02139

SUMMARY/OVERVIEW:

The objectives of this research are:

- I. The development of accurate numerical methods which can be utilized in the integration of the time-dependent, three-dimensional Navier-Stokes equations and the energy and species conservation equations for high values of the Reynolds and Peclet numbers and moderate values of the Damkohler number, and when the heat release is large with respect to the internal energy of the flow.
- II. The investigation of the mechanisms of turbulence-combustion interactions on the basis of the solutions obtained from the numerical simulations, and the study of how these interactions can be manipulated to provide more control over the burning process in turbulent shear flows.

These goals are being accomplished by developing grid-free, Lagrangian schemes: the vortex element and the transport element methods, which can be used to simulate fields that develop large velocity and scalar gradients. For the purpose of validating these schemes and analyzing turbulence-combustion interactions, we are using simulations of the reacting shear layers in two and three dimensions and in cases when the fuel and oxidizer are initially flowing in separate streams, and when the premixed reactants and products are initially flowing in separate streams. Attention has been focused on the low Mach number limit in which spatial pressure variations are neglected in the thermodynamics of the problem. Effort is underway to extend the formulation to higher Mach number flows in which this restriction is relaxed. In the following, we discuss briefly some of the results of this research during the past year. Some of these results, as well as the numerical methodology, have been described in the publications listed in the References Section.

I. Numerical Simulation of a Reacting Shear Layer

Numerical simulation is applied to study mixing of a passive scalar in a spatially-developing shear layer, and to investigate the enhancement of the rate of chemical reaction in a mixing layer formed of separate fuel and oxidizer streams. The numerical simulations are performed using the transport element method, which we have developed as an extension of the vortex element method for the solution of the species and the energy conservation equations at high heat and mass transfer Peclet numbers. The method is Lagrangian and grid-free, and is based on the accurate discretization of flow gradients among finite elements which are transported along particle paths. The core functions of the elements are chosen to guarantee high spatial accuracy, and may be deformed to capture mild strain field. Computational elements are only utilized in areas of large flow gradients, and are redistributed whenever the flow map becomes severely distorted. The strengths of the elements are updated according to the source terms in the conservation equations [1,2].

In the spatially-developing, non-reacting mixing layer, we found that instantaneous scalar profiles exhibit mixing asymmetry and that the concentration fractions within the cores are skewed in favor of the

high-speed stream due to the asymmetry in the dynamic field. The velocity statistics and mixing statistics of a passive scalar agree well with the experimental measurements of Masutani and Bowman in a two-dimensional shear layer. The rms of the passive scalar and the computed scalar PDF, which can be used as measures of the mixedness, emphasize the effect of molecular diffusion on mixing for Peclet numbers in the range of 1000-10000.

We have started extending the computations to a chemically-reacting, spatially-developing layer assuming that the heat release does not change the density of the flow (the extension to a variable-density flow is described in the next section). This calculation is expensive because the computational domain involves $O(10)$ large eddies requiring $O(10000)$ elements to resolve the gradients accurately and because the chemical kinetics imposes a limit on the time step. We are in the process of developing and implementing time-saving algorithms based on domain decomposition and multi-pole expansion of the field of vortex elements to economize the computations.

II. Flow-Combustion Interactions in Premixed Combustion

The interactions between the flow field and the combustion process in a premixed shear layer are investigated using the results of numerical simulation using the transport element method. The reaction is governed by finite-rate Arrhenius kinetics for a single reactant, the density of the flow is allowed to vary with the temperature, and the Reynolds number is high. Heat release is moderate and molecular heat and mass diffusivities are finite, while the Mach number is small. The thickness of the reaction zone and that of the vorticity layer are of the same order of magnitude, i.e. turbulence scales are relatively small. Attention is focused on a single, or two eddies in a temporal shear layer to limit the computational time. Extension to a spatially developing layer is discussed in the previous section.

Results indicate that at the early stages, a reacting layer behaves like a laminar flame. During the growth phase of the eddy, the rate of burning is strongly enhanced by the entrainment fluxes that lead to the swelling of the reaction zone. During this phase, the total rate of product formation can be approximated by the unstrained laminar burning velocity times the flame length measured along the line of maximum reaction rate. Following the burning in the eddy core, the strain field along the eddy boundaries causes a noticeable thinning of the reaction zone, thus curbing the rise in the rate of burning. During this phase, the rate of burning expression in the wrinkled laminar flame theory should be modified to account for the change of the laminar burning velocity with strain.

Baroclinic vorticity generation, due to the acceleration of fluid elements in the density gradient of the flame, is found to be the most important mechanism by which combustion alters the flow field in the low Mach number limit. The baroclinic torque augments the vorticity within the core while it reduces the vorticity on its outer edges. This enhances the overall volumetric entrainment into the eddy core, and causes entrainment asymmetry with a bias towards the products stream. The modified vorticity field extends the growth, or entrainment period of the eddy and imparts on it an extra mean convective motion in the direction of the reactants stream [3,4,5].

In all steps of development, the numerical methods are validated by comparing the numerical solutions with the results of the linear stability theory of shear layer during the initial stages of development. This strategy is used to ensure that the physical model utilized in the numerical solution matches that used in the analytical, or semi-analytical study. Results for the late, non-linear stages are compared with idealized experimental data or results of conceptual models.

We are currently working on extending the formulation of the transport element method to higher Mach numbers by allowing the change in the pressure field due to the acceleration of the material elements to affect the thermodynamics of the motion. In this formulation, the thermodynamics is described by two state variables, the pressure and entropy, whose gradients are transported, along with the vorticity, by the transport elements. Therefore, all the machinery that has been developed to implement the low Mach number model in the transport element method is extendable to perform these computations of high Mach number flows.

III. Three-Dimensional Structure of Shear Flow

The main goal of this project is the extension of vortex methods to three-dimensional flows. The numerical scheme is based on the accurate discretization of the vorticity field into a number of finite-core, spherical vortex elements, and the transport of these elements along particle paths. The vortex scheme is then used to study the formation of streamwise vorticity which is known to be a precursor to self-turbulization and mixing transition in shear flows. To validate the scheme, and understand the underlying physics of the transition process, two examples are analyzed: an isolated finite-core vortex ring perturbed in the azimuthal direction, and a periodic shear layer simultaneously perturbed in its streamwise and spanwise directions.

Results obtained for both cases show the innate tendency of vorticity, initially aligned in the direction normal to the stream, to form coherent streamwise structures which have alternating vorticity signs in the spanwise direction. The formation of streamwise vorticity follows the "maturation" of the spanwise structure and the evolution of the former is energized by the strain field of the latter. While the streamwise vorticity is responsible for the added "turbulization" of the flow, leading to further mixing enhancement, it does not seem to lead to the disintegration of the two-dimensional basic structure. Results compare favorably with the conclusions of the linear stability theory and the available experimental results [6,7].

We have started to apply the method to simulate a shear layer. This problem is complicated by the following three factors: (1) the formation of strong strain field in the streamwise plane requires the implementation of a scheme of vorticity redistribution to capture the small scales; (2) the need to extend the formulation of the transport element method to three dimensions to study the mixing enhancement associated with the formation of streamwise vorticity; and (3) the computational requirements of the method. The last issue is being addressed implementing domain decomposition and fast particle solver in three dimensions, and by exploring the potential of utilizing fine-grain parallel processing technology in performing the required particle interaction.

REFERENCES:

1. Ghoniem, A.F., Heidarnejad, G. and Krishnan, A. "Numerical simulation of a thermally-stratified shear layer using the vortex element method," J. Comput. Phys., 75, 1988, in press.
2. Ghoniem, A.F., Heidarnejad, G. and Krishnan, A. "Turbulence-combustion interactions in a reacting shear layer," Lecture Notes in Engineering, Proceedings of the France-U.S.A. Joint Workshop on Turbulent Reactive Flows, July 1987, Rouen, France, Springer-Verlag, 1988, in press.
3. Ghoniem, A.F., Heidarnejad, G. and Krishnan, A. "On mixing, baroclinicity and the effect of strain in a chemically reacting shear layer," the AIAA 26th Aerospace Sciences Meeting, January 11-14, Reno, Nevada AIAA-88-0729.
4. Ghoniem, A.F., "Vortex methods in two and three dimensions," Invited paper for presentation at the 1st National Fluid Dynamics Conference, July 25-28, 1988, Cincinnati, Ohio, AIAA-88-3577.
5. Krishnan, A. and Ghoniem, A.F. "Origin and manifestation of flow-combustion interaction in a premixed shear layer," for presentation at the 22nd Symposium (International) on Combustion, 8-13 August, 1988, Seattle, Washington.
6. Knio, O. M. and Ghoniem, A. F. "On the formation of streamwise vorticity in turbulent shear flows," the AIAA 26th Aerospace Sciences Meeting, January 11-14, 1988/ Reno, Nevada, AIAA-88-0728.
7. Knio, O.M. and Ghoniem, A.F. "Numerical study of a three-dimensional vortex method," submitted for publication at J. Comput. Phys., April 1988.

AERODYNAMIC AND KINETIC PROCESSES IN FLAMES

(AFOSR Grant No. 85-0147)

Principal Investigator: Chung K. Law

University of California
Davis, California 95616

SUMMARY/OVERVIEW:

The flame response in realistic situations is governed by the detailed kinetics of chemical reactions, the diffusion of heat and mass, and the aerodynamic processes of stretching, turbulence, and large-scale flow nonuniformity. The present program aims to experimentally and theoretically study the dynamic and kinetic structure of laminar premixed and diffusion flames under atmospheric and elevated pressure environments, with the results being interpreted on the basis of aerodynamic stretching, preferential diffusion, and dominant reaction paths. During the reporting period we have (1) experimentally and numerically determined the laminar flame speeds of methane/air mixtures and found good agreement between them for two specific kinetic mechanisms used; (2) experimentally demonstrated the importance of preferential diffusion in soot formation in stretched diffusion flames; (3) experimentally determined the soot extinction limits by aerodynamic straining; and (4) experimentally studied the velocity and scalar fields of turbulent premixed flames in stagnation flow.

TECHNICAL DISCUSSION

During the reporting period the following specific projects have been conducted/completed.

1. Experimental and Numerical Determination of Laminar Flame Speeds of Methane/Air Mixtures under Reduced and Elevated Pressures

The laminar flame speed S_L^0 is an important physico-chemical parameter of a combustible mixture because it contains the basic information regarding its diffusivity, exothermicity and reactivity. However, in spite of the extensive efforts expended to accurately determine their values, wide systematic spreads in the reported experimental data still exist even though in many instances the experiments appear to have been carefully executed. Recently, it has been suggested that these systematic discrepancies are likely caused by the coupled effects of flame stretch and preferential diffusion. Specifically, it has been

demonstrated both theoretically and experimentally that the flame response can be qualitatively reversed when the flame stretch changes from positive to negative (e.g. expanding spherical flame versus the Bunsen flame), and when the mixture's effective Lewis number crosses a critical value typically around unity (e.g. lean methane/air and rich propane/air mixtures versus rich methane/air and lean propane/air mixtures).

A particularly serious implication of the stretch-induced flame response is the potential falsification of the kinetic information determined or validated through comparison between the numerically-calculated and experimentally-determined results. In view of this concern, we have recently proposed a stagnation-flow based methodology through which stretch effects can be systematically subtracted out such that S_L^0 can be unambiguously determined.

In the present investigation we have accurately determined the S_L^0 of methane/air mixtures under reduced and elevated pressures. While these data are of practical interest in their own right in terms of high-pressure combustion, we note in addition that these data also carry significant kinetic information because pressure not only influences the frequency of molecular collision but also differentiates the relative efficiencies of the two-body branching reaction versus the three-body termination reaction. Thus they provide additional constraints for the validation of the kinetic schemes.

The experimental data have been compared with the numerically-calculated values obtained by assuming different kinetic mechanisms. Consequently, the C₁ mechanism of Miller and C₂ mechanism of Warnatz both accurately reproduce our experimental data over the extensive concentration and pressure ranges tested. The relative superiority of these two schemes cannot be further resolved.

The present experimental data also demonstrates the existence of negative overall reaction orders in that there exist situations under which the mass burning rate of the flame, $\rho_u S_L^0$, decreases with increasing pressure. This is the first conclusive experimental demonstration of such a phenomenon, which is caused by the progressive dominance of the chain termination reaction with increasing pressure.

2. Preferential Diffusion and Concentration Modification in Sooting Counterflow Flames

An experimental investigation has been conducted on the influence of the mobility of inert additives on soot formation in counterflow propane/enriched-air and ethylene/air diffusion flames. By using helium, neon, argon or krypton as the inert additive, results show that while the inert mobility has practically no effect when a small amount of the inert is added to the oxidizer side, the influence is significant when it is added to the fuel side in that krypton, being the least mobile inert, yields the least. By relating the spatially-resolved soot volume fractions to the corresponding profiles of temperature, velocity and species concentrations, it is demonstrated that this influence on soot loading is likely caused by concentration modifications of the fuel and the soot precursors due to different mobilities of the inert additives.

3. Soot Extinction by Aerodynamic Straining in Counterflow Diffusion Flames

An experimental study has been performed with axisymmetric counterflow diffusion flames to investigate the relevant soot extinction limits in these aerodynamically-strained flames. The sooting limits are defined by the critical strain rate at which either soot luminosity, soot particle scattering, or fluorescence is negligible compared to the appropriate background signal. The critical strain rate is found to be greatest for the sooting limit based on the fluorescence signal, and least for that based on luminosity. The fluorescence signal, attributed to polycyclic aromatic hydrocarbons, yields a limit that can be interpreted as the extinction of the large soot precursors and is suggested to be an appropriate limit for identifying a completely nonsooting flame condition. The separate effects of flame temperature and fuel concentration on the critical strain rates for soot extinction have also been studied. Results show that they are both important parameters affecting the sooting limits.

4. Velocity and Scalar Fields of Turbulent Premixed Flame in Stagnation Flow

Detailed experimental measurements of the scalar and velocity statistics of premixed methane/air flames stabilized by a stagnation plate are reported. Conditioned and unconditioned velocity of two components and the reaction progress variable are measured by using a two-component laser Doppler velocimetry technique and Mie scattering technique, respectively. Experimental conditions cover equivalence ratios of 0.9 and 1.0, incident turbulence intensities of 0.3 to 0.45 m/s, and global stretch rates of 100 to 150 sec⁻¹. The experimental results are analyzed in the context of the Bray-Moss-Libby flamelet model of these flames. The results indicate that there is no turbulence production within the turbulent flame brush and the second and third order turbulent transport terms are reduced to functions of the difference between the conditioned mean velocity. The results of normalization of these relative velocities by the respective velocity increase across laminar flames suggest that the mean unconditioned velocity profiles are self-similar.

PUBLICATIONS

1. "Extinction of Interacting Premixed Flames: Theory and Experimental Comparisons," by S. H. Chung, J.S. Kim and C. K. Law, Twenty-First Combustion Symposium, the Combustion Institute, Pittsburgh, PA, pp. 1845-1851, (1988).
2. "Structure and Propagation of Turbulent Premixed Flames Stabilized in A Stagnation Flow," by P. Cho, C. K. Law, J. Hertzberg, and R. K. Cheng, Twenty-First Combustion Symposium, the Combustion Institute, Pittsburgh, PA, pp. 1493-1499, (1988).
3. "Propagation and Extinction of Stretched Premixed Flames," by C. K. Law, D. L. Zhu, and G. Yu, Twenty-First Combustion Symposium, the Combustion Institute, Pittsburgh, PA, pp. 1419-1426, (1988).

4. "Theory of Nonadiabatic Flame Propagation in Dissociation Equilibrium," by B. H. Chao and C. K. Law, Twenty-First Combustion Symposium, the Combustion Institute, Pittsburgh, PA, pp. 1793-1802, (1988).
5. "Flame Curvature and Preferential Diffusion in the Burning Intensity of Bunsen Flames," by C. K. Law, P. Cho, M. Mizomoto, and H. Yoshida, Twenty-First Combustion Symposium, the Combustion Institute, Pittsburgh, PA, pp. 1803-1809, (1988).
6. "Extinction of Counterflow Diffusion Flames with Branching-Termination Chain Mechanisms: Theory and Experiment," by C. K. Law, Lecture Notes in Physics Series, Vol. 229: Mathematical Modelling in Combustion Science (J. Buckmaster and T. Takeno, eds.), Springer-Verlag, pp. 147-156, (1988).
7. "Asymptotic Structure and Extinction of Diffusion Flames with Chain Mechanics," by M. Birkan and C. K. Law, to appear in Combustion and Flame.
8. "Effects of Preferential Diffusion and Concentration Modification in Sooting Counterflow Diffusion Flames," by R. L. Axelbaum, C. K. Law, and W. L. Flower, to appear in Proc. of Twenty-Second Combustion Symposium.
9. "Velocity and Scalar Fields of Turbulent Premixed Flames in Stagnation Flow," by P. Cho, C. K. Law, R. K. Cheng, and I. Sheperd, to appear in Proc. of Twenty-Second Combustion Symposium.
10. "Dynamics of Stretched Flames," by C. K. Law, to appear in Proc. of Twenty-Second Combustion Symposium.
11. "Experimental and Numerical Determination of Laminar Flame Speeds of Methane/"Air" Mixtures as Function of Stoichiometry, Pressure, and Flame Temperature," by D. L. Zhu, F. N. Egolfopoulos, and C. K. Law, to appear in Proc. of Twenty-Second Combustion Symposium.
12. "Experiments on Soot Extinction by Aerodynamic Straining in Counterflow Diffusion Flames," by D. X. Du, R. L. Axelbaum, and C.K. Law, to appear in Proc. of Twenty-Second Combustion Symposium.
13. "Dilution and Temperature Effects of Inert Addition on Soot Formation in a Counterflow Diffusion Flame," by R. L. Axelbaum, W. L. Flower and C. K. Law, submitted.
14. "Laminar Flame Speeds of Methane/Air Mixtures Under Reduced and Elevated Pressures," by F. Egolfopoulos, P. Cho, and C. K. Law, submitted.

RESEARCH ON MIXING CONTROL IN A SUPERSONIC SHEAR LAYER

ONR Contract N00014-88-K-0242

Principal Investigators: D. K. McLaughlin, P. J. Morris, and G. S. Settles

Penn State University, Department of Aerospace Engineering,
233 Hammond Bldg., University Park, PA 16802

SUMMARY/OVERVIEW

Experimental, analytical, and computational efforts are directed at the control and enhancement of the mixing of two supersonic streams. The experimental effort consists of both high-Reynolds number studies of an axisymmetric shear layer and low-Reynolds number studies of a planar shear layer. The analytical and computational effort is based upon a wave model of large-scale mixing layer structures. Mixing control strategies to be investigated include acoustic shear layer excitation and shear layer destabilization by way of nonsteady shock wave interactions. The goals of this research are to gain a better understanding of the nature of the supersonic mixing phenomenon and to develop effective methods for supersonic mixing control and enhancement, with applications in advanced high-speed airbreathing propulsion.

TECHNICAL DISCUSSION

This research effort began in February, 1988, and is now in its early stages. The approach taken and the initial results obtained are discussed below for each of the three major elements of the effort.

I. Analysis and Computations (P. J. Morris)

We are developing *simple* models for the mixing process in supersonic shear layers. Our approach depends on the presence of large-scale coherent structures in free shear layers. These have been observed at subsonic speeds in both plane and axisymmetric mixing layers and, at high speeds, their presence has been confirmed in axisymmetric flows. For high speed plane shear layers there is also some preliminary evidence for their existence. Although the existence and importance of large-scale structures in free shear flows has been known for several years, turbulence models, using such evidence, have been slow to develop. In our model we also make use of the observed close relationship between the local characteristics of the large-scale structures and the predictions of linear stability theory.

In the present model the large-scale structures are modeled either as a train of instability waves with a broad content of frequencies and spanwise wavenumbers or as a train of instability waves with discrete frequencies. This latter case is based on the sub-harmonic model of Ho and Huang (1982) and may be viewed as providing a single realization of the flow. Our aim is to provide a sufficiently simple model of the fluid dynamic mixing process that the later inclusion of chemistry does not present an overwhelming computational problem.

The wave model consists of writing a single wave component as:

$$\phi(x,y,t) = A(x) \phi(\eta) \exp[i(\alpha x - \omega t)] + c.c.$$

where "c.c." denotes the complex conjugate, $A(x)$ is the amplitude of the wave component, ϕ is any component of the velocity or pressure fluctuation, ω is the wave frequency and α is its wave number. It is readily shown that these fluctuations satisfy the Rayleigh equation of hydrodynamic stability. Together with the boundary conditions that the fluctuations vanish far

above and below the shear layer, this gives a homogeneous boundary value problem that is readily solved. Once the distributions of the velocity and pressure fluctuations are known from this solution, the Reynolds stress associated with the instability waves or large scale structures is known, except for its amplitude. This amplitude may be obtained from an integral form of the instability wave kinetic energy equation. The mean energy equation may be solved simultaneously to obtain the width of the shear layer. For the discrete wavetrain it is possible to build a model for the time-dependent behavior of the shear layer. This enables individual fluid particles to be tracked.

The initial calculations have concentrated on the incompressible mixing layer. We have examined the effects of velocity and density ratio on the mixing rate and compared the results with experiments. Fig. 1 shows the predicted and measured variation of spreading rate of the mixing layer, based on the vorticity thickness, as a function of velocity ratio. The agreement between the predictions and experiments is remarkable. It should be noted that there are *no empirical constants in our model*. The only empiricism is in the way we truncate the equations of motion for the large scales. Fig. 2 shows our predictions of the effect of density ratio on the spreading rate. Once again the predictions are remarkably good. For this case there exists only a limited amount of experimental data, *i.e* Brown and Roshko (1974).

The extension of the model to supersonic flows is underway. The formulation of the model in this case will be guided by the experimental observations to be obtained as described below. Accordingly, we are also extending the model to the axisymmetric shear layer case.

II. High-Reynolds Number Experiments (G. S. Settles)

Initial experiments on the generation and measurement of a high-Reynolds number axisymmetric turbulent mixing layer are under way in the supersonic wind tunnel facility of the Penn State Gas Dynamics Laboratory. The choice of an axisymmetric geometry was influenced by the fact that the few available research results on high-speed mixing are primarily planar, *e.g.* Papamoschou and Roshko (1986), as are several new studies now being carried out by other investigators. Further, axisymmetry supports our intention of applying primarily optical flow diagnostics to the mixing problem, in that turbulent structures at the edge of the shear layer should be clearly visible without the difficulties of integration along the optical path.

As sketched in Fig. 3, an axisymmetric shear layer generator has been fabricated and installed in the test section of the Penn State Supersonic Wind Tunnel, which is a high-pressure blowdown-type facility. The shear layer generator consists of a cone/cylinder body with an internal plenum terminating in a converging-diverging nozzle. The plenum is fed by a secondary gas stream through its swept support strut. In operation, both the exhaust of the shear layer generator and the (primary) wind tunnel freestream are supersonic. The latter is continuously variable over the Mach number range $1.5 \leq M_1 \leq 4.0$ by way of a sliding-block nozzle. Replaceable exit nozzles of the shear layer generator cover the same M_1 range. Depending upon Mach number and stagnation pressure, the Reynolds number of either stream may be as large as $10^8/m$. Further, the secondary stream may consist either of air with variable stagnation temperature or of foreign gases such as Helium. A versatile testing capability for supersonic mixing research is thus provided.

In operation, the turbulent boundary layers in the nozzle and on the outside of the shear layer generator merge at the nozzle exit to form an axisymmetric turbulent free shear layer. Ordinarily, the primary and secondary streams are adjusted to provide a wave-free static pressure match at the nozzle exit. Such a case is illustrated in Fig. 4 by a schlieren photograph for the conditions $M_1 = M_2 = 3$, where both streams are air with a common stagnation temperature.

Optical flow diagnostics will be used to characterize both the mixing layer structure and mixing rate of the primary and secondary streams. These diagnostics include pulsed-laser holographic interferometry, high-speed schlieren cinematography (up to 1 MHz), continuous and pulsed laser light-screen imaging, and crossed-beam, time-resolved laser deflectometry. The goal of this work is the identification of large-scale turbulent structures in the mixing layer and the study of their response to acoustic and unsteady-shock inputs for mixing control.

The initial experiments, now in progress, are designed to characterize the supersonic mixing layer as a function of M_1 and M_2 , with both streams at cold flow ($\gamma = 1.4$) conditions. As is now customary, these results will be examined in terms of the convective Mach number. The effect of temperature differences will then be considered by heating the secondary airstream. Current plans for the study of mixing control include mounting an acoustic source (miniature siren) inside the plenum of the shear layer generator, so as to produce high-level, variable-frequency acoustic radiation in the secondary stream. Estimates of the natural frequency of the axisymmetric shear layer indicate that excitation up to the 40kHz range may be required. Finally, several potential schemes for the imposition of a nonsteady shock wave upon the shear layer are being studied. An oscillating oblique shock produced by the separation of a turbulent boundary layer in the primary stream is one such possibility. Shock wave generation by a pressure mismatch between the two streams is another possible strategy.

III. Low Reynolds Number Experiments (D. K. McLaughlin)

The low-Reynolds number experiments in this research effort are designed to provide two capabilities not available in those experiments just discussed. Firstly, a low-Reynolds number turbulent shear layer allows large-scale structures to be more easily identified, in that the range of turbulence scales is much narrower. As a consequence, additional information concerning the modes of the turbulent structure and the interaction in time and space of these modes may be extracted. Thus, this approach aims to simplify the complex turbulent mixing problem to some extent by way of the natural cutoff mechanism of viscous stresses at low Reynolds numbers. Secondly, the glow discharge technique is expected to provide a powerful means of artificial flow excitation for mixing control and enhancement. This excitation also provides a useful phase reference from which the character of large-scale structures may be determined from hot-wire anemometry measurements. The latter technique becomes very difficult and the former becomes impossible at the high flow densities of most past and current supersonic mixing experiments.

A low-Reynolds number shear layer facility is being fabricated for this element of the study. As diagrammed in Fig. 5, this facility will produce two supersonic streams of different Mach number which merge at the beginning of the test section to form a planar mixing layer. The high-speed leg of this facility incorporates variable Mach number by way of an asymmetric, sliding-block nozzle. Glow-discharge excitation will occur in the turbulent boundary on the splitter plate just upstream of the beginning of the free mixing layer. Hot-wire, conventional probe, and optical diagnostics will be applied to the shear layer in the test section of the facility. A large vacuum vessel connected to the output of the facility permits testing at low flow densities in order to provide low-Reynolds number conditions. The completion of this facility, flow calibration tests, and the beginning of experiments are expected to occur during 1988.

The initial experiments will parallel those described in Section II. above. Hot-wire surveys will be used to characterize the planar free shear layer over a range of Mach number conditions. Both glow-discharge and acoustic excitation will then be applied in attempts to manipulate the turbulence structure and mixing rate of the shear layer. Throughout this effort, comparisons will be made among the low- and high-Reynolds number results and the analytical modeling effort described earlier.

REFERENCES

- Brown, G. L. and Roshko, A. (1974) "On Density Effects and Large Structure in Turbulent Mixing Layers," *J. Fluid Mechanics*, Vol. 64, pp. 775-816.
- Ho, C.-M. and Huang, L.-S. (1982) "Subharmonics and Vortex Merging in Mixing Layers," *J. Fluid Mechanics*, Vol. 119, pp. 443-473.
- Papamoschou, D., and Roshko, A. (1986) "Observations of Supersonic Free Shear layers," AIAA Paper 86-0162.

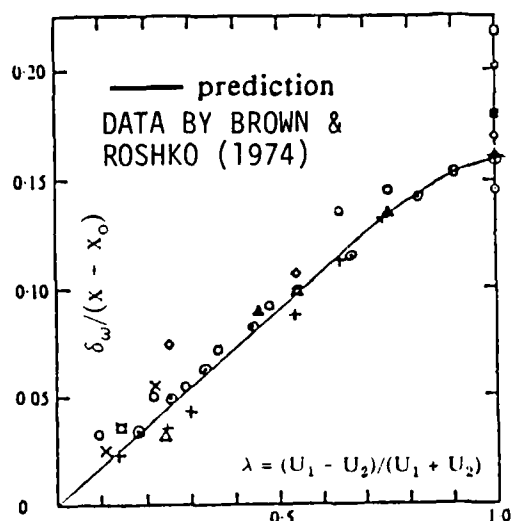


Fig. 1 - Growth rate of a two-stream mixing layer with velocity ratio.

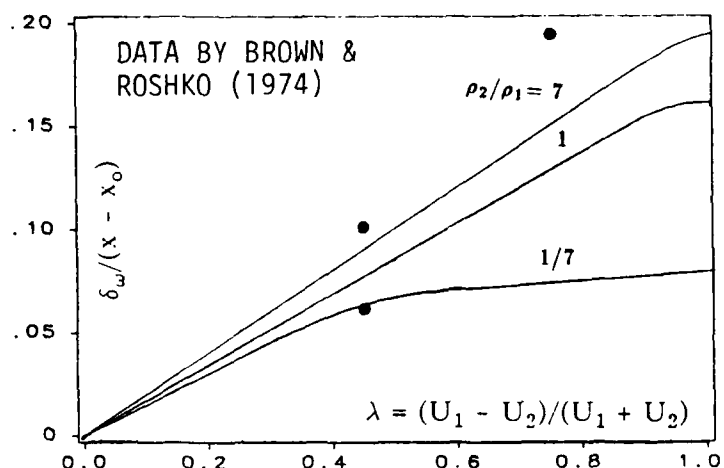


Fig. 2 - Growth rate of a two-stream mixing layer with density ratio.

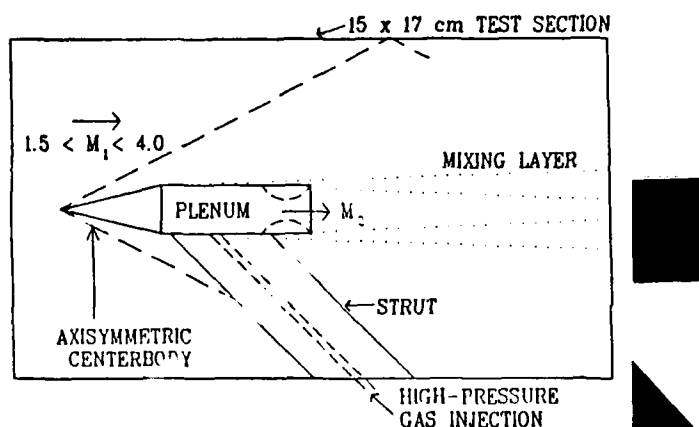


Fig. 3 - Axisymmetric shear layer generator sketch.

Fig. 4 - Schlieren photo of axisymmetric shear layer with $M_1 = M_2 = 3$.

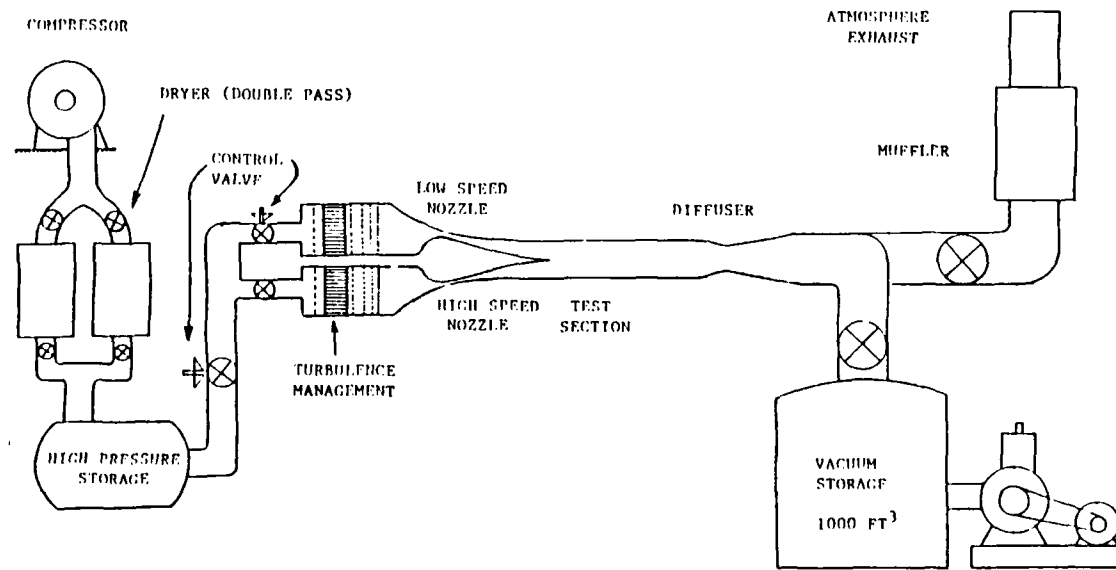


Fig. 5 - Sketch of low-Reynolds number shear layer facility

INVESTIGATION OF COMBUSTION IN LARGE VORTICES**AFOSR Grant No. AFOSR-84-0286****Frank E. Marble****Edward E. Zukoski****California Institute of Technology****Pasadena, California 91125****Summary/Overview:**

Mixing between fuel and air in a combustion chamber with supersonic air flow can be enhanced by passing shock waves over masses of a low density fuel, such as hydrogen, embedded in more dense air. The shock wave induces strong vorticity in part of the hydrogen and the large scale vortices produced by the accumulation of this vorticity can cause enhanced mixing. Combustion in such vortices is being studied in an experimental program in which vortices are produced periodically in the flow of a premixed mixture of fuel and air at a rearward facing step. Ignition occurs as hot products of combustion are entrained into the vortex and the combustion process is studied with conventional instrumentation which includes high frequency response pressure gages, ion probes, and high speed shadowgraph movies and photographs. An enhanced video camera system is used to measure the chemiluminescence produced in the combustion reactions and the intensity of this light gives a measure for the volumetric intensity of the combustion process.

Technical Discussion:

During the past year we have completed an extensive construction and instrumentation acquisition stage of this experiment and have successfully begun the experimental program. This period has been critical for us because deviations from our original conception of the hardware and significant changes in some of the instruments were necessary.

The basic combustion channel being used is a modification of that which was used for several years in the study of combustion oscillations in dump combustors. The new duct, shown in Figure 1, was modified to allow us to study the development of vortices for long periods of time after they are formed. This required that the height of the combustion chamber be increased considerably to prevent the vortices from impinging on the lower wall of the combustion chamber.

The new apparatus has a combustion chamber with a lower wall which can be positioned to allow the height of the chamber to be changed from 2.5 cm to 15 cm. Synthetic

quartz windows 15 cm square allow the entire combustion chamber to be viewed with several optical systems.

In the new apparatus we again control the frequency of the vortex shedding by adjusting the length of the plenum chamber to make the desired frequency a mode of the duct. Further control is obtained by means of a siren placed at the upstream end of the plenum chamber. The frequency can be fixed by the siren and the amplitude of the signal by the energy supplied to the selected mode by passing part of the fuel-air mixture through the siren and part through a bypass around the siren. In the absence of the siren, the period of the oscillation varied slightly about a mean value. The siren prevents this variation in the period of the individual cycles and the precisely fixed frequency aids in the interpretation of the phase averaged data.

This arrangement allows us to produce vortices with closely controlled frequencies between 100 and 600 Hz and to observe them at scales up to 15 cm. The system has been tested using cold flow and has performed satisfactorily over its entire range of frequencies and amplitudes. Our acoustic model for the new system, which is employed in the analysis and reduction of data, is in excellent agreement with the results of cold flow experiments.

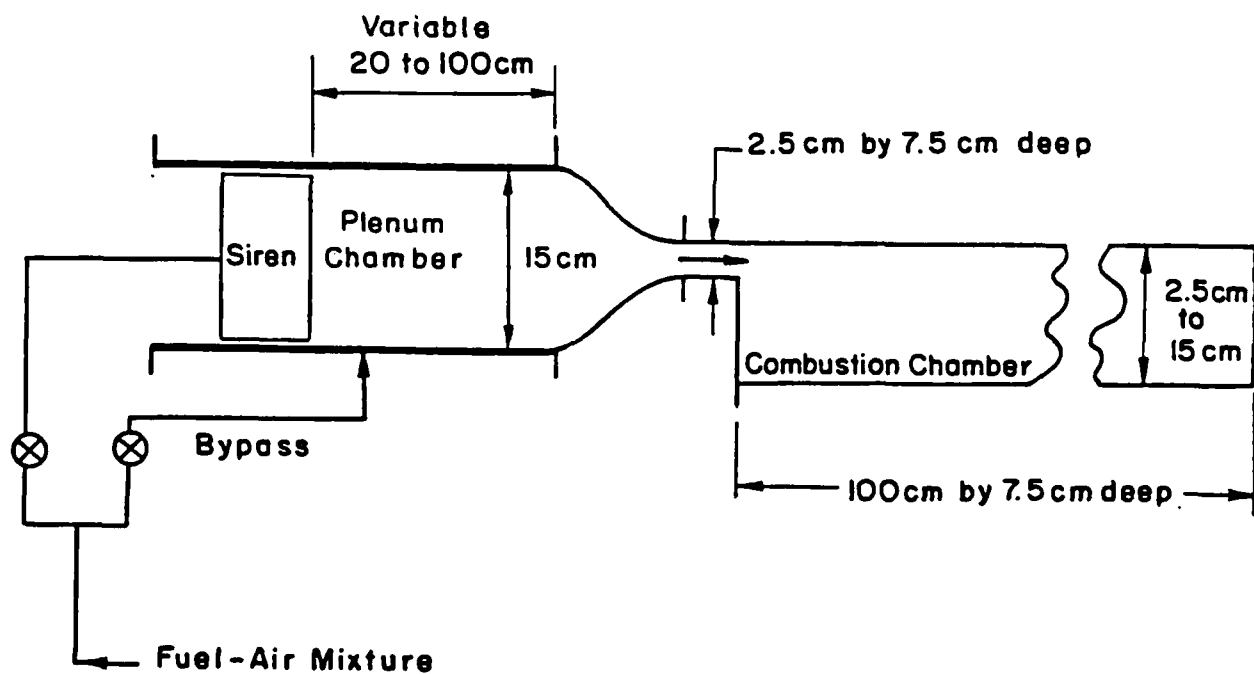


Figure 1: Diagram of the Rebuilt Experimental Facility

The burner itself and associated instrumentation has been operated extensively at a height of 2.5 cm. In addition to the array of pressure transducers, local time resolved radiation measurements and direct high-speed photography, the recently acquired intensified video camera is now operating very satisfactorily and a new array of ionization probes is being used to assure that the processes taking place in the center of the channel are essentially identical with those obtained using the video camera.

Figure 2 is an example of the print-out from our data acquisition system showing traces corresponding to i) pressure transducer 0.5 in. downstream of the step, ii) and iii) ion probes at distances of 2.0 in. and 4.0 in. respectively downstream of the step, iv) the photomultiplier output at a distance of 4.0 in. downstream of the step and finally v) a timing signal with pulse at the time a spark shadowgraph was taken. The corresponding spark shadowgraph is shown in Figure 3.

Some features should be commented upon: First, note the very close correspondence between the second ion probe and the photomultiplier output located at the same distance downstream of the step. This result confirms our previous contention that the local radiative output does correctly represent presence of chemical reaction. Second, another feature of interest is the clear displacement between the ion probe outputs at positions of 2.0 in. and 4.0. downstream of the step. The streamwise transport of the burning vortex is very clear and strongly suggests that the reacting structure is as coherent as our earlier shadowgraphs suggest. We are now in the process of assembling the data for a complete cycle, showing the complete process of vortex formation and combustion.

The image intensified video camera has an electronic shutter with a minimum open time of about one micro-second but can take pictures no more often than 30 frames per second. Thus to obtain photographs at various phases of the cycle it is necessary to use photographs assembled from a large number of cycles. This is the reason that we are interested in using the siren discussed above to carefully control the period for the shedding and keep the process as uniform in time as possible.

The output of the image intensified video camera is producing excellent results despite the weak light signals and short exposure times we must use. The camera is operating satisfactorily and the intensity of the light is high enough that even with an exposure of 10 microseconds we can obtain useful results. A frame grabber is used to digitize selected frames for storage and computer enhancement. At the flow speeds we are using at present the gas will move a maximum of 0.1 mm during this exposure time and the local resolution fixed by the camera system is a square region of about 0.5 mm on a side. Unfortunately, a Xerox copy of pictures obtained with the video camera and frame grabber does not do justice to the results and a sample will not be included.

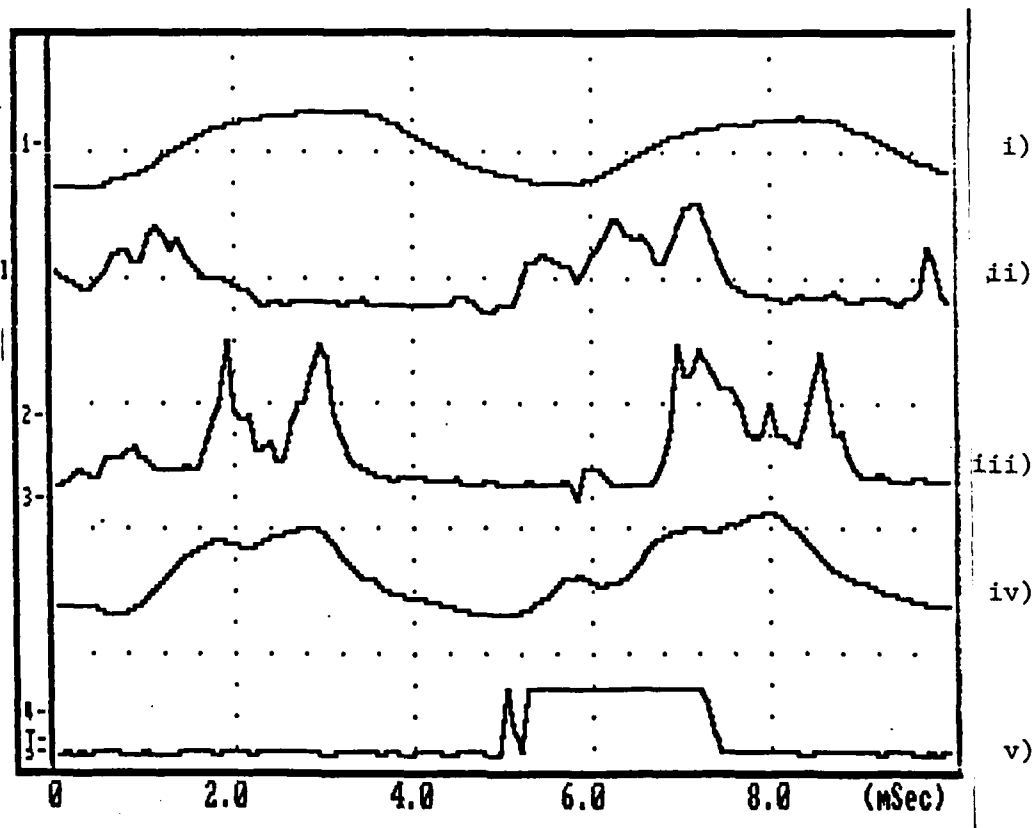


Figure 2: Typical Print-out from Data Acquisition System



Figure 3: Spark Shadowgraph at Time-mark of Figure 2

The apparatus and data acquisition system are now operating as intended and we have embarked on the main substance of the experimental program. In the immediate future the duct will be expanded to its full height of 15 cm, in order to reduce any possible interference between the vortex and the lower wall, and the complete range of vortex shedding frequencies, as set by the siren and the variable length settling chamber, will be studied. This, and accompanying variations in the gas throughput velocity, constitutes a wide variation of the fluid-dynamical time scale. The chemical time scale will be varied through changes in both the mixture ratio and the fuel composition, which will be changed from pure methane to mixtures of methane and hydrogen.

Substantial progress in this program is anticipated before the end of the current contract year.

THE EFFECTS OF COMPRESSIBILITY ON A SUPERSONIC MIXING LAYER

AFOSR Contract No. F49620-88-C-0003

Principal Investigator: David Nixon

Nielsen Engineering & Research, Inc.
510 Clyde Avenue, Mountain View, CA 94043-2287

SUMMARY/OVERVIEW

The research is concerned with identifying the physics of supersonic mixing layers by using a numerical simulation. Previous research on supersonic mixing layers revealed that such layers have a smaller spreading rate than subsonic mixing layers. It has been suggested that the effects of localized shock formation may be important. A computer code for solving the Navier-Stokes equations is being used to calculate the interaction of vortices with convective flow fields, including shock wave effects. It is expected that these studies will provide important insight to the effects of compressibility on the interaction between turbulent eddies and shear layers.

TECHNICAL DISCUSSION

One of the possible scenarios of turbulent flow in supersonic mixing layers includes the presence of shock waves (or shocklets) which could be produced either by the fluctuating turbulent eddies or by large vortical structures, if the local flow relative to some reference frame becomes supersonic. In the case of the turbulent eddies the induced velocities are not steady, and the shock developed will be very transient; the nature of such a transient shock/turbulent eddy interaction is not known at present.

In order to examine the possibility of shock waves forming within eddies or as a result of interaction between the eddy and the surrounding stream, several preliminary numerical experiments have been performed. In each, a vortex and a uniform flow are calculated as they evolve in time and space from given initial conditions.

The results for the case of a simple vortex being convected by a uniform flow are shown in Figure 1. For subsonic convection, the vortex is perturbed after a long time, but is basically still in existence as a single vortex. There are perturbations in the flow field which may be of a vortical nature, but no clear pattern of secondary flow emerges. On the other hand, supersonic convection appears to result in a clear formation of secondary vortices. However, no shock waves were noted in the evolution of this flow.

Another interesting case had the following initial conditions:

Uniform flow with $M_\infty = 2.5$ for $R > 15$
Vortex + Uniform flow with $M_c < M_\infty$ for $R > 15$

where R is the distance from the vortex center, M_∞ is the freestream Mach number and M_c is the convective velocity of the vortex center.

Thus, the initial conditions represent a localized vortical fluid mass instantaneously inserted in a free flowing stream. The convective velocity of the vortex was varied from low subsonic to low supersonic. The freestream Mach number was always 2.5, giving relative velocities between the free stream and the vortex of 0.25, 0.7, and 1.25.

Figure 2 shows the velocity field relative to the free stream velocity for the case with $M_c=2.25$. The results indicate that a splitting of the freestream flow occurs due to the presence of the slower moving vortical mass. The split flow accelerates as it moves around the vortex and forms a pair of vortices as it encounters the low pressure region behind the vortex. The flow pattern is similar to that of a flow around a solid cylinder with separation. As the flow develops further, the original vortex seems to be absorbed by the free stream vortex of the same sign and the final pattern is two vortices, one of which is primarily the original vortex and the other a weak vortex which is the result of the division of the free stream. The calculation must be extended further to determine the ultimate fate of these vortices.

Compressibility effects are to be observed in the next figure for the case with $M_c = 1.25$. As the flow develops from the initial condition, a compression occurs at the front of the vortex. The flow in the vortex does not accelerate instantaneously to the free stream. The compression must move through the inner flow. The formation of a shock wave is apparent in the pressure field ahead of the vortex. The strength of the secondary vortices formed by the splitting is increased with relative Mach number. The compression that occurs for the highest vortex velocity is weak and results in less splitting and thus weak secondary vortices (Fig 2). For the lower vortex convective speeds, the compression is greater and results in more splitting and consequently strong secondary vortices. As the primary vortex flow accelerates, the compression will disappear. The two vortices of like sign could combine, thus leaving two vortices.

This formation of a pair of vortices in place of a single vortex could be an important mechanism in the explanation of the spreading rate of compressible shear layers. More detailed results are needed as well as examination of the pressure field surrounding the vortices and an assessment of the actual process of mixing between the vortical fluid and the free stream fluid.

These studies are continuing. It is expected that the conclusion of this phase of the work will answer some important questions of how vortex splitting can occur in a compressible flow.

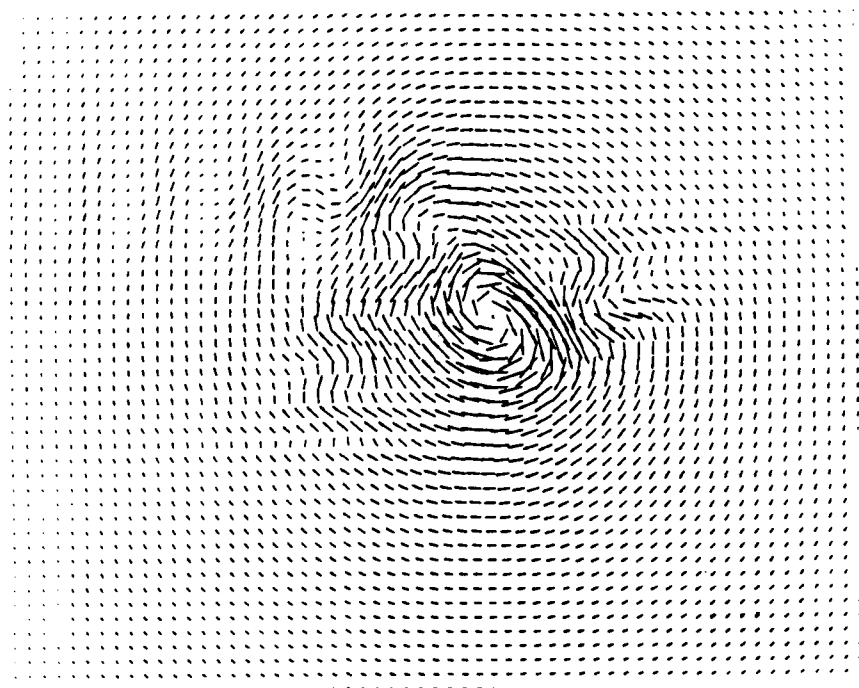
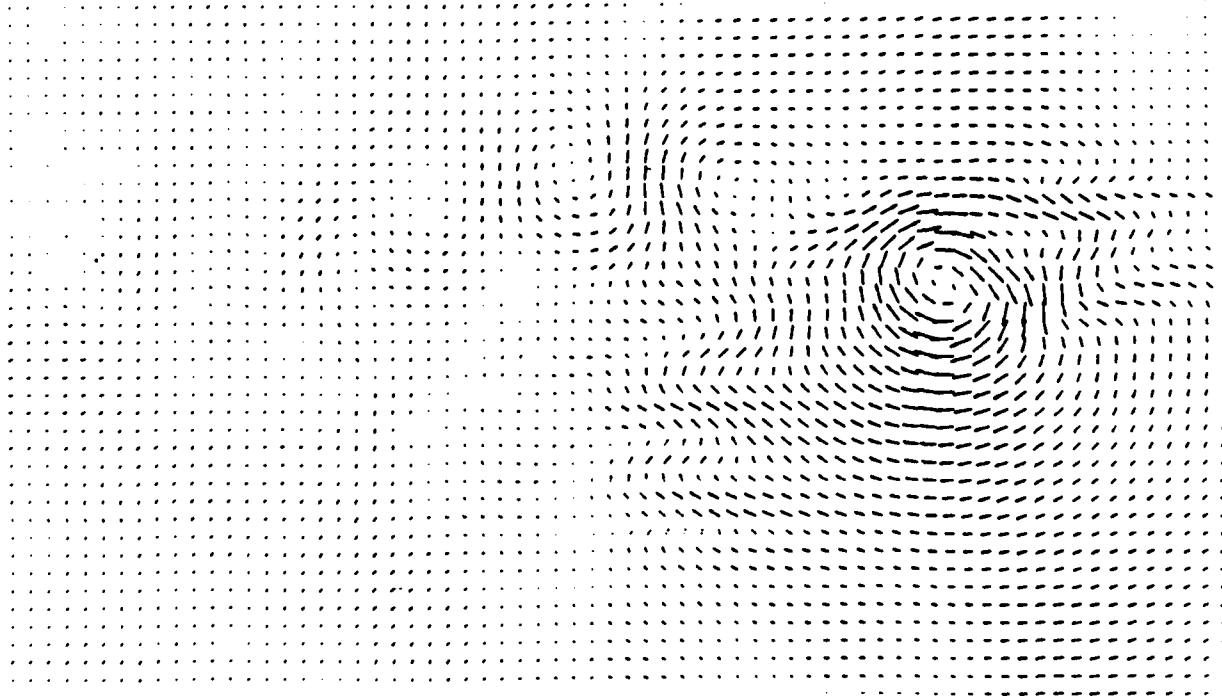
a) $M_\infty = 0.3$ b) $M_\infty = 1.1$

Figure 1.- Relative velocity vectors for a vortex in uniform flow.

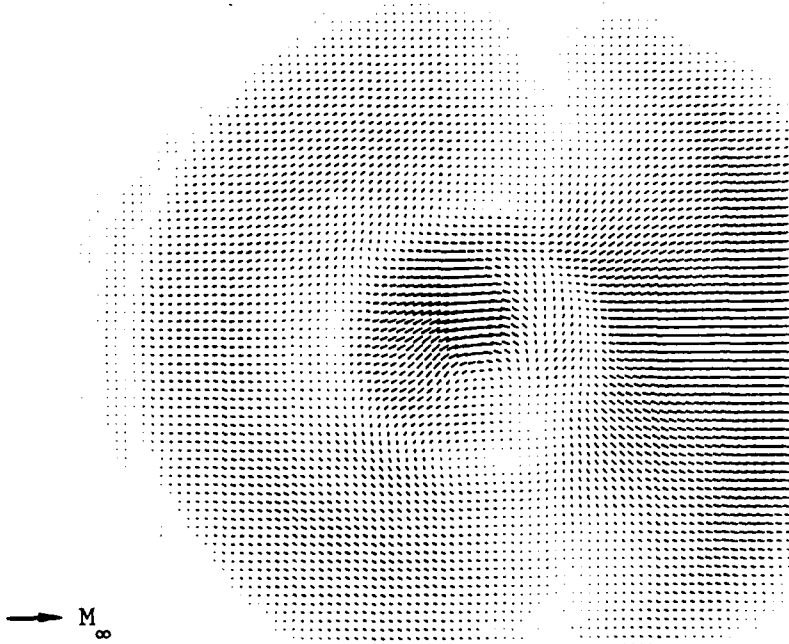


Figure 2.- High Speed Eddy

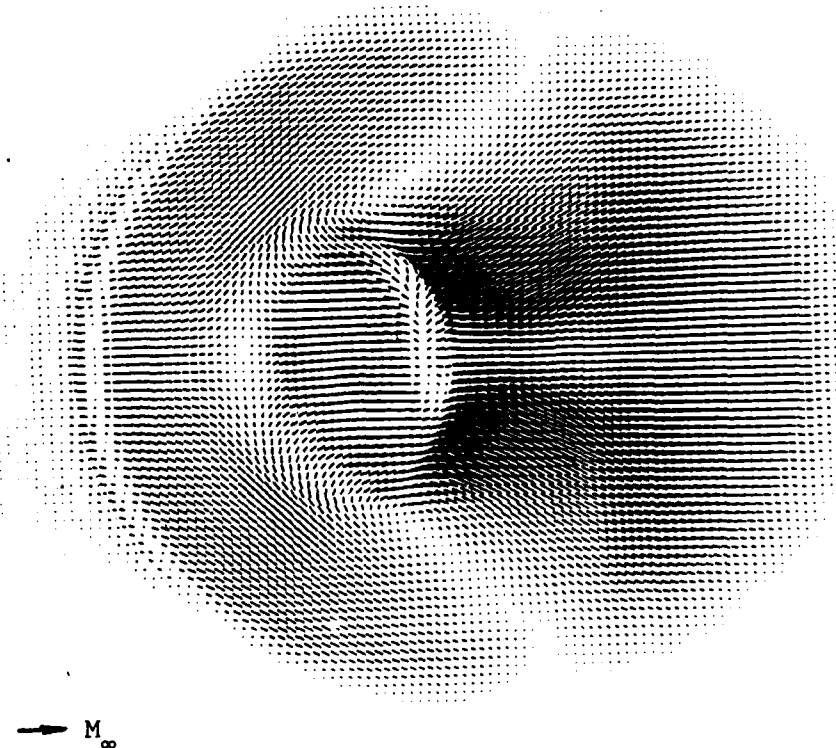


Figure 3.- Low Speed Eddy

NUMERICAL INVESTIGATION OF TURBULENT FLAME SHEETS
(AFOSR Grant No. 88-0052)

Principal Investigator: Stephen B. Pope

Sibley School of Mechanical and Aerospace Engineering
Cornell University, Ithaca, NY 14853

SUMMARY

An accurate physical model of a premixed flame (in the flame-sheet regime) is that combustion is confined to a thin sheet that can be regarded as a mathematical surface. This surface is convected by the fluid and propagates normal to itself at the (local) laminar flame speed. Many important questions related to the nature and evolution of these flame sheets are unanswered, because of inevitable experimental difficulties. This study aims at answering some of these questions through direct numerical simulations.

TECHNICAL DISCUSSION

In the last ten years, great strides have been taken in developing tools to study turbulent reacting flows. Three different approaches to the problem are simultaneously reaching maturity, are elucidating the essential physical processes, and are allowing the prediction of turbulent reactive flows of engineering importance. First, laser diagnostics are being used to extract information undreamt of a decade ago. Second, direct numerical simulations (DNS) of turbulent flows are revealing further information, inaccessible to measurement. And third, stochastic models of turbulent combustion have proved themselves on laboratory flames, and are being extended to the more complex flows of engineering practice. In spite of these strides, there remain fundamental issues on which we are ignorant. In particular, we do not have a clear understanding of the different regimes of premixed turbulent combustion, nor do we have a quantitative understanding of the effect of turbulence on flame sheets.

A straightforward application of DNS to reacting flow problems is to solve for scalar fields representing reactants, products etc. as well as for velocity. While this approach is useful to address some problems, because of the limited range of scales that can be resolved, it does not permit studies in some important parameter ranges. In particular, for premixed flames in the flame-sheet regime, the laminar flame thickness is less than the Kolmogorov scale. The flame sheet could be resolved only if very low Reynolds numbers were used.

Rather than accepting this severe restriction we will use a different approach. A well-tried approach to premixed turbulent flames is to represent the flame as a mathematical surface —a flame sheet— that separates reactants from products. This surface propagates normal to itself relative to the products ahead at a speed w . To a first approximation the propagation speed w is just the laminar flame speed u_L .

While many models and theories of turbulent premixed combustion are based on the flame-sheet concept, there is a large number of basic unanswered questions. Examples of the questions that the proposed study can answer are:

- a) How does the rate of surface stretching depend on the propagation speed w ?
- b) With the over-simple model $w = u_L$, how soon do cusps form?

- c) How rapidly does an initially plane surface develop curvature? Is there an asymptotic distribution of curvatures?
- d) When does the surface collide with itself? And by how much does this process reduce the flame area?
- e) Do pockets of unburnt reactants persist for long times?
- f) What is the fractal nature of the surface? How does it depend on u'/u_L ?

The first stage of the investigation is a "point-wise" study of flame sheets, which can address questions a), b) and c). This is done by following individual points, and extracting from the DNS calculations the velocity and its first two derivatives at the surface-point locations. Then, not only can the surface point be tracked, but the stretch-rate, orientation and curvature can be computed. A statistical analysis of these quantities is then performed.

A limitation of the constant-propagation speed model is that the surface eventually develops cusps. Once a cusp appears, the point-wise representation breaks down. We will study, therefore, the statistics of cusp development.

CURRENT STATUS AND PROGRESS

1. Several DNS production runs have been performed with 128^3 grids yielding Taylor-scale Reynolds numbers up to 90. The computations are performed on the Cornell National Supercomputer Facility's IBM 3090/600, using all six processors in parallel.
2. An accurate interpolation scheme is needed to extract the velocity and its gradients following a point on the flame surface. An existing algorithm was found to be sufficiently accurate for velocity, but not for its gradients. A much improved algorithm based on cubic splines has been developed, implemented and tested.
3. Times series of the velocity gradient following a surface point have been obtained and analyzed. Many unexpected features have been discovered — the correlation time of strain rate is much shorter than that of vorticity, for example. To fully understand the essential dynamics we are constructing a stochastic model for the process.

PREMIXED TURBULENT FLAME PROPAGATION

(AFOSR Grant 87-0097)

Principal Investigator: D. A. Santavicca

Department of Mechanical Engineering
The Pennsylvania State University
University Park, PA 16802

SUMMARY/OVERVIEW:

Turbulence-flame interactions are being studied in premixed turbulent flames over a broad range of turbulence Reynolds and Damkohler numbers. Laser Doppler velocimetry is used to characterize the mean velocity, turbulence intensity, time scale, length scale, energy spectrum, Reynolds stress and vorticity. These measurements are made as a function of time through a propagating turbulent flame in order to determine the flame's effect on the turbulent flow field both immediately upstream and downstream of the flame zone. Two-dimensional Mie scattering is used to characterize the turbulent flame structure. These measurements are analyzed to evaluate the fractal nature of the flame structure and its dependence on the incident turbulent flow field. The objective of this research is to obtain a better understanding of turbulence-flame interactions and to in turn develop improved, phenomenologically correct models of premixed turbulent flame propagation.

TECHNICAL DISCUSSION

Premixed turbulent flame propagation has been studied by numerous researchers. The common objective of these studies has been to characterize and better understand the effect of turbulence on the flame propagation or mass burning rate. Also of importance, but much less studied, is the flame generated turbulence which significantly affects post-flame heat transfer in practical combustion systems. In most experimental studies, attempts have been made to develop empirical correlations between the measured flame speed and the upstream turbulence intensity, and in a few cases, the turbulence length scale as well. Theoretical flame speed predictions have also been proposed based on various turbulent flame models. Both the empirical and theoretical flame speed predictions, however, are found to vary significantly from one study to another. The large variation between the various flame speed predictions clearly indicates the need for an improved understanding of the underlying turbulence-flame interaction. One aspect of this interaction is the effect of the incident turbulent flow field on the turbulent flame structure, since it is through changes in the flame structure that one can explicitly account for changes in the flame's mass burning rate. A second aspect is the local flow field induced by the flame which alters the turbulent flow field, not only downstream of the flame, but ahead of it as well. Therefore the incident turbulent flow field, and in turn the flame structure, are affected by the flame dynamics.

Characterization of the turbulence-flame interactions requires two types of measurements. The turbulent flow field must be characterized; not only the upstream conditions, but also immediately ahead and downstream of the flame zone. It is evident from previous studies that characterization of the turbulence intensity alone is not sufficient. In this study, the turbulence length scale, time scale, energy spectrum, Reynolds stress and vorticity are also measured. These measurements are made with a two-point, two-component LDV system. In addition to this detailed characterization of the turbulent flow field, it is necessary to characterize the turbulent flame structure and to develop an appropriate method for quantifying that structure. Two-dimensional Mie scattering and fractal analysis, respectively, are used for this purpose in this study.

All of the above mentioned measurements are made in a turbulent flow reactor (Figure 1) which has been designed specifically for this study. This flow reactor is used to generate freely propagating, premixed turbulent flames over a broad range of turbulence Reynolds and Damkohler numbers. To date, a range of turbulence Reynolds numbers from 60 to 1400 and Damkohler numbers from 1 to 100 have been studied, using both the unconfined and confined configurations illustrated in Figure 1. This corresponds to flames which extend over a significant portion of what is referred to as the wrinkled laminar flame or reaction sheet regime.

Velocity and turbulence parameters as a function of time through the propagating flame are shown in Figures 2 through 5. These measurements were made in the unconfined flow reactor using premixed stoichiometric propane-air. The upstream turbulence intensity and integral length scale are 26 cm/sec and 8mm, respectively. Note that all of these results represent ensemble averages over approximately 1000 flame events.

Figure 2 shows the mean velocity, both parallel and perpendicular to the flame front. Flame arrival is clearly indicated by the sudden change in the velocity, where the velocity perpendicular to the flame front is observed to decrease ahead of the flame and to then increase by a factor of three through the flame. Both the decrease in velocity ahead of the flame and the less than expected increase in velocity through the flame can be attributed to the unconfined nature of the flow. Figure 3 shows the effect of the flame on the turbulence intensity, again measured perpendicular and parallel to the flame front. The flame is observed to have a much greater effect on the turbulent fluctuations perpendicular to the flame front, both ahead of and behind the flame. The turbulent fluctuations perpendicular to the flame increase by ~50% ahead of the flame and by an additional factor of 4 through the flame, resulting in highly non-isotropic turbulence in the post-flame gases.

The Reynolds stress (Figure 4) is found to increase significantly from near zero ahead of the flame to approximately $30 \text{ cm}^2/\text{sec}^2$ immediately behind the flame due to the flame generated shear. The integral length scale shown in Figure 5 is a transverse length scale with the separation distance oriented parallel to the flame front. The length scale is observed to increase steadily by ~50% through the flame zone. It is expected that the length scale oriented perpendicular to the flame front will undergo a much greater increase, consistent with the non-isotropic turbulence generation shown in Figure 3.

Typical 2-D flame structure measurements are shown in Figure 6 for a range of turbulence intensity to laminar flame speed ratios (u'/S_f) from 1/4 to 12. The field of view in these images is 2 cm x 2 cm. These results show a very clear increase in the degree of wrinkling and a decrease in the scale of wrinkling as u'/S_f increases. The corresponding results from the fractal analysis of these flame structures is shown in Figure 7, where the slope of the straight line segment gives the fractal dimension of the flame surface. As indicated, the slope and hence the fractal dimension is found to increase with increasing u'/S_f . These results clearly illustrate the fractal nature of premixed turbulent flame structures over a broad range of turbulence Reynolds numbers.

Figure 8 shows the fractal dimensions obtained for all of the u'/S_f conditions which have been studied to date. Each point represents an average over from 12 to 35 measurements and the "error bars" indicate the standard deviation. These results show a clear trend of increasing fractal dimension with increasing u'/S_f . Note that at the highest u'/S_f , the flame structure fractal dimension is nearly equal to the fractal dimension which has been predicted for passive scalar surfaces at very high Reynolds numbers. In an attempt to relate the fractal dimension of the flame surface to the incident turbulent flow field, measurements of the fractal dimension of isovelocity surfaces have also been recently initiated.

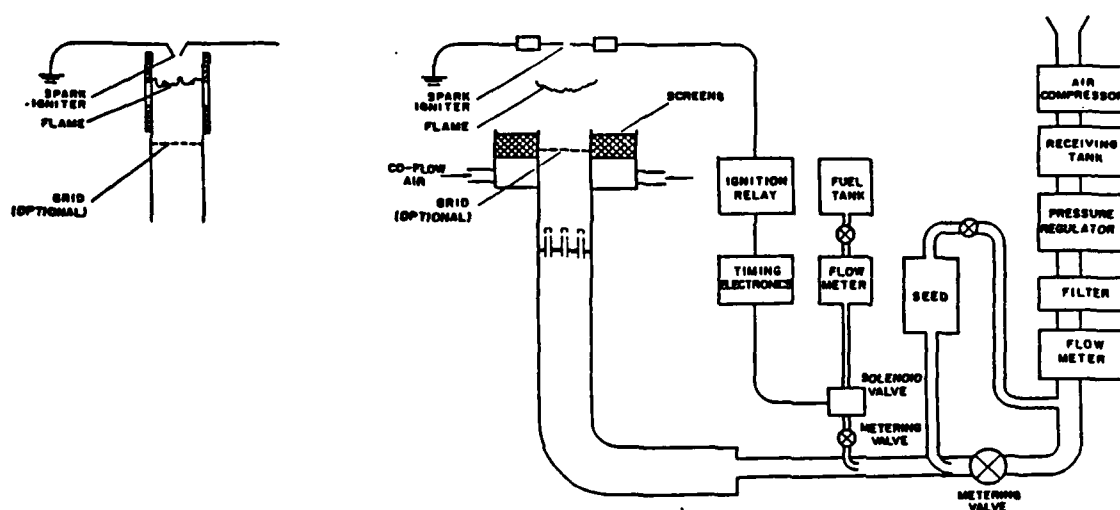


FIGURE 1 Schematic drawing of turbulent flow reactor, with unconfined and confined test sections.

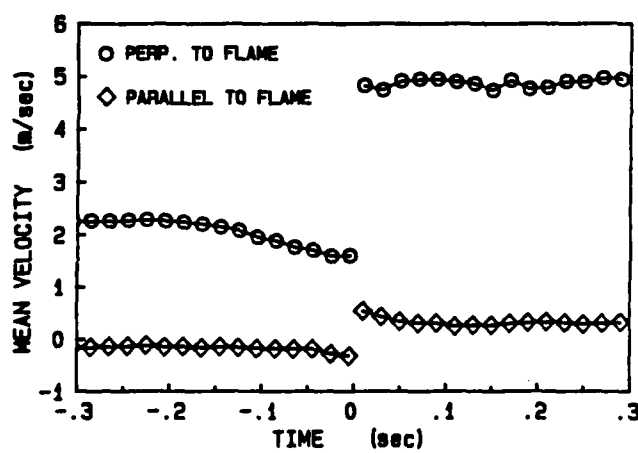


FIGURE 2 Ensemble averaged velocity versus time through propagating flame.

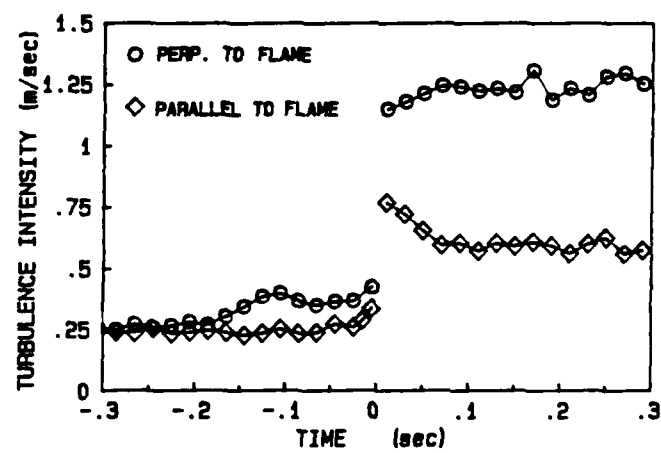
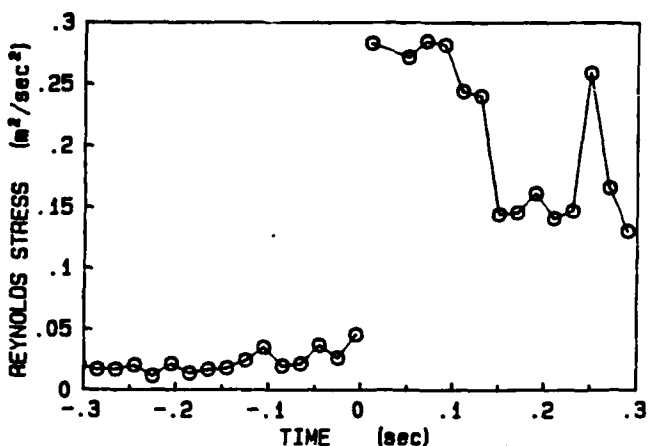


FIGURE 3 Ensemble averaged turbulence intensity versus time through propagating flame.



EXPERIMENTAL INVESTIGATION OF OPPOSED JET TURBULENT DIFFUSION FLAMES

AFOSR Grant 88-0011

Principal Investigator: L. Talbot
Mechanical Engineering Department
University of California
Berkeley, CA 94720

SUMMARY/OVERVIEW:

Our interest in this program is in certain features of transverse jet injection which is under consideration as a method for introducing fuel into the combustion chamber of a supersonic ramjet engine. Numerical modelling and experiments have revealed that some of the reaction occurs in the shock-separated subsonic boundary layer region upstream of the injected jet (1,2,3). This reaction zone is essentially a recirculation region containing fuel, bounded by an airstream, with the interface being a turbulent diffusion flame having in part the characteristics of a shear layer and in part the characteristics of a stagnation point flow. Our investigation is aimed at gaining some understanding of the characteristics of this reaction zone through the study of a simpler model, that of the opposed jet turbulent diffusion flame. Various laser-based diagnostic and tomographic techniques are being employed to determine the structure and properties of this flame configuration. A parallel numerical modelling study will also be carried out to make comparisons with the experimental results.

TECHNICAL DISCUSSION

The principal combustion configuration to be investigated will be that of a hydrogen jet directed toward an opposed airstream, with the jet directed vertically downward (See Figure 1). During the initial stages of the program, while our existing combustion flow system is being modified to accomodate hydrogen, preliminary cold flow tests have been carried out for the purpose of determining empirically the parameters controlling the jet penetration and the location of the stagnation point in the flow field, and for the purpose of obtaining cold flow field data with which the numerical model studies can be compared before introducing the additional complications of chemical reaction. Our initial cold flow investigations have employed time-resolved Schlieren flow visualization. To produce conditions comparable to hydrogen cold jet flow we have employed helium as the gas injected into the oncoming turbulent flow. The Schlieren observations revealed immediately that buoyancy effects played a dominant role in determining the configuration of the recirculation region. To further explore the effects of buoyancy, we have replaced helium with freon as the jet fluid. We are currently comparing the Schlieren studies of the flow field structure under conditions of positive jet buoyancy (helium) and negative jet buoyancy (freon). These Schlieren studies will serve as preliminaries to more detailed Rayleigh scattering and LDV measurements of the flow fields in the two cases (4,5), and these will in turn be followed by the same types of measurements for the reacting hydrogen-air flow field which is the primary

interest of this study. The ultimate objective of these measurements is to quantify the nature of the entrainment, mixing and reaction processes and the effect of stretch for the turbulent opposed jet flow (6,7,8,9.)

Numerical studies of this flame configuration will be carried out as a collaborative effort with Dr. Janet Ellsey of the Laboratory for Computational Physics and Fluid Dynamics of the Naval Research Laboratory, Washington, D.C. The method to be employed in the calculations will make use of the "Barely Implicit Correction to Flux Corrected Transport" (BIC-FCT) algorithm to solve the two-dimensional compressible conservation equations for mass, momentum and energy, modified to apply to the axisymmetric case. This algorithm eliminates the sound speed limitation on the time step and allows efficient simulation of low-speed flows. The effects of viscous diffusion, species diffusion, buoyancy, and conduction are included through a time step splitting technique, such that each of these processes may be studied individually. A flame sheet model of the reaction zone has already been investigated and "tuned" by comparing the results to a detailed simulation on an H₂ - O₂ flame.

References

- 1) White, M.E., Drummond, J.P. and Kumar, A. (1986). Evolution and Status of CFD Techniques for Scramjet Applications, AIAA Paper 86-0158.
- 2) Waltrip, P.J. (1986). Liquid Fueled Supersonic Combustion Ramjets: A Research Perspective of the Past, Present and Future, AIAA Paper 86-0158.
- 3) Shetz, J. (1984) in Combustion in Supersonic Flow, Workshop Report 21st JANNAF Combustion Meeting NASA Langley Research Center, October, 3-4, 1984.
- 4) Namazian, M. Talbot, L. Robben, F.A. and Cheng, R.K. (1982). Two-point Rayleigh scattering measurements in V-shaped turbulent flames, Nineteenth Symposium (International) on Combustion, The Combustion Institute, pp. 487-493.
- 5) Cheng, R.K. (1984). Conditional sampling of turbulence intensities and Reynolds stress in premixed turbulent flames, Combustion Science and Technology, 41, pp. 109-142.
- 6) Bilger, R.W. (1976). Turbulent jet diffusion flames, Prog. Energy Combust. Sci., 1, pp. 87-109.
- 7) Cho, P., Law, C.K., Hertzberg, J.R. and Cheng, R.K. (1986). Structure and propagation of turbulent premixed flames stabilized in a stagnation flow. To appear in 21st Symposium (International) on Combustion, The Combustion Institute.
- 8) Law, C.K. (1984). Dynamics of stretched flames, Invited paper, 1984 Technical Meeting, Eastern States Section of the Combustion Institute.
- 9) Liew, S.K., Bray, K.N.C. and Moss, J.B. (1983). A stretched laminar flamelet model of turbulent nonpremixed combustion, Combustion and Flame, 56, pp. 199-213.

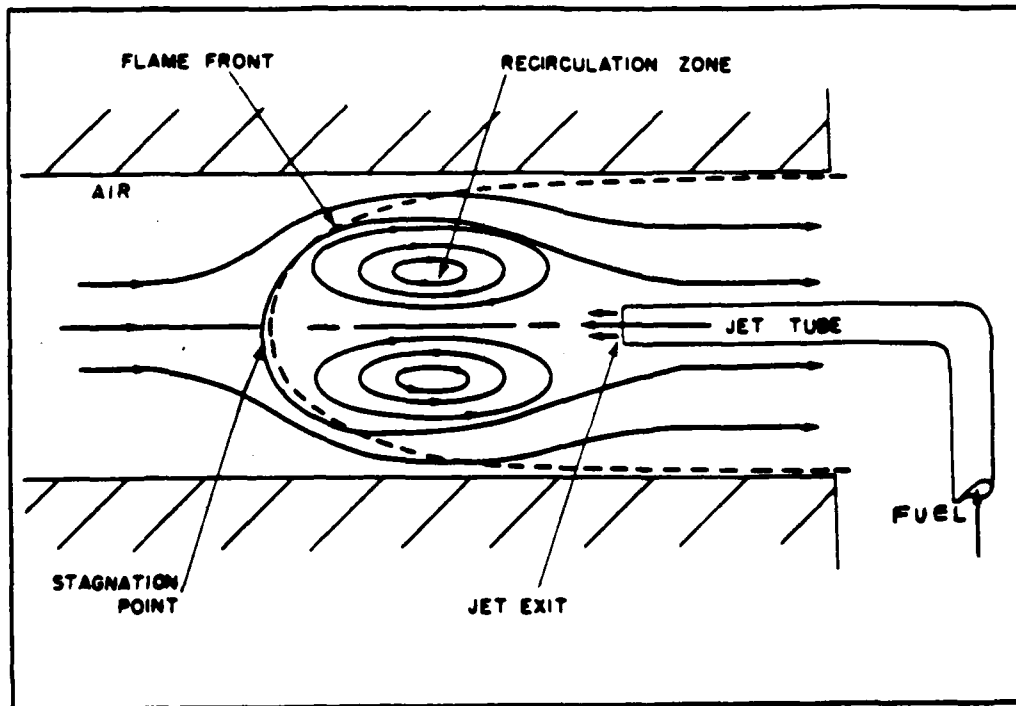


FIG. 1. Opposed reacting jet flowfield.

THERMAL AND FLOW STRUCTURES OF TURBULENT V-FLAMES AT LOW DAMKÖHLER'S NUMBERS

(AFOSR Grant No. 83-0373)

Principal Investigator: Tau-Yi Toong

Massachusetts Institute of Technology
Cambridge, Massachusetts 02139

SUMMARY/OVERVIEW:

Despite recent important advance in the study of turbulent combustion, physical understanding of turbulence-combustion interactions is still obscure. The main objective of this research is to determine and elucidate the mechanisms governing these interactions in different spectral regimes. Both theoretical and experimental investigations are conducted. It is hopeful that this coordinated study will help to advance our understanding of the physics of turbulence-combustion interactions and to provide sound guidelines for improving combustion efficiency and reducing emissions.

TECHNICAL DISCUSSION

The theoretical and the experimental studies reported earlier showed the importance of turbulence-combustion interactions in determining the structure of premixed turbulent flames. In order to shed light on the nature of these interactions, experiments were conducted to examine the relationship between simultaneous temperatures and velocities (either normal or tangential to the flame brush) at different distances apart and at different relative orientations within a turbulent V-flame. This study showed that the high-frequency fluctuations in temperatures and normal velocities were highly correlated and were associated with changes in flame shapes, thicknesses and propagation speeds. Furthermore, their RMS values were higher within the reaction zone than in either the cold or the hot regions. However, the fluctuations in tangential velocities were less well correlated with temperatures and their RMS values remained almost constant within the flame brush.

Figure 1 shows the profiles of the "instantaneous" mean temperatures and normal velocities (\bar{T} , \bar{V}) within the slowly drifting turbulent flame and of the most probable temperatures and normal velocities (T , V) in the presence of the high-frequency fluctuations. The distributions of the corresponding high-frequency RMS temperature and normal-velocity fluctuations were also shown. Their maximum values occurred near the inflection points of the respective profiles.

Simultaneous measurements of temperatures and velocities were made at different locations within the turbulent flame. In one configuration (cf. inset in Fig. 2), the temperatures T_2 at positions A, B, C and D were compared with those at a fixed position T_1 . Figure 2 shows the corresponding cross-correlation coefficients of the high-frequency temperature fluctuations at different delay times. The temperature fluctuations at position A were found to lag behind T_1 while those at positions B, C and D, to lead T_1 . The delay time at the peak cross-correlation coefficients were plotted in Fig. 3, which showed increasing lead in T_2 as its position moved farther away from T_1 in the vertical direction.

Figure 3 also shows the variation of the peak cross-correlation coefficients and the spatial cross-correlation coefficients (at zero delay time) at the four positions A, B, C and D. The peak values were about the same, while the spatial coefficients dropped sharply with increasing distance.

Associated with the high-frequency fluctuations, the turbulent flame changed its shape. Figure 4 shows a comparison of the most probable temperature profiles when the temperatures were rising and when they were dropping. Note that the spatial gradients were steeper and the thickness was thinner when the temperatures were rising.

On the basis of the temporal changes in the average temperatures and temperature gradients between two positions separated at a small distance apart normal to the flame brush, one could estimate the speed of the flame movement in the laboratory coordinate system. Figure 5 shows a comparison of the computed flame speed with the measured gas speed normal to the flame brush. Similar high-frequency fluctuations were observed. Cross-correlation coefficients of the measured temperature and computed flame speed were shown in Fig. 6 at different delay times. The relationship was nearly an odd function with peak values at about -0.8 and 1.0 ms. The crossing of the correlation curve near the origin suggested that the flame-speed fluctuation led the temperature fluctuation by about 90 degrees.

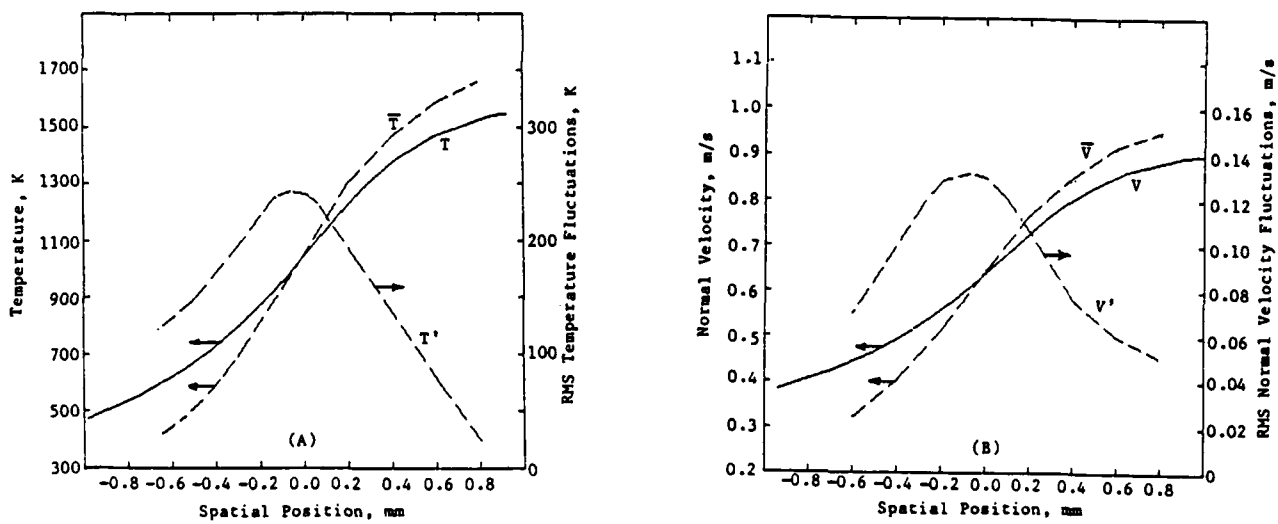


Fig. 1 Profiles of "Instantaneous" Mean Temperatures and Normal Velocities (\bar{T} , \bar{V}) and Most Probable Temperatures and Normal Velocities (T , V), Together with Corresponding High-Frequency RMS Values.

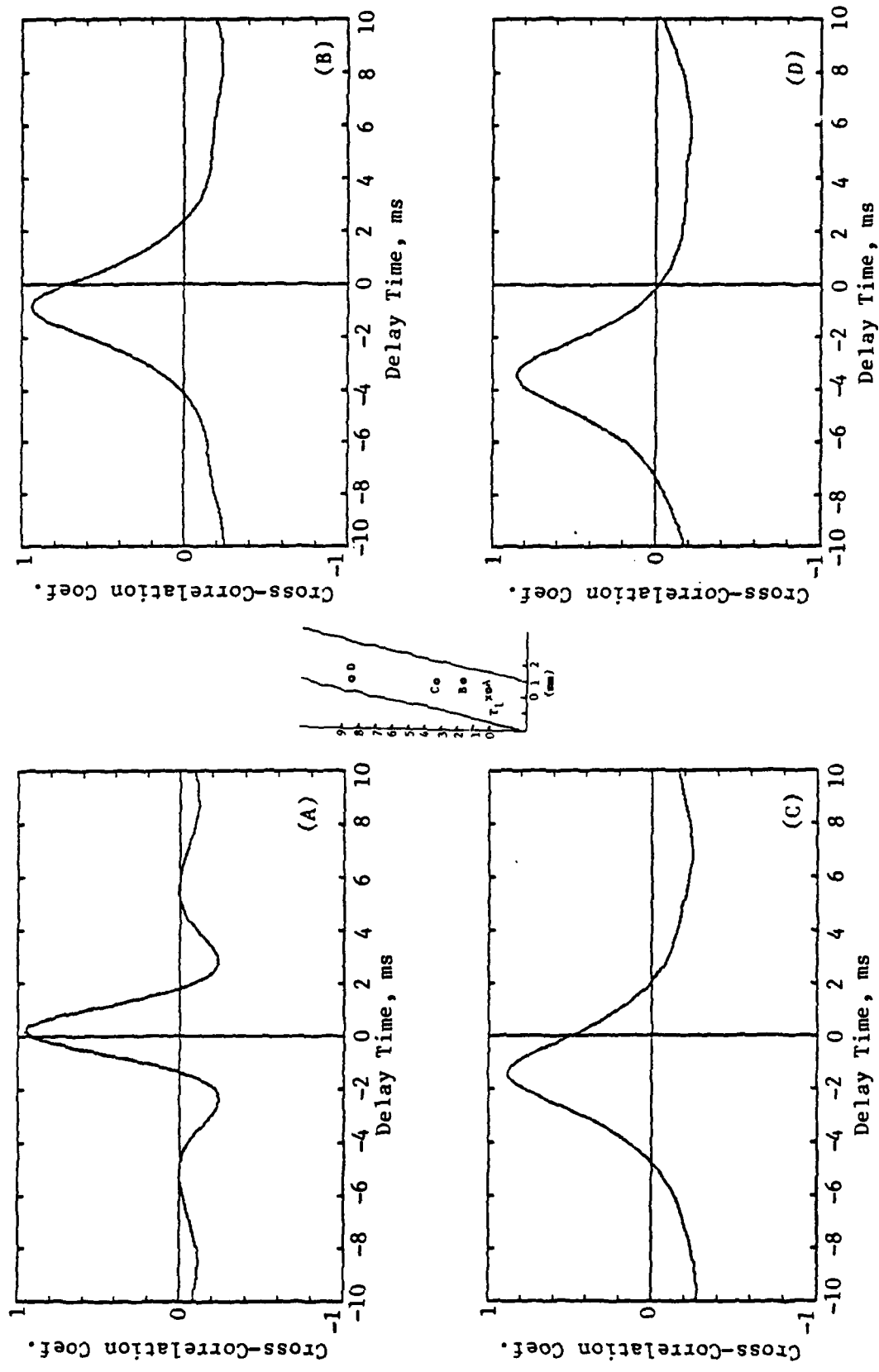


Fig. 2 High-Frequency T_1-T_2 Cross-Correlation Coefficient versus Delay Time for Different Positions Shown in Inset.

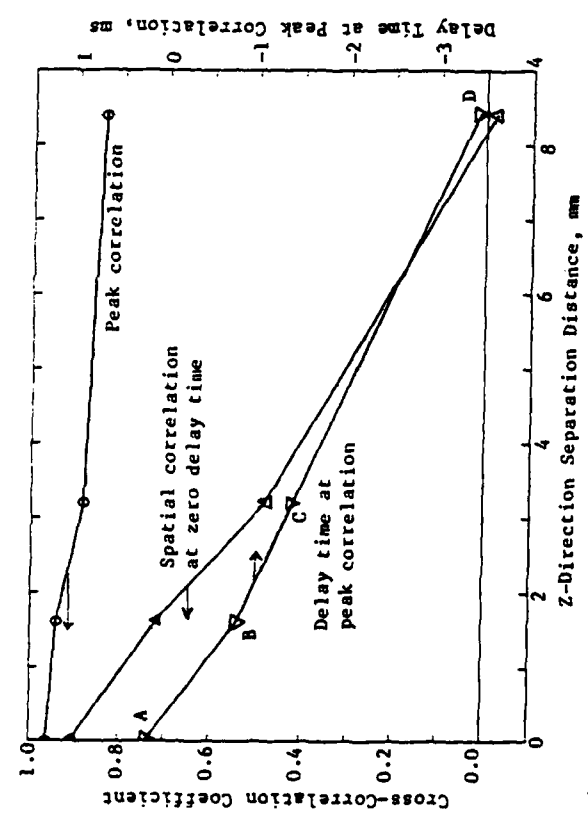


Fig. 3 High-Frequency T_1-T_2 Cross-Correlation Coefficient versus Vertical Separation Distance, Showing Peak Values, Delay Time at Peak Correlation, and Spatial Values at Zero Delay Time.

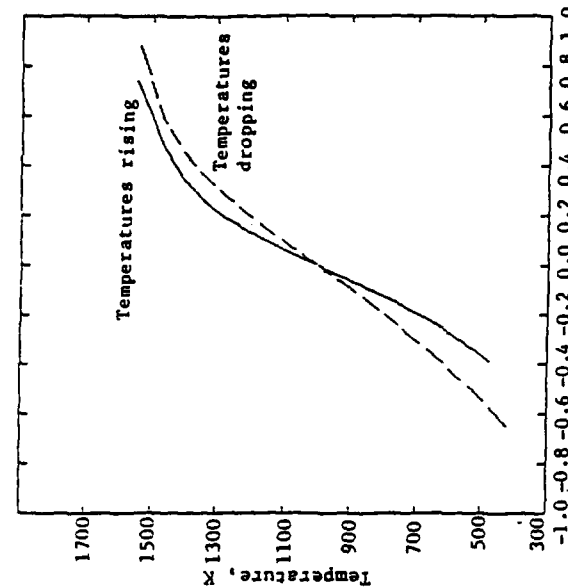


Fig. 4 Comparison of Most-Probable Temperature Profiles for Rising and Dropping Temperatures during Fluctuations.

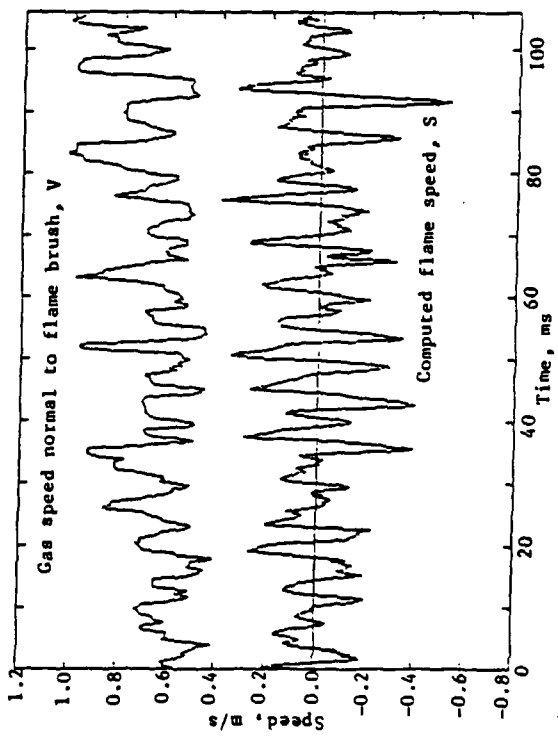


Fig. 5 Measured Gas Speed and Computed flame speed Normal to Apparent Flame Brush.

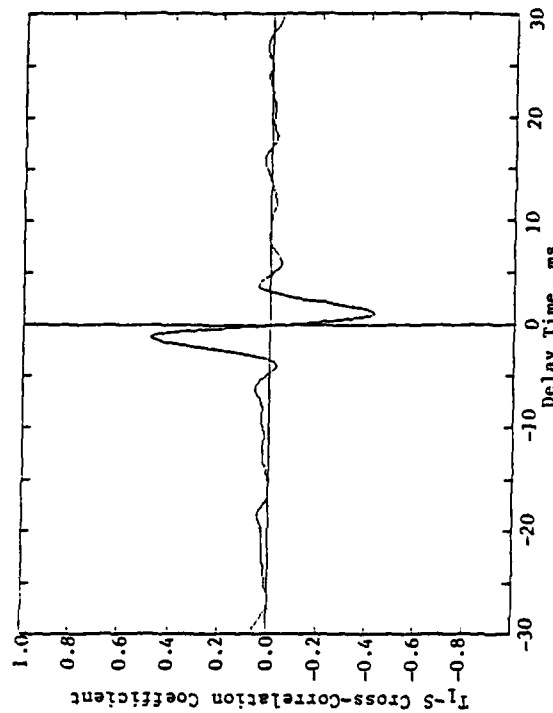


Fig. 6 Cross-Correlation Coefficient of Temperature T_1 and Computed Flame Speed S versus Delay Time.

AFOSR/ONR CONTRACTORS MEETING ON COMBUSTIONInvitees

Dr. Scott L. Anderson
Department of Chemistry
State University of New York
Stony Brook NY 11794-3400
(516) 632-7915

Dr K Annamalai
Mechanical Engineering Dept
Texas AM University
College Station TX 77843-3123

Dr K Annen
Aerodyne Research, Inc.
45 Manning Road
Manning Park Research Center
Billerica MA 01821
(617) 663-9500

Dr Simon H Bauer
Department of Chemistry
Cornell University
Ithaca NY 14853-1301

Dr. S. L. Baughcum
Spectra Technology
2755 Northrup Way
Bellevue WA 98004-1495
(206) 828-3517

Dr. H. R. Baum
National Bureau of Standards
Center for Fire Research
Gaithersburg MD 20899
(301) 975-6668

Dr John Bdzil
Los Alamos National Laboratory
Los Alamos NM 87545

Dr. H. L. Beach
NASA Langley Research Center
MS 168
Hampton VA 23665-5225
(804) 865-3772
(804) 865-2658

Dr. Josette Bellan
Applied Technologies Section
Jet Propulsion Laboratory
4800 Oak Grove Drive
Pasadena CA 91109
(818) 354-6959

Dr. Paul A. Bonczyk
United Technologies Research
Center
Silver Lane
East Hartford CT 06108
(203) 727-7162

Dr Kevin G Bowcutt
Rockwell International
Mail Code WA40
2770 East Carson Street
Lakewood CA 90712
(213) 420-0317

Dr. C. T. Bowman
Department of Mechanical
Engineering
Stanford University
Stanford CA 94305-3032
(415) 723-1745

Dr Robert E Breidenthal
 Department of Aeronautics and
 Astronautics
 University of Washington, FS10
 Seattle WA 98195
 (206) 545-1098

Dr. J. E. Broadwell
 Graduate Aeronautical Labs
 California Institute of
 Technology
 Pasadena CA 91125

Dr Garry L Brown
 Aeronautical Research Labs
 506 Lorimer St, Fishermen's Bn
 Box 4331, P. O.
 Melbourne, Victoria AUSTRALIA 3001
 03-647-7511

Dr R C Brown
 Aerodyne Research, Inc.
 45 Manning Road
 Manning Park Research Center
 Billerica MA 01821
 (617) 663-9500

Dr Dennis Bushnell
 NASA Langley Research Center
 Mail Stop 168
 Hampton VA 23665
 (804) 865-4546

Dr Ron Butler
 AFWAL/POSF
 Wright-Patterson AFB OH 45433-6563

Dr. T. D. Butler
 Group T-3
 Los Alamos National Laboratory
 Los Alamos NM 87545
 (505) 667-4156

Dr. H. F. Calcote
 AeroChem Research Laboratories
 Inc.
 P. O. Box 12
 Princeton NJ 08542
 (609) 921-7070

Dr. B. J. Cantwell
 Department of Mechanical
 Engineering
 Stanford University
 Stanford CA 94305-3032
 (415) 723-4825

Dr. T Charalampopoulos
 Mechanical Engineering Dept.
 Louisiana State University
 Baton Rouge LA 70803
 (504) 388-5792
 (504) 388-5799

Dr. Robert E. Childs
 Nielsen Engineering and
 Research, Inc.
 510 Clyde Avenue
 Mountain View CA 94043-2287
 (415) 968-9457

Dr S Y Cho
 Department of Mechanical and
 Aerospace Engineering
 Princeton University
 Princeton NJ 08544

Dr M-S Chou
 Building R1, Room 1044
 TRW Space and Technology Group
 One Space Park
 Redondo Beach CA 90278
 (213) 535-4321

Mr. Anthony Cifone
 Research and Technology Group
 Naval Air Propulsion Center
 Trenton NJ 08628
 (609) 896-5753

Mr. R. W. Claus
 NASA Lewis Research Center
 21000 Brookpark Road
 Cleveland OH 44135-3127
 (216)433-5869

Dr. M. B. Colket
 United Technologies Research
 Center
 Silver Lane
 East Hartford CT 06108
 (203) 727-7481

Dr. S. M. Correa
 General Electric - Corporate
 Research and Development
 P. O. Box 8
 Schenectady NY 12301
 (518) 387-5853

Dr. E. T. Curran
 AFWAL/CA-P
 Wright-Patterson AFB OH 45433-6563
 (513) 255-2246
 AV785-2246

Dr Eli K Dabora
 Mechanical Engineering Dept
 University of Connecticut
 Box U-139 ME
 Storrs CT 06268
 (203) 486-2415
 (203) 486-2189

Maj Larry P Davis
 AFOSR/NC
 Bolling AFB DC 20332-6448
 (202) 767-4963
 AV297-4963

Dr. R. W. Dibble
 Department of Mechanical
 Engineering
 University of California
 Irvine CA 92717

Dr. P. E. Dimotakis
 Graduate Aeronautical Labs
 California Institute of
 Technology
 Pasadena CA 91125
 (818) 356-4456

Mr Lee G L D
 Southwest Research Institute
 P O Drawer 28510
 San Antonio TX 78284
 (512) 684-5111
 Ext 3251

Dr. M. C. Drake
 Physical Chemistry Department
 General Motors Research Labs
 Twelve Mile and Mound Roads
 Warren MI 48090-9055

Dr. Fredrick L. Dryer
 Department of Mechanical and
 Aerospace Engineering
 Princeton University
 Princeton NJ 08544
 (609) 452-5206

Dr. H. A. Dwyer
 Department of Mechanical
 Engineering
 University of California
 Davis CA 95616

Dr Raymond B Edelman
 Science Applications
 International Corporation
 9769 Owensmouth Avenue
 Chatsworth CA 91311
 (818) 709-5222

Dr Phillip Emmerman
 Harry Diamond Laboratories
 Attn. SLCHD-ST-RD
 2800 Powder Mill Road
 Adelphi MD 20783-1197
 (301) 394-3000

Dr. K. C. Ernst
 Pratt and Whitney Aircraft
 Group
 Government Products Division
 West Palm Beach FL 33402

Dr. G. M. Faeth
 Department of Aerospace
 Engineering
 University of Michigan
 Ann Arbor MI 48109-2140
 (313) 764-7202

Dr. Francis E. Fendell
 TRW Space and Technology Group
 Building R1, Room 1022
 One Space Park
 Redondo Beach CA 90278
 (213) 536-3534

Capt Nannette Founds
 AFWL/ARDF
 Kirtland AFB NM 87117-6008
 (505) 844-0196
 AV244-0196

Dr Michael Frenklach
 202 Academic Projects Building
 The Pennsylvania State
 University
 University Park PA 16802
 (814) 865-4392

Dr David E Fyfe
 Laboratory for Computational
 Physics
 Naval Research Laboratory
 Washington DC 20375
 (202) 767-6583
 AV297-6583

Dr Alon Gany
 Department of Aeronautical Eng
 Technion-Israel Institute of
 Technology
 32000 Haifa, ISRAEL
 04-292308

Dr. A. F. Ghoniem
 Department of Mechanical
 Engineering
 MIT
 Cambridge MA 02139
 (617) 253-2295

Mr. R. Giffen
 General Electric Company
 Aircraft Engine Group
 Neumann Way
 Cincinnati OH 45215

Dr. P. Givi
 Department of Mechanical
 and Aerospace Engineering
 State University of New York
 Buffalo NY 14260

Dr. Irvin Glassman
 Department of Mechanical and
 Aerospace Engineering
 Princeton University
 Princeton NJ 08544
 (609) 452-5199

Dr Frederick C Gouldin
 Department of Mechanical and
 Aerospace Engineering
 Cornell University
 Ithaca NY 14853-1301

Dr Ephraim Gutmark
 Research Department
 Code 3892
 Naval Weapons Center
 China Lake CA 93555-6001
 (619) 939-1079
 AV437-1079

Dr Robert J Hansen
 Office of Naval Research
 Code 1215
 800 North Quincy Street
 Arlington VA 22217-5000
 (202) 696-4715

Mr. Dale A. Hudson
 AFWAL/POTC
 Wright-Patterson AFB OH 45433-6563
 (513) 255-5974
 AV785-5974

Dr. T. A. Jackson
 AFWAL/POSF
 Wright-Patterson AFB OH 45433-6563
 (513) 255-6462
 AV785-6462

Dr Sheridan C Johnston
 Combustion Sciences
 Sandia National Laboratories
 Livermore CA 94550
 (415) 294-2138

Dr. W-H Jou
 Flow Industries, Inc.
 21414 68th Avenue South
 Kent WA 98031
 (206) 872-8500

Dr. Ann R. Karagozian
 Mechanical, Aerospace and
 Nuclear Engineering Department
 University of California, LA
 Los Angeles CA 90024
 (213) 825-5653

Dr. Arnold A. Kelly
 Department of Mechanical and
 Aerospace Engineering
 Princeton University
 Princeton NJ 08544
 (609) 452-5221

Dr. John T. Kelly
 109 Via De Tesoros
 Los Gatos CA 95030-1638

Mr. M. Kenworthy
 General Electric Company
 Aircraft Engine Group
 Neumann Way
 Cincinnati OH 45215

Maj Paul Kerch
 HQ AFESC/RDV
 Tyndall AFB FL 32403-6001
 (904) 283-4234
 AV970-4234

Dr. J. A. Kezerle
 Gas Research Institute
 8600 West Bryn Mawr Avenue
 Chicago IL 60631
 (312) 399-8331

Dr. G. B. King
 Department of Mechanical
 Engineering
 Purdue University
 West Lafayette IN 47907
 (317) 494-2713

Mr. R. Kirby
 Garrett Turbine Engine Company
 111 South 34th Street
 P. O. Box 5217
 Phoenix AZ 85010

Dr Charles E Kolb
 Aerodyne Research, Inc.
 45 Manning Road
 Manning Park Research Center
 Billerica MA 01821
 (617) 663-9500

Dr. W. Kollman
 Department of Mechanical
 Engineering
 University of California
 Davis CA 95616

Mr. Gil Kraemer
 Combustion Section, D-12
 AVCO-Lycoming
 550 South Main Street
 Stratford CT 06497
 (203) 385-3283

Dr Kenneth K Kuo
 Department of Mechanical
 Engineering
 Pennsylvania State University
 University Park PA 16802
 (814) 865-6741

Dr. John C. Larue
 Department of Mechanical
 Engineering
 University of California
 Irvine CA 92717

Dr. N. M. Laurendeau
 Department of Mechanical
 Engineering
 Purdue University
 West Lafayette IN 47907
 (317) 494-2713

Dr. C. K. Law
 Department of Mechanical
 Engineering
 University of California
 Davis CA 95616
 (916) 752-8928

Dr J Carl Leader
 McDonnell Douglas Research Lab
 McDonnell Douglas Corporation
 PO Box 516
 St Louis MO 63166-0516
 (314) 232-4687

Dr. Anthony Leonard
 Graduate Aeronautical Labs
 California Institute of
 Technology
 Pasadena CA 91125
 (818) 356-4465

Dr C R Krishna
 Department of Nuclear Energy
 Brookhaven National Laboratory
 Upton NY 11973

Dr. Marshall Lapp
 High Temperature Interfaces
 Division
 Sandia National Laboratories
 Livermore CA 94550
 (415) 294-2435

Dr. A. Laufer
 Office of Energy Research
 U. S. Department of Energy
 1000 Independence Avenue, N.W.
 Washington DC 20585
 (202) 353-5820

Dr. Moshe Lavid
 ML Energia, Inc.
 P. O. Box 1468
 Princeton NJ 08540
 (609) 799-7970

Dr Stan Lawton
 McDonnell Douglas Research Lab
 McDonnell Douglas Corporation
 PO Box 516
 St Louis MO 63166-0516
 (314) 233-2547

Dr Spiro Lekoudis
 Office of Naval Research
 Mechanics Division, Code 432
 800 North Quincy Street
 Arlington VA 22217-5000
 (202) 696-4406

Dr. R. S. Levine
 National Bureau of Standards
 Center for Fire Research
 Gaithersburg MD 20899
 (301) 921-3845

Dr. Erwin A. Lezberg
 NASA Lewis Research Center
 21000 Brookpark Road
 Cleveland OH 44135-3127
 (216) 433-4000
 Ext. 6161

Dr. P. A. Libby
 Dept. Of. Appl. Mech. and
 Engrg. Sci.
 University of California
 La Jolla CA 92093
 (619) 534-3168

Dr. Wilbert Lick
 Department of Mechanical and
 Environmental Engineering
 University of California
 Santa Barbara CA 93106

Dr. Hans W. Liepmann
 Graduate Aeronautical Labs
 California Institute of
 Technology
 Pasadena CA 91125
 (818) 356-4535

Dr. Pei Lin
 2008 NE 102nd Street
 Seattle WA 98125

Dr. F. E. Lytle
 Department of Chemistry
 Purdue University
 West Lafayette IN 47907
 (317) 494-5261

Dr James Madison
 McDonnell Douglas Research Lab
 McDonnell Douglas Corporation
 PO Box 516
 St Louis MO 63166-0516

Dr. Edward T. Mahefkey
 AFWAL/POOC-5
 Wright-Patterson AFB OH 45433-6563
 (513) 255-6241
 AV785-6241

Dr Oscar Manley
 US Department of Energy
 Office of Energy Research
 1000 Independence Avenue, SW
 Washington DC 20585

Dr. Nagi N. Mansour
 Computational Fluid Mechanics
 Branch, M/S 202A-1
 NASA Ames Research Center
 Moffett Field CA 94035
 (415) 694-6420

Dr. F. E. Marble
 Engrg. and Appl. Sci. Dept.
 California Institute of
 Technology
 Pasadena CA 91125
 (818) 356-4784

Dr. John C Marek
 NASA Lewis Research Center
 21000 Brookpark Road
 Cleveland OH 44135-3127

Mr. C. R. Martel
 AFWAL/POSF
 Wright-Patterson AFB OH 45433-6563
 (513) 255-7431
 AV785-7431

Dr Bruce Masson
 AFWL/ARDF
 Kirtland AFB NM 87117-6008
 (505) 844-0208
 AV244-0208

Dr. James McDonald
 Code 6110
 Naval Research Laboratory
 Chemistry Division
 Washington DC 20375
 (202) 767-3340
 AV297-3340

Dr James McMichael
 AFOSR/NA
 Bolling AFB DC 20332-6448
 (202) 767-4936
 AV297-4936

Dr. Lynn A. Melton
 Programs in Chemistry
 University of Texas, Dallas
 P. O. Box 668
 Richardson TX 75080
 (214) 690-2913

Dr. Andrzej W Mizolek
 Ignition and Combustion Branch
 Interior Ballistics Division
 Ballistic Research Laboratory
 Aberdeen Proving Gnd MD 21005-5066
 (301) 278-6157

Dr P J Morris
 233-L Hammond Building
 Pennsylvania State University
 University Park PA 16802
 (814) 863-0157

Dr. M. G. Mungal
 Department of Mechanical
 Engineering
 Stanford University
 Stanford CA 94305-3032
 (415) 723-1745

Dr. Abdollah Nejad
 AFWAL/POPT
 Wright-Patterson AFB OH 45433-6563
 (513) 255-9991
 AV785-9991

Dr D K McLaughlin
 233 Hammond Building
 Pennsylvania State University
 University Park PA 16802
 (814) 865-2569

Dr A M Mellor
 Mech Matls Eng Department
 Station B, Box 6019
 Vanderbilt University
 Nashville TN 37235
 (615) 343-6214

Dr. R. Metcalfe
 Department of Mechanical
 Engineering
 University of Houston
 Houston TX 77004
 (713) 749-2439

Dr. H. Mongia
 General Motors Corporation
 Allison Gas Turbine Operations
 P. O. Box 420
 Indianapolis IN 46206-0420
 (317) 242-5945

Dr. E. J. Mularz
 Aviation Res. and Tech. Activ.
 NASA Lewis Res. Ctr., MS 5-11
 21000 Brookpark Road
 Cleveland OH 44135-3127
 (216) 433-5850

Dr Arje Nachman
 AFOSR/NM
 Bolling AFB DC 20332-6448
 (202) 767-5028
 AV297-5028

Dr Herbert Nelson
 Code 6110, Chemistry Division
 Naval Research Laboratory
 Washington DC 20375
 (202) 767-3686

Dr. David Nixon
 Nielsen Engineering and
 Research, Inc.
 510 Clyde Avenue
 Mountain View CA 94043-2287
 (415)968-9457

Dr. G. B. Northam
 NASA Langley Research Center
 MS 168
 Hampton VA 23665-5225
 (804)865-2803

Dr. R. C. Oldenborg
 Chemistry Division
 Los Alamos National Laboratory
 Los Alamos NM 87545
 (505)667-2096
 (505)667-3758

Dr. A. K. Oppenheim
 Department of Mechanical
 Engineering
 University of California
 Berkeley CA 94720
 (415)642-0211

Dr. E. S. Oran
 Laboratory for Computational
 Physics
 Naval Research Laboratory
 Washington DC 20375
 (202)767-2960

Dr Richard B Peterson
 Department of Mechanical
 Engineering
 Oregon State University
 Corvallis OR 97331-6001
 (503)754-2567

Dr. W. M. Pitts
 National Bureau of Standards
 Center for Fire Research
 Gaithersburg MD 20899
 (310)975-6486

Dr. Robert W. Pitz
 Department of Mechanical and
 Materials Engineering
 Vanderbilt University
 Nashville TN 37235
 (615)322-0209

Dr. S. B. Pope
 Department of Mechanical and
 Aerospace Engineering
 Cornell University
 Ithaca NY 14853-1301
 (607)255-4314

Dr. C. L. Proctor II
 Department of Mechanical
 Engineering
 University of Florida
 Gainesville FL 32611
 (904)392-7555

Dr. Herschel Rabitz
 Department of Chemistry
 Princeton University
 Princeton NJ 08544
 (609)452-3917

Dr. S. R. Ray
 National Bureau of Standards
 Center for Chemical
 Engineering
 Washington DC 20234

Dr. R. G. Rehm
 National Bureau of Standards
 Center for Fire Research
 Gaithersburg MD 20899

Dr M Renksizbulat
 Department of Mechanical
 Engineering
 University of Waterloo
 Waterloo, Ontario CN N2L 3G1
 (519)885-3977

Dr. W. C. Reynolds
 Department of Mechanical
 Engineering
 Stanford University
 Stanford CA 94305-3032
 (415) 723-3840

Dr James J Riley
 Mechanical Engineering Dept
 University of Washington
 Seattle WA 98195
 (206) 543-5347

Dr. U. S. Rohatgi
 Department of Nuclear Energy
 Brookhaven National Laboratory
 Upton NY 11973
 (516) 282-2475

Dr. W. M. Roquemore
 AFWAL/POSF
 Wright-Patterson AFB OH 45433-6563
 (513) 255-6813
 AV785-6813

Dr. Anatol Roshko
 Graduate Aeronautical Labs
 California Institute of
 Technology
 Pasadena CA 91125
 (818) 356-4484

Dr. D. E. Rosner
 Department of Chemical
 Engineering
 Yale University
 New Haven CT 06520
 (203) 432-4391

Dr John Ross
 Department of Chemistry
 Stanford University
 Stanford CA 94305-3032
 (415) 723-9203

Dr Mohammad Samimy
 Ohio State University
 206 West 18th Avenue
 Columbus OH 43210
 (614) 422-6988

Dr. G. S. Samuels
 Department of Mechanical
 Engineering
 University of California
 Irvine CA 92717
 (714) 856-5468

Mr. John Sanborn
 Garrett Turbine Engine Company
 111 South 34th Street
 P. O. Box 5217
 Phoenix AZ 85010
 (602) 231-2588

Dr. B. R. Sanders
 Thermofluids Division, 8363
 Combustion Research Facility
 Sandia National Laboratories
 Livermore CA 94550
 (415) 294-3113

Dr. J. J. Sangiovanni
 United Technologies Research
 Center
 Silver Lane
 East Hartford CT 06108
 (203) 727-7328

Dr Lakshmi Sankar
 School of Aerospace Engrg
 Georgia Institute of
 Technology
 Atlanta GA 30332
 (404) 894-3014

Dr. Domenic Santavicca
 Department of Mechanical
 Engineering
 Pennsylvania State University
 University Park PA 16802
 (814) 863-1863

Dr. R. J. Santoro
 Department of Mechanical
 Engineering
 Pennsylvania State University
 University Park PA 16801
 (814) 863-1285

Dr Klaus Schadow
 Naval Weapons Center
 Code 3892
 China Lake CA 93555-6001
 (619) 939-1086
 AV437-1086

Dr. John W. Schaefer
 Energy and Environmental Div.
 Acurex Corporation
 555 Clyde Ave., P. O. Box 7555
 Mountain View CA 94039

Dr. D. J. Seery
 United Technologies Research
 Center
 Silver Lane
 East Hartford CT 06108

Dr. H. G. Semerjian
 National Bureau of Standards
 Center for Chemical
 Engineering
 Washington DC 20234
 (301) 975-2609

Dr. K. Seshadri
 Dept. Of. Appl. Mech. and
 Engrg. Sci.
 University of California
 La Jolla CA 92093
 (619) 534-4876

Dr G S Settles
 309 Mechanical Engrg Building
 Pennsylvania State University
 University Park PA 16802
 (814) 863-1504

Mr. Harold C. Simmons
 Parker Hannifin Corporation
 Gas Turbine Fuel Systems Div.
 17325 Euclid Avenue
 Cleveland OH 44143
 (216) 531-3000
 Ext 2309

Dr. W. A. Sirignano
 School of Engineering
 University of California
 Irvine CA 92717
 (714) 856-6002

Dr Bernard Spielvogel
 U S Army Research Office
 P O Box 12211
 Research Triangle Park NC 27709-2211

Dr David S Stewart
 Department of Theoretical and
 Applied Mechanics
 University of Illinois
 Urbana IL 61801

Dr. F. D. Stull
 AFWAL/POPS
 Wright-Patterson AFB OH 45433-6563
 (513) 255-5210
 AV785-5210

Dr B Sturtevant
 Engrg and Appl Sci Dept
 California Institute of
 Technology
 Pasadena CA 91125

Dr. Dexter Sutterfield
 National Institute for
 Petroleum and Energy Research
 Post Office Box 2128
 Bartlesville OK 74005
 (918) 337-4251

Dr. L. Talbot
 Department of Mechanical
 Engineering
 University of California
 Berkeley CA 94720
 (415)642-6780

Julian M. Tishkoff
 AFOSR/NA
 Bolling AFB DC 20332-6448
 (202)767-0465
 AV297-0465

Dr. T. Y. Toong
 Department of Mechanical
 Engineering
 MIT
 Cambridge MA 02139
 (617)253-3358

Dr Michael Trenary
 Department of Chemistry
 The University of Illinois
 Chicago IL 60680

Capt Martin Trout
 AFWL/ARDF
 Kirtland AFB NM 87117-6008
 (505)844-0196
 AV244-0196

Dr. C. J. Ultee
 United Technologies Research
 Center
 Silver Lane
 East Hartford CT 06108

Dr. S. P. Vanka
 Argonne National Laboratory
 9700 South Cass Avenue
 Argonne IL 60439

Dr. P. J. Waltrip
 Applied Physics Laboratory
 Johns Hopkins University
 Johns Hopkins Road
 Laurel MD 20707-6099
 (301)953-5000
 Ext. 4186

Dr. C. K. Westbrook
 Lawrence Livermore National
 Laboratories
 P. O. Box 808
 Livermore CA 94550

Dr. R. W. Whitehead
 Office of Naval Research
 Mechanics Division, Code 432
 800 North Quincy Street
 Arlington VA 22217-5000
 (202)696-4404

Dr James Whitelaw
 Department of Mechanical Engrg
 Imperial College of Science
 and Technology
 London SW7 2BX UK

Dr. Forman A. Williams
 Department of Mechanical and
 Aerospace Engineering
 Princeton University
 Princeton NJ 08544
 (609)452-5271

Dr. Francis Wodarczyk
 AFOSR/NC
 Bolling AFB DC 20332-6448
 (202)767-4960
 AV297-4960

Dr Richard A Yetter
 Department of Mechanical and
 Aerospace Engineering
 Princeton University
 Princeton NJ 08544

Dr. E. E. Zukoski
Engrg. and Appl. Sci. Dept.
California Institute of
Technology
Pasadena CA 91125
(818) 356-4785